

1995 108256

349255

P. 17

JPL Publication 94-19

Proceedings of the Eighteenth NASA Propagation Experimenters Meeting (NAPEX XVIII)

and the

Advanced Communications Technology Satellite (ACTS) Propagation Studies Miniworkshop

Held in Vancouver, British Columbia,
June 16-17, 1994

Faramaz Davarian
Editor

(NASA-CR-196959) PROCEEDINGS OF
THE EIGHTEENTH NASA PROPAGATION
EXPERIMENTERS MEETING (NAPEX 18)
AND THE ADVANCED COMMUNICATIONS
TECHNOLOGY SATELLITE (ACTS)
PROPAGATION STUDIES MINIWORKSHOP
(JPL) 455 p

N95-14670
--THRU--
N95-14684
Unclas

August 1, 1994

G3/32 0025990



National Aeronautics and
Space Administration

Jet Propulsion Laboratory
California Institute of Technology
Pasadena, California

JPL Publication 94-19

Proceedings of the Eighteenth NASA Propagation Experimenters Meeting (NAPEX XVIII)

and the

Advanced Communications Technology Satellite (ACTS) Propagation Studies Miniworkshop

Held in Vancouver, British Columbia,
June 16–17, 1994

Faramaz Davarian
Editor

August 1, 1994

NASA

National Aeronautics and
Space Administration

Jet Propulsion Laboratory
California Institute of Technology
Pasadena, California

The research described in this publication was carried out by the Jet Propulsion Laboratory, California Institute of Technology, under a contract with the National Aeronautics and Space Administration.

Reference herein to any specific commercial product, process, or service by trade name, trademark, manufacturer, or otherwise, does not constitute or imply its endorsement by the United States Government or the Jet Propulsion Laboratory, California Institute of Technology.

PREFACE

The NASA Propagation Experimenters (NAPEX) meeting is a forum convened each year to discuss studies supported by the NASA Propagation Program. The reports delivered at this meeting by program managers and investigators present our recent activities and future plans. Representatives from domestic and international organizations who have an interest in radio wave propagation studies are invited to NAPEX meetings for discussions and an exchange of information. This Proceedings records the content of NAPEX XVIII and the ACTS Propagation Studies miniworkshop that preceded it.

NAPEX XVIII, which took place at Le Meridien Hotel, Vancouver, Canada, on June 17, 1994, consisted of opening remarks and two sessions. Faramaz Davarian made the opening remarks, which described last year's achievements and next year's plans. Session 1, entitled "Slant Path Propagation Studies and Experiments," was chaired by David Rogers of Communications Research Centre (CRC), Canada. Session 2, entitled "Propagation Studies for Mobile, Personal, and Sound Broadcast Systems," was jointly chaired by Rod Olsen of CRC and Faramaz Davarian of the Jet Propulsion Laboratory (JPL).

The main objective of the NASA Propagation Program is to enable new satellite communication applications. This program has always enjoyed a high level of interaction with the space communications community. During these slow economic times with ever more stringent budgetary constraints, this program needs industry's support more than ever. We are looking to industry to share the cost of some of our most urgent studies.

I would like to express my sincere gratitude to Professor Mos Kharadly and his staff for hosting this meeting. They did a splendid job in making this meeting a pleasant one. Thank you Professor Kharadly. Mardy Wilkins was also invaluable in helping us organize the meetings. Furthermore, I would like to thank the participants of both the workshop and NAPEX XVIII for their valuable contributions. Finally, I would like to express my appreciation to Janice Jones of the JPL Technical Information Section for coordinating the publication of this document.

Professor V. N. Bringi of Colorado State University will host NAPEX XIX in June 1995. The exact date of this meeting will be announced later. The fifth ACTS Propagation Studies Workshop will take place in Florida on November 29 and 30, 1994. Professor Rudy Henning of the University of Southern Florida has kindly offered to be the local host for this meeting.

Faramaz Davarian

ABSTRACT

The NASA Propagation Experimenters Meeting (NAPEX), supported by the NASA Propagation Program, is convened annually to discuss studies made on radio wave propagation by investigators from domestic and international organizations. NAPEX XVIII was held on June 17, 1994, in Vancouver, British Columbia, Canada. Participants included representatives from Canada, the Netherlands, England, and the United States, including researchers from universities, government agencies, and private industry. The meeting was organized into two technical sessions. The first session was dedicated to slant path propagation studies and experiments. The second session focused on propagation studies for mobile, personal, and sound broadcast systems. In total, 14 technical papers and some informal contributions were presented.

Preceding NAPEX XVIII, the Advanced Communications Technology Satellite (ACTS) Propagation Studies Miniworkshop was held on June 16, 1994, to review ACTS propagation activities with emphasis on ACTS experiments status and data collection, processing, and exchange. Eleven technical papers were presented by contributors from government agencies, private industry, and university research establishments.

CONTENTS

NAPEX XVIII MEETING

OPENING REMARKS	1
<i>F. Davarian</i>	
 SESSION 1. SLANT PATH PROPAGATION STUDIES AND EXPERIMENTS	5
<i>D. Rogers, Chair</i>	
PROGRESS REPORT ON OLYMPUS PROPAGATION EXPERIMENTS.....	7
<i>B. Arbesser-Rastburg (ESA)</i>	
SLANT PATH PROPAGATION MODELS RESULTING FROM OLYMPUS EXPERIMENTS IN THE U.S.....	11
<i>W. Stutzman (VPI)</i>	
PROPAGATION CHARACTERISTICS OF 20/30 GHz LINKS WITH A 40° MASKING ANGLE.....	47
<i>F. Davarian, A. Kantak, C. Le (JPL)</i>	
PROPAGATION DATA AT 20/40 GHz AND THE PROPAGATION NEEDS OF MILSTAR.....	77
<i>F.I. Shimabukuro, Y.S. Kim, P. Ayotte (Aerospace & USN)</i>	
THE 40 AND 50 GHz PROPAGATION EXPERIMENTS AT THE RUTHERFORD APPLETON LABORATORY, UK, USING THE ITALSAT BEACONS	83
<i>J. M. Woodroffe, P.G. Davies, D.N. Ladd, J.R. Norbury (RAL)</i>	
A DATABASE FOR PROPAGATION MODELS	87
<i>A.V. Kantak, K. Suwitra, C. Le (JPL)</i>	
 SESSION 2. PROPAGATION STUDIES FOR MOBILE, PERSONAL, AND SOUND BROADCAST SYSTEMS	103
<i>R. Olsen and F. Davarian, Chairs</i>	
CHANNEL CHARACTERISATION FOR FUTURE KA-BAND MOBILE SATELLITE SYSTEMS AND PRELIMINARY RESULTS.....	105
<i>M. Sforza, S. Buonomo, B. Arbesser-Rastburg (ESA)</i>	
ACTS MOBILE EXPERIMENTS SUMMARY	117
<i>D.S. Pinck (JPL)</i>	
ACTS MOBILE PROPAGATION CAMPAIGN.....	135
<i>J. Goldhirsh, W.J. Vogel, G.W Torrence (APL & Texas)</i>	

SLANT PATH L- AND S-BAND TREE SHADOWING MEASUREMENTS	151
<i>W.J. Vogel, G.W. Torrence (Texas)</i>	
PROTOGRAMMETRIC MOBILE SATELLITE SERVICE PREDICTION	159
<i>R. Akturan, W. J. Vogel (Texas)</i>	
PROPAGATION CONSIDERATIONS FOR THE ODYSSEY SYSTEM DESIGN	165
<i>H.H. Ho (TRW)</i>	
COMMUNICATIONS AVAILABILITY: ESTIMATION STUDIES AT AMSC	181
<i>C.E. Sigler, Jr. (AMSC)</i>	
S-BAND PROPAGATION MEASUREMENTS (<i>Not Presented</i>)	211
<i>R.D. Briskman (CD Radio)</i>	
SATELLITE FADE STATISTICS AND DIVERSITY GAIN FOR PERSONAL AND BROADCAST SATELLITE COMMUNICATIONS SYSTEMS DERIVED FROM TDRS OBSERVATIONS	223
<i>W.J. Vogel, G.W. Torrence (Texas)</i>	

CONTENTS ACTS MINIWORKSHOP

OPENING REMARKS..... <i>F. Davarian, Chair</i>	239
ADVANCED COMMUNICATIONS TECHNOLOGY SATELLITE (ACTS) PROGRAM..... <i>R. Bauer (NASA Lewis)</i>	243
ACTS PROPAGATION TERMINAL MAINTENANCE, SUPPORT AND UPDATES..... <i>D. Westenhaver (WWW, Inc.)</i>	267
RADIOMETER CALIBRATION PROCEDURE AND BEACON ATTENUATION ESTIMATION REFERENCE LEVEL <i>R.K. Crane (Oklahoma)</i>	273
DATA CENTER STATUS REPORT <i>W.J. Vogel, A. Syed (Texas)</i>	287
ALASKA ACTS PROPAGATION TERMINAL: DATA ANALYSIS PROCEDURE, SYSTEM STATUS, AND RESULTS <i>B. Jaeger, C. Mayer (Alaska)</i>	297
U.B.C. ACTS PROPAGATION EXPERIMENT..... <i>I. Dommel, R. Hulays, M. Kharadly (British Columbia)</i>	323
KA-BAND PROPAGATION MEASUREMENTS USING THE ACTS PROPA- GATION TERMINAL AND CSU-CHILL MULTIPARAMETER RADAR..... <i>V.N. Bringi, J. Beaver, J. Turk (Colorado)</i>	351
ACTS UP-LINK POWER CONTROL EXPERIMENT..... <i>A. Dissanayake (COMSAT)</i>	385
FLORIDA'S PROPAGATION REPORT <i>H. Helmken, R. Henning (Florida Atlantic & South Florida)</i>	399
NEW MEXICO ACTS PROPAGATION TERMINAL STATUS REPORT..... <i>S. Horan, G. Feldhake (New Mexico)</i>	415
ACTS PROPAGATION MEASUREMENTS PROGRAM..... <i>L.J. Ippolito (Stanford Telecommunications/New Mexico)</i>	429
GEORGIA TECH ACTS EXPERIMENT <i>D. Howard (Georgia Tech)</i>	453
REPORT OF THE WORKING GROUPS PLENARY MEETING <i>D.V. Rogers, R.K. Crane (CRC & Oklahoma)</i>	457

NAPEX XVIII AND ACTS MINIWORKSHOP ATTENDEES

Bertram Arbesser-Rastburg
ESA-ESTEC
Postbus 299
NL-2200
The Netherlands
+31-1719-84541
+31-1719-84999 (FAX)
E-mail: bertram@xe.estec.esa.nl

Robert Bauer
NASA Lewis Research Center
21000 Brookpark Rd., MS 54-6
Cleveland, OH 44135
216-433-3431
216-433-6371 (FAX)
E-mail: acbauer@lims01.lerc.nasa.gov

John Beaver
Colorado University
Dept. of EE
Ft. Collins, CO 80523
303-491-7678
303-491-2249 (FAX)
E-mail: jb686028@longs.lance.
colostate.edu

Greg Brooke
University of British Columbia
Dept. of EE
2356 Main Mall
Vancouver, British Columbia
Canada V6T 1Z4
604-822-3980
604-822-5949 (FAX)
E-mail: acts@ee.ub.ca

Aimee Chan
University of British Columbia
2356 Main Mall
Vancouver, British Columbia
Canada V6T 1Z4
604-293-6094
604-293-5787 (FAX)
E-mail: achan@mprgate.mpr.ca

Robert K. Crane
University of Oklahoma
100 East Boyd St., Room 1248
Norman, OK 73019-0628
405-325-4419
405-325-7689 (FAX)
E-mail: bcrane@geohub.gcn.uoknor.edu

Faramaz Davarian
Jet Propulsion Laboratory
MS T-1708
4800 Oak Grove Drive
Pasadena, CA 91109
818-354-4820
818-393-0096 (FAX)
E-mail: davarian@java.jpl.nasa.gov

Asoka Dissanayake
COMSAT Labs
22300 Comsat Drive
Clarksburg, MD 20871
301-428-4411
301-428-3638 (FAX)
E-mail: asoka_dissanayake@mr_mail.
trans.comsat.com

Irmgard I. Dommel
University of British Columbia
Dept. of EE
2356 Main Mall
Vancouver, British Columbia
Canada V6T 1Z4
604-822-3980
604-822-5949 (FAX)
E-mail: acts@ee.ub.ca

Barry Fairbanks
NASA Lewis Research Center
21000 Brookpark Rd., MS 54-6
Cleveland, OH 44135
216-433-3541
216-433-6371 (FAX)
E-mail: acfair@lims01.lerc.nasa.gov

Glen Feldhake
New Mexico State University
Department SG
P. O. Box 30001
Las Cruces, NM 88003-0001
505-646-3042
505-646-1435 (FAX)
feldhake@shanon.nmsu.edu

Julius Goldhirsh
Applied Physics Lab.
Johns Hopkins University
Johns Hopkins Road
Laurel, MD 20723-6099
301-953-5042
301-953-6141 (FAX)
E-mail: julius@nansen.jhuapl.edu

Henry F. Helmken
Florida Atlantic University
P.O. Box 3091, MS SE/456
Boca Raton, FL 33431
407-367-3452
407-367-2336 (FAX)
helmkenh@acc.fau.edu

Rudolph Henning
University of South Florida
Dept. of EE
Tampa, FL 33620
813-974-4782
813-974-5250 (FAX)
E-mail: henning@ec.usf.edu

Hau H. Ho
TRW
MS R6-1587
One Space Park
Redondo Beach, CA 90278
310-812-1658
310-813-4719 (FAX)

Stephen Horan
New Mexico State University
P. O. Box 30001, Dept. SG
Las Cruces, NM 88003-3001
505-646-5870
505-646-1435 (FAX)
E-mail: shoran@nmsu.edu

Daniel H. Howard
Georgia Tech Research Institute
Information Tech. and Telecom Lab
Atlanta, GA 30332-0800
404-894-3541
404-894-3906 (FAX)
E-mail: dan.howard@gtri.gatech.edu

Rafel Hulays
University of British Columbia
2356 Main Mall
Vancouver, B.C.
Canada V6T 1Z4
604-822-2872
604-822-5949 (FAX)
E-mail: acts@ee.ubc.ca

Louis J. Ippolito
Stanford Telecom.
1761 Business Center Drive
Reston, VA 22090
703-438-8061
703-438-8112 (FAX)
E-mail: lji@sed.stel.com

Brad Jaeger
University of Alaska
Dept. of EE
539 Duckering Bldg.
Fairbanks, AK 99775
907-474-7815
907-474-6087 (FAX)
E-mail: fsfejl@aurora.alaska.edu

Jeff Jenkins
New Mexico State University
P. O. Box 30001, ECE Dept.
Las Cruces, NM 88003-3001
505-646-6287
505-646-1435 (FAX)
E-mail: jejenkn@nmsu.edu

Anil V. Kantak
Jet Propulsion Laboratory
MS-1708
4800 Oak Grove Drive
Pasadena, CA 91109
818-354-1825
818-393-0096 (FAX)
E-mail: kantak@java.jpl.nasa.gov

M. M. Z. Kharadly
Dept. of EE
University of British Columbia
2356 Main Mall
Vancouver, British Columbia
Canada V6T 1Z4
604-822-2816
604-822-5949 (FAX)
E-mail: acts@ee.ubc.ca

Takis Mathiopoulos
University of British Columbia
Dept. of EE
2356 Main Mall
Vancouver, British Columbia
Canada V6T 1Z4
604-822-6942
604-822-5949 (FAX)
mathio@ee.ubc.ca

Charlie Mayer
University of Alaska, Dept. of EE
539 Duckering Bldg.
Fairbanks, AK 99775
907-474-6091
907-474-6087 (FAX)
E-mail: ffcem@aurora.alaska.edu

Daniel I. Nakamura
Jet Propulsion Laboratory
MS 238-420
4800 Oak Grove Drive
Pasadena, CA 91109
818-354-2643
818-354-6825 (FAX)
dnakamur@bv.jpl.nasa.gov

Demetre Nicolaidis
Teleglobe Canada
625 Belmont Street
Montreal, Quebec
Canada H3B 2M1
514-868-8322
514-868-8350 (FAX)

John R. Norbury
Rutherford Appleton Laboratory
Radio Communication Research
Building R.25
Chilton, Didcot
Oxfordshire, OX110QX
U.K.
+44-235-445508
+44-235-446140 (FAX)
E-mail: JRN@IB.RL.AC.UK

Roderic L. Olsen
Communications Research Centre
3701 Carling Avenue
Ottawa, Ontario
Canada K2H 8S2
613-998-2564
613-998-4077 (FAX)
E-mail: rod.olsen@crc.doc.ca

Michael Penner
University of British Columbia
Dept. of EE
2356 Main Mall
Vancouver, British Columbia
Canada V6T 1Z4
604-822-3980
604-822-5949 (FAX)
E-mail: acts@ee.ubc.ca

Deborah Pinck
MS 161-241
Jet Propulsion Laboratory
4800 Oak Grove Drive
Pasadena, CA 91109
818-354-8041
818-393-4643 (FAX)
pinck@zorba.jpl.nasa.gov

David J. Rochblatt
Jet Propulsion Laboratory
MS 238-725
4800 Oak Grove Drive
Pasadena, CA 91109
818-354-3516
818-354-2825 (FAX)
E-mail: David-j-rochblatt@jplpost.
jpl.nasa.gov

David V. Rogers
Communications Research Centre
3701 Carling Avenue
Ottawa, Ontario
Canada K2H 8S2
613-998-5174
613-998-4077 (FAX)
E-mail: dave.rogers@crc.doc.ca

Fred I. Shimabukuro
Aerospace Corporation
P.O. Box 92957
Los Angeles, CA 90009
310-336-6903
310-336-6225 (FAX)

Charles Sigler, Jr.
American Mobile Satellite Corp.
1150 Connecticut Ave, NW 4th Floor
Washington DC, 20036
202-872-7626
202-331-5861 (FAX)

Daniel Stern
NASA Headquarters
Code OX
Washington DC, 20546
202-358-4829
202-358-3525 (FAX)
dstern@qmgate.osc.hq.nasa.gov

Warren L. Stutzman
Virginia Tech.
Bradley Dept. of Electrical Engineering
Blacksburg, Virginia 24061-0111
703-231-6834
703-231-3355 (FAX)
E-mail: stutzman@vtvm1.cc.vt.edu

Krisjani S. Suwitra
Jet Propulsion Laboratory
4800 Oak Grove Drive, MS T-1708
Pasadena, CA 91109
818-354-9250
818-393-0096 (FAX)
E-mail: suwitra@java.jpl.nasa.gov

Geoffrey Torrence
University of Texas
10100 Burnet Road
Austin, TX 78758-4445
512-471-8608
512-471-8609

Wolf Vogel
EE Research Laboratory
University of Texas
10100 Burnet Road
Austin, TX 78758
512-471-8608
512-471-8609 (FAX)
E-mail: wvogel@globe.ece.utexas.edu

David B. Westenhaver
Auburn CCDS
746 Lioness Ct. S.W.
Stone Mountain, GA 30087-2855
404-925-1091
404-931-3741 (FAX)
E-mail: 72622.3404@CompuServe.Com

Administrative Assistant

JPL:

Mardy Wilkins
818-354-1723
818-393-0096 (FAX)
E-mail: wilkins@java.jpl.nasa.gov

ACTS Electronic Mailing List Address:

acts@java.jpl.nasa.gov

**NAPEX XVIII AGENDA
NASA Propagation Experimenters' Meeting
Le Meridien Hotel, Vancouver
June 17, 1994**

- 8:00 Registration and continental breakfast
- 8:15 Opening Remarks
F. Davarian and W. Rafferty (JPL)
- Session 1: Slant Path Propagation Studies and Experiments**
- 8:45 Progress Report on Olympus Propagation Experiments
B. Arbesser-Rastburg (ESA)
- 9:15 Slant Path Propagation Models Resulting from Olympus Experiments in the U.S.
W. Stutzman (VPI)
- 9:35 A Summary of ACTS Propagation Measurements (not presented)
R. Crane (Oklahoma) and W. Vogel (Texas)
- 10:00 Break
- 10:25 Ka-Band Propagation Effects with a 40° Masking Angle
F. Davarian, A. Kantak, and C. Le (JPL)
- 10:45 Propagation Data at 20/40 GHz and the Propagation Needs of Milstar
S. Shimabukuro, Y. S. Kim (Aerospace), and P. Ayotte (USAF)
- 11:05 The Propagation Studies at Rutherford Appleton Laboratory using the 40 and 50 GHz Beacons from ITALSAT
J. Norbury (RAL)
- 11:20 A Database for Propagation Models and Computer Demo
A. Kantak, K. Suwitra, and C. Le (JPL)
- 11:45 Lunch Break (lunch served at 12:00 noon)
- Session 2: Propagation Studies for Mobile, Personal, and Sound Broadcast Systems**
- 1:15 Channel Characterisation for Future Ka-Band Mobile Satellite Systems and Preliminary Results
M. Sforza, S. Buonomo, and B. Arbesser-Rastburg (ESA)
- 1:35 ACTS Mobile Experiments Summary
D. Pinck (JPL)
- 1:55 ACTS Mobile Propagation Campaign
J. Goldhirsh (APL), W. Vogel, G. Torrence (Texas)
- 2:15 Slant Path L- and S-Band Tree Shadowing Measurements
W. Vogel and G. Torrence (Texas)
- 2:35 Photogrammetric Mobile Satellite Service Prediction
W. Vogel and R. Akturan (Texas)
- 2:50 Propagation for Odyssey
H. Ho (TRW)
- 3:05 Break
- 3:30 Communications Availability Estimation Studies at AMSC
E. Sigler (AMSC)
- 3:45 S-Band Propagation Measurements (not presented)
R. Briskman (CD Radio)
- 4:00 Satellite Fade Statistics and Diversity Gain for Personal and Broadcast Satellite Communications Systems Derived from TDRS Observations
W. Vogel and G. Torrence (Texas)
- 4:20 Closing Remarks
- 5:00 Meeting Adjourned

AGENDA
ACTS PROPAGATION MINIWORKSHOP
Hotel Le Meridien, Vancouver
June 16, 1994

- 8:00 Registration and Continental Breakfast
- 8:15 Opening Remarks
F. Davarian (JPL)
- 8:45 An Update from LeRC on the Beacons, Satellite, etc.
R. Bauer (LeRC)
- 9:15 Terminal Maintenance
D. Westenhaver (WWW, Inc.)
- 9:45 Radiometer Calibration Procedure
R. Crane (Oklahoma)
- 10:15 Break
- 10:40 Beacon Attenuation Estimation Reference Level
R. Crane (Oklahoma)
- 11:00 ACTS Propagation Data Center
W. Vogel (Texas)
- 11:30 ACTS Propagation Experimenter Update
Alaska, British Columbia, Colorado, Florida, Maryland, New Mexico, Oklahoma
- 12:00 Lunch Break (lunch served at 12:15)
- 1:30 Experimenter Update Continues
- 3:15 Break
- 3:35 Plenary
R. Crane (Oklahoma) and D. Rogers (CRC)
- 5:00 Meeting Adjourned
- 5:30 Leave for a visit to ACTS site at UBC
- 7:30 Salmon Dinner at UBC
Host: M. Kharadly (UBC)

OPENING REMARKS RECENT ACCOMPLISHMENTS AND FUTURE PLANS

Faramaz Davarian

It is customary to review the progress of the NASA Propagation Program during the opening remarks of the annual NAPEX meeting. In line with this practice, the accomplishments of the Program during the past year and our plans for the next year are presented here. We hope that the meeting participants, particularly members of the space communications industry, will provide us with feedback to insure that our plans will meet their needs.

Our Olympus campaign, which began in 1988, was completed during this reporting period by the experiment team at Virginia Polytechnic Institute and State University (VPI). This experiment consisted of beacon measurements at 12, 20, and 30 GHz at an elevation angle of 14° for one year. Although the final reports were distributed in December 1993, the VPI team is continuing the publication of the results in the open literature. A week ago, I received two papers from VPI that I copied to the ACTS experimenters. We will take advantage of lessons learned from the Olympus effort in the ACTS campaign. Dr. Warren Stutzman will provide a summary of the Olympus experiment in his presentation this morning.

During this reporting period, the ACTS terminals were installed and Ka-band propagation measurements began at seven sites. Since December 1993, experimenters have been sending data to the ACTS Data Center at the University of Texas. Most of the terminal hardware and software problems have been dealt with, and we are ready to address the remaining ones. Our experimenters will focus on data processing and analysis in the coming year. Since a one-day session was devoted to ACTS propagation work yesterday, no presentation is scheduled on this subject today.

In 1992, we made low-elevation-angle L-band measurements of land mobile-satellite channels. The analyses of these measurements took place in 1993 with the final report published in early 1994. The principal investigator of this effort, Dr. Wolfhard Vogel, will make a presentation on this subject.

A few months ago, NASA offered Tracking and Data-Relay Satellite System (TDRSS) satellites to industry for communication experiments and field measurements. This is a great opportunity for us to make S-band measurements in support of future satellite broadcast radio services. Currently we are using two of the TDRSS satellites for field trials. The goal is to collect fade statistics and multisatellite diversity data. Dr. Vogel will make a presentation on this subject. The result of this campaign will be published in 1995.

Dr. Vogel will also talk on a number of L- and S-band measurement efforts that we started about a year ago. These include tree shadowing, in-building measurements, and more. The purpose of this campaign is to support the development of low-earth-orbit (LEO) satellite communications systems for mobile and personal applications.

We have been conducting two long-term measurement campaigns over the past several years. Using a 12-GHz Intelsat beacon, we have made low-elevation angle measurements for six years (*will go for eight years*). This campaign will conclude when eight years of data have been collected. The final report will be published by the University of Texas. Similarly we have collected eight years of rain-rate data using a network of rain gauges in the Mid-Atlantic coast of the United States. This network consists of ten sites. The measurement phase of this campaign has been completed, and a report is due soon.

Last year we released Version 1 of the *Database for Propagation Models* software. This program has been improved considerably since a year ago and now both PC and Mac versions are available. A presentation and demonstration of this program will be given in this meeting. You will also receive a copy of this program free of charge. However, after you have had a chance to try it out, we request that you share your comments with us. We would like to use your feedback to improve the program. This software will facilitate the use of propagation models by the user community, particularly system planners and designers. System engineers will be able to link the output of this program to their design control tables.

Last year CCIR was renamed ITU-R and Study Groups 5 and 6 were merged into a new Study Group 3. As you may recall, more than a year ago I submitted an input document to CCIR on modeling land mobile-satellite effects. This document was considered at the meeting of WP5/B of ITU-R in Geneva, Switzerland in October 1993. WP5/B adopted the models presented in our document as a new ITU-R recommendation for predicting land mobile-satellite propagation effects. We also provided land mobile-satellite data to the ITU-R data bank at the October meeting. I continue to be ITU-R table keeper for land mobile-satellite data, and Bob Crane continues to maintain rain rate and scintillation tables. In the coming years, we expect to provide the ITU with improved and expanded mobile-satellite, direct-satellite-broadcast, and Ka-band models.

The working parties of Study Group 3 will meet in September 1994 in Boulder, Colorado. A task group on LEO systems is also scheduled to meet during the same period. This task group will consider, for the first time, the propagation needs of LEO mobile and personal communication systems. I will participate in both the working party meeting and the task group meeting.

With the new changes in NASA's priorities, a strong emphasis has been placed on industry interaction and participation in NASA's programs. The NASA Propagation Program has always worked with industry and has considered the space communications community its main customer. Therefore, I would like to reiterate our goal of helping industry to expand and develop new services and applications. We achieve our goal by conducting propagation studies to enable the development of necessary technologies and by working with regulatory organizations to secure radio spectrum for satellite communications applications. We invite industry to actively participate and support our efforts. We will consider these industry inputs as the basis for our future plans.

NAPEX XVIII

Session 1

**SLANT PATH PROPAGATION STUDIES AND
EXPERIMENTS**

Chair:

David Rogers

Communications Research Centre

PROGRESS REPORT ON OLYMPUS PROPAGATION EXPERIMENTS

Bertram Arbesser-Rastburg

349252

P37

European Space Agency - ESTEC,
Wave Interaction and Propagation Section (XEP)
Keplerlaan 1, NL-2200 AG Noordwijk, The Netherlands
Tel:+31-1719-84541 Fax:+31-1719-84999 Internet: bertram@xe.estec.esa.nl

ABSTRACT

A summary of the activities of the OPEX (Olympus Propagation EXperimenters) group is given and some of the recent findings are presented.

1. BACKGROUND

OLYMPUS, a telecommunication satellite owned by the European Space Agency, was launched on 12 June 1989. After the in-orbit tests were completed (in September 1989) the first propagation experiments started. Throughout 1990 the spacecraft functioned very well and a large number of experimenters received the beacon signals. On 29 May 1991 the spacecraft became in-operational after a major technical problem. With a series of complicated procedures OLYMPUS was recovered on 15 August 1991 - the first time in history that a civilian telecommunications satellite was brought back to service after losing power and telemetry. The propagation experiments were back on the track. However, the recovery had used up so much fuel that the North-South station keeping had to be abandoned, which led to a natural increase of inclination at a rate of about 0.8° per year. On 10 October 1992 the second 30 GHz beacon tube failed, causing a loss of this beacon signal. The other two beacon frequencies continued to deliver a stable signal for more than two years. On 12 August 1993 the spacecraft experienced another problem with the attitude control, but this time there was not enough fuel left for a recovery maneuver and thus the mission had come to an end.

The table below gives a summary of the operational status of the OLYMPUS beacon payload:

	1989	1990	1991	1992	1993
Spacecraft bus	=====	=====	=====	=====	=====
B0 beacon (12.5 GHz)	=====	=====	=====	=====	=====
B1 beacon (19.7 GHz)	=====	=====	=====	=====	=====
B2 beacon (29.6 GHz)	=====	=====	=====	=====	=====

Table 1: Availability of beacon signals from OLYMPUS

During the operational phase of the OLYMPUS satellite, the OPEX group met twice per year (OPEX 13 to OPEX 20) to discuss the measurements, the data processing and analysis

procedures and to interpret the first results.

AFTER the early demise of OLYMPUS on 12 August 1993, the propagation experimenters concentrated on the analysis of the data collected.

2. DATA ANALYSIS AND COLLECTION OF STATISTICAL RESULTS

The data of most experiments were pre-processed using the DAPPER software [1] which was jointly defined by the members of the OPEX group. Also the analysis was done with DAPPER, although alternate approaches which followed the same philosophy were also used. In order to allow easy access to the statistical results of the different experiments and in particular to use the results for testing prediction methods, a database management system named DBOPEX has been set up which is completely compatible with the ITU-R SG5 electronic databank [2]. The experimenters convert their data to the DBOPEX flat file format and upload them to the ESTEC FTP server. There the data are imported into the existing database and stored in DBF (dBASE) format. The DBOPEX package itself is a self contained database management system written in CLIPPER (designed to run on MS-DOS compatible platforms). The user can:

- inspect the data (Browse-mode),
- set up the print format and print the data,
- make queries on the database to select data that meet certain conditions,
- extract the data to an ASCII file for further processing (e.g. for model tests),
- edit existing data and append new data,
- import data from a flat ASCII file which has the format of the "EXPORT"-file.

Compatibility with the ITU-R database facilitates the submission of the data to the ITU-R Study Group 3.

3. AVAILABLE ATTENUATION STATISTICS

The following table was prepared by the coordinator of the Attenuation Working Group [3].

Location and Country		Source	Analysed time period (MO/YR)
Darmstadt	DE	B1V, B2	01/90 - 12/90 & 10/91 - 09/92
Oberpfaffenhofen	DE	B1H	01/92 - 06/92
Eindhoven	NL	B0 B1V B1H B2 Radiometer (12/20/30)	09/90 - 08/93 12/90 - 08/93
Martlesham	GB	B0 B1V B2	11/89 - 05/91
Chilton	GB	B2	06/90 - 05/91
Albertslund	DK	B1V B2 Radiometer (20/30)	10/91 - 09/92 10/91 - 09/92
Spino d'Adda	IT	B0 B1V	08/92 - 08/93
Rome	IT	B0 B1H	01/92 - 12/93
Verona	IT	B1H	04/92 - 12/92
Naples	IT	B1H	03/92 - 12/92
Lessive	BE	B0 B1V B1H	01/90 - 12/90 & 01/92 - 12/92

Table 2: Completed analysis of OPEX attenuation data (Status as of May 1994)

4. RECENT FINDINGS

This section presents some results published since the OLYMPUS Utilization Conference in Seville [4], namely at OPEX 20 [5] and at OPEX 21 [6].

○ Attenuation and scintillation

A few experiments have so far provided cumulative statistics of attenuation [7]. Comparison with predictions (according to ITU-R Rec 618) generally shows reasonable agreement. In the low-margin region from 1 to 10 percent of the year however, the non-rain effects become dominant and here the current prediction methods which are based on Ku-band observations are not sufficient.

For fade durations several investigations were carried out [8],[9]. A modelling exercise [10] showed that the previously held assumption that the statistics of short fades can be described by a power-law function and that of long fades by a log-normal function ("COST 205 model" [11]) is still valid. However, the breakpoint between long and short fades is no longer 32 seconds but rather 1 minute.

Scintillations are particularly important for low margin systems. Spectral analysis of scintillation events at 20 and 30 GHz confirm the expected $-8/3$ slope of the power density with a corner frequency of between 0.1 and 0.5 Hz.

○ XPD

Depolarization can become a problem when frequency re-use is employed. For obtaining good depolarization data, complex procedures had to be established to remove all equipment effects [1],[3]. Comparison of experimental results with existing prediction models (ITU BR Rec 618) showed that ice induced XPD (which also occurs at clear sky conditions) is not properly accounted for in the prediction. This observation already led to the development of "two population" hydrometeor models, where a clear distinction of the rain and ice induced depolarization mechanisms is made .

○ Impairment Restoration

Uplink power control was traditionally suffering from the need to scale the fade measured at the downlink frequency to the frequency used for transmitting. Instantaneous frequency scaling from 20 to 30 GHz has been studied by many experimenters and prediction errors of up to ± 3 dB were found when applying a constant conversion factor. A small cell of intensive rain (large drops) can give the same path attenuation at 20 GHz as a long path through moderate rain (small drops) but at 30 GHz the two different events would have different attenuation values. Besides the drop size distribution, also the melting layer can influence the scale factor.

Site diversity may be the only viable means of meeting high availability requirements on Ka-band links. A first analysis of OPEX site diversity arrangements shows that the site diversity

gain predicted by the ITU BR Rec 618 is within acceptable bounds. It has been shown however, that deriving site diversity gain from cumulative statistics (equiprobable approach) tends to underpredict. Analysing site diversity gain straight from the raw data gives more realistic results [12].

CONCLUSIONS

In spite of the shorter than expected lifetime of OLYMPUS the OPEX campaign brought the propagation research an important step forward. A major contributing factor to this success was the good collaboration between the different groups within OPEX. The exchange of data, ideas and expertise generated a most fruitful synergistic effect which is reflected in a number of jointly published papers. A joint presentation of the findings will be given at the OPEX Workshop from 8 to 10 November 1994 at ESTEC.

REFERENCES

1. Siemens Austria "DAPPER Software Users Manual, Preprocessing and Analysis Software", ESA Contract 7609
2. CCIR "Acquisition, Presentation and Analysis of Data in Studies of Tropospheric Propagation", ITU-R Recommendation 311-6, RPN Series, Geneva 1992
3. P.G. Davies, "Summary of Attenuation Statistics from OPEX Members", Proc. OPEX 21, Louvain, May 1994
4. OLYMPUS Utilization Conference, Seville, April 1993, ESA WPP-60
5. Proceedings of the 20th Meeting of OLYMPUS Propagation Experimenters, Darmstadt, November 1993
6. Proceedings of the 21st Meeting of the OLYMPUS Propagation Experimenters, Louvain-la-Neuve, May 1994
7. P G Davies, "Summary of Attenuation Statistics from OPEX Experiments", Proc OPEX 21, Louvain, May 1994
8. S. Upton, "Fade Durations and Intervals Measured in Denmark with Olympus", Proc. OPEX 21, Louvain, May 1994
9. A.P. Gallois, "Further Fade Duration Statistics", Proc OPEX 21, Louvain, May 1994
10. A. Paraboni, "A New Method for Fade Duration Statistics Prediction", Proc. OPEX 21, Louvain, May 1994
11. COST Project 205 "The Influence of the Atmosphere on Wave Propagation", European Community Commission Report 9923, Brussels 1985
12. P. Golé and J. Lavergnat, "Diversity Results at 20 and 30 GHz - Investigation of Instant Diversity Gain", Proc OPEX 21, Louvain, May 1994

**SLANT PATH PROPAGATION MODELS
RESULTING FROM OLYMPUS
EXPERIMENTS IN THE U.S.**

**Warren Stutzman
Virginia Tech**

NAPEX - June 1994

Vancouver, BC



wis\slant.ovr
06/10/94

OVERVIEW

Propagation Effects

Data Presentation

Modeling

Rain Rate

Attenuation

Attenuation Ratio

Fade Slope

Fade Duration



PROPAGATION EFFECTS



SUMMARY OF PROPAGATION EFFECTS

● EFFECTS

Effect	Responsible Mechanisms	Level	Time Scale
Attenuation (fading) (amplitude reduction)	Gases	A few dB	Slow
	Rain	Many dB	Fast (seconds to minutes)
	Clouds, fog, wet snow	A few dB	Fast
	Ice, dry snow	Small	-----
Scintillations (Rapid fade/enhancement)	Gases	Several dB	Very fast (seconds)
Depolarization	Precipitation	Can reduce dual polarized channel isolation to unusable levels	Fast (seconds to minutes)
Dispersion			
Frequency variations over signal bandwidth	Gases	Not significant	-----
	Hydrometeors	Not significant	

● SYSTEM IMPLICATIONS

- Reduced quality of analog links
- Increased error rate on digital links

● FREQUENCY DEPENDENCE OF EFFECTS

<u>Mechanism</u>	<u>Frequency Dependence</u>
Gaseous Attenuation	Increases with frequency Spectral line of water vapor at 22 GHz
Scintillations	RMS signal $\sim f^{7/12}$ [dB]
Rain Attenuation	$A \sim f^2$ [dB]
Rain Depolarization	$XPD_2 = XPD_1 - 21.5 \log \frac{f_2}{f_1}$ [dB]

DATA PRESENTATION

- Quantities

Rain rate R

Attenuation AFS, ACA, ARD

Other: Crosspolarization, Phase

- Types

- Instantaneous (time histories)

Quantities as a function of time



- Statistics (average annual)

 - Primary

 - Rain rate

 - Attenuation

 - Attenuation ratio

 - Secondary

 - Fade rate

 - Fade duration

 - Interfade interval



MODELING

Rain Rate

Attenuation

Attenuation Ratio

Fade Slope

Fade Duration



● CCIR Rain Regions

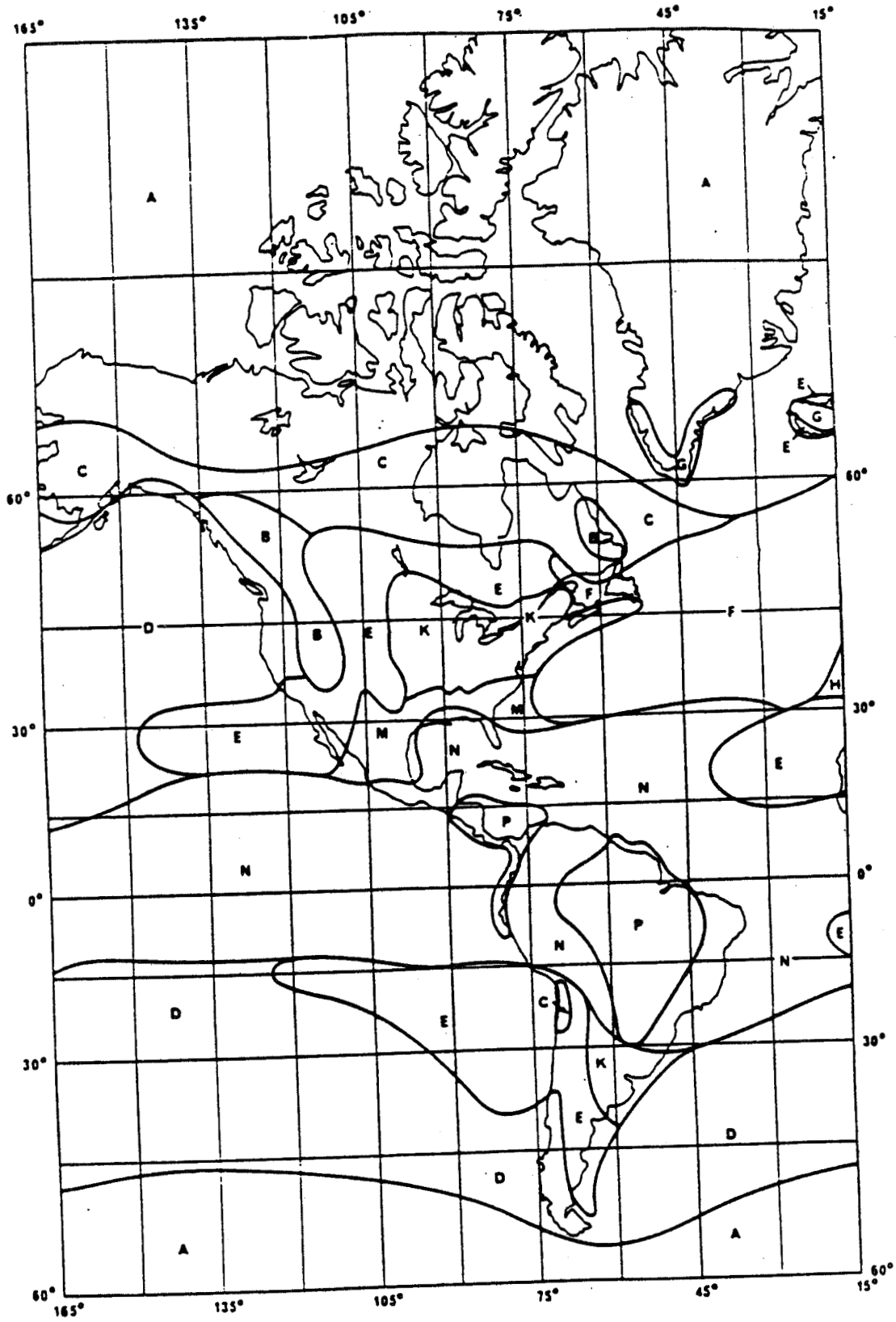
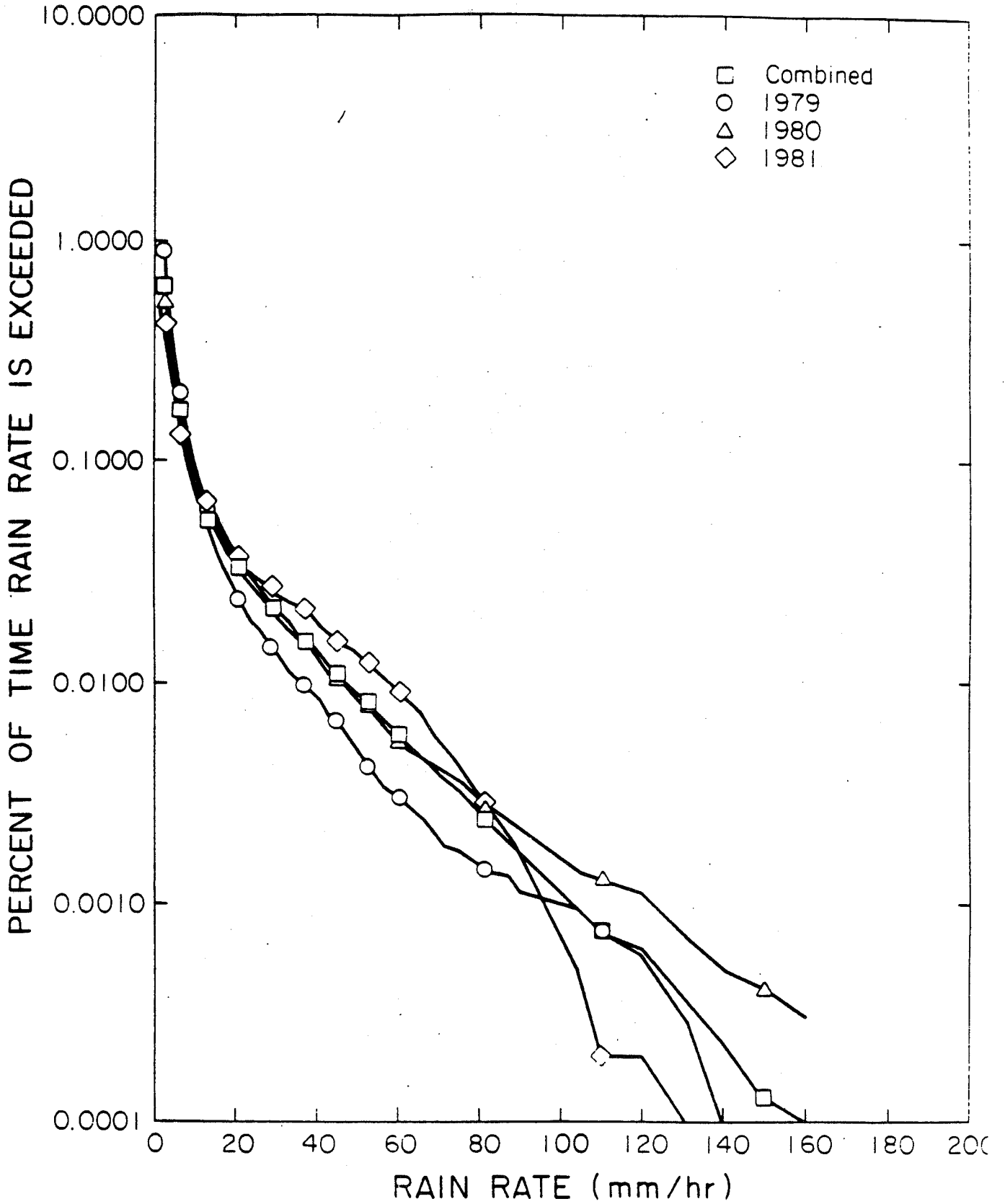


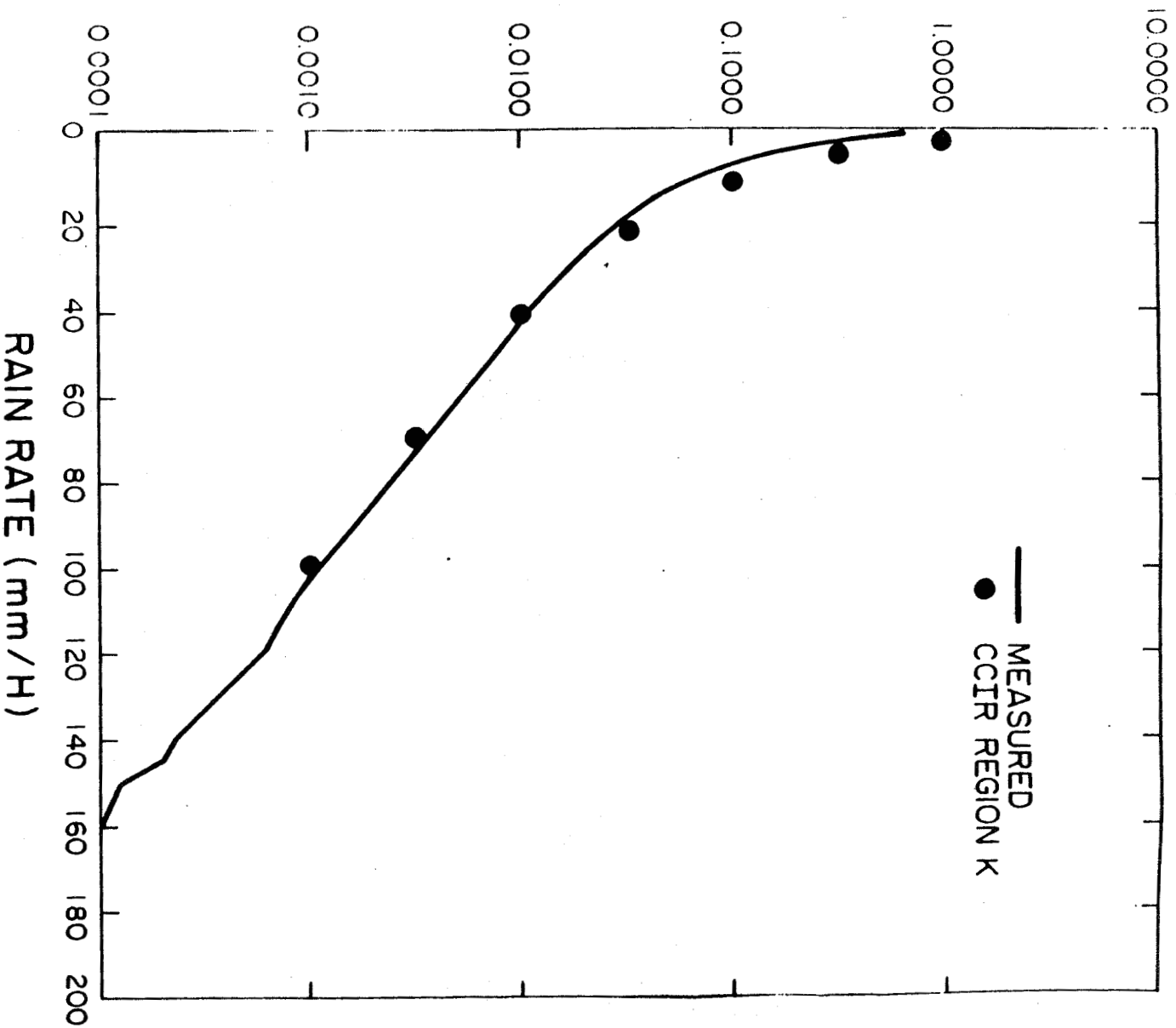
FIGURE 15
(see Table I)

RAIN RATE

● Example of Multiple Years of Measured Data

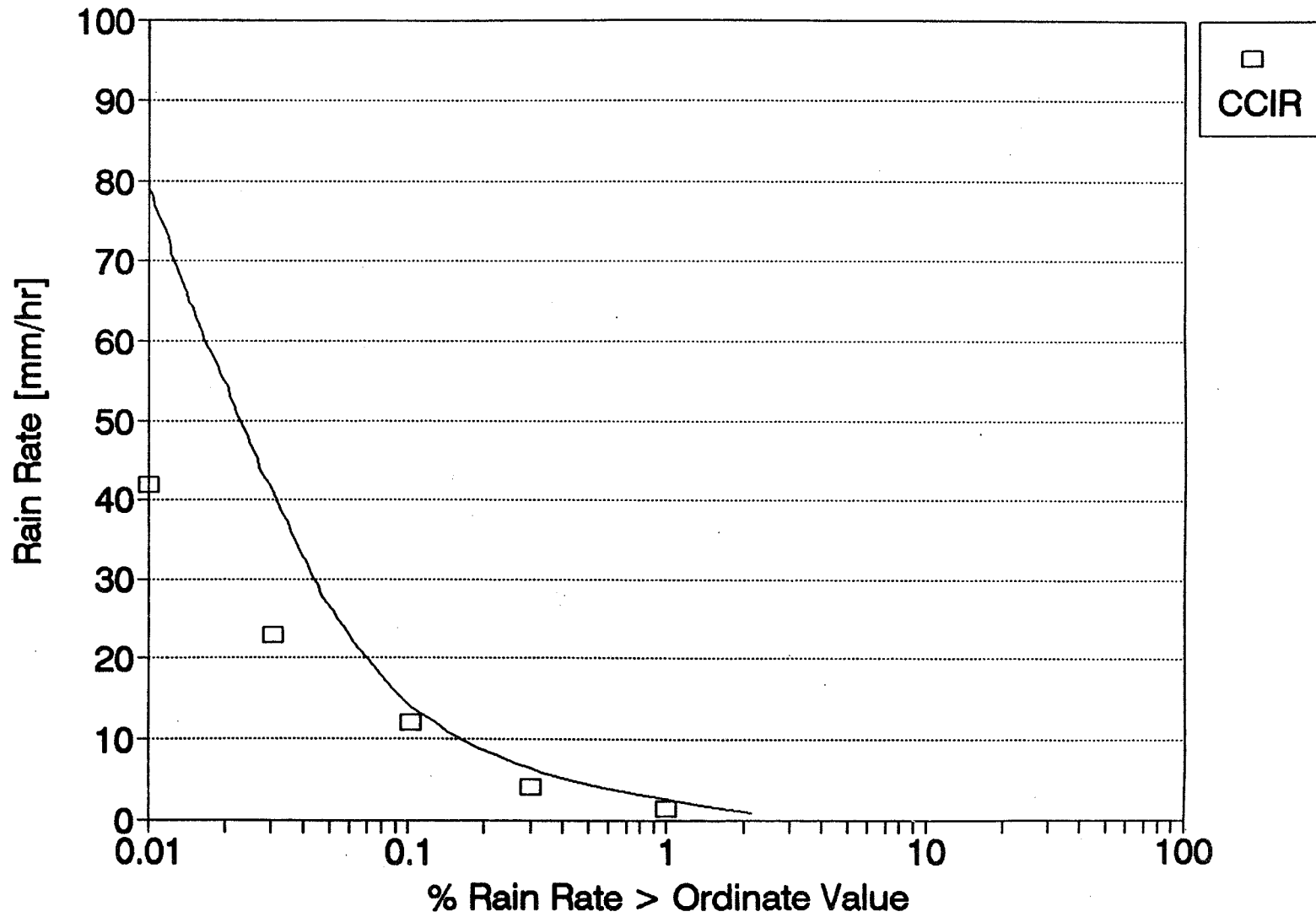


PERCENT OF TIME RAIN RATE IS EXCEEDED



1979-81

MEASURED RAIN RATE AT BLACKSBURG, VA One Year (91/92)



MODELING OF RAIN ATTENUATION

- Attenuation Prediction Formulation

$$A = L_e \alpha \quad [\text{dB}]$$

$$\alpha = \text{specific attenuation} = aR^b \quad [\text{dB/km}]$$

R = point rain rate at earth terminal [mm/h]

L_e = effective path length [km] which is a function of R, elevation angle, . . .

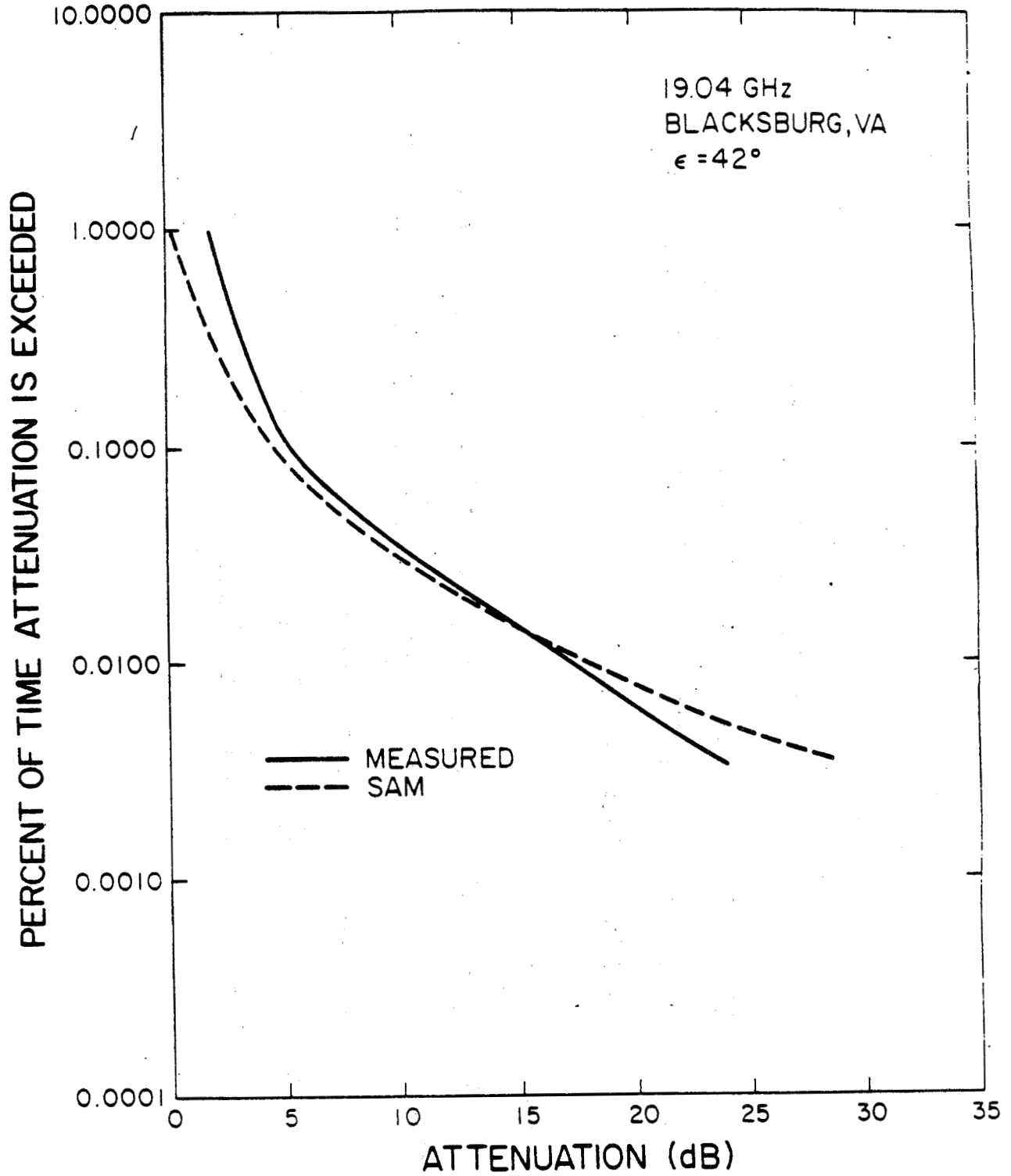
- Some Models

CCIR [Rept. 564-3] is based on 0.1% rain rate value

Global [Crane, Radio Science, Nov/Dec 1982] is based on own rain rate model

SAM [Yon and Stutzman, Radio Science, Jan/Feb 1986] can use any rain rate distribution

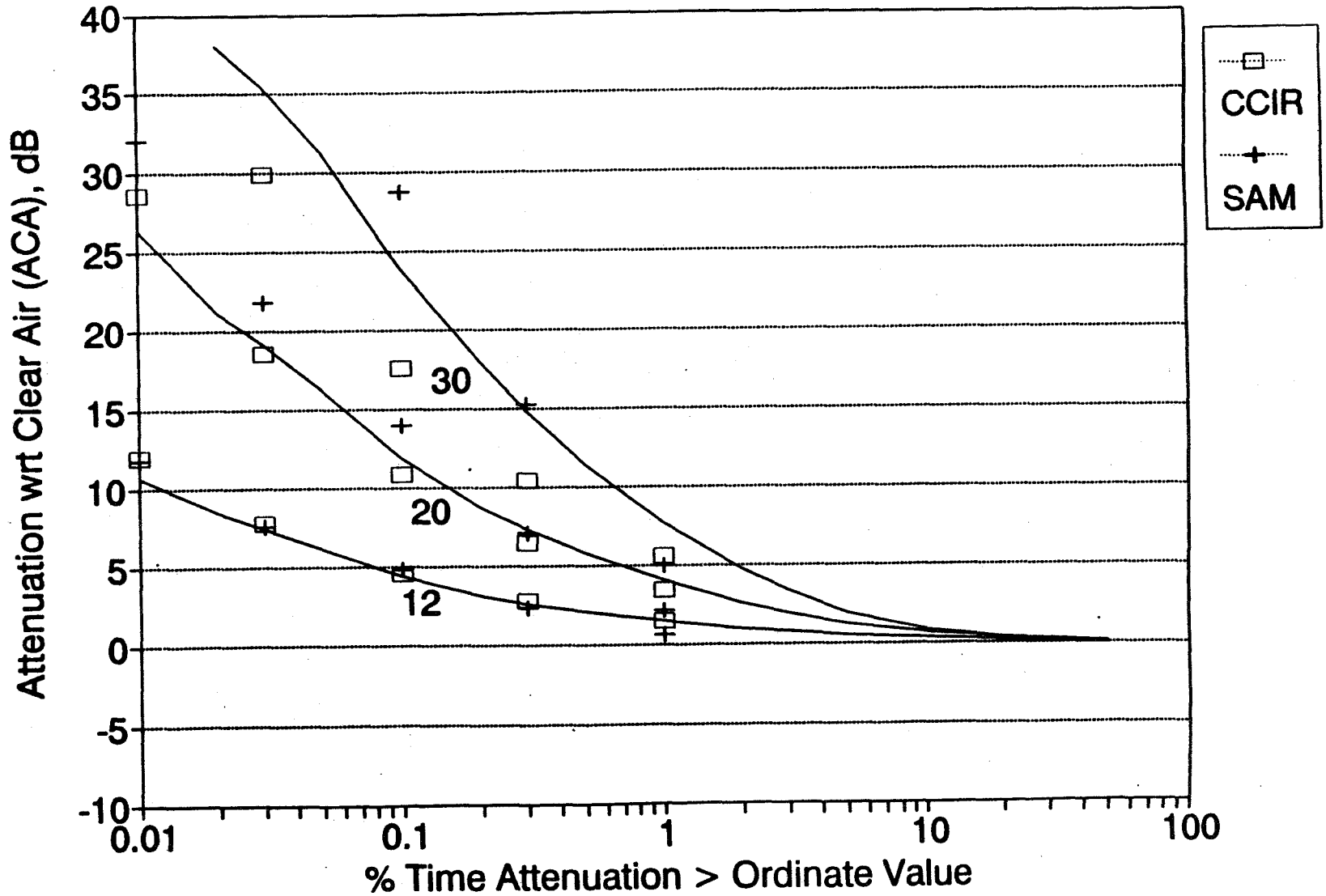
EXAMPLE OF MODEL PREDICTIONS COMPARED TO MEASUREMENTS



32 months of data from the COMSTAR
satellite (solid curve)

globe.pfl
globe15.drw
07/17/92

ATTENUATION WITH RESPECT TO CLEAR AIR 12, 20, & 30 GHz - One Year (91/92)



ATTENUATION RATIO

Instantaneous Attenuation Ratio

$$RA(f_L, f_U, t) = \frac{ACA(f_U, t)}{ACA(f_L, t)}$$

(smoothed using a 30-s moving average to remove scintillations)

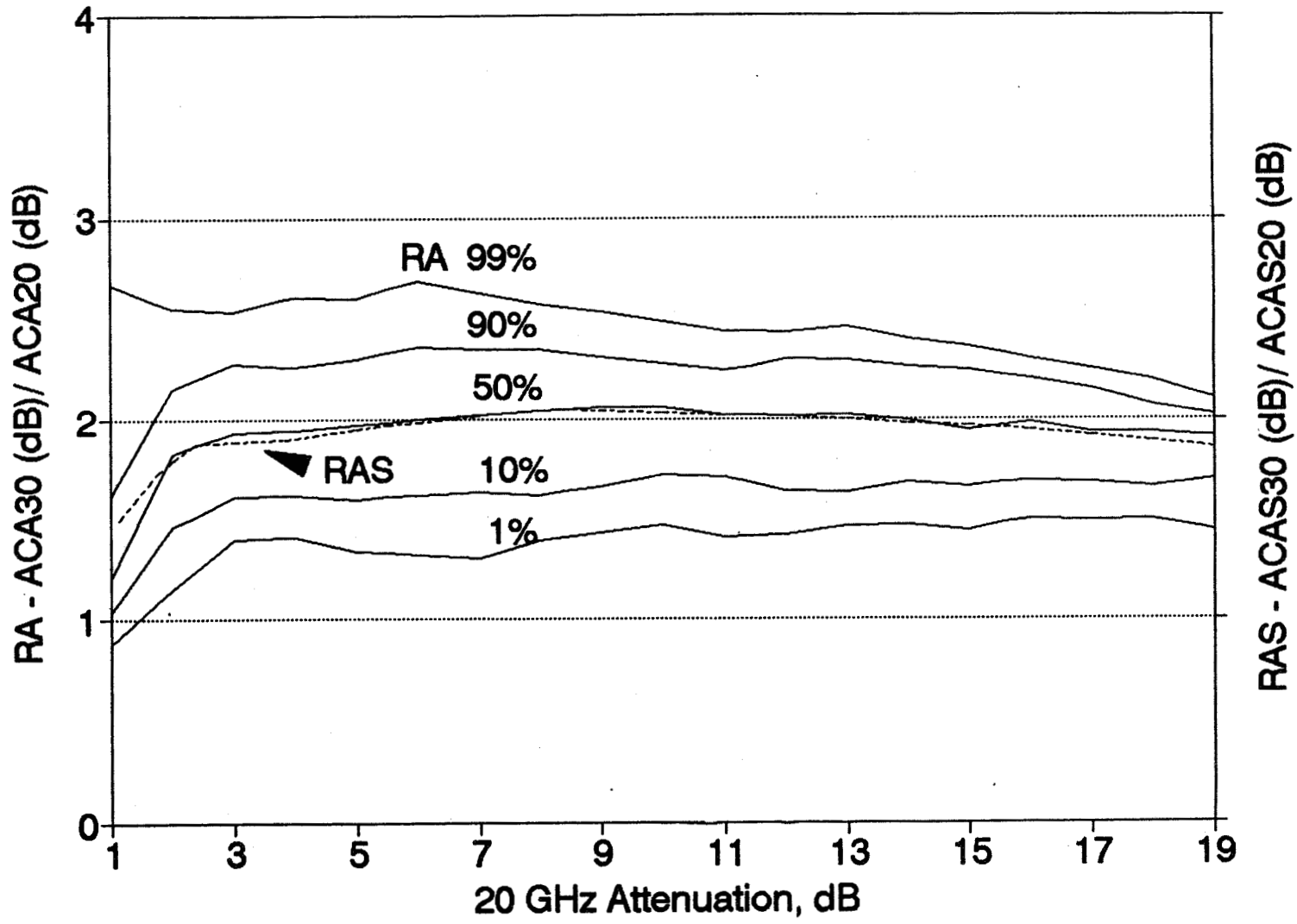
RA_{med} = 50% value of $RA(t)$ over year

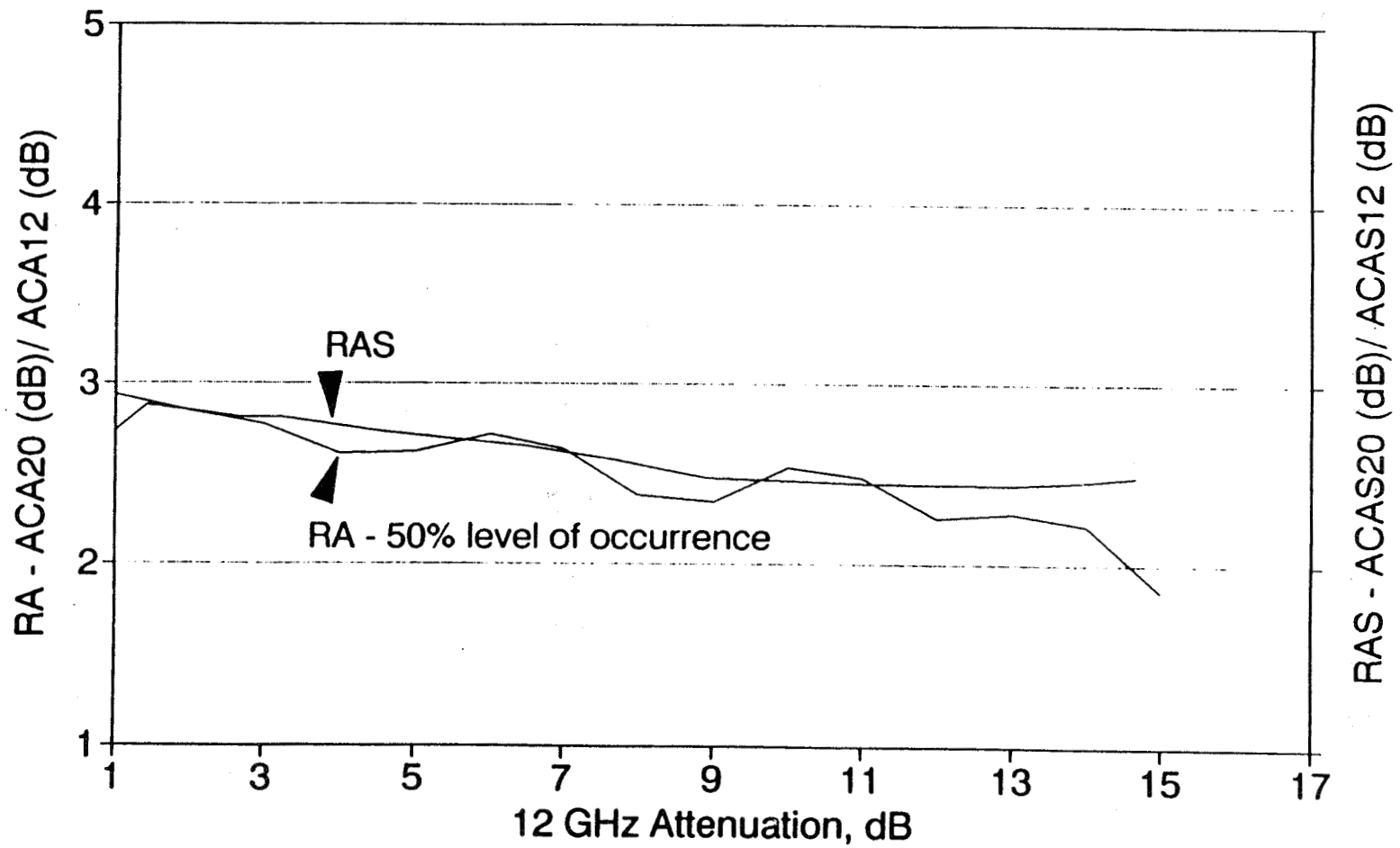
RA_{med_i} = median for i th 1-dB bin on the base frequency attenuation

RA_{ave} = average of RA_{med_i} over all valid bins

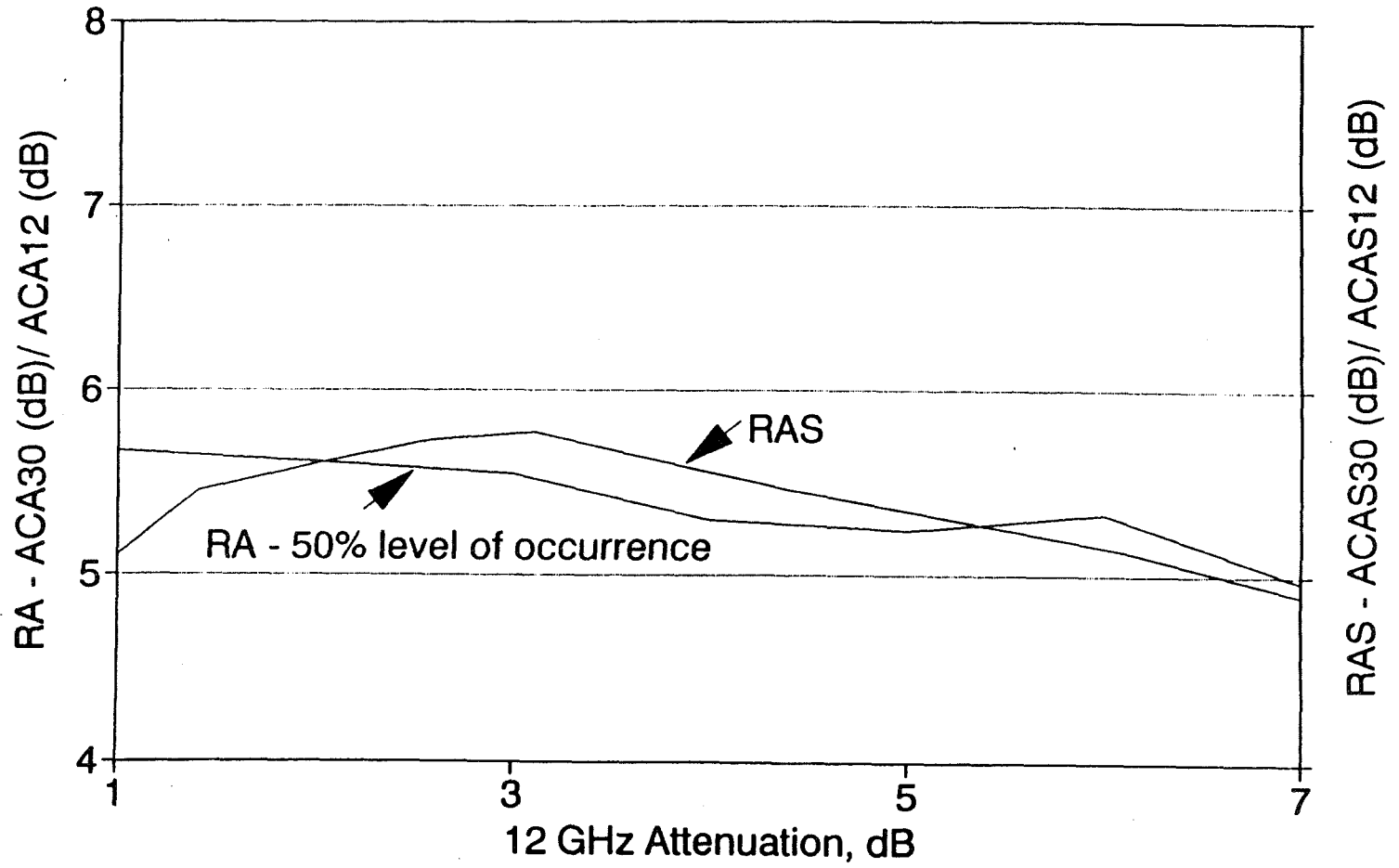
Statistical Attenuation Ratio

$$RAS(f_L, f_U, P) = \frac{ACAS(f_U, P)}{ACAS(f_L, P)}$$



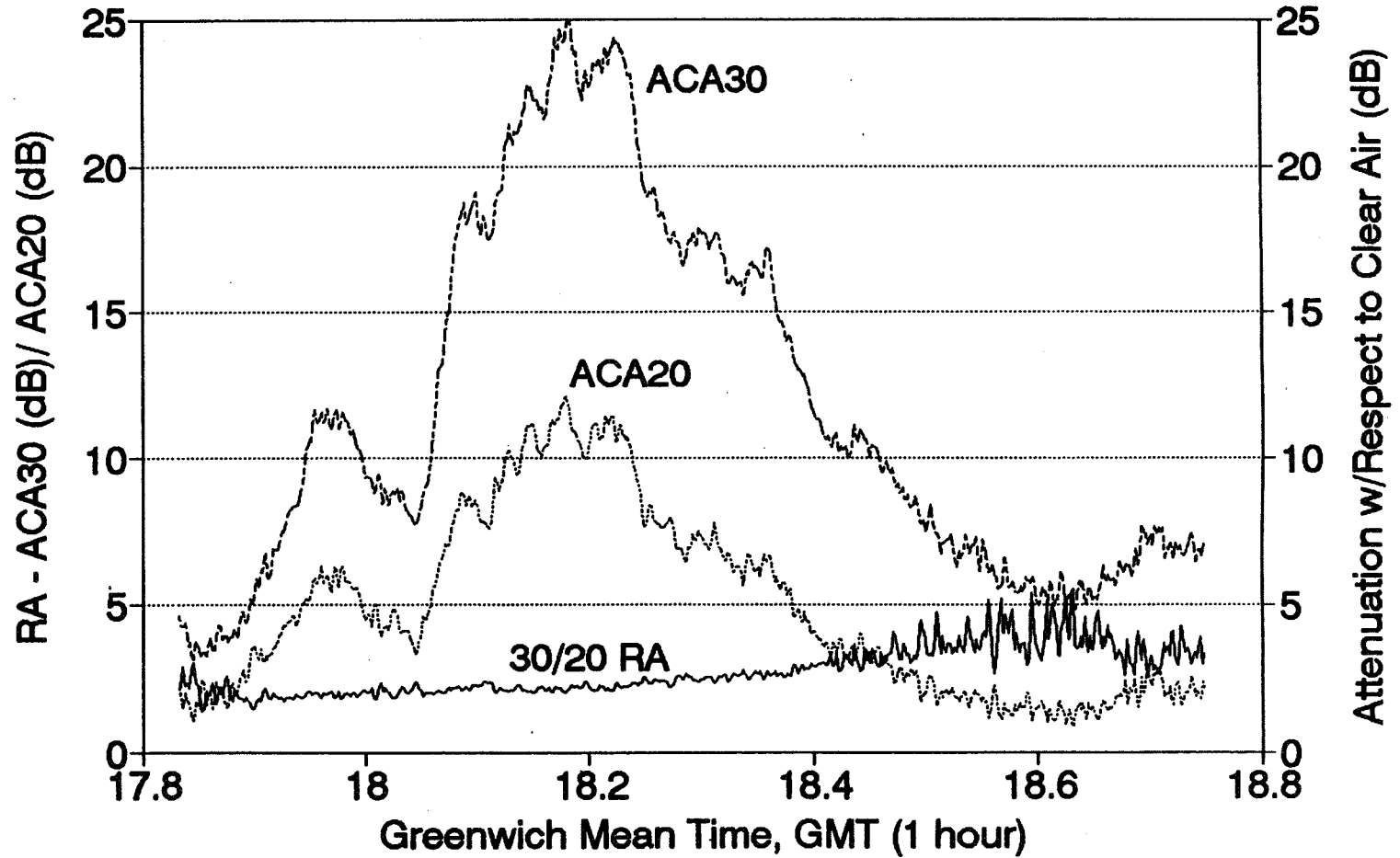


Comparison of statistical attenuation ratio (RAS) to median instantaneous attenuation ratio (RA_{med}) for 20/12 GHz.



Comparison of statistical attenuation ratio (RAS) to median instantaneous attenuation ratio (RA_{med_i}) for 30/12 GHz.

30/20 Attenuation Ratio vs. Time May 14, 1991 Rain Event



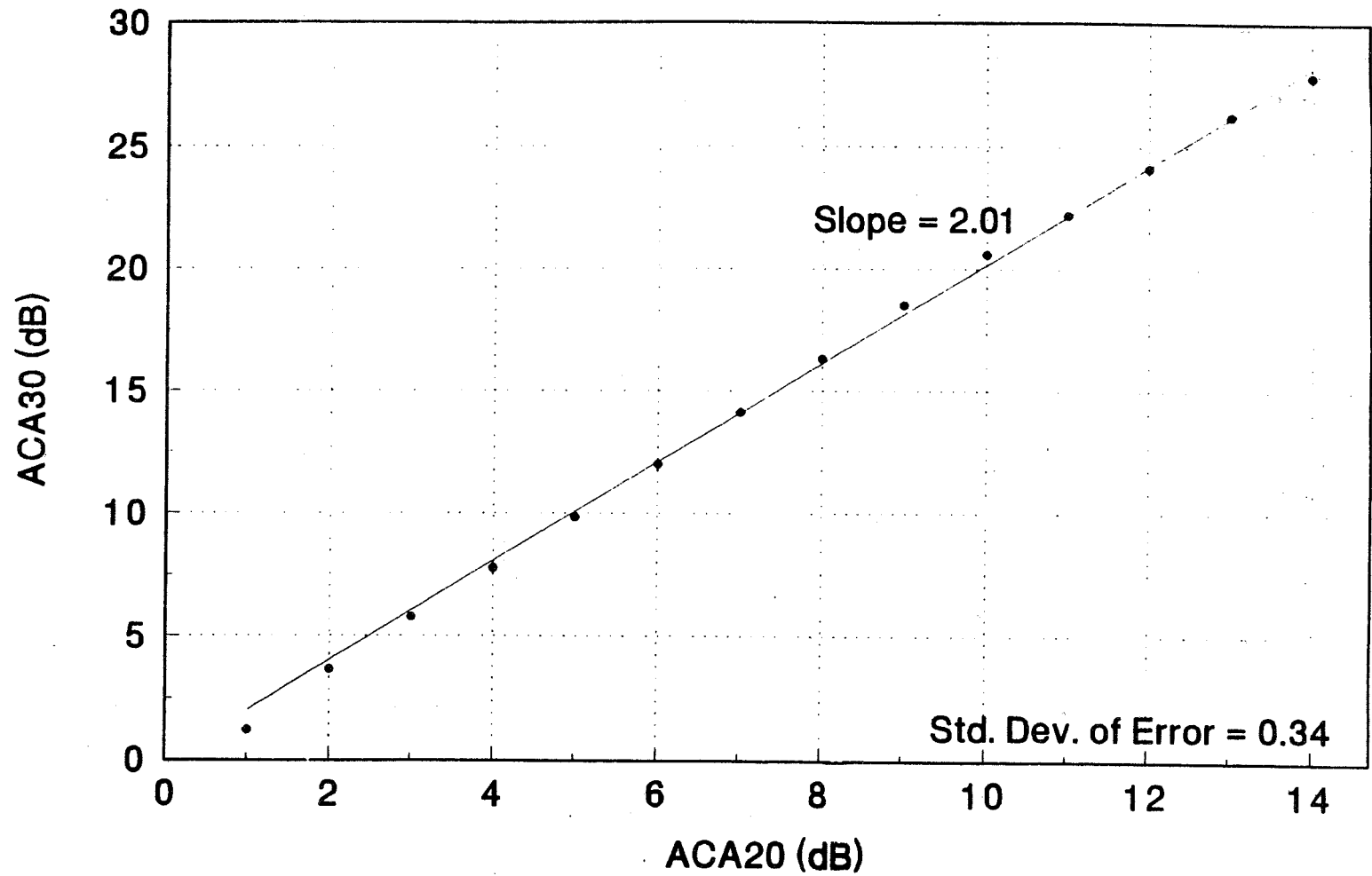
30/20 Attenuation Ratio vs. Time (with ACA30 & ACA20), May 14, 1991

Statistics of Attenuation Ratio for One Year of Olympus Data

$$(ACA(f_L) > 1 \text{ dB})$$

Frequency Pair, f_U/f_L	30/20	20/12	30/12
VA Tech RA_{med}	1.93	2.86	5.56
VA Tech RA_{ave}	2.01	2.52	5.43
Std. Dev. of Error of RA_{ave}	0.34	0.90	0.44



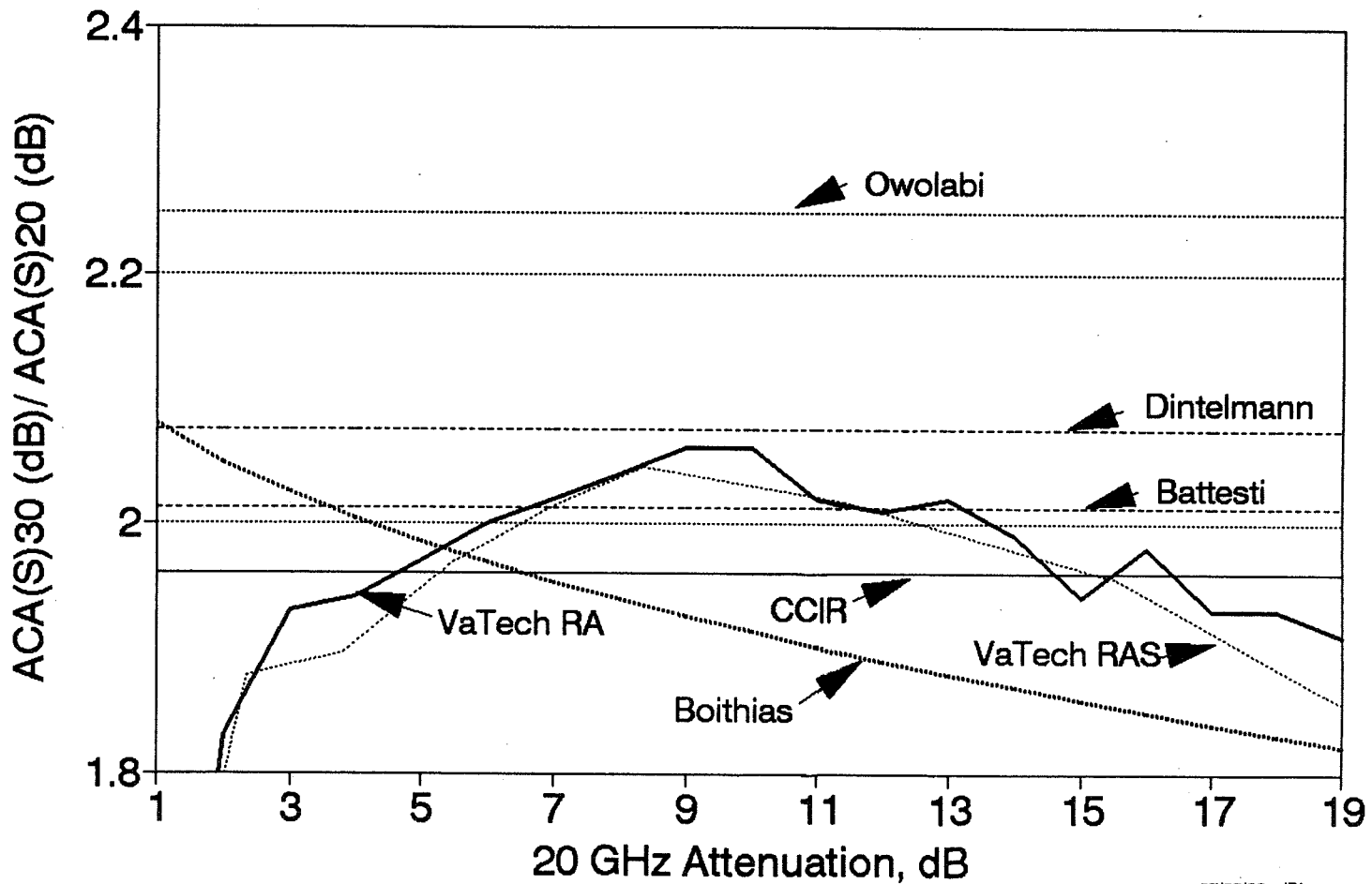


Median 30-GHz attenuation for each 1-dB interval of 20-GHz attenuation using all data from the analysis year. The least mean squared derivation straight line fit is also shown.

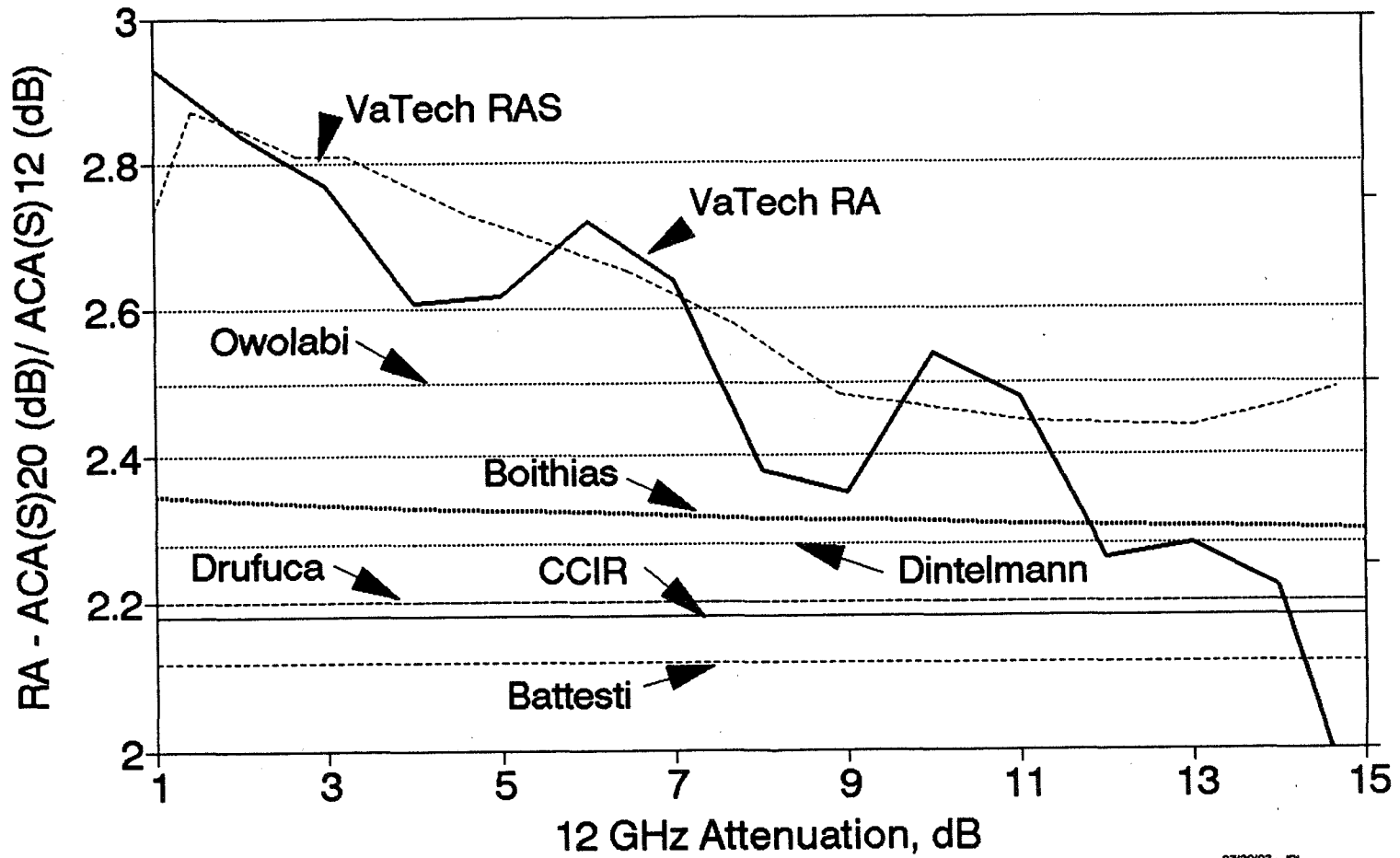
Statistics of Attenuation Ratio Compared to Model Predictions for OLYMPUS Frequencies

Model or Data	Frequency pair, f_U/f_L		
	30/20	20/12	30/12
VA Tech RA_{med} data	1.93	2.86	5.56
VA Tech RA_{ave} data	2.01	2.52	5.43
Battesti model	2.01	2.12	4.23
CCIR model	1.96	2.18	4.28
Dintelmann model	2.07	2.28	4.74
Drufuca model	----	2.20	----
Owolabi/Ajayi model	2.25	2.50	5.63

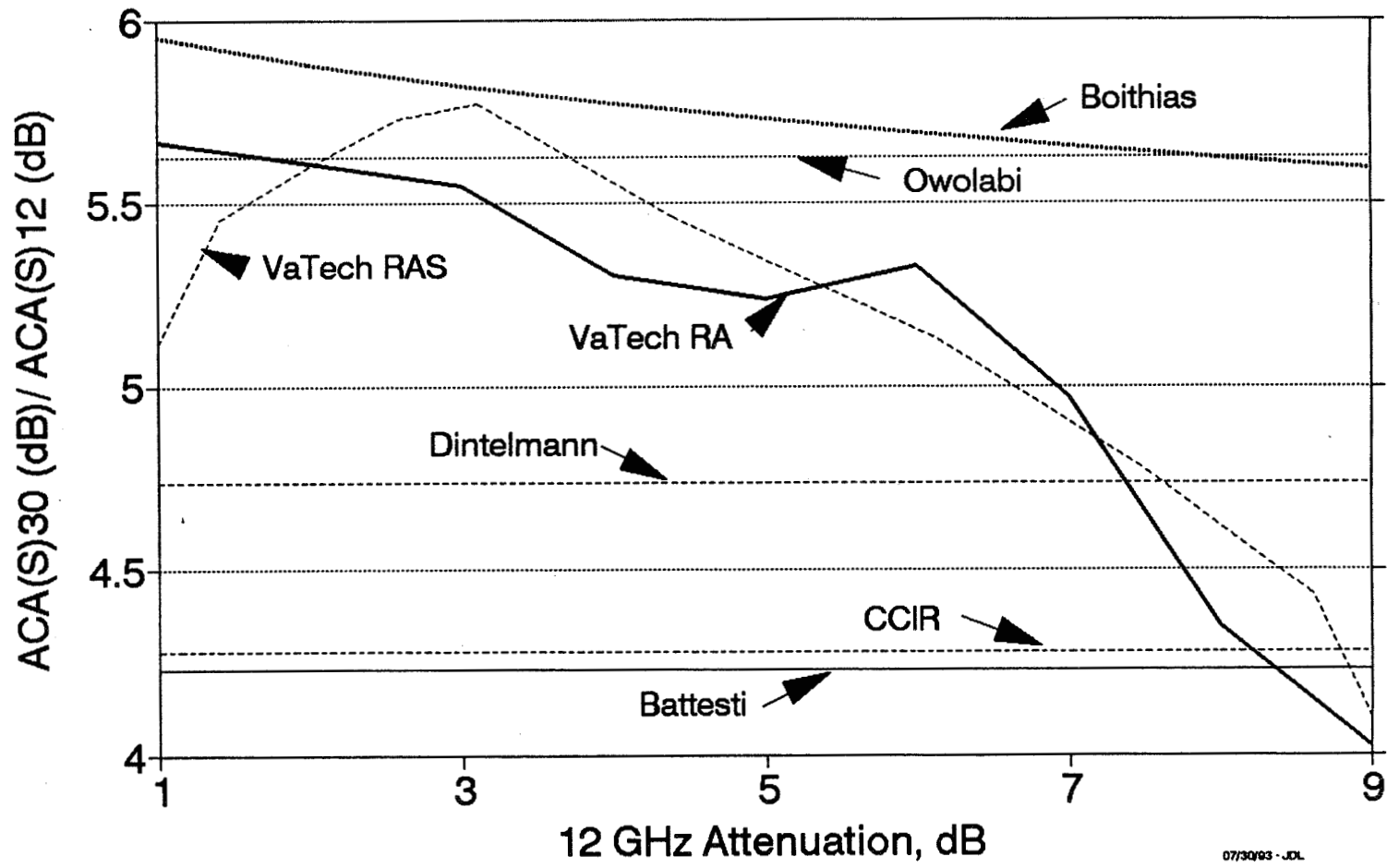
30/20 RA, RAS, and MODELS One Year (91/92) -vs. 20GHz Attenuation



20/12 RA, RAS, and MODELS One Year (91/92) -vs. 12GHz Attenuation



30/12 RA, RAS, and MODELS One Year (91/92) -vs. 12GHz Attenuation



36

Simple Power Law Model $RA = (f_U / f_L)^n$

	Frequencies f_U / f_L			Average n
	30/20	20/12	30/12	
Power n for RA_{med}	1.62	2.29	1.99	1.97
Power n for RA_{ave}	1.72	2.02	1.96	1.90



Comparison of Attenuation Ratio Values for Three Long Term Experiments Using OLYMPUS

	Frequencies f_U/f_L		
	30/20	20/12	30/12
BT Labs (best fit slope of $A(f_U)$ vs. $A(f_L)$)	1.8	2.5	4.3
Dintelmann (RA computed with n = 1.8)	2.07	2.28	4.28
Virginia Tech Measured RA_{ave}	2.01	2.52	5.43

FADE SLOPE

Block average of attenuation

$$\overline{AFS}_i = \left(\frac{1}{100} \right) \left(\sum_{j=i-49}^{i+50} AFS_j \right) \quad [\text{dB}]$$

where AFS_j is the instantaneous value of attenuation at each 0.1-s interval.

Fade slope is defined as the 10-s block average of attenuation centered at 5 s before a threshold subtracted from a 10-s block average of attenuation centered at 5 s after the threshold, divided by 10 s:

$$FSB_i(\overline{AFS}_i) = \left(\frac{1}{10} \right) \left(\overline{AFS}_{i+50} - \overline{AFS}_{i-50} \right) \quad [\text{dB/s}]$$

Empirical model of percent time P the fade slope for 12 to 30 GHz is in the bin centered on FSB:

$$P(FSB) = a \cdot e^{b|FSB|}$$

where

$$a(A_T, f) = \frac{a(A_T, 20) - a(A_T, 12)}{20 - 12} \cdot (f - 12) + a(A_T, 12) \quad \text{for } A_T > 3, 12 \leq f \leq 20$$

$$a(A_T, f) = \frac{a(A_T, 30) - a(A_T, 20)}{30 - 20} \cdot (f - 20) + a(A_T, 20) \quad \text{for } A_T > 3, 20 \leq f \leq 30$$

$$b(A_T, f) = \frac{b(A_T, 20) - b(A_T, 12)}{20 - 12} \cdot (f - 12) + b(A_T, 12) \quad \text{for } A_T > 3, 12 \leq f \leq 20$$

$$b(A_T, f) = \frac{b(A_T, 30) - b(A_T, 20)}{30 - 20} \cdot (f - 20) + b(A_T, 20) \quad \text{for } A_T > 3, 20 \leq f \leq 30$$

where A_T is the threshold attenuation (AFS) level in dB and f is the frequency in GHz.

$$a(A_T, 12) = 52.93 e^{(0.07 A_T - 1.45 A_T^2 - 0.0013 A_T^3)}$$

$$a(A_T, 20) = 717.71 e^{(-1.07 A_T + 0.038 A_T^2 - 0.00056 A_T^3)}$$

$$a(A_T, 30) = 404.22 e^{(-1.05 A_T + 0.063 A_T^2 - 0.0018 A_T^3)}$$

$$b(A_T, 12) = -0.0315 A_T^3 + 1.168 A_T^2 - 14.94 A_T + 72.72$$

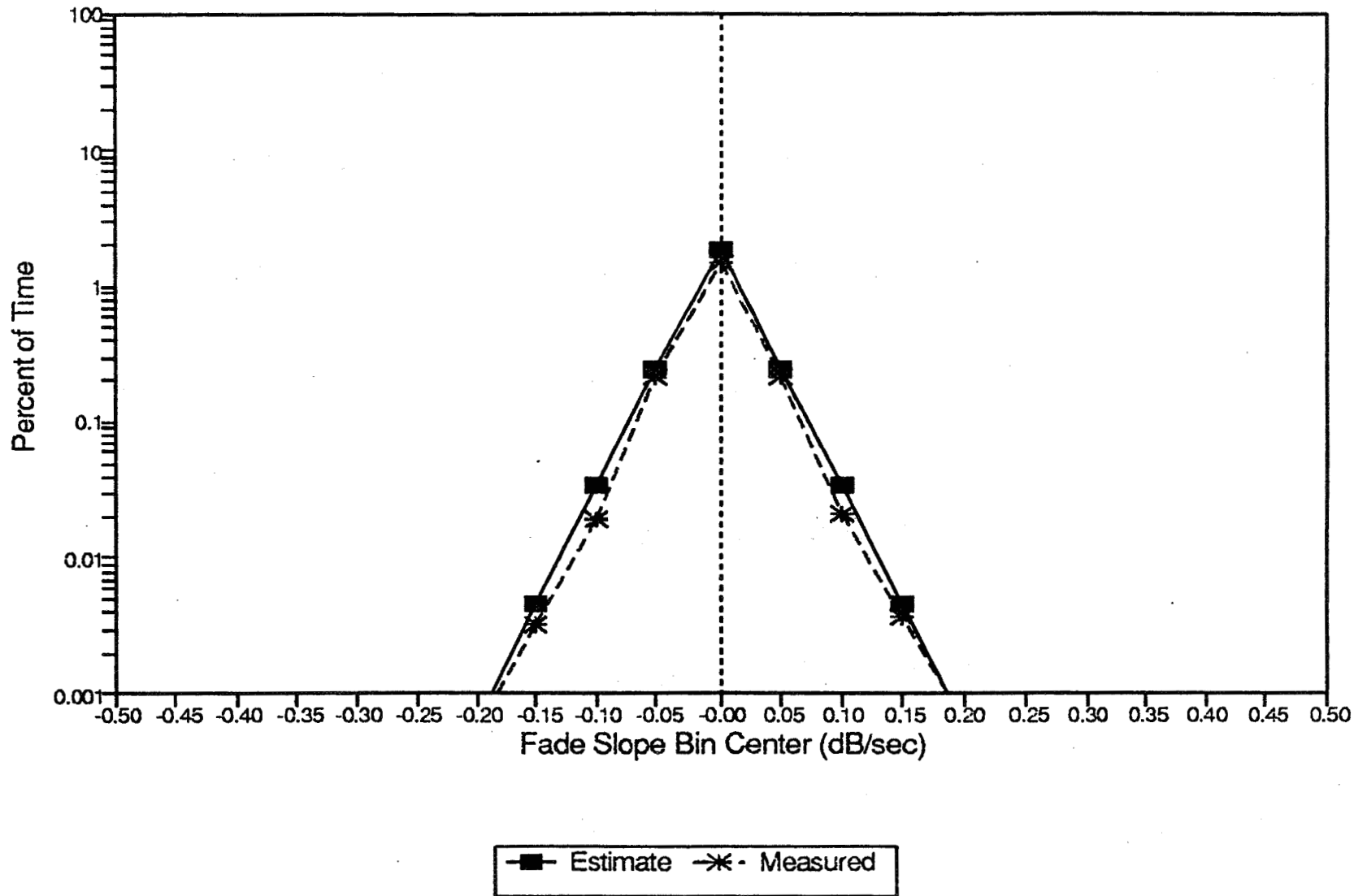
$$b(A_T, 20) = 0.0202 A_T^3 - 0.3149 A_T^2 - 3.105 A_T + 61.62$$

$$b(A_T, 30) = 0.0134 A_T^3 - 0.2647 A_T^2 - 1.178 A_T + 47.82$$

This third order model agrees to Olympus measured data within 5%.
A seventh order model fits to within 1%.

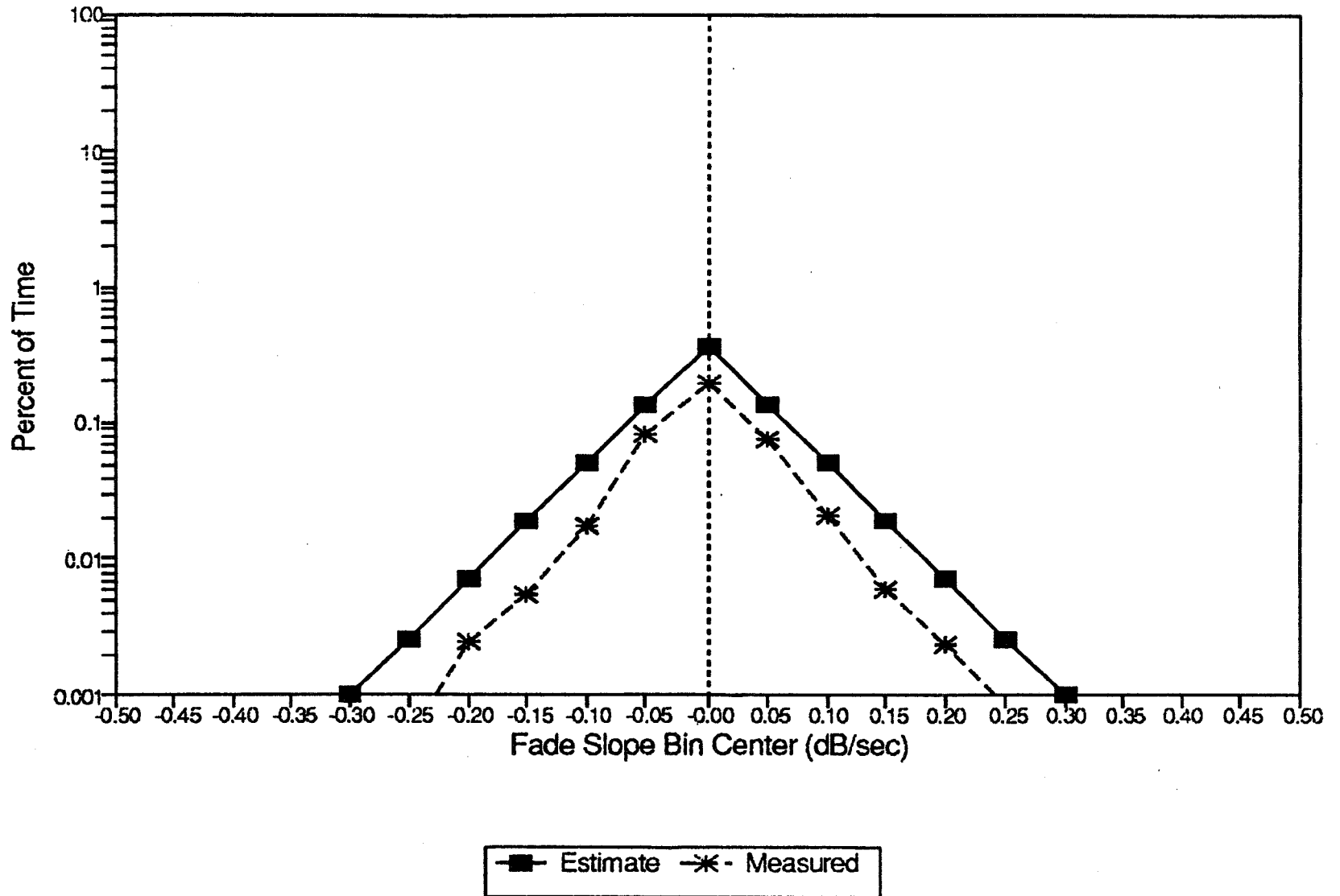
MEASURED VS MODELED FADE SLOPE

One Year In Rain -- 12 GHz at 3 dB



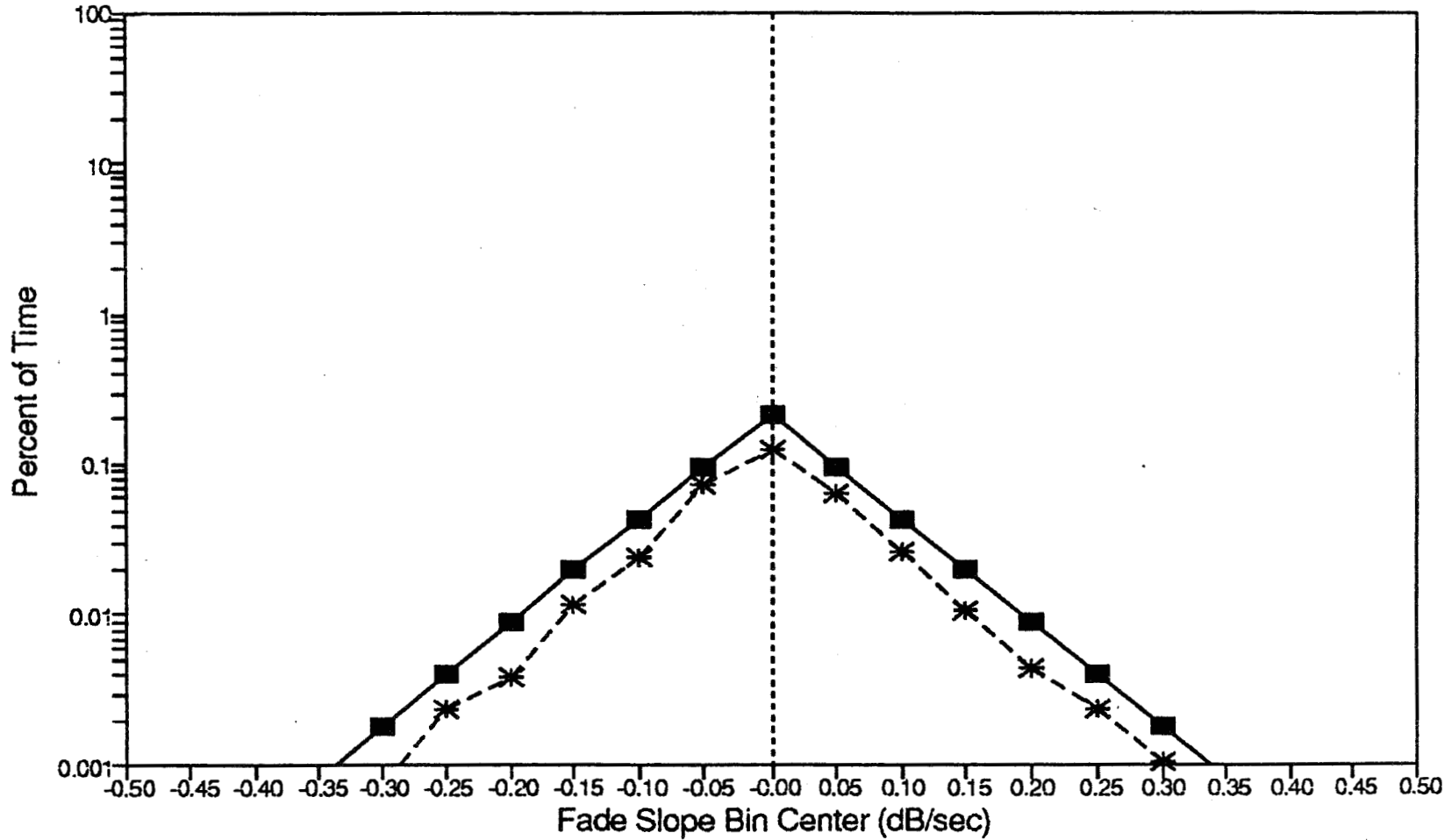
MEASURED VS MODELED FADE SLOPE

One Year In Rain -- 20 GHz at 10 dB



MEASURED VS MODELED FADE SLOPE

One Year In Rain -- 30 GHz at 15 dB



SUMMARY

Models that agreed well with Olympus data:

Rain Rate	CCIR
Attenuation	CCIR, SAM
Attenuation Ratio	CCIR, $n = 1.90$

Models developed during Olympus investigation:

Attenuation Ratio

$RA \approx RAS$

Power law ($n = 1.90$)

Empirical model for A ($P = 99\%$)

Empirical model for fade slope statistics for any frequency in 12 to 30 GHz range and any attenuation threshold

Empirical model for fade duration

Propagation Characteristics of 20/30 GHz Links with a 40° Masking Angle

F. Davarian, A. Kantak, And C. Le
Jet Propulsion Laboratory
California Institute of Technology

1. Introduction

Because of a great demand for wireless communications, the available spectrum at frequencies lower than 18 GHz cannot meet the rapidly growing needs of the satellite communications industry. In contrast, K_a -band frequencies, which span from about 18 to over 30 GHz, offer large segments of the radio spectrum for satellite communication applications. The International Telecommunications Union (ITU) spectrum allocation for satellite communications at the K_a -band exceeds 3 GHz in each direction and currently is underutilized.

The scarcity of bands below about 18 GHz coincides with an explosive increase in demand for wireless communication services in the U.S. and elsewhere during the 1990s. Hence, spectrum shortage can severely impede industrial development as well as growth in certain sectors of the economy. Therefore, the recent interest in K_a -band frequencies for Earth/space communications is expected and should be encouraged.

On the negative side, atmospheric effects are considerably higher at K_a -band than at frequencies below about 18 GHz. It is therefore recognized that frequencies above about 18 GHz cannot be successfully exploited unless the atmospheric-induced anomalies are understood, accounted for, and mitigated. For over two decades, the United States' NASA Propagation Program and other investigators abroad have studied K_a -band propagation to improve our knowledge of the field and to find means of enhancing channel availability. These investigations have been fruitful, producing data and models that can be used for Earth/space propagation effects prediction.

An effective means of reducing K_a -band propagation loss is the use of high elevation angle paths, i.e., a large masking angle, between Earth stations and the space platform. Experimental data have shown that the signal loss associated with most atmospheric effects is inversely proportional to $\sin(\theta)$, where θ denotes the path elevation angle. A large masking angle and a

generous link margin are the primary tools used in the Teledesic Corporation network to minimize atmospheric-related signal outages. This report documents the results of a study sponsored by Teledesic Corporation to characterize the effect of radiowave propagation on Teledesic's links.

CCIR recommendations and NASA Propagation Handbooks are the main sources of propagation data and models [1,2]. The recent Olympus campaign in Europe and the U.S. has provided new information that is not included in these sources yet. Therefore, CCIR recommendations and NASA Propagation Handbook models constitute the base of this study, and, when applicable, data from other sources have been used to improve the predictions. Furthermore, attention has been given to data from the Olympus campaign.

The effects investigated during this study include gas, rain, fog, sand, and cloud attenuation, diversity gain, scintillation, and depolarization.

2. Gaseous Attenuation

Although gaseous absorption for frequencies below about 18 GHz may be ignored for most applications, K_a -band atmospheric attenuation may exceed 1 dB for small percentages of the time. Gaseous absorption is mainly due to oxygen and water vapor in the atmosphere. Oxygen produces a small but constant loss, whereas water vapor attenuation demonstrates diurnal and seasonal variations that can become much larger than the oxygen contribution.

Oxygen attenuation gradually increases by frequency, greater for 30 GHz than 20 GHz. Water vapor attenuation peaks around 22 GHz, and it is less at 30 GHz than 20 GHz. Since water vapor attenuation is proportional to water density in the atmosphere, large values of attenuation occur during warm and humid days.

Both the oxygen and water vapor effects can be estimated by a CCIR recommendation on this subject. The procedure involves the calculation of the specific attentions in dB/km and scale heights in km. The scale height used in calculating the water vapor effect is less for no-rain periods than rainy periods. Figure 1 shows the atmospheric K_a -band attenuation as a function of relative humidity at surface temperatures of 20° C and 30° C, assuming site location at sea level and no rain. Gaseous attenuation during rain is shown in Figure 2 for temperatures of 20° C and 30° C. Both figures use a path elevation angle of 40°.

For dry regions of the Earth, i.e., where relative humidity is about 20% at a temperature of 20° C, it appears that a gaseous attenuation margin of 0.3 dB is adequate. For warm and humid regions, i.e., where relative humidity is 90% and temperature is 30° C, margins are about 1.3 and 1.1 dB for 20 and 30 GHz,

respectively. These margins moderately decrease for site locations above sea level. Note that for high-altitude locations, such as mountainous regions, hot and humid scenarios are unlikely; it is a very rare meteorological event if Denver, Colorado, experiences a 30° C temperature with relative humidity 90%, whereas the same event is not unusual for Austin, Texas.

3. Rain Attenuation

Rain attenuation is the most severe form of slant path atmospheric loss at 20/30 GHz frequencies. To predict the rain outage on Teledesic links, Crane's global model is used [2]. Crane's rain regions and their corresponding rain rate statistics are given in Table 1. This model divides the globe into twelve rain regions according to rain rate statistics and develops a procedure to predict the attenuation. This model was used to generate the global attenuation characteristics for the downlink and uplink of Teledesic's communications system, and the results are shown in the form of bar charts in Figures 3 and 4, respectively. For the downlink at 20 GHz frequency, the proposed communication system design assumes that the link has a rain margin of 9 dB. To see the sensitivity of link outage hours to the rain margin, we have taken 9 ± 3 dB, i.e., 6, 9, and 12 dB levels for the chart in Figure 3. Similarly for the uplink at 30 GHz frequency, the link design assumes a rain margin of 19 dB, and we have taken 19 ± 3 dB, i.e., 16, 19, and 22 dB levels for the chart in Figure 4. In both figures the path elevation angle is assumed to be 40°.

Table 1. Point Rain Rate Distribution Values (mm/h)
Versus Hours per Year Rain Rate Exceeded

Hours per Year	Climate Regions											
	A	B1	B	B2	C	D1	D2	D3	E	F	G	H
0.44	14	22	29	35	41	50	65	81	118	34	121	178
0.88	10	16	20	24	28	36	49	63	98	23	94	147
1.75	7	11	14	16	18	24	35	48	78	15	72	119
4.38	4	6.4	8	9.5	11	15	22	32	52	8.3	47	87
8.77	2.5	4.2	5.2	6.1	7.2	9.8	15	22	35	5.2	32	64
17.5	1.5	2.8	3.4	4	4.8	6.4	9.5	15	21	3.1	22	44
43.8	0.7	1.5	1.9	2.3	2.7	3.6	5.2	7.8	11	1.4	12	23

Figure 3 shows a bar chart of the average number of service outage hours per year for the downlink at 20 GHz for all climatic regions without diversity in the global model. This chart shows that for the climatic regions A to D2 the average number of link outage hours per year is under 10 hours, and in some cases, as in regions A, B1, and B, it is in the vicinity of only 1 hour. For the regions D3

to F, the average number of link outage hours per year are larger than 10 hours, and in some cases, such as regions E, G, and H, the outage hours are substantially greater than 10.

Figure 4 shows a similar bar chart for the uplink frequency of 30 GHz. This chart is also drawn using the climatic zones in the global model. As in Figure 3, Figure 4 shows that for the regions A to D2, the average link outage hours per year are less than 10 hours, and in some regions (A, B1, and B) it is about 1 hour. For the regions D3 through H, the average outage hours per year are more than 10 hours, in some regions (E, G, and H) the outage is substantially greater than 10 hours.

Figure 5 shows measured rain attenuation statistics at Blacksburg, Virginia, resulting from Olympus measurements for a one-year period. From this figure, it can be seen that rain attenuation margins of 11 dB (20 GHz) and 21 dB (30 GHz) result in annual outage times of 9 and 10 hours for 20 and 30 GHz frequencies, respectively. Note that to account for gaseous and cloud attenuation, 2 dB is added to the margins of 9 dB and 19 dB at 20 GHz and 30 GHz, respectively. Blacksburg is in Region D2 of the global model, and the measurement year of Figure 5 received slightly more rainfall than the average year in Blacksburg [3].

4. Diversity

Teledesic is planning to use site diversity to improve link availability at gateway stations. The diversity principle is based on the fact that most high rain-rate cells are not very large and hence all the spatially diverse receiving stations provided in a diversity system may not suffer the worst rain attenuation at the same time. Obviously, more receiving stations as well as larger separating distances between the stations imply a better system performance, however, we will assume only two ground stations separated by a distance of 30 km.

The CCIR model for diversity rain attenuation prediction was used to predict the performance. The CCIR model computes the outage time percentage of the diversity system as a function of the outage time percentage of a single site. We have found good agreement between measured K_a -band diversity data reported in [4] and the CCIR prediction. The data had a diversity separation of 9 km and a path elevation angle of 26 degrees.

Figure 6 shows the percentage of time for two sites to exceed the desired level as a function of the percentage of time for a single site. The parameter is the diversity distance. Figures 7 and 8 show the average number of service outage hours per year for all climatic regions with diversity in the global model. Figure 7 is for the downlink at 20 GHz and at 6, 9, and 12 dB attenuation levels, and Figure 8 is for the uplink at 30 GHz frequency with 16, 19, and 22 dB attenuation

levels. The spatial diversity is assumed to be 30 km, and the ground station antenna elevation angle is assumed to be 40 degrees. These figures show that the link outage hours per year for both uplink and downlink are reduced compared with the earlier charts (Figures 3 and 4).

Figures 7 and 8 indicate that for large single-site outage times, i.e., larger than 10 hours per year, diversity improvement is small. However, this may be partly due to the inability of the CCIR model to accurately predict diversity improvement at large percentage values for Teledesic's links. It is possible that the CCIR diversity predictions for rain climate regions E, G, and H are pessimistic. This is an area that deserves further investigation.

5. Cloud Attenuation

The treatment of slant path cloud attenuation is not a simple task because it is difficult to separate cloud contribution from gaseous and rain contributions. For this reason there are no simple models for cloud attenuation that can be applied. Both analytical and experimental studies show that cloud attenuation is higher at 30 GHz than 20 GHz. Main contributing factors to signal attenuation are moisture content of the cloud and the slant path length through the cloud. Measurements have shown that at the 5% level, total zenith attenuation can vary from about 0.5 dB to more than 2 dB depending on the location of the site (from very dry to very wet regions) for 30 GHz signals [2]. These values, of course, include gaseous absorption.

Figures 9 and 10 show radiometrically produced statistics of total atmospheric attenuation at Denver, Colorado, for December 1987 and August 1988, respectively. At the 0.5% level, total attentions for 30 GHz are 0.75 and 2.1 dB, for December 1987 (dry) and August 1988 (humid), respectively.

In summary, it is difficult to separate clouds from other atmospheric contributors. For clear weather (no rain) conditions a 1-dB margin may be suggested for Teledesic's 20 and 30 GHz links. It is, however, difficult to associate reliable outage statistics to a 1-dB cloud margin. This is an area that deserves more research.

6. Fog Attenuation

The fog attenuation is very small and is not usually a factor in satellite link system design for frequencies below 100 GHz. Therefore, this attenuation could be ignored for Teledesic's 20- and 30-GHz links.

7. Sand and Dust Attenuation

Sand and dust can cause signal attenuation by scattering electromagnetic energy. Simulated measurements have shown that at 10 GHz and concentration of 10^{-5} g/m³ the measured specific attenuation was less than 0.1 dB/km for sand and 0.4 dB/km for clay [2].

Sand and dust storms occur in certain regions of the world. The vertical extent of these storms is unknown, but it is unlikely that high concentrations would exceed 1 km. The slant path length in the case of Teledesic is expected to vary between zero and 2 km, generally resulting in a total additional attenuation due to sand less than 1 dB [2]. No measured satellite beacon data is available to confirm these results.

8. Depolarization

In radiowave propagation, depolarization refers to a change in the polarization state of the signal. This change is usually caused by wave propagation in the atmosphere. At frequencies below 10 GHz, the main cause of depolarization is the Faraday rotation: a rotation of the plane of polarization due to the interaction of radiowaves with electrons in the ionosphere. For frequencies above about 10 GHz, ionospheric effects can be ignored; however, for these frequencies hydrometeor-induced depolarization may pose a problem.

In satellite communications, rain and ice crystals are the prominent sources of signal depolarization. Radiowave propagation through rain and clouds with ice crystals can transfer a portion of the signal energy to an orthogonal polarization state. As will be demonstrated in this section, hydrometeor depolarization is often too small to affect the performance of single-polarized satellite communications links, however, it could have an adverse effect on dual-polarized systems.

Rain depolarization is usually associated with large rain attenuation, i.e., 15 dB, whereas ice depolarization can occur at relatively low attenuation levels, i.e., 2 dB. In general, depolarization due to rain is more frequent than due to ice. Ice depolarization is mainly observed in high-density, high-altitude clouds, such as clouds associated with thunderstorms. Low-latitude clouds are usually too warm to contain substantial amounts of ice. For predicting polarization effects at 20/30 GHz frequencies, the CCIR model can be used. In addition to the CCIR model, measured data from Olympus and other experiments are also available. A common measure of depolarization is a parameter known as cross-polarization discrimination (XPD). This parameter is defined as

$$\text{XPD} = \frac{\text{Power in the received co-pol signal}}{\text{Power in the received cross-pol signal}} \quad (1)$$

For an ideal system, XPD is infinity.

The CCIR prediction model for depolarization due to rain has the following form:

$$\text{XPD}_{\text{rain}}(p) = a - b \log_{10}(A) \quad (2)$$

where A is the total attenuation due to rain in dB, a and b are two empirical constants that depend on frequency, elevation angle, θ , and the polarization tilt angle with respect to the local horizon, τ . Note that dependence on p , time percentage, is implicit in A , a , and b . To also account for ice depolarization, the following model gives the total depolarization prediction

$$\text{XPD}_{\text{T}}(p) = [0.85 - 0.05 \log_{10}(p)] \text{XPD}_{\text{rain}}(p) \quad (3)$$

Long-duration measurements of Olympus linearly polarized signals in Germany have yielded the following empirical relationship for the measured medians [5], where $\theta = 27^\circ$ and $\tau = 21^\circ$

$$\begin{aligned} \text{XPD}_{20} &= 44.0 - 21.8 \log_{10}(A_{20}) \quad (\text{dB}) \\ \text{XPD}_{30} &= 46.5 - 21.4 \log_{10}(A_{30}) \quad (\text{dB}) \end{aligned} \quad (4)$$

Because the above models are obtained from one year of measurement data in Germany, its applicability to other climatic and geographic zones should be made with caution.

To demonstrate the effect of depolarization, Figure 11 shows the cumulative distribution of XPD for Darmstadt, Germany, for $\theta = 27^\circ$ and $\tau = 21^\circ$ [6]. This site was selected because multiyear Olympus measurements exist at this site. Figure 11 also shows the measured values. For this particular data set, the CCIR model underestimates the effect of depolarization.

Figure 12 shows the cumulative distribution of predicted XPD for Blacksburg, Virginia, assuming circular polarization. Measured Olympus rain attenuation data at 14° elevation angle [7] were scaled to 40° and then used to obtain Figure 12. Note that there are no XPD measured data at Blacksburg.

Olympus 20 and 30 GHz data are also available from the British Telecom site near Ipswich, England [8]. Although these measurements were made at a low elevation angle of 27.5° , the measured values of XPD are high at the percentage values of interest to Teledesic as shown in Figure 13. For example, at a percentage value of 0.1, XPD is higher than 20 dB for both frequencies.

Considering the predicted and measured data provided in this section, the following conclusion can be reached: At a percentage level of 0.1, XPD measurements, as well as predictions, are higher than 20 dB for both frequencies. This value of XPD provides a comfortable margin for Teledesic links. Therefore, assuming that Teledesic does not intend to use dual polarization transmissions, the effect of depolarization can safely be ignored. However, if Teledesic plans in the future to employ dual polarization transmissions to a cell as a means of frequency reuse, depolarization is likely to play a role. In summary, depolarization does not seem to be an issue for the present design of the Teledesic network.

9. Scintillation Effects

Tropospheric scintillation implies rapid fluctuation of signals caused by electromagnetic wave scattering and diffraction due to small scale turbulent refractive index inhomogeneities in the troposphere. Low-latitude tropospheric layers and clouds (especially fair weather cumuli) are considered the prime sources of K-band scintillation. The estimation of scintillation intensity in satellite links is obtained via a model that attributes scintillation to a thin turbulent layer about 1 km above the Earth station [1]. Scintillation intensity is a function of humidity, temperature, path elevation angle, and frequency. The size of the Earth station antenna also has a weak-to-moderate effect on the observed intensity of scintillation. The relationship is of inverse type with larger aperture sizes producing less scintillation fading than the smaller ones. The existing CCIR model has been frequently tested at Ku-band frequencies with good results. The available K_a -band database, however, is small compared to the Ku-band, and therefore, only a limited number of tests have been performed on the CCIR model at 20/30 GHz. The few examinations of the CCIR model at K_a -band have been positive so far.

Because Blacksburg, Virginia, is one of the rare sites in the U.S. with K_a -band scintillation data, we have chosen this site to produce Figures 14 and 15. These figures show cumulative fade statistics due to scintillation estimated for Teledesic links using the CCIR method. K_a -band scintillation data collected at Blacksburg have shown good-to-moderate agreement with the CCIR model for a 14° elevation angle [9]. These data were collected during the Olympus campaign at Blacksburg. Figure 14 shows the average yearly effect, whereas, Figure 15 is based on a one-month period in late spring when scintillation

intensity is high because of high humidity and warm weather conditions. These figures indicate that for climate regions exemplified by Virginia, USA, 1 dB of margin is sufficient to protect the Teledesic link from scintillation fading for more than 99.99% of the time. No spatial diversity is assumed for combating scintillation.

Figure 16 shows the cumulative fade statistics of scintillation for average conditions at Austin, Texas. Austin has warm and humid weather -- a high scintillation region. The worst case situation in Austin is shown in Figure 17. According to this figure, in rare occasions, fades deeper than 1-dB can be observed in Austin.

10. Propagation Margin Summaries

Recommended gaseous attenuation margins in dB are given in Table 2.

Table 2. Gaseous Attenuation in dB

Region	20 GHz		30 GHz	
	No Rain	Rain	No Rain	Rain
Dry	0.3		0.3	
Warm & Humid	1.3	1.8	1.1	1.5

The global model predicts rain attenuation with respect to clear air, whereas the CCIR model predicts total attenuation (cloud and atmospheric attenuations are partially included). Hence when using the global model, gaseous attenuation during rain should be obtained from Table 2 minus 0.3 dB (e.g., 1.5 dB and 1.2 dB for 20 GHz and 30 GHz frequencies, respectively). For the CCIR model, there is no need to add gaseous attenuation to rain attenuation, because gaseous attenuation is already included in the rain attenuation model.

Average outage hours per year due to rain attenuation assuming margins of 9 and 19 dB for 20 and 30 GHz frequencies, respectively, are given in Table 3. This table contains values with and without space diversity.

Table 3. Rain Attenuation

Region	A	B1	B	B2	C	D1	D2	D3	E	F	G	H
Hours	0.2	0.8	0.5	1.0	4.0	3.5	6.5	15	31	3.0	50	89
Hours with Diversity	0.0	0.0	0.0	0.0	0.2	0.2	0.7	2.5	5.5	0.1	18	41

The recommended **cloud attenuation** (above gaseous attenuation) margin is 1 dB.

Fog attenuation can be ignored.

Sand and dust attenuation can generally be ignored for most regions of the world. In regions with high probability of heavy sand or dust storms, a 1-dB margin is recommended.

Depolarization loss can be ignored for single-polarization transmissions to the same location.

For **scintillation fading** a margin of 1 dB is recommended for hot and humid locations (high scintillation conditions).

11. International Telecommunications Union

The International Telecommunications Union is an intergovernmental organization, and any sovereign state may become a member of this union. Their governments (in most cases represented by their telecommunications administrations) are constitutional members with special obligations, but also enjoy special rights, e.g., the right to vote. Other organizations such as network and service providers, manufacturers, scientific, and other international organizations (e.g., Teledesic), may be admitted through their national administrations to certain ITU activities, such as standardization, but enjoy a lower legal status with no right to vote.

Three main functions that are carried out globally by ITU are as follows:

1. Standardization of telecommunications.
2. Development of telecommunications.
3. Regulation of telecommunications (mainly for radio communications).

The standards developed by ITU are called *recommendations*. This term implies that they constitute nonbinding, voluntary agreements in contrast to the term *standard*, which is often used for mandatory, binding norms.

Consistent with its international nature, Teledesic can and should play a strong role in the first two functions of ITU. Participation in ITU functions will provide visibility in the international scene as well as pave the road for receiving regulatory support from future Teledesic client states. Because of the obvious benefits to its objectives, ITU welcomes and encourages the participation of international network and service providers in its activities.

Recommendations are developed in the Study Groups of the Radio Communications and Telecommunications sectors. These sectors are also known as ITU-R and ITU-T¹, respectively. Each study group deals with a specific area in radio communications or telecommunications. Study group members are *delegates* sent by their administrations. Other organizations may also participate by sending their experts as *participants* if their organization has been admitted by their national administration to the activities of ITU-R or ITU-T.

Study groups of interest to Teledesic are ITU-R Study Groups 4 and 8, dealing with the areas of fixed and mobile satellite communications, respectively. Teledesic's specific approach in treating propagation problems should also be brought to the attention of Study Group 5 of ITU-R since microwave propagation is in the domain of this study group. The contact with Study Group 5 can be made either directly or through Study Groups 4 and 8.

12. References

1. 1992 *CCIR Recommendations*, RPN Series, Propagation in Non-Ionized Media, ITU, Geneva, 1992.
2. L. Ippolito, *Propagation Effects Handbook for Satellite Systems Design*, NASA Reference Publication 1082 (04), NASA, Washington, DC, 1989.
3. J. Laster and W. Stutzman, *Attenuation Scaling by frequency in the Ku/Ka-Band Using the Olympus Satellite*, SATCOM Report No 93-16, Virginia Tech, Sept. 1993.
4. K. Lin and C. Levis, "Site Diversity for Satellite Earth Terminals and Measurements at 28 GHz," *Proc. of the IEEE*, Vol 81, No 6, June 1993, pp. 897-904.
5. R. Jakoby and F. Rucker, "Three Years of Crosspolar Measurements at 12.5, 20, and 30 GHz with the Olympus Satellite," *Proc. Olympus Utilization Conf.*, Sevilla, Spain, Apr. 20 - 22, 1993, pp. 567 - 672.
6. F. Dintelman, G. Ortgies, F. Rucker, and R. Jakoby, "Results from 12- to 30-GHz German Propagation Experiments Carried Out with Radiometers and the Olympus Satellite," *Proc. IEEE*, Vol. 81, No. 6, June 1993, pp. 876 - 884.
7. W. Stutzman, et al., "Statistical Results from the Virginia Tech Propagation Experiment Using the Olympus 12, 20 and 30 GHz Satellite Beacons," *Proc.*

¹In December 1992, an ITU Plenipotentiary Conference introduced three new sectors: *Radio Communications* (formerly CCIR and IFRB), *Telecommunications Standardization* (formerly CCITT), and a new *Development Sector*.

Seventeenth NASA Propagation Experimenters Meeting (NAPEX XVII), JPL Publication 93-21, JPL, Pasadena, CA, Aug. 1, 1993, pp. 33 - 45,

8. R. Howell, J. Harris, and M. Mehler, "Satellite Crosspolar Measurements at BT Laboratories," *BT Technology Journal*, Vol. 10, No. 4, Oct. 1992, pp. 52 - 67.
9. T. Pratt and F. Haidara, "Results from a Study of Scintillation Behavior at 12, 20, and 30 GHz Using the Results from the Virginia Tech Olympus Receivers," *Proc. Seventeenth NASA Propagation Experiments Meeting (NAPEX XVII)*, JPL Pub 93-21, JPL, Pasadena, CA, Aug. 1, 1993, pp. 47-58.

Acknowledgment

The research described in this publication was carried out by the Jet Propulsion Laboratory, California Institute of Technology, and was sponsored by Teledesic corporation.

GASEOUS ABSORPTION

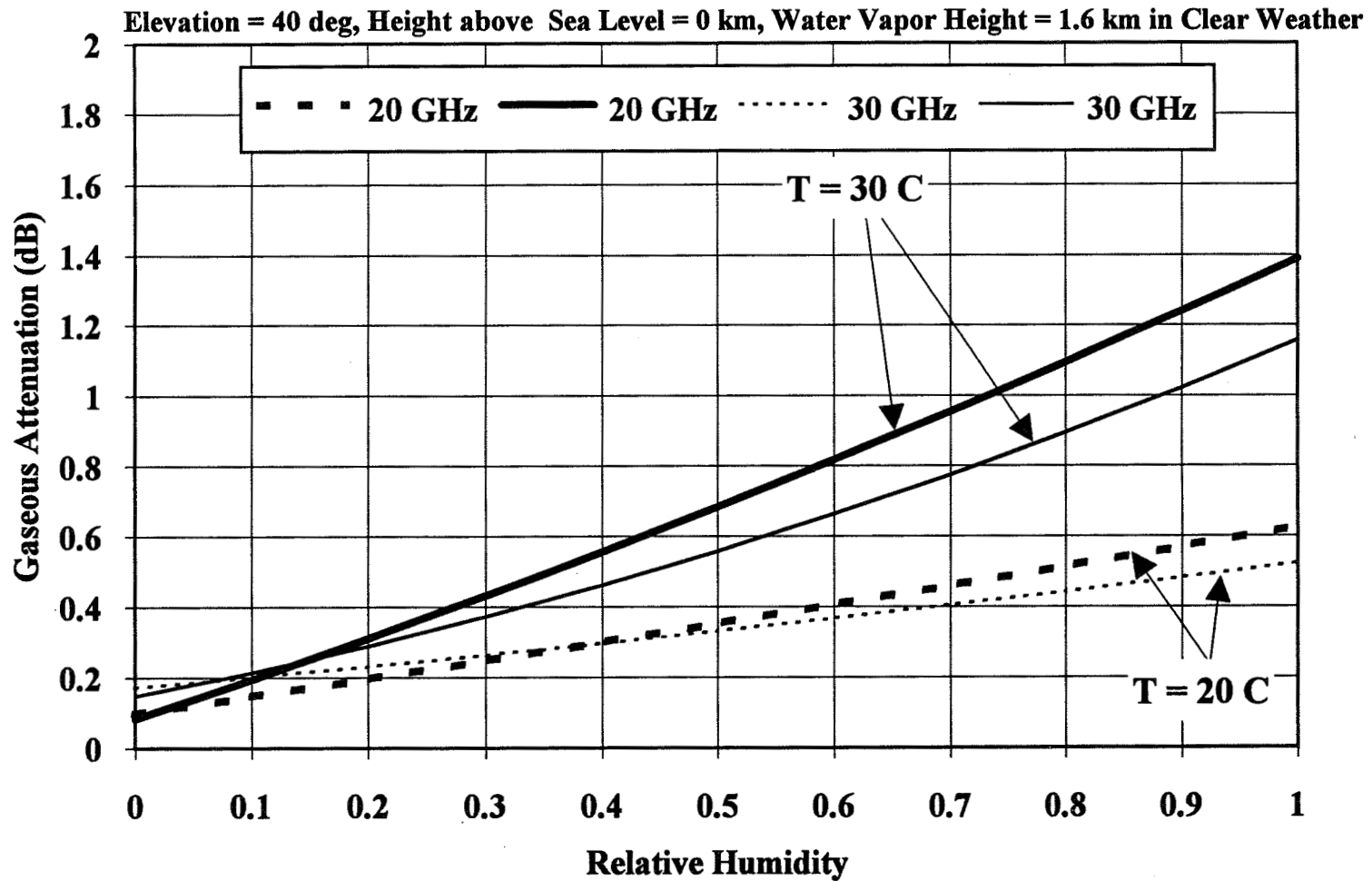


Figure 1: Gaseous Attenuation due to Oxygen and Water Vapor in Clear Weather.

GASEOUS ABSORPTION

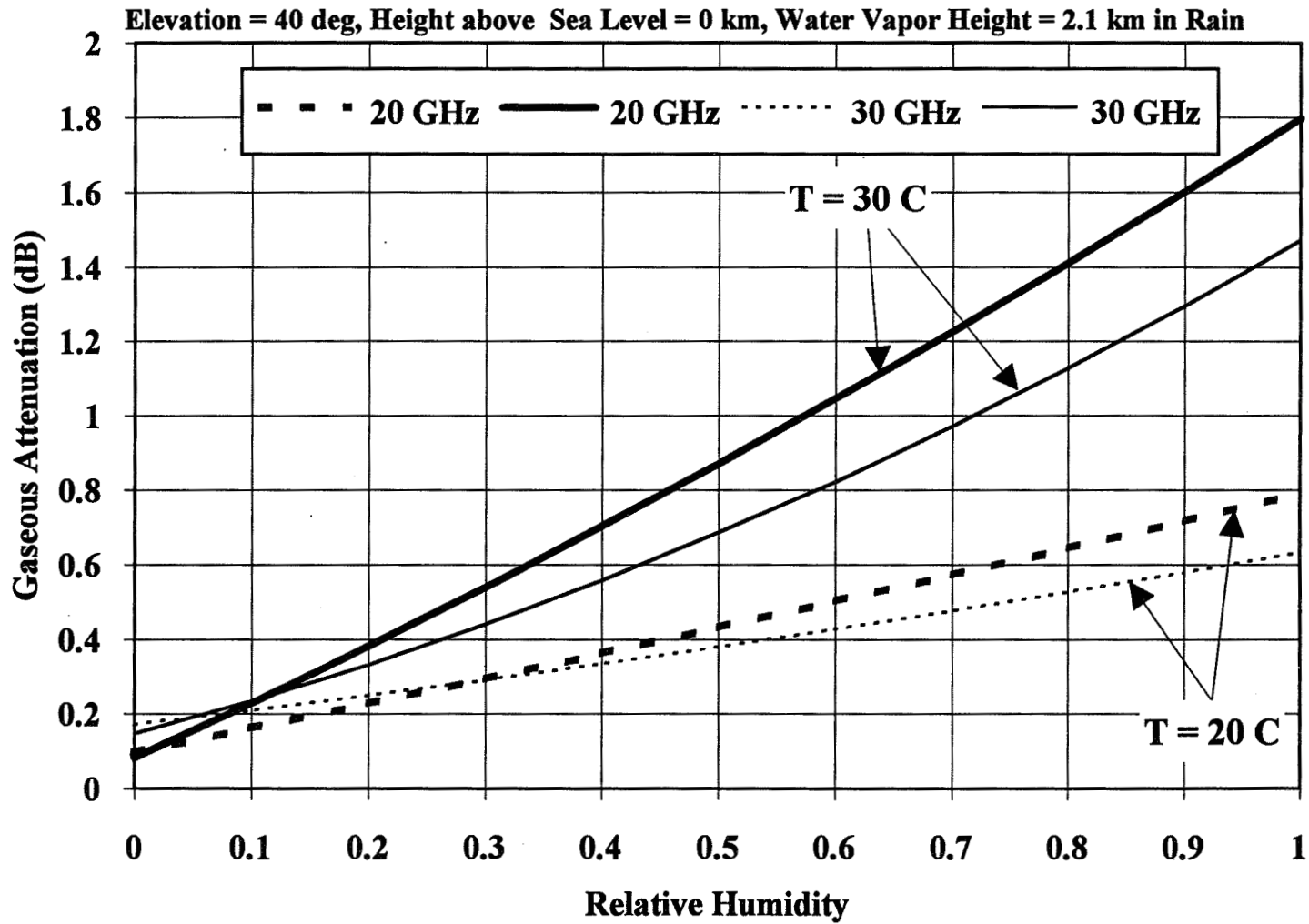


Figure 2: Gaseous Attenuation due to Oxygen and Water Vapor in Rain.

RAIN ATTENUATION

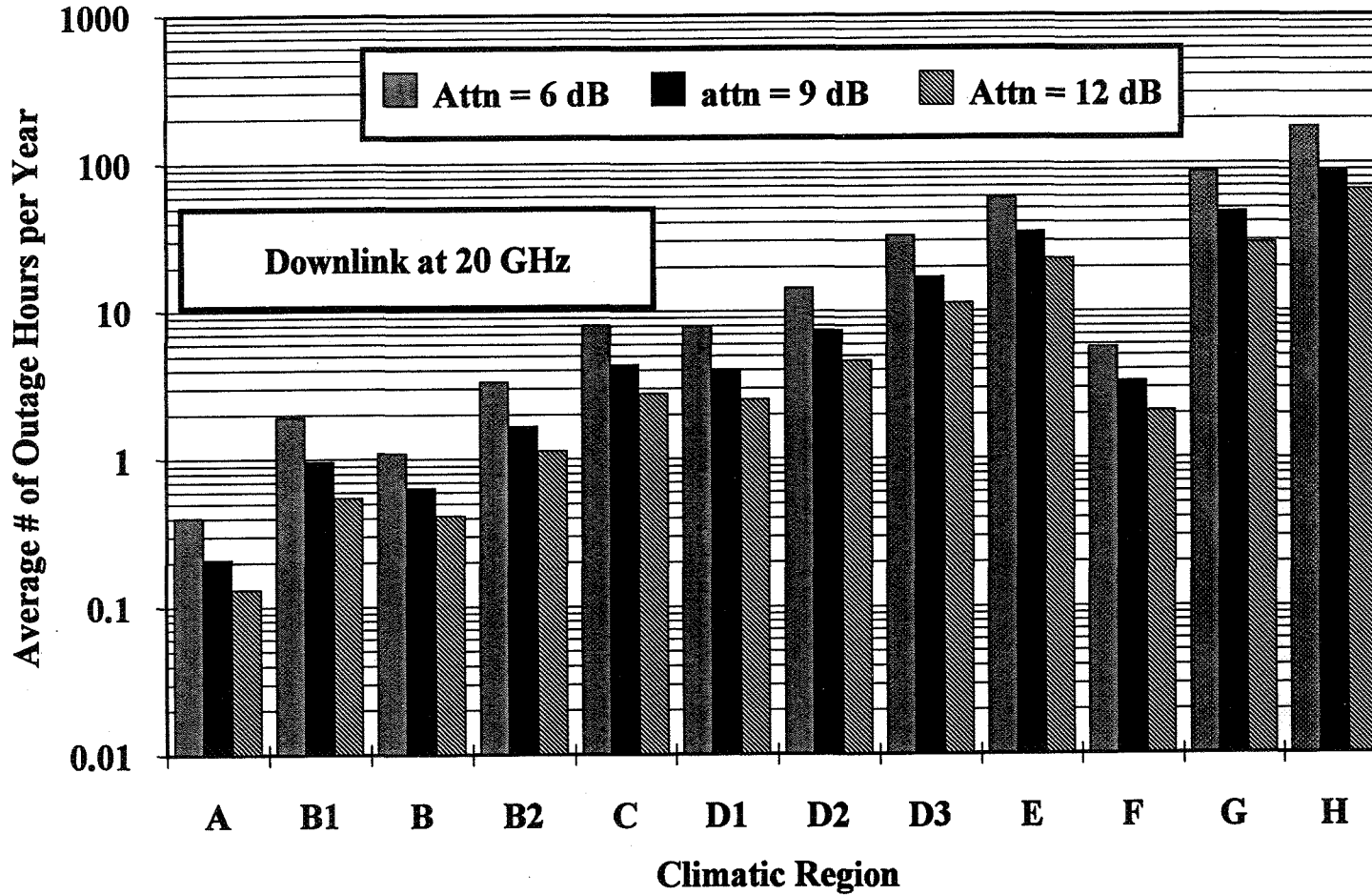


Figure 3: Average Number of Link Outage Hours per Year with No Spatial Diversity.

RAIN ATTENUATION

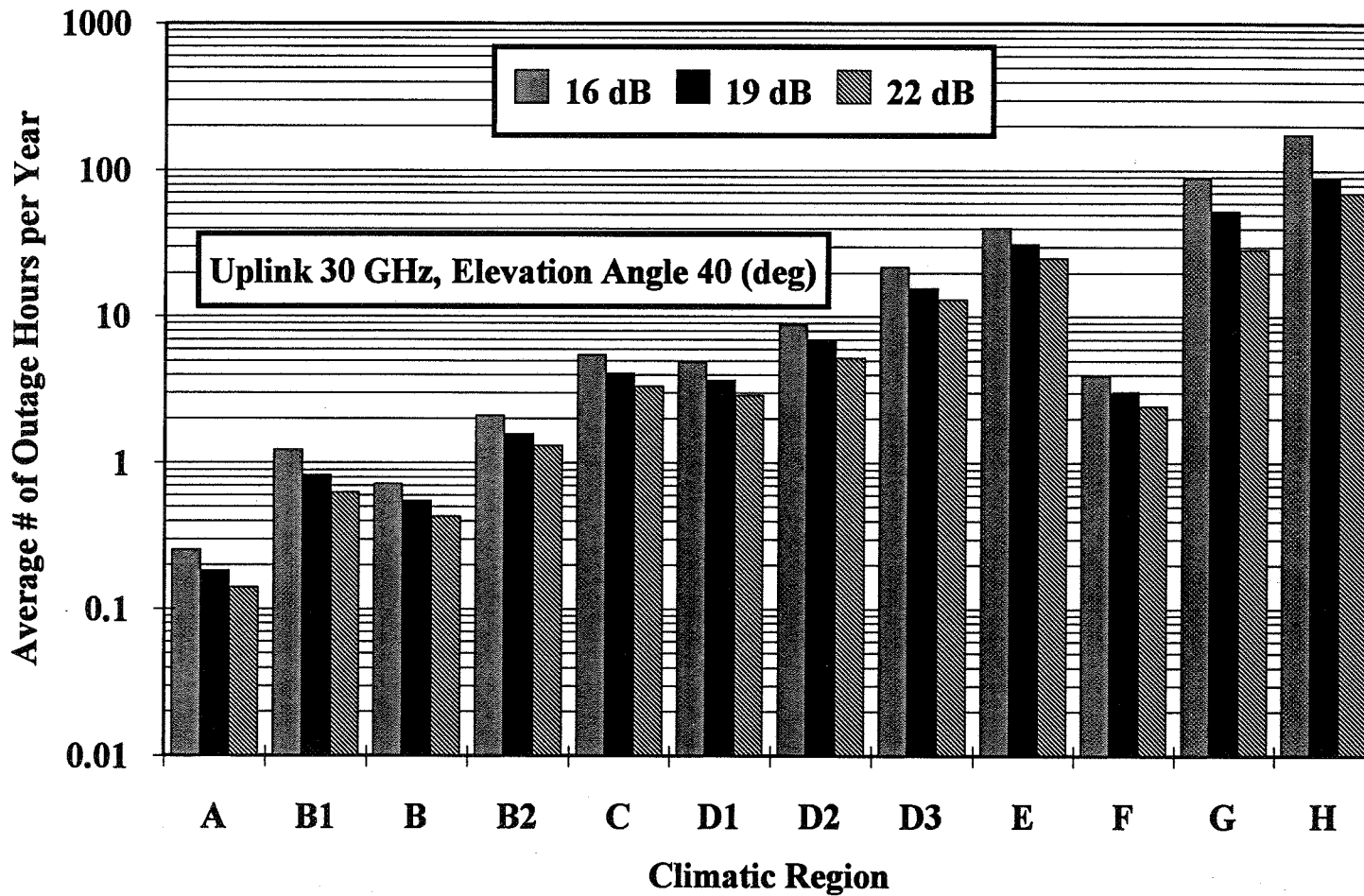
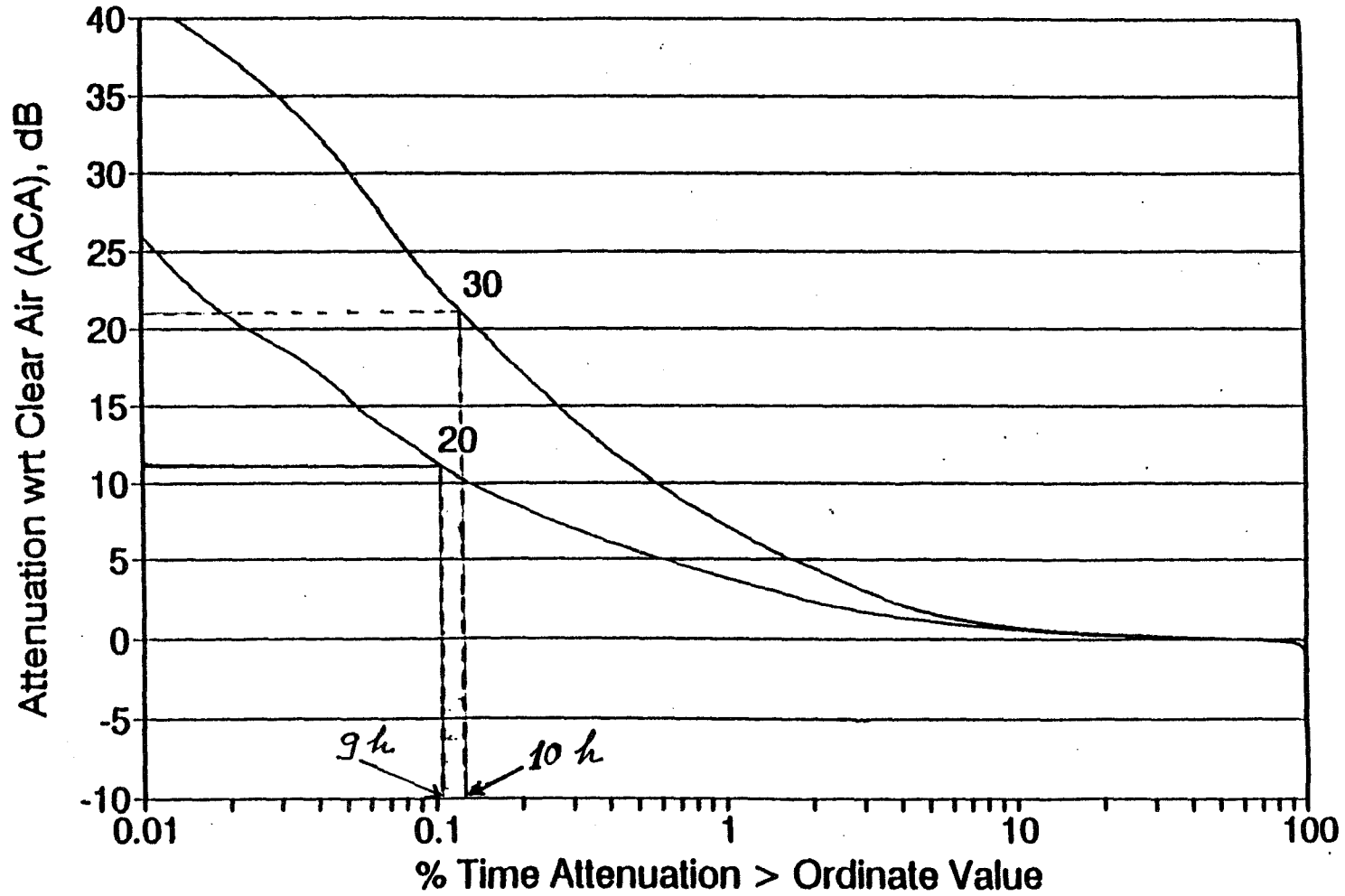


Figure 4: Uplink Average Number of Link Outage Hours per Year with No Spatial Diversity.

RAIN ATTENUATION



* Common Time Base

Figure 5: Attenuation with Respect to Clear Air at 20 & 30 GHz (91/92)-Blacksburg, Virginia.

CCIR DIVERSITY MODEL

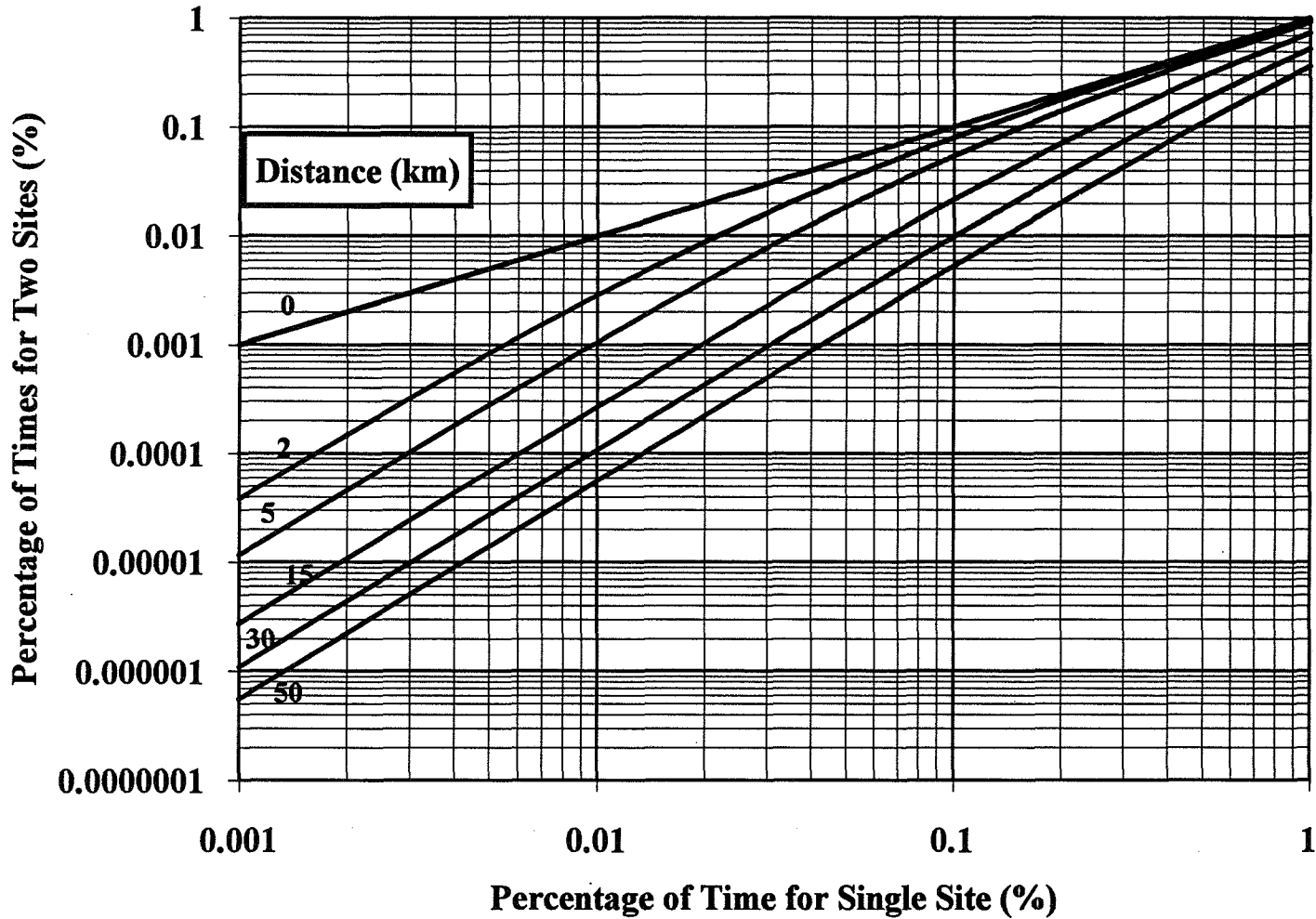


Figure 6: Diversity Improvement with Two Sites.

RAIN ATTENUATION

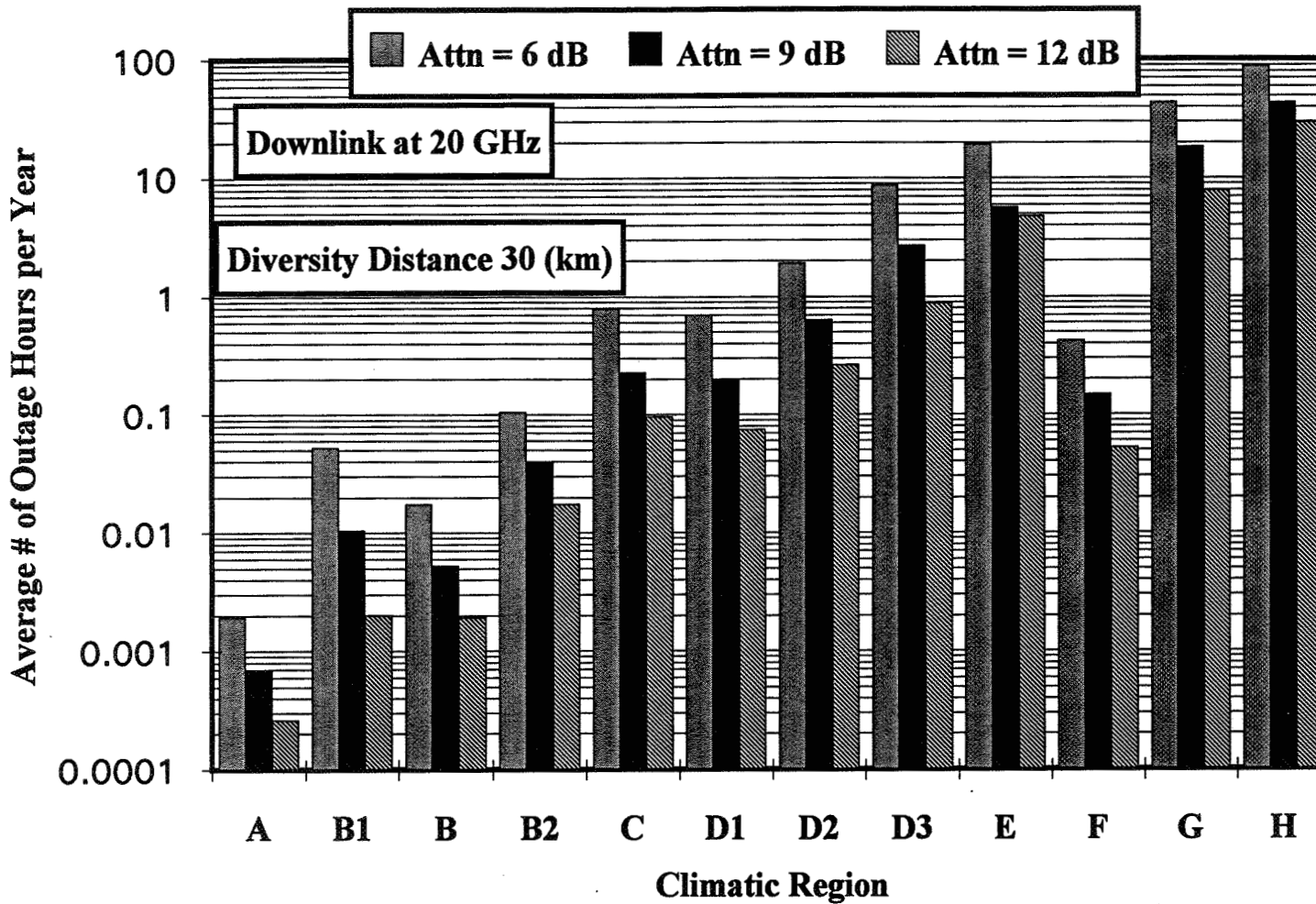


Figure 7: Average Number of Link Outage Hours per Year with Spatial Diversity.

RAIN ATTENUATION

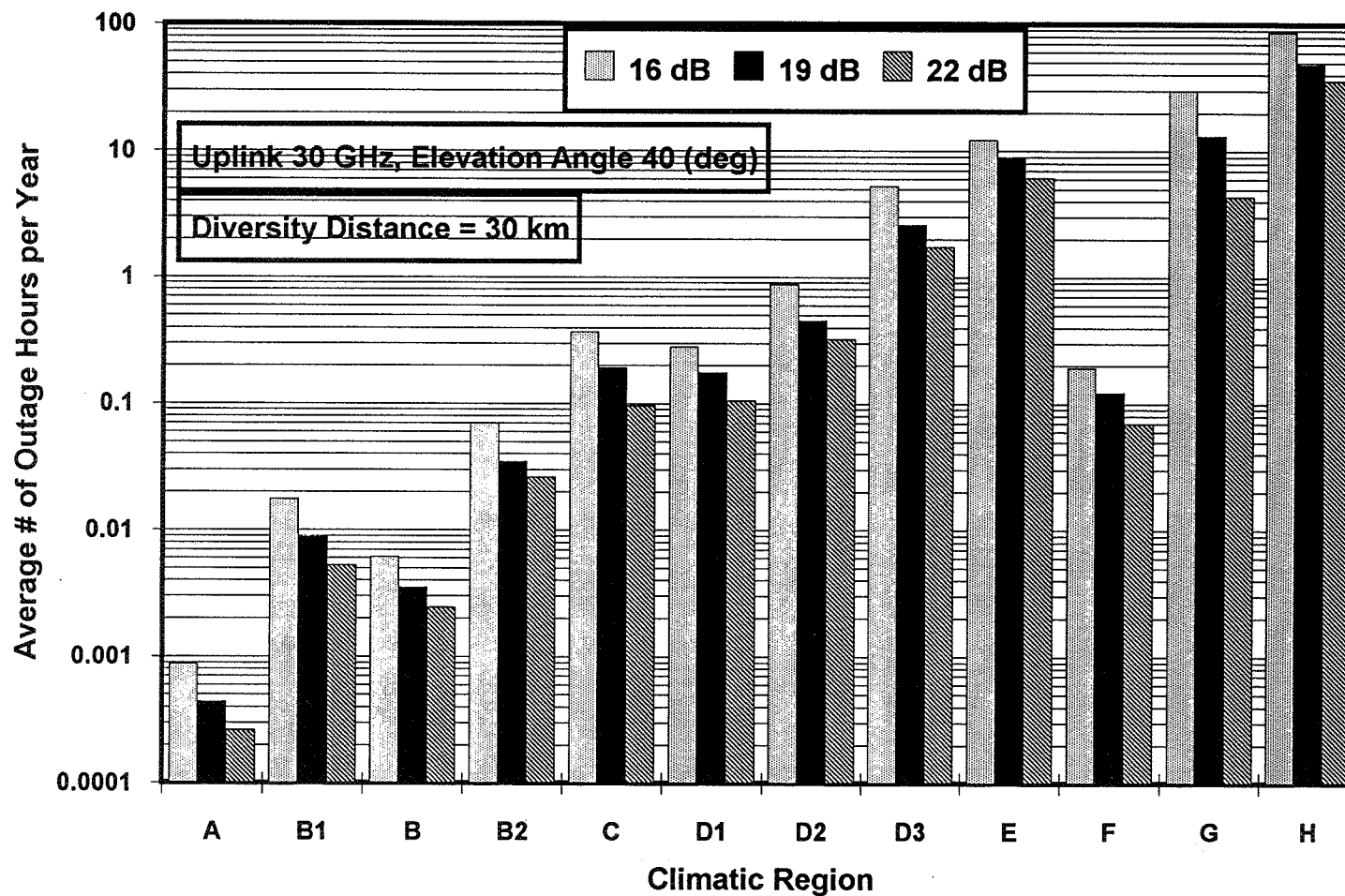


Figure 8: Average Number of Link Outage Hours per Year with Spatial Diversity

ZENITH ATTENUATION

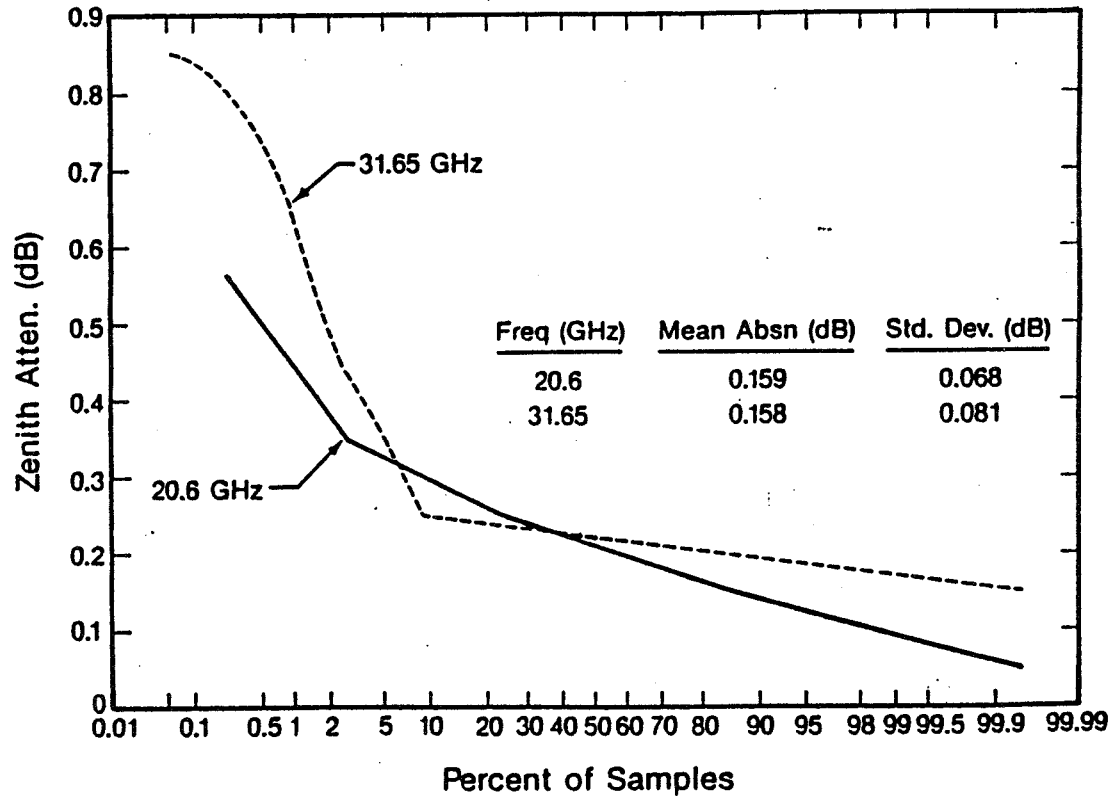


Figure 9: Cumulative Distribution of Zenith Attenuation Measured by a Three-Channel Radiometer at Denver, Colorado, December 1987. Data Consist of 14181 2-min Averages.

ZENITH ATTENUATION

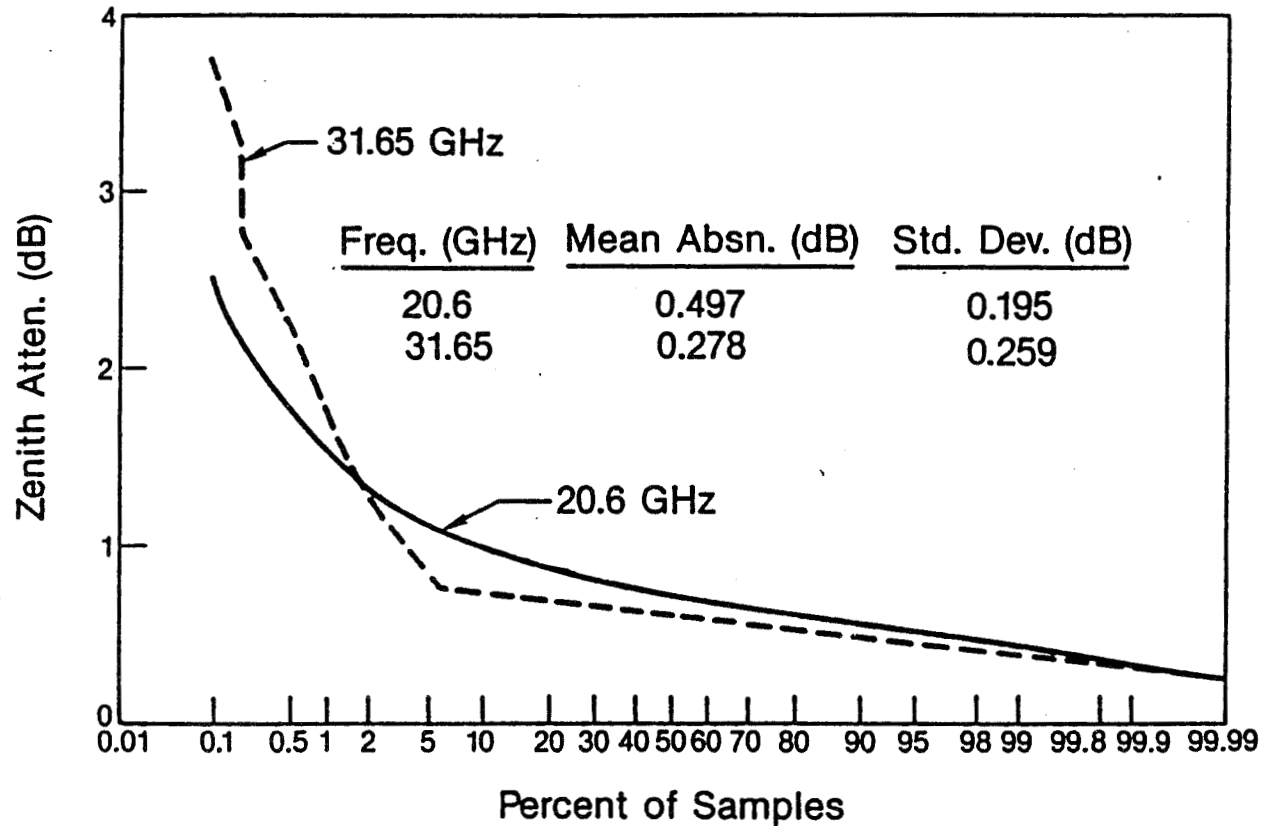


Figure 10: Cumulative Distribution of Zenith Attenuation Measured by a Three-Channel Radiometer at Denver, Colorado, August 1988. Data Consist of 17792 2-min Averages.

DEPOLARIZATION

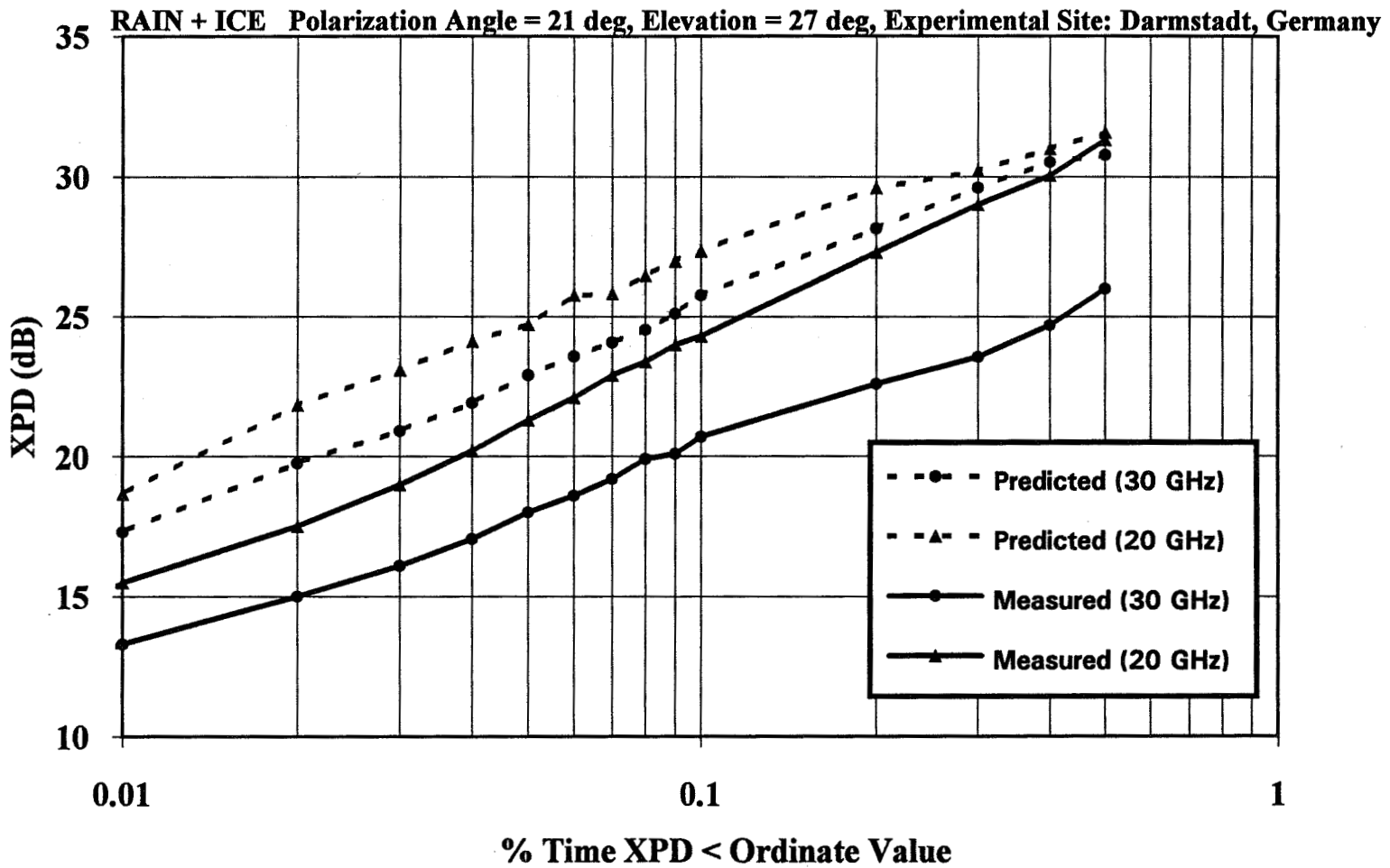


Figure 11: Cumulative Distributions of Measured XPD and CCIR Predictions Based on Measured Attenuation at 20 and 30 GHz.

DEPOLARIZATION

RAIN + ICE Circular Polarization Elev. Angle = 40 deg Experimental Site: Blacksburg, Virginia, U.S.A.

70

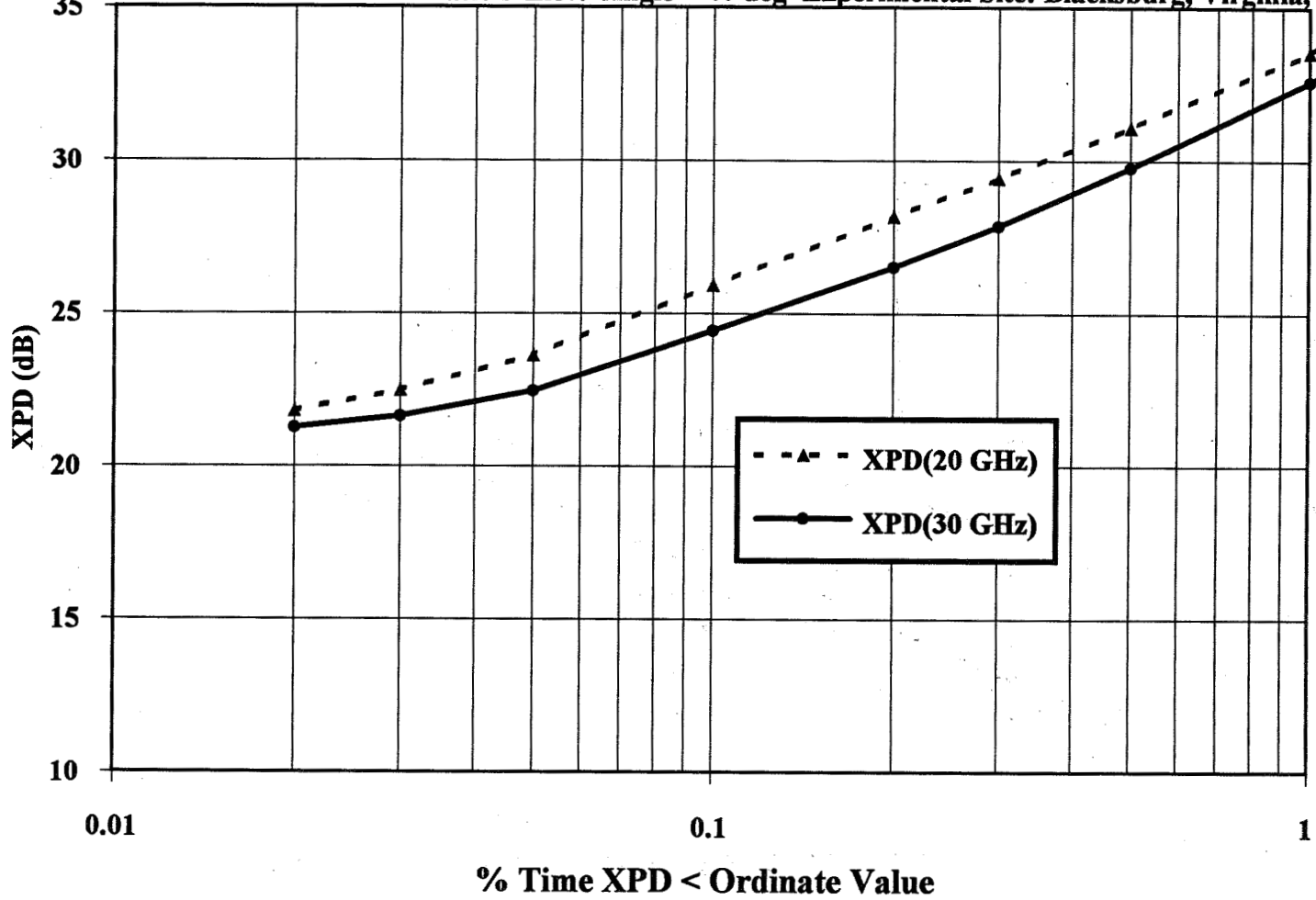


Figure 12: Cumulative Distribution of XPD for Blacksburg, Virginia.

DEPOLARIZATION

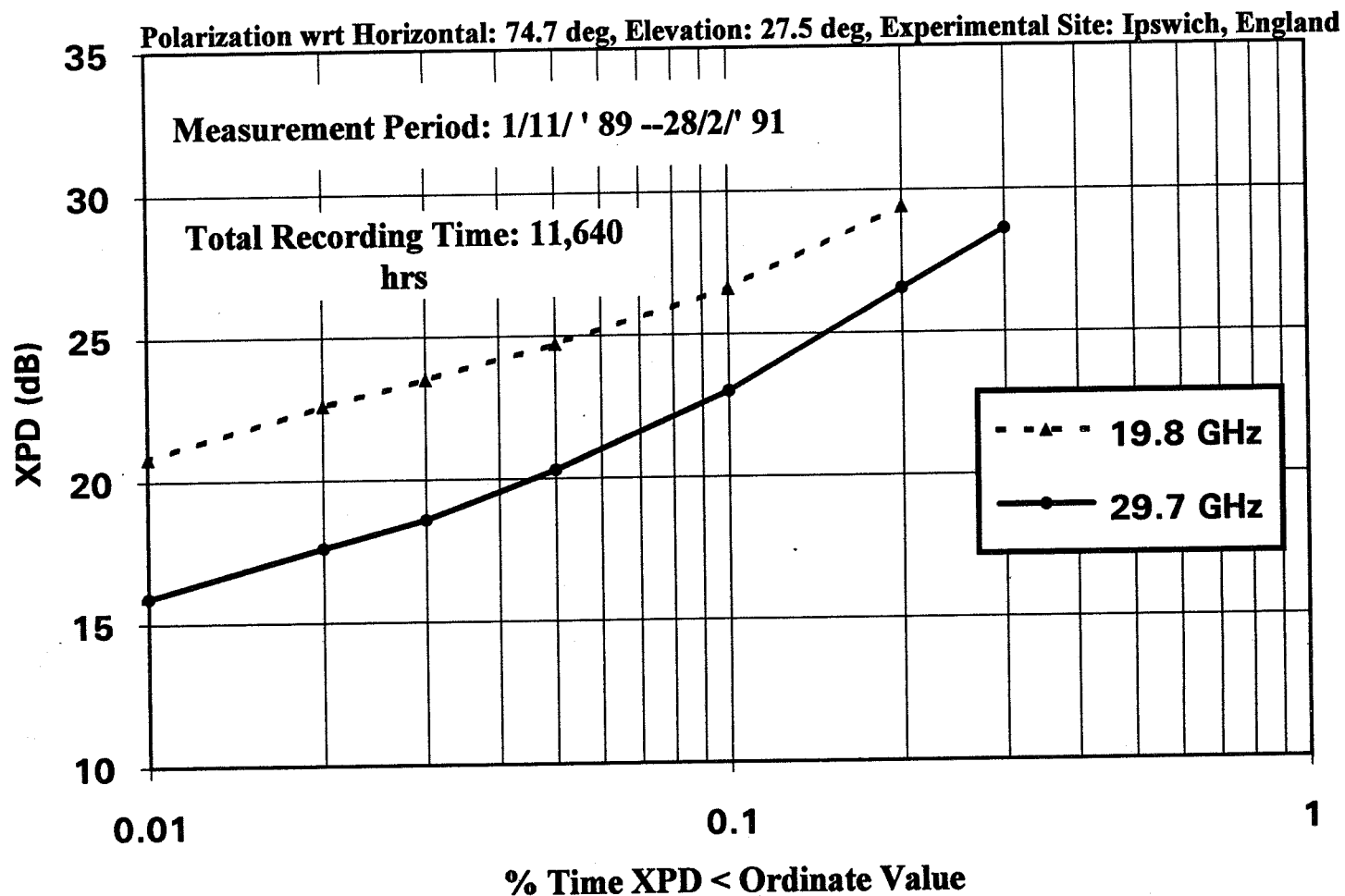


Figure 13: Crosspolar Discrimination Measured Data from OLYMPUS at 19.8 and 29.7 GHz.

SCINTILLATION

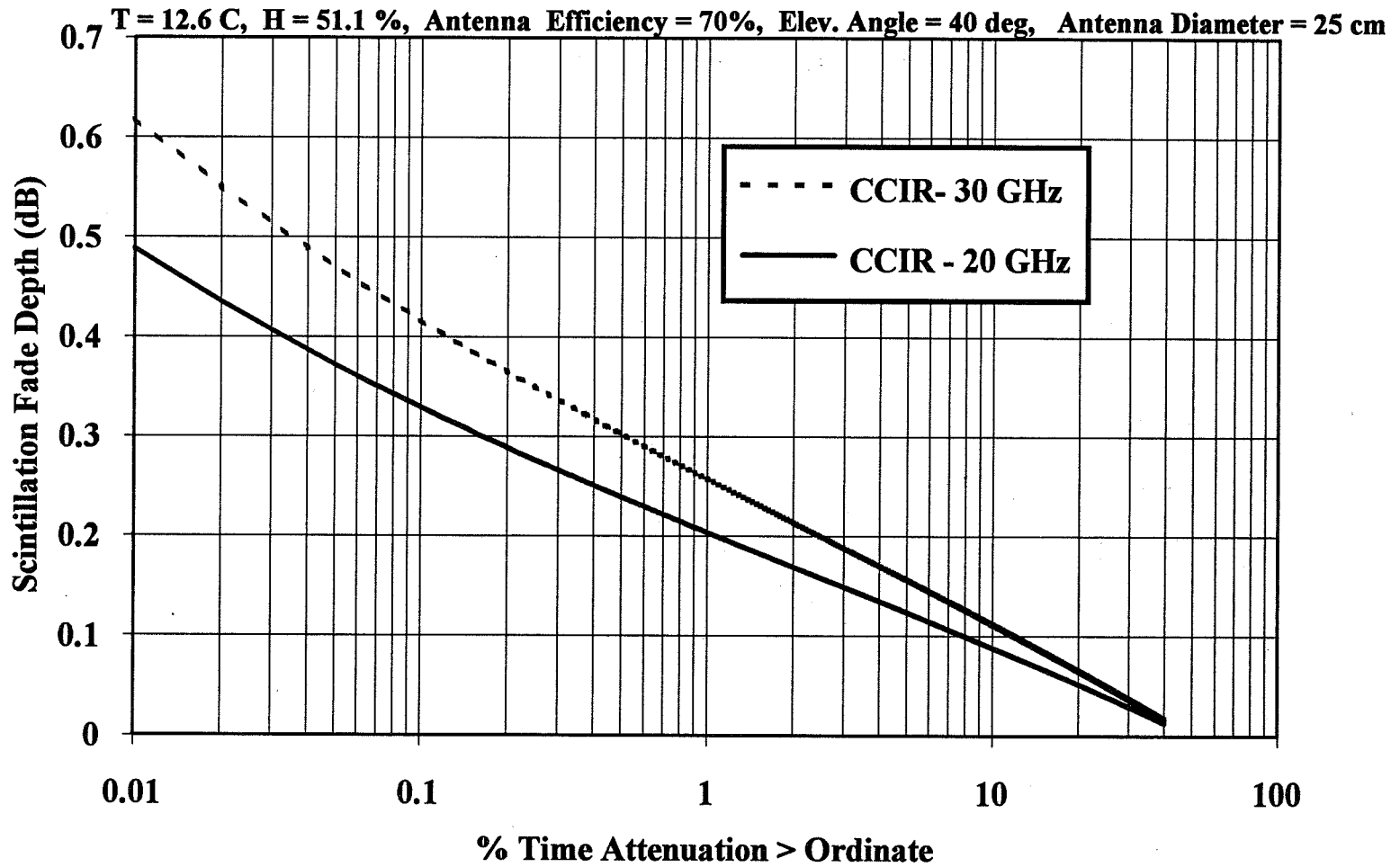


Figure 14: Cumulative Scintillation Fade Distribution, Blacksburg, VA, Average Conditions.

SCINTILLATION

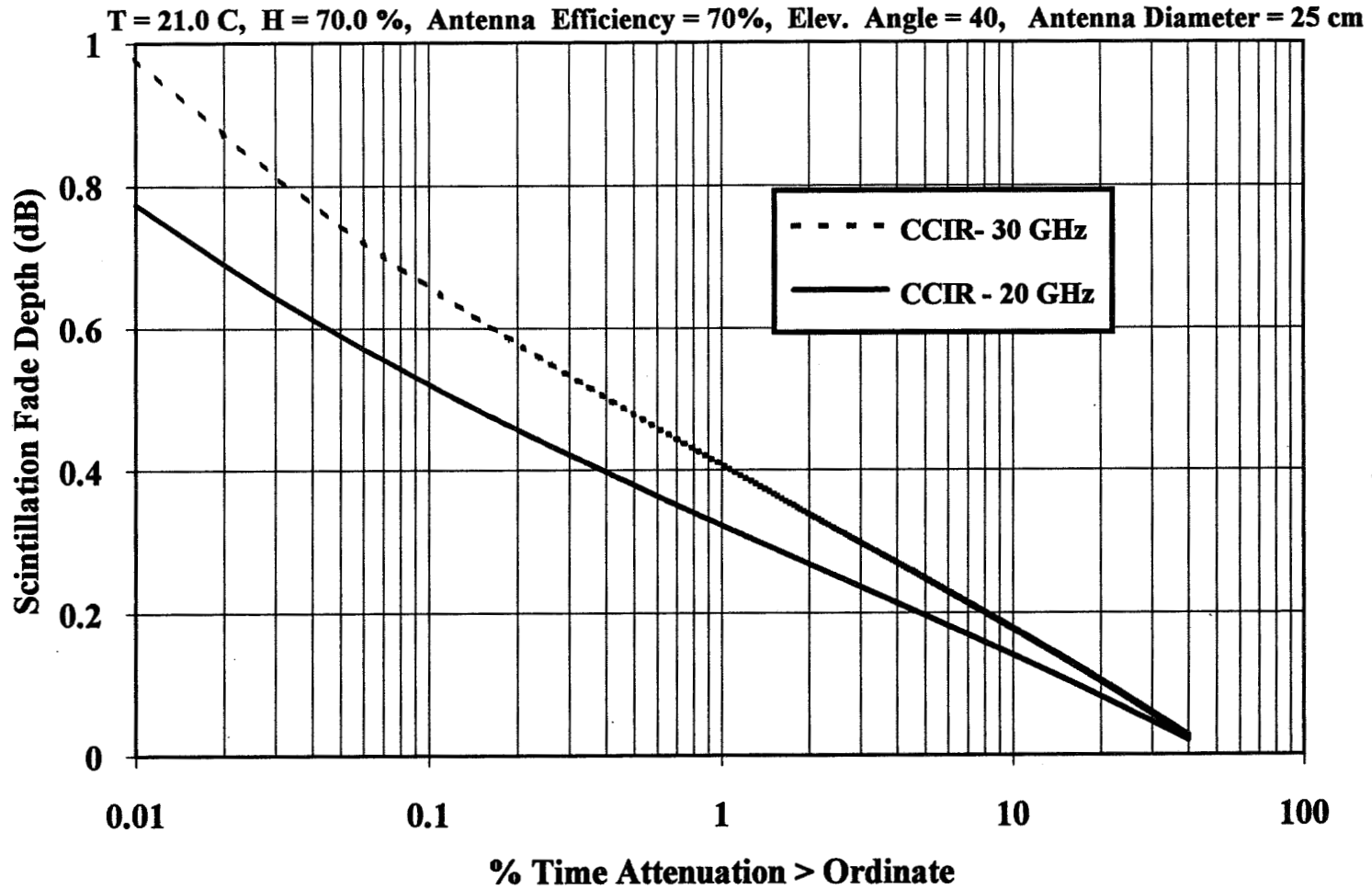


Figure 15: Cumulative Scintillation Fade Distribution, Blacksburg, VA, Spring/Summer Conditions.

SCINTILLATION

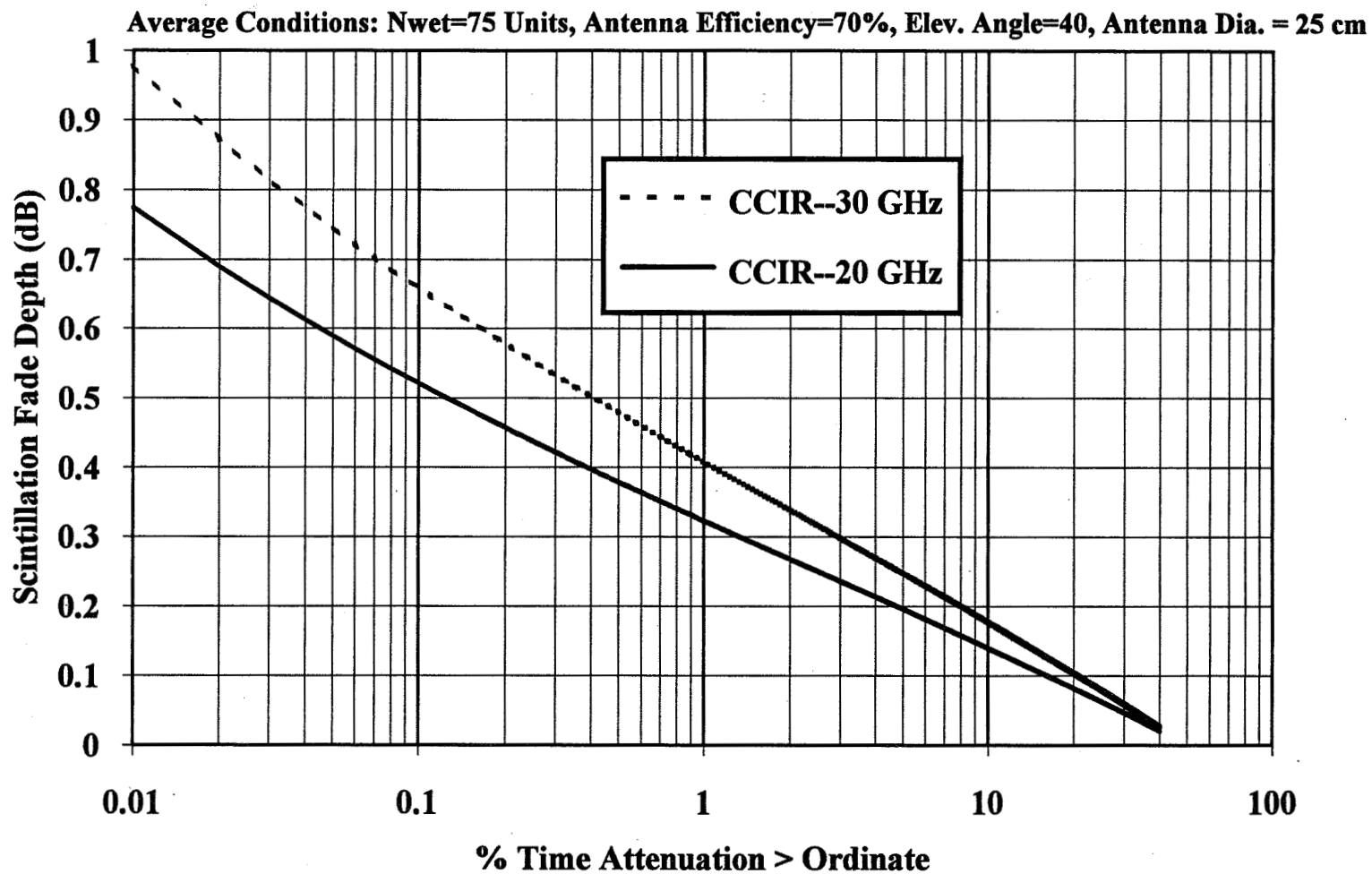


Figure 16: Cumulative Scintillation Fade Distribution, Austin, TX, Average Conditions.

SCINTILLATION

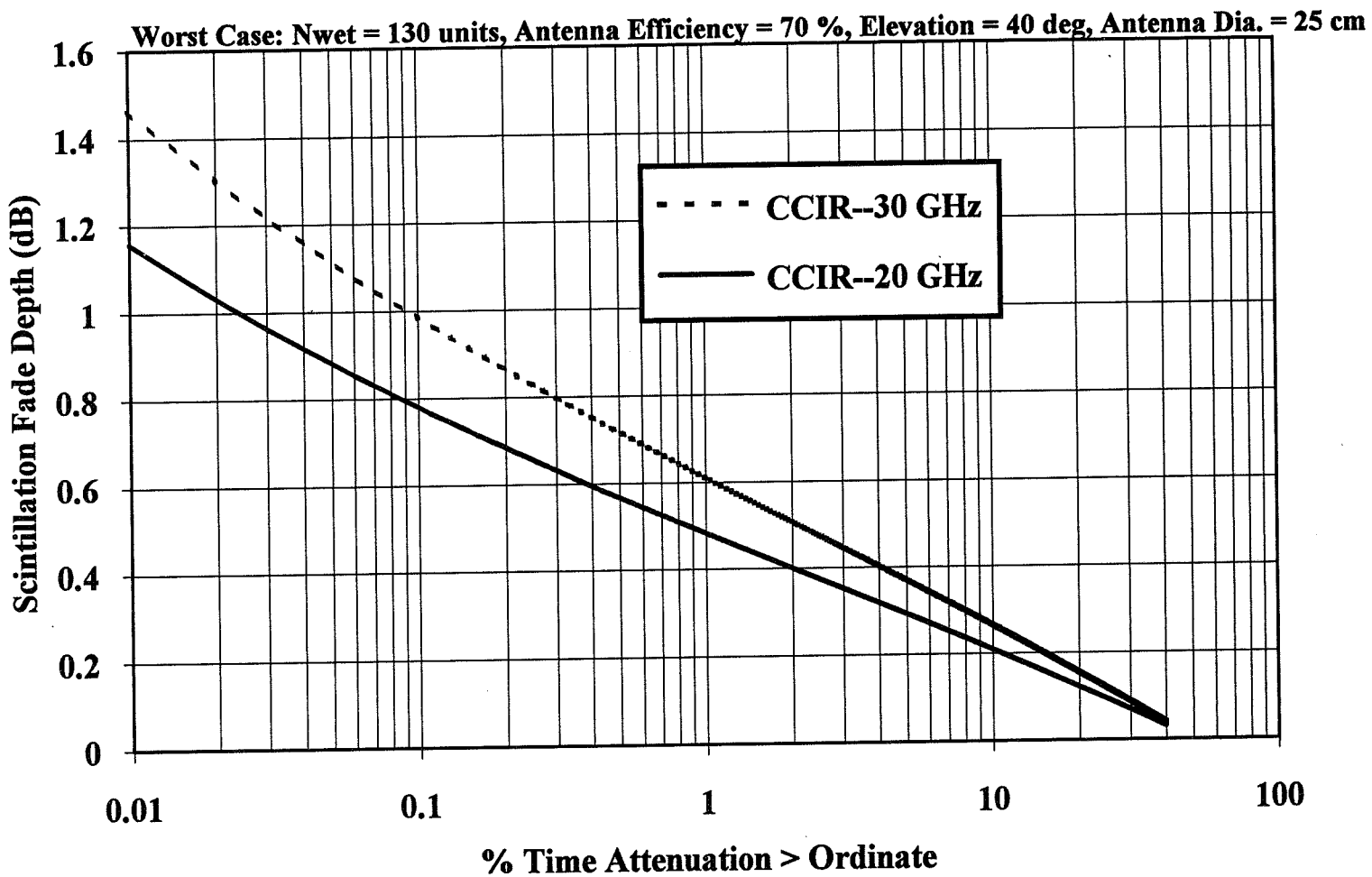


Figure 17: Cumulative Scintillation Fade Distribution for Worst Case Conditions at Austin, Texas.

PROPAGATION DATA AT 20/40 GHZ
AND THE PROPAGATION NEEDS OF MILSTAR

349270

F. I. Shimabukuro and Y. S. Kim
The Aerospace Corporation

P.5

Cdr. P. Ayotte
USN

1. Introduction

Milstar system planners are in the process of creating accurate service definitions, evaluating resource requirements, and assessing performance. An important factor in the determination of the resource allocations to provide acceptable network performance is accurate link analysis. The Milstar system utilizes EHF communication links, 44 GHz on the uplink and 20 GHz on the downlink. There are various environmental factors which can affect the link performance at these frequencies, and the propagation factors for which there are inadequate characterizations are of most concern. These inadequacies result from either an inadequate data base which precludes the derivation of a proper propagation model, or, if the data do exist, they have not been assimilated in a form which is readily utilized.

The Milstar system incorporates terminals of varying sizes, and the performance of the small field terminals, which have relatively small link margins, are most affected by atmospheric phenomena. With small link margins, clouds, foliage, light rain, and molecular absorption can affect link closure. At low elevation angles, the effects are more pronounced, and in addition, multipath, refraction, and turbulence effects may become significant. Especially important for Milstar system planning is an adequate characterization of cloud and rain effects on link performance. The interaction of the electromagnetic field with cloud particles is well understood, but a usable statistical description of the integrated liquid water content along an arbitrary earth-to-space path at locations of interest is lacking. Measured data, taken for a limited time, are available for a few locations, but for system planning, cloud effects cannot be adequately modeled for most sites. As with clouds, the effects of rain on radio propagation are also well understood. Unlike clouds, there are sufficient rain data to provide viable global rain models which can be used to give annually averaged statistical estimates of link outages in many regions of the world. In many cases the data will support more detailed rain models which would be more helpful to system planners. For example, the user is not usually interested in the statistics of annual averages over large climate regions, but rather in the statistics in the deployment area, while he is there. Therefore, monthly and worst

month statistics for many and smaller regions are much more useful. The assimilation of all available data of this type to derive a monthly global rain model would greatly benefit system planning. Long term weather patterns may change, and when predictable, should be incorporated in the rain model. Also, the planner would like to have an indication of how long the link outage is likely to last, and how often the outages occur. This information can serve as a guide on whether to drop the data rate, design for a backup, etc. Rain data are available to provide information for some of these concerns, and in this paper one of the rain induced statistics of interest, outage duration, will be examined.

2. Estimates of Outage Duration Statistics

Available experimental data, with some theoretical justification [1], indicate that rain rate, and thereby rain attenuation, is approximately lognormally distributed. Also, for the same reasons, the time durations for given rain rates are lognormally distributed. When it rains at a particular rain rate or greater, the probability density for the time duration, t , is modeled as

$$p(t) = \frac{1}{\ln(s) \sqrt{2\pi}} \frac{1}{t} \exp\left[-\left(\frac{\ln(t) - \ln(m)}{\sqrt{2} \ln(s)}\right)^2\right] \quad (1)$$

where $\ln(m)$ and $\ln(s)$ are the mean and standard deviation of the logarithm of the variable, t . The value m is the median time duration. Given that it is raining at a given rain rate or greater, the probability that the duration T is greater than t is given by

$$P(T > t) = \frac{1}{2} \operatorname{erfc}\left[\frac{\ln(t) - \ln(m)}{\sqrt{2} \ln(s)}\right] \quad (2)$$

where erfc is the complementary error function.

Tattelman and Knight [2] described a method for extracting one minute rain rates from original raingage recordings. Using this method, Tattelman and Larson [3] obtained 1 minute average

rain rate data over a 10 year period at 41 locations in the contiguous U. S. In particular, they have plots of the average number of occurrences of rain at particular rain rates for 6 duration times at these locations. A sample plot is shown for International Falls, Mn. The event occurrences are counted in the following way. As an example, a contiguous period of 23 minutes during which the rain rate exceeds the critical rate is counted as twenty three 1-minute events, four 5-minute events, two 10-minute events, one 15-minute event, and one 20-minute event.

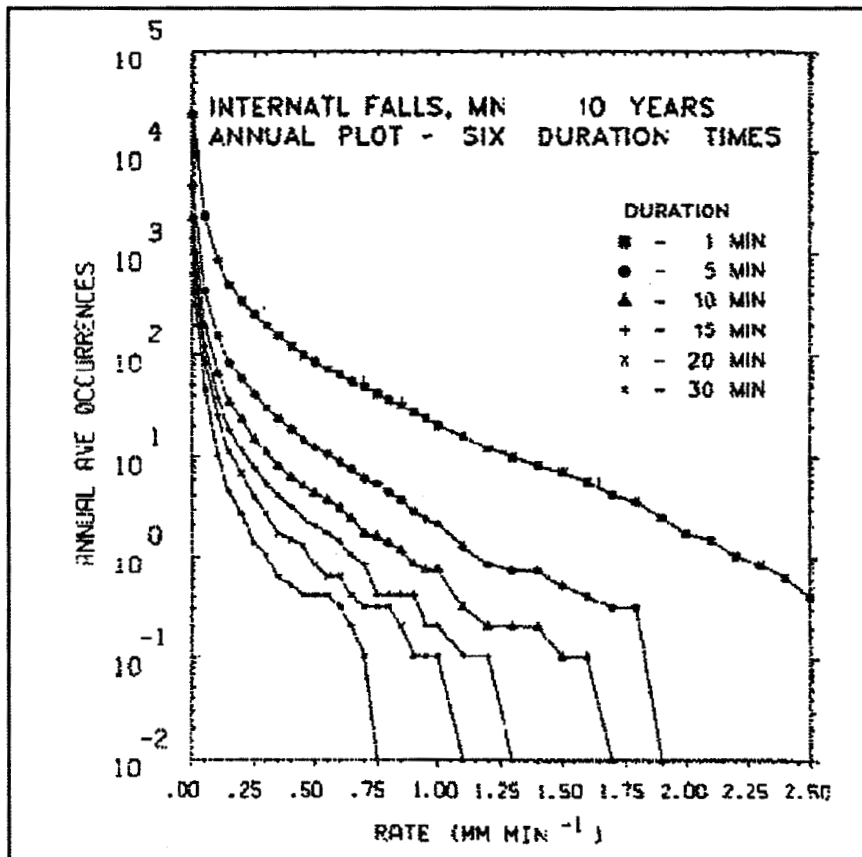


Fig. 1. Annual average number of occurrences of 1-minute rain rates for 6 duration times. Rain rates are those equalled or exceeded during each minute of the specified duration.

If the duration times are truly lognormally distributed, the data above can be used to estimate the median, m , and s for a particular rain rate. The predicted occurrences of 1-minute duration events are given by

$$N_1 = K[n_1 + 2n_2 + 3n_3 + \dots] \quad (3)$$

where n_i is the normalized number of events between i and $i+1$ minutes, as given by (1), and K is a constant which converts the normalized values to the actual observed 1-minute occurrences in a year. In general, the number of occurrences for the time duration t is given by

$$N_t = K \left[\sum_{i=t}^{2t-1} n_i + 2 \sum_{i=2t}^{3t-1} n_i + \dots \right] \quad (4)$$

The procedure for estimating the median and standard deviation in the lognormal distribution is as follows. For a given rain rate, the average number of occurrences of the 1, 5, 10, 15, 20, and 30-minute durations are obtained from Fig. 1. Then a value of m and a value of s are assumed and the predicted number of the 1, 5, 10, 15, 20, and 30-minute occurrences are obtained from (4). The process is repeated with a range of values for m and s and the best least squares fit for m and s will give the minimum value of L , where

$$L = \sum_t [N_{mt} - N_t]^2 \quad t=5,10,15,20,30 \quad (5)$$

where N_{mt} is the measured occurrence for duration t and N_t is the predicted occurrence.

As an example, suppose a rain rate of 9 mm/hr will cause an outage on the uplink for an EHF terminal located at International Falls. From Fig. 1, for this rain rate (9 mm/hr or 0.15 mm/min), there will be an average of approximately 500 1-minute events, 88 5-minute events, 37 10-minute events, 19 15-minute events, 11 20-minute events and 5.5 30-minute events in a year. For this example, the best least squares fits for the median, m , and s are 11 and 2.4 minutes, respectively. Plots of the average number of occurrences as a function of outage duration and the probabilities that the outage will be greater than a given duration are shown in Fig. 2. Also shown on the plot are the measured occurrences of the 1, 5, 10, 15, 20, and 30-minute durations.

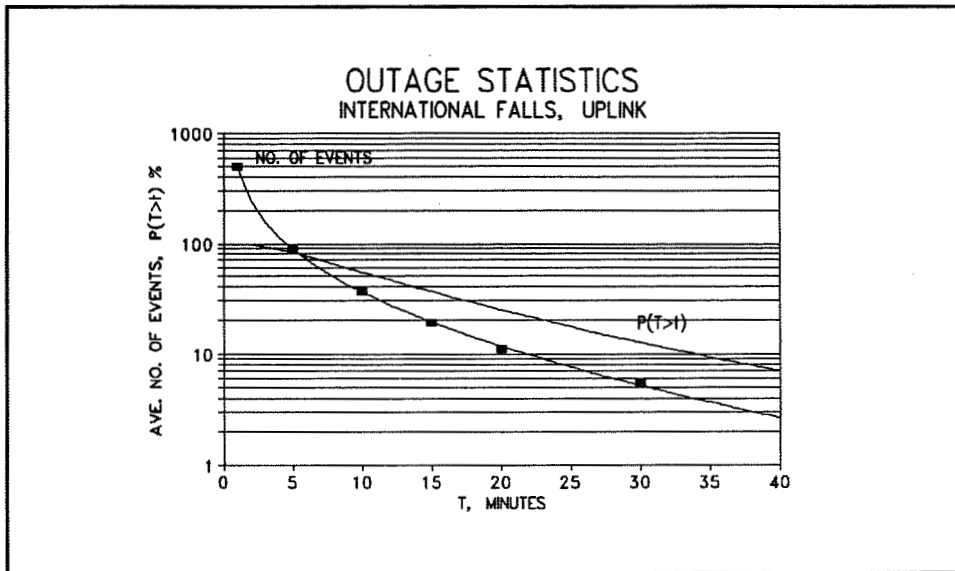


Fig. 2. Annual average number of outage events of duration t and the probability that the duration will be greater than t . The rain rate is 9 mm/hr. The solid rectangles are the values obtained from Fig. 1, and the solid curve is that for the best fit values of m and s .

3. Summary

There are a number of propagation issues that need further investigation for efficient system planning for EHF communication systems. Especially needed are better cloud and rain characterizations. A method for estimating one of the rain induced effects of interest, outage duration, is presented.

4. References

1. S. H. Lin, "Statistical Behavior of Rain Attenuation", Bell Syst. Tech. Journ. 52, 557, 1973.
2. P. Tattelman and R. W. Knight, "Analyses of 1-min Rain Rates Extracted from Weighing Raingage Recordings", Journ. of Appl. Meteorolgy 27, 928, 1988.
3. P. Tattelman and K. P. Larson, "Effects on Rain Attenuation on Satellite Communications in the United States", AFGL Report AFGL-TR-89-0012, Jan. 8, 1989.

1995 14674 60

The 40 and 50 GHz propagation experiments at the Rutherford Appleton Laboratory, UK, using the ITALSAT beacons

349277

J. M. Woodroffe, P. G. Davies, D.N.Ladd and J. R. Norbury

Rutherford Appleton Laboratory, Chilton, U.K.

29

ABSTRACT

This paper describes the current experimental programme and future plans for the reception of transmissions from the 18.7, 39.6 and 49.5 GHz beacons from the ITALSAT satellite by the Radio Communications Research Unit at Rutherford Appleton Laboratory, UK.

The 49.5 GHz beacon on ITALSAT has very similar characteristics to that of the 20 GHz beacon on Olympus. The similarities between the design of this beacon and the 20 GHz transmission from Olympus were considered desirable, in that experimental systems and analysis techniques, developed for the Olympus project, could then be directly applied to these higher wavebands. The signal, which is switched between vertical and horizontal polarization at a rate of 933 Hz, has a specified EIRP of 26.8 dBW, after five years' operation. The coverage area of both 39.6 and 49.5 GHz beacons (3 dB footprint) includes most of Europe.

1. INTRODUCTION

The Radio Communications Research Unit at Rutherford Appleton Laboratory, which has had considerable experience in developing experimental millimetric equipment for propagation studies (1), has initiated the development of a single-channel receiver and a triple channel receiver to measure propagation effects at 49.5 GHz and 39.6 GHz respectively. The initial location of the receivers will be at Chilbolton, Hampshire, UK.

More details of this beacon and the other two on ITALSAT can be obtained through the ITALSAT Propagation Experiment Users guide (2).

2. CHARACTERISTICS OF THE ITALSAT 39.6 and 49.5 GHz BEACON

ITALSAT is situated in a geostationary orbit at 13° East longitude and is maintained in a ± 0.15° orbit box. The satellite was launched in January 1991 with a scheduled five year operational lifetime. The 39.6 GHz beacon is modulated to produce side bands ± 505 MHz from the carrier with an EIRP of 24.8 dBW. The polarization of this beacon is right-hand circular. The two side bands can be used to measure amplitude and phase distortions produced by the medium and to assess the quality of its coherence bandwidth up to ~ 1 GHz.

3. SINGLE CHANNEL RECEIVER DESIGN

The 49.5 GHz system consists of a single polarization receiver for reception of one polarization and a 51 GHz radiometer. The construction of these systems can be seen in Figures 1 and 2. The receiving dish comprises a small 60 cm cassegrain dish, which feeds the signal through a polarization switch to allow selection of either vertical or horizontal polarization. The down conversion to 70 MHz is accomplished through a single balanced mixer with a noise figure of 6 dB. The local oscillator (LO) consists of a VHF crystal source which phase locks to an X- band generator, and is then multiplied to 49.42GHz by a times- four multiplier. The IF signal is amplified and filtered, before final detection by a conventional phase-locked loop (PLL) beacon receiver. This PLL system had been originally developed for the single channel beacon receiver operating in conjunction with the B1 beacon (20 GHz) of the Olympus satellite experiment. The received signal level achieved was 34 dB above the noise

level in clear sky conditions and quite adequate for observing significant propagation effects.

The 51 GHz radiometer (Figure 2), follows the conventional design of a Dicke switched radiometer, where the input to the radiometer signal is switched at 1 KHz between the sky temperature, to be measured, and a reference load controlled by a Peltier junction device. The design is very similar to radiometers at 78 GHz and 95 GHz which had been developed for earlier studies (3). As the necessity for having a stable, low phase noise, local oscillator is not as high as in the receiver, a Gunn oscillator with fundamental frequency near 51 GHz has been used. The frequency drift is reduced to acceptable variations through controlling the temperature of this oscillator, again with a Peltier junction controlled heat-sink. The signal is detected after amplification through a 400 MHz bandwidth IF by a phase sensitive detector, synchronized to the input switching signal. The output from the system produces a measure of the medium temperature to an accuracy of $<1^{\circ}\text{K}$ over a range of 0 to 300°K .

3.1 Mechanical construction

The mechanical layout is based on a fabricated box section aluminium alloy chassis with the antenna mounting plate fixed at right angles to one end. This construction provides a rigid and stable platform for the waveguide components. The top plate carries the LO section, the RF and IF sections. The control circuits, protection circuits and power supplies are mounted on the lower plate. The system is temperature controlled to 20°C and enclosed in a RAE type case. The RF head unit is mounted on an outside broadcast tripod fitted with an elevation over azimuth steerable mount. The gross weight of the receiver system is approximately 20 kg.

4. EXPERIMENTAL RESULTS

Experimental results from an engineering trial were reported in more detail in the ICAP'93 paper (4). However the cumulative distributions derived over a 4 month period (Figure 3) in 1992 have also been included again and compared with the CCIR predictions (4) for 50 GHz at 30° elevation angle. Caution should be exercised in drawing any conclusion from these data as the period of observation was very limited and coincided

with a particularly low rainfall period in the UK.

The final version of this 49.5 GHz system has been operational since July 1993 and analysis of propagation measurements is in progress.

5. THE 39.6 GHz RECEIVING SYSTEM

The 39.6 GHz receiving system is currently in its development phase. The overall design is shown in block diagram form, in Figure 4 is a slightly more complex version of the single channel 49.5 GHz receiver. The RF section consists of an initial down conversion to frequencies in the 1.4 to 2.5 GHz band. A three way multiplexer splits the carrier and two side bands into separate channels, before a second down conversion to 70 MHz. The radiometer which operates near 41 GHz is a conventional Dicke switched system. Calibration of the system is important to monitor any changes in the relative amplitudes and phases between the carrier and side bands. The scheme shown uses the same basic local oscillator for both the second down conversion and calibration signal.

The final stage, a triple channel phase locked loop receiver, is a modification of a single channel design, produced by Ferranti International, which had been used extensively on the Olympus experiment (5).

6. EXPERIMENTAL ARRANGEMENTS

The initial testing of the 49.5 GHz and 39.6 GHz has been performed at Chilbolton. Currently the 49.5 GHz has been operational for nearly 12 months and trials of the prototype 39.6 GHz system started in late April 1994. However it is intended to move both these two receivers together with an 18.7 GHz receiver to Sparsholt, a site 8 km from Chilbolton. The 18.7 GHz receiver will monitor the Ku band beacon on the ITALSAT satellite, intended initially for only Italian coverage. Although the EIRP is 12 to 14 dB lower than at beam centre, the fade margin of about 17 dB is adequate to compare fades at millimetric wavelengths with those at the lower frequencies, which were extensively researched through the Olympus project (5). A 12.5 GHz receiver monitoring the EUTELSAT F4 satellite at 16°E , a 30 GHz radiometer, a rapid response rain gauge and a

distrometer complete the instrumentation at Sparsholt. The multiparameter radars (6) situated at Chilbolton will also be used as a diagnostic instrument to monitor selected events. The experimental measurements at Sparsholt will continue for at least two years assuming a start of operations in late 1994 and the continued transmissions from of ITALSAT.

7. ACKNOWLEDGEMENT

The research activity reported in this paper has been performed as part of the National Radio Propagation Programme at RAL and has been funded by the Radiocommunications Agency of DTI.

8. REFERENCES

- 1) C J Gibbins et al; "A 500m experimental range for propagation studies at millimetre, infra red and optical wavelengths"; J of IEE Vol 57, No 5, pp 227-234, 1987.
- 2) ITALSAT Propagation Experiment - Users Guide. Consiglio Nazionale delle Ricerche, Rome 1987.
- 3) J. M. Woodroffe et al, "Preliminary results from an ITALSAT propagation experiment at 49.5 GHz in the UK". ICAP'93, IEE Conf. No. 370, p.458-461, Edinburgh 1993.
- 4) CCIR Rep 564-7; Propagation data and prediction methods required for earth-space telecommunication systems; Reports of CCIR, 1990, Annex to Vol V, p447-505.
- 5) P G Davies; "Cumulative statistics of rain attenuation at 20 and 30 GHz". Olympus Utilization Conference, (ESA-WPP-60). Seville, April 1993, p521-525.
- 6) J W F Goddard, J D Eastment and M Thurai; "The Chilbolton advanced meteorological radar: a tool for multidisciplinary atmospheric research". Electronics and Communications Eng. Journal, April 1994, p77- 86.

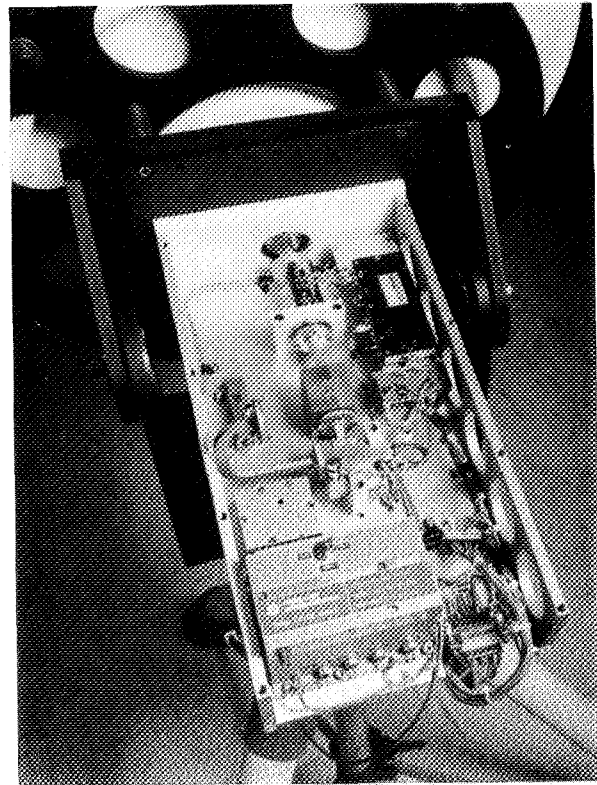


Figure 1
ITALSAT RECEIVER
at 49.5 GHz

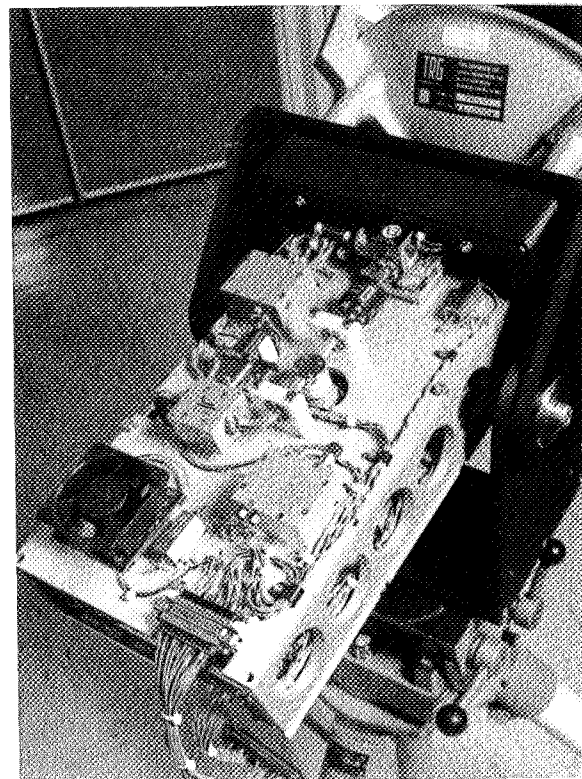


Figure 2
ITALSAT Radiometer
at 51.0 GHz.

INITIAL STATISTICS FROM RECEPTION
OF 49.5 GHz ITALSAT BEACON,
LOCATION CHILBOLTON, UK.

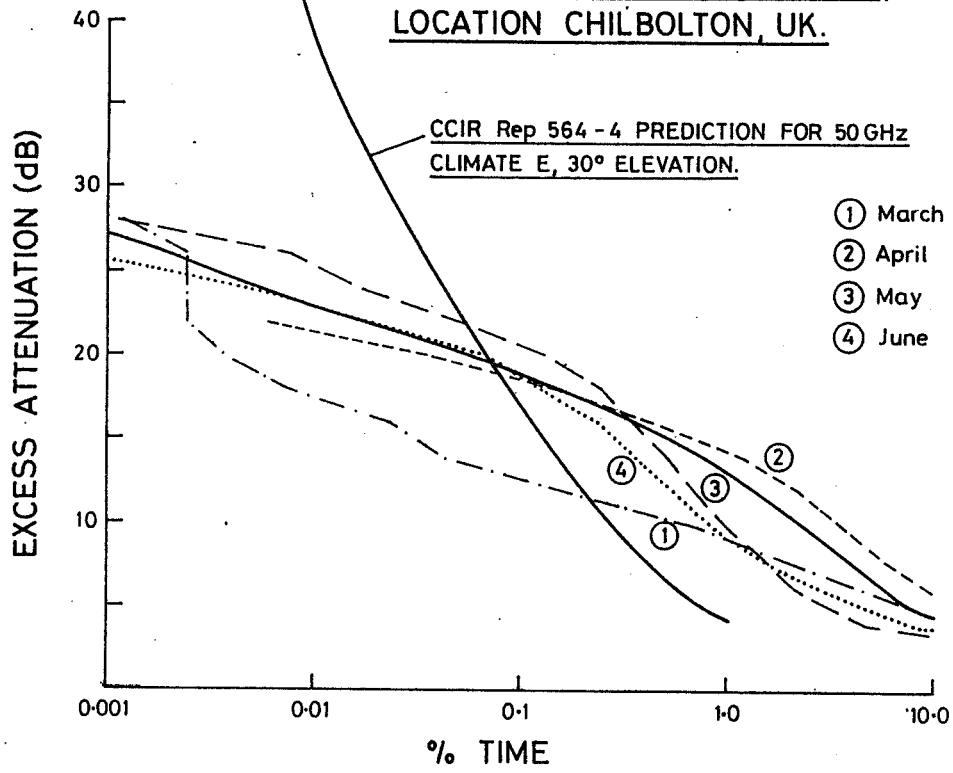


Figure 3

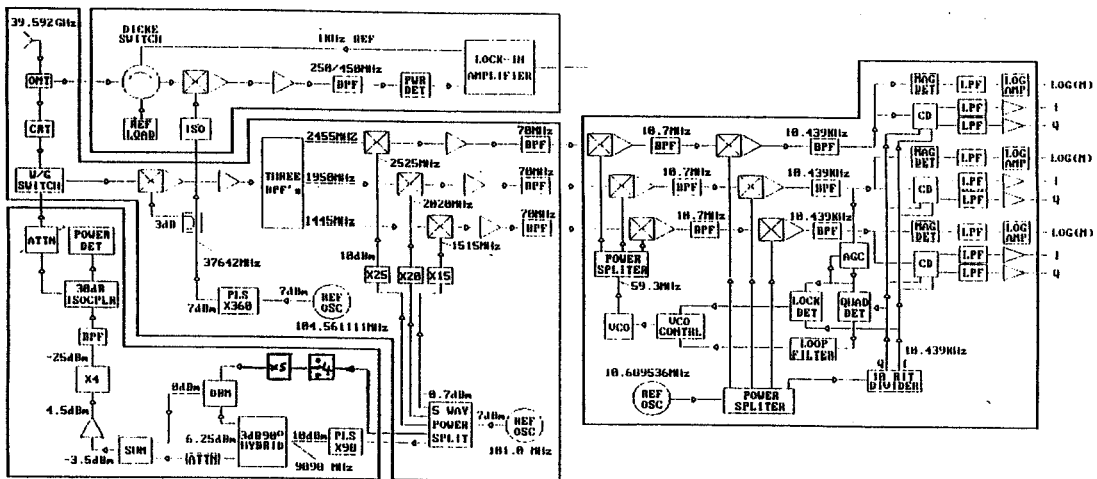


Figure 4
The Triple Channel 40 GHz
ITALSAT Receiver

A Database for Propagation Models

Anil V. Kantak, Krisjani Suwitra and Choung Le
Jet Propulsion Laboratory,
California Institute of Technology
Pasadena, California 91109.

P. 16

1.0 Introduction

The National Aeronautics and Space Administration's (NASA's) Propagation Program supports academic research that models various propagation phenomena in the space research frequency bands. NASA supports such research via schools and institutions prominent in the field. The products of these efforts are particularly useful for telecommunications systems engineers and researchers in the field of propagation phenomena.

The systems engineer usually needs a few propagation parameter values for a system design. Published literature on the subject, such as the Consultative Committee for International Radio (CCIR) publications, may help, but often the parameter values given in such publications use a particular set of conditions that may not quite include the requirements of the system design. The systems engineer must resort to programming the propagation phenomena models of interest to obtain the parameter values to be used in the system design. Furthermore, the researcher in the propagation field must then program the propagation models either to substantiate the model or to generate a new model. The researcher or the systems engineer must either be a skillful computer programmer or must hire a programmer. This, of course, increases the cost of the effort; an increase in cost due to the inevitable programming effort may seem particularly inappropriate if the data generated by the experiment is to be used to substantiate the already well-established models, or a slight variation thereof.

To help the researcher and the systems engineers, it was recommended by the conference participants of NASA Propagation Experimenters (NAPEX) XV (London, Ontario, Canada, June 28 and 29, 1991) that software should be constructed that contains propagation models and the necessary prediction methods of most propagation phenomena. Moreover, the software should be flexible enough for the user to make slight changes to the models without expending a substantial effort in programming.

2.0 Properties of the Propagation Database

The Propagation Model Database described here creates a user friendly environment that makes using the database easy for experienced users and novices alike. The database allows sufficient freedom for users to custom fit the propagation phenomena model of interest to their requirements. The database is designed to pass data through the desired models easily and generate relevant results quickly. The database contains many propagation phenomena models accepted by the propagation community. Only minimal computer operations knowledge is necessary to run the database.

The models included in the database are published in the NASA Propagation Effects Handbook, CCIR publications, or other publications such as the IEEE Journal, etc. Every model included in the software contains a reference to the document from which the model was obtained, and a brief description of the model itself. Also, when applicable, the related model names are also indicated. The parameters of every model in the database are shown explicitly, and the units of the parameters are defined completely so that the user does not have to invest time investigating them. Wherever possible, to make the use of the model obvious to the user, default values of the parameters are given. The default values are generally values that are used most frequently with the model, the user is free to change them to more appropriate ones. One possible use of the default values is to compare the already known results using the default values with the newly obtained values in an experiment.

User friendly procedures are used to call the available mathematical functions of Excel software, such as curve fitting, statistical analysis, etc. This allows the user to apply these functions to the data whenever needed.

3.0 Software Selection to Host the Propagation Database

A study was conducted to evaluate the advantages and disadvantages of a compiler-based program versus a spreadsheet-based program hosting the propagation database software. The results indicated that spreadsheet or database software (because of its very nature of dealing with data in columns without extra effort) will easily create a final database-type product such as the Propagation Models Database.

Of the many commercially available spreadsheet programs, Microsoft Excel was selected to host the Propagation Models Database. Excel provides an extensive list of the database and mathematical functions necessary to implement the propagation models. Excel also has excellent charting capabilities that include many versions of two- and three-dimensional charts, which can be easily used or automated using the macro language. Excel also offers the dialog box utility, which can be effectively used for input and output functions of the Propagation Models Database.

Another notable advantage of Excel is that it can call any executable programs written in C, which is a compiler-based program. This arrangement is ideal because it combines the advantages of a spreadsheet environment with the speed of the compiler-based software for number-crunching purposes.

The Propagation Models Database Software was created using Excel version 4.0 and uses the dialog box as well as the charting capabilities of this version quite extensively.

4.0 Software and Hardware Requirements

To run the Propagation Models Database, Microsoft Windows 3.1 and Microsoft Excel 4.0, or later versions are required. A personal computer equipped with an 80386 cpu, accompanied by its 80387 math coprocessor chip, with at least 4 Mbytes of RAM, is required to run the software. The clock speed should be at least 20 MHz. An 80486-based system with a higher clock speed is preferable. Any other computer (e.g., an 80286-based PC) with sufficient RAM will run the software, however, it will be very slow.

For the Macintosh version of the database, a Macintosh IIci or better computer accompanied with its coprocessor chip and having at least 4 Mbytes of RAM are needed to run the software. The clock speed should be at least 20 MHz.

It is recommended that a color monitor be used so that the charting can be done more effectively. Also, needed is a hard disk with at least several megabytes of storage space available for the software.

5.0 The Propagation Database

The Propagation Database is divided into six categories: the Ionospheric models, the Tropospheric models, the Land Mobile Systems models, the Effects of Small Particles models, the Rain models, and the Radio Noise models. These six categories are further divided into subcategories to include all the models to be housed in the software.

Ionospheric Models:

Absorption Model and Scintillation Model

Tropospheric Models:

Index of Refraction Profile Model, Gaseous Attenuation Model, Refraction and Fading Model

Land Mobile Satellite System Models:

Cumulative Distribution of Fade Duration Model, Cumulative Distribution of Non-Fade-Duration Model, Cumulative Distribution of Phase Fluctuation Model, Diffusely Scattering Model, Empirical Regression Models, Empirical Roadside Shadowing Model, Large Scale - Small Scale (LS-SS) Coverage Model, Fade State Transition Model, Faraday Rotation Model, Frequency Scattering Model, Geometric Analytic Models, Single Object Model, Multiple Object Scattering Model, Loo's Distribution Model, Log normal Shadowing Model, Raleigh Model, Reflection Coefficient Model, Simplified Log normal Shadowing Model, and Total Shadowing Model

Effect of Small Particles Models:

Cloud Model

Rain Models:

CCIR Model, CCIR Model (Proposed Modification), Global Model, Dutton Dougherty Model, Lin Model, Rice Holmberg Model, and Simple Attenuation Model

Radio Noise Models:

Noise Model

The access to any model is carried out using Excel's dialog box user interface. Each dialog box is divided into six distinct areas to help the user to provide the inputs easily.

The six areas of the dialog box are described below. The first area is used to provide general information about the model selected by the user. This step describes any particular conditions required by the model, the parameter ranges as well as the number of steps the model has, and so on. The second area is used to display formulas describing the model selected. The formula can be modified by the users to a certain extent using legal expressions in Excel. Once the formula is created, the software will use this formula for the current run only. Loading the software again will bring back the original formula. The third area is the input area. This area is used to acquire input parameter(s) for the model. The fourth area is used to display definitions of the input and output parameter(s) used by the model. The fifth area is used to display intermediate or final result(s) of the particular model. The sixth area has a few buttons to help the user and to produce the output(s) of the model (or step). For some models, this area also has buttons to allow creation of a table of output values of the model as a function of the range of the selected input parameter. The following figures show the run of the CCIR rain attenuation model included in the database software.

6.0 Conclusion

A database of various propagation phenomena models that can be used by telecommunications systems engineers to obtain parameter values for systems design is presented. This is an easy-to-use tool and is currently available for either a PC using Excel software under Windows environment or a Macintosh using Excel software for Macintosh. All the steps necessary to use the software are easy and many times self-explanatory; however, following is a sample run of the CCIR rain attenuation model presented.

A Sample Run of the CCIR Rain Attenuation Model

The following pages show a sample run of the CCIR model, which contains 6 steps:

The model used for the effective rain height, h_R , is as follows:

$$h_R = 3.0 + 0.028 * Phi \quad 0 \leq Phi < 36^\circ$$

$$h_R = 4.0 - 0.075 * (Phi - 36) \quad Phi \geq 36^\circ$$

where

Phi is the station's latitude in degrees.

- Enter Phi (the station's latitude) in degrees, e.g., 30 degrees.
- Click the Output button to see h_R (the effective rain height).
- Click the Step 2 button to go to the next step.

The screenshot shows a software window titled "CCIR". The text inside reads: "This Rain model is used to calculate the long-term statistics of the slant-path rain attenuation at a given location for frequencies up to 30 GHz. This model has 6 steps, each will appear in a separate dialog box." Below this, it says "Step 1 of 6." The interface is divided into sections: "MODEL" with the instruction "Calculate the Effective Rain Height," "INPUT" with a field for "Phi (deg)" containing the value "37", "DEFINITION" with "Phi: Station's Latitude" and "hR: Effective Rain Height", and "OUTPUT" with a field for "hR (km)" containing the value "3.99". At the bottom, there are four buttons: "Reference", "Output", "Step 2", and "Close".

Step 2: Calculates L_S , the slant-path length below rain height in km. The model used for the slant-path length, L_S , is as follows:

$$L_s = \frac{(h_r - h_s)}{\sin(\text{Theta})} \quad \text{Theta} \geq 5^\circ$$

$$L_s = \frac{2(h_r - h_s)}{\left(\sin^2(\text{Theta}) + \frac{2(h_r - h_s)}{R_e} \right)^{1/2} + \sin(\text{Theta})} \quad \text{Theta} < 5^\circ$$

where

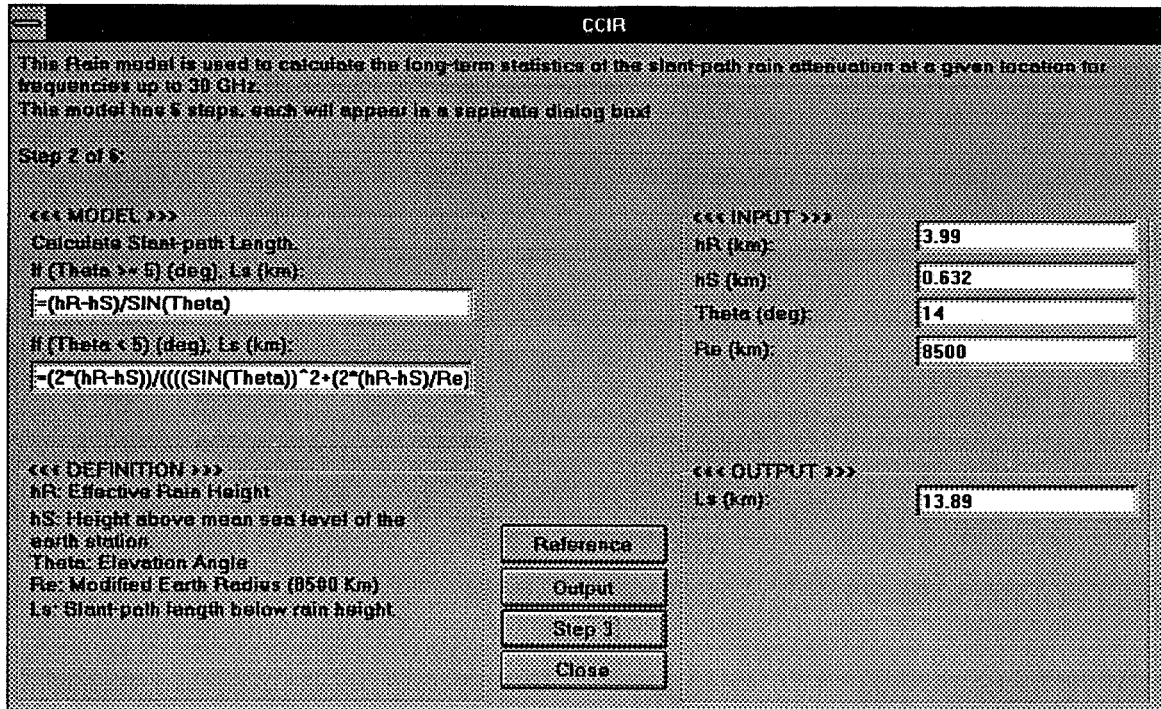
h_R is the effective rain height in kilometers.

h_S is the height mean sea level of the Earth station in kilometers.

Theta is the elevation angle in degrees.

R_e is the modified Earth radius (defaulted to 8500 km).

- h_R was computed in Step 1.
- Enter h_S (the height mean sea level of the Earth station) e.g., 0.632 km.
- Enter Theta (the elevation angle) e.g., 14 degrees.
- Change R_e (the Earth radius) if necessary.
- Click the Output button to see L_S (the slant-path length).
- Click Step 3 to go to the next step.



Step 3: Calculates L_g , the horizontal projection of the slant-path length in kilometers.

The model used for the horizontal projection of the slant-path length, L_g , is

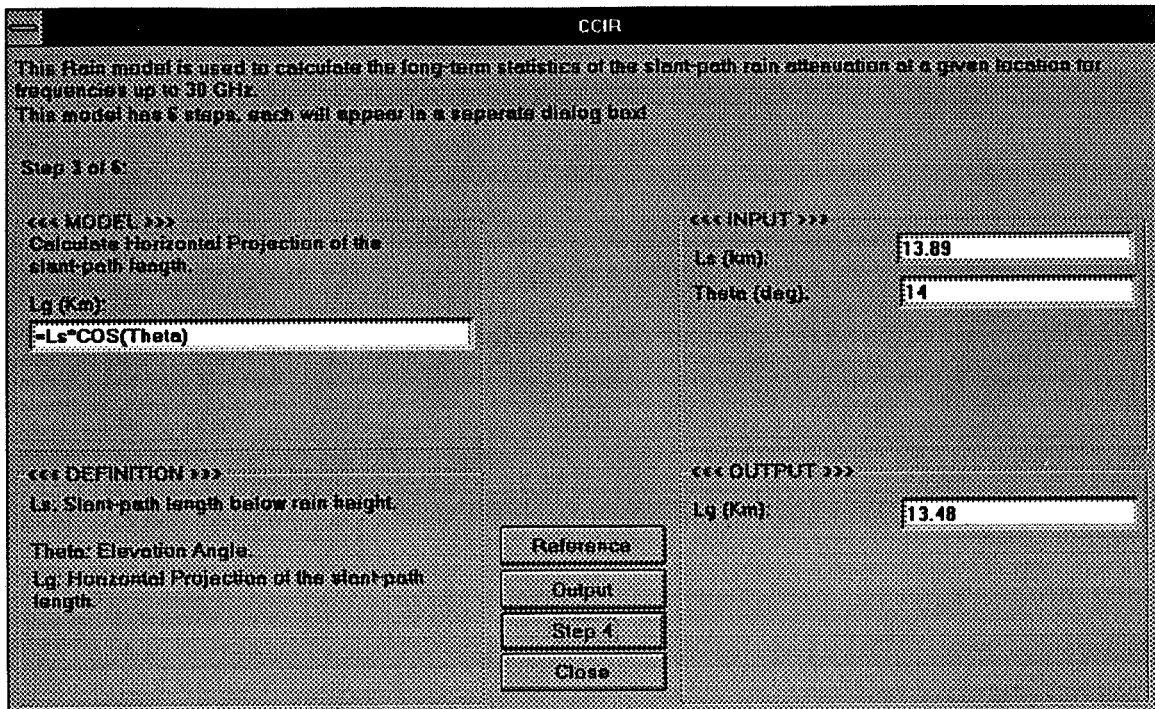
$$L_g = L_s \cos(\theta)$$

where

L_s is the slant-path length below rain height in kilometers.

θ is the elevation angle in degrees.

- No input is required for this step.
- Click the Output button to see L_g (the horizontal projection of the slant-path length).
- Click the Step 4 button to go to the next step.



Step 4: Obtains $R_{0.01}$ (dB), the rain intensity exceeded for 0.01% of an average year and calculates $r_{0.01}$, the reduction factor.

The model used for the reduction factor, $r_{0.01}$, is

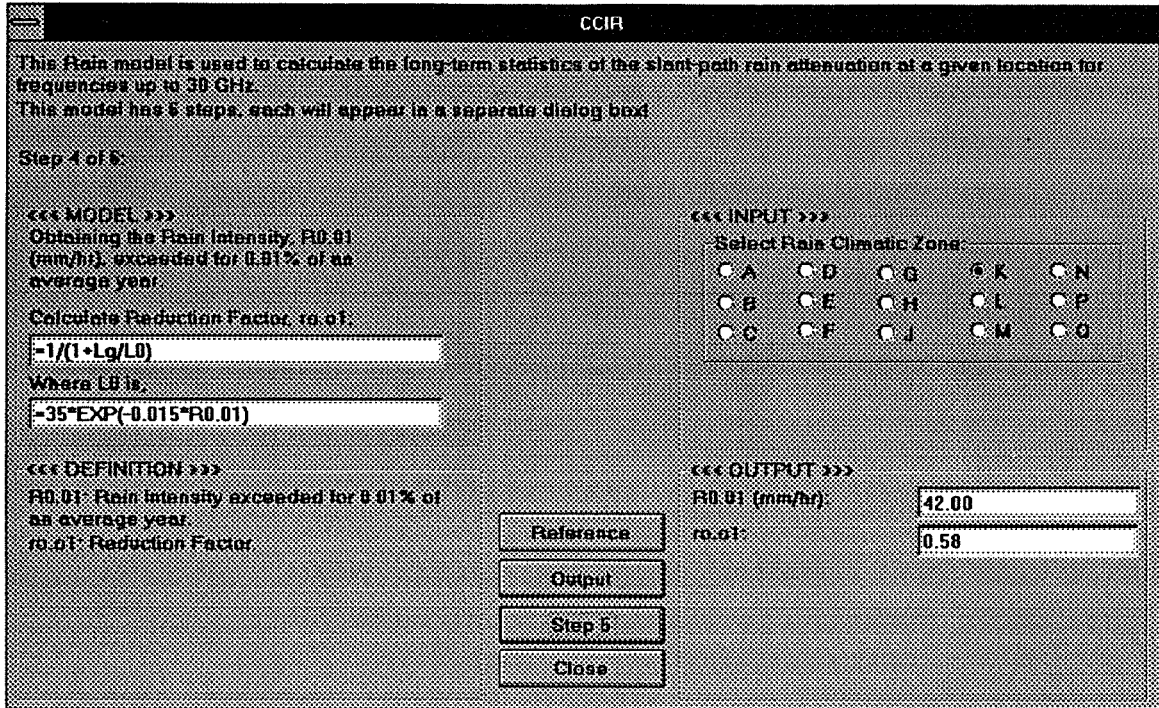
$$r_{0.01} = \frac{1}{1 + L_g/L_o}, \quad L_o = 35 \exp(-0.015 R_{0.01})$$

where,

$R_{0.01}$ is the rain intensity exceeded for 0.01% of an average year in mm/hr.

$r_{0.01}$ is the reduction factor.

- Select the Rain Climatic Zone, such as K for this example.
- Click the Output button to see $r_{0.01}$ (the reduction factor).
- Click the Step 5 button to go to the next step.



Step 5: Calculates ΓR , the specific attenuation using the frequency-dependent coefficient in dB/km. The formula used to calculate ΓR is as follows:

$$\Gamma R = k R_{0.01}^a,$$

$$k = [k_H + k_V + (k_H - k_V) \cos^2(\Theta) \cos(2\tau)] / 2$$

$$a = [k_H \alpha_H + k_V \alpha_V + (k_V \alpha_H - k_H \alpha_V) \cos^2(\Theta) \cos(2\tau)] / 2k$$

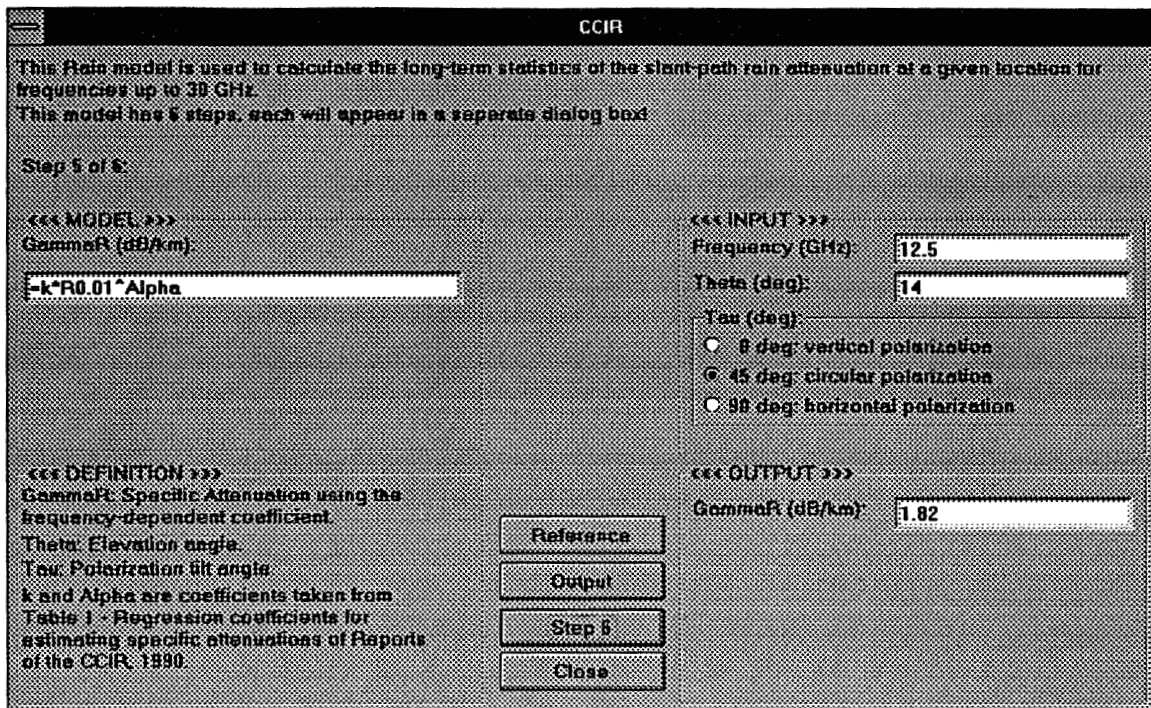
where

Θ is the elevation angle in degrees.

τ is the polarization tilt angle in degrees.

k and a are coefficients taken from Reports of the CCIR, 1990. Table 1. Regression Coefficients for Estimating Specific Attenuation.

- Enter *Frequency*, e.g., 12.5 GHz.
- Select *Tau*, e.g., 45 degrees for circular polarization.
- Click the Output button to see ΓR .
- Click the Step 6 button to go to the next step.



Step 6: Calculates $A_{0.01}$, the attenuation exceeded for 0.01% of an average year in decibels.

The formula used for the attenuation exceeded for an average year, $A_{0.01}$ is:

$$A_{0.01} = \text{GammaR} * L_s * r_{0.01}$$

where

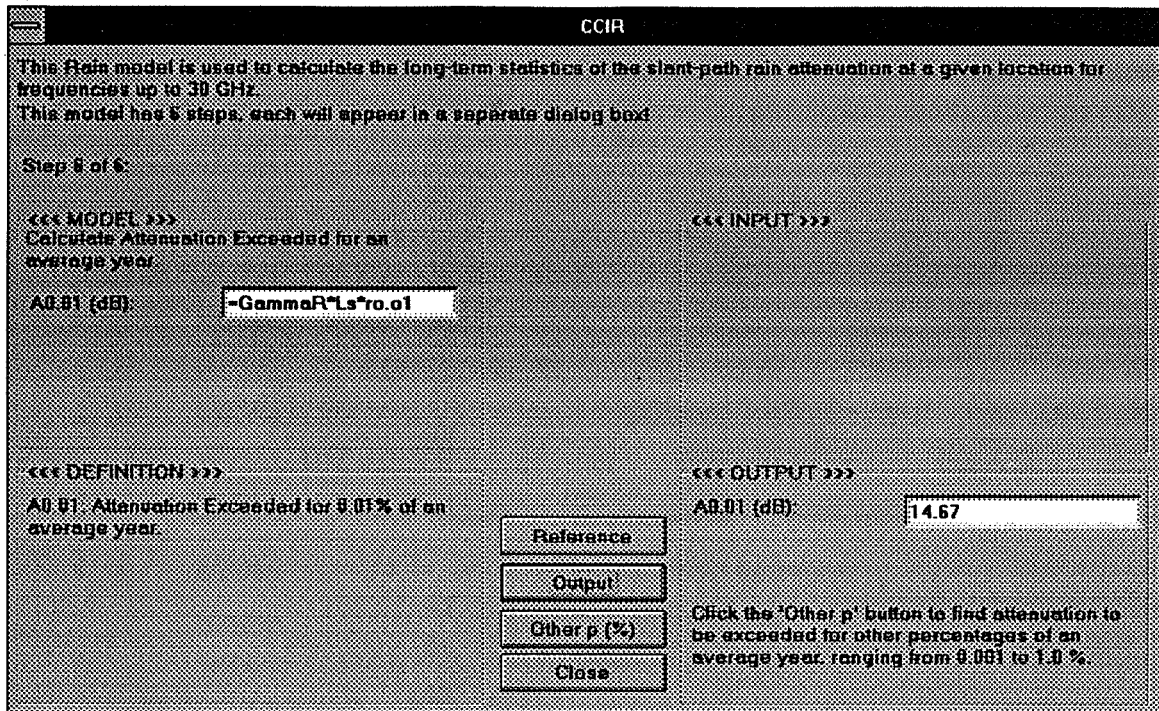
GammaR is the specific attenuation using the frequency dependent coefficient in dB/km.

L_s is the slant-path length below rain height in kilometers.

$r_{0.01}$ is the reduction factor.

Click the Output button to see $A_{0.01}$ (the attenuation exceeded for 0.01% of an average year).

Click the "Other p (%)" button to find attenuation exceeded for other percentages of an average year (0.001 to 1.0 %).



This step also calculates attenuation exceeded of an average year for other percentages (0.001 - 1.0 %).

The formula used for p percent of the attenuation exceeded of an average year is as follows:

$$A_p = A_{0.01} * 0.12 * p^{-(0.546+0.043\log(p))}$$

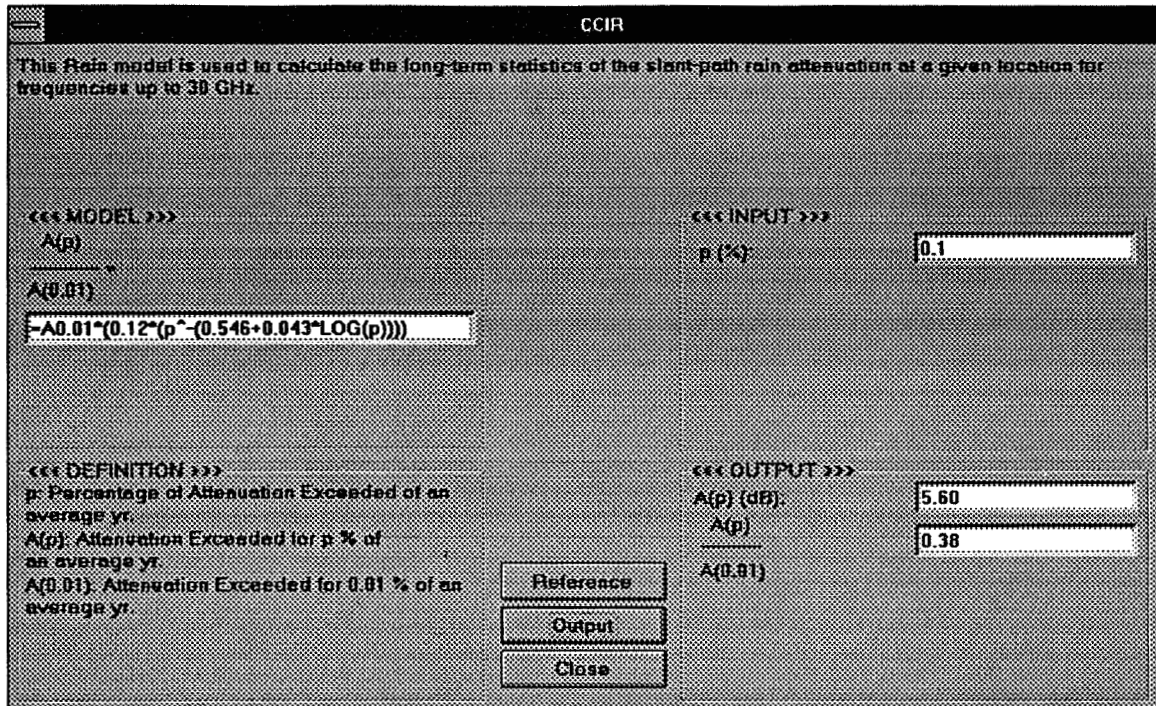
where

p is the percentage of the attenuation exceeded.

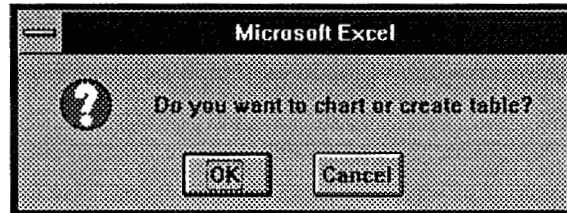
A_p is the attenuation exceeded for p percent.

$A_{0.01}$ is the attenuation exceeded for 0.01 percent.

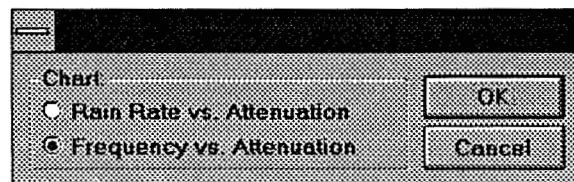
- Enter the p (percentage) of an average year.
- Click the Output button to see A_p , attenuation of p percentage and ratio of $A_p / A_{0.01}$



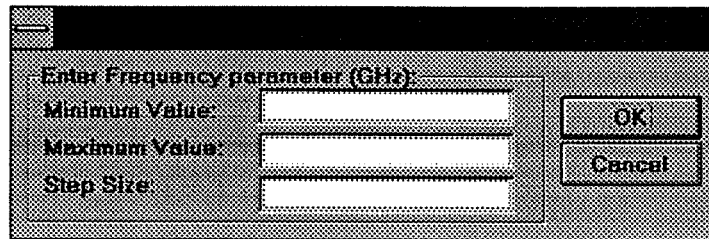
When the close button is clicked the following dialog box appears



- Click OK to see the response.



- Select one of the options, e.g., the Frequency vs. Attenuation.
- Click OK.



Enter Frequency parameter (GHz):

Minimum Value:

Maximum Value:

Step Size:

OK

Cancel

- Enter the minimum, maximum and step values
- Click OK

A new worksheet will then be invoked to store all of the parameters used, and the table, as well as the selected chart.

The 'Print' option is available after this step.

This ends the sample run of the CCIR model.

Acknowledgment

The research described in this paper was carried out by the Jet Propulsion Laboratory, California Institute of Technology, under a contract with the National Aeronautics and Space Administration.

NAPEX XVIII

Session 2

**PROPAGATION STUDIES FOR
MOBILE, PERSONAL, AND SOUND
BROADCAST SYSTEMS**

Chairs:

Rod Olsen

Communications Research Centre

and

Faramaz Davarian

Jet Propulsion Laboratory

Channel Characterisation for Future Ka-band Mobile Satellite Systems and Preliminary Results

Mario Sforza, Sergio Buonomo, Bertram Arbesser-Rastburg

The European Space Research and Technology Centre
Keplerlaan 1, 2200 AG Noordwijk, The Netherlands
Telefax: (31) 1719 84999

Abstract

Mobile Satellite Systems (MSS) are presently designed or planned to operate, with the exception of OMNITRACKS, in the lower part of the frequency spectrum (UHF to S-bands). The decisions taken at the last World Administrative Radio Conference in 1992 to increase the allocated L- and S-bands for MSS services will only partly alleviate the problem of system capacity. In addition the use of L- and S-band frequencies generally requires large antenna apertures on board the satellite terminal side. The idea of exploiting the large spectrum resources available at higher frequencies (20-30 GHz) and the perspective of reducing user terminal size (and possibly price too) have spurred the interest of systems designers and planners ([1]-[3]). On the other hand, Ka-band frequencies suffer from increased slant path losses due to atmospheric attenuation phenomena.

The European Space Agency (ESA) has recently embarked on a number of activities aimed at studying the effect of the typical mobile propagation impairments at Ka-band. This paper briefly summarizes ESA efforts in this field of research and presents preliminary experimental results.

1 Introduction

The advantages of Ka-band for future Land Mobile (LMS) and Personal Access Satellite Systems (PASS) can be summarized as follows:

- large spectrum resources (more than 1 GHz at Ka-band, downlink) would dramatically relax the requirements on frequency reuse and efficient on-board channel routing and processing, currently envisaged for L-band LMS systems;
- mobile terminal and spacecraft antenna sizes could be considerably reduced hence increasing market potential and lowering payload mass, respectively;

- share of the on-board resources of Fixed Satellite Services (FSS) (e.g. EUTELSAT with its EUTELTRACKS system) could be of great benefit for the satellite operators.

The price to pay, at least from the channel viewpoint, is an increased attenuation effect due to tropospheric phenomena such as rain, clouds, water vapour, and to blockage. In order to compensate for these propagation impairments, link margins higher than at L- or S-bands should be budgeted for. Unlike for UHF to S-bands ([4]-[5]), the typical mobile propagation phenomena, blockage and multipath, have not been thoroughly studied so far in the Ku-/Ka-band frequency range.

The lack of comprehensive and consistent information on the mobile propagation channel was one of the reasons which led ESA to fund two activities: the design and development of a multifrequency narrowband mobile receiver, and the first extended Ka-band LMS experimental campaign, in different European locations and environments. The identification of an empirical law linking RF signals and optical images was the second objective of these two research activities; at these high frequencies, in fact, the terminal antenna radiation pattern is highly directive (in our test case, we had a beamwidth of 2.4 degrees, [6]) and rather insensitive to multipath effects. An empirical law could be therefore found which uniquely associates RF shadowing to optical shadowing (see [7] for previous experiences) hence information on blockage effects can be obtained from passive rather than active experimental campaigns. In order to achieve these objectives ESA placed two contracts, the first on 1992 with the Danish company RESCOM to design and build a mobile Ka-band beacon receiver, and the second one in 1993 with the Joanneum Research Institute, Austria, to run a narrowband experimental campaign in different European locations. This paper shortly reports on the main features of the mobile beacon receiver and also presents preliminary results of the narrowband measurement campaign.

2 The Ka-band Land Mobile Beacon Terminal (LMBT)

The Ka-band LMBT is a narrowband receiver installed in a van, conceived and built to carry out LMS experimental measurements. It is currently equipped with a Ka-band antenna but has been designed as a multifrequency receiver so that experimental propagation data can be recorded and stored at up to three different frequency bands, simultaneously. This feature could allow for the possibility of frequency scaling empirical fade laws in a more rigorous way.

The Ka-band LMBT was originally designed to operate with the Olympus polarization-switched B1 beacon, at 19.8 GHz; on a later stage of the contract and due to the premature demise of Olympus, the LMBT RF front-end was eventually modified and it presently operates with the Italsat F1 18.7 GHz beacon. Italsat is an Italian telecommunication satellite which in addition to a number of communication payloads also carries on board three beacons for propagation experiments. The 18.7 GHz beacon has a reduced coverage in comparison with Olympus (Italy and the alpine region with its main beam) and offers a slightly less dynamic range at the receive mobile terminal.

Fast signal acquisition and tracking combined with stringent operational constraints (van speed and resulting Doppler, medium to long fade durations and related re-acquisition performance) were indoubtely the driving factors in the design of the Ka-band LMBT. Particular attention was also given to the data acquisition and video subsystems which had to handle a considerable amount of data, in real-time. Finally the whole receiver needed to be built and integrated in the van to insure robustness and sturdiness in mobile operational scenarios. The final LMBT configuration resulting from this set of requirements presently consists of the following subsystems:

1. Antenna: Cassegrain antenna with rotatable feed and radome;

NAPEX XVIII. Ka-band LMS channel characterisation

2. Pointing: gyro-stabilized elevation-over-azimuth platform;
3. Receiver: RF units mounted on the platform and a rack-mounted detector unit, inside the van;
4. Data Acquisition System: a high capacity tape streamer for data recording and a computer for acquisition and handling of measurements data;
5. Central Control System: the operator PC and the interfacing network;
6. Video System: two colour CCD cameras and a video mixer;
7. Power System: a motor/generator unit and a 24V battery pack;
8. Van: a Mercedes-Benz 208D passenger van with heater and air-conditioning units.

The rotating platform is mounted on a metallic chassis and can be lowered down through the chassis inside the van to ease maintenance and house-keeping operations. Vibration dampers connect the chassis and the two 19" racks to the passenger van to filter out the effects of vibrations produced by the movement of the vehicle, and by the engine and generator. A functional block diagram of the LMBT and the layout of its physical configuration are given in Figs. 1 and 2, respectively. A short description of the performance and features of the LMBT subsystems is hereafter presented.

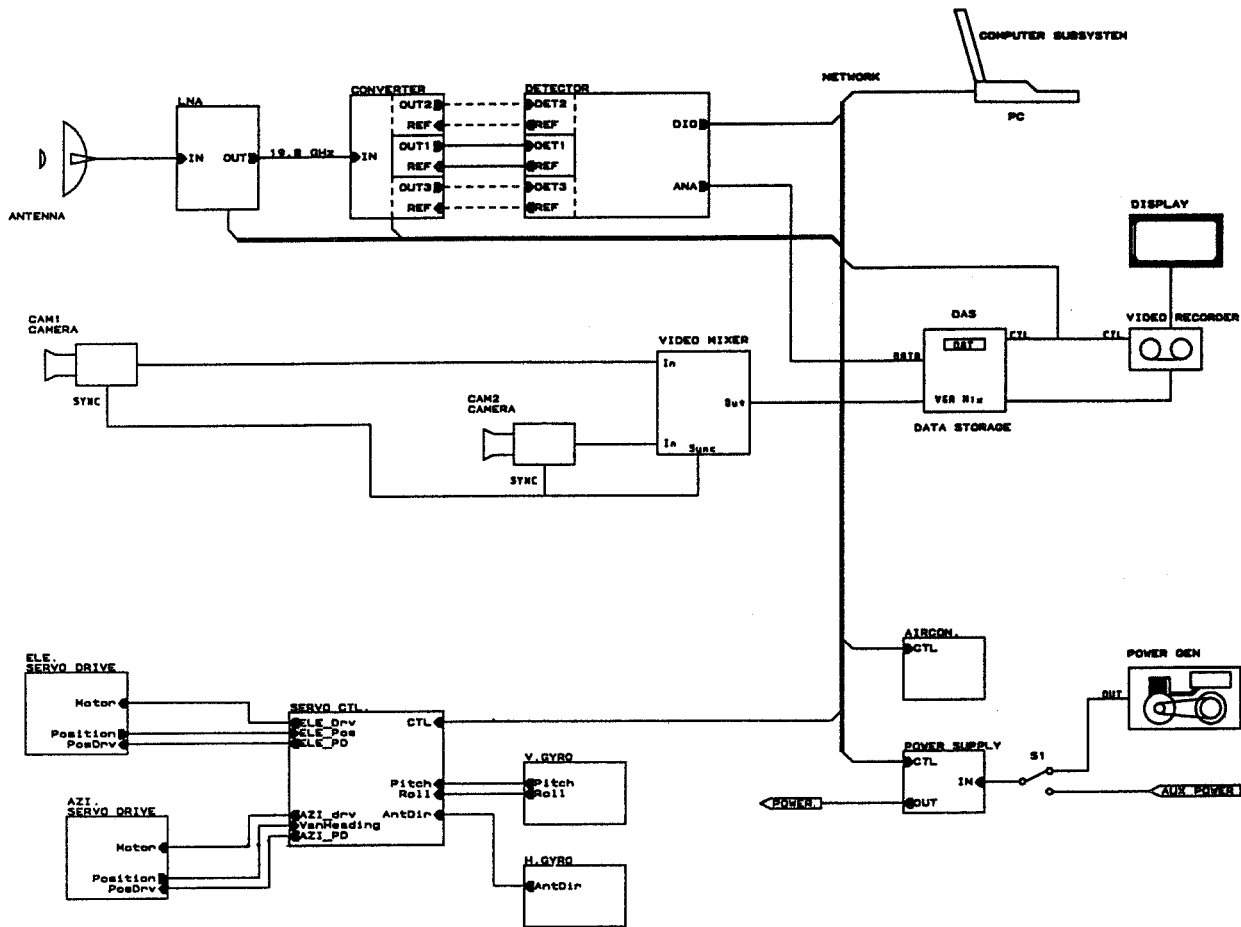


Figure 1: LMBT functional block diagram

2.1 The antenna subsystem

The antenna was designed to provide a gain able to ensure a minimum dynamic range of 30 dB (with a 50 Hz PLL bandwidth, locked mode) in all experimental scenarios and to achieve a good pointing accuracy. The trade-off between gain and beamwidth led to the design of an antenna with the following characteristics (measured):

Antenna type	Cassegrain
Main reflector diameter	50 cm
Subreflector diameter	9.5 cm
Gain at 18.7 GHz	35.8 dBi
Beamwidth, 3 dB	2.4°
Return loss at 18.7 GHz	35.0 dB

Table 1: LMBT antenna characteristics

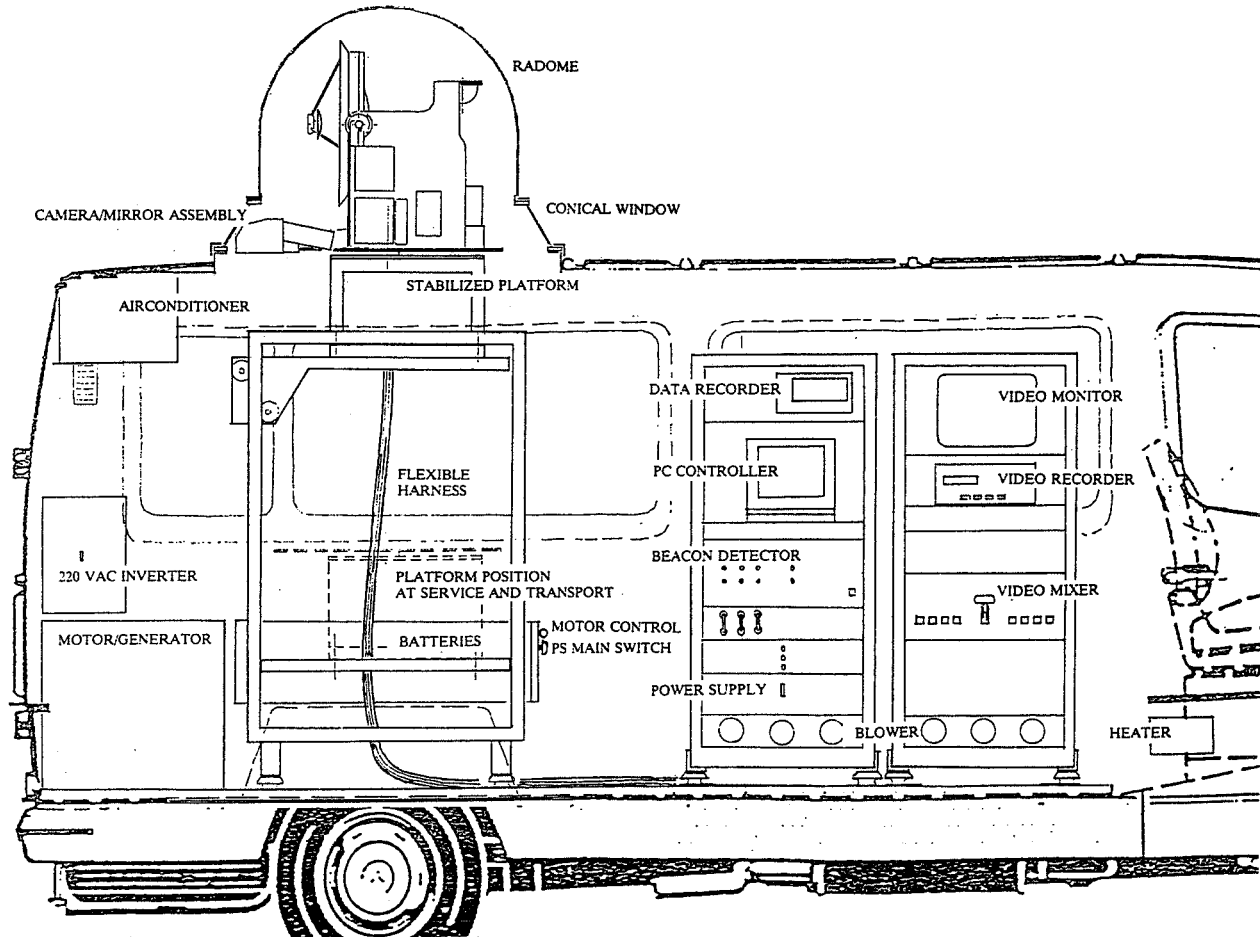


Figure 2: LMBT layout

The antenna is mounted on the elevation gimbal of the stabilization system. The glass-fibre radome has an insertion loss of less than 0.5 dB and it is screwed down on a truncated cone made of a light-transparent material such as to provide full optical visibility to the antenna-slaved video camera.

2.2 The platform subsystem

The platform is the most complicated and demanding amongst all the LMBT subsystems. Correct pointing towards the satellite has to be granted in all operational conditions and for a period of time equivalent to the duration of a measurement run, originally fixed in 15 minutes. A figure of 1 dB of maximum pointing loss, i.e. a pointing error of less than 0.7° at 18.7 GHz, was the baseline objective. In its final experimental configuration, the LMBT platform showed pointing losses of less than 0.4-0.6 dB throughout the acceptance tests.

The servo-controlled stabilized platform is a gyro based system with sensors designed to be as insensitive as possible to horizontal and vertical accelerations in order to stabilize the platform and the units mounted on it on all three axis. The solution selected for the design of our Ka-band LMBT was to use two gyroscopes, a vertical one providing information on the pitch and roll angles, and a directional one (gyro-compass) giving read-outs of the North angle, i.e. heading. Both vertical and directional gyros, which are standard avionic equipment, are mounted on the azimuth turntable, controlled to maintain a constant heading. The major drawback of this solution is that the directional gyro has an in-built circuit slaved to a flux valve magnetic sensor providing the gyro a fixed heading reference. This magnetic sensor (compass) is unfortunately strongly influenced by all sorts of magnetic fields generated by the van metallic structure and instrumentation, and by nearby buildings, cars, power lines and so forth. So only at the platform start-up the compass is used to give an initial reference; in mobile measurements, the directional gyro is operated in unslaved mode.

Particular attention was also given in the initial design and later in the fine tuning of the system to the mechanical construction and balancing of the stabilization platform, which also hosts the antenna-slaved video camera and some RF units. The servo control electronics circuits are implemented on five PCBs.

2.3 The receiver subsystem

The principal requirements at the receiver level were basically low noise figure, low phase noise and high medium term stability. An overall noise figure of 2 dB, referenced to the antenna output port, has been achieved thus providing a satisfactory C/N_o level during the measurements. The phase noise of the receiver mainly due to the reference oscillator was kept within that one of the satellite signal itself. Finally a gain variation of ± 0.2 dB was measured; this low figure is considered not to contribute significantly to the overall uncertainty of each measurement run. The receiver consists of two major subsystems, the Front End and the Detector.

The Front End, schematically drawn in Fig. 3, is made of a Low Noise Amplifier (LNA), a downconverter, and microwave and reference oscillator units. The LNA is mounted directly on the antenna feed horn to reduce losses whereas the remaining units are placed on the platform turntable. The measured LNA gain and bandwidth at 18.7 GHz are 28.0 dB and 1 GHz, respectively; the corresponding noise figure is 1.4 dB.

The Detector unit processes the 70 MHz signal from the downconverter and provides in digital form the signal I and Q components to the Data Acquisition subsystem and to the operator PC. There are three identical detector chains to allow for simultaneous multifrequency measurements although only one is used in the current LMBT configuration. The basic functions of the detector subsystem are to establish a phase-locked acquisition to the correct transmitted satellite signal, to compensate for potential large Doppler shifts and to perform a fast and efficient reacquisition after long fades exceeding the maximum LMBT dynamic range. Signal acquisition, tracking and recapture functions

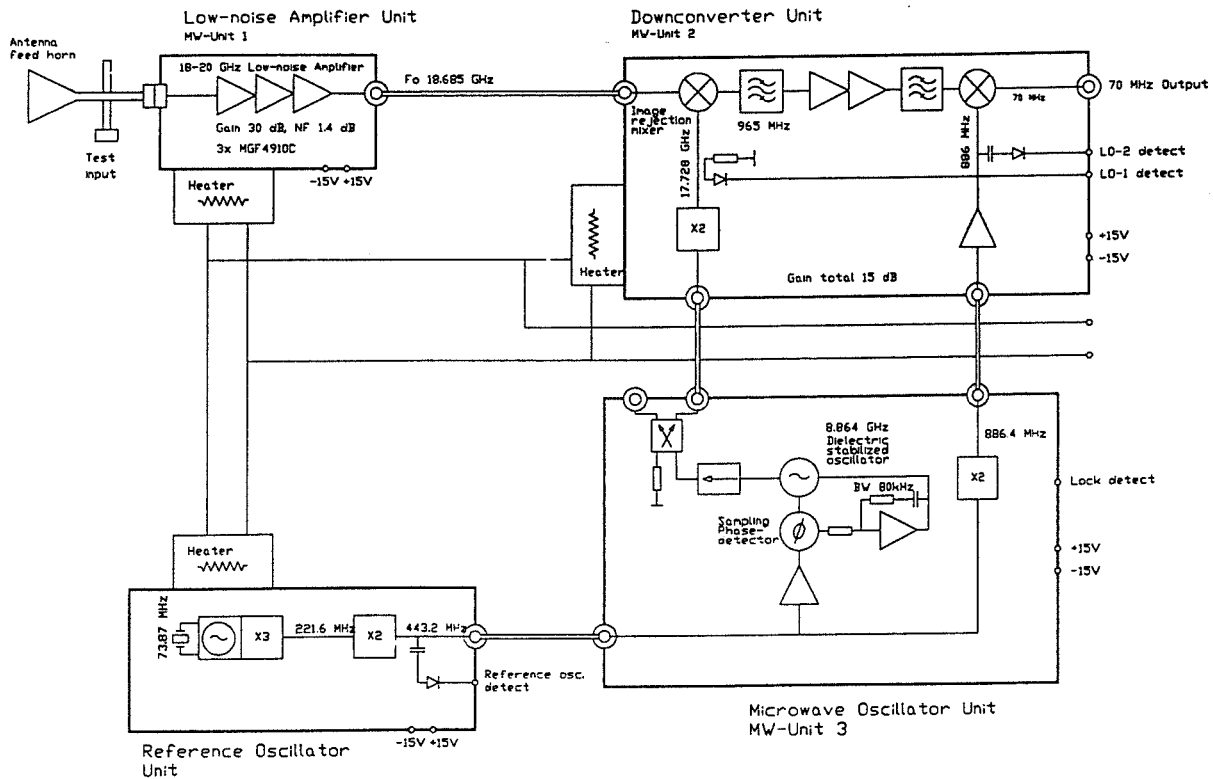


Figure 3: LMBT Front-End functional block diagram

are of course essential in the design of any receiver designed to operate in mobile scenarios; these requirements are even more stringent at Ka-band and with such narrow antenna beamwidth. The solution adopted was a rather conventional one, a Phase Lock Loop (PLL) with four bandwidths (50, 100, 200 and 400 Hz), but proved to be simple and suitable for the specified system requirements. A substantial number of measurements was carried out at RESCOM premises during the acceptance tests at different vehicle speeds, headings and PLL bandwidths, and in acceleration and constant speed modes; in all these tests a recapture time of less than 0.1 s was found.

2.4 The data acquisition subsystem

The Data Acquisition Subsystem (DAS) essentially collects and store information on the received beacon signal and on the status of the overall system. A functional block diagram is given in Fig. 4. The computer is equipped with an Intel 80386 CPU, 33 MHz clock and 2 Mbytes of RAM, and operates under MS-DOS environment. There are three boards connected to the computer: the A/D converter providing the signal from the detector, the video board which receives the pictures from the two video cameras properly combined in a video mixer, and the I/O board which collects all the environmental and system status data. The sampling rate can be selected from 1 up to 15 KHz, therefore a high capacity storage medium is required: an ExaByte EXB-8500 tape streamer with 8mm cartridges of 5 GBytes capacity. Amongst other functions, the DAS generates the time stamp which synchronizes the signals and images recording so that, during off-line analyses, signal fades can be uniquely associated to actual natural or man-made obstacles.

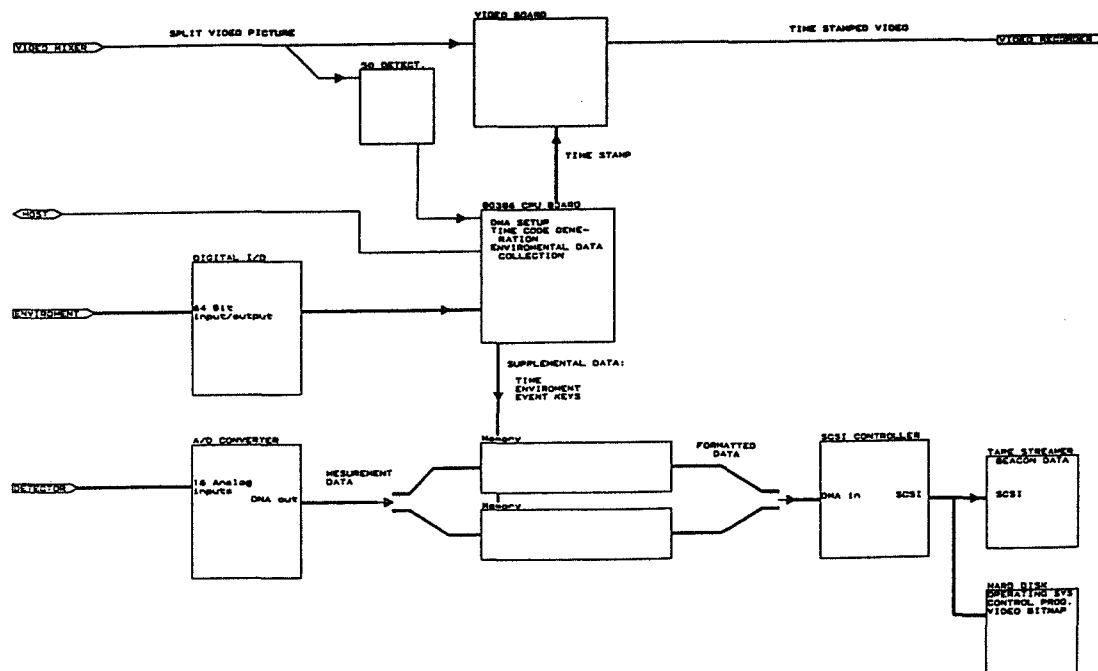


Figure 4: LMBT Data Acquisition System

2.5 The video subsystem

The main purpose of this subsystem is to provide the experimenter with real-time and synchronized optical information on environmental attributes and landscape. Two video cameras are used to achieve this objective: one antenna-slaved and the other, forward-looking and wide-angle. The former is placed on the platform turntable and is slaved to the antenna movements hence it allows the operator to closely watch and indentify any obstruction along the line-of-sight; the latter (with an opening angle of 107°) is placed behind the windshield of the van and provides a general description of the environmental scenarios. The video signals from both cameras are combined in a mixer and they are time synchronized with the DAS. In order to ensure full optical visibility to the side-looking antenna-slaved camera, an acryl truncated cone is assembled with the glass-fibre radome (the solution of a fully RF and light transparent radome was not viable); a two-mirrors arrangement, where one mirror is controlled by a servo loop slaved to the antenna one and the other is fixed, allows the video camera to point at the satellite direction with an error of $\pm 0.5^\circ$.

2.6 The other LMBT subsystems

The remaining LMBT subsystems (Central Control, Power Supply, Racks and Passenger Van) are only briefly described. The Central Control Subsystem (CSS) is responsible for all the interfacing network of the LMBT; making use of the CSS features the operator is able to control and monitor all the LMBT functions. The CSS is executed from the operator PC while the actual interconnections between subsystems are dealt with by a network of locally intelligent nodes and a simple CAN (Controller Area Network) bus which is a serial communication protocol supporting distributed real-time control, originally developed for automotive applications. The operator PC is of a laptop type, with a 386 SX-20 MHz, 12 Mbytes of RAM and coprocessor; an 80 Mbytes hard disk is integrated in the PC.

From this PC, the operator controls data acquisition and presentation, the latter being displayed on the PC screen in several user-selectable menu pages.

As the whole receiver needs power in the order of 2 kW, a 24 V DC system has been implemented where the primary supply source is a pack of four 12 V truck batteries. The battery pack is charged by a gasoline generator, placed in the van inside a sound-insulated compartment. Two 19" racks are used; they are installed on the van floor through shock absorbers. Finally, the vehicle selected for this activity is a Mercedes-Benz 208/33 passenger van large enough to accommodate the Ka-band LMBT and possible future upgrade at other frequency bands, e.g. L- and S-bands. Air-conditioning and heating units are foreseen to keep the platform temperature correctly controlled and to ensure comfortable working conditions. The passenger van speed is measured by means of a proximity sensor mounted in the vicinity of the flange connecting the gear box and the drive shaft.

3 The experimental Ka-band LMS campaign

A contract was placed by ESA in late 1993 with the Joanneum Research, Institute for Applied System Technology (IAS) in Graz, Austria, to collect and analyse experimental data for the characterisation of the Ka-band LMS narrowband propagation channel. After a careful campaign planning phase needed to identify suitable European LMS scenarios, a large number of measurements was carried out in France, Germany and Austria in spring 1994; in all these countries a strong satellite signal was always experienced ensuring an optimum dynamic range. The experimental campaign was performed in open, wooded, suburban and urban areas at different speeds and azimuth angles. From an operational point of view, a reference level (0 dB) was measured and recorded in line-of-sight conditions, at the beginning and at the end of each experimental run; the average duration of each run was of 10-15 minutes. Video images were also recorded and will be intensively studied on a second stage of the data analyses to find an empirical law linking RF to optical signals, i.e. active to passive measurements. The following set of narrowband statistics will be produced for each of the environments and azimuth angles (where applicable):

- Probability Distribution Functions (PDF)
- Cumulative Distribution Functions (CDF)
- Average Fade Durations (AFD)
- Level Crossing Rates (LCR)
- Durations of Fades (DoF)
- Time Shares of Fades (TSoF)
- Durations of Connections (DoC) (or of Non-Fades)
- Time Shares of Connections (TSoC) (or of Non-Fades)

Few preliminary results are presented in the following figures. In Fig. 5 a sample of a time series recorded in a suburban area around the city of Munchen, Germany, is given; the corresponding Cumulative Distribution Function (CDF) is drawn in Fig. 6. The average van heading during this specific run was 65 degrees thus offering an almost orthogonal position with respect to the satellite signal (Italsat F1 is in a geostationary orbit at 13E). In Figs. 7 and 8 an example of time series and

corresponding CDF for an urban area in Munchen is presented, this time with an average van heading of 170 degrees; the van position during the entire run was therefore almost constantly parallel to the transmitted satellite signal hence with very few blockages. For all the runs, the average elevation angle was of 30 degrees.

Although the results presented in this paper represent a very small sample of the large amount of data recorded during the IAS Ka-band experimental campaign, few interesting considerations can be drawn from a preliminary analysis of these results. At Ka-band the signal received at the mobile terminal looks very much like an on-off (binary) signal; the temporary blockage offered by man-made or natural obstacles can most of the times drive the receiver out of its dynamic range. The propagation channel could be therefore characterised using state-models like the ones defined in previous works ([8]-[10]). In addition, we think that an empirical law relating RF to optical signals could well describe the propagation channel behaviour highlighted in Fig. 5 and 6. The importance of the latter consideration lies in the fact that passive measurements could be effectively envisaged to characterise the Ka-band LMS propagation channel, rather than the more expensive and time-consuming active ones. Whether this approach can be also applied to L- or S-band LMS channels is still to be seen; considerations of the radiation pattern of the mobile terminal antenna (vehicle-mounted or hand-held) hence of the overall impact of multipath shall be part of the modelling effort. Finally, the quite different results

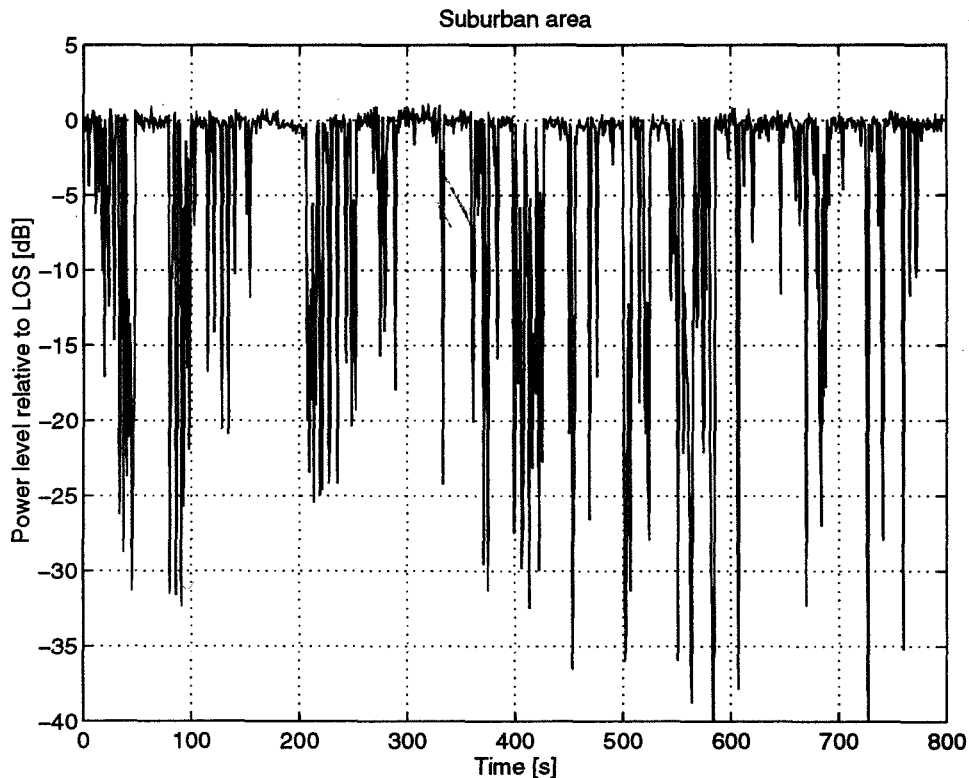


Figure 5: Time series in a suburban area around Munchen, Germany ($f=18.7$ GHz)

shown in Fig. 5 and 7 prove again that information on azimuth angle is essential in the data analysis and that considerations made for link availability estimation in multisatellite LMS systems can not be drawn without it.

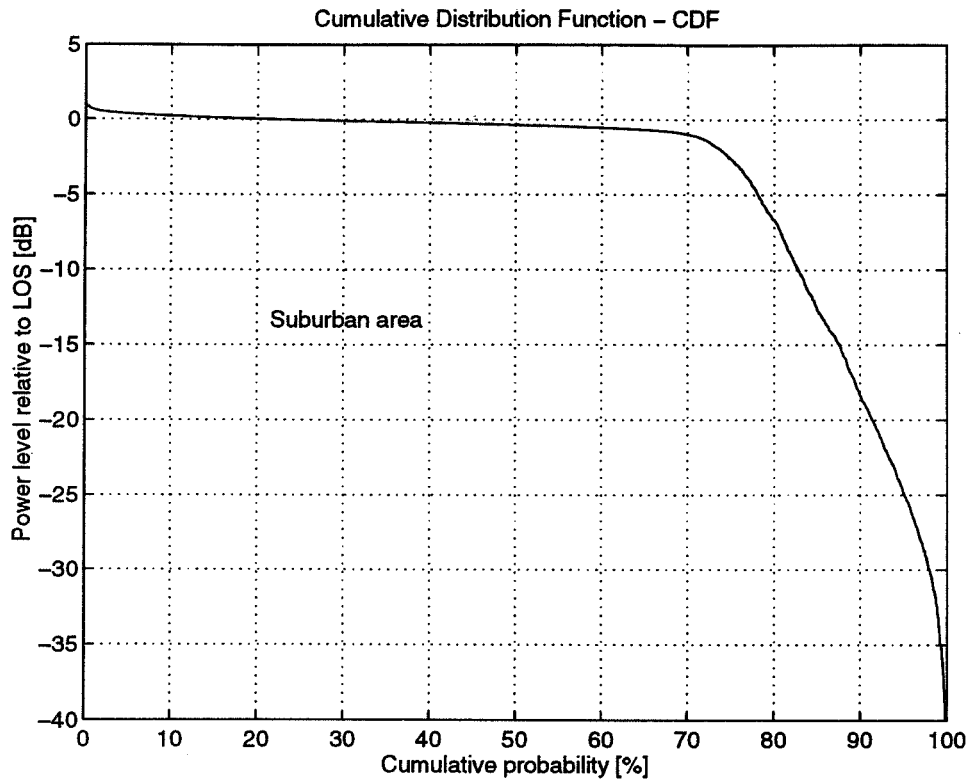


Figure 6: CDF, suburban area (f=18.7 GHz)

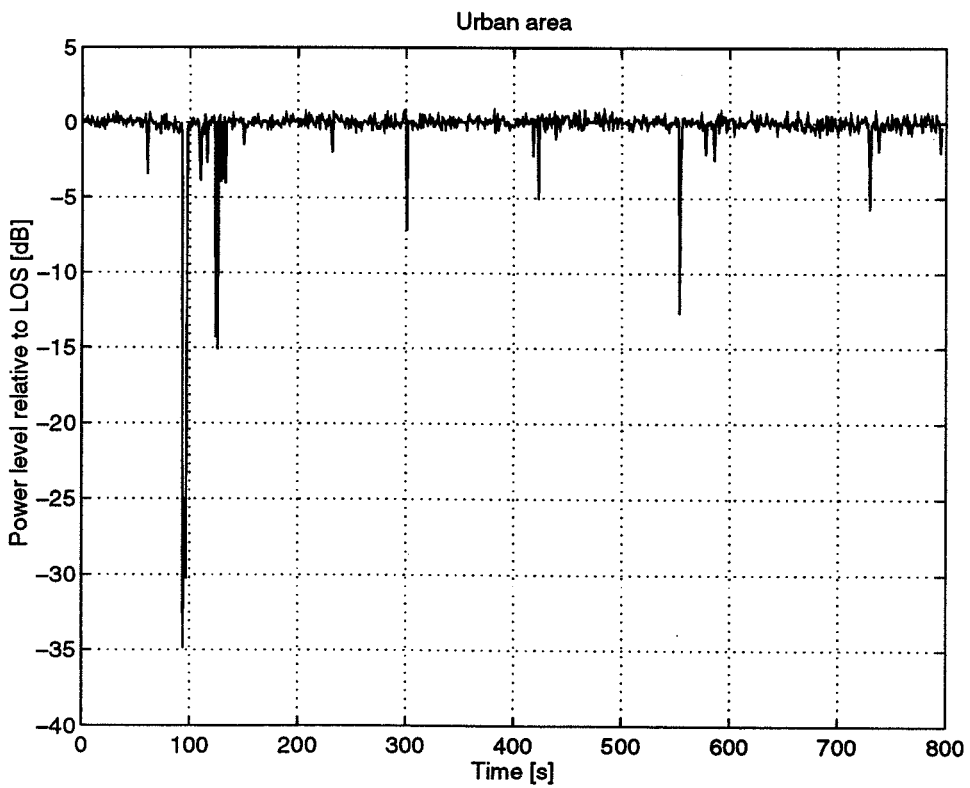


Figure 7: Time series in an urban in Munchen, Germany (f=18.7 GHz)

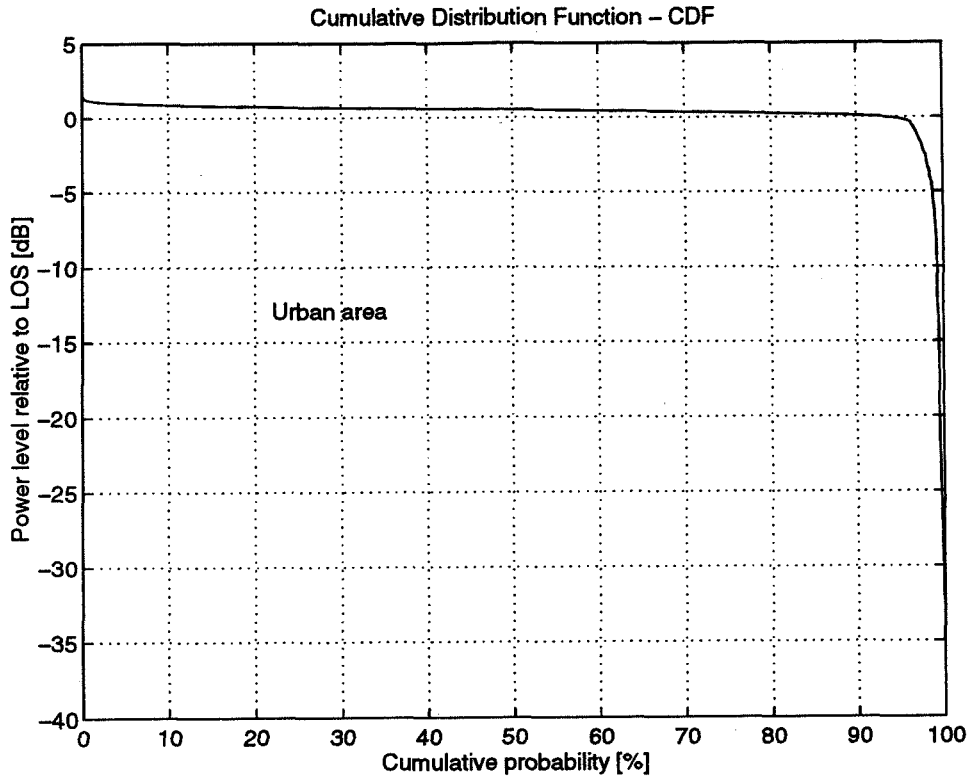


Figure 8: CDF, urban area (f=18.7 GHz)

4 Conclusions

In this paper a Land Mobile Beacon Terminal designed to carry out LMS experimental narrowband campaigns at Ka-band has been presented and briefly described. The terminal presently operates with the Italsat 18.7 GHz propagation beacon but it is inherently capable to receive simultaneously three RF signals, just changing or upgrading the RF front-ends. A combined data and video acquisition system allows to uniquely link RF Ka-band to optical signals so that the propagation engineer can effectively derive information on channel blockage phenomena from passive optical measurements. The terminal installed in a passenger van has been already use to complete the first extended Ka-band LMS experimental campaign, in different European locations and operational scenarios; preliminary results have been also presented.

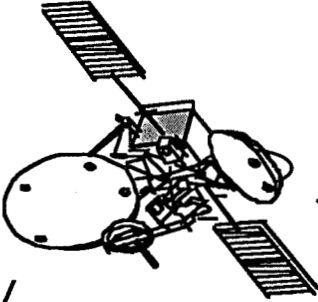
It is foreseen to upgrade the existing LMBT configuration with L- and S-band front-ends and to integrate it with wideband channel sounders presently under development. The final objective is to have a comprehensive experimental equipment to use intensively in narrow- and wideband multifrequency LMS and terrestrial measurements which should ensure an optimum characterization and modelling of the propagation channel for mobile communication services of the next generation.

Acknowledgements

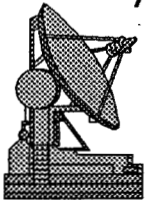
We are sincerely grateful to Messrs F. Murr and M. Richter from IAS for the enthusiasm and technical competence shown throughout the preliminary calibration tests and later during the extended experimental campaign. We also acknowledge the support of the entire RESCOM staff and the committment they put in the development of the first Ka-band land mobile test terminal.

References

- [1] M.K. Sue et al., *A Satellite-based Personal Communication System for the 21st century*, Proc. 2nd International Mobile Satellite Conf., Ottawa, Canada, 17-20 June 1990.
- [2] M.K. Sue et al., *A 20/30 GHz Personal Access Satellite System Study*, Proc. 38th IEEE Vehicular and Technology Conf., June 1988.
- [3] J. Fortuny, M. Sforza, *Mobile Satellite Systems at Ku- and Ka-band*, Proc. 2nd European Conf. on Satellite Communications, Liege, Belgium, 22-24 October 1991.
- [4] J. Goldhirsh, W.J. Vogel, *Propagation Effects for Land Mobile Satellite Systems: Overview of Experimental and Modelling Results*, NASA Ref. Publ. 1274, February 1992.
- [5] M. Sforza, S. Buonomo, *Characterisation of the Propagation Channel for Non-Geostationary LMS Systems at L- and S-bands: Channel Modelling*, Proc. XVII NAPEX Conf., Pasadena, USA, 14-15 June 1993.
- [6] *Land Mobile Beacon Terminal*, Final Report of ESA Contract 9896/92, Vedbaek, Denmark, February 1994.
- [7] W.J. Vogel, U. Hong, *Measurement and Modelling of Land Mobile Satellite Propagation at UHF and L-band*, IEEE Trans. Antennas and Propag., vol. 36, pp. 707-719, May 1988.
- [8] M. Sforza, S. Buonomo, A. Martini, *Channel Modelling for Land Mobile Satellite Systems: Markov Chain Approach*, Proc. PIERS'94, Noordwijk, The Netherlands, 11-15 July 1994.
- [9] Lutz E. et al., *The Land Mobile satellite communication channel. Recording statistics and channel model*, IEEE Trans. Vehic. Techn., vol. 40, pag. 375-385, May 1991.
- [10] Vucetic B., Du J., *Channel model and simulation in Satellite Mobile Communication Systems*, IEEE Trans. Vehic. Techn., vol. , pag. 1209-1218, October 1992.



*ACTS Mobile
Experiments Summary*

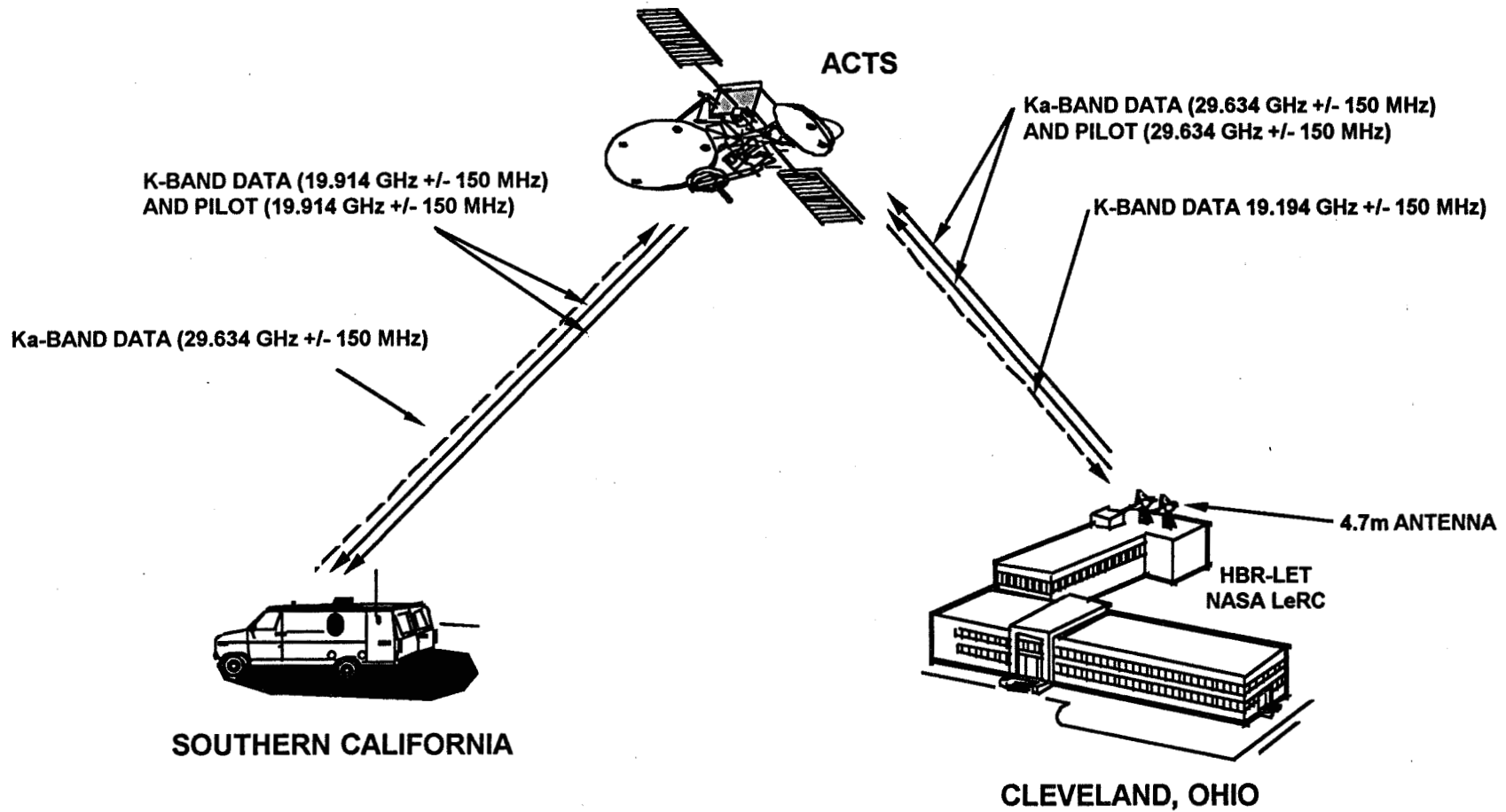


*Deborah S. Pinck
ACTS Mobile Terminal Task
JPL- California Institute of Technology*

Outline

- **AMT Experiments Configuration**
- **ACTS Mobile Terminal Configuration**
- **AMT Experiments**
- **Experiment Results**
 - **Satellite Characterization - Linearity Tests**
 - **AMT Baseline Performance - BERs**
 - **Shadowing Events**
- **Conclusions**

AMT Experiments Configuration

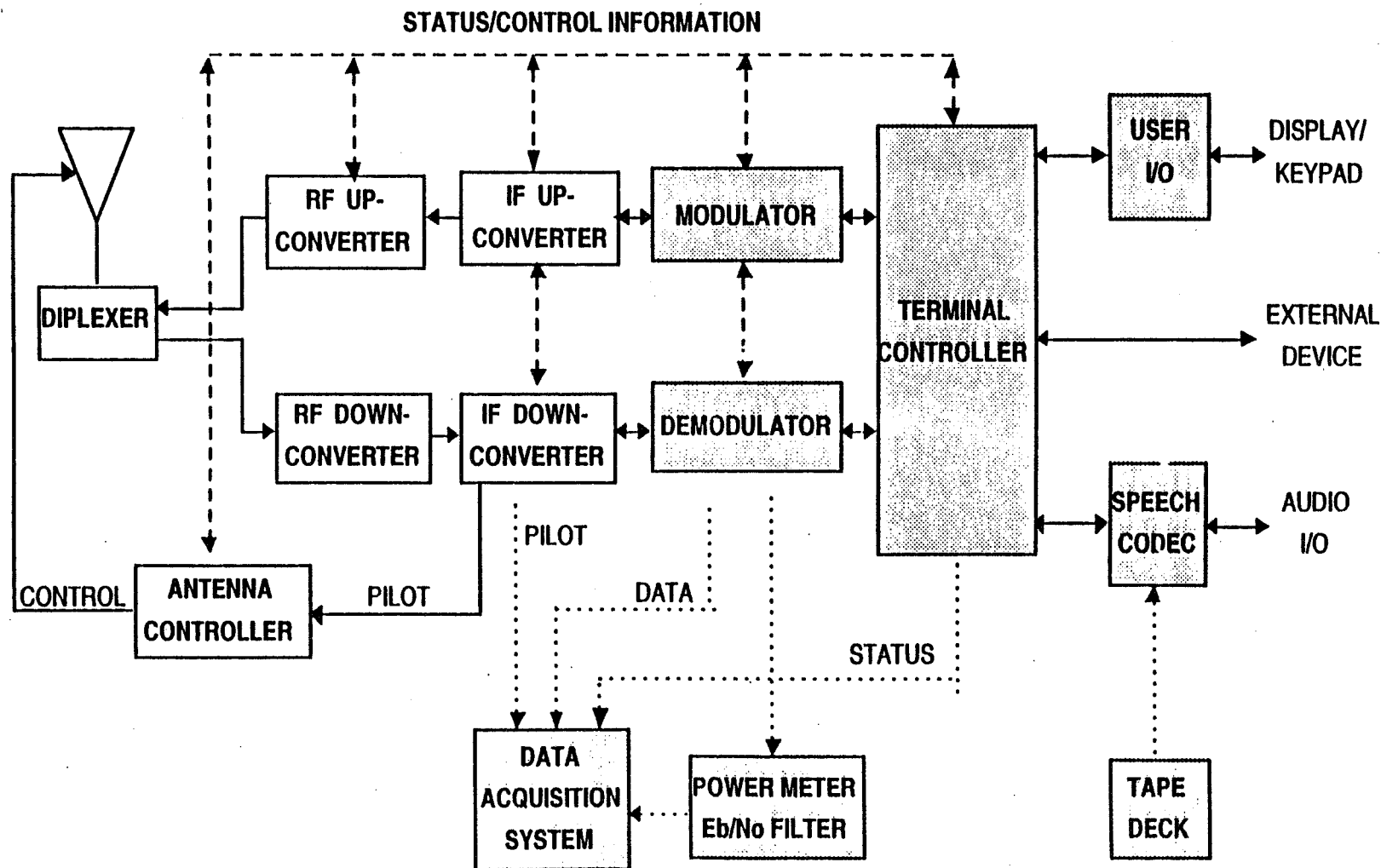


ACTS GENERATED BEACONS AT 20.185, 20.195, AND 27.505 GHz ARE NOT SHOWN.

6/13/94



ACTS Mobile Terminal Configuration



120

6/13/94

AMT Experiments

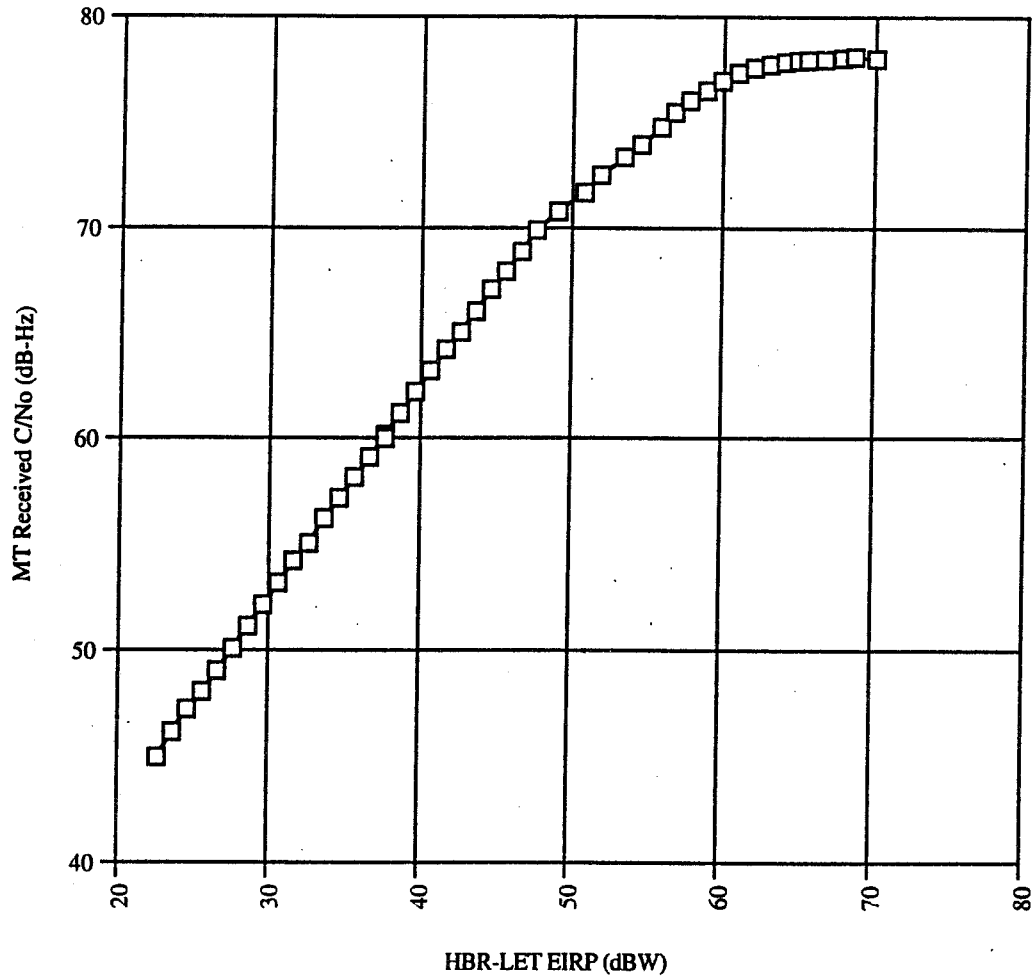
- **Land-Mobile**
- **Satellite News Gathering**
- **Communications-on-the-Move**
- **High Quality Audio**
- **Satellite PCS**
- **Emergency Medical**
- **Telemedicine**
- **Secure Communications**
- **Aero-X**
- **Broadband Aeronautical**

6/12/94



Satellite Characterization:

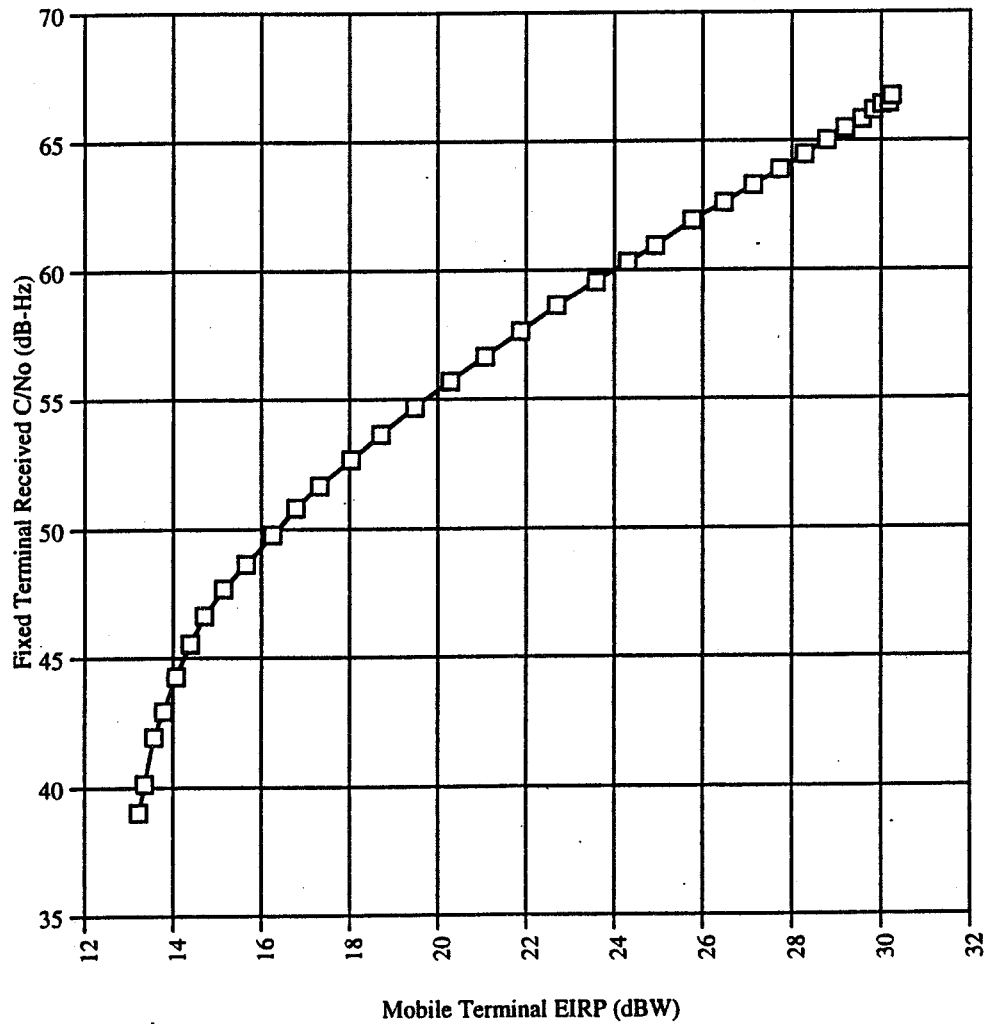
ACTS Linearity Test
Fixed-to-Mobile Transmission
Single Unmodulated Data Signal



6/12/94

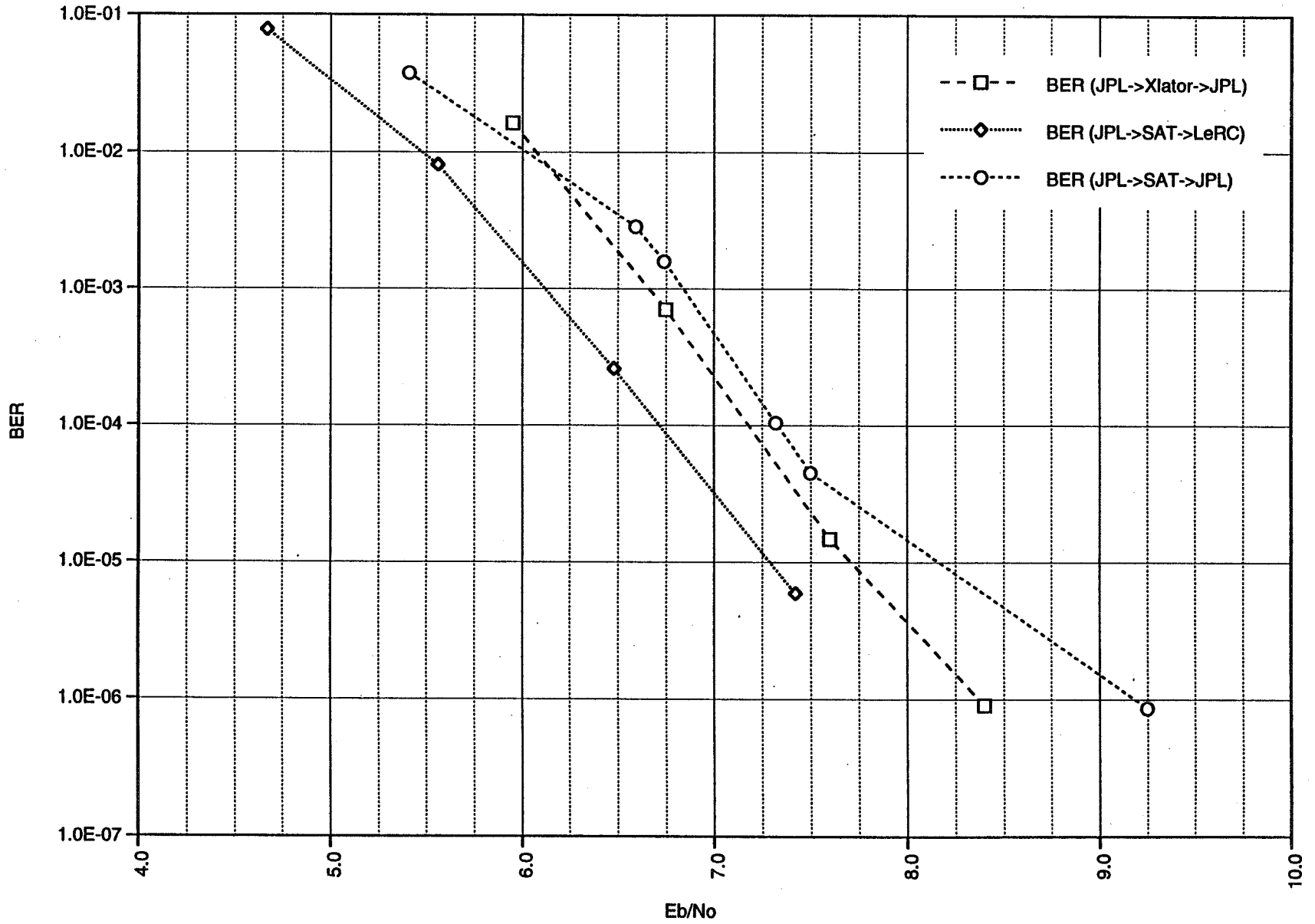
Satellite Characterization:

ACTS Linearity Test
Mobile-to-Fixed Transmission
Single Unmodulated Data Signal

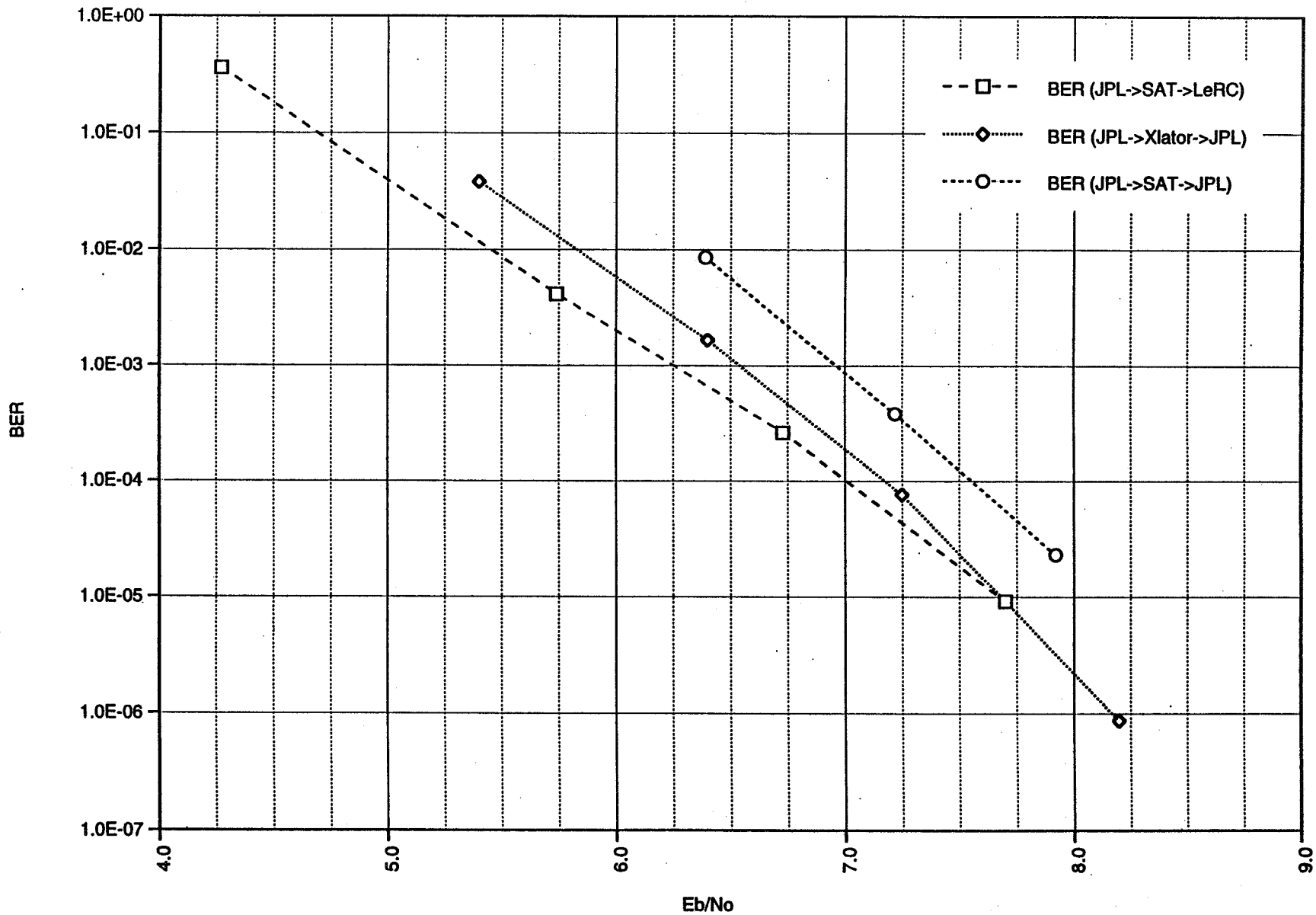


6/12/94

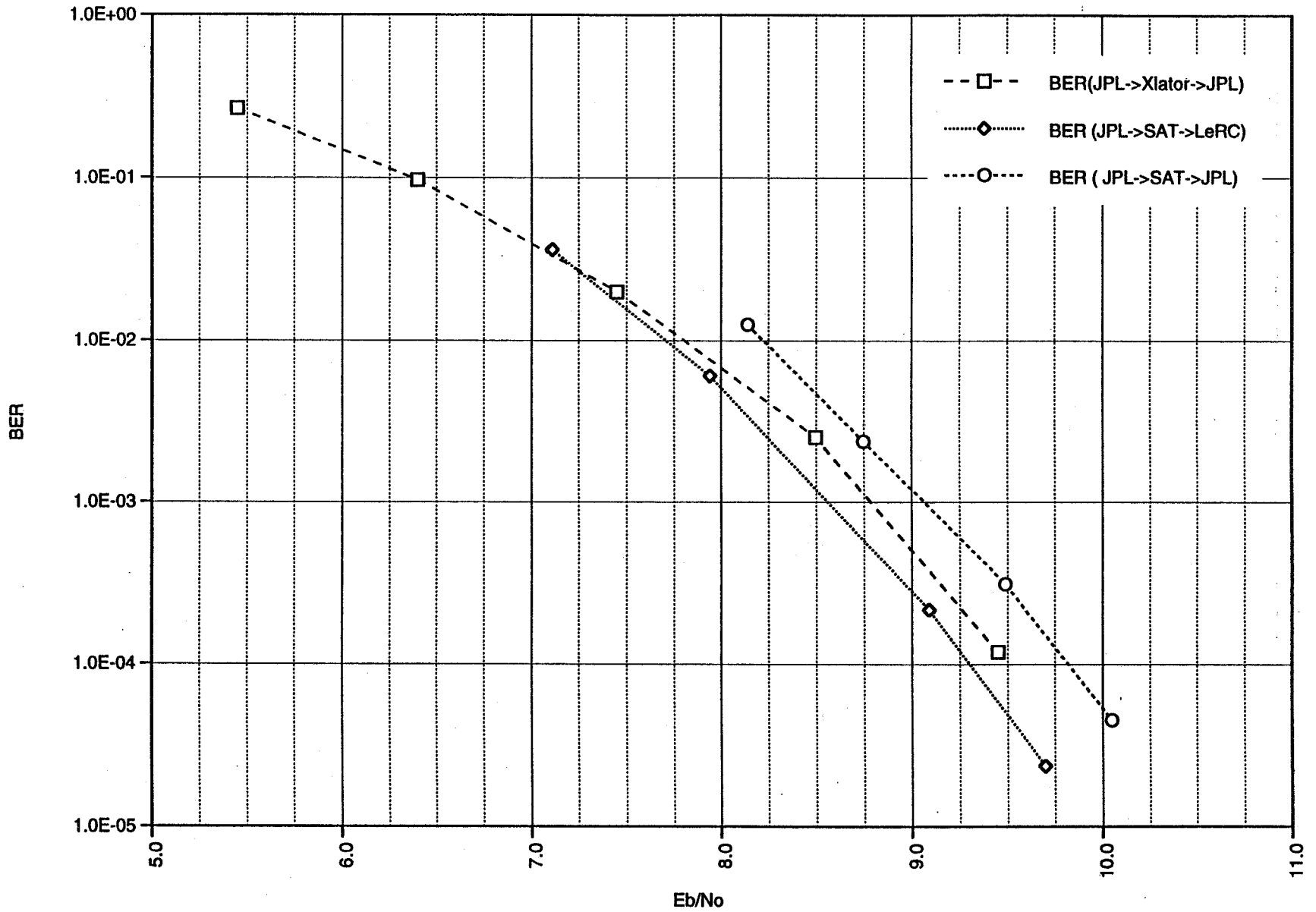
9.6K BER BASELINE COMPARISON
FOR MODEM #2; No PI Tracking, No Ant
Tracking, No Doppler Precompensation

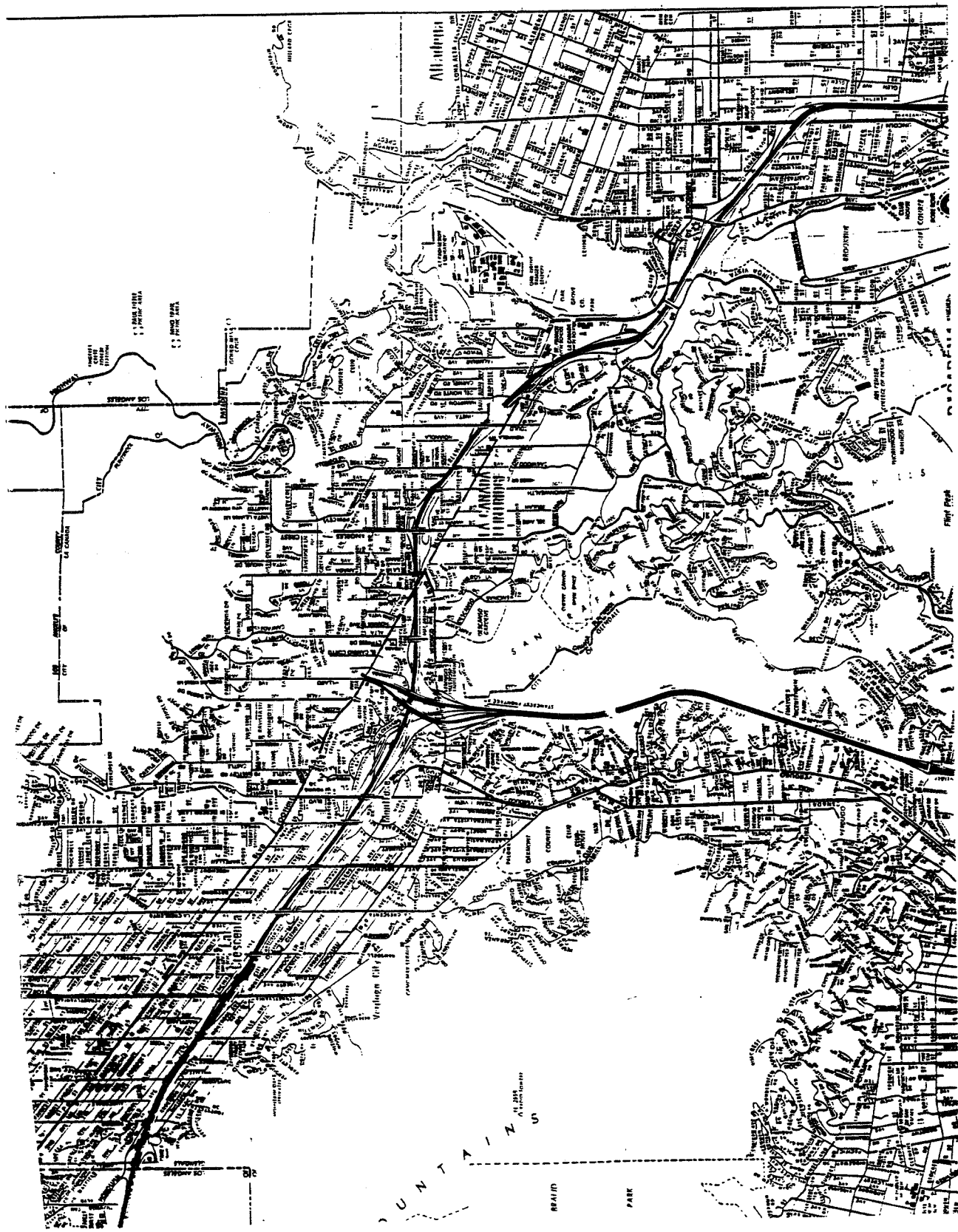


4.8K BER BASELINE COMPARISON
FOR MODEM #2; No Plt Tracking, No Ant
Tracking, No Doppler Precompensation

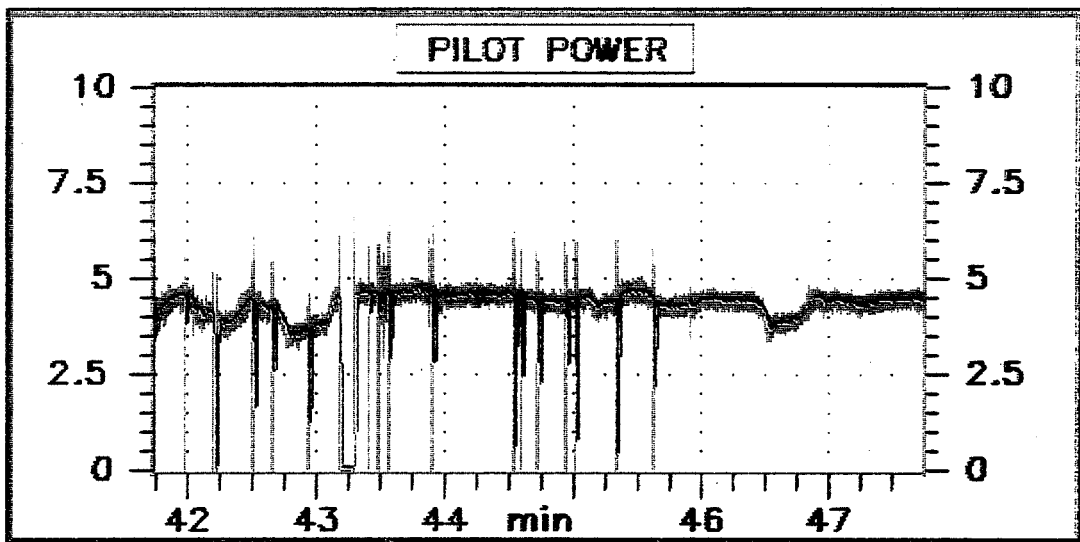
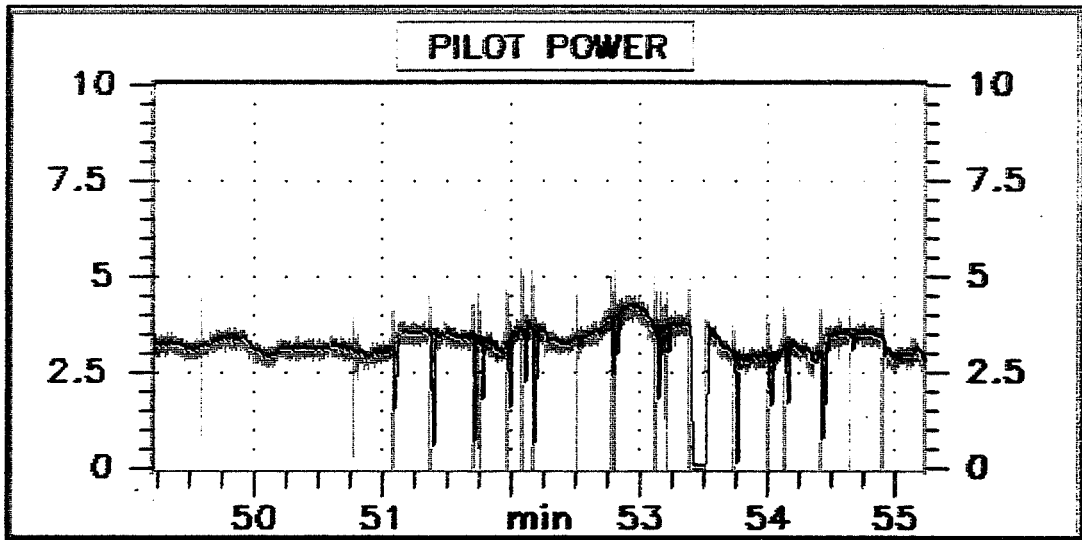


2.4K BER BASELINE COMPARISON
FOR MODEM #2; No Pit Tracking, No Ant
Tracking, No Doppler Precompensation

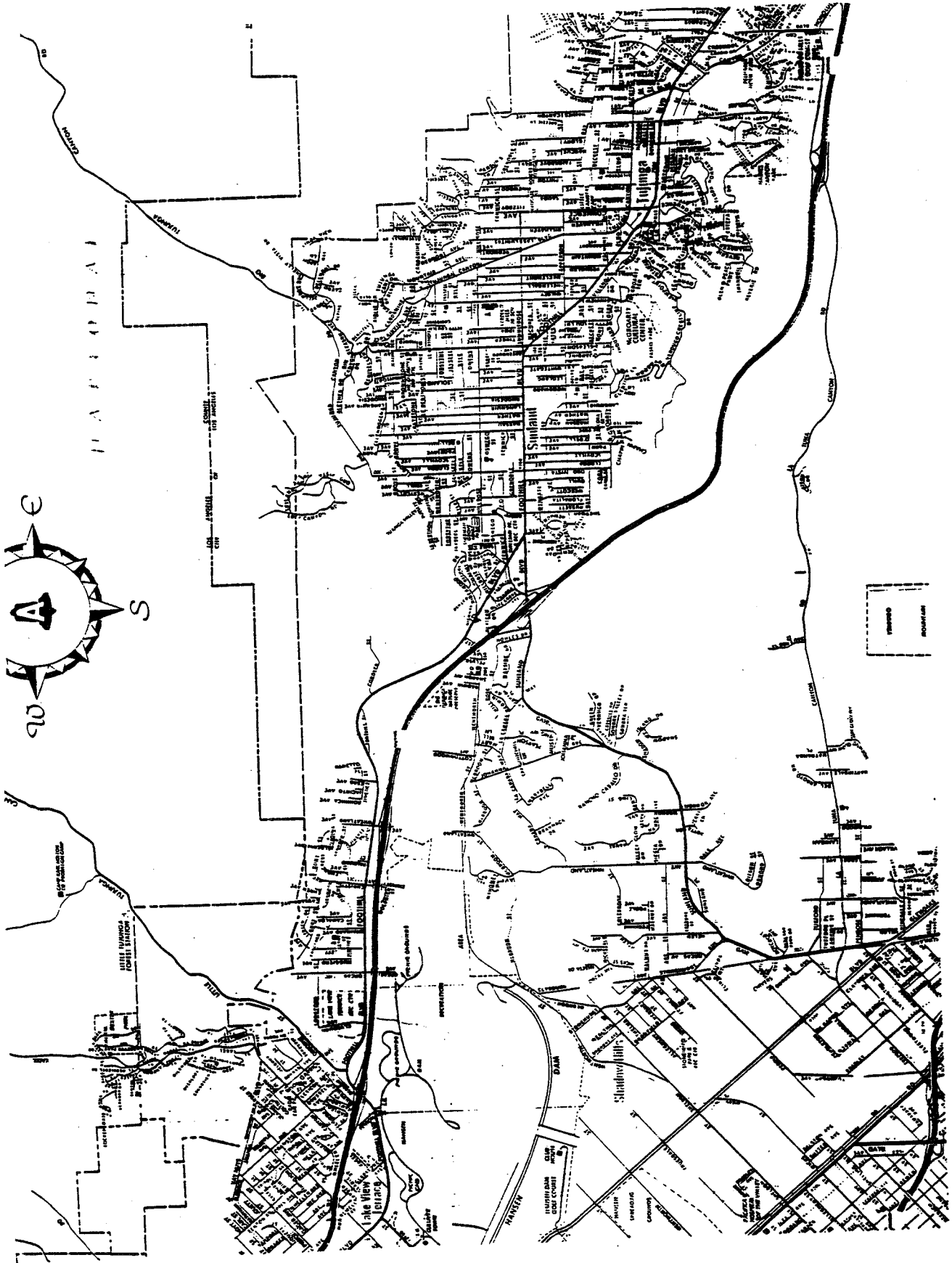




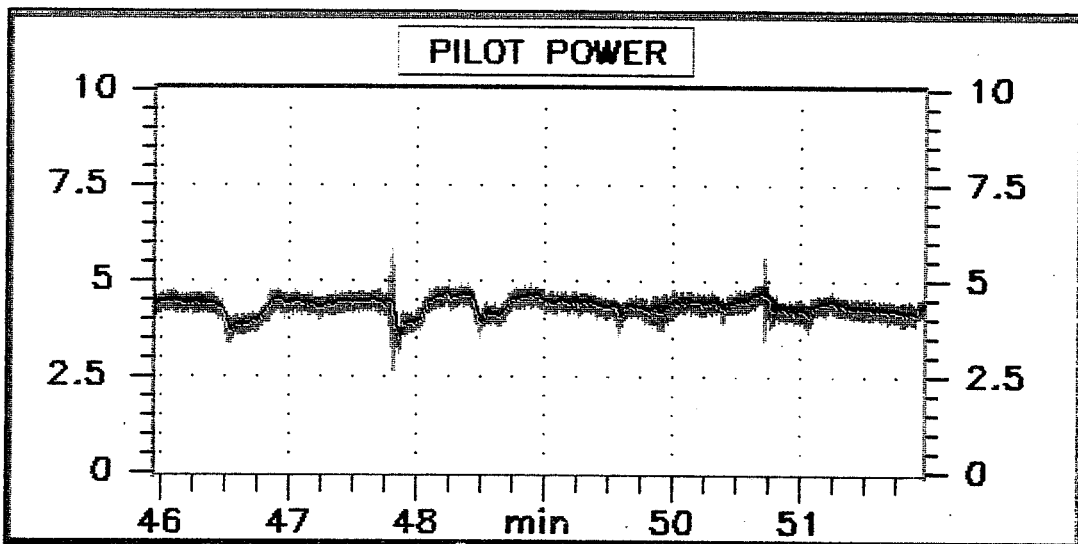
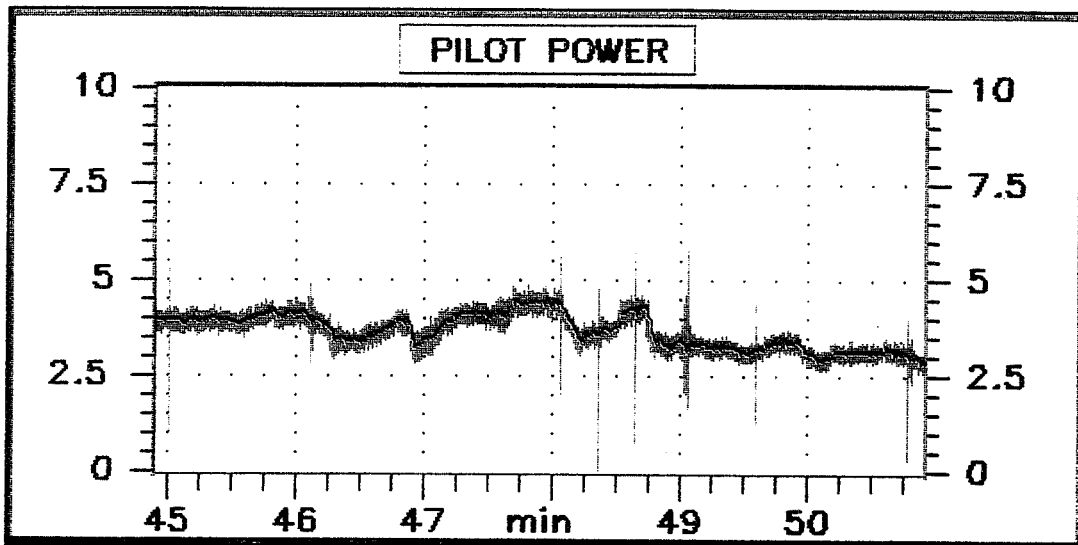
**I-210 Eastbound, overpasses west of Oak Grove Exit
NCS-1 MT, 2 February 1994**



**I-210 Westbound, overpasses west of Oak Grove Exit
NCS-1 MT, 2 February 1994**

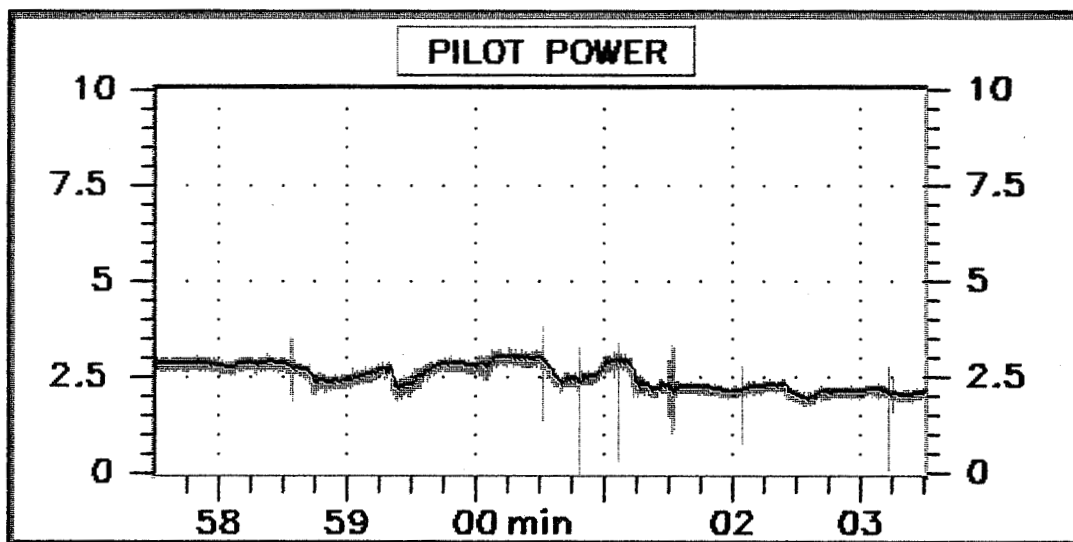
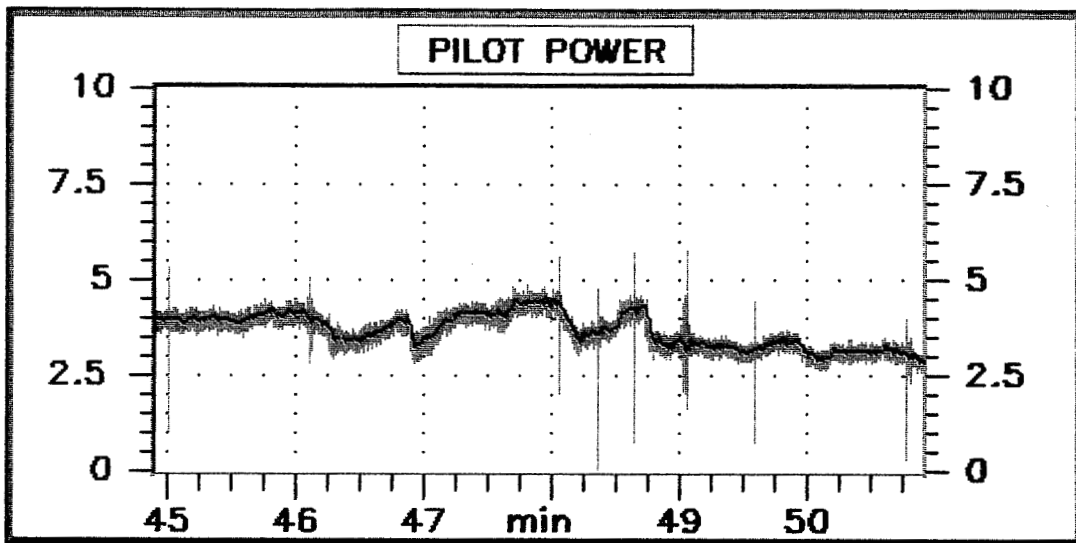


I-210 Eastbound
Hilly terrain between La Crescenta and San Fernando Valleys
NCS-1 MT, 2 February 1994



I-210 Westbound
Hilly terrain between La Crescenta and San Fernando Valleys
NCS-1 MT, 2 February 1994

**I-210 Eastbound
Hilly terrain between La Crescenta and San Fernando Valleys
NCS-1 MT, 2 February 1994**



**I-210 Eastbound
Hilly terrain between La Crescenta and San Fernando Valleys
NCS-1 MT, 1 February 1994**

Conclusions

- **Satellite Characterization:**
 - MT to FT: linear for complete useful range of the MT's transmit EIRP
 - FT to MT: linear for transmit EIRPs less than 50 dBW
 - received C/N_0 of 78 dB-Hz, 28 dB higher than that required to operate the terminal at 9.6 kbps
- **Baseline System Performance:**
 - in agreement with satellite simulator tests
 - for a BER of 10^{-3} from FT to MT
 - » @ 9.6 kbps, $E_b/N_0 = 6.8$ dB
 - » @ 4.8 kbps, $E_b/N_0 = 6.7$ dB
 - » @ 2.4 kbps, $E_b/N_0 = 8.5$ dB

Conclusions (cont.)

- **Baseline System Performance:**
 - for a BER of 10^{-3} from MT to FT
 - » @ 9.6 kbps, $E_b/N_0 = 6.2$ dB
 - » @ 4.8 kbps, $E_b/N_0 = 6.3$ dB
 - » @ 2.4 kbps, $E_b/N_0 = 8.7$ dB
- **Shadowing: tbd**
- **Near Toll Quality Voice**

ACTS Mobile Propagation Campaign

349293

Julius Goldhirsh
Applied Physics Laboratory, The Johns Hopkins University
Johns Hopkins Road, Laurel, Maryland 20723-6099

P. 6

Wolfhard J. Vogel, Geoffrey W. Torrence
Electrical Engineering Research Laboratory, The University of Texas at Austin
10100 Burnet Road, Austin, Texas, 78758-4497

Abstract

Preliminary results are presented for three propagation measurement campaigns involving a mobile receiving laboratory and 20 GHz transmissions from the Advanced Communications Technology Satellite (ACTS). Four 1994 campaigns were executed during weekly periods in and around Austin, Texas in February and May, in Central Maryland during March, and in Fairbanks, Alaska and environs in June. Measurements tested the following effects at 20 GHz: (1) attenuation due to roadside trees with and without foliage, (2) multipath effects for scenarios in which line-of-sight paths were unshadowed, (3) fades due to terrain and roadside obstacles, (4) fades due to structures in urban environs, (5) single tree attenuation, (6) effects of fading at low elevation angles (8° in Fairbanks, Alaska) and high elevation angles (55° in Austin, Texas). Results presented here cover sampled measurements in Austin, Texas for foliage and non-foliage cases and in Central Maryland for non-foliage runs.

1.0 Objectives

The objectives of the 20 GHz ACTS mobile propagation campaigns are to measure and analyze fading effects for the following scenarios: (1) roadside trees in rural regions, (2) trees near homes and structures in suburban communities, (3) trees with and without foliage, (4) line-of-sight elevation angles at low (8°) and high (55°) values, (5) highway obstacles such as signs, overpasses, and terrain, and (6) buildings and other structures in urban regions. The analysis involves examining multipath, shadowing, and blockage effects and extending to K-Band previous models valid at the lower UHF to S-Band [1-3].

During the first six months of 1994, four mobile propagation measurement campaigns were successfully executed by investigators from the Electrical Engineering Research Laboratory (EERL) of The University of Texas at Austin and the Applied Physics Laboratory of The Johns Hopkins University, enabling all of the above objectives to be realized. In this paper, we describe the mobile propagation system and present preliminary results associated with objectives (1)-(3).

2.0 Overview of Campaigns

An overview of the ACTS mobile propagation campaign locations, dates, elevation angles, and foliage condition is shown in Table 1. In total, four field tests were conducted during the first six months of 1994. Each test consisted of five contiguous days on which approximately four hours of measurements were made. Two field tests were undertaken in Austin, Texas where the elevation angle was approximately 55° ; one during February when the deciduous trees were bare, and another during May when the deciduous trees were in full blossom. Measurements were made within the city of Austin as well as nearby suburban and rural environs. In March, tests were made in Central Maryland along the same system of roads where mobile propagation measurements were previously made at UHF and L-Band by the authors [1,3-5]. The rationale for replicating the same system of roads was to combine the results of previous measurements so that developed models could be extended to K-Band (20 GHz). In addition, measurements were made within the cities of Baltimore and Washington, DC, as well as suburban and rural communities in the vicinity of these cities.

Table 1: Locations, dates, elevation angles, and condition of foliage for 1994 ACTS mobile propagation campaigns.

Site Location	Date (1994)	Elevation Angle ($^\circ$)	Deciduous Trees
Austin, Texas	February 14-18	54.5°	Bare
Central, Maryland	March 14-18	38.7°	Bare
Austin, Texas	May 2-6	54.5°	Full Bloom
Fairbanks, Alaska	June 6-10	7.9°	Full Bloom

3.0 Experimental Aspects

3.1 Configuration

In Figure 1 is depicted the general configuration associated with the ACTS mobile propagation campaign. A CW signal from a tone generator at approximately 3.4 GHz was injected at the upconverter input of the Link Evaluation Terminal at the NASA Lewis Research Center in Cleveland, Ohio. This resulted in an uplink signal of approximately 30 GHz and a downlink transmission at approximately 20 GHz employing the microwave switch matrix mode of ACTS. These downlink signals were received at either Austin Texas, Fairbanks

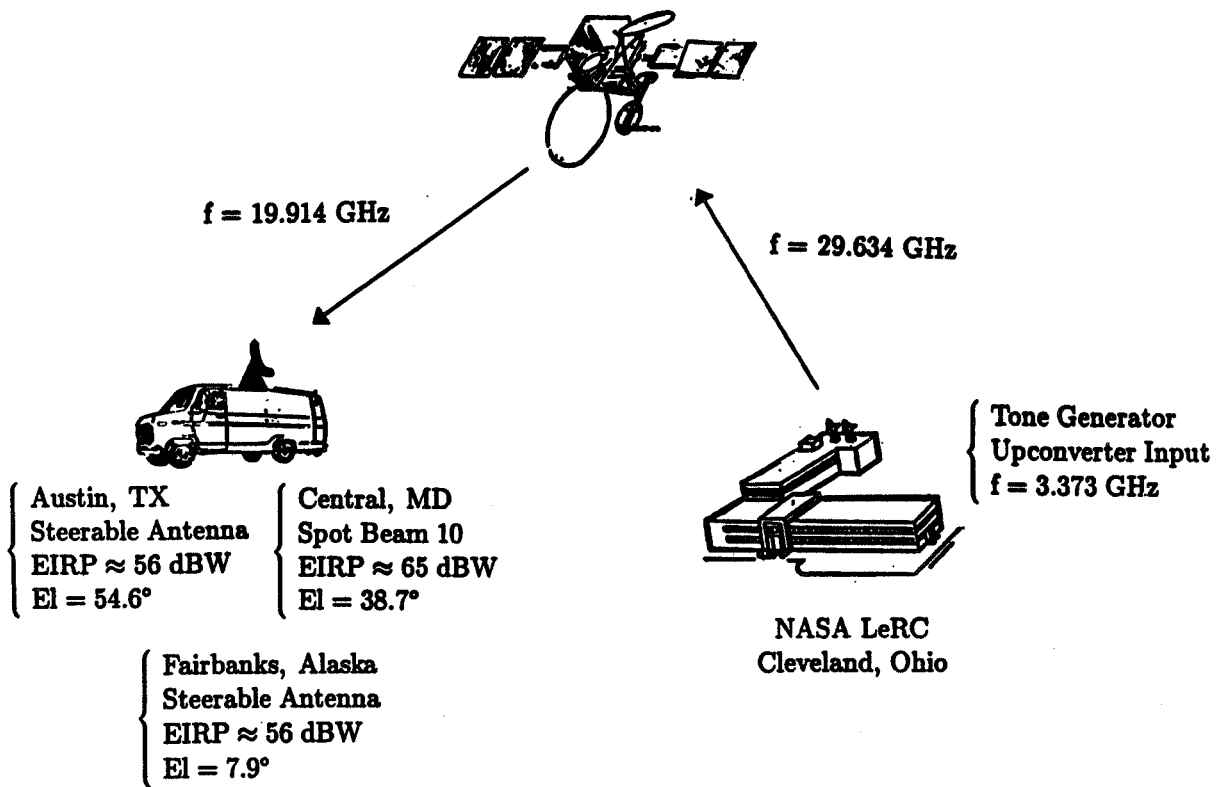


Figure 1: Experimental configuration for the ACTS Mobile Propagation Campaign.

Alaska using the steerable antenna or Central MD employing a spot beam antenna. The EIRP of the spot beam antenna (Central Maryland) was approximately 9 dB greater than that of the steerable antenna.

3.2 Link Budget

A summary of the link budget parameters is given in Table 2 for the different site locations. Utilizing a receiving horn antenna with a 1.5 inch aperture, we achieved a beamwidth of 27° and antenna gain of approximately 16 dB. With a 400 Hz bandwidth, the carrier-to-noise ratios were in excess of 30 dB in Austin Texas and Alaska and greater than 40 dB in Central Maryland. Measurements at these locations confirmed these carrier-to-noise ratios.

3.3 Elements of the Antenna Tracking System

The passive tracking system has as major elements an angular rate sensor, a flux gate compass, a horizontal rotary turn-table and a computer which points the antenna towards the satellite given the known coordinates of the satellite and the receiver location. Absolute tracking in azimuth is maintained to within a few degrees. Because the receiving antenna beamwidth is approximately 27°, the peak gain variability due to pointing errors was generally less than 1 dB for most road and city driving conditions.

The antenna and angular rate sensor rest on the rotary table which is driven by a step-motor system. When the vehicle under the rotary table turns, the rate sensor develops an output voltage proportional to the angular turn rate. This voltage is integrated to give a "turning angle" voltage which is fed into a frequency converter whose output gives a series of pulses at a frequency proportional to the turning angle. These pulses and a direction signal are interfaced with the stepping motor driver such that the rotary table is driven in the direction reducing the turning angle. When the error angle reduces to zero, no further pulses are injected into the stepping motor driver. Because the rate sensor experiences drift, the computer system also senses the drift rate relative to the average absolute vehicle direction received with a flux-gate compass mounted to the vehicle. It subsequently compensates the drift and the antenna is pointed in the correct direction. An algorithm mitigates compass errors caused by magnetic anomalies due to roadside structures.

3.4 Elements of the Receiver System/Data Acquisition System

The major elements of the receiver system are a microwave spectrum analyzer, a frequency synthesizer, the aforementioned antenna tracker system, a low noise frequency down-converter, an intermediate frequency stage with automatic frequency control (AFC), and a PC-based data acquisition system. Ancillary sensors give vehicle speed and direction. The receiver operates at 19.914 GHz, has a nominal noise bandwidth of 400 Hz, and measures both in-phase and quadrature-phase voltages at a sampling rate of 1000 Hz. The AFC tracks the satellite frequency and compensates for Doppler shift due to relative vehicle motion over a ± 1000 Hz capture range.

The resulting propagation data are stored on the computer's hard disk which has the

capacity to hold over four hours of continuous data. The time, vehicle speed, and vehicle direction are stored once per second and the antenna pointing parameters are stored at a 5 Hz rate. More complete details of the antenna tracker system and receiver system are given by Goldhirsh et al. [6].

Table 2: ACTS 1994 mobile propagation link budgets.

PARAMETER	BOTH SITES	TX Austin	MD Central	AK Fairbanks
Satellite:				
Longitude (°W)	100			
Downlink Frequency (GHz)	19.914			
Uplink Frequency (GHz)	29.634			
Polarization	Vertical			
Receiver Geometry:				
Latitude (°N)		30.4	39.25	65.0
Longitude (°W)		97.7	77.0	147.7
Elevation (°)		54.5	38.7	7.9
Azimuth (°)		184.5	213.9	129.5
Receiver Parameters:				
Polarization	Circular			
Antenna Efficiency	0.6			
Antenna Diameter (in)	1.5			
Antenna Gain (dB)	15.8			
Beamwidth (°)	27			
System Temperature K	430			
Link Budget:				
EIRP (dBW)		56	65	56
Polarization Loss (dB)	3			
Free Space Loss (dB)		-209.7	-210.0	-210.6
Atmospheric Gas Loss (dB)		0.4	0.5	2.2
Radome Loss (dB)	2.0			
Mobile G/T (dB/K)	-10.5			
Signal Power Received (dBW)		-143.3	-134.7	-146.0
Noise Power (dBW/Hz)	-202.2			
Carrier/Noise (dB per Hz)		58.9	67.5	56.2
Carrier/Noise (dB; 400 Hz)		32.9	41.5	30.2

4.0 Measurement Results

4.1 Fading Due to Roadside Trees with Foliage

In February 1994, the attenuation effects of an approximate 8 km stretch of a tree lined

road were measured in Bastrop, which is located approximately 30 km southeast of Austin. The road examined (Route 21) is comprised of two lanes in each direction with a median strip containing trees. Both the roadside and median strip contain approximately 75% evergreens known as loblolly pines (*Pinus taeda*). This is a coniferous tree predominant in the southeastern United States which contains bundles of stout often twisted needles and blackish-gray bark. The canopies of these trees were relatively closely spaced with overhanging regions in which they often formed a virtual tunnel of foliage above the road.

Shown in Figure 2 are fade-time series representations, where the vertical scale is the signal level relative to the unshadowed case, and the abscissa is elapsed time covering an approximate ten minute period. Three sets of curves are shown; the top and bottom curves (thin curves) represent the maximum and minimum signal levels, respectively, derived from 1000 samples during each second. The thick middle curve represents the one second average of the 1000 samples. The "average" relative signal level is shown to vary between 0 and -20 dB during the run, whereas the "minimum" relative signal level frequently is smaller than -30 dB. The "maximum" curve represents the largest signal received during the one second interval and this signal ranges from approximately +4 dB multipath enhancement to approximately -11 dB signal loss. The average speed of the vehicle was 32 mph for this run.

In Figure 3 are given cumulative distributions for the mobile Bastrop run (dashed curve) and two static runs obtained previously employing a fixed 20 GHz source and receiver [7]. The dot-dashed curve corresponds to an unshadowed line-of-sight distribution signifying multipath fading conditions, and the solid curve is a static distribution for a pecan tree with foliage representing attenuation due to shadowing. The ordinate for the mobile run case (Bastrop, Texas) represents the percentage of distance for which the fade is greater than the abscissa, whereas the static runs represent the percentage of shadowed locations in which the fade is greater than the abscissa.

The relative azimuth angle between the vehicle direction and the satellite ranged from 38°-80° with an average of approximately 57°, where 90° represents the case in which the line-of-sight path is orthogonal to the line of roadside trees. The slopes for the first few dB of the "clear line-of-sight" and the "pine tree" distributions are similar, indicating multipath effects for the Bastrop run. On the other hand, the slopes of the pine tree run distribution for fades in excess of 5 dB tend to match those for the pecan distribution, signifying the shadowing effects. Hence, the 20 GHz Bastrop distribution may be separated into two segments separated by an inflection region; an approximately exponential multipath part and a shadowing part, which at fades exceeding 10 dB is also exponential. We note that for 10% of the driving distance, the fades were in excess of 15 dB. Since the elevation angle was relatively high (approximately 55°), the distribution fade depth is nevertheless mitigated relative to lower angle scenarios.

The matching of distribution slopes for multipath and shadowing cases may be demonstrated using the following simple modeling concepts. We assume that the trees are identical and equally spaced with shadowing arising due to optical blockage by the tree foliage and

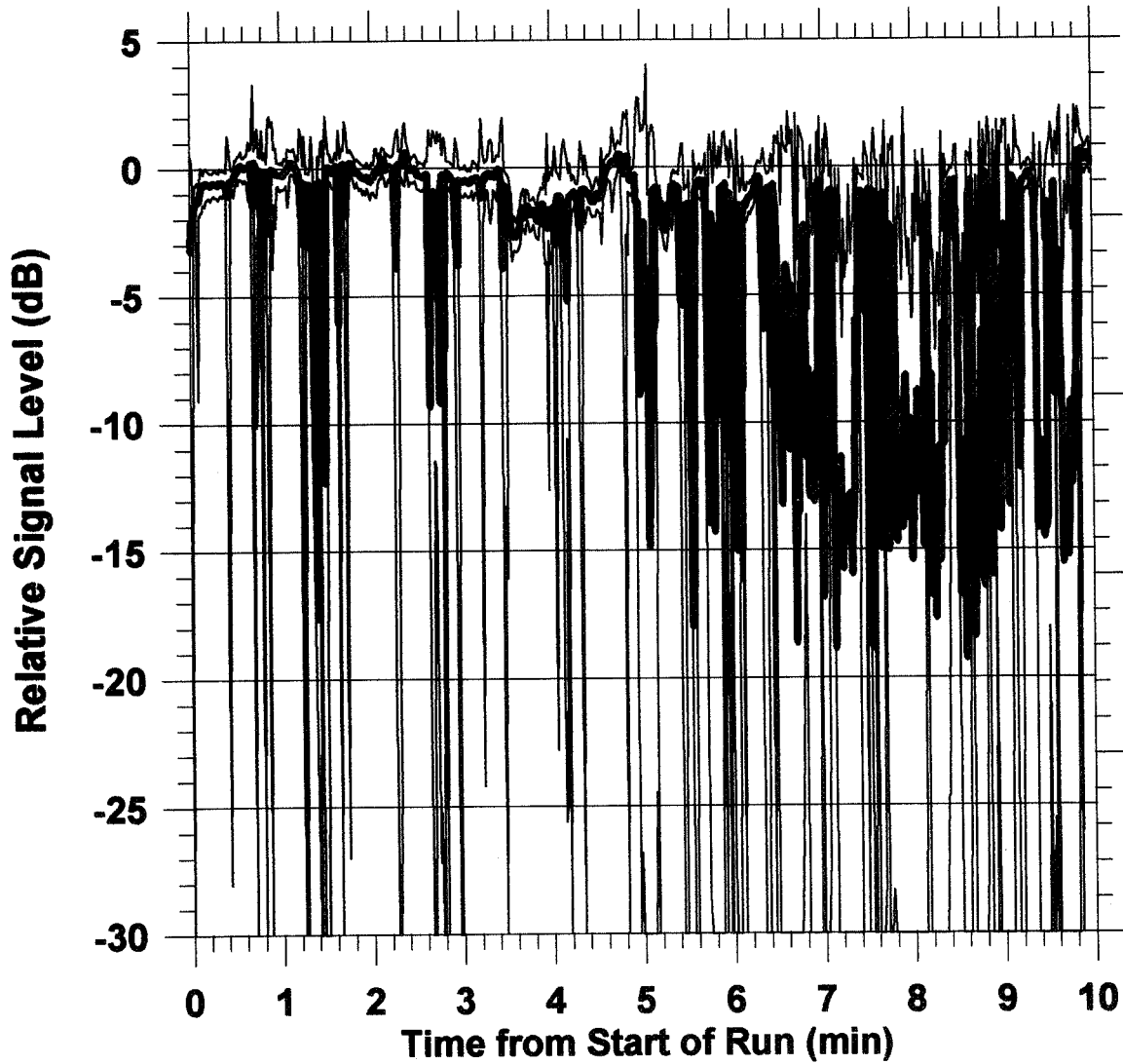


Figure 2: Relative signal time-series of maximum, minimum, and average levels for a 10 minute run (32 km) along an evergreen tree-lined road in Bastrop, Texas in February 1994.

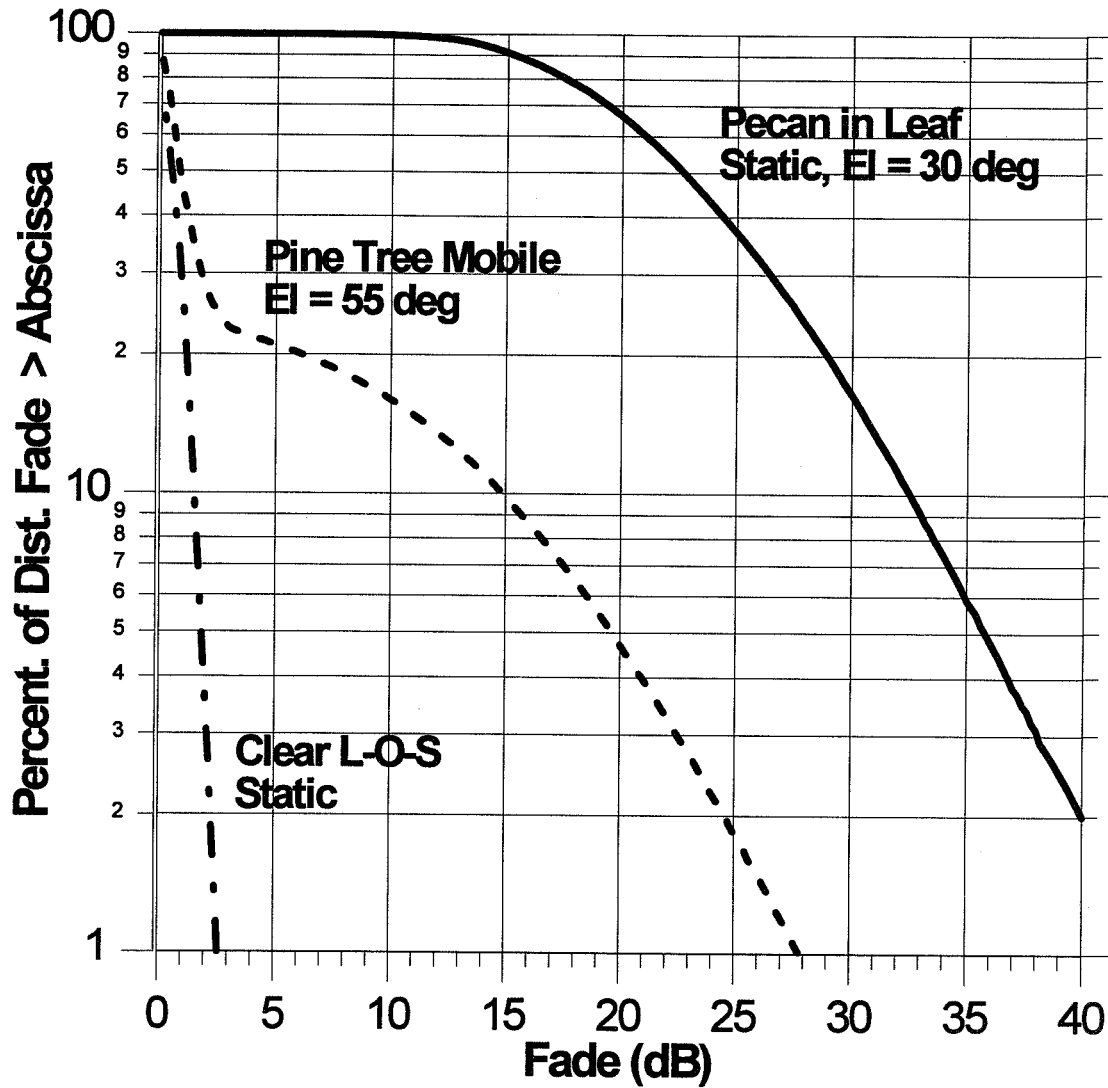


Figure 3: Cumulative distribution (dashed curve) for a 10 minute run (32 km) of an evergreen tree-lined road in Bastrop, Texas in February 1994. Also shown are static distribution for a pecan with foliage (solid curve) and a clear line-of-sight case.

only multipath occurring during times the line-of-sight path is pointing in between the tree canopies. An expression for total shadowing probability may then be derived which is equal to the shadowing probability for a single tree times a constant factor containing the combined effects of all the trees. On a logarithmic scale, the slope of the distribution is maintained and the constant factor translates the curve up or down. An analogous methodology may be employed for the multipath case. Here, the resultant probability may be demonstrated to relate to the probability for a single multipath scenario corresponding to unshadowed line-of-sight propagation between a single pair of tree canopies times a constant representing the combined effects caused by all such scenarios in the run. The multipath distribution plotted on a logarithmic scale will have a slope for a single tree case identical to the slope of the distribution for the multiple tree scenario.

4.2 Fading Along Rural and Highway Roads

A stretch of road in Central Maryland was examined (Route 108) which is a relatively narrow, has one lane in each direction, and contains approximately 55% roadside deciduous trees. The sampled runs along Route 108 corresponded to directions southwest and northeast between Route 32 and Route 97, a distance of approximately 15 km in which the satellite path intersected the roadside trees and obstacles broadside. During the sampling period (March, 1994), the deciduous trees were without foliage.

In Figure 4 is shown an 18 minute time-series fade example for the case in which the vehicle was traveling in the northeast direction and the satellite path cut the line of roadside trees from the right. This scenario approximately replicates runs previously executed at UHF and L band employing helicopter and satellite platforms [1, 3-5]. As in Figure 2, the top and bottom thin curves represent the maximum and minimum signal levels for each 1 second period and the thick curve corresponds to the one second average. We note that occasionally average relative signal levels smaller than -25 dB occur.

In contradistinction, Figure 5 shows a set of time series corresponding to Route 295, driving south in the right lane, with the satellite generally directly in front of the vehicle and occasionally to the right. Route 295 is a four lane highway connecting Baltimore, Maryland and Washington, DC, having two lanes in each direction. The roadside foliage optical shadowing for the Route 295 run was approximately 75% as opposed to 55% along Route 108. Nevertheless, we observe significantly less fading for Route 295 because the line-of-sight paths to the satellite minimally cut the tree lines and were generally unshadowed.

In Figure 6 we combine the cumulative distributions for Route 295 (dashed) and Route 108 (solid). Shown also is the distribution for the Bastrop, Texas run (dashed-dot curve), which corresponded to a higher elevation case with trees in foliage. The following features are evident: (1) All the distributions show an inflection at approximately 3 dB separating multipath from shadowing. (2) Although Route 295 has the largest roadside tree population, fade levels are smallest because the line-of-sight path to the satellite was generally unshadowed (i.e., satellite in front of vehicle). (3) The Bastrop run showed the largest fades at percentages of 20% and smaller because this run was one in which the roadside trees contained foliage and

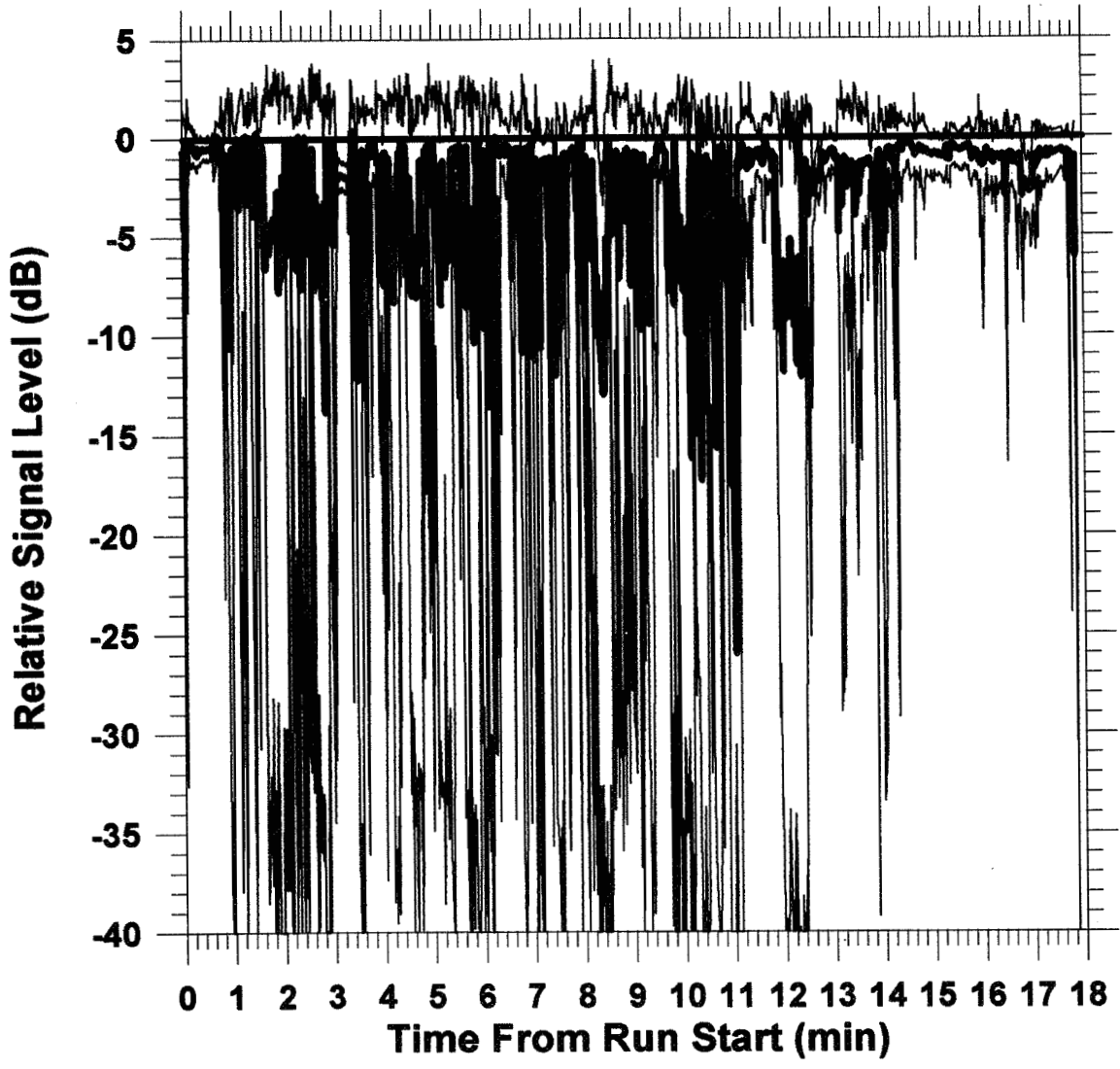


Figure 4: Relative signal time-series of maximum, minimum, and average levels for an 18 minute run (15 km) along Route 108 in Central Maryland which contains 55% deciduous trees.

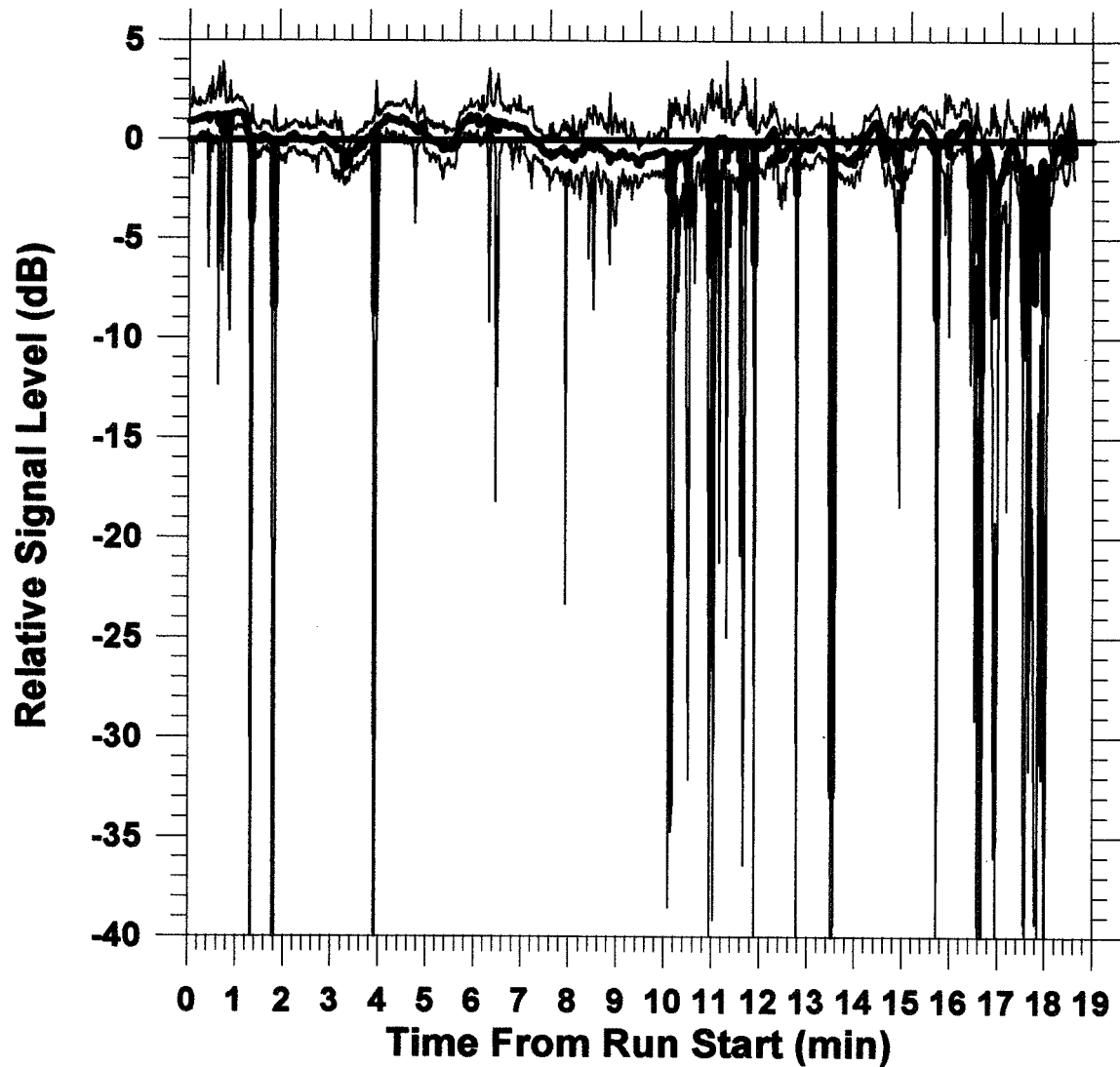


Figure 5: Relative signal time-series of maximum, minimum, and average levels for a 19 minute run (25 km) along Route 295 in Central Maryland which contains 75% deciduous trees.

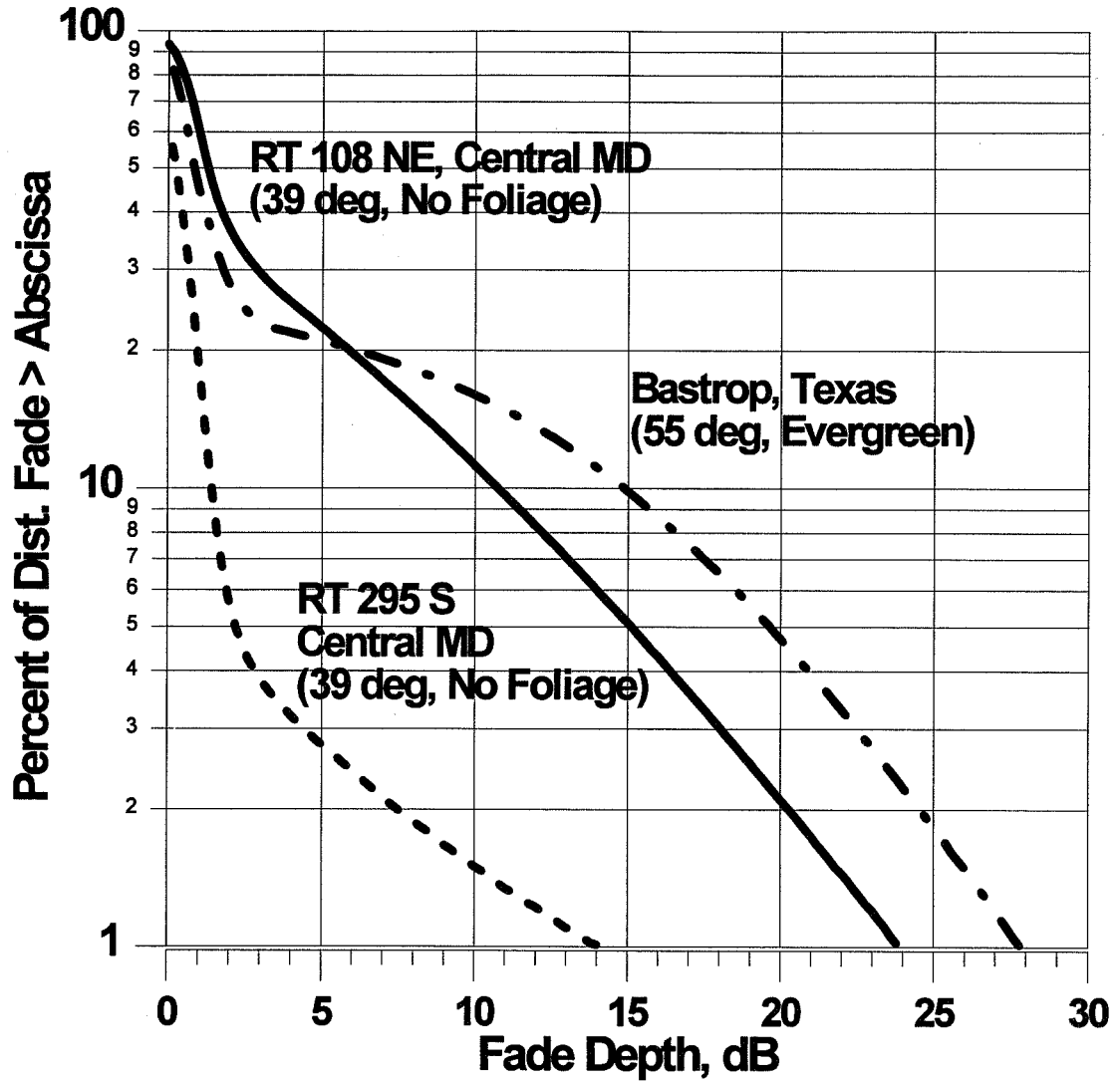


Figure 6: Comparison of cumulative fade distributions for Routes 295 and 108 in Central Maryland (no foliage) and Route 21 in Bastrop, Texas (foliage).

the line-of-sight path generally passed through the canopies. Nevertheless, the level of fades was mitigated because the higher elevation angle (55°) resulted in a reduced shadowing path length through the canopies.

4.3 Effects of Foliage on Fading

To quantify the effects of foliage during mobile runs, measurements were examined of the same tree-lined suburban streets obtained in Austin, Texas in February and May of 1994 during which time the trees were “without” and “with” foliage, respectively. As an example, we present here the foliage effects for 42nd Street between Duval and Avenue A, a stretch of road which is 0.75 km long, and is directed approximately east-west. The example run considered corresponds to the case where the receiving van was moving westward, where the line-of-sight path was above the roof-tops of the homes, but passed through the canopies of dense overhanging roadside trees (approximately 90% population) which were primarily pecan.

In Figure 7 are time series runs depicting the average 1 s relative signal levels for the foliage and non foliage cases which exhibit remarkable differences. We note the average foliage relative signal level (thick curve) is smaller than -18 dB, whereas the non-foliage relative signal level (thin curve) is greater than -9 dB. The fading effects difference between the foliage and non-foliage cases are further emphasized in Figure 8, which shows the cumulative distributions for both runs. The foliage distribution (solid curve) exhibits fades which are more than double those of the non-foliage case (dashed curve) for percentages of 50% and smaller. These results are consistent with 20 GHz signal tree measurements made previously for the static case by Vogel and Goldhirsh [7].

The effects of foliage on 20 GHz fading is very much different than those at UHF (870 MHz). Increases of fading of only approximately 25% were noted at 870 MHz [5]. The differences are explained in terms of the wavelength size relative to the spacing between branches (non-foliage case) and leaves (foliage case). At 870 MHz, the wavelength is approximately 35 cm and the spacing between branches is generally smaller than a wavelength. Hence, for both the foliage and non-foliage cases at 870 MHz, the dominant fading is due to the wood part of the tree. On the other hand at 20 GHz, the wavelength is 1.5 cm and the spacing between branches generally tends to be larger resulting in mitigated attenuation vis-a-vis the UHF non-foliage case. An analog to the above corresponds to the example of propagation through a conducting screen where minimal and maximum attenuation occur when the screen segments are large and small, respectively, relative to a wavelength. When the trees are in full foliage, the leave spacings are generally small relative to a wavelength for the 20 GHz transmissions, and hence the signal experiences substantially greater attenuation than for the non-foliage case.

5.0 Summary and Conclusions

Assuming communications between a satellite and a mobile vehicle with a 90% connectivity, fade margins at 20 GHz should be capable of compensating for 15-25 dB of tree shadowing for worst-case earth-satellite path aspects (Figures 6 and 8) when trees are in full

foliage, and 7-11 dB when trees are without leaves (Figures 8 and 6). The 20 GHz cumulative distributions show two characteristic segments separated by distinct curve inflections at approximately 3 dB (Figure 6). Fade levels smaller than 3 dB tend to be characterized by multipath fading, whereas larger fading is representative of attenuation due to shadowing. Large differences in the cumulative distributions were observed for the same tree runs during different seasons in which the trees were devoid of leaves (February) and were in full blossom (May) (Figure 8). For percentages of 50% and smaller, the fading levels with leaves were more than double those without leaves. This result is in contradistinction to the UHF case (870 MHz), where the foliage case resulted in only a 25% increase relative to the non-foliage case [5]. These differences are explained in terms of the relative wavelength size and the spacing between branches and leaves. Further efforts are planned to analyze a larger data set and address the objectives cited in Section 1.0

6.0 Acknowledgements

This effort was supported by NASA Lewis Research Center, Cleveland, Ohio under Contract N00039-91-C-0001 for the Applied Physics Laboratory, The Johns Hopkins University and Contract NAS3-26403 for the Electrical Engineering Research Laboratory, The University of Texas at Austin.

7.0 References

- 1 Goldhirsh, J. and W. J. Vogel, "Propagation Effects for Land Mobile Satellite Systems: Overview of Experimental and Modeling Results," *NASA Reference Publication 1274*, February, 1992.
- 2 Vogel, W. J., J. Goldhirsh, and Y. Hase, "Land-Mobile-Satellite Fade Measurements in Australia," Vol. 29, No. 1, pp. 123-128, Jan.-Feb., 1992.
- 3 Vogel, W. J., and J. Goldhirsh, "Mobile Satellite Propagation Measurements at L-Band Using MARECS-B2," *IEEE Trans. Antennas and Propagation*, Vol. 38, No. 2, pp. 259-264, February, 1990.
- 4 Goldhirsh, J., and W. J. Vogel, "Roadside Tree Attenuation Measurements at UHF for Land-Mobile Satellite Systems," *IEEE Trans. Antennas and Propagation*, Vol. AP-35, pp. 589-596, May, 1987.
- 5 Goldhirsh, J., and W. J. Vogel, "Mobile Satellite Fade Statistics for Shadowing and Multipath from Roadside Trees at UHF and L-Band," *IEEE Trans. Antennas and Propagation*, Vol. AP-37, No. 4, pp. 489-498, April, 1989.
- 6 Goldhirsh, J. and W. J. Vogel, "Mobile Satellite Propagation Measurements from UHF to K Band, *Proceedings of the 15th AIAA International Communications Satellite Systems Conference*, 28 February-3 March, 1994, San Diego, California, pp. 913-920.
- 7 Vogel, W. J., and J. Goldhirsh, "Earth-Satellite Tree Attenuation at 20 GHz; Foliage Effects," *IEE Electronics Letters*, Vol. 29, No. 18, 2 Sept. 1993.

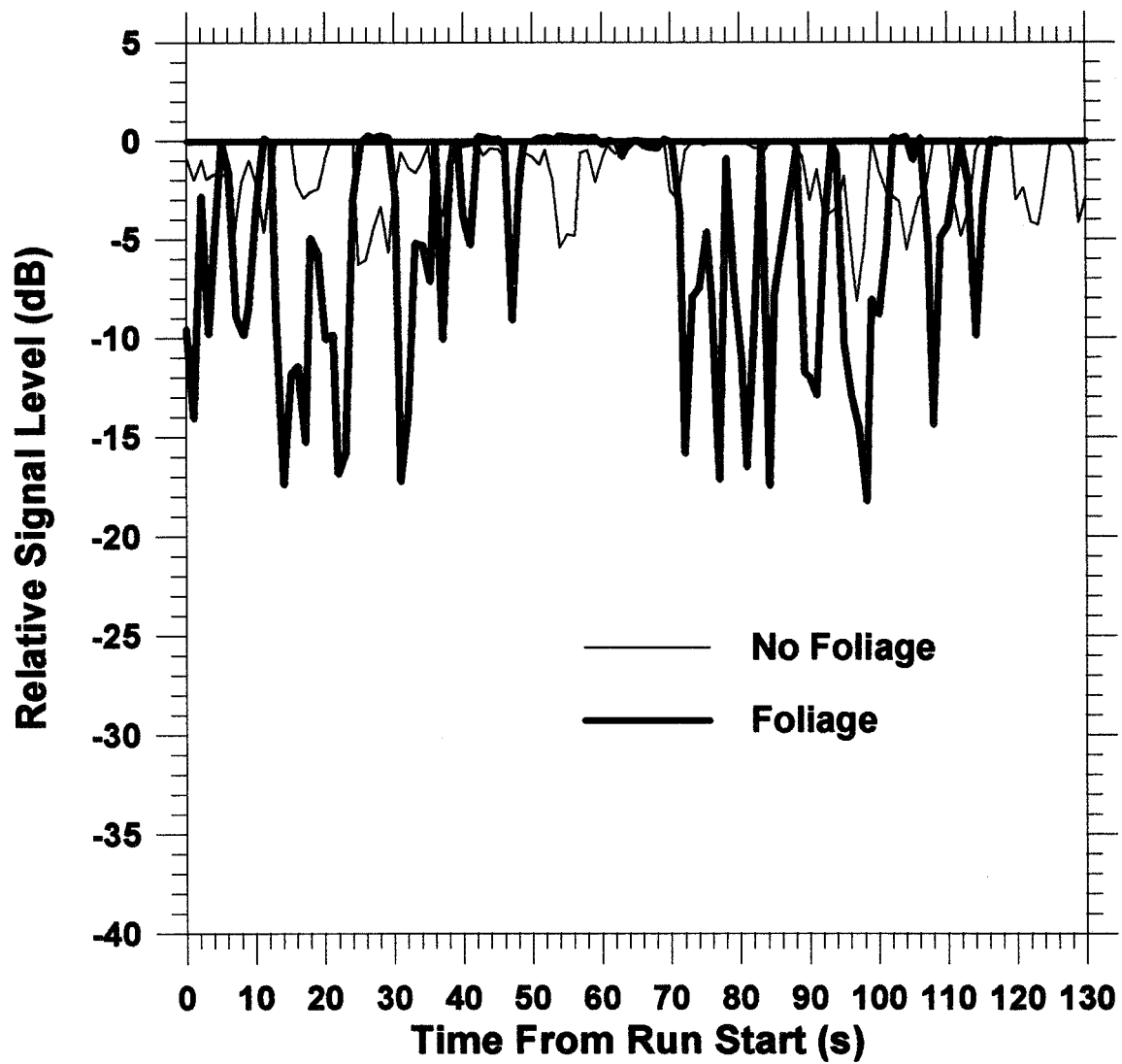


Figure 7: Comparison of average signal time-series runs for the full foliage (thick curve) and no foliage (thin curve) cases for 42nd Street run in Austin, Texas.

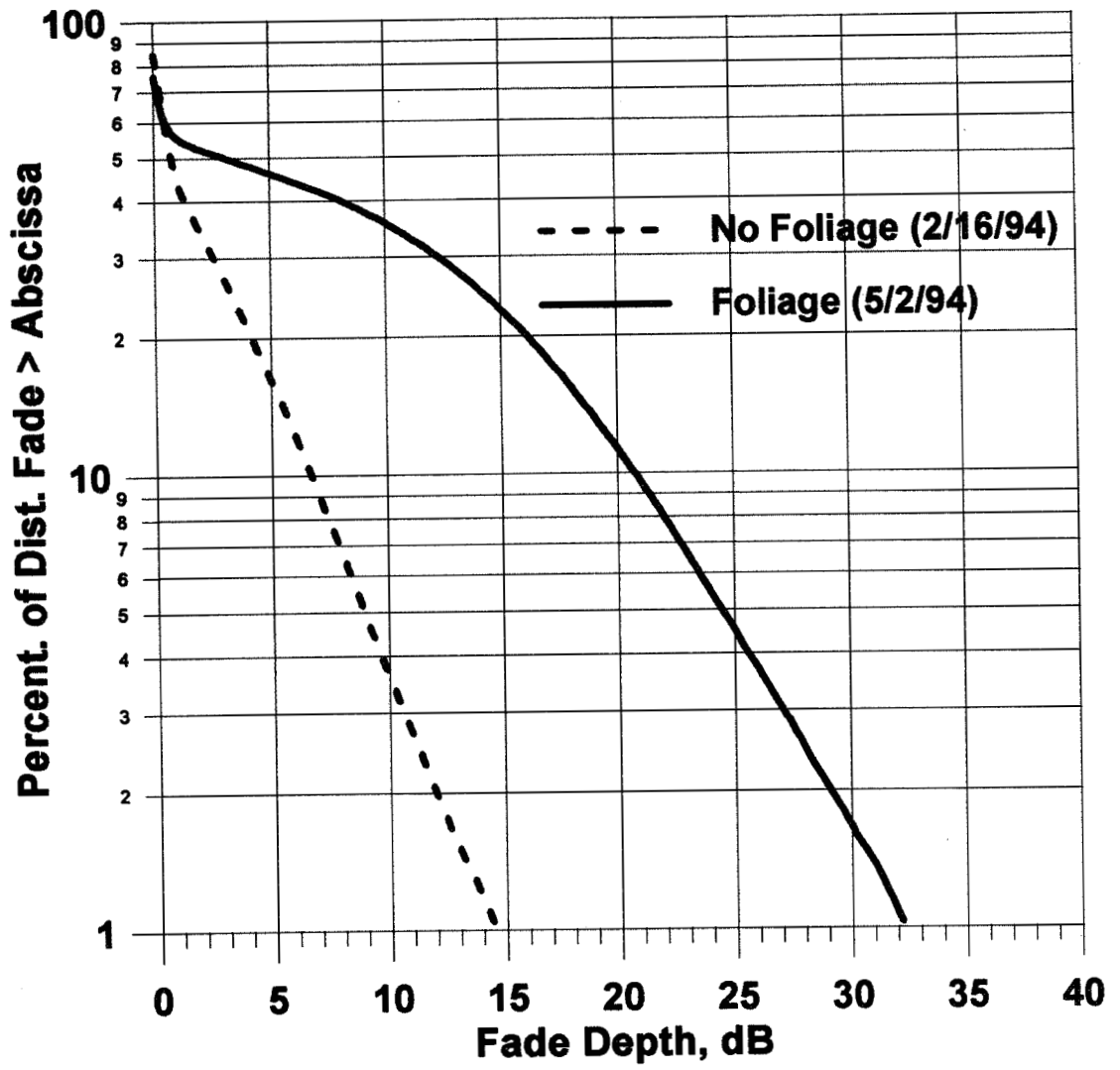


Figure 8: Cumulative distributions for foliage (thick curve) and non-foliage (thin curve) cases for 42nd Street run in Austin, Texas.

SLANT PATH L- AND S-BAND TREE SHADOWING MEASUREMENTS

Wolfhard J. Vogel and Geoffrey W. Torrence
Electrical Engineering Research Laboratory
The University of Texas at Austin
Austin, Texas 78758, USA

349296

p. 7

Abstract - This contribution presents selected results from simultaneous L- and S-Band slant-path fade measurements through a Pecan, a Cottonwood, and a Pine tree employing a tower-mounted transmitter and dual-frequency receiver. A single, circularly-polarized antenna was used at each end of the link. The objective was to provide information for personal communications satellite design on the correlation of tree shadowing between frequencies near 1620 and 2500 MHz. Fades were measured along 10 m lateral distance with 5 cm spacing. Instantaneous fade differences between L- and S-Band exhibited normal distribution with means usually near 0 dB and standard deviations from 5.2 to 7.5 dB. The Cottonwood tree was an exception, with 5.4 dB higher average fading at S- than at L-Band. The spatial autocorrelation reduced to near zero with lags of about 10λ . The fade slope in dB/MHz is normally distributed with zero mean and standard deviation increasing with fade level.

I. INTRODUCTION

Several proposed personal satellite communications systems in the 1610-1626.5 and 2483.5-2500 MHz bands envision employing CDMA modulation, for which high system efficiency requires keeping every user's signal power in the transponder at a similar level. Propagation effects such as tree shadowing, terrain multipath, and obstacle blockage, however, impose variations on each user's power level and therefore may require mitigation. One way of achieving this is through active transmitter power control, which could be most conveniently implemented by setting the power to be transmitted using the known received signal level. This method also has the benefit of not requiring hub-station feed-back with its inherent round-trip delay of at least several tens of milliseconds.

Multi-frequency propagation measurements of roadside tree fading have previously been reported for UHF and L-Band [1,2] and at UHF, L-Band and S-Band [3]. In these measurements, however, spatially separated receiving antennas were used for each band, allowing only statistical comparisons between the power levels observed at each frequency. Also, the propagation data were obtained at just a single frequency in each band. This experiment differs in two key aspects. It used a single aperture at both ends of the dual-frequency transmission link and it generated data in either fixed- or swept-cw modes, thus permitting a deterministic comparative assessment of the temporal, spatial, and frequency structure of the received power levels at L- and S-Band. In addition, data were obtained for co-polarized and cross-polarized reception, although at separate times.

II. EXPERIMENTAL SETUP

The measurement system consists of a dual-frequency sweeping transceiver located in a van, a 20 m crank-up transmitter tower mounted to the van, and a wired remote receiving antenna, filter, and preamplifier mounted on a linear positioner. A simplified block diagram of the transmitter and receiver is shown in Figure 1. The signals at L- and S-Band are generated as the upper and lower sidebands mixing products of a stable 2055 MHz oscillator combined with a tracking generator. After the mixing stage, the two signals are separated and leveled to account for differences in system and spreading losses at the two frequencies, with the objective of achieving approximately equal powers in the final receiver stage. Before transmission through a single, wideband, cavity-backed conical spiral antenna on top of the tower, the signals are recombined and amplified. The system can be operated in two modes: (1) constant cw-tone mode for measuring time series data and (2) swept cw-tone mode for measuring the frequency variability of the channel. In Mode 1, the tracking generator frequency is set to 437 MHz, resulting in

test frequencies of 1618 and 2492 MHz. These frequencies are approximately centered in the up- and down-link LEO bands. In Mode 2, the tracking generator frequency sweeps ± 100 MHz centered on 375 MHz, resulting in simultaneous sweeps over the 1580-1780 MHz and 2330-2530 MHz ranges. All frequencies in the transmitter are phase-coherent with a stable 10 MHz reference oscillator.

The receiving antenna is of the same type as the transmitting antenna, but alternately a left- or right-hand polarized antenna can be used. All antennas have a 3 dB beamwidth of about 90° at both frequency bands. The received signals are high-pass filtered, low-noise amplified, and returned through a 100 m long cable to the equipment in the measurement van. The processed Mode 1 output is a power level time series with a 0.01 s sampling rate. Mode 2 processing results in frequency spectra over 160 MHz with about 1 MHz resolution obtained in 0.1 s sweep duration. The outer 20 MHz regions of each spectrum are not used to eliminate edge effects due to the digital signal processing. The advantage of this dual-frequency system implementation is that it allows making simultaneous dual-band measurements through shared antennas with a single-channel receiver.

The receiver positioner holds the receiving antenna on a computer-controlled linear motion arm. The motion can be along any direction and over a range of 80 cm. When the axis of motion is vertical, as during the clear-path calibrations, the antenna moves from 1.8 to 2.6 m above the ground, when it is horizontal, the axis is 1.4 m above ground. To take data over a wider range of receiver positions, the entire positioner has to be moved in 80 cm increments.

III. MEASUREMENT DETAILS

Measurements were made through three different trees, a Pecan (*carya illinoensis*), a Cottonwood (*populus deltoides*), and a Loblolly Pine (*pinus taeda*) during the Fall of 1993, while the deciduous trees were still in leaf. Photographs of the test trees are shown in Figure 2, in which the deciduous trees have been pictured without foliage to make the limb-structure visible. All trees had heights in the range from 9 to 12 m, maximum crown diameters of 6 to 10 m, and trunk diameters of 0.25 to 0.38 m. The transceiver-van was parked on one side of the tree under test with the transmitter tower fully extended. The receiver positioner was placed on the opposite side of the tree and moved along a horizontal arc centered on the tower base such that the propagation path would initially be clear of obstructions and subsequently, after moving laterally, pass through the tree crown. With each tree about 1/3 of the way from the receiver to the transmitter tower, the foliage was in the far-field of both antennas in all cases. Only the Pine was entirely free-standing, the other two trees had neighbors of the same species on one side. At the end of the measurement arc, therefore, only the signal in the Pine tree case returned to the clear-path level. In that case, the projected shadow zone from the part of the crown intercepted by the transmission was nearly 10 m wide at the receiver. The path elevation angle was 30° for the Pecan, 23° for the Cottonwood, and 20° for the Pine tree.

The two deciduous trees stand on lawns at the J. J. Pickle Research Campus in Austin, Texas, and have buildings, roads, and chain-link fences in their vicinity; the coniferous tree grows on a park-road median in the 'Lost Pines' area of Bastrop, Texas, and has no adjacent buildings or fencing. Mode 2 (swept-cw; frequency spectrum) data were obtained in 5 cm steps over 13 m for the Pecan and Pine and over 10.5 m for the Cottonwood. Mode 1 (fixed-cw; time series) data were taken at every sixteenth Mode 2 position (every 80 cm), when the receive antenna positioner was moved. Although the antennas have large beamwidths, the transmitter antenna was repointed repeatedly (by remote control) to track the moving receiver direction to within $\pm 10^\circ$. The measurements were performed in dry weather with variable light to gusty winds. After completing a measurement set with one receiving antenna, the set was repeated with the opposite receiving polarization.

The measurements also included a calibration procedure. During calibration, the co-polarized receiver antenna was scanned vertically while measuring the power levels at 16 points. This was repeated at four horizontal positions separated by 0.3 m along the beginning of the measurement arc with clear path conditions. At each frequency, the clear-path co-polarized power level was obtained as the (linear) mean over the 64 (16×4) measurements, thus averaging out the effects of specular ground reflections and diffuse multipath reflections from the nearby trees and/or buildings. All results are presented relative to the co-polarized clear-path level.

IV. RESULTS

A. Spatial Variability

Figure 3 shows the spatial variation of power levels received at 1618 and 2492 MHz with co-polarized and cross-polarized antennas as a function of position in the shadow of the Pecan, Cottonwood, and Pine trees. As mentioned, the Pine was the only free-standing tree, allowing the power levels at both ends of the horizontal scan to return to the clear-path value. For the Pecan and Cottonwood, the crowns of other trees were intercepted by the line-of-sight path towards the end of each scan. Some general observations can be made from inspecting the plots. As expected, there is a macroscopic correlation between power levels at the two frequencies, i.e., both L- and S-Band are attenuated by the intervening tree, with 5 to 20 dB being typical values. On a finer distance scale, however, there are many deviations from equality which will be quantified below. Co-polar fades at the two frequencies occupy a similar range for the Pecan and Pine, but fades for the Cottonwood tend to be deeper at S-Band than at L-Band. Cross-polar power levels do not show as much dependence as the co-polar levels on how much tree crown is intercepted at each position, they range from -10 to -25 dB relative to the co-polar clear-path level and this indicates a relatively constant illumination intensity with scattered, depolarized power at locations both to the side and behind each tree. Considering that data for RHC and LHC polarizations were obtained successively, the cross-polar isolation, i.e. difference of co-polar and cross-polar levels, was not derived. The mean, median, minimum, maximum and standard deviation for each tree, polarization, and frequency band are summarized in Table 2. Also given in the table are the differences between the received power levels at 1618 and 2492 MHz.

Figure 4 summarizes the difference between the two frequencies for co-polarization, in the form of normal probability plots. The straight line in the graph represents a best fit normal approximations. The data show the Cottonwood difference and overall somewhat normal behavior.

To assess the sensitivity of received power to horizontal motion, the L-Band spatial autocorrelation functions for each tree have been plotted in Figures 5. The autocorrelation decreases from near 0.9 at the measurement increment to near 0 at a lag of about 10 wavelengths. Similarly, the S-Band autocorrelation was found to decrease to near 0 with a lag of about 20 to 30 wavelengths. The difference between the two frequency bands may be due to the dominant effect of the size of the tree branches as opposed the wavelengths on the scattering patterns.

B. Frequency Variability

Variations of the received power levels were measured at L- and S-Band frequencies over a 160 MHz span for all trees and polarizations. Both co- and cross-polarization show similar characteristics. A close-up analysis of the frequency selectivity of tree fading (Pine) for the allocated mobile satellite service bands from 1600 to 1626.5 (upper panel) and 2483.5 to 1500 MHz (lower panel) revealed that at low fade levels only limited frequency selectivity is exhibited.

An indicator for frequency variability is the fade slope vs. frequency, defined by

$$fadeslope = \frac{dS}{dF} \quad (\text{dB/MHz}) \quad (1)$$

where dS is the change in received co-polarized power over the measurement frequency resolution dF , i.e. 1.55 MHz for the Pecan and 1.0 MHz for the Cottonwood and Pine trees. The fade slope was found to depend on the mean signal level. Regression coefficients for the standard deviation of the fade slope as a function of the mean signal level have been derived using

$$\sigma_{fs} = a + b\mu + c\mu^2 \quad (2)$$

where σ_{fs} is the standard deviation of the fade slope and μ is the mean signal level over the frequency span. The mean fade slope is very nearly equal to zero in all cases. The coefficients for the standard deviation are given in Table 1.

Table 1: Regression Coefficients for the Standard Deviation of the Fade Slope as a Function of the Mean Signal Strength.

	L-Band			S-Band		
	a	b	c	a	b	c
Cottonwood	0.137	-0.006	0.002	0.113	-0.041	0.003
Pecan	0.253	0.027	0.004	0.230	-0.082	0.003
Pine	0.253	0.046	0.005	0.231	-0.063	0.003

For a 5 dB faded signal at L-Band the central 90% of the fade slopes (± 1.96 Std. Dev.) are within a 0.7 dB/MHz range, compared to a 1.9 dB/MHz range at S-Band. All fade slope distributions were tested for normality using the Kolmogorov-Smirnov procedure and for most the hypothesis of normality could not be rejected. Probability plots of L- and S-Band fade slopes for selected Pine tree measurements with mean signal levels of -5, -10, -15, and -20 dB are shown in Figure 6 to illustrate the approximately normal fade slope distribution.

V. CONCLUSIONS

We have observed the space and frequency domain structures of L- and S-Band simulated satellite power levels in both circular polarizations after slant-angle propagation through three representative trees. Our findings are:

- Power level variations at L-Band are not correlated with those measured simultaneously at S-Band in any of the domains. Spatial means of power levels are weakly correlated, however.
- Power level variability in the three domains increases with increasing attenuation, because as the direct signal is reduced, multipath scattering has a greater effect.
- Power levels as a function of space measured with a cross-polarized receiving antenna were in the mean 15 to 20 dB below the co-polarized clear-path level and more variable than the co-polarized signal. These characteristics were independent of position with respect to the tree.
- The fade slope with frequency, measured in dB/MHz, was found to be normally distributed with zero mean and standard deviation increasing with fade level.

ACKNOWLEDGMENT

This effort was supported jointly by Loral Aerospace Corporation and the NASA Propagation Program under Contract JPL 956520, via the JPL Technology Affiliates Program, coordinated by the JPL Commercialization Office.

REFERENCES

- [1] Vogel, W. J. and U. S. Hong "Measurement and Modeling of Land Mobile Satellite Propagation at UHF and L-Band," *IEEE Transactions on Antennas and Propagation*, Vol. 36, No. 5, May 1988
- [2] Goldhirsh, J. and W. J. Vogel, "Mobile Satellite System Fade Statistics for Shadowing and Multipath from Roadside Trees at UHF and L Band," *IEEE Transactions on Antennas and Propagation*, Vol. 37, No. 4, April 1989
- [3] Bundrock, A. and R. Harvey, "Propagation Measurements for an Australian Land Mobile-Satellite System," *Proc. of International Mobile Satellite Conference*, Pasadena, California, pp. 119-124, May 1988

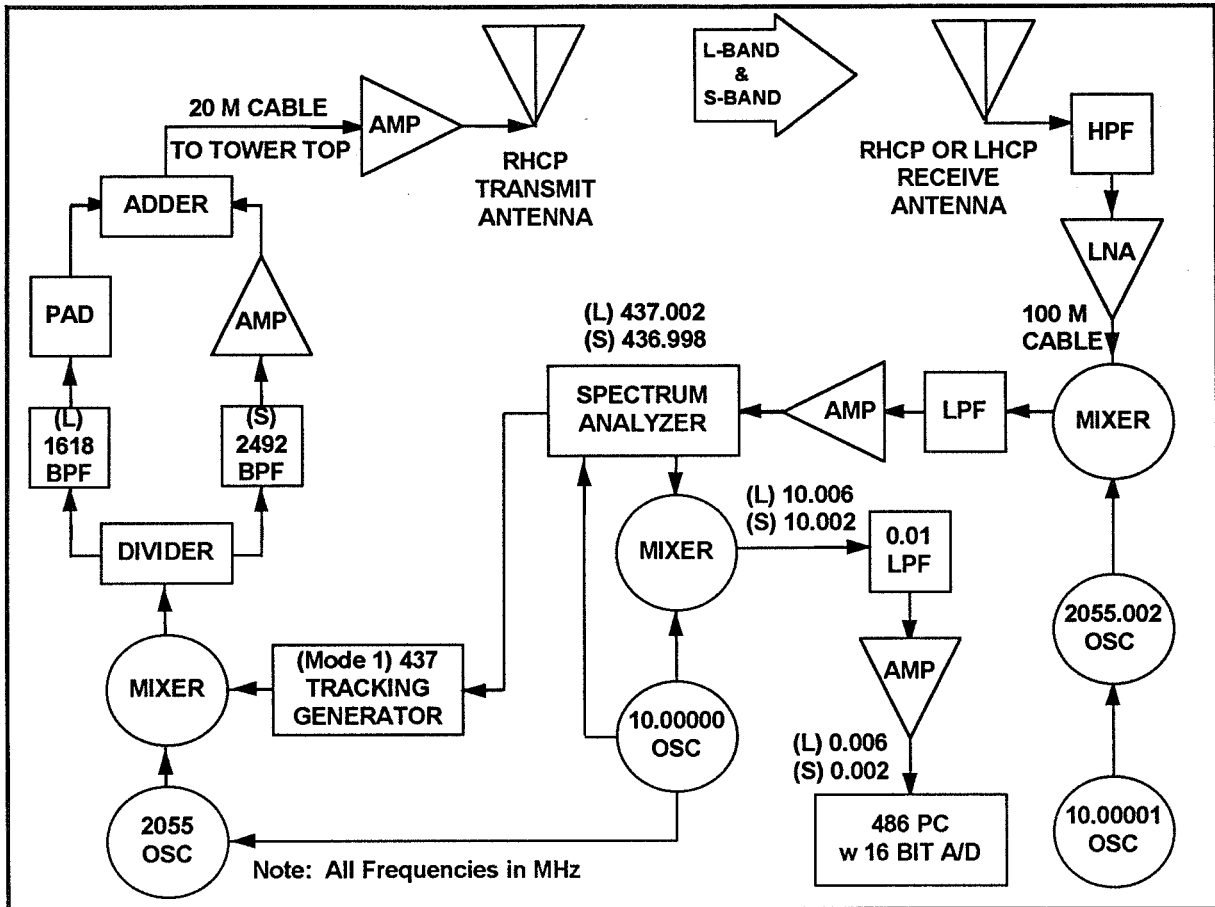


Fig. 1 Simplified blockdiagram of the dual-frequency measurement system.

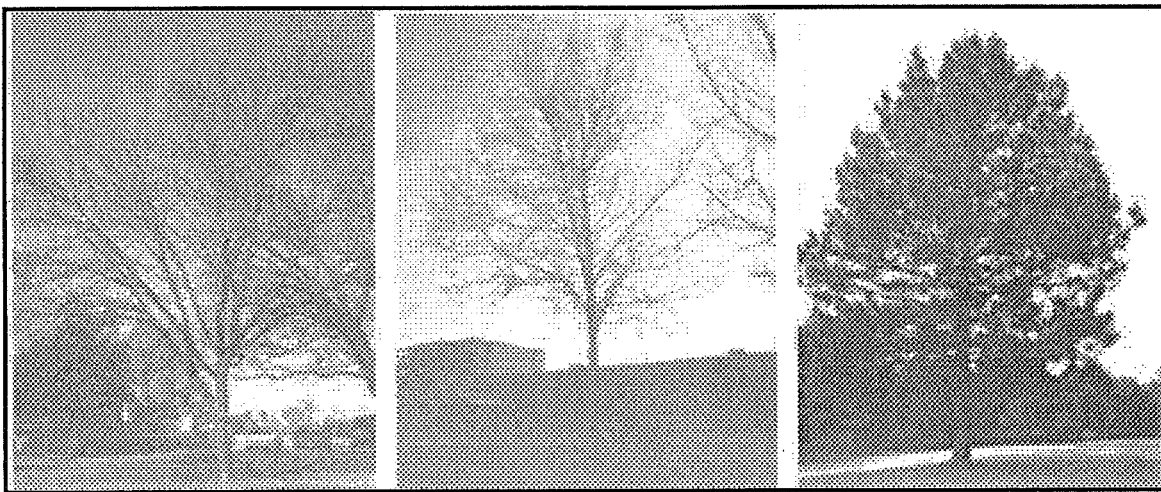


Fig. 2 Photographs of the Cottonwood, Pecan, and Pine trees (left to right). Although bare deciduous trees are shown, the data were taken while they were still in leaf.

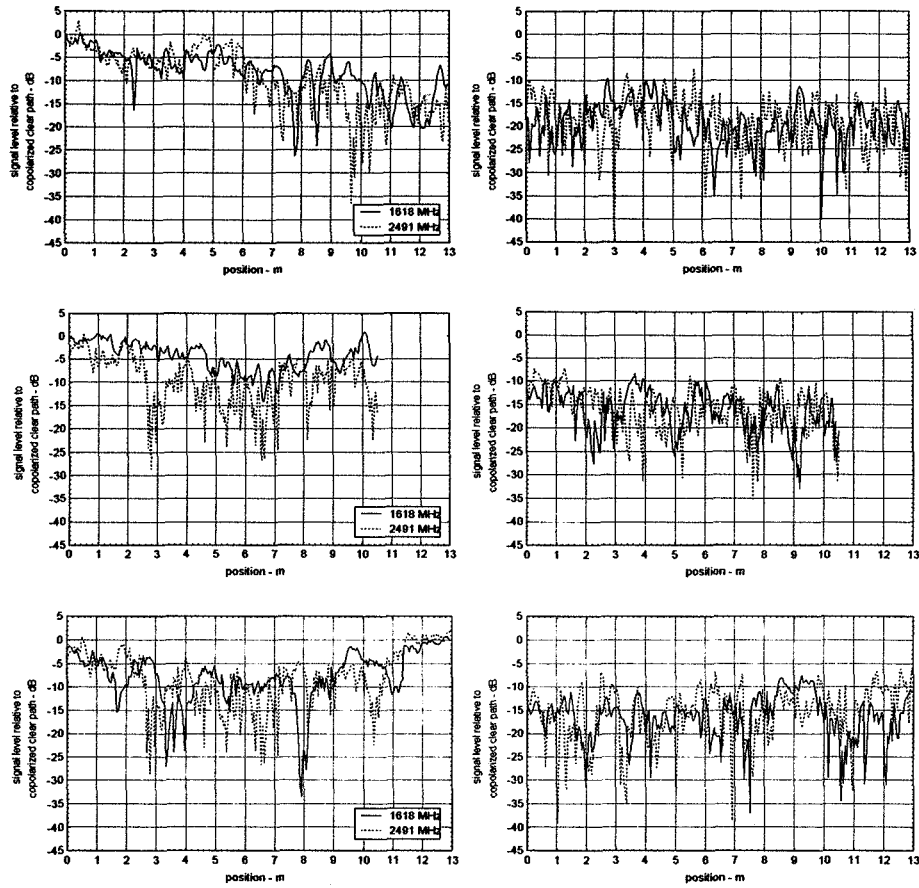


Fig. 3 Signal Levels received at 1618 Mhz (solid line) and 2491 Mhz (dashed line) with a co-polarized (left panels) and a cross-polarized (right panels) antenna versus position in the shadow of a Pecan (top), Cottonwood (middle), and Pine (bottom) tree .

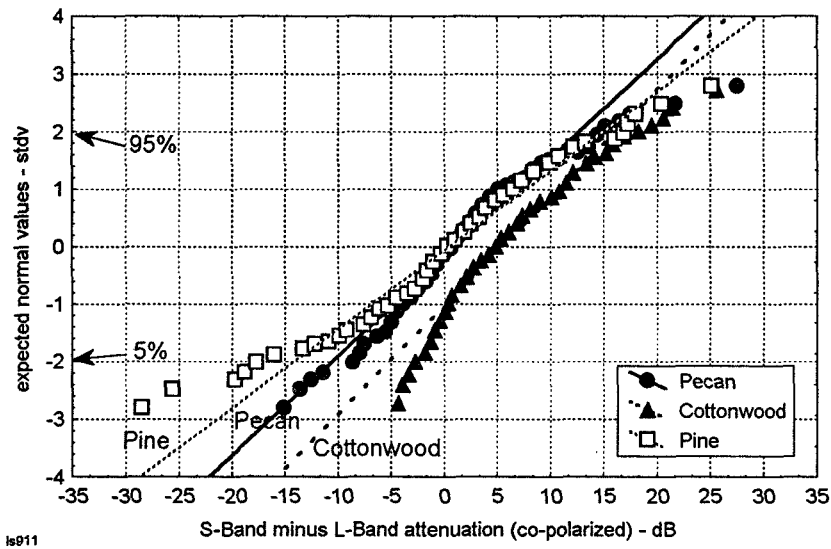


Fig. 4 Probability plot of the difference between S-Band and L-Band co-polarized attenuation for the three trees.

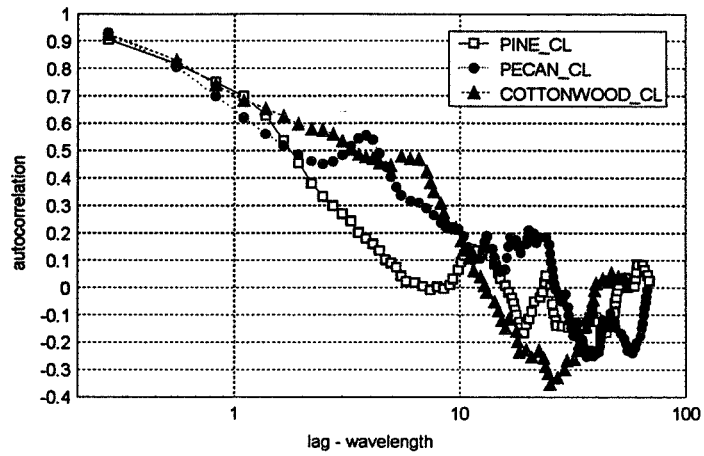


Fig. 5 The autocorrelation of the spatial data as a function of lag (in wavelengths) for the co-polarization case at L-Band.

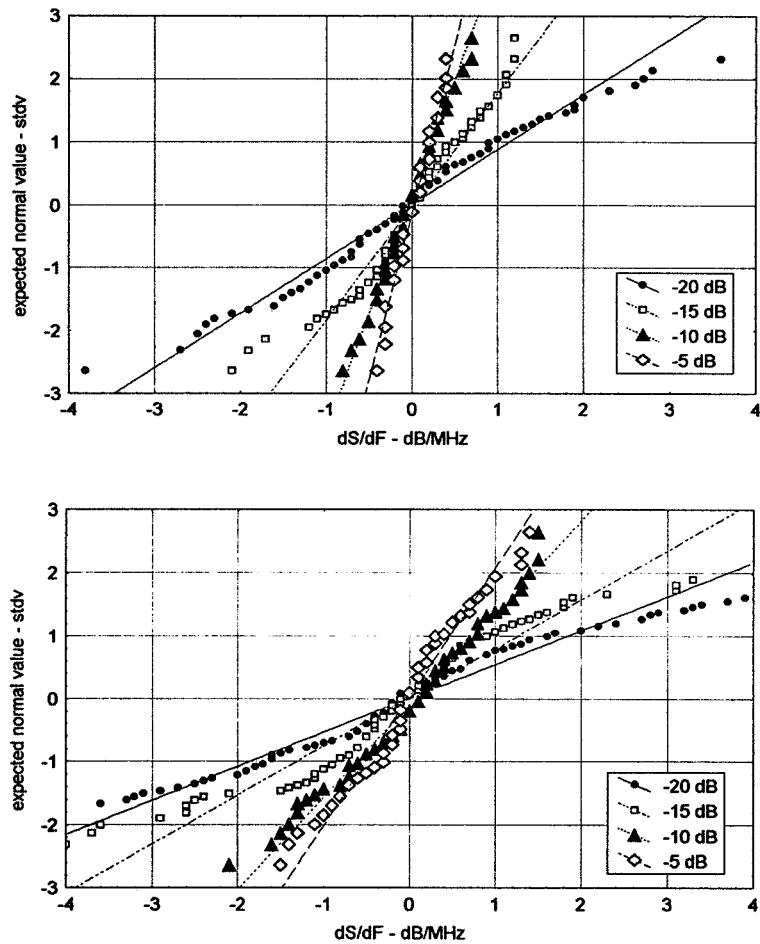


Fig. 6 Probability plot of co-polarized fade slopes for the Pine tree exhibit near-normal behavior at L-Band (top) and S-Band (bottom).

1995108265

349298

P.5

Photogrammetric Mobile Satellite Service Prediction

Riza Akturan
Wolfhard J. Vogel

Electrical Engineering Research Laboratory
The University of Texas at Austin

ABSTRACT - Photographic images of the sky were taken with a camera through a fisheye lens with a 180° field-of-view. The images of rural, suburban, and urban scenes were analyzed on a computer to derive quantitative information about the elevation angles at which the sky becomes visible. Such knowledge is needed by designers of mobile and personal satellite communications systems and is desired by customers of these systems. The 90th percentile elevation angle of the skyline was found to be 10°, 17°, and 51° in the three environments. At 8°, 75%, 75%, and 35% of the sky was visible, respectively. The elevation autocorrelation fell to zero with a 72° lag in the rural and urban environment and a 40° lag in the suburb. Mean estimation errors are below 4°.

reasonably well understood. However, efforts of generalized modeling of the effects engendered by these three states and of producing reliable system performance predictions are hampered by the requirement that one needs to possess knowledge of the environment near the MES at a large number of possible locations. Obtaining such knowledge by carrying out systematic measurement campaigns using real or simulated satellite transmissions is very time-consuming and expensive. A more convenient method of determining the incidence of the three fade states is needed.

INTRODUCTION

All economically feasible mobile satellite communications systems, whether targeted for vehicular or personal use, and whether operating at UHF-, L-, S-Band frequencies or higher, are ultimately performance limited by the three non-exclusive propagation states in which the mobile earth station (MES) can find itself. The MES can either be

1. shadowed by trees,
2. blocked by mountains and structures such as buildings and overpasses,
3. or receiving multipath echoes generated by reflectors such as terrain and buildings or scatterers such as trees, utility poles and building edges.

Many measurement campaigns have been carried out in the US and abroad [1] to establish a database for system simulation as well as for statistical and analytical performance prediction. At this time, the significant environmental parameters and their electromagnetic repercussions are

Previous measurements of optical brightness along the line-of-sight to a balloon-borne transmitter have demonstrated that there exists a statistical linkage between fading and optical intensity [2]. We expand on that *point measurement* by developing a system that evaluates full images of the upper half-sphere and determines where the sky is clear, where it is shadowed by vegetation, and where it is blocked. Assuming that enough images are acquired in a specified environment, one can develop statistics for the three fade states as a function of elevation and azimuth angles and these can later be combined with state-dependent propagation data to produce realistic simulated data or attenuation statistics. The image data can then be used, for instance, to predict fading probability as a function of elevation angle or to forecast the diversity gain of a satellite system employing satellite diversity, all in a chosen environment.

The ultimate goal of this research is to develop automatic image-recognition

techniques that can be employed to derive personal and mobile satellite propagation predictions from video images taken with a fish-eye lens. If fully successful, then images will be analyzed in real time at the 30 frames/second rate to identify each fade state as a function of azimuth and elevation. Our near-term goal was more modest. We acquired and analyzed images taken through a fish-eye lens with a 35 mm still-camera in a rural, a suburban, and two urban locales. Instead of the ternary classification, we restricted the recognition to just two states: clear sky or not.

In the following, we present a brief system description, some information about the detection algorithms, and the statistical results from the initial batch of images. We will also outline the future direction of our efforts and offer some conclusions.

SYSTEM DESCRIPTION

The images described and evaluated here were acquired with a 35 mm camera and a fisheye lens with a full 180° field of view. The camera was always mounted on a leveled tripod and a compass was used to align the top of each frame towards north. The photos were taken on slide film and the slides were scanned into a personal computer. The fisheye lens has also been coupled to a video camera in a system which can be mounted to the roof of a car and includes a GPS receiver, which provides location, vehicle speed and heading. At a later time, the video recordings will be played into a frame-grabber for analysis.

SOFTWARE ALGORITHMS

The current binary image-identification software starts by reducing the color image to a 256-level gray-scale and then unwrapping it, i.e., converting from a circular image in which the zenith direction is at the center to a rectangular coordinate system in which zenith is at the top of the frame. The second

derivative of the histogram of the image, after filtering, is then used to estimate the gray-level threshold value separating sky and objects [3]. After this procedure, a binary image can be produced from which all the results presented here are derived. These are, for each image, (1) the elevation angle of the sky-line as a function of azimuth [4] and (2) the fraction of visible sky as a function of elevation. As a visual aid to interactively assess the validity of the calculations, a contour line representing the first result can be drawn over the rectangular picture.

To derive ternary instead of just binary object identification, more processing will be required and is now under development. This includes object locating, and object identification, edge-detection, low-pass filtering, derivatives and statistical algorithms. Artificial intelligence procedures [5] will be used for classifying the objects into three separate groups. Pre-defined templates [6] have been avoided for the sake of faster execution. The result of these additional procedures will be a clear-shadowed-blocked image description, which will allow us to calculate the necessary statistics for a given image.

INITIAL RESULTS

Four environments in Central Texas were sampled, rural, suburban, and two cities (Austin and San Antonio). In the rural case, a total of 43 images were acquired along a sparsely tree-lined rural route connecting a small city to Austin, about one picture per mile on the side of the road. In the suburban case, 90 images were taken in a neighborhood with mostly single-story houses and relatively young trees, which did not form canopies over the road. In the central business districts (CBD) of Austin and San Antonio, 119 and 105 images were taken, respectively. For the last three cases, pictures were taken mid-block and at block corners with the camera at the street-side of the sidewalk.

After determining the skyline for each image (see the example in Fig. 1), i.e., the highest elevation angle separating sky and terrestrial objects at each azimuth, statistics of skyline angles were calculated and averaged over all images in a particular environment. As expected, the average elevation angle of the skyline at each location strongly depends on the environment. The mean, 90th percentile and maximum elevation for the rural, suburban and Austin CBD environs are shown in Figs. 2 to 4.

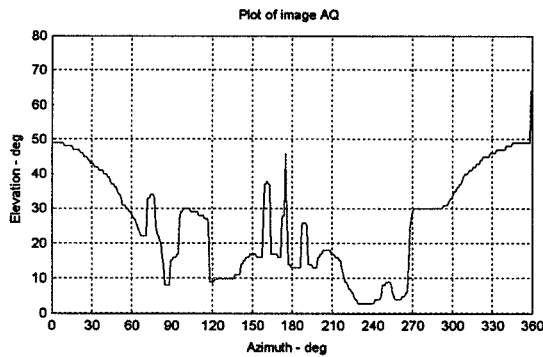


Fig. 1 Example of a skyline image (SA)

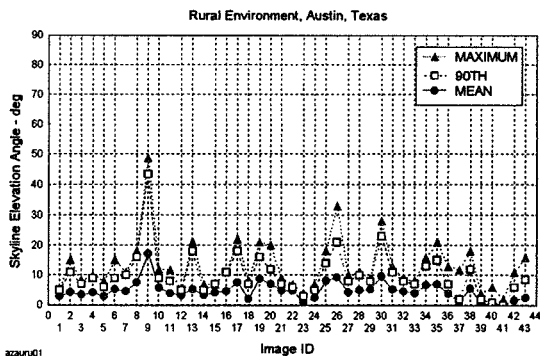


Fig. 2 Rural image statistics

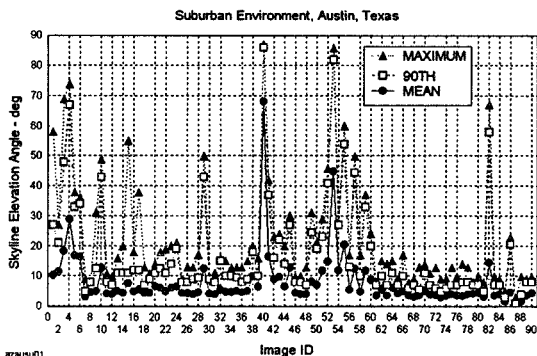


Fig. 3 Suburban skyline statistics

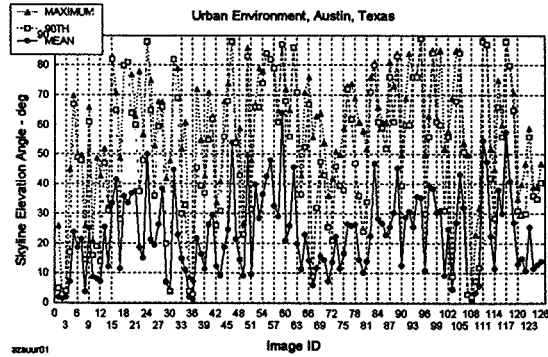


Fig. 4 Austin urban skyline statistics

After averaging over all images in a specific environment, the overall statistics in Table 1 are found.

Environment	Mean (°)	STD (°)	90% (°)
rural	4.8	3.5	10.0
suburban	7.9	5.9	16.9
Austin CBD	23.5	18.8	50.5
San Ant. CBD	26.4	18.1	52.6

The 90th percentile of the skyline elevation angle follows a normal distribution, except in the suburban case.

The percentage of sky visible at a given elevation angle has been plotted in Figs. 5 and 6 for the Austin rural and urban environments. In the former, at 8° elevation over 75% of the sky are visible (median), in the latter, only 35% of the sky can be seen.

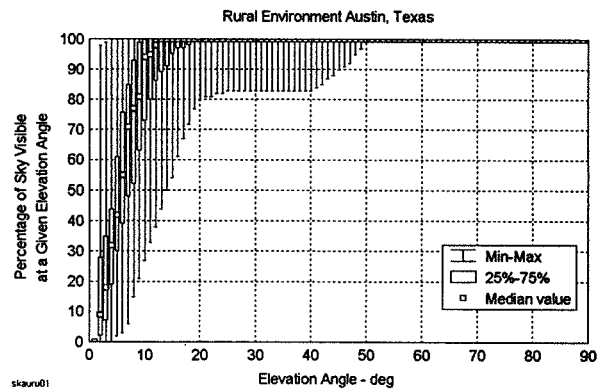


Fig. 5 Percent sky visible in rural Austin

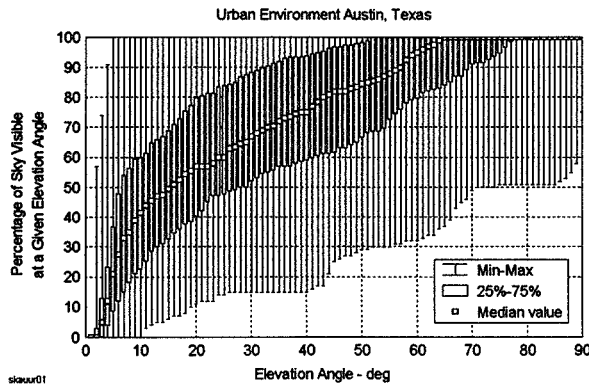


Fig. 6 Percent sky visible in urban Austin

The elevation angle distributions of the skylines for selected images (all with nearly environment-average mean elevation) are depicted in Fig. 7. The lognormal distribution has been fit to each histogram, but the fit is not very close.

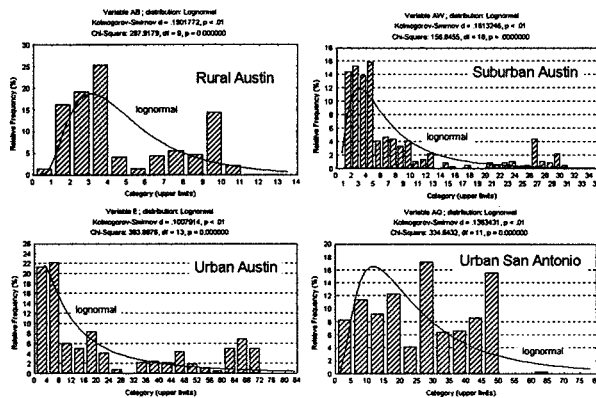


Fig. 7 Skyline elevation histograms

The autocorrelation of the skyline elevation vs. azimuth angle for the above selected images falls off linearly to 0 at a lag of near 70°, except for the suburban environment, where it reduces to 0 at 40° lag. Figs. 8 and 9 show the autocorrelation for the suburban and urban Austin environs. The skyline image is also inserted into these graphs.

Autocorrelation Function for Suburban Austin Image AW

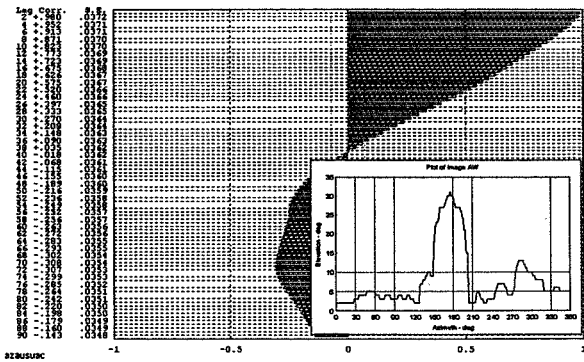


Fig. 8 Suburban skyline autocorrelation

Autocorrelation Function for Urban Austin Image E

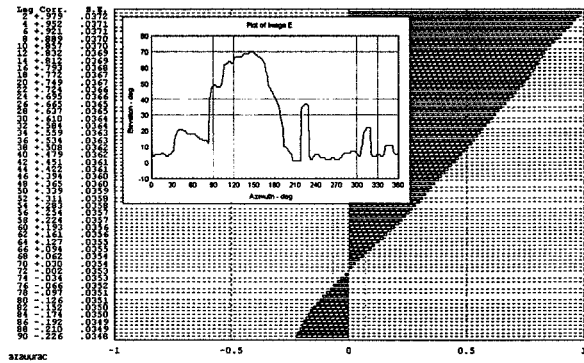


Fig. 9 Urban skyline autocorrelation

Errors in recognizing the correct skyline elevation angles were quantified by comparing the elevations found by the program with those derived by manually tracing selected images with a mouse. The difference, although to some degree dependent on the skill of the mouse operator, is taken as the error of the image recognition program. Fig. 10 summarizes the errors on an image-by-image basis, Fig. 11 depicts an overall box plot of the error for the four environments. The largest error, with a mean of 4° and a standard deviation of about 3°, arose in the suburban environment. As this was the only environment with significant numbers of trees, the error can be explained by the uncertainty in defining the tree-sky boundary.

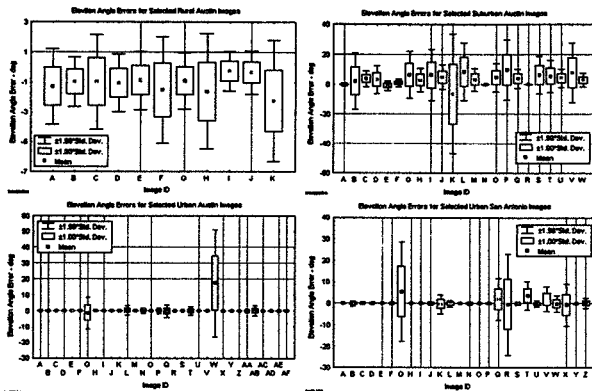


Fig. 10 Elevation errors by image

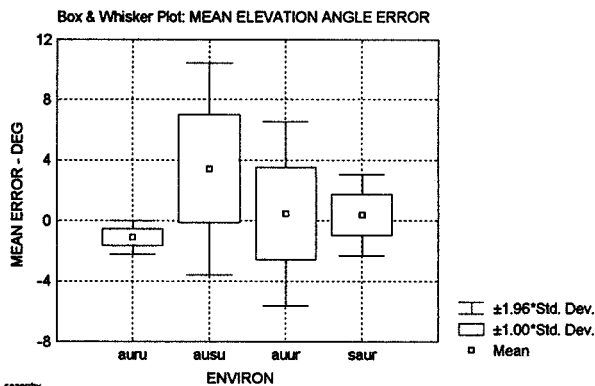


Fig. 11 Mean elevation angle error

The error is nearly normally distributed for the rural and suburban environments, but not for the urban ones.

FUTURE EFFORTS

Efforts are now under way to derive a full three-state description of images. This will allow the connection of image data to propagation statistics for simulation and prediction purposes.

The programming is being done in C on a 486-33 platform. Most of the effort so far has been directed towards developing reliable algorithms as opposed to achieving processing speed. The analysis in this report took 120 s/image. Recompiling the program as written to run on a Sun workstation and a Cray supercomputer resulted in time reductions to 7.2 and 13.5 s/image, respectively. This is not yet fast enough to analyze video at a 30 images/s rate, but

speed optimization has yet to be implemented.

CONCLUSION

Photogrammetry will provide a powerful tool to derive service predictions for personal and mobile satellite communications systems in any environment. Initial results, although restricted to a binary description of sky visibility, are encouraging and should be of immediate use to satellite system designers. However, more work needs to be done to derive a ternary description for clear, shadowed and blocked states. This will allow one to combine satellite orbit design with propagation statistics to predict performance such as fade probability or diversity gain in a specified environment.

ACKNOWLEDGMENTS

This effort was supported jointly by Loral Aerospace Corporation, Motorola Inc., and the NASA Propagation Program.

BIBLIOGRAPHY

- [1] Goldhirsh, J. and W. J. Vogel, "Propagation Effects for Land Mobile Satellite Systems: Overview of Experimental and Modeling Results," *NASA Reference Publication 1274*, February 1992
- [2] Vogel, W. J. and U. S. Hong, "Measurement and Modeling of Land Mobile Satellite propagation at UHF and L-Band," *IEEE Trans. Ant. and Prop.*, Vol. 36, No. 5, May 1988
- [3] Bovik, A. C., "Digital Image Processing," The University of Texas at Austin, Austin, Texas, 1991
- [4] Birdwell, B. N., "Design of an optical sensor system to replicate the effects of signal blockage and shadowing on satellite signal propagation," M.S. Thesis, The University of Texas at Austin, Austin, Texas, May 1993
- [5] Rosenfeld, A. and A. C. Kak, *Digital Picture Processing*, Academic Press, Inc., Orlando, Florida, 1982
- [6] Bichsel, M. and P. Seitz, "Object recognition with optimum neural networks," in *Neural Networks*, Lisboa, P. G. J., Ed., Chapman & Hall, London, 1992

19210723

349300

8.16

PROPAGATION CONSIDERATIONS FOR THE ODYSSEY SYSTEM DESIGN

Hau H. Ho, Odyssey Systems Engineer
TRW, Inc.
One Space Park
Redondo Beach, CA 90278

ABSTRACT

This paper presents an overview of the Odyssey system with special emphasis given to the link availability for both mobile link and feeder link. The Odyssey system design provides high link availability, typically 98% in the primary service areas, and better than 95% availability in other service areas. Strategies for overcoming Ka-band feeder link rain fades are presented. Mobile link propagation study results and summary link budgets are also presented.

SYSTEM OVERVIEW

The Odyssey system, illustrated in Figure 1, provides high quality world wide personal and mobile communication services on a regional basis. The system consists of three segments: space, ground, and handset. The gateways interconnect with both public switched telephone networks (PSTN), and other gateways. The Odyssey handset is a dual mode; it can access either the Odyssey system or a terrestrial cellular network. These services include voice and data provided by a constellation of medium-altitude Earth orbiting (MEO) satellites.

Communication can be established either between mobile and fixed users or between pairs of mobile users. A fixed user is one who is connected to the terrestrial network. Mobile customers use inexpensive hand-held transceivers. These transceivers are self-powered and generally require only 0.5 watts of average transmitted power to provide quality communications. The Odyssey handset provides at least 60 minutes talk time and 24 hour standby.

Each satellite is placed in circular orbit at an altitude of 10354 Km. There are three orbit planes inclined at 52° to the equatorial plane. Deployment of the satellites permits phased introduction service. After only three launches, in which two satellites are launched in each plane, service can be provided to three major service regions. The Odyssey six satellite constellation coverage is shown in Figure 2. After three more launches for a total of 12 satellites, service can be expanded to all populated regions of the

Earth with dual coverage to most regions. Figure 3 shows 12-satellite constellation coverage.

Each satellite covers more than 14.5% of the earth surface with a multibeam antenna that divides its coverage area into thirty-seven contiguous beams. Figure 4 shows the mobile link antenna pattern. The mobile link antennas are fixed mounted to the satellite body. The attitude control system orients the satellite to ensure constant coverage of land mass and coastal areas. Pointing can be reprogrammed by ground control to ensure optimized coverage of the desired service areas.

The frequency bands for satellite-based personal mobile communications were designated at the 1992 WARC. In L-band, 1610 to 1626.5 MHz is allocated for the mobile return link from the user to satellite. The mobile forward link from satellite to user is allocated 2483.5 to 2500 MHz in S-band. However, 11.35 MHz bandwidth of L-band and 16.5 MHz bandwidth at S-band are our current baseline design. Circular polarization is used for mobile link. Part of Ka-band, 19.7 to 20.2 GHz and 29.5 to 30.0 GHz are used for the feeder return link (from the satellite to gateway) and feeder forward link (from gateway to satellite), respectively. Linear polarization is used for the feeder link.

Each beam carries an 11.35 MHz in L-band, which is fully reused in each beam. The forward link includes a Ka-band link from the gateway to the satellite and an S-band link down to the users. The return link from the user to the gateway includes an L-band link to the Odyssey satellite and a Ka-band link down to the gateway. The satellite payload functions as a simple bent pipe, frequency translating transponder. For the mobile link, each satellite has a 37-beam antenna with 38° field-of-view (40° field-of-coverage). The S-band, downlink from the satellite to users, provides a dynamic capacity distribution through the use of five matrix amplifiers. This allows each beam to support up to 20% of satellite capacity. In the feeder link, each satellite has three independent steerable antennas for both transmitting and receiving signals to/from multiple gateways. Each Ka-band antenna can support the full satellite capacity on each polarization. Each satellite weighs 1971 Kg at launch, and the solar array provides 3126 watts of power. Capacity is 2800 voice circuits per satellite. The payload block diagram is shown in Figure 5.

In order to provide the global coverage, the Odyssey system requires only seven earth stations. Each earth station is equipped with four 7 m tracking antennas. Three of the antennas are used simultaneously to communicate with three of the in-view satellites. The fourth antenna can be used to acquire an additional satellite, or used for satellite handover, or it can be used as a diversity function in the event of heavy rainfall. Separation between the antennas must be at least 10 Km to provide the diversity function. Depending on the location of the earth station, site diversity may or may not be needed.

Odyssey provides high quality voice service. Our design is based on the 4.8 kbps IMBE (Improved Multi-Band Excitation) speech codec. DVSI is the owner and developer of this codec; INMARSAT, OPTUS/ AUSSAT, and MSAT selected IMBE as their voice coding standard. The BER of 10^{-3} will provide high voice quality with 3.5 MOS (Mean Opinion Score)

Digital data from 2.4 kbps to 19.2 kbps is also accommodated in the Odyssey system. The transmitted data rate depends on the modem. The handset supports rates up to 2.4 kbps. A more powerful modem is required for the higher data rates. Digital data service quality is assured by maintaining system BER of 10^{-5} or better.

The Odyssey system uses spread spectrum CDMA techniques for forward and return links that are compatible with the service as initially authorized for these L and S-bands.

COMMUNICATION SYSTEM SIGNAL PARAMETERS

To provide high voice quality, low hand held transmitted EIRP, and minimum time delay, the following signal parameters are used in the Odyssey system:

- * Digitally encoded voice data : 4800 bps
- * Channel error correction encoding
 - ** Convolutional code rate = 1/3, k=7
 - ** Soft decision decoding
- * Concatenated code is used in digital data transmission
- * Modulation: filtered OQPSK
- * Access method: CDMA
- * Spread bandwidth: 2.5 MHz
- * Voice duty cycle: 50%
- * Required $\frac{E_b}{N_0}$: 4.0 dB, including 1.5 dB implementation loss
- * Digital data rates: 2.4 kbps, 4.8 kbps, 9.6 kbps, and 19.2 kbps. Handset supports up to 2.4 kbps; 4.8 kbps, 9.6 kbps and 19.2 kbps are supported by higher power modem.

SUMMARY COMMUNICATION SIGNAL REQUIREMENTS

Mobile Link

- Satellite L& S-bands
 - * Received frequency: 1610 to 1621.35 MHz
 - * Transmitted frequency: 2483.5 to 2500 MHz
 - * Polarization: circular
 - * Number of beams: 37 beams
 - * Field-of-view: 38° (40° field-of-coverage)
 - * Average G/T over field-of-view ≥ 1.0 dB/K

- * S-band transmitted EIRP ≥ 53.4 dBW
- * Satellite capacity: 2800 users
- * Each beam can support up to 20% satellite capacity
- Handset transceiver
 - * Received frequency: 2483.5 to 2500 MHz
 - * Transmitted frequency: 1610 to 1621.35 MHz
 - * Polarization: circular
 - * Handset received G/T: -22.1 dB/K
 - * Handset transmitted EIRP: 0.2 dBW

Feeder Link

- Satellite Ka-band
 - * Received frequency: 29.5 to 29.76 GHz
 - * Transmitted frequency: 19.7 to 19.96 GHz
 - * Polarization: linear
 - * Three independently steerable Ka-band antenna spot beams
 - * Each beam can support up to 2800 users on each polarization
 - * Satellite receiving G/T ≥ 6.1 dB/K
 - * Satellite transmitting EIRP ≥ 48.5 dBW
- Earth station
 - * Earth station receiving G/T: 32.5 dB/K
 - * Earth station transmitting EIRP: 85.7 dBW
 - * Polarization: linear
 - * Received frequency: 19.7 to 19.96 GHz
 - * Transmitted frequency: 29.5 to 29.76 GHz

LINK BUDGETS

Odyssey system uses the spread spectrum CDMA techniques, the link budgets must take into account both the receiver noise and interference noise from other users. The multiple access interference in the link budget is the total interference power including other users in the same beam and the users from other beams. We assume that power control is used for both forward and return links with 2 dB accuracy.

Return Link

The return link is a link from a mobile user to the earth station through the satellite. The return link includes an L-band link from the mobile users to the satellite and Ka-band downlink to the gateways through three independent Ka-band steerable antennas.

The data from a mobile user is transmitted according to a conventional CDMA scheme. The total noise is the sum of thermal noise and the mutual interference noise. The return link budgets are shown in Table 1

Forward Link

The forward link includes a Ka-band link from the gateway to the satellite and an S-band link down to the users. The forward link receives its signal at 30 GHz from either of the three Ka-band antennas, which provides coverage of regions of interest. The signal is bandpass filtered, fed to a low noise amplifier (LNA), and down converted to an intermediate frequency (IF).

The LNA outputs are 18 and 19 (one from vertical, and the other one from horizontal pol.) way power divided by the total of 37 separate signals for the downlink beams. The 37 separate signals are then filtered, upconverted to S-band prior to amplification by solid state amplifier for transmission to the users on the 37 beam S-band antenna.

The forward link uses orthogonal CDMA. The summary link budgets are shown in Table 2.

LINK MARGIN AND LINK AVAILABILITY

Mobile Link Margin

Return Link (User-to-satellite): The minimum return link margin for the Odyssey system is 6 dB for elevation angles above 20°. If the users are uniformly distributed over field-of-view, then the user's elevation angles are greater than 30° more than 95% of the time. Indeed, elevation angles are greater than 55° more than 50% of the time. The percent of time versus elevation angles is shown in Figure 6.

The return link margin depends on the user elevation angle, which in turn is a function of the user position within the field-of-view. The user position is measured by the angular displacement from the satellite antenna boresight. The return link margin and user elevation angle are shown as a function of user position in the field-of-view in Figure 7.

In order to provide the service down to 20° elevation angle, 40° field-of-view will need to be pointed up to 2 degrees off nadir. More than 50% of the time, the link margins are greater than or equal to 8.0 dB, which can be seen by combining the data in Figures 6 and 7.

Forward link (Satellite-to-Users): To achieve both high capacity and good voice quality, the Odyssey system employs power control for both forward and return link. Also, to account for the fact that the mobile users may be in a disadvantaged location due to antenna contours, vegetation loss, or fading, the satellite Tx S-band RF power allocated to each user can be varied depending on its need. The required forward link propagation margin is calculated as follows:

- The users are uniformly distributed in a beam and over field-of-view.
- The elevation angle distribution at several latitudes is shown in Figure 8.
- Propagation statistics representative of suburban areas were used to calculate the required propagation margin [1].
- The attenuation at S-band can be estimated as:

$$A(2.5 \text{ GHz}) \approx A(1.6 \text{ GHz}) \sqrt{\frac{2.5 \text{ GHz}}{1.6 \text{ GHz}}} \quad \text{dB}$$

Where A(1.6 GHz) is the attenuation at 1.6 GHz

Based on all the listed conditions above, the required average down link margin is approximately 4.0, which is allocated in the forward link budgets.

Mobile Link Availability

The Odyssey system design will provide reliable, excellent quality phone service, typical 98% availability in all primary service areas, and better than 95% availability in other service areas. The Odyssey link availability is calculated by using statistics obtained from experimental data [2]& [3]. The link availability is calculated as follows:

- For each location, link availability is defined as the percentage of time that the return link margin exceeds the propagation loss.
 - * Available return link margin is a function of satellite elevation angle and user location within satellite beam.
 - * Probability distribution of propagation loss is a function of satellite elevation angle.
 - * Link availability is determined by integrating over joint distribution of satellite elevation angle and user location.
- Satellite elevation angle histograms were developed for a number of user locations, based on the highest satellite providing directed coverage of each location.
- Propagation statistics representative of suburban areas were used to calculate the required propagation margin.

Twelve cities at different latitudes were selected from the highest demand regions to obtain a measure of Odyssey system availability. Figure 9 shows that the calculated availability for 12 satellites is typically 98% . Six Odyssey satellites provide single satellite availability between 91% and 97%.

Feeder Link Margin And Link Availability

The Odyssey system needs only seven earth stations to provide worldwide coverage. Seven potential earth stations are Los Angeles (CA - USA), Buenos Aires (Argentina), Fucino (Italy), Cape Town (South Africa), Ahmadabad (India), Yamaguchi (Japan), and Sydney (Australia).

The forward link, earth station-to-satellite operates at 30 GHz band. The return link, satellite-to-earth station operates at 20 GHz band. In our baseline design, each satellite has three transmitted and three received antennas. Dual polarization is used in the feeder link. Each antenna, and each polarization can support the full system capacity. In terms of power, each antenna (dual pol.) can support twin system capacity. 10 dB and 18 dB rain margins are allocated for the return, and the forward link, respectively. Since the Ka-band is used for the feeder link, rain attenuation is very severe in some locations depending on their rain zones.

The minimum required link availability is 99.5% (43.8 hours outage per year), with 99.9% (8.76 hours outage per year) as a goal. In order to achieve this requirement, some earth stations may need site diversity.

In our link availability calculations, we assume the following conditions:

- Global rain attenuation model is used.
(Global Model Rain Attenuation Prediction Technique as Described in Propagation Effects Handbook for Satellite Systems Design, NASA Reference Publication 1082 (04), February 1989 by Louis J. Ippolito)
- Horizontal polarization is used.
- The Hodge model is used here for diversity gain and site separation
- Rain zone of seven potential earth stations are:
 - @ Los Angeles, CA: rain zone F
 - @ Buenos Aires, Argentina: rain zone D
 - @ Fucino, Italy: rain zone D2
 - @ Cape Town, South Africa: rain zone C
 - @ Ahmadabad, India: rain zone G
 - @ Yamaguchi, Japan: rain zone D
 - @ Sydney, Australia: based on the map, it is very difficult to see that Sydney either belongs to rain zone D or C. In this paper, we will present the link availability of two rain zones.

The link availability calculations are based on the following:

- Percent of time versus elevation angle.
- The feeder link availability is the minimum link availability of two links namely forward and return links.
- 10 dB and 18 dB are allocated for rain attenuation in the return and forward link, respectively.

Figure 10 shows the percent of time that a given elevation angle is exceeded at the Los Angeles earth station. For example, an elevation angle of $\geq 20^\circ$ occurs 82% of the time.

However, to compute the availability of particular location, the probability density function (pdf) of elevation angle is required. The pdf of Los Angeles earth station is shown in Figure 11. Figure 12 shows the diversity gain versus site separation. The curves of link availability versus elevation angle (with and

without site diversity) are shown in Figure 13 that were computed for Los Angeles earth station based on the Global Model Rain Attenuation.

The feeder link availability for Los Angeles earth stations is founded by combining data from Figures 11 & 13 and the result is shown in Table 3. Table 3 contains the feeder link availability of the other six earth stations.

With no site diversity, the link availability for most earth stations is greater than or equal to 99.75%, which meets our requirements, except for Ahmadabad, India. With site diversity, an earth station at Ahmadabad achieves 99.6% link availability, and greater than 99.9% for the other six earth stations. There is only one earth station at Ahmadabad, India, that needs site diversity. In this analysis, horizontal polarization was assumed. If vertical polarization is used, then the rain attenuation is less, and achieved link availability is higher. Also, we assume satellite Ka-band antenna supports full satellite capacity on each polarization.

Note that, the calculated rain attenuation is based on the current available global data. The actual rain attenuation will be calculated with local rain rate data or in some cases testing may be needed.

ADVANTAGES

Odyssey, with its medium Earth orbit altitude and direct coverage of mobile link antenna patterns, has several advantages over other proposed systems as listed below:

- Time delay of Odyssey is more acceptable than the GEO satellite
- The Odyssey satellite moves only 1° per minute so that they seem almost fixed to the user.
- With medium Earth orbit altitude, the user's elevation angle is higher than LEO satellite. Indeed, the elevation angles are greater than 30° and 55° more than 95% and 50% of the time, respectively.
- With directed pointing, most users can be served by a single beam of one satellite for the duration of telephone conversation.

CONCLUSION

The Odyssey system design will provide high link availability, typical 98% link availability for mobile link, and more than 99.5% link availability for feeder link. This system will deliver an excellent voice quality, and digital data transmission.

ACKNOWLEDGMENT

The author gratefully acknowledges the work of the Odyssey team, especially Drs. M. Horstein, E. Siess, E. Wiswell and Mr. Tom Zeiller for their comments and suggestions.

REFERENCES

- [1] J. Goldhirsh, W. J. Vogel, "An Overview of Results Derived from Mobile-Satellite Propagation Experiments," International Mobile Satellite Conference, Ottawa, 1990.
- [2] J. Goldhirsh, W. J. Vogel, "Mobile Satellite System Fade Statistic for Shadowing and Multipath from Roadside Trees at UHF and L-band," IEEE Transactions on Antennas and Propagation, April, 1989.
- [3] Lutz, et al, " The Land Mobile Satellite Communication Channel - recording, Statistics, and Channel Model," IEEE Transactions on Vehicular Technology, May 1991.

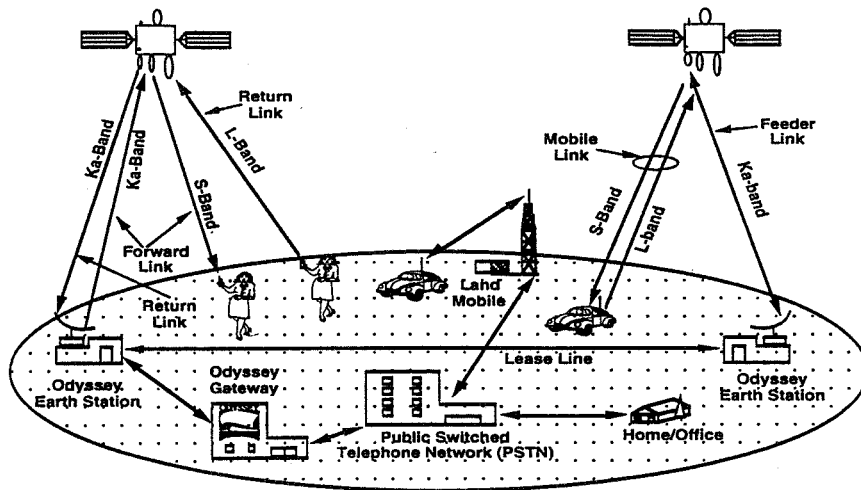


Figure 1: Odyssey Communication Concept

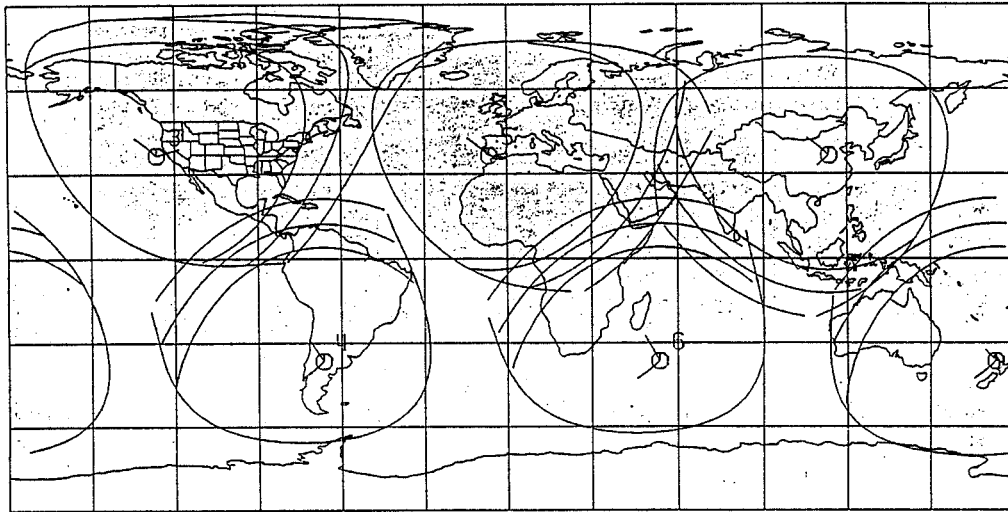


Figure 2: Example Of 6-Satellite Coverage

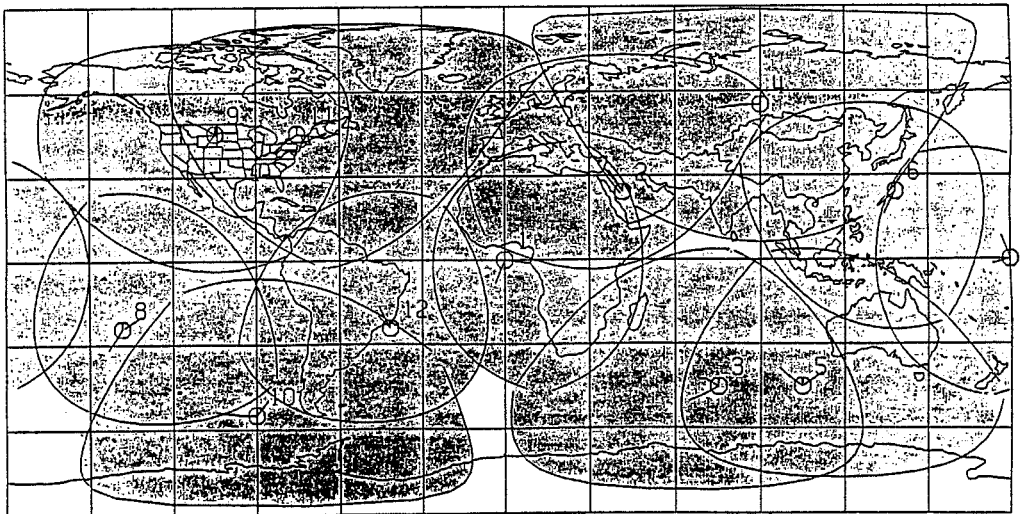


Figure 3: Example Of 12-Satellite Coverage

Table 1: Summary Return Link Budgets

ASSUMPTIONS			
USER-TO-SATELLITE LINK		SATELLITE-TO-EARTH STATION	
FREQUENCY	1.62 GHz	FREQUENCY	19.83 GHz
HANDSET TRANSMIT ERP	0.2 dBW	TOTAL TRANSMIT ERP	48.5 dBW
VOICE DUTY CYCLE	50.0 %	SYSTEM CAPACITY	2800.0 Users
AVERAGE ELEVATION ANGLE	55.0 degrees	MINIMUM ELEVATION ANGLE	10.0 Degrees
NUMBER OF USERS/25 MHz CHANNEL	150.0 Users	EARTH STATION GT	32.6 dBK
NOISE FIGURE OF POWER CONTROL	2.0 dB	SATELLITE C/N ₀	15.0 dB
SPACECRAFT GT	1.0 dBK		

PARAMETERS	CLEAR	RAIN	UNIT
HANDSET ERP	0.2	0.2	dBW
PATH LOSS	177.5	177.5	dB
ATMOSPHERIC LOSS	0.2	0.2	dB
RAIN LOSS	0.0	-0.0	dB
POLARIZATION LOSS	0.5	0.5	dB
REQUIRED UPLINK MARGIN	6.0	6.0	dB
FX SIGNAL	-184.1	-184.1	dBW
SPACECRAFT GT	1.0	1.0	dBK
BOLTZMANN'S CONSTANT, k	-228.6	-228.6	dBK-Hz
UPLINK RECEIVED C/N ₀	45.5	45.5	dB-Hz
UPLINK DEGRADATION DUE TO MM (α)	4.1	4.1	dB
UPLINK RECEIVED C/N ₀ (α)	41.4	41.4	dB-Hz

PARAMETERS	CLEAR	RAIN	UNIT
TOTAL TRANSMIT ERP	48.5	48.5	dBW
RETRANSMITTED NOISE LOSS	7.9	8.0	dB
NUMBER OF USER	31.5	31.5	dB
EFFECTIVE ERP PER USER	9.1	9.1	dBW
PATH LOSS	201.6	201.6	dB
ATMOSPHERIC LOSS	0.6	0.6	dB
SCINTILLATION LOSS	0.4	0.4	dB
RAIN LOSS*	0.0	10.0	dB
POLARIZATION LOSS	0.1	0.5	dB
FX SIGNAL	-193.5	-203.9	dBW
EARTH STATION GT	32.6	32.6	dBK
BOLTZMANN'S CONSTANT, k	-228.6	-228.6	dBK-Hz
DOWNLINK RECEIVED C/N ₀	67.7	57.3	dB-Hz

COMBINED UPLINK & DOWNLINK			
PARAMETERS	CLEAR	RAIN	UNIT
UPLINK RECEIVED C/N ₀ (α)	41.4	41.4	dB-Hz
DOWNLINK RECEIVED C/N ₀	67.7	57.3	dB-Hz
SATELLITE C/N ₀ + SPURIOUS	51.8	51.8	dB-Hz
COMBINED C/N ₀ + N ₀	41.0	40.9	dB-Hz
DATA RATE (4.8 Kbps)	36.8	36.8	dB-Hz
RECEIVED E _{IR} (α)	4.2	4.1	dB
REQUIRED E _{IR} (α)	4.0	4.0	dB
EXCESS MARGIN (OVER 6 dB)	0.2	0.1	dB

NOTE: * INCLUDING NOISE TEMPERATURE INCREASE DUE TO RAIN
 ** INCLUDING 1.5 dB IMPLEMENTATION LOSS

Table 2: Summary Forward Link Budgets

ASSUMPTIONS			
EARTH STATION-TO-SATELLITE		SATELLITE-TO-USER	
FREQUENCY	28.63 GHz	FREQUENCY	2.49 GHz
TRANSMIT ERP (CLEAR)	67.3 dBW	TOTAL TRANSMIT ERP	53.4 dBW
TRANSMIT ERP (RAIN)	65.7 dBW	SYSTEM CAPACITY	2800.0 Users
SYSTEM CAPACITY	2800.0 USERS	VOICE DUTY CYCLE	50.0 %
VOICE DUTY CYCLE	50.0 %	AVERAGE USER ELEVATION ANGLE	55.0 Deg
UPLINK RAIN LOSS (ALLOWABLE)	18.0 dB	HANDSET GT	-22.1 dBK
SPACECRAFT GT	6.1 dBK	SATELLITE C/N ₀	14.0 dB

PARAMETERS	CLEAR	RAIN	UNIT
TRANSMIT ERP	67.3	65.7	dBW
NUMBER OF USERS	31.5	31.5	dB
EFFECTIVE TRANSMIT ERP PER USER	35.9	34.3	dBW
PATH LOSS	206.1	206.1	dB
ATMOSPHERIC LOSS	0.6	0.6	dB
SCINTILLATION LOSS	0.4	0.4	dB
RAIN LOSS*	0.0	18.0	dB
POLARIZATION LOSS	0.1	0.5	dB
FX SIGNAL	-170.3	-170.3	dBW
SPACECRAFT GT	6.1	6.1	dBK
BOLTZMANN'S CONSTANT, k	-228.6	-228.6	dBK-Hz
UPLINK RECEIVED C/N ₀	64.5	64.5	dB-Hz

PARAMETERS	CLEAR	RAIN	UNIT
TOTAL TRANSMIT ERP	53.4	53.4	dBW
RETRANSMITTED NOISE LOSS	0.4	0.4	dB
SIGNALING REQUIRED POWER (10%)	0.5	0.5	dB
NUMBER OF USER	31.5	31.5	dB
EFFECTIVE ERP PER USER	21.1	21.1	dBW
PATH LOSS	181.3	181.3	dB
ATMOSPHERIC LOSS	0.2	0.2	dB
RAIN LOSS	NA	0.1	dB
POLARIZATION LOSS	0.5	0.5	dB
REQUIRED AVERAGE DL MARGIN	4.0	4.0	dB
FX SIGNAL	-165.0	-165.0	dBW
HANDSET GT	-22.1	-22.1	dBK
BOLTZMANN'S CONSTANT, k	-228.6	-228.6	dBK-Hz
DOWNLINK SPURIOUS DUE TO MM	0.1	0.1	dB
DOWNLINK RECEIVED C/N ₀ (α)	41.5	41.4	dB-Hz

COMBINED UPLINK & DOWNLINK			
PARAMETERS	CLEAR	RAIN	UNIT
UPLINK RECEIVED C/N ₀	64.5	64.5	dB-Hz
DOWNLINK RECEIVED C/N ₀ (α)	41.5	41.4	dB-Hz
SATELLITE C/N ₀ + SPURIOUS	50.8	50.8	dB
COMBINED C/N ₀ + N ₀	41.0	40.9	dB-Hz
DATA RATE (4.8 Kbps)	36.8	36.8	dB-Hz
RECEIVED E _{IR} (α)	4.2	4.1	dB
REQUIRED E _{IR} (α)	4.0	4.0	dB
EXCESS MARGIN (OVER 4 dB)	0.2	0.1	dB

NOTE: * INCLUDING 1.5 dB IMPLEMENTATION LOSS

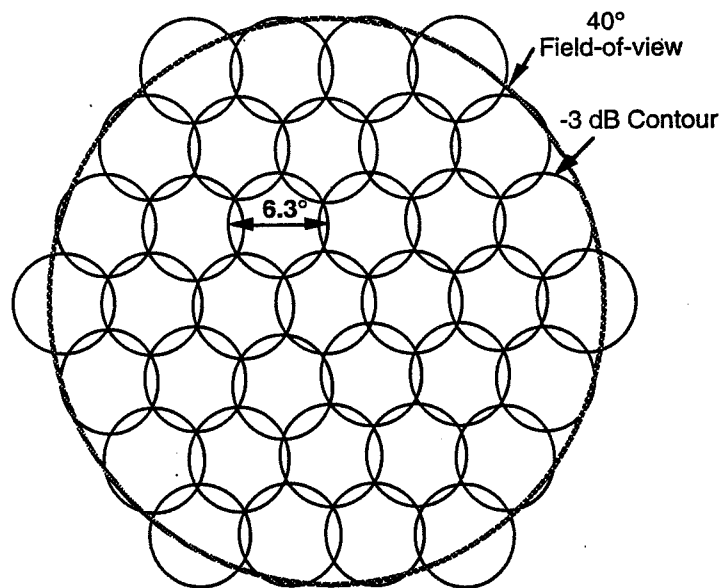


Figure 4: L And S-Band Antenna Beam Pattern

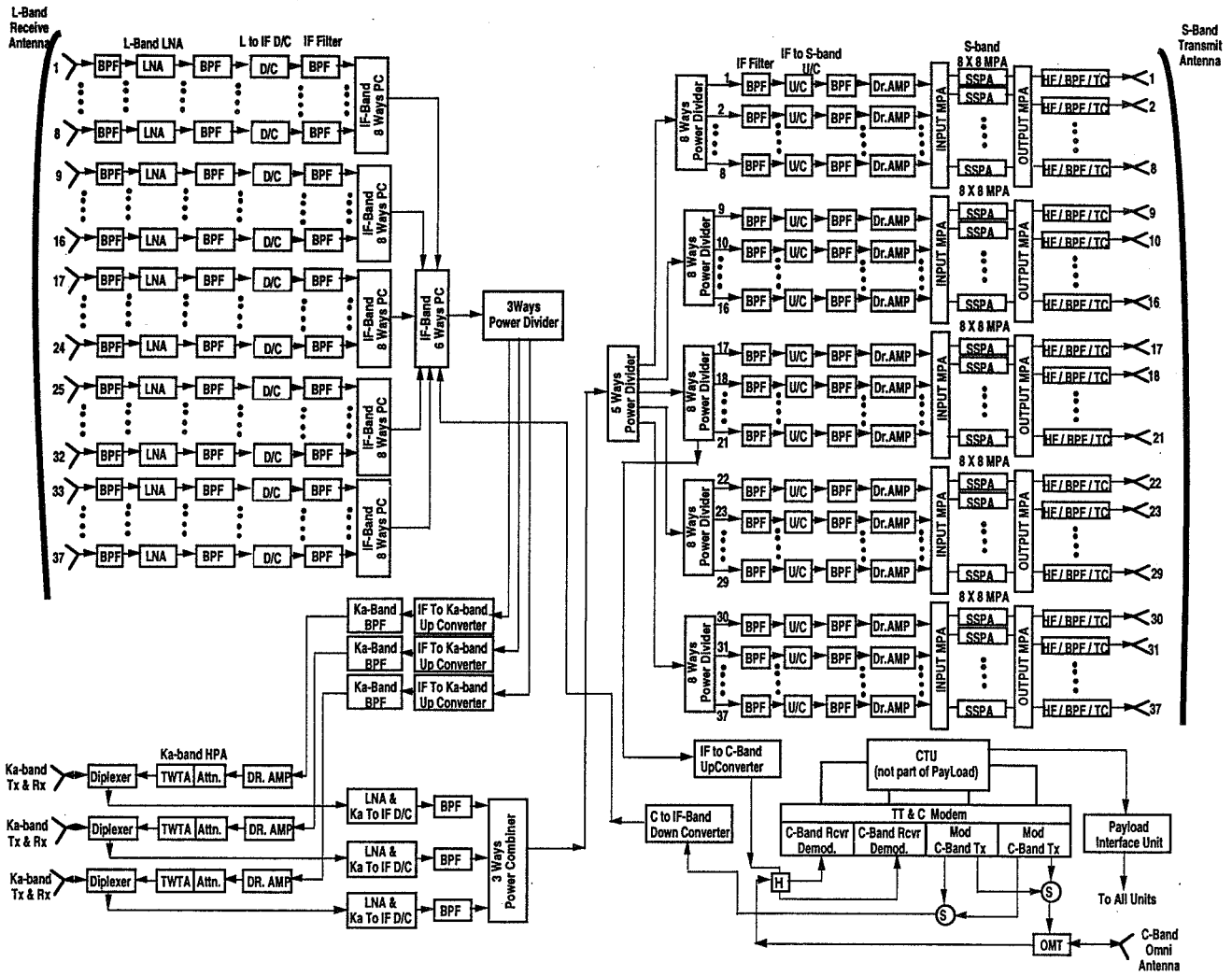


Figure 5: Odyssey Communication Payload Block Diagram

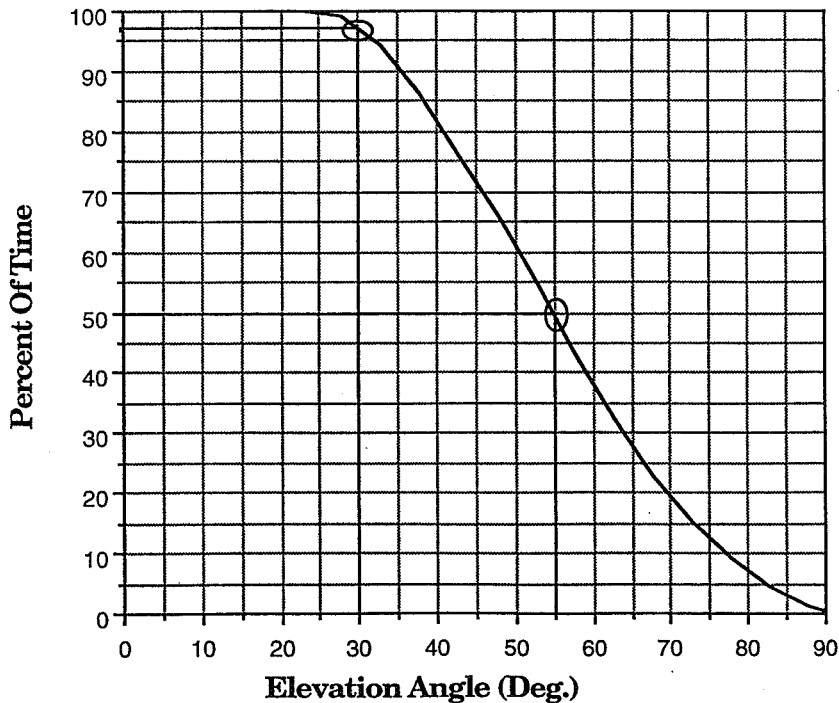
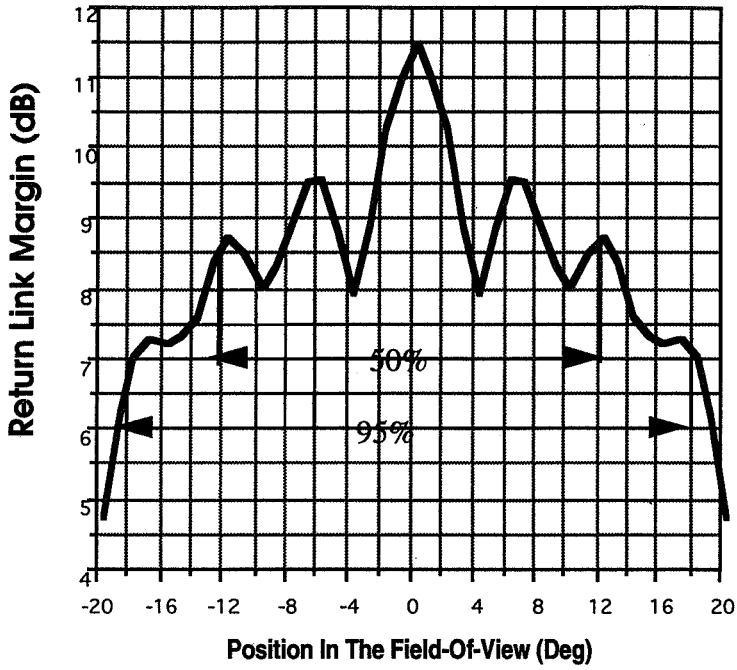


Figure 6: The Percent Of Time Elevation Angle Is Exceeded



Position In The Field-Of-View	Elevation Angle
± 0°	87°
± 2°	82°
± 4°	77°
± 6°	71°
± 8°	66°
± 10°	60°
± 12°	54°
± 14°	47°
± 16°	40°
± 18°	31°
± 20°	20°

(2° Off Nadir)

Figure 7: Odyssey Uplink Margin

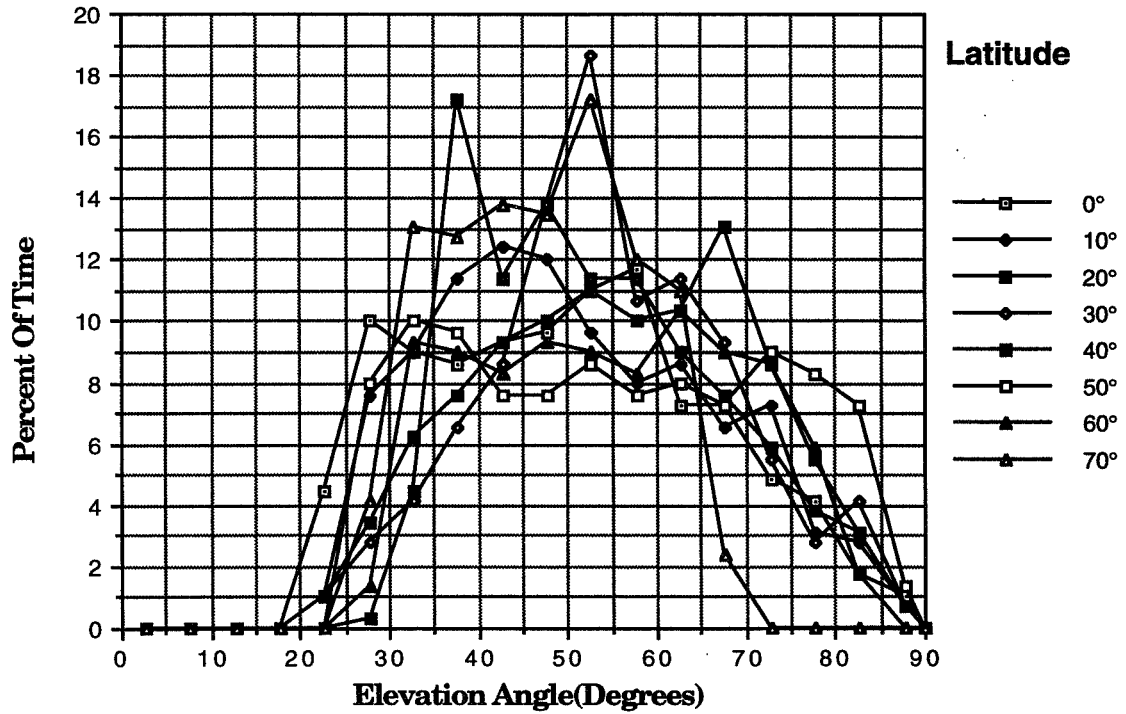


Figure 8: Users Elevation Angle Distribution

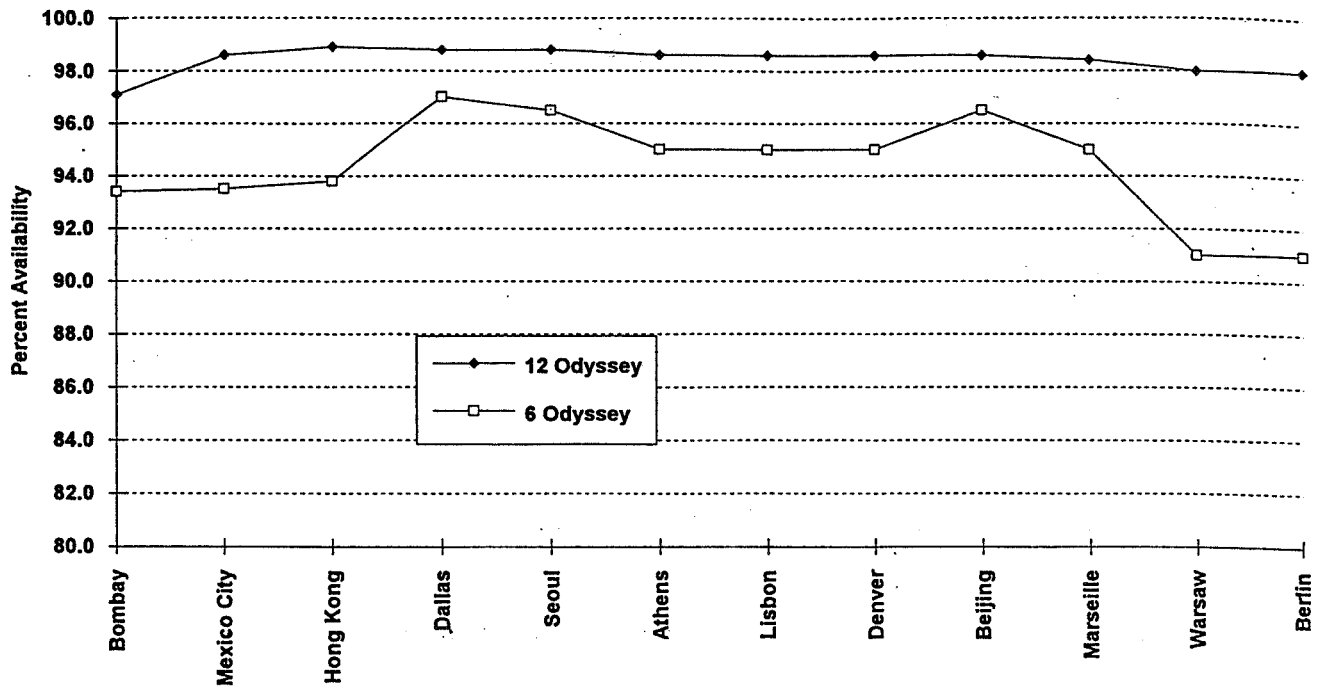


Figure 9: Calculated Availability For Odyssey Constellations

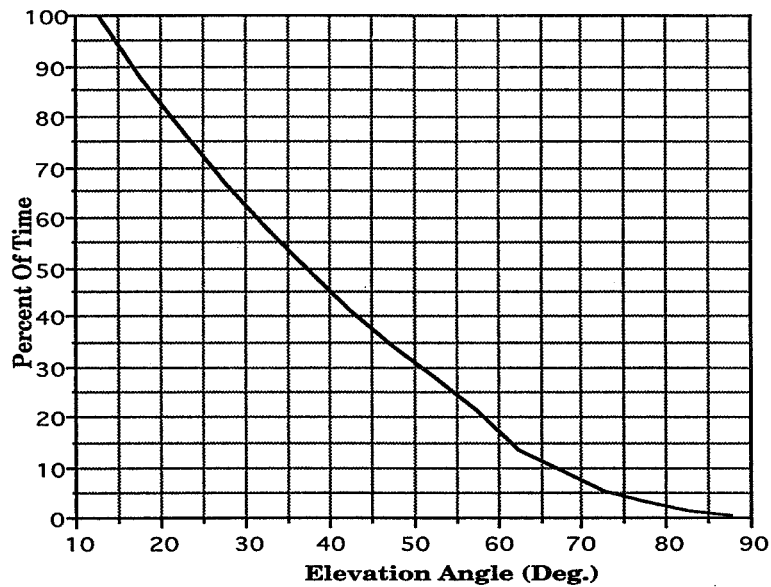
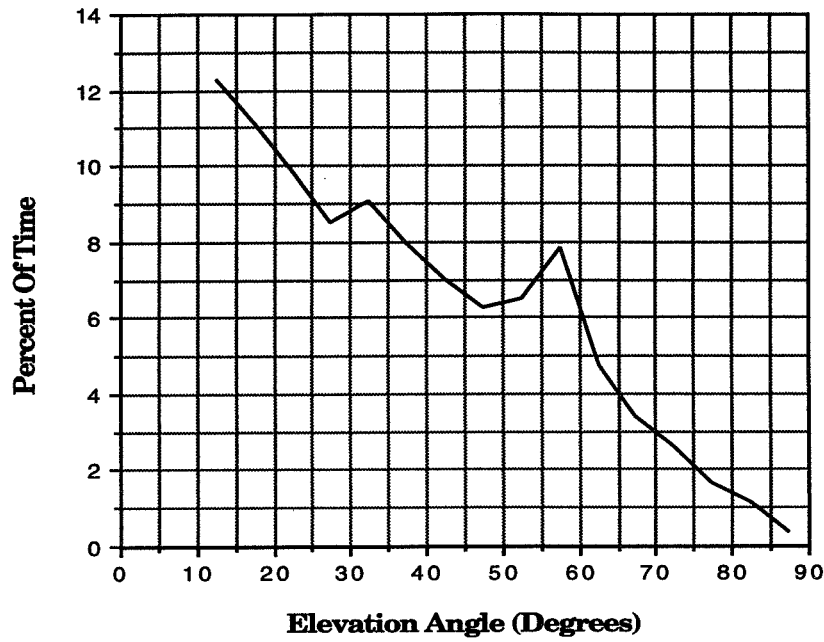
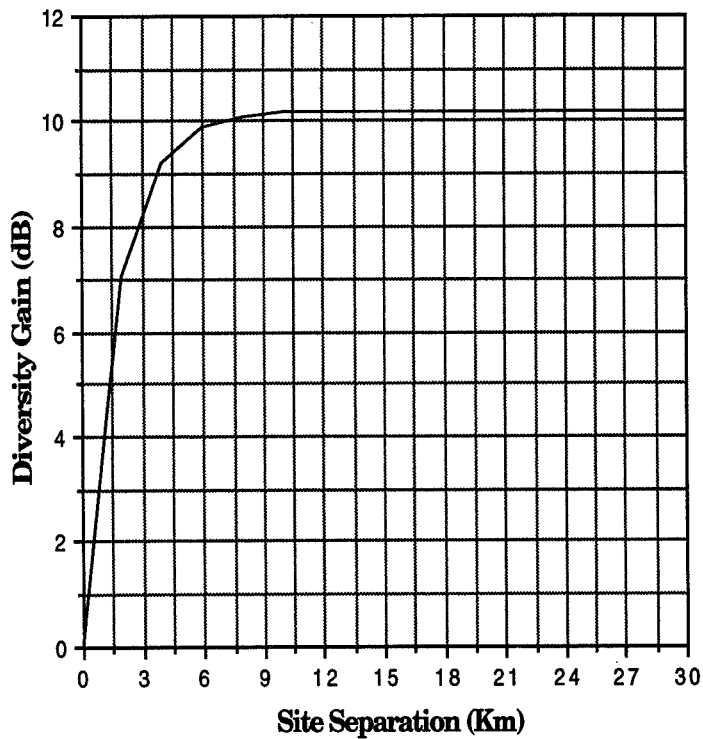


Figure 10: Percent Of Time Elevation Angle Is Exceeded (Los Angeles, CA - Earth Station)



**Figure 11: Elevation Angle Distribution
(Los Angeles, CA - Earth Station)**



**Figure 12 : Path Diversity Gain (Hodge Model)
(Los Angeles, CA - Earth Station
@ 30 GHz & 10° elevation Angle)**

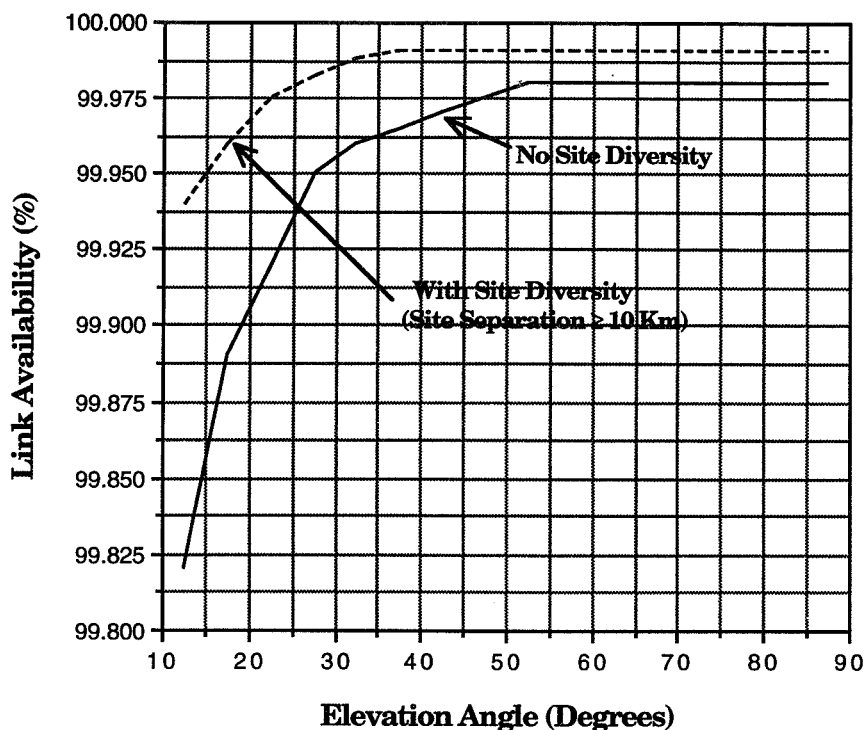


**Figure 13 : Link Availability Versus Elevation Angle
(Los Angeles, CA - Earth Station
@ 30 GHz with 18 dB Link Margin)**

Table 3 : Feeder Link Availability

Feeder Link Availability		
Site	No Site Diversity	With Site Diversity Site Separation ≥ 10 Km
Los Angeles, CA	99.94%	99.98%
Buenos Aires, Argentina	99.76%	99.91%
Fucino, Italy	99.86%	99.95%
Cape Town, South Africa	99.91%	99.97%
Ahmadabad, India	98.76%	99.61%
Yamaguchi, Japan	99.76%	99.92%
Sydney, Australia (Zone C)	99.89%	99.96%
Sydney, Australia (Zone D)	99.75%	99.91%

399304
1.30

**Communications Availability:
Estimation Studies at AMSC**

C. Edward Sigler, Jr.
American Mobile Satellite Corporation
10802 Parkridge Boulevard
Reston, Virginia 22091

ABSTRACT

This paper presents the results of L-band communications availability work performed to date. Results include a L-band Communications Availability Estimate Model and field propagation trials using an INMARSAT-M terminal. AMSC's primary concern centers on availability of voice communications intelligibility, with secondary concerns for circuit-switched data and fax. The model estimates for representative terrain/vegetation areas are applied to the contiguous US for overall L-band communications availability estimates.

Introduction

The AMSC Mobile Satellite (MSAT) program uses Mobile Terminal (MT) receive and transmit frequency ranges of 1525-1559 MHz and 1626.5 - 1660.5 MHz, respectively. These ranges lie within the portion of RF spectrum commonly referred to as "L-Band." Unfortunately, vegetation, especially deciduous and coniferous trees, and terrain present significant obstacles to L-Band signals in a land mobile environment. The amount of signal degradation depends significantly upon tree height, tree density, road backoff from trees, terrain gradient, and tree placement with respect to terrain.

In order to adequately estimate operational end-user voice quality and overall MSAT availability, AMSC launched a program to model the effects of terrain and vegetation on MSAT L-band communications. Within this effort, an internal propagation estimation tool was produced along with a methodology of applying averaged point-wise propagation estimates to the contiguous US.

This paper provides an overview of the L-band propagation estimation model and the methodology that applies the model predictions to the contiguous US. Additionally, this paper presents limited initial results with accompanying assumptions and parameter values.

2.0 Communications Availability Model

Numerous sources have empirically documented the effects of terrain and vegetation on Radio Frequency (RF) L-Band propagation. Different authors (Ref. Goldhirsh, Vogel, Stutzman, etc.) have developed L-band propagation estimation models based on varying premises and parameters. The empirical models provide sufficient representation of the expected propagation losses produced by vegetation, but only for adequately described routes. The term adequate does not imply detailed, but merely described with more parameters than can easily be gathered for long routes over diverse sections of the US. AMSC faces this larger task of predicting L-Band propagation degradation due to vegetation and terrain for the contiguous U.S. The models developed to date cannot be easily combined and tailored to such a large task with minimal data. As such, AMSC elected to develop an internal Communications Availability Model that produced results specifically designed to the project needs.

2.1 Communications Availability Model Overview

Since AMSC required large scale and statistical L-band communication availability estimates, a basis for a model was very important. Essential requirements include: electronic data availability for terrain and vegetation; an existing model framework; flexibility in design and future enhancements; and minimal development time and effort. The Satellite Communications Availability Simulation Model (AMSIM) was developed for this purpose. Major features and capabilities of AMSIM include:

- USGS Electronic Topographic Data
- USGS Land Use/Land Cover Electronic Data
- US Census Bureau TIGER File Data Processing
- Full Compliment of dBase features
- User Friendly Man-Machine Interface

LDMap, a product providing integrated data base and mapping capabilities, was modified to process U.S. Geologic Survey (USGS) electronic 7.5° quadrature topographic maps. 7.5° topographic maps were selected for their 30 meter resolution. To further customize LDMap the base program was augmented to process electronic USGS Land-Use/Land-Cover (L-series) data maps. The L-series maps contain vegetation information across the US. The vegetation information is contained in complex polygons with the predominate vegetation type (if any) listed within the polygon.

Types include deciduous trees, coniferous trees, mixed trees, grasslands, tree covered and non-tree covered wetlands, etc. No information is provided on the vegetation densities, species, or heights. Even with these limitations the L-series maps provide the best data on vegetation across the US in a consistent format.

2.2 AMSIM Basic Operation

Operation of AMSIM requires scanning the area of interest on paper topographic map copy into the computer to use as a display. Electronic terrain data must also be loaded from tape/disk and registered with the scanned image. The registration process provides information to AMSIM necessary to plot on the map image at the correct geographic coordinates.

Once the maps are input and registered, the user selects a route of interest using a point & click interface. Parameters selected for the propagation model are input and stored in a database file. The model then predicts the L-band communications availability for equally spaced points along the defined route. The model calculates the availability estimate using the user defined parameters. These parameters include:

- Tree heights (varies for type and elevation angle range)
- Tree Backoff from road
- MT RF Link Margin
- RF Absorption per meter of tree foliage
- Antenna height above roadway.

Tree backoff refers to the distance from the center of the lane closest to the tree vegetation to the start of the tree line. RF absorption per meter depends upon the type of tree and the density. Please refer to Section 4.1 for a complete description of the simulation parameter set.

Given an arbitrary area, the availability for routes may differ greatly. A selected route may align with the satellite azimuth, may be shadowed by a ridge line, etc. To minimize the variability in route selection from one area to the next, a generic route pattern, contained in Figure 2-1, was generated. The generic pattern attempts to remove route biases that may be present due to satellite, terrain, and/or vegetation location.

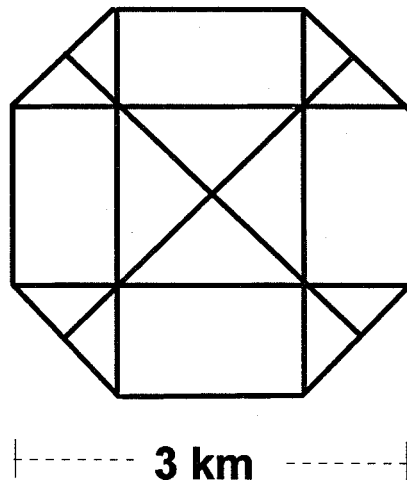


Figure 2-1 Generic Route Pattern

3.0 Availability Estimate Methodology

3.1 Detailed Overview

The US contains extremely diverse terrain and vegetation combinations. Applying the communications availability estimation model to the entire US requires large amounts of time and a significant investment in electronic and paper maps. The contiguous US was divided into 0.5° x 0.5° areas: a size selected to capture regional terrain and vegetation features while maintaining a manageable number of areas. Each area was categorized based upon three features: terrain, tree vegetation cover, and elevation angle. Five types of terrain and five types of tree vegetation density were selected. Three elevation angle ranges were selected. Combined, these attributes produce 75 possible overall terrain/vegetation/elevation angle choices to describe each of the 0.5° x 0.5° areas.

The five terrain categories are: 1) Flat; 2) Rolling; 3) Hilly; 4) Rugged; and 5) Mountainous. Table 3-1 details each terrain category.

Terrain Category	Definition	Examples
Flat	Little or no terrain gradient; gentle sloping terrain	Great Plains Florida
Rolling	Minor terrain gradient; low rolling hills	Central Maryland Central Carolinas
Hilly	Moderate terrain gradient; clustered large hills	Central Pennsylvania
Rugged	Large terrain gradient; clustered large hills/mountains	Upstate New York Ranges of California
Mountainous	Severe terrain gradient; mountain range peaks	Olympia Mountains Rocky Mountains

Table 3-1 Terrain Category Definitions

Similarly, the five tree vegetation categories are: 1) Clear; 2) Light; 3) Moderate; 4) Heavy; and 5) Dense. Table 3-2 present definitions of each tree vegetation category.

Vegetation Category	Definition
Clear	Tree Coverage < 10% of area
Light	Tree Coverage >10% & < 25% of area
Moderate	Tree Coverage >25% & <50% of area
Heavy	Tree Coverage >50% & <80% of area
Dense	Tree Coverage >80% of area

Table 3-2 Tree Vegetation Category Definition

3.2 Terrain Characterization

Terrain characterization of the 0.5° x 0.5° areas began with the 1:1,000,000 Map of the World series. These maps contain topographic information using color tinting and contour lines. For this project, all map reference materials were obtained from the US Geologic Survey (USGS) Cartographic Library in Reston, Virginia.

The main point in characterizing the terrain is to look at the gradient of the terrain vice the elevation. Parts of the Great Plains have somewhat high altitudes but are relatively flat. Selecting the proper characterization requires a subjective interpretation of the terrain guidelines applied to the terrain at hand. Some individual areas may not be characterized correctly; however, the error should only be one category level. Moreover, the statistical nature of the model and the number of 0.5° x 0.5° areas (appr. 2000) renders minor characterization errors statistically insignificant.

3.3 Vegetation Characterization

Vegetation characterization of the 0.5° x 0.5° areas used the Land Use/Land Coverage map series for the US. These maps contain complex polygons defining areas of similar vegetation. Area tree vegetation characterization was performed manually from these maps.

Manual area tree vegetation characterization consisted of three steps. First, the area was physically partitioned on the map. Second, the portions of the area with tree vegetation were visually 'integrated' to estimate the percent of the area with tree vegetation. For this model, no distinction was made for the percentage of each tree type within the area, only total tree coverage. Third, the percentage of tree coverage determined the tree vegetation category to apply to the area. Due to the nature of the percentage tree coverage estimation, the conservative approach desired for the simulation results dictated that a bias be applied towards the more heavily treed categories. Also note that for urban areas, the tree cover may be very light but man-made obstructions dominate. As such, the tree vegetation estimates may produce optimistic results for urban areas.

3.4 Representative Area Selection and Communication Availability Model Integration

A representative area was selected for each of the fifteen terrain/elevation angle types. The areas were selected based on geographic diversity, terrain type, and elevation angle. Tree Vegetation was added via five 'standardized' overlays. The standardized overlays contained deciduous, coniferous, and mixed trees in equal proportions. A small percentage (5%) of the Heavy and Dense overlays were dedicated to Wetland trees.

The simulations performed produced consistent results, exhibiting a general decrease in estimated availability as the terrain roughness increased and as the tree vegetation cover increased.

4.0 Availability Analysis Results, Interpretation, and Limitations

4.1 Parameter Set Description

A complete model of the communications availability of the contiguous US requires many variables. In order to maintain a tractable model, many parameters were fixed in generating this particular set of results. The parameter set for this set of simulations is given below in Table 4-1. An attempt was made to select conservative values for all simulation parameters. Interpretation of the availability results must include a review of the model parameter values. Variations of these parameters may greatly change the resultant communications availability estimates. Man-made obstructions (overpasses, bridges, buildings, etc.) were not modeled. Availability estimates may not apply to primarily urban areas.

Parameter	Value
Deciduous Tree Height	30°-40° - 50'
	40°-50° - 40'
	50°-60° - 40'
Coniferous Tree Height	30°-40° - 50'
	40°-50° - 30'
	50°-60° - 30'
Mixed Tree Height	30°-40° - 50'
	40°-50° - 30'
	50°-60° - 30'
Wetland Tree Height	30°-40° - 30'
	40°-50° - 30'
	50°-60° - 25'
RF absorption per meter (L-Band) for Tree Foliage	Absorption - 0.5dB/Meter
Road Type	Interstate/Primary Routes
Tree Backoff from Roadway	20'
Link Margin with Minimal Acceptable CODEC Performance	Margin - 6 dB, Voice only (Assumes AWGN Channel)
MT Antenna Height Above Roadway	Height - 0'

Table 4-1 Availability Estimation Parameter Set

4.1.1 Tree Height

The USGS Land Use map series contains information regarding tree coverage. The maps divide the tree information into 4 broad categories: Deciduous, Coniferous, Mixed, and Wetland. The maps provide no information regarding tree species, height or density. Due to this lack of detailed information, tree heights were selected for the broad categories based on elevation angle. The position of the satellite and the elevation angle ranges selected essentially divide the US into thirds, running North-South. The tree heights were selected for the top, middle, and bottom thirds of the US, assuming 'typical' species within the tree type. Unfortunately, tree heights vary significantly between species even within the same type. Moreover, tree height is major factor in the availability estimate. Thus, proper operation of the availability models requires accurate and consistent tree height information. Although this can be done for individual simulations for know routes and areas, accurate tree height information over large areas proves difficult. To reemphasize, the communications availability model results apply in the aggregate: care must be exercised in applying the model results to specific routes.

4.1.2 Vegetation Absorption

The tree species sets the density of leaves and branches and the thickness of the branches. At L-band, tree leaves and branches readily absorb RF energy. Thus, the total absorption along a path through the tree vegetation is determined by the absorption per tree and the number of tree along the path. Using data from [1] and a generic tree to tree density, an average absorption of 0.5 dB/Vegetation-Meter was selected. The model calculates and applies this absorption for communications paths through tree vegetation. As with tree height, the simulation results for heavily treed areas depend significantly on the selected tree vegetation absorption per meter.

4.1.3 Tree Backoff

Tree backoff refers to the distance from the center of the roadway lane closest to the trees to the tree vegetation. For purposes of this parameter set, only Interstate and primary routes were considered. Typically, highway designers and State transportation departments maintain a tree backoff for Interstate and Primary roads. To maintain a conservative approach, 20 feet was selected for the tree backoff. Note, if a vehicle is on the side of the road closest to the satellite, then there is a 20 foot backoff; however, if the vehicle were on the other side of

the road (or in another lane), then the backoff greatly increases. Because of this, the availability estimates are the average of the simulation results for the 'bad side' and the 'good side'. Simulations of the 'bad side' use a 20 foot backoff. Simulations of the 'good side' use a 50 foot backoff. The significance of tree backoff depends on the tree heights and the elevation angle. Simulations results for treed areas with tall trees and elevation angles of 30°-40° are the most affected by tree backoff variations.

4.1.4 RF Link Margin

The RF link margin refers to additional link power available above the minimum power necessary to maintain the link performance at or above a specified level. For purposes of this parameter set, a 6 dB link margin was selected corresponding to a AWGN channel. The selected margin does not include beam illumination variation -- edge of beam gain considered in all cases.

4.1.5 MT Antenna Height

The MT antenna was assumed to be on the roadway surface. Typical passenger vehicle installations provide an antenna height of 3-4 feet. Installations for trucks give the antenna a height of 7+ feet. The higher the antenna, the better the performance through roadside tree foliage. Thus an antenna height of 0 feet provides for a conservative availability estimate with respect to antenna height.

4.2 Results

The Communications Availability estimate model was used on the representative terrain areas detailed in Section 3. Table 4-2 contains the results for these Representative areas. Note that the general results are favorable. However, the overall results of the modeling exercise are proprietary. The results for Maryland, Kansas, and California are provided in Table 4-3 as examples.

The overall L-band Communications availability estimate for each state cannot be directly applied on a per call basis. For instance, a call of infinite duration that traversed the entire state could expect an overall availability for the duration of that equal to the estimated availability for that state. However, calls of anticipated duration (1 - 2 minutes) within certain terrain and vegetation combinations with a low elevation angle may experience a much smaller availability for the duration of the call. In fact, the link may degrade so significantly that

the call is dropped. Conversely, a call of anticipated duration for most terrain and vegetation combinations will have an availability approaching 100%. For example, a call from a MT located in the Great Plains will likely have an availability approaching 100%.

The design of the voice CODEC removes or reduces intelligibility loss due to small signal dropouts produced by tree trunks, telephone poles, etc, while producing natural sounding voice. As such, the actual communications availability for voice communications may be higher than the estimated values.

Terrain	Vegetation	30-40	40-50	50-60	Elevation (deg)
		Voice Avail Avg	Voice Avail Avg	Voice Avail Avg	
Flat	Clear	100	100	100	
Flat	Light	98.5	100	100	
Flat	Moderate	94	100	100	
Flat	Heavy	93.5	100	100	
Flat	Dense	91.5	100	100	
Rolling	Clear	99.5	100	100	
Rolling	Light	97.5	100	100	
Rolling	Moderate	92	99.5	100	
Rolling	Heavy	89.5	99.5	100	
Rolling	Dense	87	99	100	
Hilly	Clear	98.5	100	100	
Hilly	Light	97.5	99.5	100	
Hilly	Moderate	95.5	99	100	
Hilly	Heavy	91.5	99	100	
Hilly	Dense	90.5	98	100	
Rugged	Clear	99	99	100	
Rugged	Light	96.5	99	100	
Rugged	Moderate	90.5	98	100	
Rugged	Heavy	86	98	100	
Rugged	Dense	84	97.5	100	
Mountainous	Clear	98.5	99.5	100	
Mountainous	Light	94.5	99	100	
Mountainous	Moderate	87	98	99.5	
Mountainous	Heavy	84	97.5	99.5	
Mountainous	Dense	77.5	97	99	

Figure 4-2
Representative Area Communications Availability Estimates

State	Estimated Voice Availability
California	95.6 %
Kansas	100 %
Maryland	94.9 %

Figure 4-3
Communications Availability Estimate Examples

4.3 Model Validation and Verification

The AMSIM propagation estimation model has undergone limited field validation; however, additional validation and verification is necessary for high confidence in the model outputs. Validation and verification will continue with appropriate model adjustments, as necessary.

The AMSIM model was verified by comparison of measured data with the output of the model for the same terrain/vegetation combinations. An INMARSAT Standard M terminal mounted in a truck was used to gather direct information on L-band propagation through vegetation. INMARSAT Standard M has a similar link margin to that simulated and uses a variation of the CODEC designed into the AMSC system. Because of this, the INMARSAT propagation results can be directly compared to the propagation model results.

The tests conducted used a tape recorded message (length 30 minutes) connected to a PSTN phone. The Standard-M phone dialed this phone number. An audio pick-up collected the recorded message as received by the Standard-M phone. The pick-up was fed into the audio port of a Video Cassette recorder which (approximately) recorded the Line-of-Site to the INMARSAT AORW or AORE satellite. Availability of a given route was taken as the amount of time that the recorded message was intelligible divided by the total length of the call. Experiment runs located in central Maryland, with sustained Standard-M terminal to PSTN phone connectivity, compared consistently with the model results for similar terrain, within the constraints of the experimental arrangement.

5.0 Conclusions

This task has produced useful and documentable results. The resultant Communications availability values indicate that AMSC's customers will enjoy 'on the average' acceptable or better voice quality over nearly the entire contiguous US.

6.0 References

- [1] **Propagation Effects for Land Mobile Satellite Systems: Overview of Experimental and Modeling Results**, J. Goldhirsh and W. Vogel, NASA Reference Publication 1274, February 1992.



Communications Availability Studies at AMSC

194



- ◆ **AMSC's Mission:** Provide Mobile Telephony Service via Geo-synchronous Satellite and Low Cost Earth Terminals.
- ◆ **Issue:** Given Satellite & Mobile Earth Terminal (MT) design constraints, what is expected voice communications availability for U.S.?
- ◆ **Resolution:** Undertake task to determine communications availability throughout U.S.





Communications Availability Estimation Development

◆ Restrictions:

- Low Cost
- Minimal Information
- Marketing Department Applications



Communications Availability Estimation Development (cont.)

◆ Solution:

- Divide contiguous U.S. into $0.5^\circ \times 0.5^\circ$ area blocks;
- Categorize area blocks into terrain type and tree vegetation type;
- Select 'Representative Areas' for each terrain/vegetation combination and elevation angle range;
- Develop tool to estimate communication availability for each representative area; and
- Apply results for 'Representative Areas' to all area blocks.



Terrain/Vegetation Characterization

- ◆ Define terrain and vegetation categories.
- ◆ Use USGS 1:1,000,000 and L-series Land Use/Land Cover maps for terrain and vegetation information.
- ◆ Apply categories to $0.5^\circ \times 0.5^\circ$ areas.





Terrain Category Definitions

Terrain Category	Definition	Examples
Flat	Little or no Terrain Gradient; gentle sloping terrain	Great Plains Florida
Rolling	Minor Terrain Gradient; low rolling hills	Central Maryland Central Carolinas
Hilly	Moderate Terrain Gradient; large hills	Central Pennsylvania
Rugged	Large Terrain Gradient; clustered large hills/mountains	Upstate New York Ranges of California
Mountainous	Severe Terrain Gradient; mountain range peaks	Olympia Mountains Rocky Mountains





Tree Vegetation Category Definition

Vegetation Category	Definition
Clear	Tree Coverage < 10% of area
Light	Tree Coverage > 10% & < 25% of area
Moderate	Tree Coverage > 25% & < 50% of area
Heavy	Tree Coverage > 50% & < 80% of area
Dense	Tree Coverage > 80% of area

200



Terrain/Vegetation Characterization (cont.)

					46°
	State = MT Terrain = F Veg = L El Ang = 36.8°	State = MT Terrain = F Veg = C El Ang = 36.9°			45.5°
	State = MT Terrain = F Veg = M El Ang = 37.4°	State = MT Terrain = F Veg = L El Ang = 37.4°			45°
	State = WY Terrain = R Veg = L El Ang = 37.9°	State = WY Terrain = R Veg = L El Ang = 38.0°			44.5°
	106°	105.5°	105°		
	LONGITUDE				
					L A T I T U D E

201





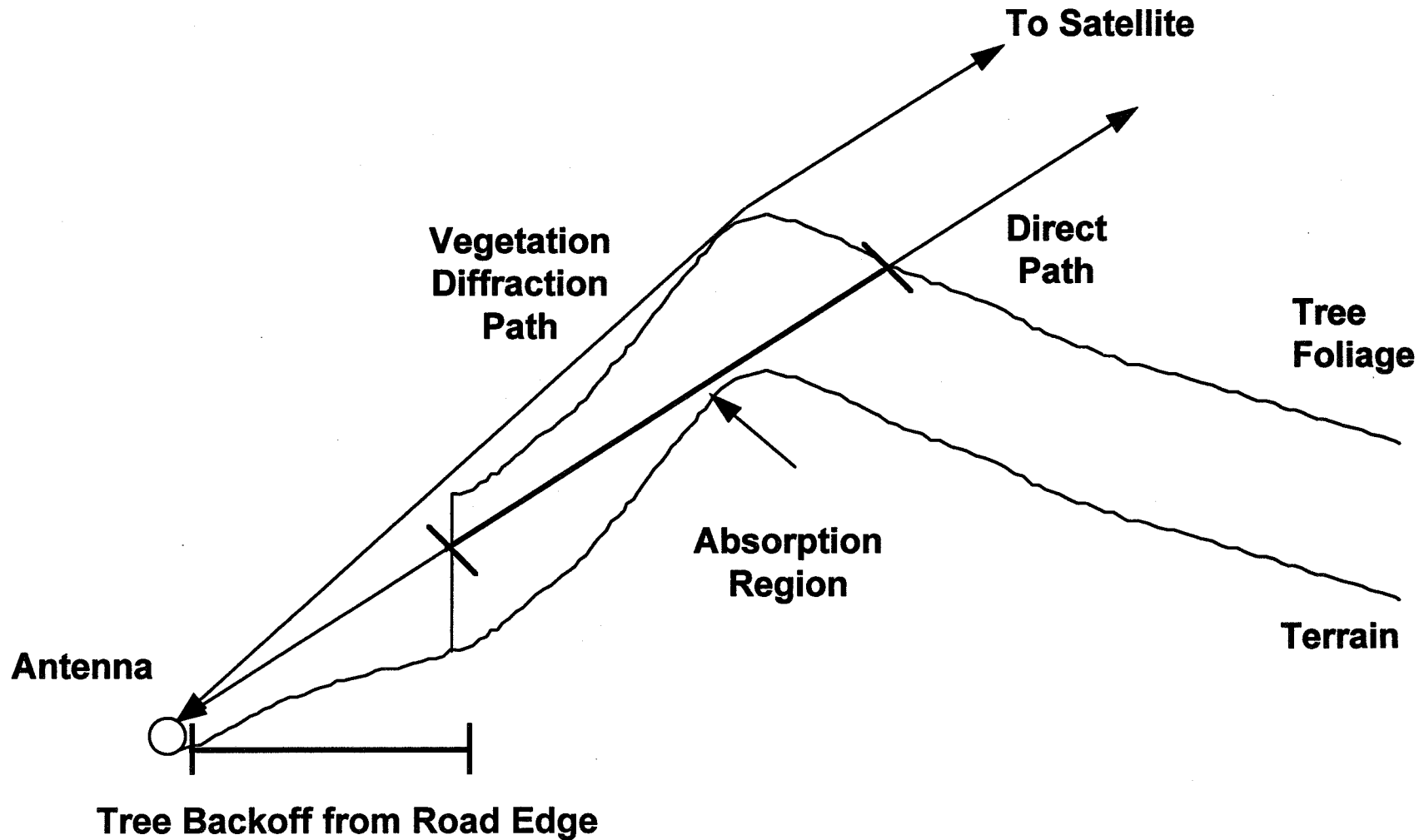
Communications Availability Model

- ◆ Considers 2 propagation paths.
- ◆ Uses USGS Electronic Topographic and L-Series Data.
- ◆ Bases availability estimate on ratio of route points with acceptable margin versus total points.
- ◆ Generic route pattern selected to reduce terrain, vegetation and elevation angle biases.

Propagation Paths

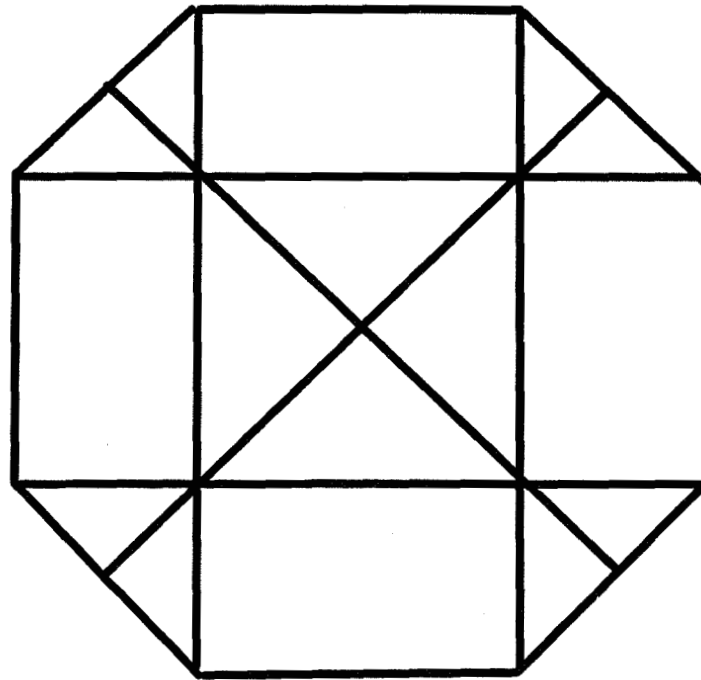


203





Generic Route Pattern



----- 3 km -----



Result:

- Process and tool combined to form a communication availability estimate for contiguous U.S.



Results



Availability Estimation Parameter Set

Parameter	Value
Deciduous Tree Height	30° - 40° - 50' 40° - 50° - 40' 50° - 60° - 40'
Coniferous Tree Height	30° - 40° - 50' 40° - 50° - 30' 50° - 60° - 30'
Mixed Tree Height	30° - 40° - 50' 40° - 50° - 30' 50° - 60° - 30'
Wetland Tree Height	30° - 40° - 30' 40° - 50° - 30' 50° - 60° - 25'
RF absorption per meter (L-Band) for Tree Foliage	Absorption - 0.5 dB/Meter
Road Type	Interstate/Primary Routes
Tree Backoff from Roadway	20' and 50'
Link Margin with Minimal Acceptable CODEC Performance	Margin - 6dB, Voice Only (Assumes AWGN Channel)
MT Antenna Height Above Roadway	0'

207

Representative Area Communications Availability Estimates



Terrain	Vegetation	30-40	40-50	50-60	Elevation (deg)
		Voice Avail Avg	Voice Avail Avg	Voice Avail Avg	
Flat	Clear	100	100	100	
Flat	Light	98.5	100	100	
Flat	Moderate	94	100	100	
Flat	Heavy	93.5	100	100	
Flat	Dense	91.5	100	100	
Rolling	Clear	99.5	100	100	
Rolling	Light	97.5	100	100	
Rolling	Moderate	92	99.5	100	
Rolling	Heavy	89.5	99.5	100	
Rolling	Dense	87	99	100	
Hilly	Clear	98.5	100	100	
Hilly	Light	97.5	99.5	100	
Hilly	Moderate	95.5	99	100	
Hilly	Heavy	91.5	99	100	
Hilly	Dense	90.5	98	100	
Rugged	Clear	99	99	100	
Rugged	Light	96.5	99	100	
Rugged	Moderate	90.5	98	100	
Rugged	Heavy	86	98	100	
Rugged	Dense	84	97.5	100	
Mountainous	Clear	98.5	99.5	100	
Mountainous	Light	94.5	99	100	
Mountainous	Moderate	87	98	99.5	
Mountainous	Heavy	84	97.5	99.5	
Mountainous	Dense	77.5	97	99	

208



Communications Availability Estimate Examples

State	Estimated Voice Availability
California	95.6 %
Kansas	100.0 %
Maryland	94.9 %

209



Conclusion: Significant majority of contiguous U.S. will, on the average, enjoy 'acceptable' or better voice quality on the AMSC MSAT System.

199510828

N95-14682



309305

p. 63

S-Band Propagation Measurements

Robert D. Briskman
CD Radio Inc., Washington, D.C.

INTRODUCTION

A geosynchronous satellite system capable of providing many channels of Digital Audio Radio Service (DARS) to mobile platforms within the contiguous United States using S-band radio frequencies is being implemented. The system is designed uniquely to mitigate both multipath fading and outages from physical blockage in the transmission path by use of satellite spatial diversity in combination with radio frequency and time diversity. Figure 1 shows the generalized system configuration. The system also employs a satellite orbital geometry wherein all mobile platforms in the contiguous United States have elevation angles greater than 20° to both of the diversity satellites. Since implementation of the satellite system will require three years, an emulation has been performed using terrestrial facilities in order to allow evaluation of DARS capabilities in advance of satellite system operations. The major objective of the emulation was to prove the feasibility of broadcasting from satellites 30 channels of CD quality programming using S-band frequencies to an automobile equipped with a small disk antenna and to obtain quantitative performance data on S-band propagation in a satellite spatial diversity system.

DARS SATELLITE SYSTEM

The satellite system consists of two geosynchronous satellites, one located over the east coast of the United States at 80° West Longitude and the second over the west coast of the United States at 110° West Longitude. The satellites receive in the 6720 MHz band and transmit in two 8 MHz segments of the 2310-2360 MHz band. The satellites each receive the same transmission from the system's up-link/programming center essentially simultaneously and retransmit the signal through an antenna beam covering the contiguous United States. Figure 2 shows the block diagram of the satellite's transmission payload. The retransmission frequencies of the two satellites are separated by 20 MHz and the beam edge EIRP is 57 dBW. The high EIRP is required due to the low gain of the mobile platform antenna. The transmission consists of 30 stereo CD music channels, a 128 kb/s service channel and several information channels. The CD stereo music channels are compressed prior to transmission using a joint encoding algorithm based on perceptual audio coding so only a 128 kb/s output data rate is required for each. The channels are digitally multiplexed together (i.e., TDM-time division multiplex) with interleaving in time, resulting in a 4 Mb/s output signal.

The output signal is convolutionally encoded, a Reed-Solomon code added and then transmitted to the satellites using offset quadrature phase shift keying.

The satellite retransmissions are received by the mobile platforms, particularly passenger automobiles. The mobile platform G/T at worst operational aspect angle is -19 dB/K. The antenna is designed to provide 3 dBi gain within a 20°-60° elevation angle range at all azimuths. The antenna is physically 2.5 cm in radius and 0.4 cm thick, designed for embedment in automobile rooftops. A photograph of the antenna is shown in Figure 3. After radio frequency reception, amplification and down conversion, the transmission from each satellite is individually demodulated. The two signals are time phased together using a maximal ratio combiner and then de-multiplexed. The user selects the specific music channel desired which is then routed to the decompressor, the digital-to-analog converter and the audio amplifier-loud speaker subsystem. Figure 4 shows a block diagram of the mobile platform receiver. The mobile platform receiver just described enjoys great resistance to multipath fading and outage from blockage since its mechanization takes advantage of satellite spatial, frequency and time diversity as depicted in Figure 5.

EMULATION IMPLEMENTATION

It is difficult to emulate the capabilities of the previously described DARS satellite system using terrestrial facilities to simulate the satellites. This is because achieving a 20° elevation angle to the mobile platform from a terrestrial transmitter simulating the satellite over a reasonably large area requires buildings or towers of great height. Also, the demonstration of spatial diversity requires two transmitters covering the same geographical area resulting in the need for several transmitters. A satellite system emulation range was constructed in Northern Virginia close to Washington D.C. Figure 6 is a roadmap of the range. Five high-rise building tops were used as transmit locations to a vehicle driving a route through the area configured so that two transmit locations are nominally at 10° or more elevation angle from the vehicle, and only one transmit path at a time experiences physical blockage. The particular driving route included areas representing both urban and suburban environments as well as areas with trees and a roadway overpass.

The 30 CD music channels and service channel were generated at a programming/up-link earth station in Washington, D.C. using the compression, multiplexing and modulation described earlier. The uplink station transmitted the signal at Ku-band to the SBS-6 satellite which relayed the signal to standard VSATs on the high-rise building roofs. The VSAT received signal was translated by a stable frequency converter to the 2310-2360 MHz band and was then re-radiated using a small S-band transmitter and omni-directional antenna. The S-band EIRP of the transmitters was adjusted to provide a signal strength equal to that which would have been received at the mobile platforms from the previously described geosynchronous satellites

throughout the nominal vehicle route. The standard passenger vehicle used for the emulation was outfitted with a prototype receiver electronically almost identical to those that would be used in the operational satellite system. A small depression was made in the car roof, the antenna inserted and the roof area repainted to make the antenna invisible. The automobile radio was modified with a single button to select Satellite Radio in addition to AM and FM, and an expanded display was used to show the driver the music composition name and composer being played on the CD channel selected. A photograph of the display is shown in Figure 7.

EMULATION OPERATIONS

An application was submitted to the FCC in December 1992 for an Experimental License to conduct the previously described emulation using rooftop mounted transmitters in the 2310-2360 MHz radio frequency band. The license was granted on February 25, 1993 and the measurements subsequently cited were performed primarily from April 1993 through early June 1994.

A simplified block diagram of the system used for the emulation is shown in Figure 8. Note that the automobile used a four channel receiver, rather than the two to be used in the actual DARS satellite system, to avoid self interference from the relatively closely spaced rooftop antennas and that the 30 music channels were compressed individually and then multiplexed. Twenty minute music segments were then placed on the computer disk at the up-link earth station for transmission during the demonstration. The music segments would repeat automatically at the end of the twenty minutes.

PROPAGATION DATA

Accumulation of propagation data is performed when satellite transmission time is available and when the emulation automobile is not used for demonstrations of service capability. Data on transmission performance are logged on a monitoring UNIX based computer in the automobile trunk and then transferred to a large office computer at headquarters. Essentially received transmission data are logged four times per second as a record containing time, location, signal strength and bit error rate. Data reduction may be performed as a function of either time period or car wheel rotations.

The results to date fall into three categories:

1. **Blockage** Considerable data were taken on blockage avoidance by satellite spatial diversity, especially overpasses. Some selected measurements of interest are presented. Figures 9, 10, 11 show that no blockage occurred at measuring points around the driving range. At least one receiver channel always had a signal above threshold. A special test of blockage avoidance was made on one of the largest freeway

overpasses in the Washington, DC area, and the measurements are summarized in Figure 12. The measurements show that no blockage outage would occur in vehicles passing under the overpass with the diversity satellite DARS system for the geometry utilized but would always occur for a single satellite DARS system.

2. **Multipath** The nominal margin over threshold in the DARS satellite system for each received transmission without diversity combining is 5dB. This required operation of the test range at increased transmitter power for statistical measurement of multipath fading up to 20dB. The data acquired to date indicate that greater than 12dB improvement was almost always obtained from diversity but the statistical distribution above 12dB awaits further data taking.

3. **Frequency Selective Fading** There was observed, on occasion, unanticipated high levels of frequency selective fading. Figure 13 shows two examples of such fades; the left hand plot containing a narrowband (0.5MHz) fade of 15dB in the lower frequency transmission and the right hand plot containing a wideband (4MHz) fade of 20dB in the upper frequency transmission. In both cases, the satellite frequency diversity scheme would have prevented a service outage.

SUMMARY

The propagation data obtained to date at S-band demonstrate the effectiveness of satellite spatial diversity in mitigating DARS service outages from blockage and multipath. Further data will be accumulated for determining accurate multipath improvement performance statistics.

Figure 1 -- The CD Radio System

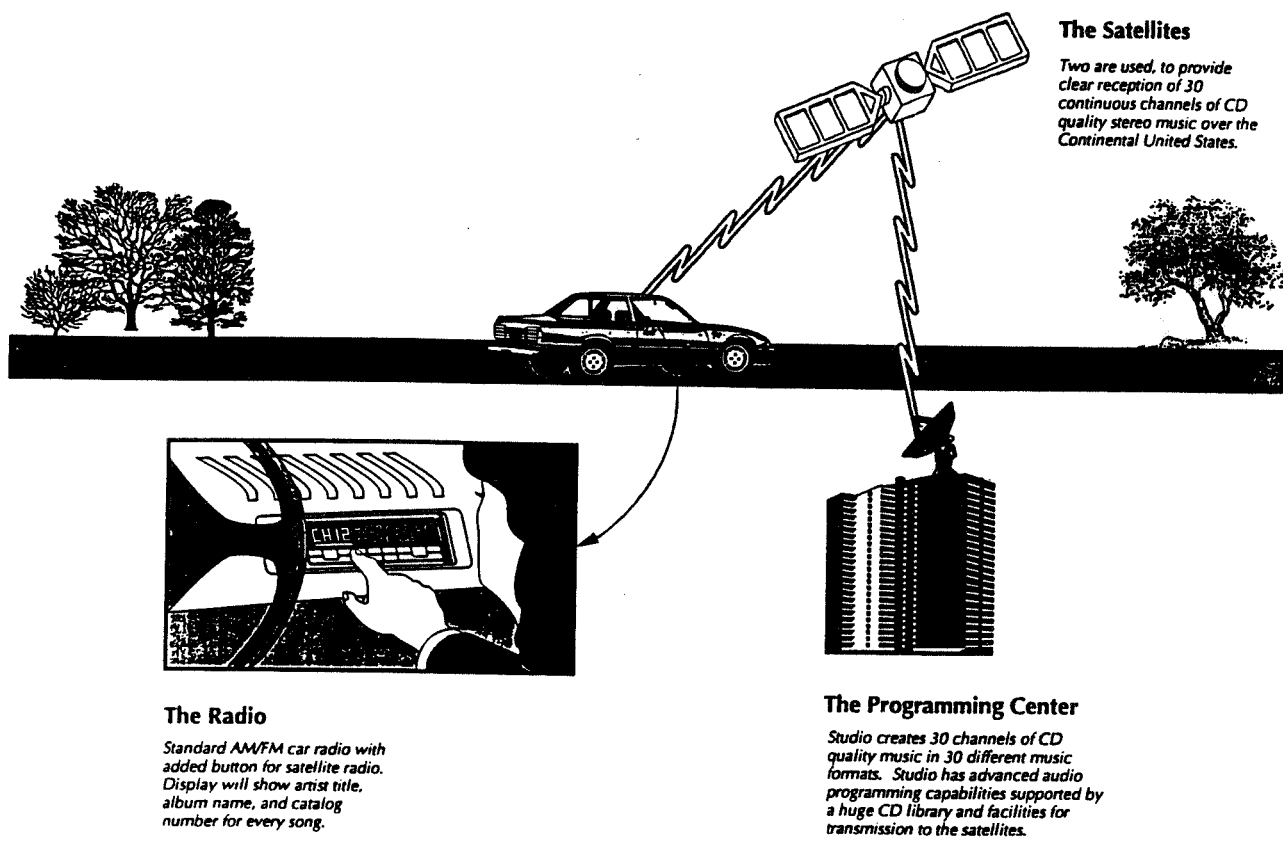


Figure 2 -- CD Radio Satellite Communications Block Diagram

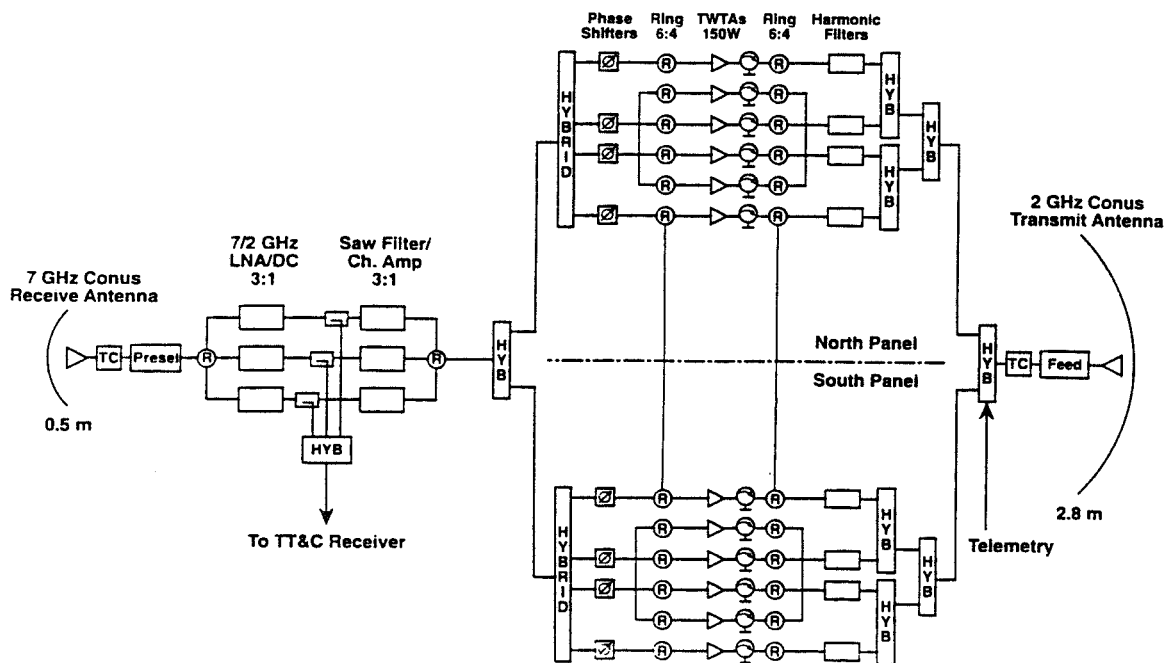


Figure 3 -- CD Radio Antenna



Figure 4 -- Vehicle Receiver

Analog AM & FM/Digital Satellite & Terrestrial

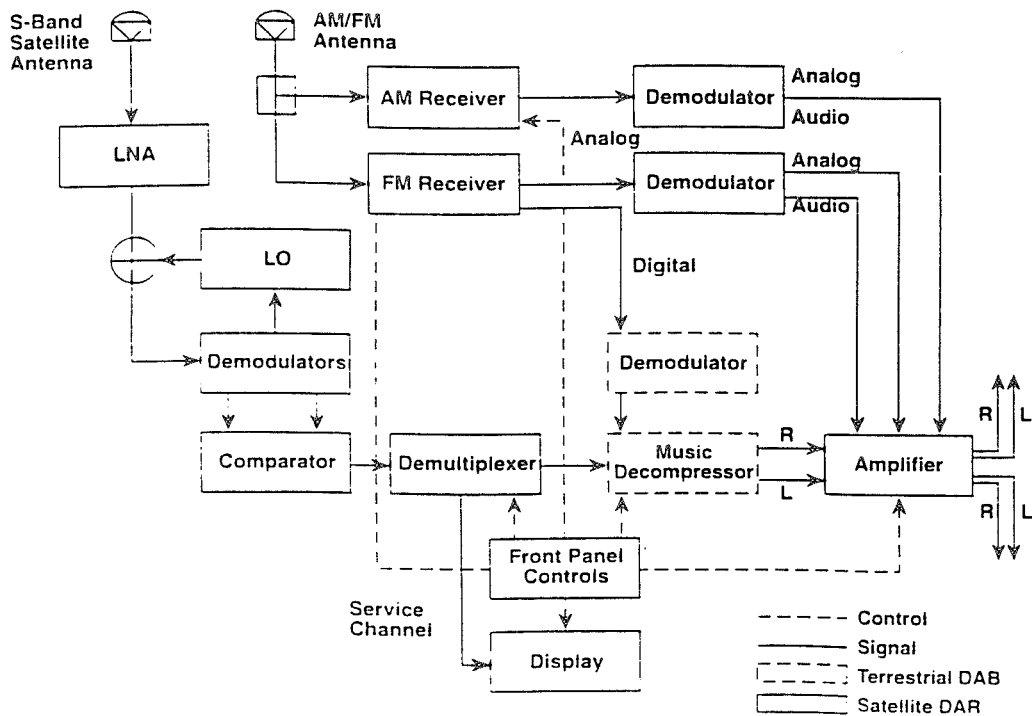


Figure 5 -- Reduction of Blockage Outages*
By Use of Two Radio Broadcast Satellites

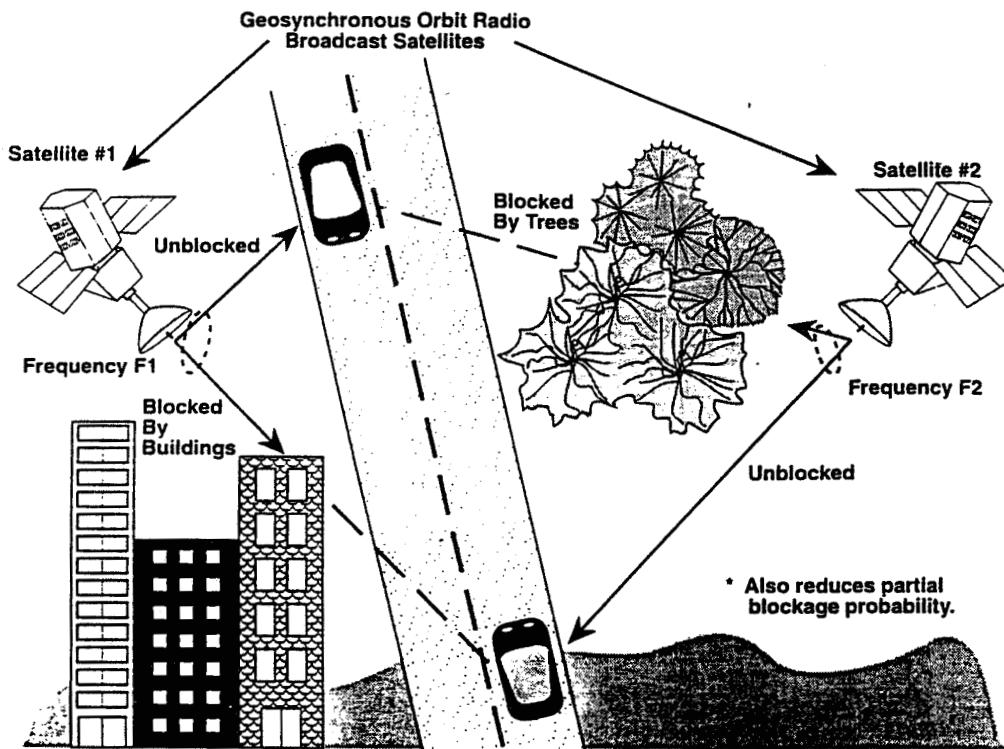


Figure 6 -- Test Range Road Map

Note: The test range is in Arlington, Virginia,
part of metropolitan Washington, D.C.

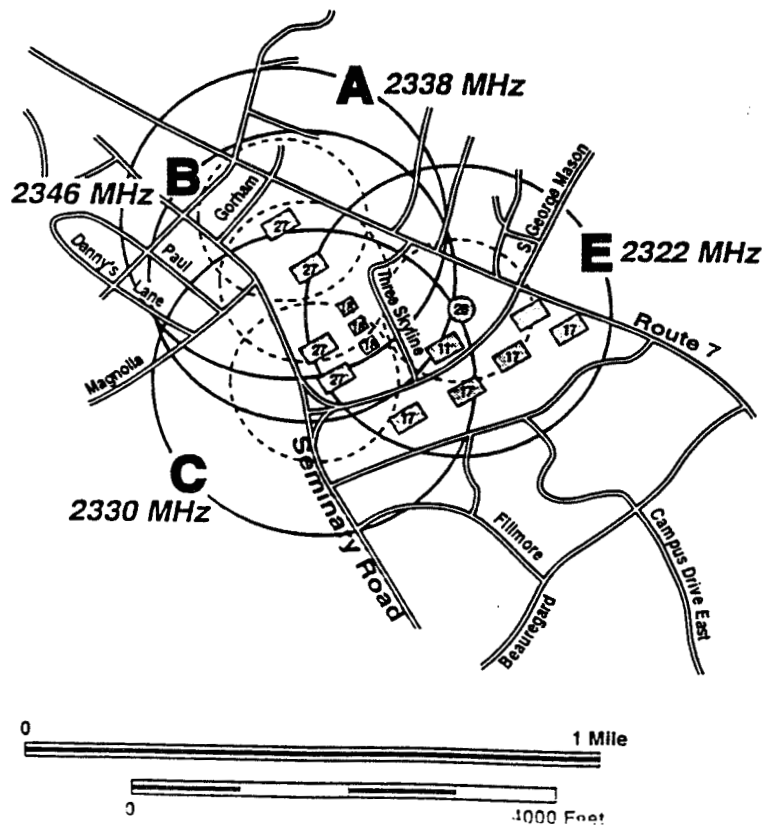


Figure 7 -- Car Radio Display

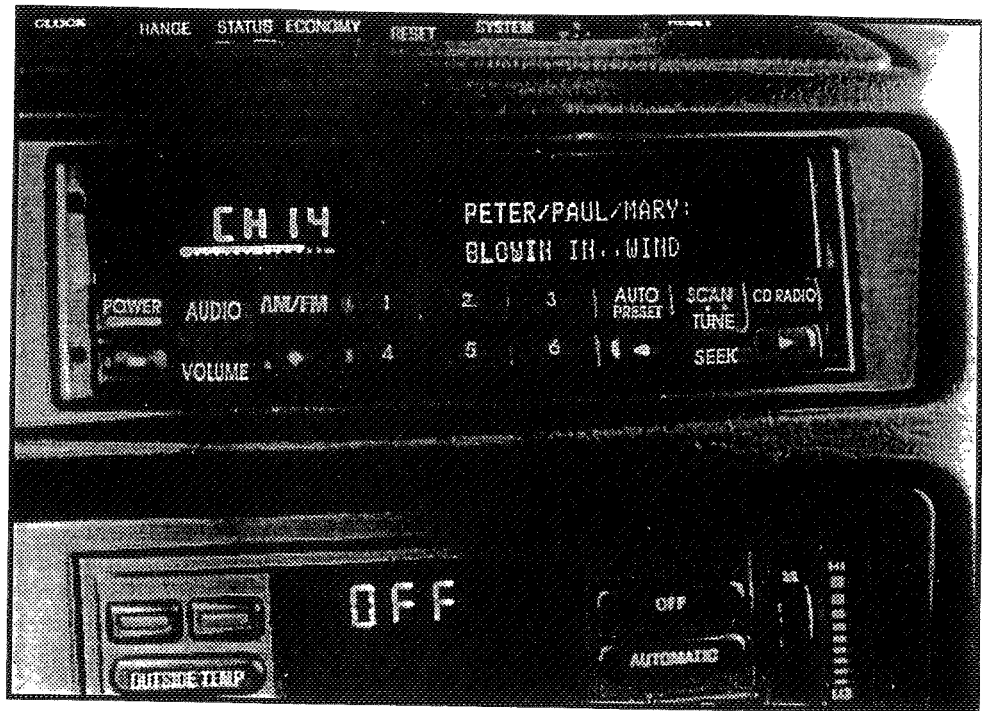


Figure 8 -- CD Radio Test System - Block Diagram

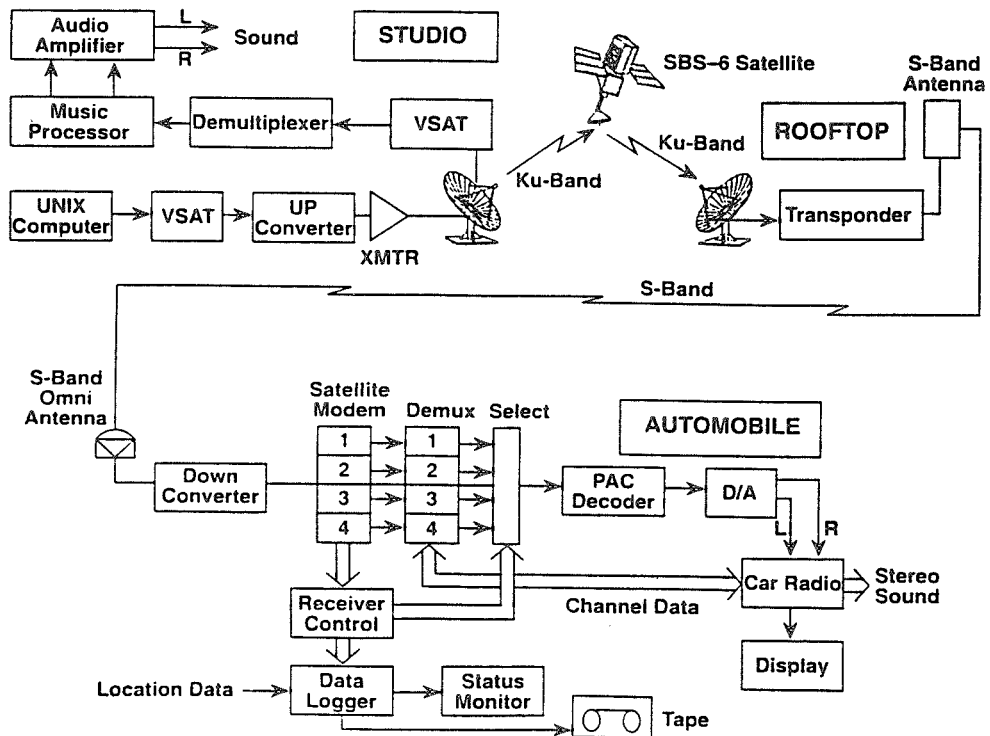


Figure 9 -- Test Range Measurement Points

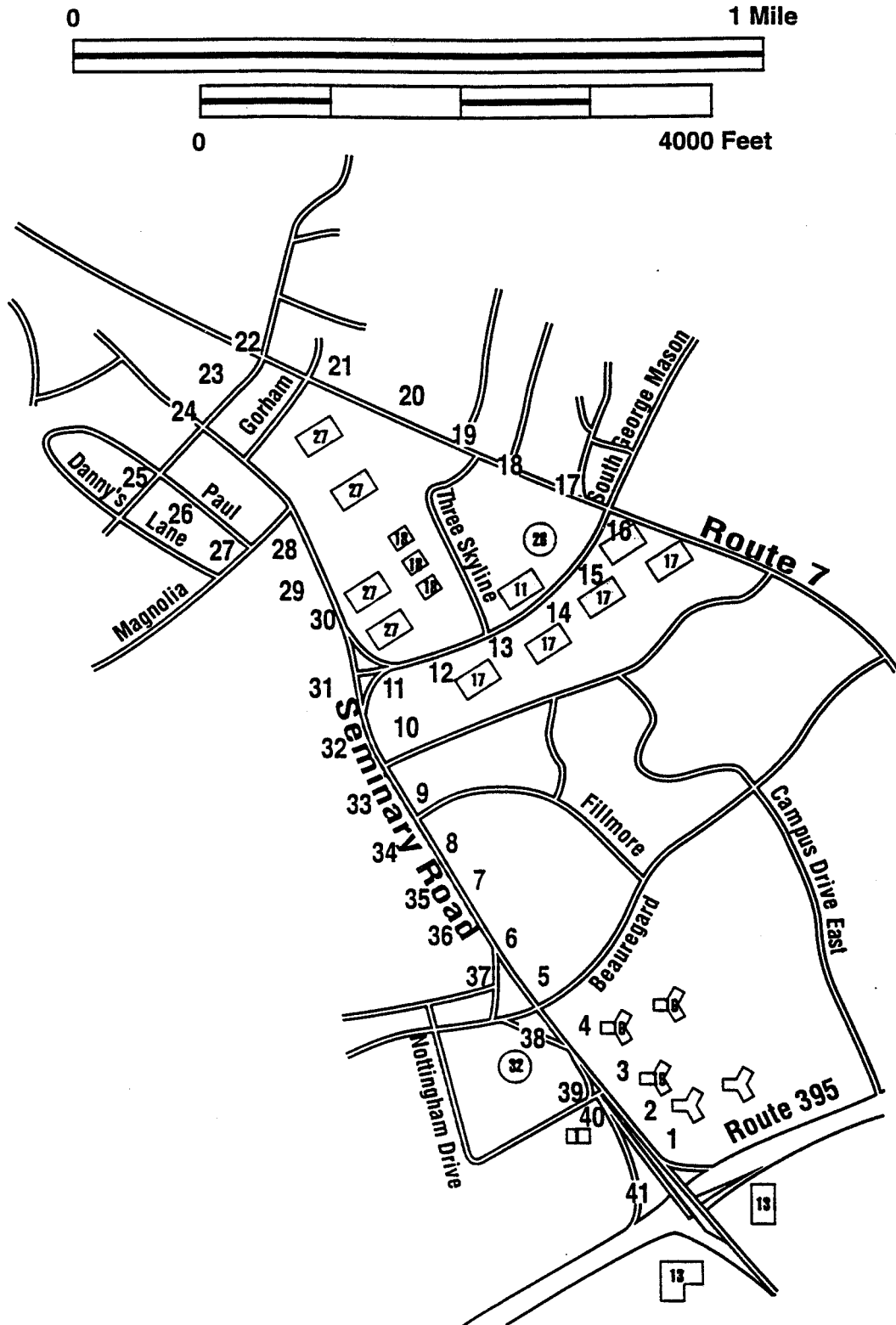


Figure 10 -- Test Range AGC Measurements - Sheet 1 of 2

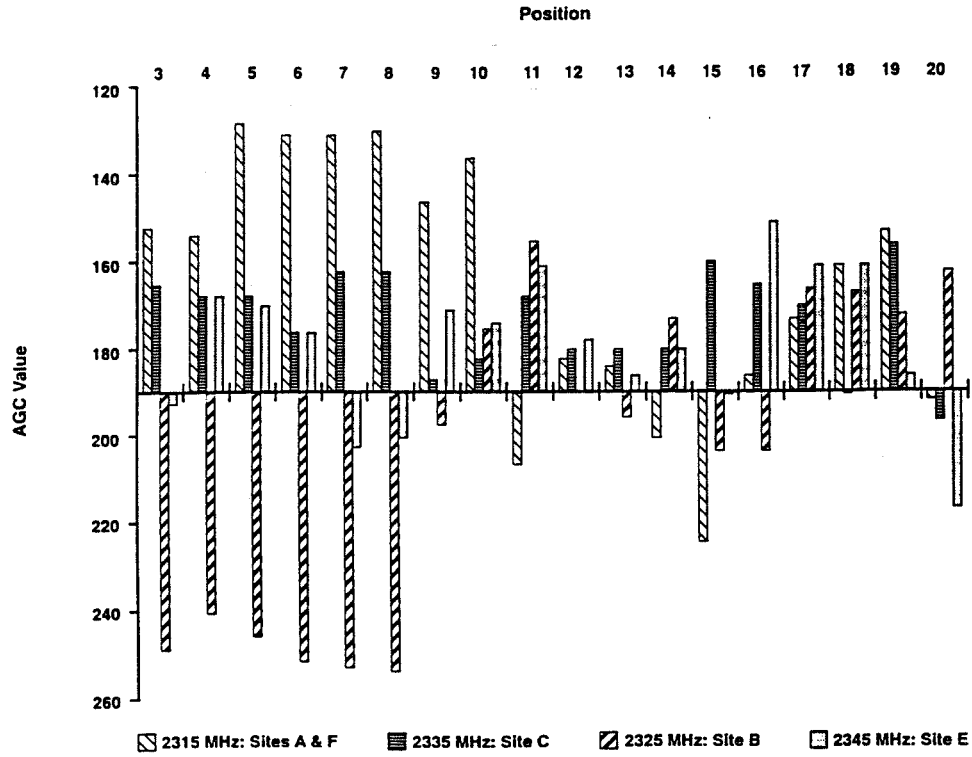


Figure 11 -- Test Range AGC Measurements - Sheet 2 of 2

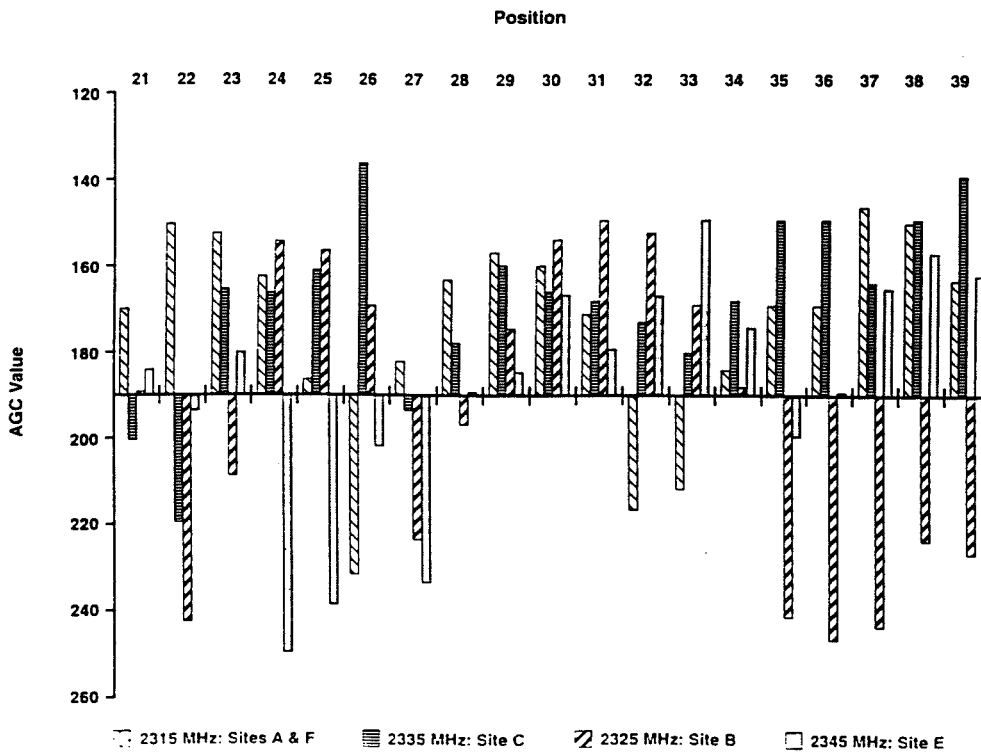


Figure 12– Highway Overpass, Test Results Summary

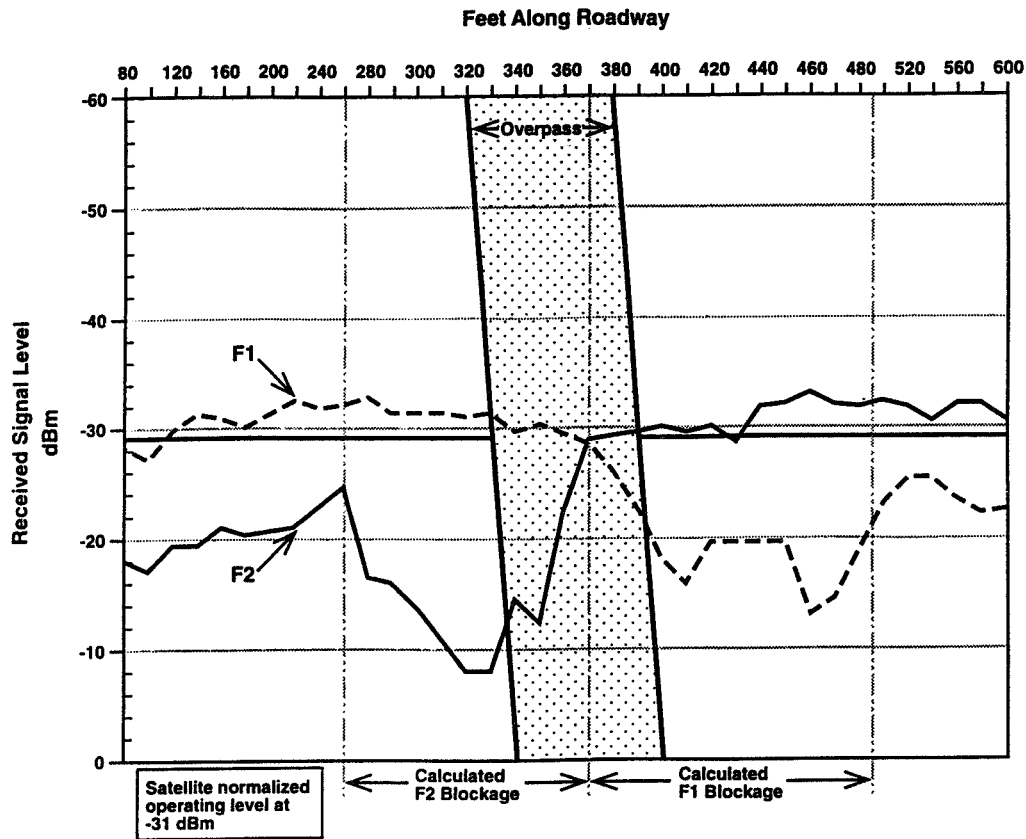
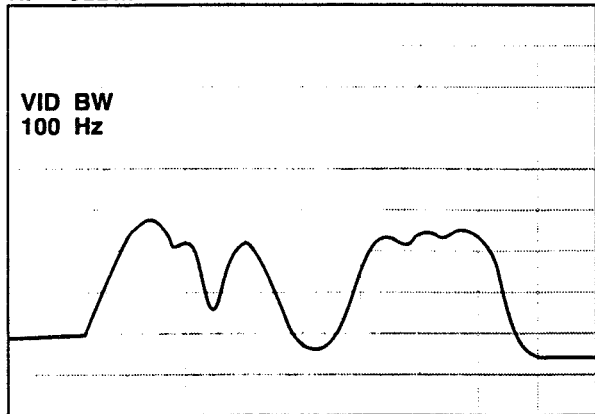


Figure 13– Test Range Spectrum Plots

ATTEN 10dB

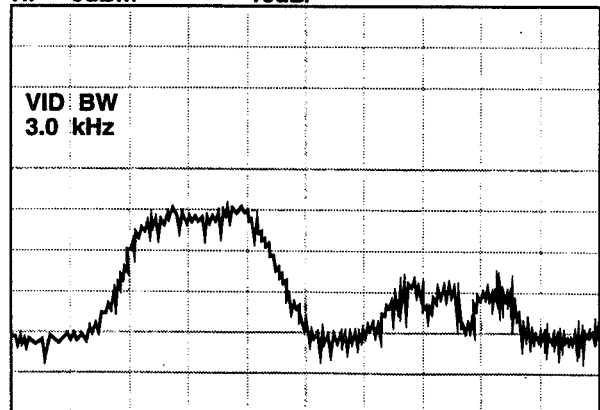
RI 0dBm 10dB/



*RBW 100kHz *VBW 100 Hz SWP 5.0sec

ATTEN 10dB

RI 0dBm 10dB/



*RBW 100kHz *VBW 3.0 kHz SWP 170 ms

EERL / Univ. of Texas

Satellite Fade Statistics and Diversity Gain for Personal and Broadcast Satellite Communications Systems Derived from TDRS Observations

**Wolfhard J. Vogel and Geoffrey W. Torrence
Electrical Engineering Research Laboratory
The University of Texas**

**Presented at NAPEX XVIII
Vancouver, BC Canada
June 17, 1994**

Background

- **NASA Propagation Program has supported mobile satellite propagation research since 1983.**
- **Results have been used to support industry, government, and regulatory bodies.**

Propagation Problems

- **multipath fading (flat)**
- **shadowing by trees**
- **blockage by structures**

User Scenarios

- **mobile**
 - vehicle-mounted antenna
 - antenna hand-held inside vehicle
- **ported**
 - outdoors
 - in building

Mobile Earth Station (MES) Environments

- rural
- suburban
- urban
- terrain
- vegetation

Applications for TDRS Propagation Data

- DBS fade and performance prediction
- LEO satellite diversity gain prediction
- mobile fade prediction
- modeling of frequency scaling

Available Tools to Acquire Data

- **TDRS**
 - cw transmissions
 - from one or two satellites
- **MES**
 - portable narrowband receiver
 - user antennas
 - » vehicle-mounted
 - » portable

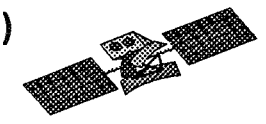
EERL / Univ. of Texas

TDRS-3
(62°..171°)

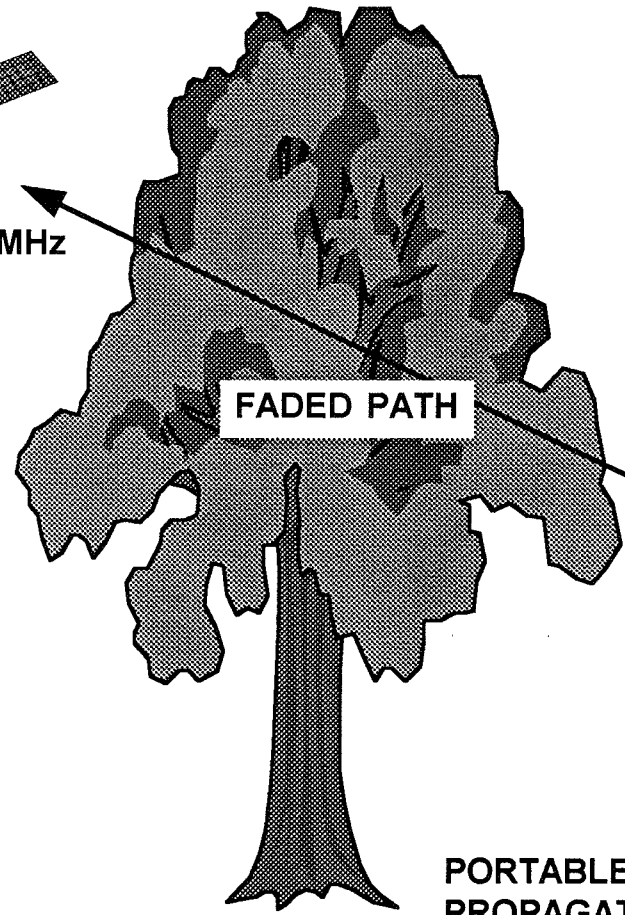


2055.001 MHz

TDRS-6
(46°)



2054.999 MHz



FADED PATH

angular
separation

UNFADED
PATH



receive
~2055 MHz

PORTABLE
PROPAGATION
RECEIVER

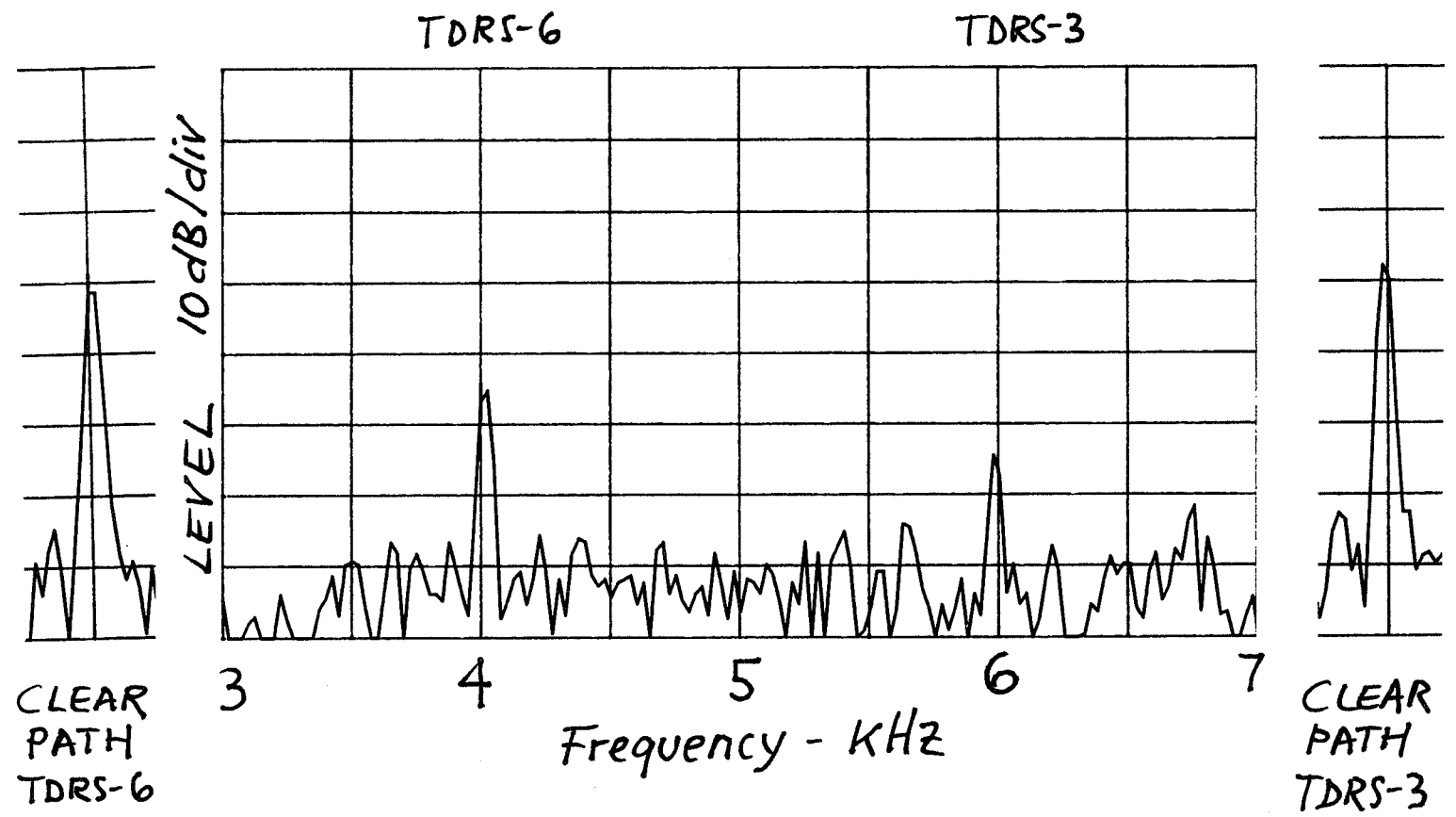
record 5 ± 2 kHz
i.f. on DAT

DIVERSITY MEASUREMENT CONCEPT

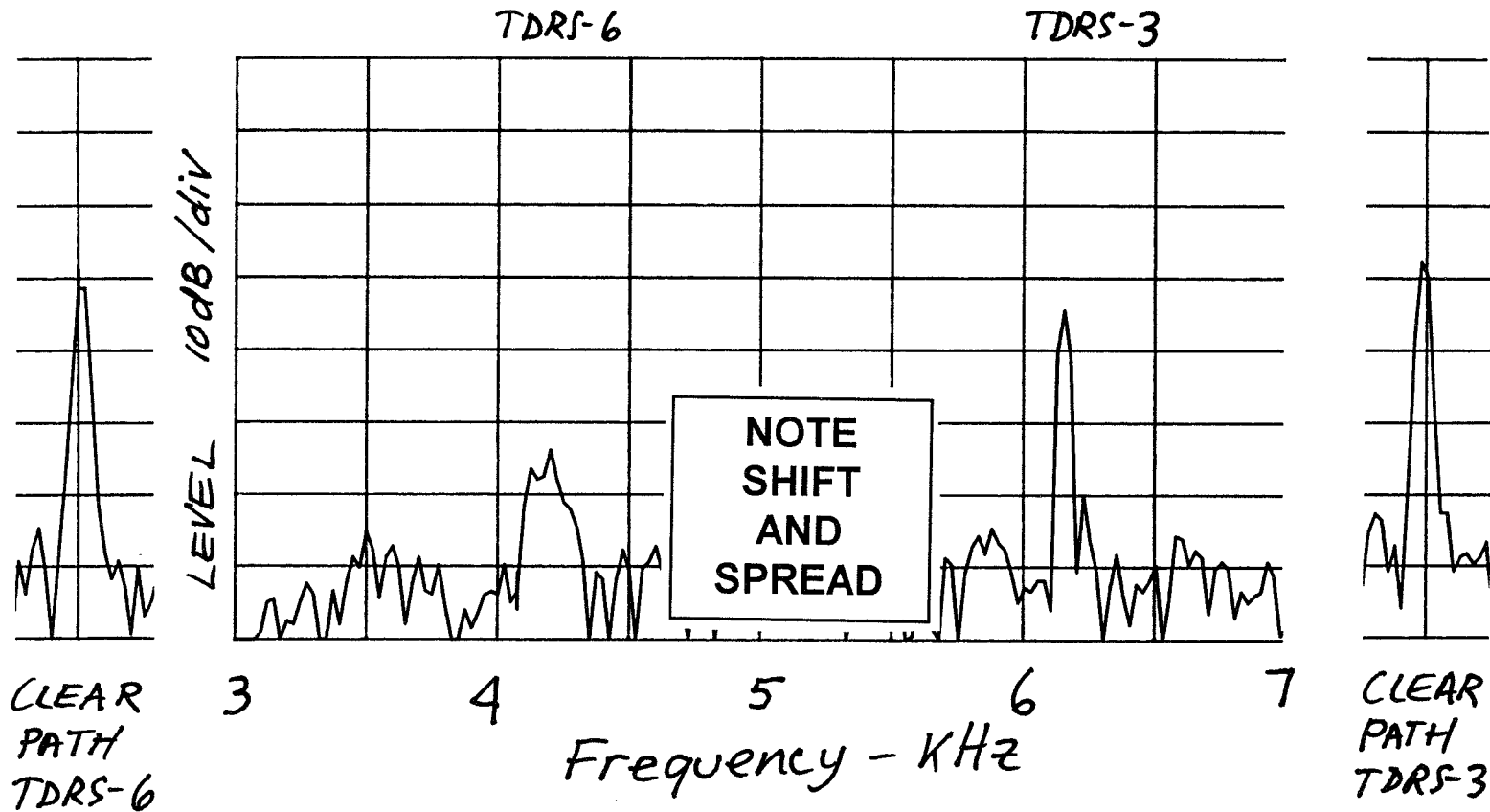
MEASUREMENT EXAMPLES

- TDRS-3 and TDRS-6 on 03/19/94 in Austin, TX
- abscissa: center frequency = 5 kHz, 1 kHz/div
- ordinate: 10 dB/div

Example 1: Walking Inside a House



Example 2: Driving in a Car



Data Reduction and Analysis

- transfer digital i.f. data from DAT recorder (16 bit, 48,000 sps) to PC
- programmed filtering and IQ detection
- derive log amplitude and phase timeseries
- classify by experimental parameters
- calculate cumulative fade statistics for each satellite observed
- calculate joint fade statistics
- calculate diversity gain

Experiment Plan

- **observe TDRS-3 and -6 simultaneously**
- **in Austin, Texas**
- **every $\sim 10^\circ$ during move of TDRS-3**
- **with repeated MES scenarios**
 - mobile with antenna on and in car
 - ported with receiver at head
 - in suburban and urban areas
 - in a few buildings
- **reduce and analyze as funds become available**

ACTS MINIWORKSHOP

**A MINIWORKSHOP
ON
ADVANCED COMMUNICATIONS
TECHNOLOGY SATELLITE (ACTS)
PROPAGATION STUDIES**

ACTS Opening Remarks

F. Davarian

Our ACTS propagation campaign has made considerable progress since the last time we met in New Mexico. We have gathered here today to review the status of our campaign and discuss issues needing our attention.

As you recall, in our previous meetings we had the NASA headquarters representative addressing us. He reviewed NASA's organization and objectives. However now that our NASA contact, John Kiebler, has retired, I will try to describe NASA's organization and its expectations of this campaign to the best of my ability. Please see Chart 1.

Changes in national priorities combined with a slow economy have had their effect on NASA. Headquarters has been going through transitions for the last two or three years. NASA is seriously reevaluating its priorities and is reconsidering the way it conducts business. In this climate NASA managers are sometimes too preoccupied to pay close attention to some of the ongoing programs such as ours. Fortunately for us and largely because of the good work of our community, the NASA Propagation Program is enjoying a good level of visibility at NASA.

I am happy to announce that in a recent review of NASA's communications projects, the NASA Propagation Program, and specifically the ACTS campaign, received positive feedback from the review committee. This committee consisted of the members of the space communications industry. I am also pleased to report that NASA funding of the ACTS campaign will continue.

NASA's requirement is that we help the satellite communications industry to develop and introduce new applications and services. Our community should rely on its own resources for success. I am asking our experimenters to continue their work with the same enthusiasm and dedication as before.

Many of the terminal bugs have been resolved, but not all have been corrected. I had to work hard to get renewed funding for Dave Westenhaver. Dave is funded now, and he is dedicated to quickly resolving all the remaining terminal issues. I am hoping that with help from the experimenters, Dave will be able to solve the remaining problems and, by the next time we gather, we will not have to be concerned about the terminals anymore.

At this stage, we should focus on data processing and analysis. I expect Bob Crane will continue his leadership role in this area. He has written a report on terminal calibration. We hope to be able to finalize our calibration scheme soon. I also expect that Wolf Vogel will play a strong role in these areas since

he is a sophisticated experimenter with years of experience. In short, we should be sending calibrated preprocessed data to Wolf every month and be able to conduct analysis and modeling efforts.

Bob Bauer is requesting a one-year extension for our campaign. If he succeeds, we will have funding to continue our measurements for three years. He is also asking for a little more money after the measurements end to allow time to finalize our analysis and modeling. He will elaborate on this issue in his talk.

The evening plenary session jointly chaired by Bob Crane and Dave Rogers will serve to capture the essence of this meeting. I expect a summary report including a list of recommendations from them. This report will be published in the proceedings of our meeting.

ISSUES FROM THE LAST MEETING:

A) REPORTING

1. There is no longer a need for weekly reports. Please send a brief monthly status report to JPL. This report will indicate accomplished milestones and problem areas. Its size should be about half a page. To allow other experimenters to see your progress, I encourage the use of the ACTS e-mail system for status reporting.
2. Quarterly reports required under contract will continue to be sent to NASA Lewis with a copy to JPL.
3. Monthly data will continue to be sent to Texas.

B) OTHERS

1. Capacitor rain gauge
2. Digital receiver post-detection filter
3. Antiwetting agent to coat the antenna
4. Beacon-level changes
5. Calibration

In this workshop, we will focus on calibration and preprocessing. In the next one, we will focus on analysis and modeling. Please see Chart 2.

PROGRAM ORGANIZATION

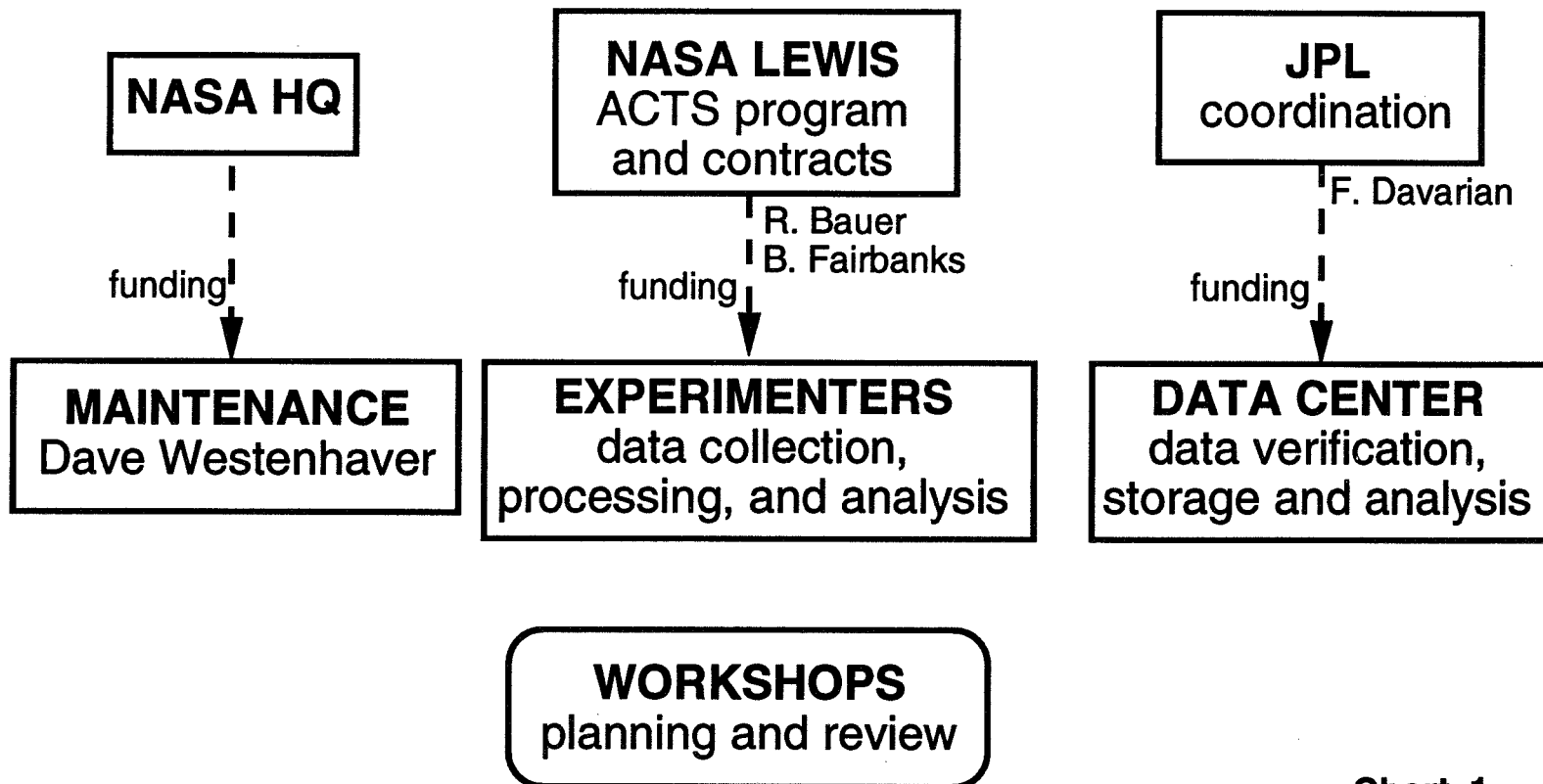


Chart 1

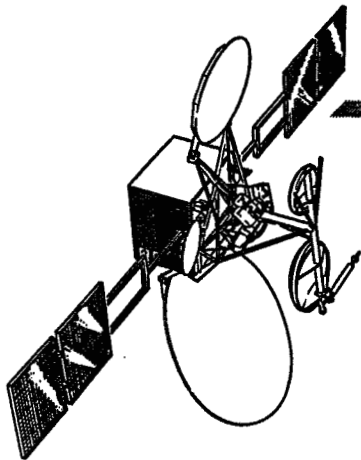
Focus Areas in ACTS Propagation Workshops

- **November 1993**
 - Terminal hardware/software
 - Calibration/ Preprocessing
- **June 1994**
 - Calibration/ Preprocessing
 - Analysis
 - Terminal hardware/ software
- **November 1994**
 - Data analysis
 - Modeling
 - Results

Chart 2

Advanced Communications Technology Satellite (ACTS) Program

243



ROBERT BAUER
NASA LEWIS RESEARCH CENTER

"ACTS STATUS AND UPDATE"

ACTS MINI WORKSHOP/NAPEX XVIII
VANCOUVER, BRITISH COLUMBIA
JUNE 16, 1994

ACTS

NASA

ACTS OPERATIONS STATUS

- AS OF MAY 01, 1994 FOUR YEARS OF STATIONKEEPING PROPELLANT REMAIN ON ACTS!
- OPERATIONS CAN NOW BE CALLED ROUTINE.

SPACECRAFT ATTITUDE

- S/C WAS BIASED IN PITCH & ROLL TO MAINTAIN CONSTANT DOWNLINK SIGNAL FOR MBA CHECKOUT AND TO BETTER COVER EXPTR. SITE ON EDGE OF BEAM.
 - Roll bias adjusted (removed) on 5/23/94 by 0.12° South to optimize MBA pointing.
 - 02/05/94 S/C pitched $+4.84^\circ$ inadvertently (instead of -0.28°). C-band back-up used to re-establish control. S/C returned to normal within 5 hrs.

ACTS OPERATIONS STATUS, cont.

- OPERATIONS CONTINUE UNDER EARTH SENSOR CONTROL INSTEAD OF AUTOTRACK. YAW ESTIMATOR USED SINCE JUNE 01 AND HAS BEEN PERFORMING WELL.
 - Algorithm estimates position of Sun when it's not in view of Sun sensors.

ECLIPSE

- FIRST COMPLETE ECLIPSE CYCLE FROM 02/26-04/13/94.
- ANNULAR ECLIPSE ON 05/10/94.
 - 78% obscuration of ACTS @ ~11:00PM EDT.
 - System shut-down as during a seasonal eclipse.

THERMAL EFFECTS

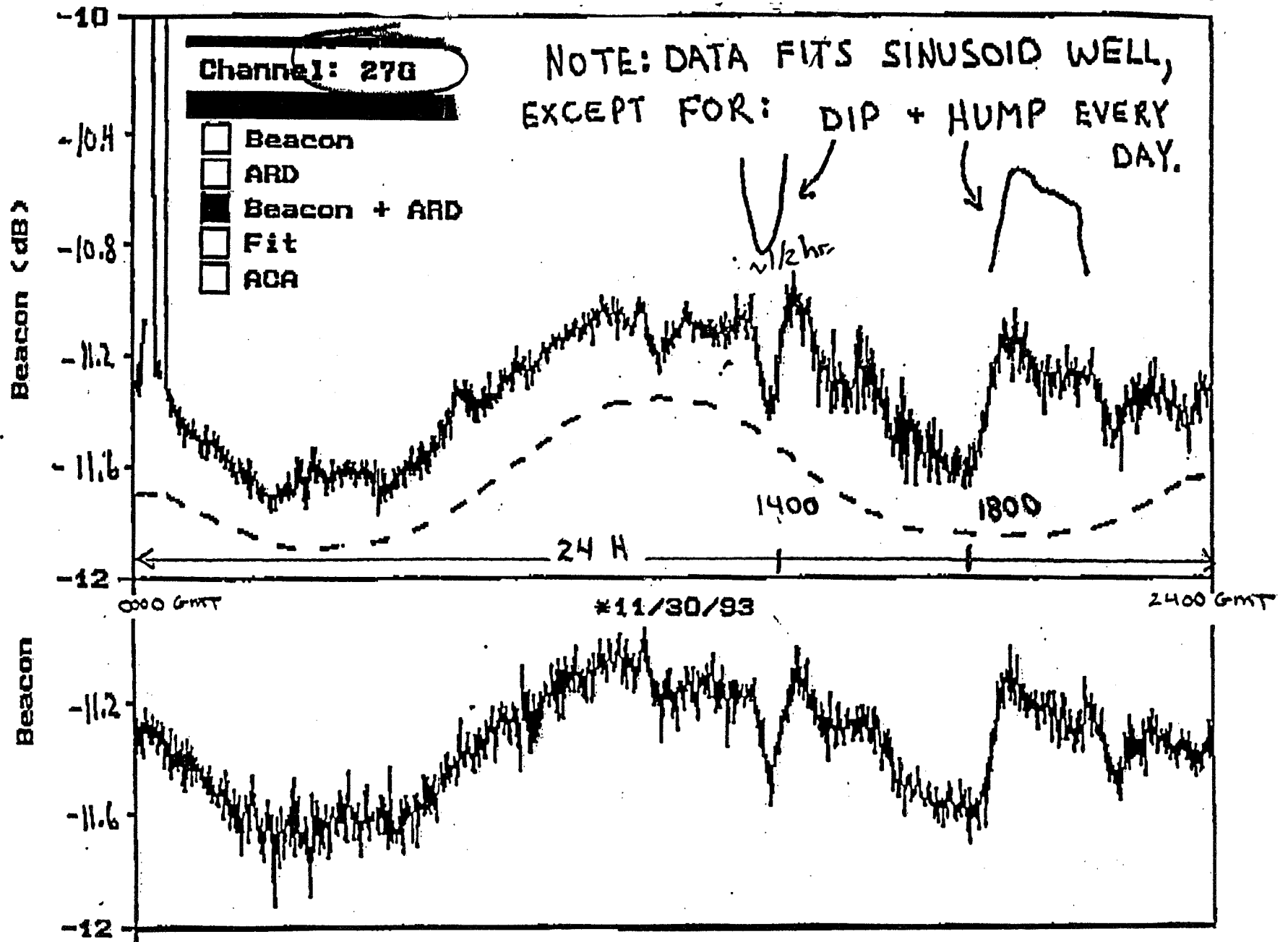
- MBA CHECKOUT - VARIOUS TESTS PERFORMED TO MEASURE BEAM CENTERS AND PATTERNS.
 - Thermal effects mostly understood. Impact to spot beam users is negligible.

ACTS OPERATIONS STATUS, cont.

- "DIP" & "HUMP" IDENTIFIED BY PROP. EXPTRS. IN LATE NOV. '93 DUE TO AUTOTRACK ROLL PERFORMANCE.
 - S/C reacted to beam wandering due to thermal effects of MBA.
- DAILY HUMP & DIP ($\sim\pm 0.3$ dB) REPORTED IN JAN. '94 OCCURRING AT ~ 0900 AND 1100 DUE TO LARGE ($>100^\circ$ C) TEMP CHANGE IN BEACON TOWER.

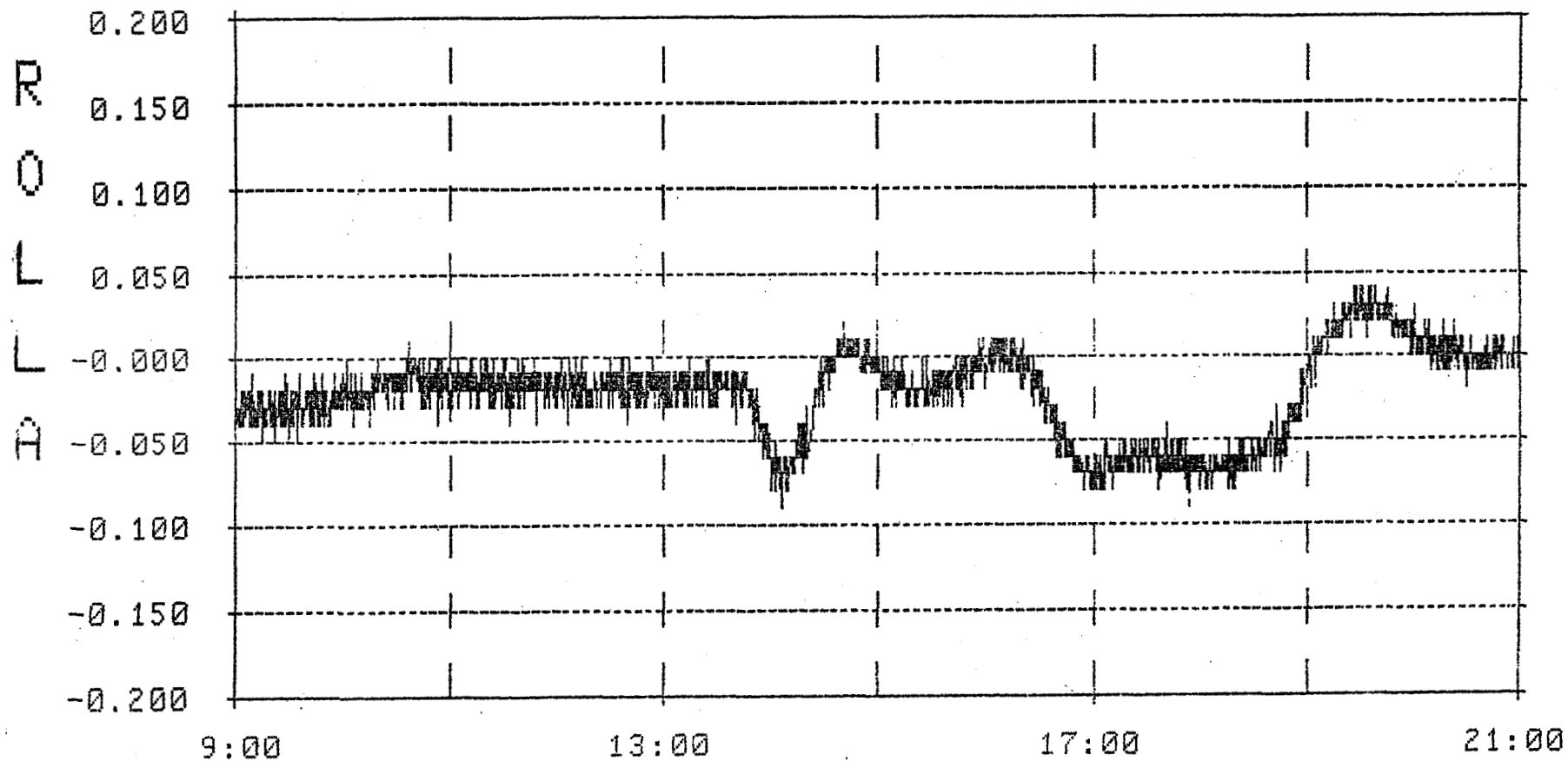
PAYLOAD

- APPROXIMATELY 6 MOS. OF OPERATIONS AND ALL SYSTEMS OPERATING WELL.
- BBP NETWORK CRASHES BY UNIQUE WORD/TRACKING ERROR WORD MISSES STILL UNDER INVESTIGATION.



UNIVERSITY OF ALASKA - "DIP & HUMP" PHENOMENA

1 = ROLL ANGLE



93/11/30 09:00:00

SPACECRAFT RECORDED ROLL ANGLE - AUTOTRACK

ACTS OPERATIONS STATUS, cont.

- **QUANTITY OF CRASHES HAS BEEN ON DECLINE.**
 - Were occurring daily, typically one crash per day.
 - Occurrence now more erratic, sometimes none for weeks.
- **1 HZ ANOMALY BEING INVESTIGATED.**
 - A 0.015° p-p variation in beam results in ~ 1 dB change in S/C D/L signal (at -10 dB beam contour) observed at LET, HDR and T1 VSAT's.
 - Theory is TX main reflector oscillates due to mechanical impulse by momentum wheel system.

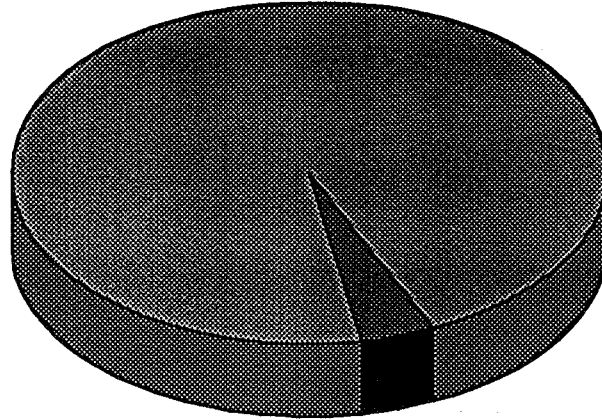
MGS OPERATIONS

- **MGS STAFFED 24 H/D, 7 D/W; INCREASE TO 12 FULL TIME POSITIONS.**
- **SOME TWTA DIFFICULTIES (BBP UPLINK).**



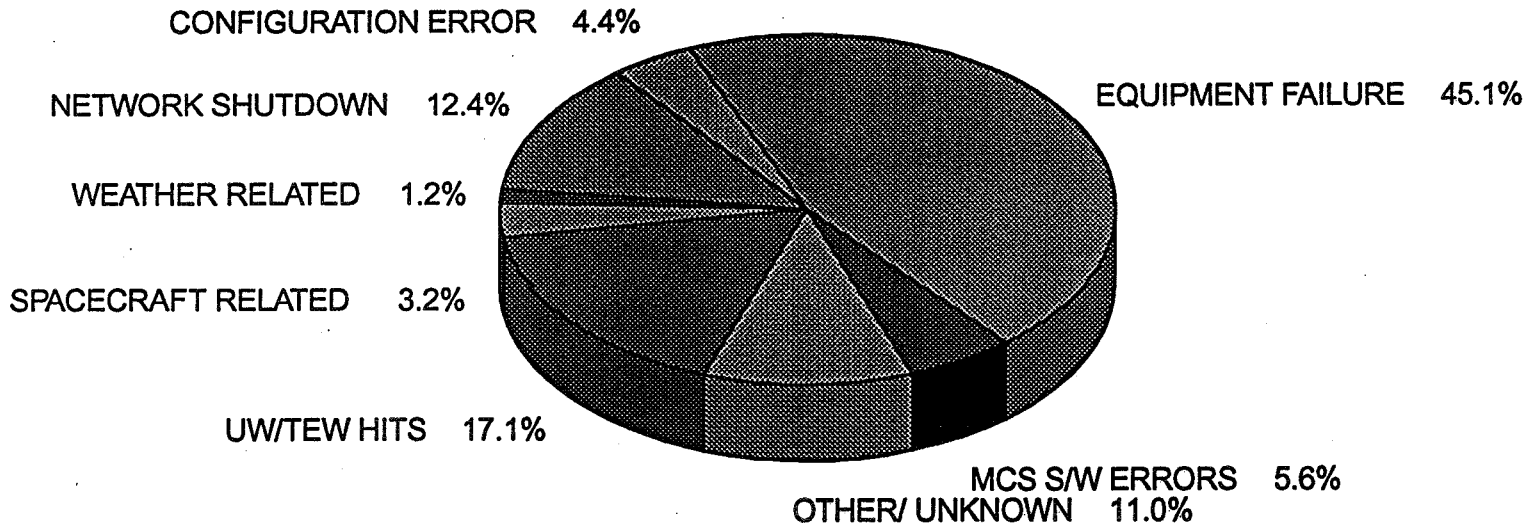
BBP MODE RELATED OUTAGES FOR LAST 60 DAYS

NORMAL OPS 95.9%

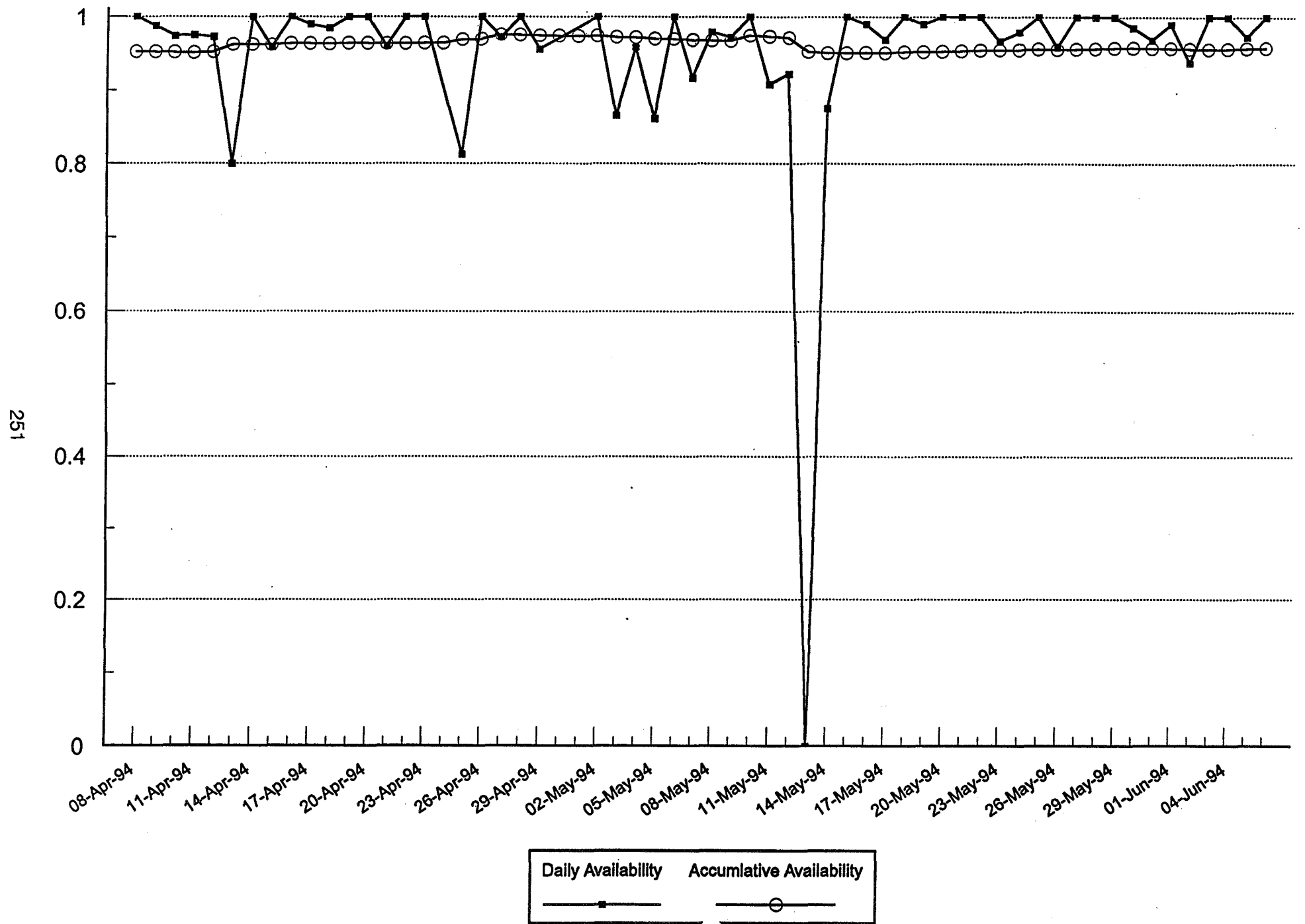


TOTAL OUTAGES 4.1%

BREAKDOWN OF OUTAGES



BBP NETWORK AVAILABILITY FOR LAST 60 DAYS





252

ORIGINAL PAGE
COLOR PHOTOGRAPH

ACTS MASTER CONTROL STATION, LEWIS RESEARCH CENTER

ACTS EXPERIMENTS PROGRAM

- EXPERIMENTS APPROVED 76

- PIs, CO-PIs & AFFILIATED ORGANIZATIONS

INDUSTRY	39
UNIVERSITY	24
GOVERNMENT	23
CCDS	2
	88

EXPERIMENTS					
TYPES	INDUSTRY	UNIVERSITY	CCDS	GOV'T	TOTAL
APPLICATION	23	10	1	12	46
TECHNOLOGY VERIFICATION	4	0	1	12	17
PROPAGATION	5	8	0	0	13
TOTAL	32	18	2	24	76

STATUS 5/13/94

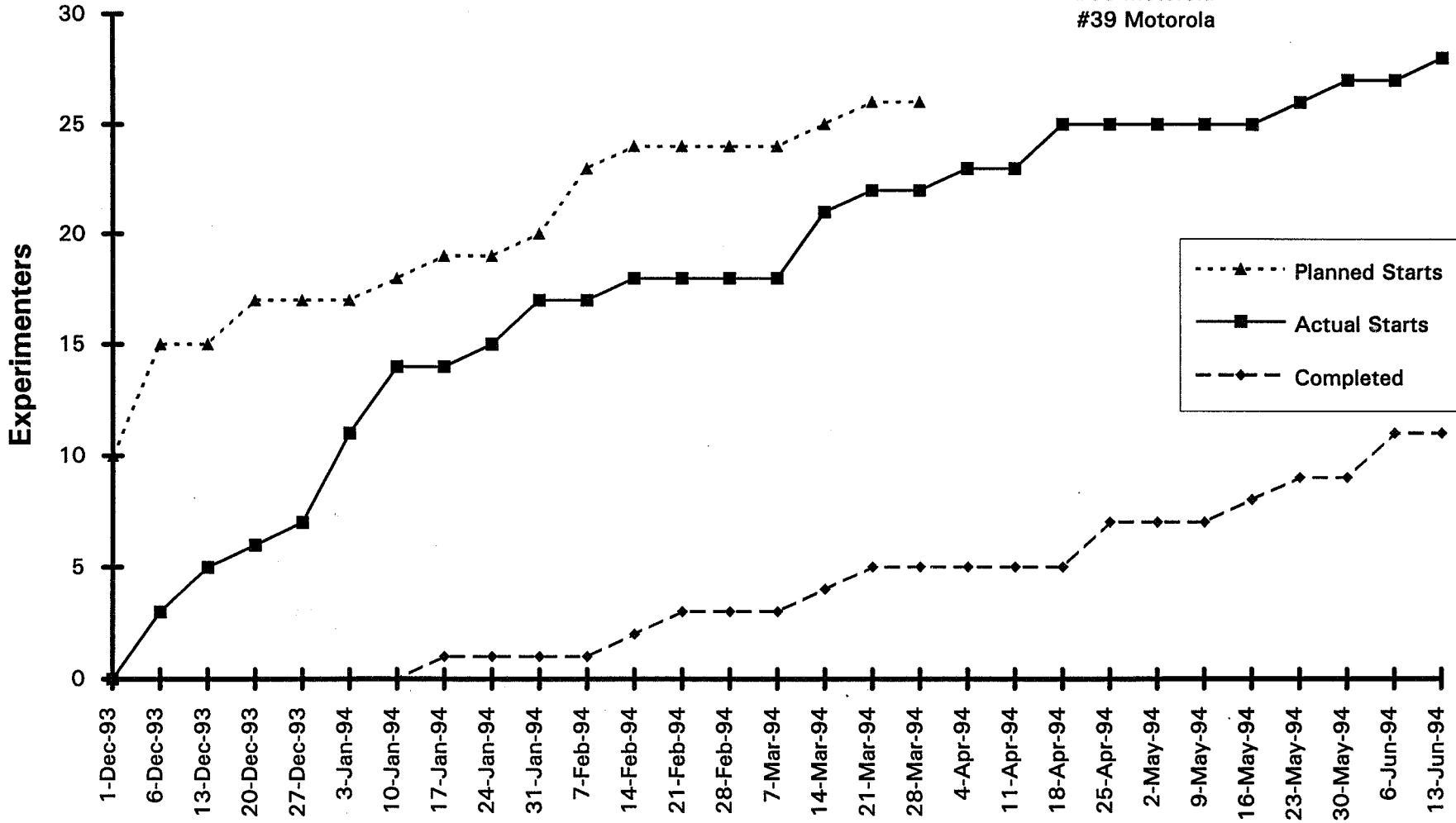
HOMAY94

Not Started
#909 Digital Tv

ACTS Experiment Starts/Completes

Completed

#1,2,3 NCS	#43 OU/Huntington Bank
#13 Krug Life/JSC	#54 Univ of Florida
#27 MITRE	#58 EMSAT
#38 Motorola	#809 JHU/UT
#39 Motorola	



Note: 7 Propagation Experiments currently running

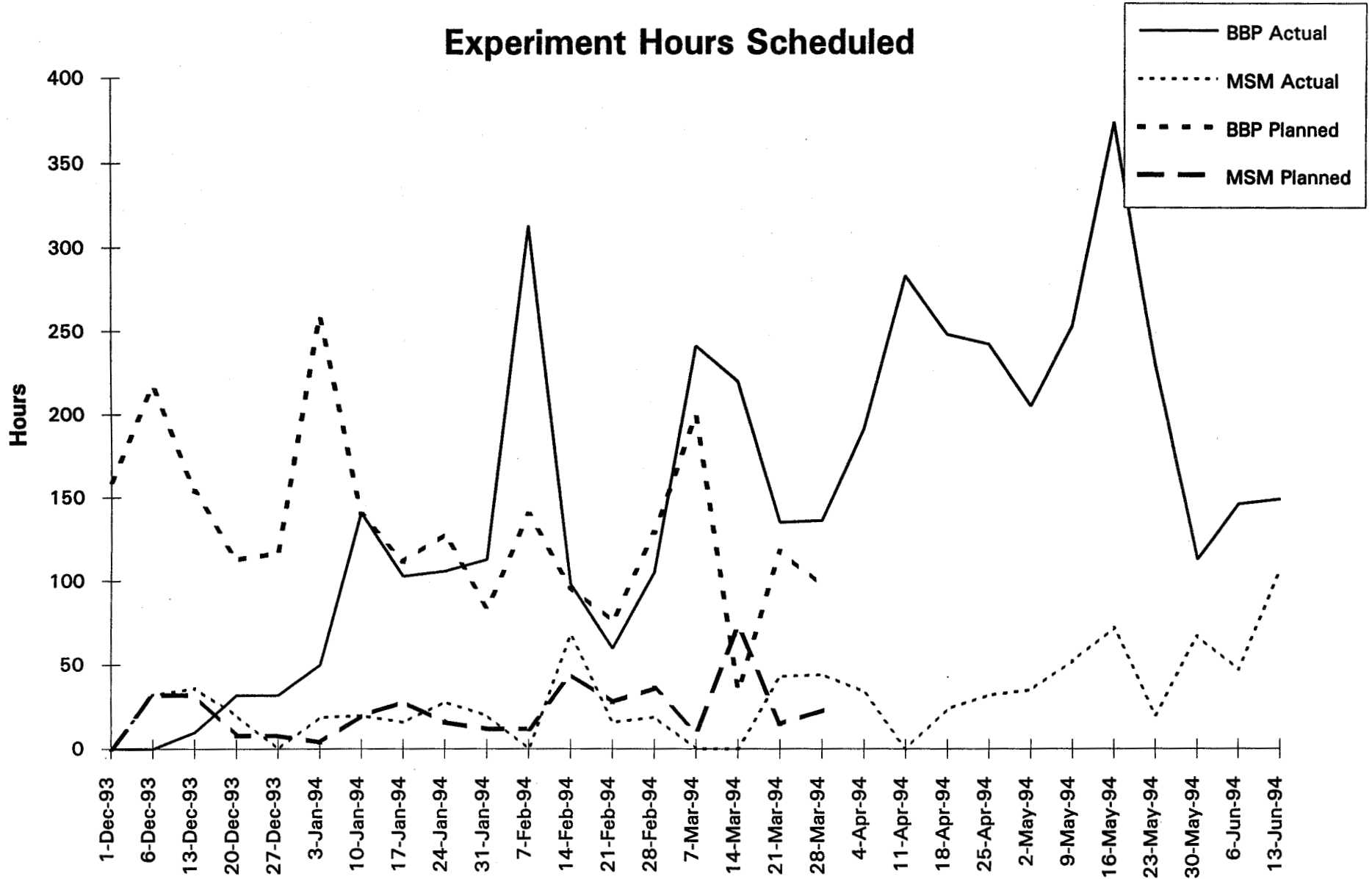
Experiment Starts and Completes by Week (actuals)

Line #	Date	Expt. #	Organization	Mode	Earth Station
1	6-Dec-93	8	JPL	MSM	AMT/LET
2		808	FAU	MSM	LET
3		908	INTEX	MSM	LET
4	13-Dec-93	38	Motorola	BBP	2, 13
5		39	Motorola	BBP	13
6	20-Dec-93	49	COMSAT	BBP	1, 7
7	27-Dec-93	45	TEC	BBP	19, 20
8	03-Jan-94	1	NCS	BBP	1, 4, 5
9		13	JSC/Krug	BBP	9, 12
10		43	OU/Huntington Bank	BBP	10, 11
11		58	EMSAT	MSM	AMT/LET
12	10-Jan-94	2	NCS	BBP	4, 5
13		7	Army	BBP	16, 17, 19
14		27	Mitre	BBP	5, 7
Completed	17-Jan-94	39	Motorola	BBP	13
15	24-Jan-94	901	MBA Performance	BBP	As Required
16	31-Jan-94	4	NCS	MSM	AMT/LET
17		701	NASA Demo	BBP	1, 9
18	14-Feb-94	809	JHU/UT	MSM	LET
Completed		2	NCS	BBP	4, 5
Completed	21-Feb-94	13	JSC/Krug	BBP	9,12

Experiment Starts and Completes by Week (actuals)

	19	14-Mar-94	5	NTIA	BBP	9
	20		6	ARL	BBP	2, 7, 8
	21		17	COMSAT	BBP	5, 7
Completed			38	Motorola	BBP	2, 13
	22	21-Mar-94	21	MAYO	BBP	12,13
Completed			58	EMSAT	MSM	AMT/LET
	23	04-Apr-94	53	AERO-X	MSM	LET
	24	18-Apr-94	54	University of Florida	BBP	3
	25	18-Apr-94	3	NCS	BBP	1, 4, 5
Completed		25-Apr-94	1	NCS	BBP	1, 4, 5
Completed		25-Apr-94	3	NCS	BBP	1, 4, 5
Completed		16-May-94	54	University of Florida	BBP	3
	26	23-May-94	804	COMSAT Uplink Power Control	MSM	LET
Completed			43	OU/Huntington Bank	BBP	10, 11
	27	30-May-94	903	LET MSM Performance	MSM	LET
Completed		6-Jun-94	27	Mitre	BBP	5, 7
			809	JHU/UT	MSM	LET

Experiment Hours Scheduled



EXPERIMENTER EARTH STATIONS

		<u>ACTS OWNED</u>	<u>EXPT'R OWNED</u>	<u>JOINT</u>
<u>BBP MODE:</u>				
NGS TRAFFIC TERMINAL	1	1		
T1-VSAT	19	8	11	
 <u>MSM MODE:</u>				
LINK EVALUATION TERMINAL	1	1		
HIGH DATA RATE	5	2	3	
ULTRA SMALL APERTURE TERMINAL (LeRC/SCE)	5	2		3
ACTS MOBILE TERMINAL (JPL)	3	3		
AERO (JPL)	1	1		
MINI-TERMINAL (LeRC)	1		1	
SETS (LeRC)	1		1	
FAU (RCV ONLY)	1		1	
COMSAT/INTELSAT	3		3	
NASA GSFC	1		1	
<u>PROPAGATION:</u>				
BEACON RECEIVER TERMINALS	11	8	3	
TOTAL	53	26	24	3
 POTENTIAL:				
<u>MSM MODE:</u>				
BB AERO (ROCKWELL)	1		1	
HDR (NCS)	1		1	
TOTAL	2		2	

258

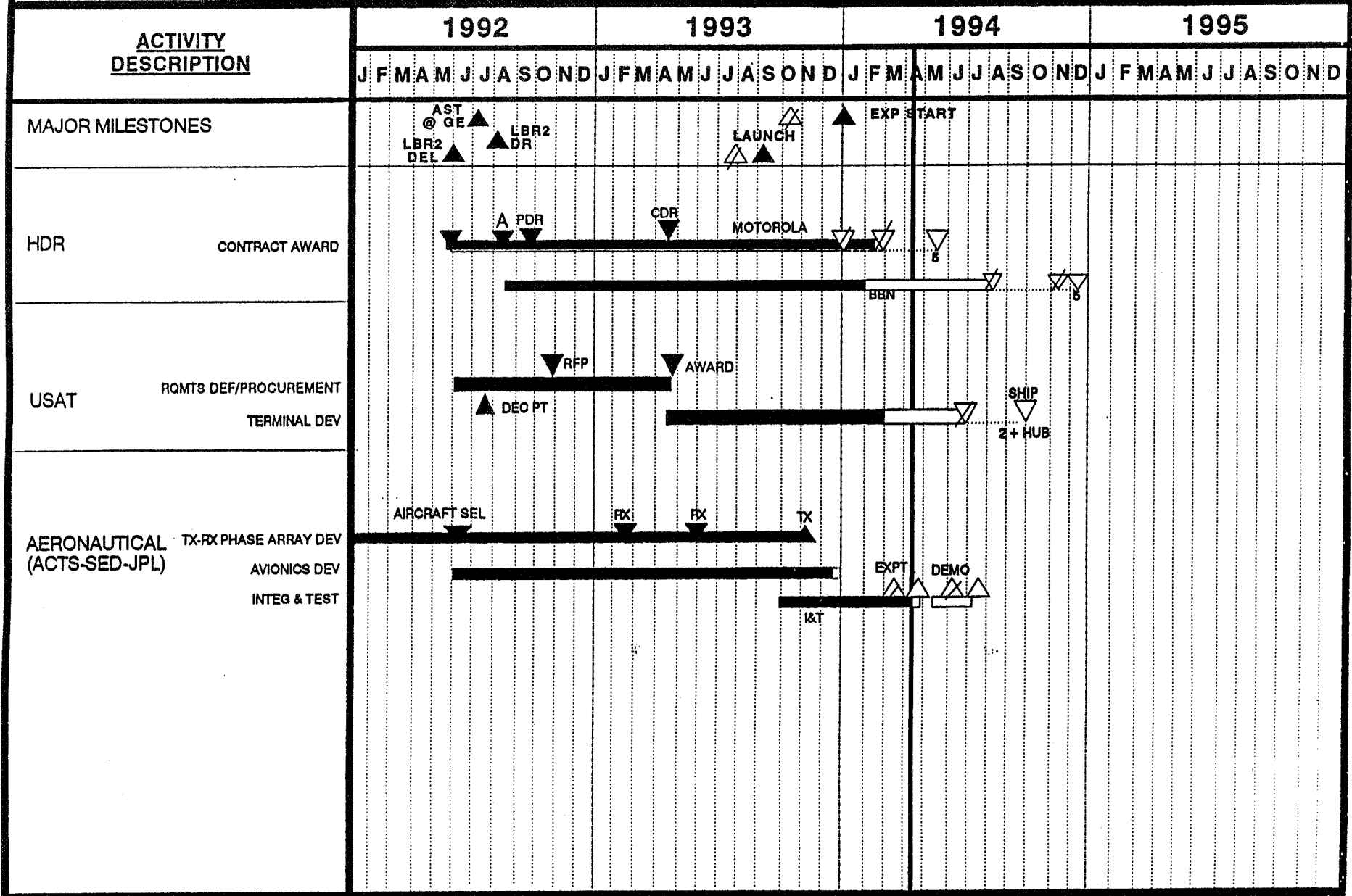
STATUS 5/13/94

T1 VSAT EARTH STATION LOCATIONS



ACTS Experiments Program Terminal Development Schedule

PLAN DATE:
REV 4: 5/14/93
STATUS: 4/25/94
PREPARED BY: B. BEZOSKA



260

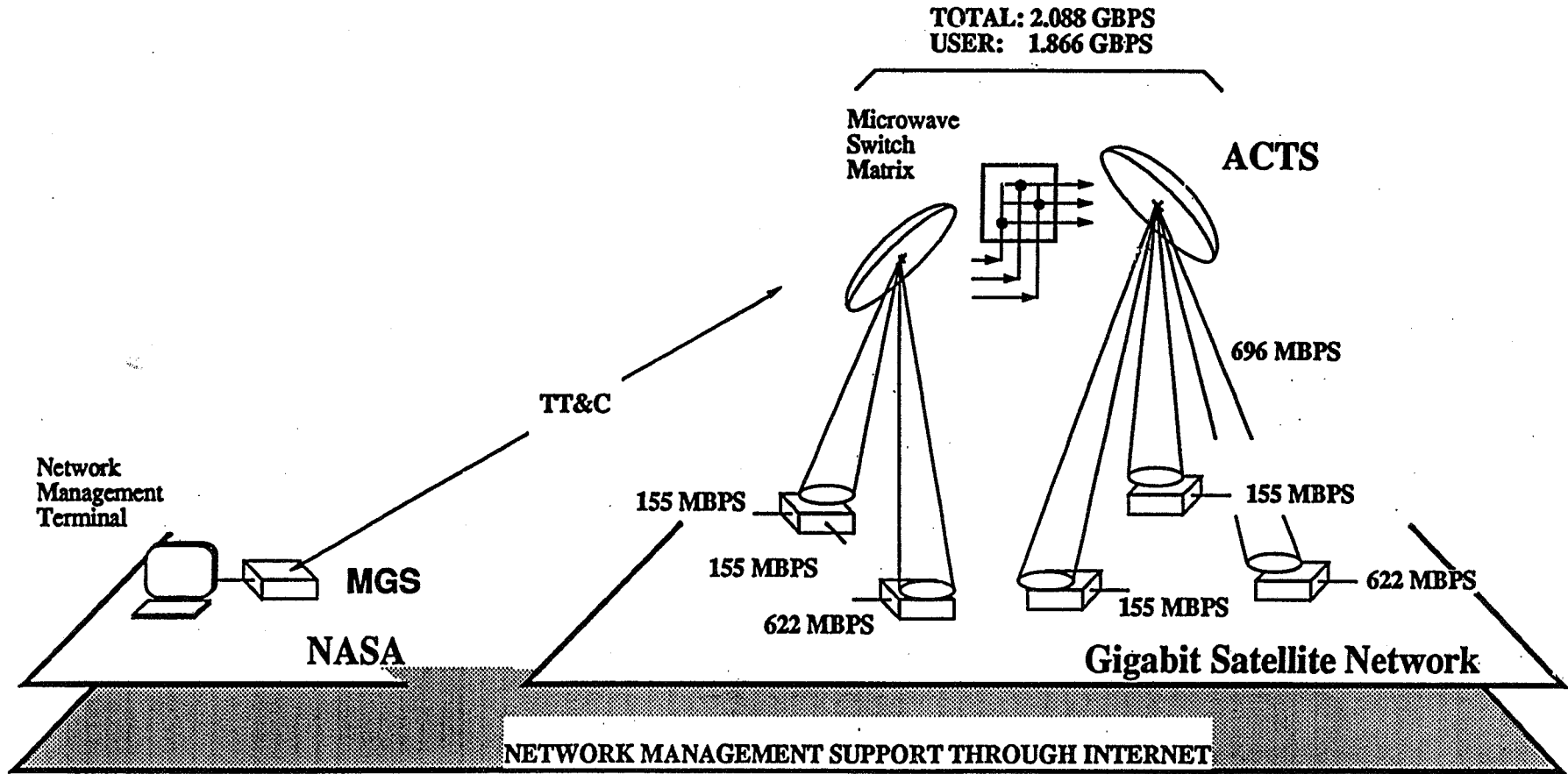


HDR Station at Motorola GSTG, Chandler, AZ
3.4 m, 622 Mbps

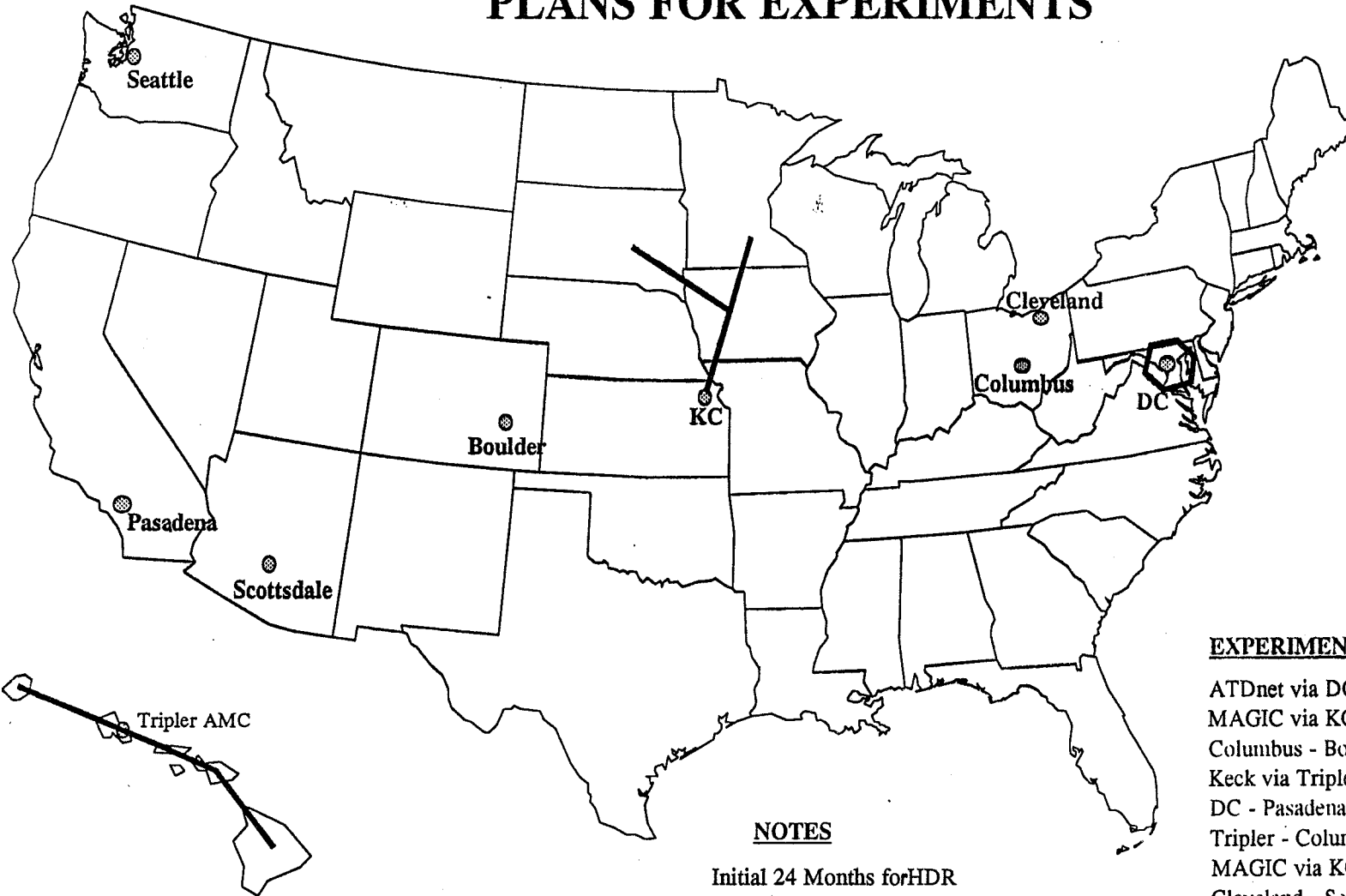
The Network Supports Sonet Interfaces at OC-3 and OC-12 Speeds and Provides Network Operators at NASA's Master Ground Station (MGS) with Direct Access to all Earth Stations.

BBN

262



HDR EARTH STATION LOCATIONS PLANS FOR EXPERIMENTS



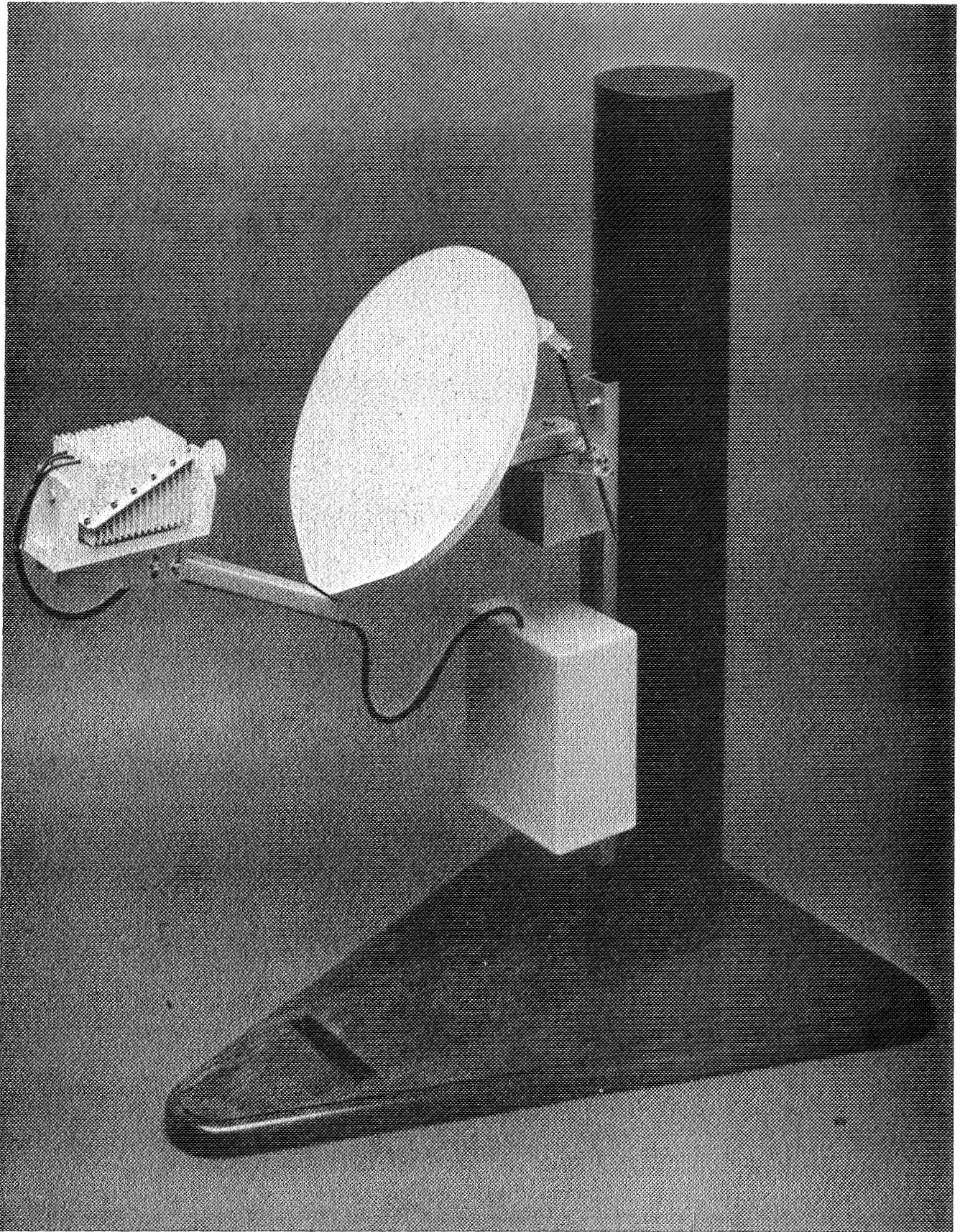
263

EXPERIMENT CONNECTIVITY

ATDnet via DC - Hawaii
 MAGIC via KC - Scottsdale
 Columbus - Boulder
 Keck via Tripler - Pasadena
 DC - Pasadena
 Tripler - Columbus - ATDnet
 MAGIC via KC - DC via ATDnet
 Cleveland - Seattle

NOTES

Initial 24 Months for HDR
 5 HDR Earth Stations
 8 Experiments
 9 Geographic Sites
 3 Terrestrial Fiber Networks



ACTS ULTRA SMALL APERTURE TERMINAL (USAT)
0.35 m diameter reflector; 4.8 kbps

AERONAUTICAL EXPERIMENT
(AERO-X)

SUCCESSFULLY TESTED THE AERONAUTICAL TERMINAL WITH THE ACRYLIC WINDOW AND POSITIVE LINK MARGINS.

CONTINUOUS PILOT TONE MONITORING AS WELL AS VOICE CONNECTIONS AT 9.6 AND 4.8 Kbps WERE ACHIEVED.

TUESDAY 26 APRIL 1994: MAIDEN VOYAGE

LEAR JET SPEED: 320 NAUTICAL MILES/HR

ALTITUDE: 41,000 FT

LOCATION: 150 MILES NW OF CLEVELAND

TIME OF 1ST CONVERSATION: 8:36 AM

CODEC RATE: 9.6 Kbps

LAST VERIFICATION FLIGHT: THURSDAY 12 MAY

FIRST DEMO FLIGHT: MONDAY 11 JULY

Acts Propagation Terminal Maintenance, Support and Updates

David Westenhaver
Westenhaver Wizard Works, Inc.
June 16, 1994

Westenhaver Wizard Works, Inc.

The GOAL of the Propagation experiments is to collect the maximum of meaningful propagation data from the ACTS satellite during the measurement period, so that any proposed propagation solution will have a solid experimental data base to be used to accurately predict the communication system performance AND to provide data to encourage inventive solutions to propagation problems in a system.

The GOAL of the Maintenance and Support effort is to assist the Users in keeping the propagation data collection system operational to maximize the quantity of meaningful propagation data.

Status / Deficiencies and Known Problems

DACS / TSR Hardware / Software status:

DACS / TSR Software status:

Revised, Version 5 Shipped Dec.14,1993

Revised, Version 7 Shipped Jun. 2,1994

Software Bugs Status:

Commutation Protocol errors; Version 5.

Compiler warnings removed; Version 6.

ADC and DAC logic system review; Version 6.

Analog voltages can have overflow; Version 6.

Incorrect WWV time causes loss of data;Version 7

Setup takes too long and is dumb; To Be Addressed.

Radiometer calibration can occur during a fade; TBA.

DACS needs updated EPROMS; TBA.

Pressing Problems:

Problem: Crashes and Reboots.

Solution: Rework code to limit effect.

Save settings and download passed on reboot.

Keep searching for the hardware problem.

RF Temperature Controller:

Problems: Generates noise , FETs over stressed,
lack of regulation.

Solution: New design is in progress.

New units will be sent in exchange for current
units.

Westenhaver Wizard Works, Inc.

Receiver Enclosure temperature regulation:

Problem: The air temperature OK but IF's follow outside temperature.

Solution: Larger fan, Move thermostat, Air flow baffles.

DRX Hardware / Software status:

DRX software status:

Revised, Version 12 Shipped Dec. 14, 1993

1Hz Filters Removed; Version 12.

20 Samples / second data is limited to 2-3 Hz BW; To Be Addressed.

Missing synchronization command / responses; TBA.

Pressing Problems:

Problem: 20 S/S Data Is Limited.

Solution: Rework Algorithm.

Problem: At least one unit fails above 48 Degrees.

Solution: Replace Temperature sensitive chip.

Westenhaver Wizard Works, Inc.

Status of Software:

ActsView software status:

Revised, Version 2.1 Shipped Nov. 15, 1993

System Crash at 23:59:59 if on status screen; TBA

Fails to "remember" last "custom" axis scaling; TBA.

Tape Backup Crashes system; TBA.

Data Problem with Daily Plots; TBA.

"Phase Noise" plot labels incorrect; TBA.

File Handles Need to be consistent; TBA.

Time axis not in integer minutes; TBA.

Unable to request "plot xx:xx:xx time"; TBA.

ActsEdit software status:

Version 1.2 Shipped Jan. 10, 1994 (Gaff)

Flags errors for Bad data; Version 2.

Review Edit w/o removing work files; TBA.

Add Range Tones Correction; TBA.

1995107269

N95-14683

349309

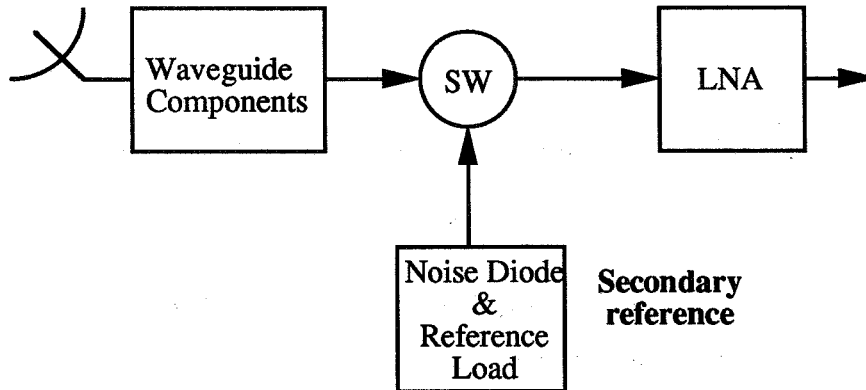
f 125

**Radiometer Calibration Procedure
and
Beacon Attenuation Estimation
Reference Level**

by

**Robert K. Crane
University of Oklahoma**

RADIOMETER SYSTEM



- **VSWR through switch is high (~ 2:1)**
- **Match secondary reference to LNA not the same as match antenna to LNA**
- **Hot/Cold load measurements not necessary match probably different from other loads**
- **No absolute calibration possible using loads and secondary reference**

RADIOMETER CALIBRATION

PRIMARY:

- Compare Radiometer Attenuation with Beacon Attenuation
- Compare Sky Temperature Estimates with Calculations Using Simultaneous Meteorological Data

SECONDARY:

- Noise Diode and Reference Load Measurements
- Adjust for Outside Temperature and Component Temperature Changes

RADIOMETER CALIBRATION MODEL

$$\mathbf{T_r = A + B V}$$

$$\mathbf{T_s = C T_r + D T_o + E}$$

$$\mathbf{A_r = -4.343 \ln ((T_m - T_s)/(T_m - T_b))}$$

A, B from noise diode, reference load measurements

C from beacon attenuation vs radiometer attenuation measurements

D, E from radiometer estimates of sky temperature vs calculated sky temperature

T_m from calculations

T_b from theory

SYSTEM CALIBRATION IS ITERATIVE

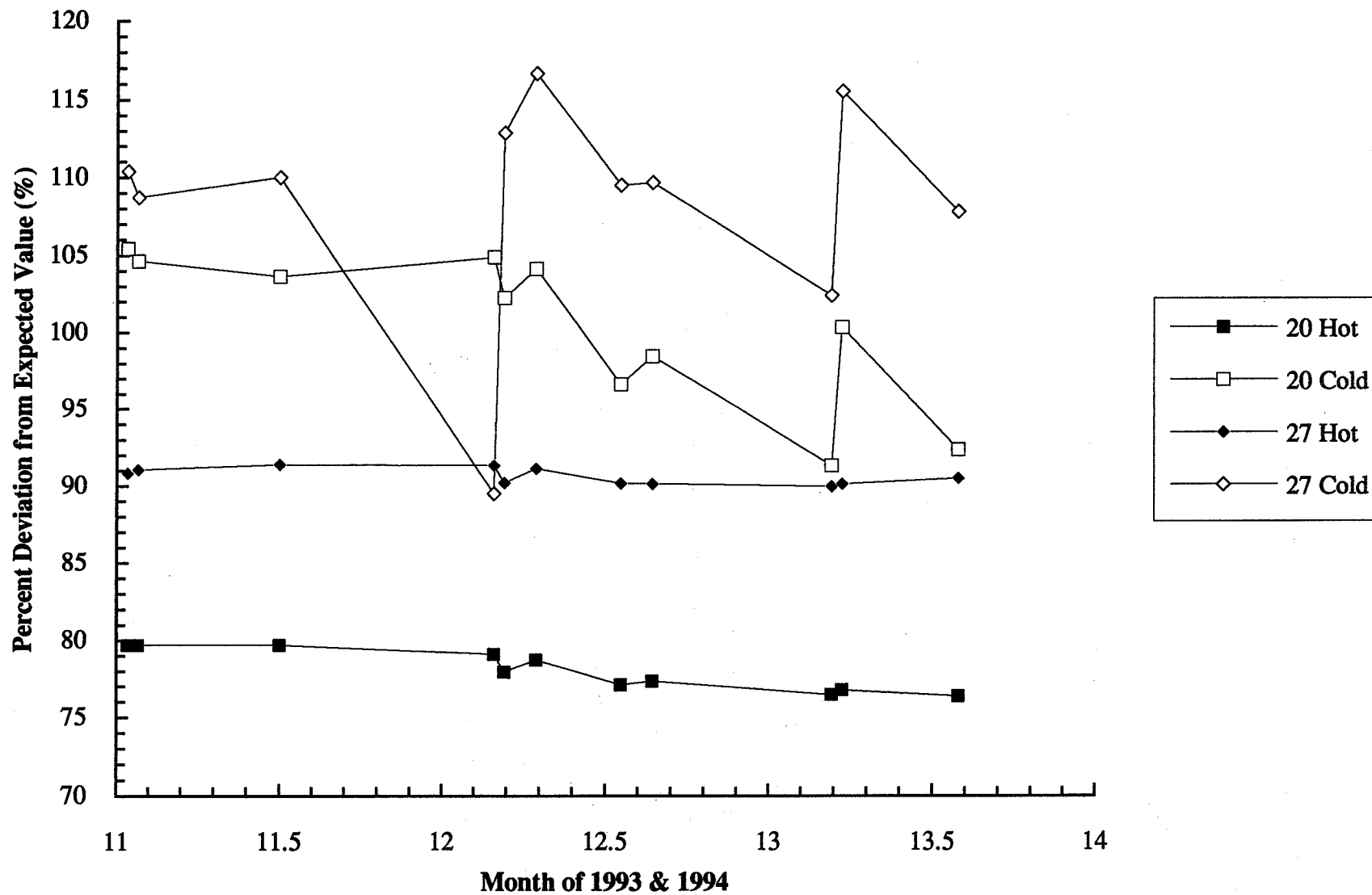
- **Need beacon attenuation to compare to radiometer**
- **Need radiometer attenuation to set beacon reference level**

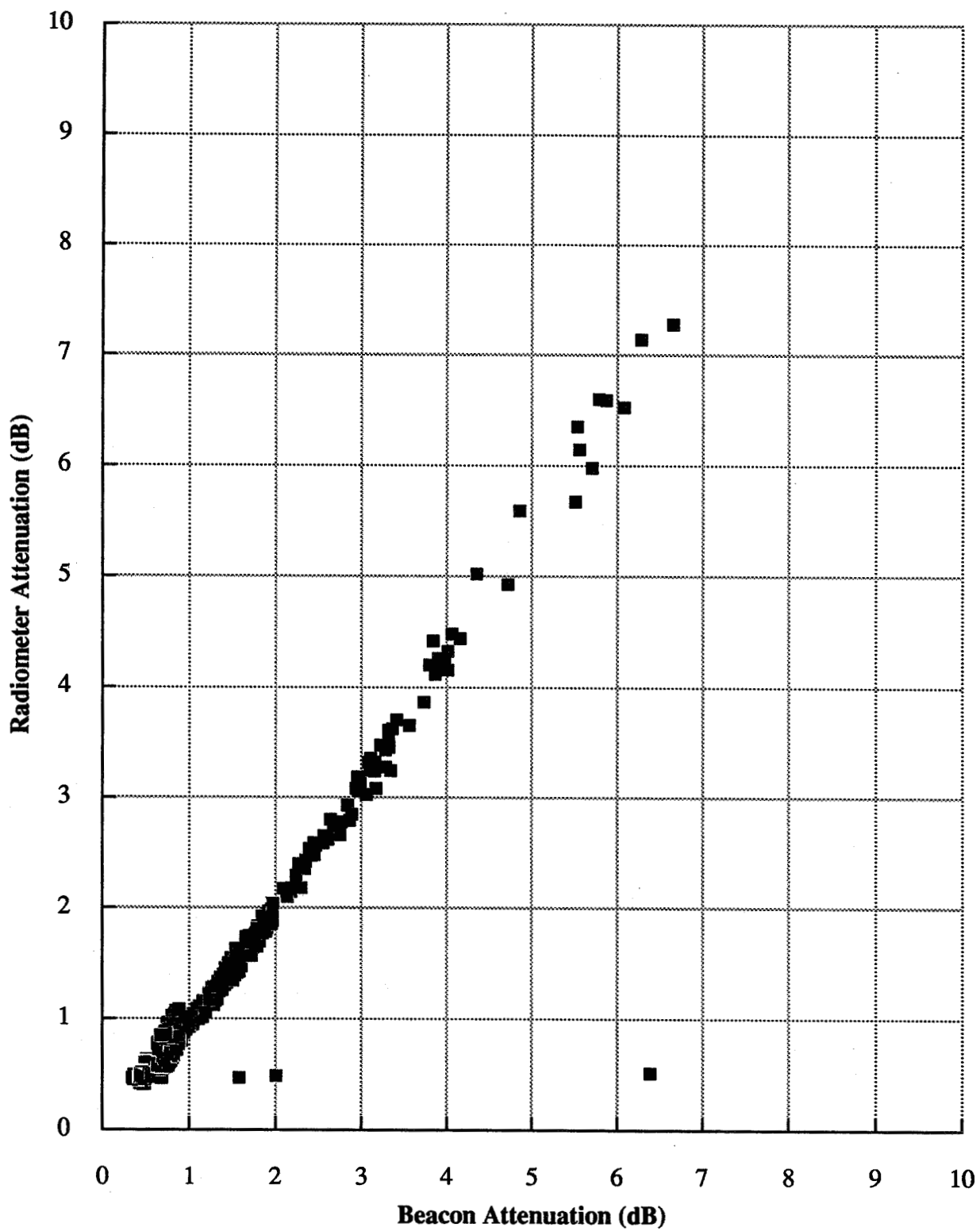
Assumptions

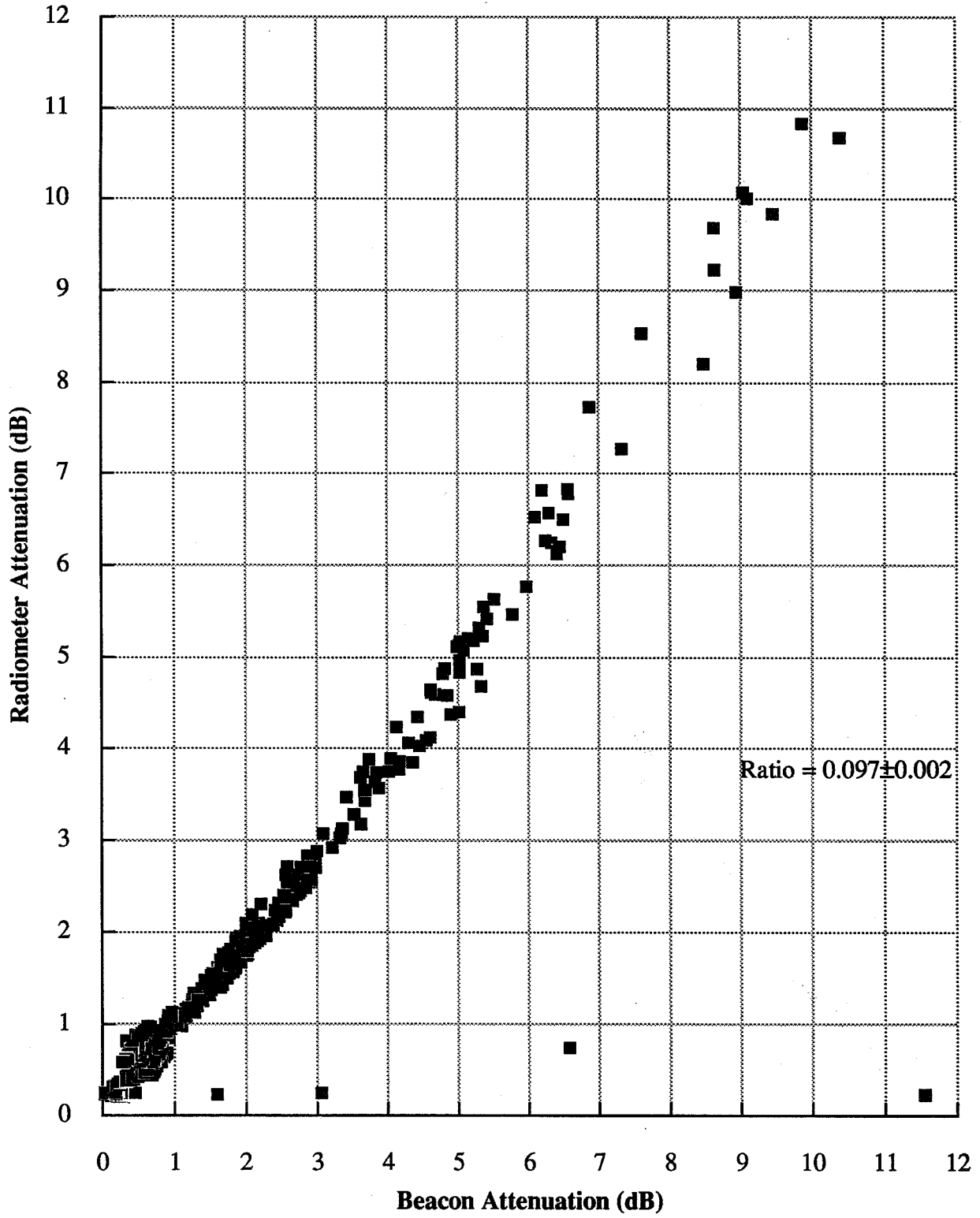
- **Beacon receiver is linear, need only find reference level to estimate beacon attenuation**
- **Radiometer receiver temperature is a linear function of radiometer output voltage, need only estimate gain and offset**
- **Sky temperature is a linear function of radiometer receiver temperature, need only estimate efficiency and background temperature**
- **Radiometer attenuation may be estimated from sky temperature if the medium temperature is known**

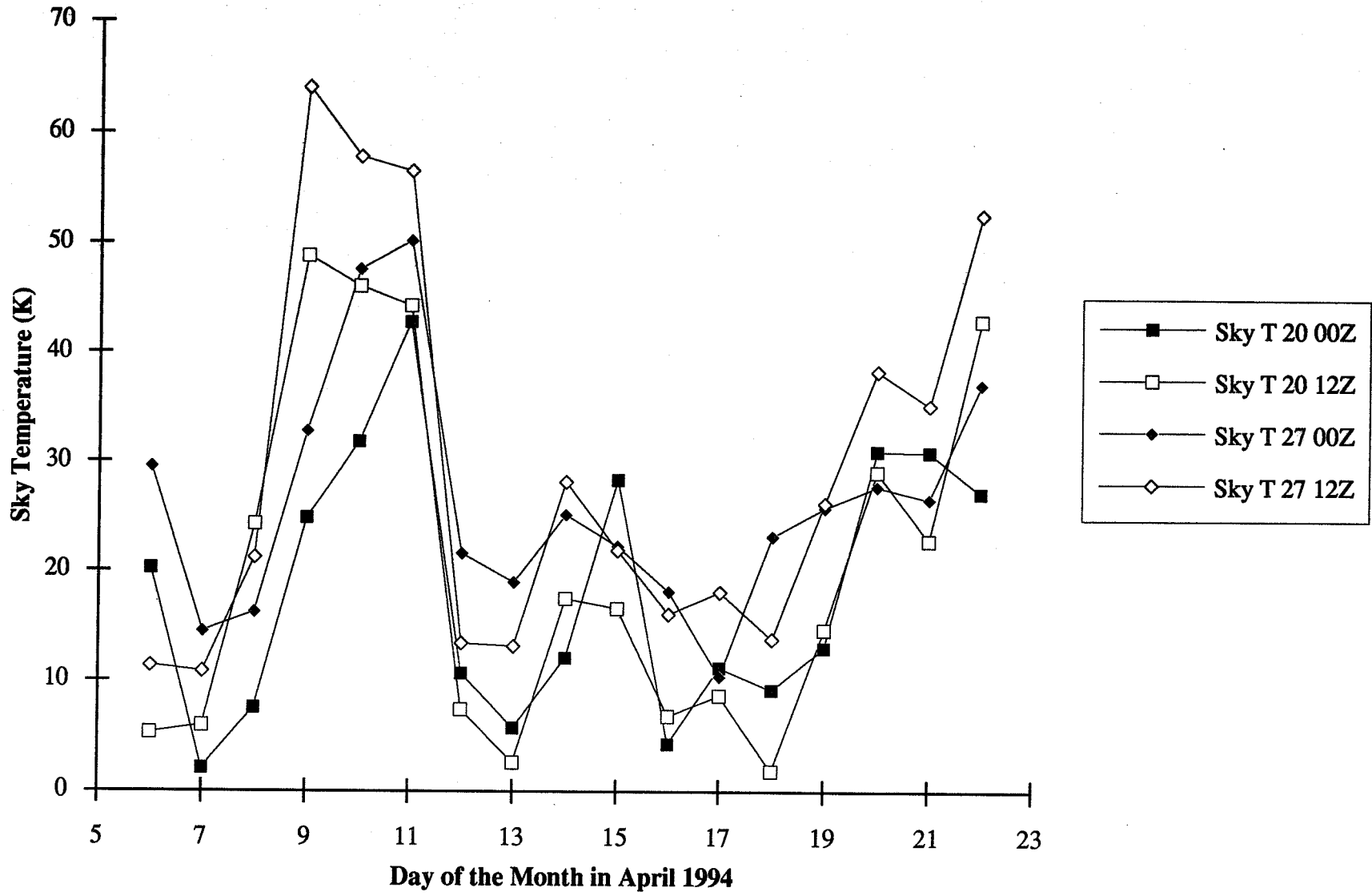
Hot/Cold.plt

278

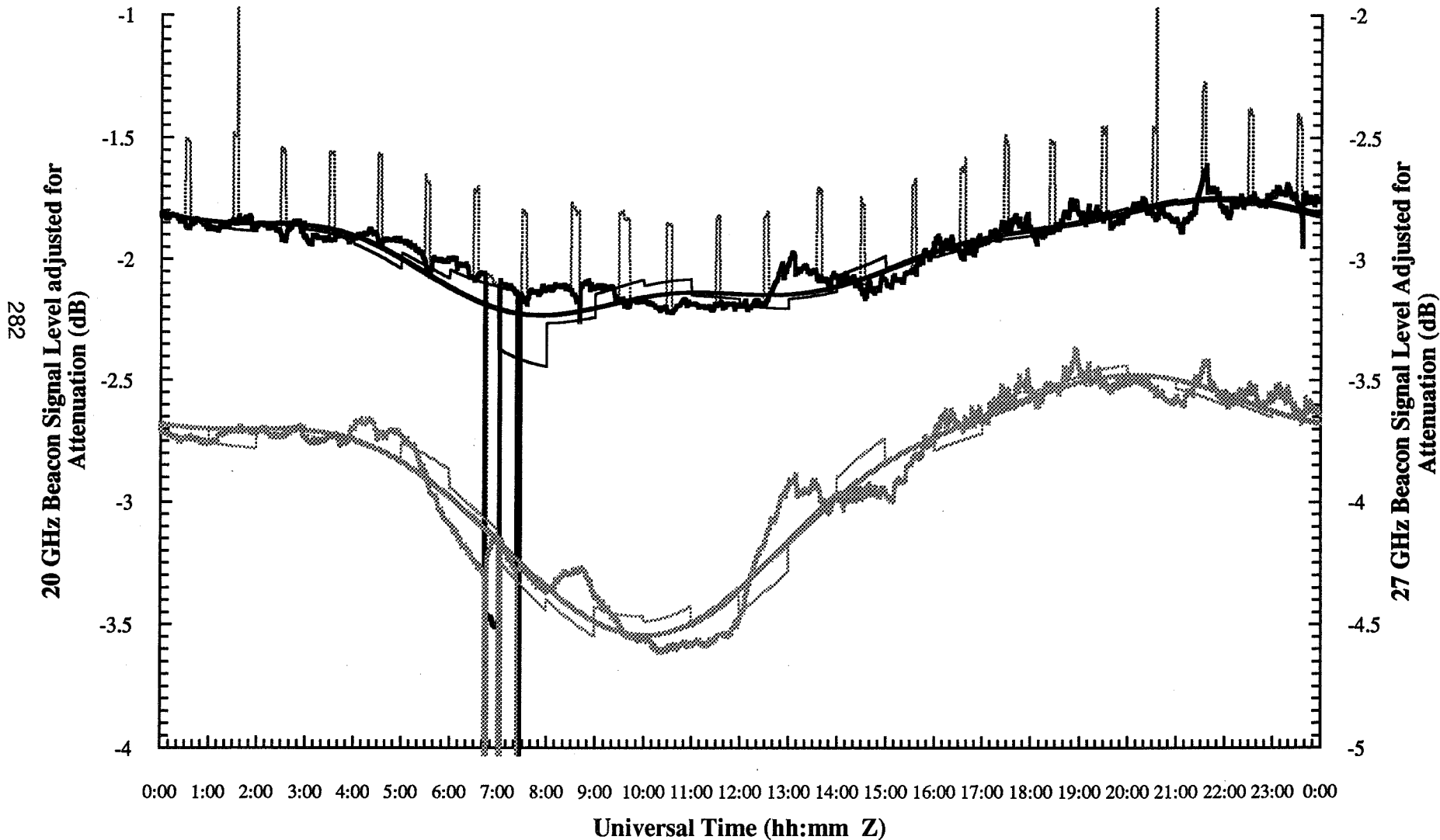








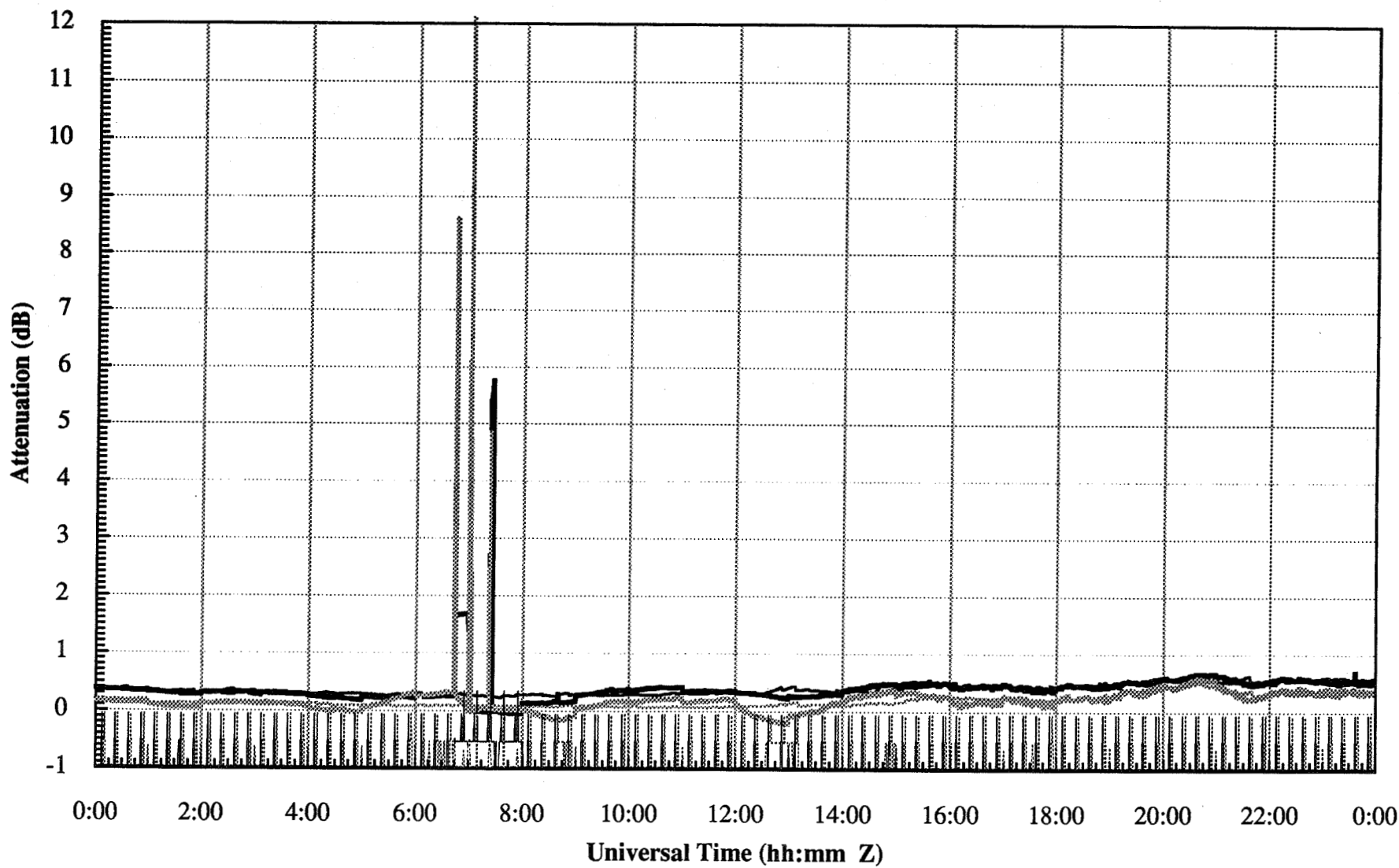
----- 20 Beacon + Arad + Ranging ——— 20 Beacon + Arad ——— 20 Beacon Diurnal Variation ——— 20 GHz Diurnal Variation
..... 27 Beacon + Arad 27 Beacon Diurnal Variation 27 GHz Diurnal Variation



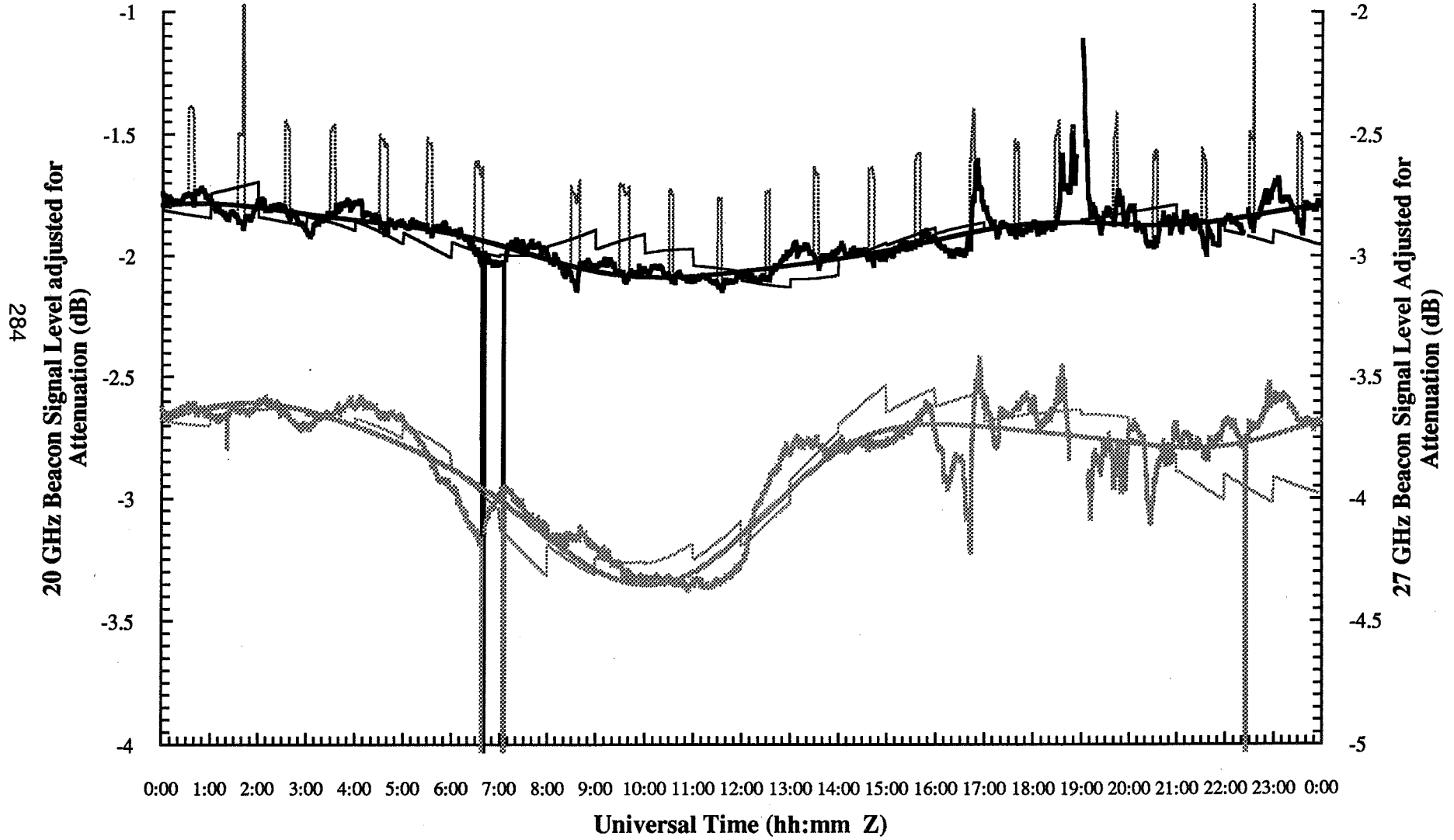
940227OK.na

— Atten 20 GHz Beacon — Atten 20 GHz Radiometer - - - Atten 27 GHz Beacon
- - - Atten 27 GHz Radiometer — 20 Beacon Flag - - - 27 Beacon Flag

283

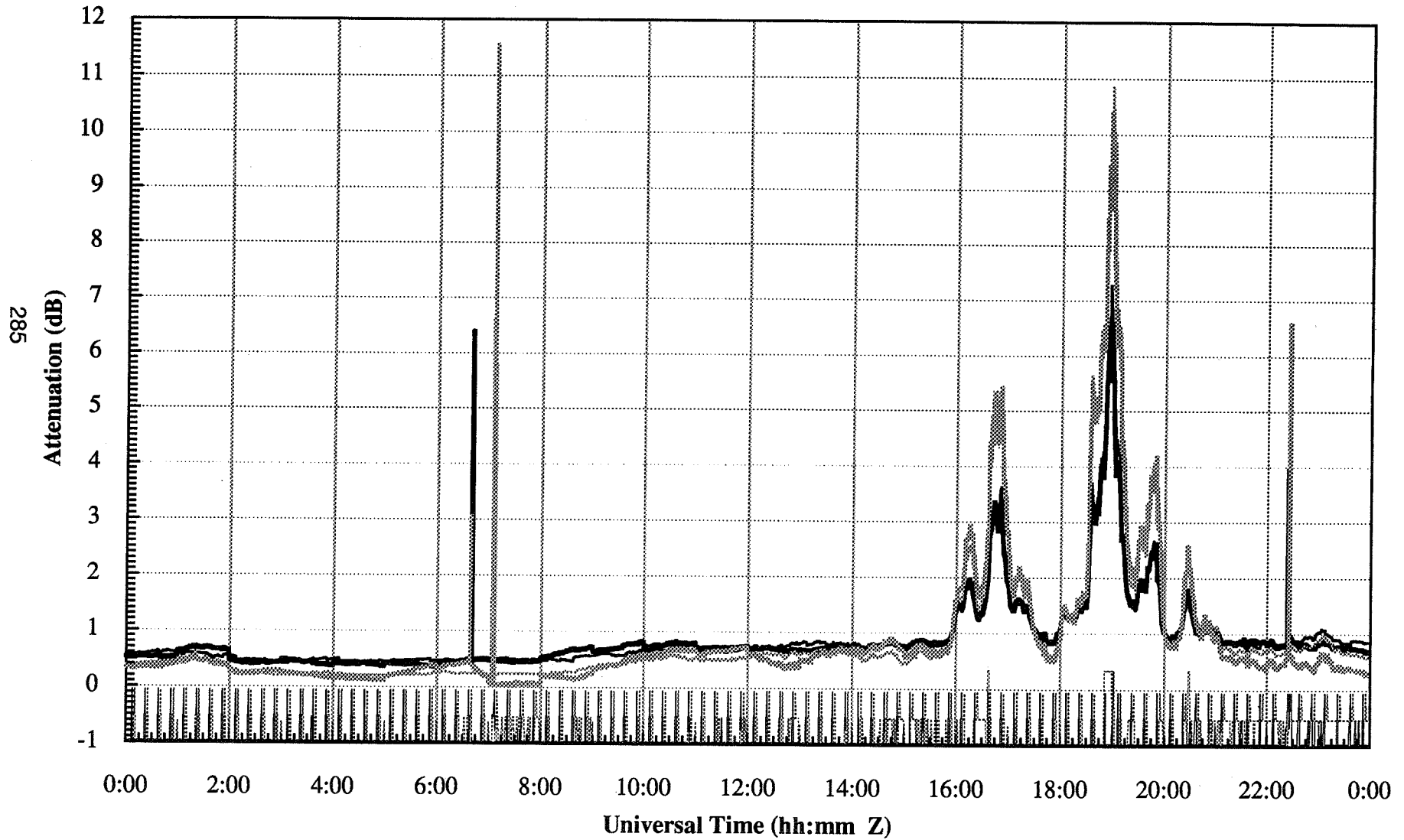


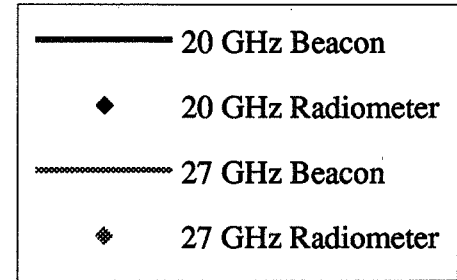
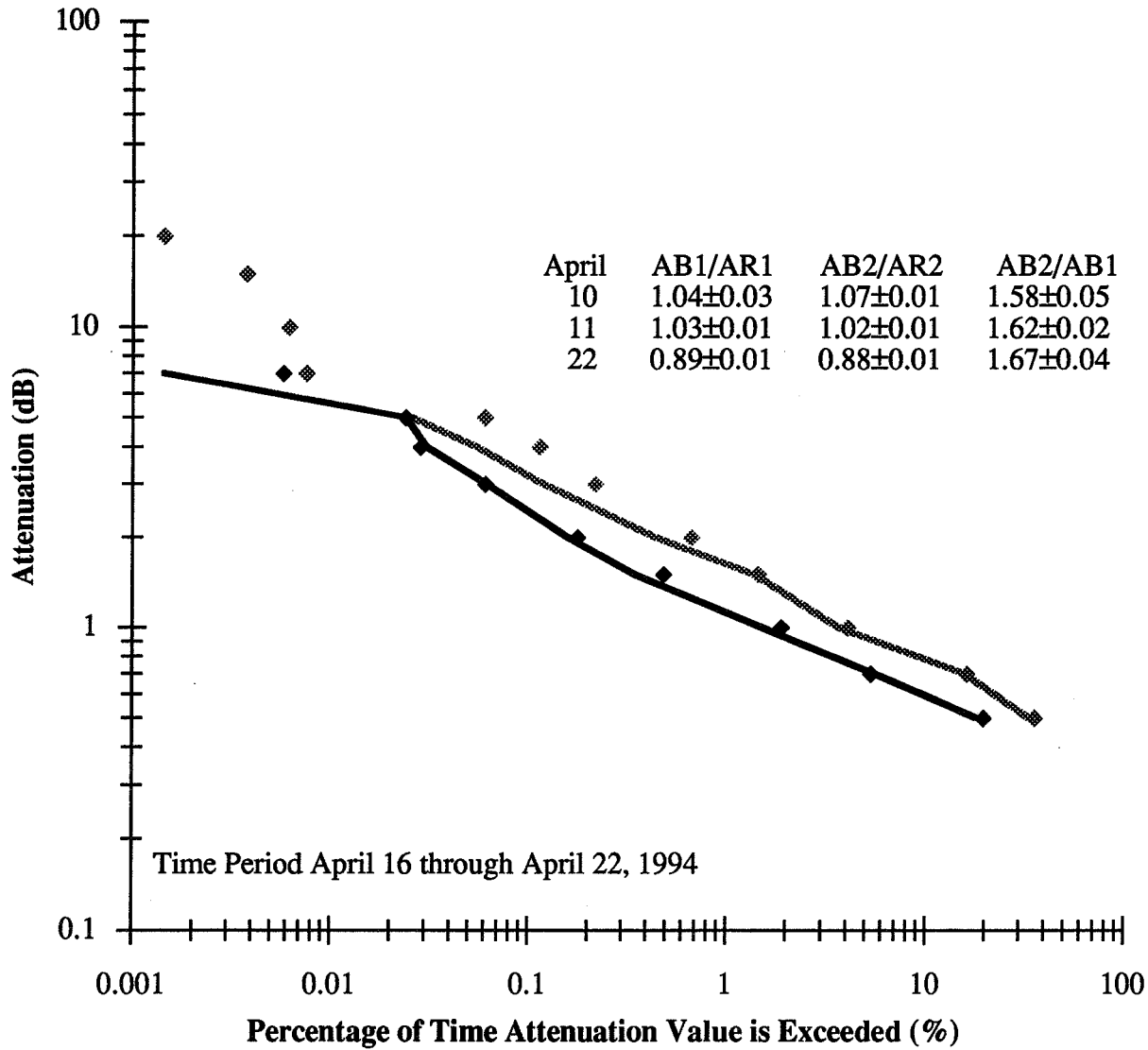
----- 20 Beacon + Arad + Ranging ———— 20 Beacon + Arad ———— 20 Beacon Diurnal Variation ———— 20 GHz Diurnal Variation
..... 27 Beacon + Arad 27 Beacon Diurnal Variation 27 GHz Diurnal Variation



940228OK.na

— Atten 20 GHz Beacon — Atten 20 GHz Radiometer Atten 27 GHz Beacon
..... Atten 27 GHz Radiometer — 20 Beacon Flag 27 Beacon Flag





EERL / Univ. of Texas

DATA CENTER STATUS REPORT

BY
WOLFHARD J VOGEL
&
ALI SYED

EERL/UTAU
10100 BURNET RD
AUSTIN, TX 78758-4497
PRESENTED AT APSW-VI
VANCOUVER, BC
JUNE 16, 1994

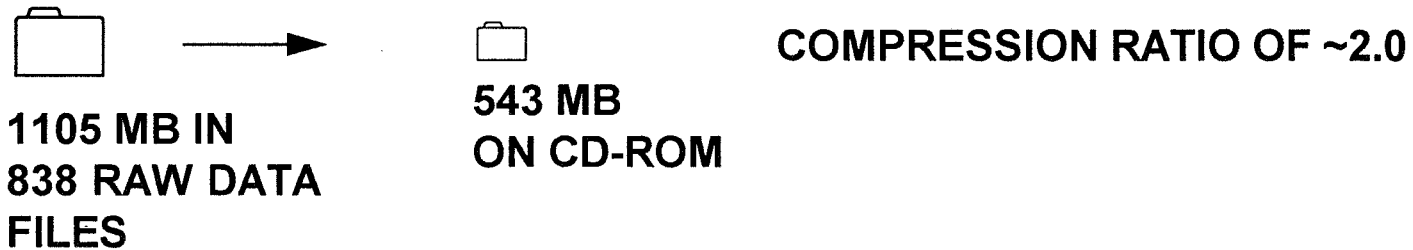
ACTS DC Services

- ☑ Archive Raw and Pre-processed Data from Stations
- ☑ Archive Event & Fault Logs from Stations
- ☑ Audit Pre-processed Data
- ☑ Distribute Monthly Audit Reports to Stations
- ⌚ Distribute Archived Data to Propagation Community

Raw Data Status

	New	Open	Save	Close	Print	Undo	Cut	Paste	Del	Prev	Find	Next	Help	Exit								
S	9	9	9	9	9	9	9	9	9	9	9	9	9	9	9	9	9	9	9	9	9	9
T	3	4	4	4	4	4	4	4	4	4	4	4	5	5	5	5	5	5	5	5	5	5
A	1	0	0	0	0	0	0	0	0	1	1	1	0	0	0	0	0	0	0	0	1	1
T	2	1	2	3	4	5	6	7	8	9	0	1	2	1	2	3	4	5	6	7	8	9
AK	31	31	28	31	30
BC	31	31	28	31	30
CO	30	31	28	31	XX
FL	29	31	28	29	30
MD	XX	XX	XX	17	30
NM	29	31	25	18	30
OK	31	31	28	31	XX

Data Archival Status



Audit & Analysis Status

☹ **INCORRECT DATA STRUCTURE CAUSED ERROR IN AUDIT & ANALYSIS. BUG FIXED.**

<input checked="" type="checkbox"/>	Time Stamp	Beacon at 20 GHz	Radiometer at 20 GHz	Beacon at 27 GHz	Radiometer at 27 GHz	Status 1	Status 2
-------------------------------------	------------	------------------	----------------------	------------------	----------------------	----------	----------

<input checked="" type="checkbox"/>	Time Stamp	Beacon at 20 GHz	Beacon at 27 GHz	Radiometer at 20 GHz	Radiometer at 27 GHz	Status 1	Status 2
-------------------------------------	------------	------------------	------------------	----------------------	----------------------	----------	----------

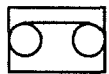
☹ **INCORRECT SCALING FOR STATUS QUANTITIES CAUSED ERROR IN AUDIT REPORT. BUG FIXED.**

<u>QUANTITY</u>	<u>CORRECT SCALE</u>	<u>RANGE</u>
RainGauge [Volts]	1000	0 to 500 mm/Hr
AirTemp. [C]	100	-50 to 70 C
Rel.Humd [%]	100	0 to 100 %

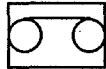
DC System Status

- CD WRITER OK
- 📀 120 MB TAPE DRIVE OK
- 📀 HARD DRIVE SCSI CARD FAILURE IN 3/94 RESULTED IN ~2 WEEKS DOWNTIME
- 👉 SYSTEM & DATA RESTORED FROM TAPES
- 👉 DAILY BACKUP SCHEDULE ADOPTED

Data Tapes Status



44 DATA TAPES RECEIVED FROM STATIONS



DIFFERENT BACKUP PATHS NOT A PROBLEM



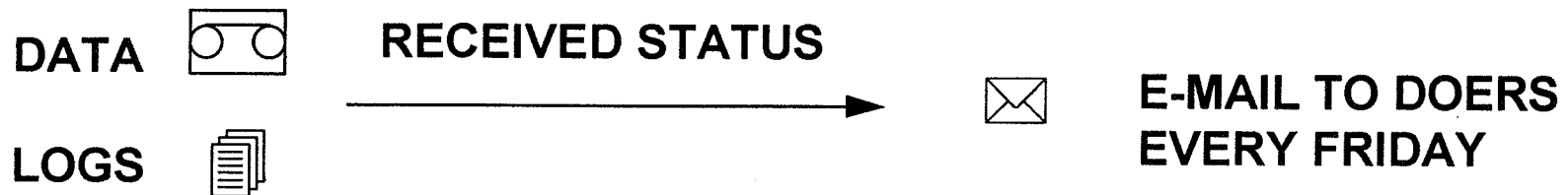
***COLORADO BACKUP LITE VER 1.20 USED
BY DATA CENTER***



DATA TAPES WILL BE RECYCLED



Feedback Schedule



CONCLUSION

- DATA COMPRESSION AND ARCHIVAL HAS WORKED WITH REAL DATA
- BUGS FOUND IN AUDIT & ANALYSIS ROUTINES HAVE BEEN FIXED
- WEEKLY DATA RECEIVED STATUS REPORT WILL BE DISTRIBUTED VIA E-MAIL
- MONTHLY AUDIT REPORT FOR STATIONS WILL BE DISTRIBUTED VIA E-MAIL
- SOME FINE TUNING IS EXPECTED IN THE FOLLOWING MONTHS

**ALASKA ACTS PROPAGATION TERMINAL:
DATA ANALYSIS PROCEDURE,
SYSTEM STATUS AND RESULTS**

**ACTS PROPAGATION MINIWORKSHOP
AND NAPEX-XVIII
VANCOUVER, BC
JUNE 16, 1994**

**BRAD JAEGER
CHARLIE MAYER
UNIVERSITY OF ALASKA FAIRBANKS**



Alaska ACTS Propagation



OUTLINE

- I. DATA ANALYSIS PROCEDURE AND RESULTS**
 - JAEGER
- II. SYSTEM STATUS AND RESULTS**
 - MAYER
- III. FUTURE PLANS**
 - MAYER



Alaska ACTS Propagation



I. DATA ANALYSIS PROCEDURE

- A. COUNT EVENTS**
- B. ANALYZE INDIVIDUAL EVENTS**
- C. ANALYZE CUMULATIVE STATISTICS**
- D. FORMULATE MODELS OF VARIOUS PARAMETERS**

Alaska ACTS Propagation

A. COUNT EVENTS

- RAIN EVENTS**
- SNOW EVENTS**
- SCINTILLATION EVENTS**

**CATEGORIZE THESE EVENTS IN TERMS OF
MAXIMUM FADE, FADE SLOPE, FADE
DURATION, ETC.**

Alaska ACTS Propagation

B. ANALYZE INDIVIDUAL EVENTS

- **TIME SERIES ANALYSIS**
- **POWER SPECTRAL DENSITY ANALYSIS**
- **SCINTILLATION INTENSITY**
- **FADE SLOPE**



Alaska ACTS Propagation



C. ANALYZE CUMULATIVE STATISTICS

- **BIN THE VARIABLES**
- **RUNNING AVERAGE TO REMOVE SCINTILLATIONS**
- **CUMULATIVE BINS**
 - DAY
 - MONTH
 - YEAR
 - EXPERIMENT LENGTH



Alaska ACTS Propagation



C. ANALYZE CUMULATIVE STATISTICS

- **STATISTICAL ANALYSIS**
 - CDFs
 - TIME PERCENTAGES VALUES EXCEEDED
 - WORST MONTH
 - » WORST MONTH TO ANNUAL AVERAGE
 - » WORST MONTH TO OTHER MONTHS
 - FREQUENCY SCALING
 - » ATTENUATION RATIOS
 - » SCINTILLATION RATIOS
 - SCINTILLATION DIURNAL AND ANNUAL VARIABILITY PLOTS
 - RAIN RATE ANALYSES
 - » DIURNAL VARIABILITY
 - » ANNUAL VARIABILITY

Alaska ACTS Propagation

D. FORMULATE MODELS OF VARIOUS PARAMETERS

- **ATTENUATION RATIO VS. FREQUENCY**
- **SCINTILLATION RATIO VS. FREQUENCY**
- **SCINTILLATION INTENSITY VS. ELEVATION ANGLE**
- **ULTIMATE FADE DEPTH**
- **FADE DURATION**
- **TIME BETWEEN FADES**

Alaska ACTS Propagation

BINNING PROCEDURE

Variable	Small Bin	Large Bin	Increment
Rain Rate	0 mm/hr	>200 mm/hr	2 mm/hr, R<30 mm/hr
			5 mm/hr, R>30 mm/hr
Beacon Attenuation	-8 dB	30 dB	1 dB or 0.2 dB
Attenuation Ratio	0	15	0.05
Radiometric Attn.	0 dB	15 dB	1 dB or 0.2 dB
Fade Slope	-1.25 dB/s	1.25 dB/s	0.05 dB/s
Ultimate Fade Depth	1 dB	30 dB	1 dB or 0.2 dB
Fade Duration	0-1 s; 1-2, 2-3, 3-5, 5-10, 10-20, 20-30, 30-60 s & min., >60 min.		for fade levels of -8 to
			30 dB in 1 dB
			increments
Time Between Fades	as above		as above
Sky Temperature	0 K	>300 K	2 K
Scintillation Intensity	0	4	0.05

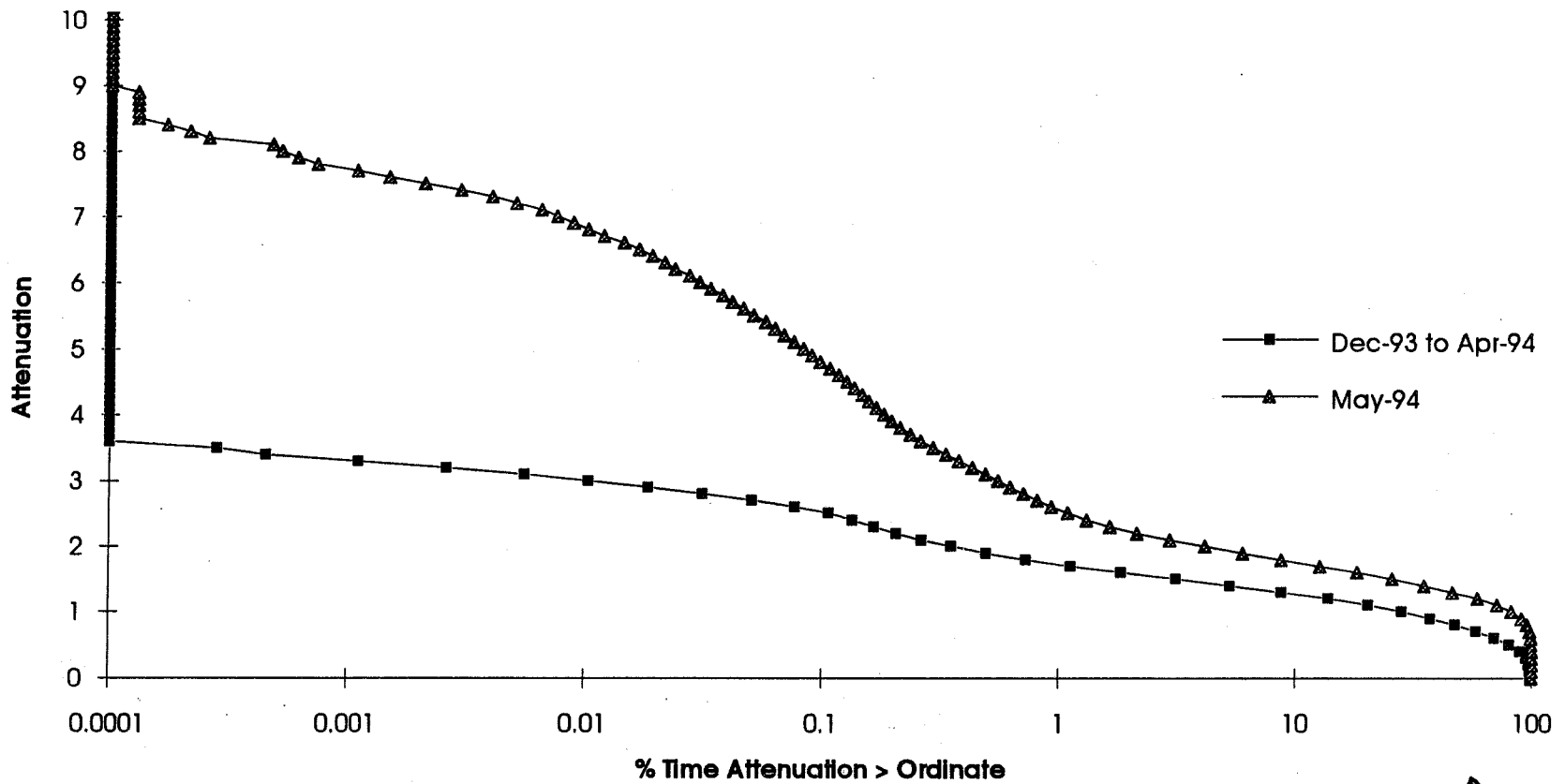
Alaska ACTS Propagation

II. SYSTEM STATUS

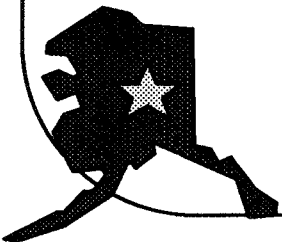
- **APT MODIFICATIONS**
 - ANGLED MOUNT POLE
 - RF BOX BRACING
 - SNOW FAN
 - ADDITIONAL INSULATION WITH REFLECTIVE COATING
- **PROBLEMS**
 - EMI
 - DYNAMIC RANGE LIMITATIONS
 - SATELLITE POINTING VARIATIONS
- **OPERATION**
 - POWER OUTAGES

Alaska ACTS Propagation

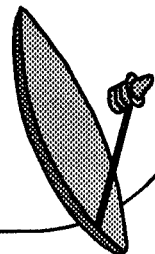
20.185 GHz Beacon CDFs



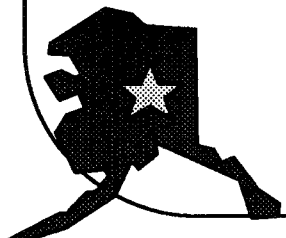
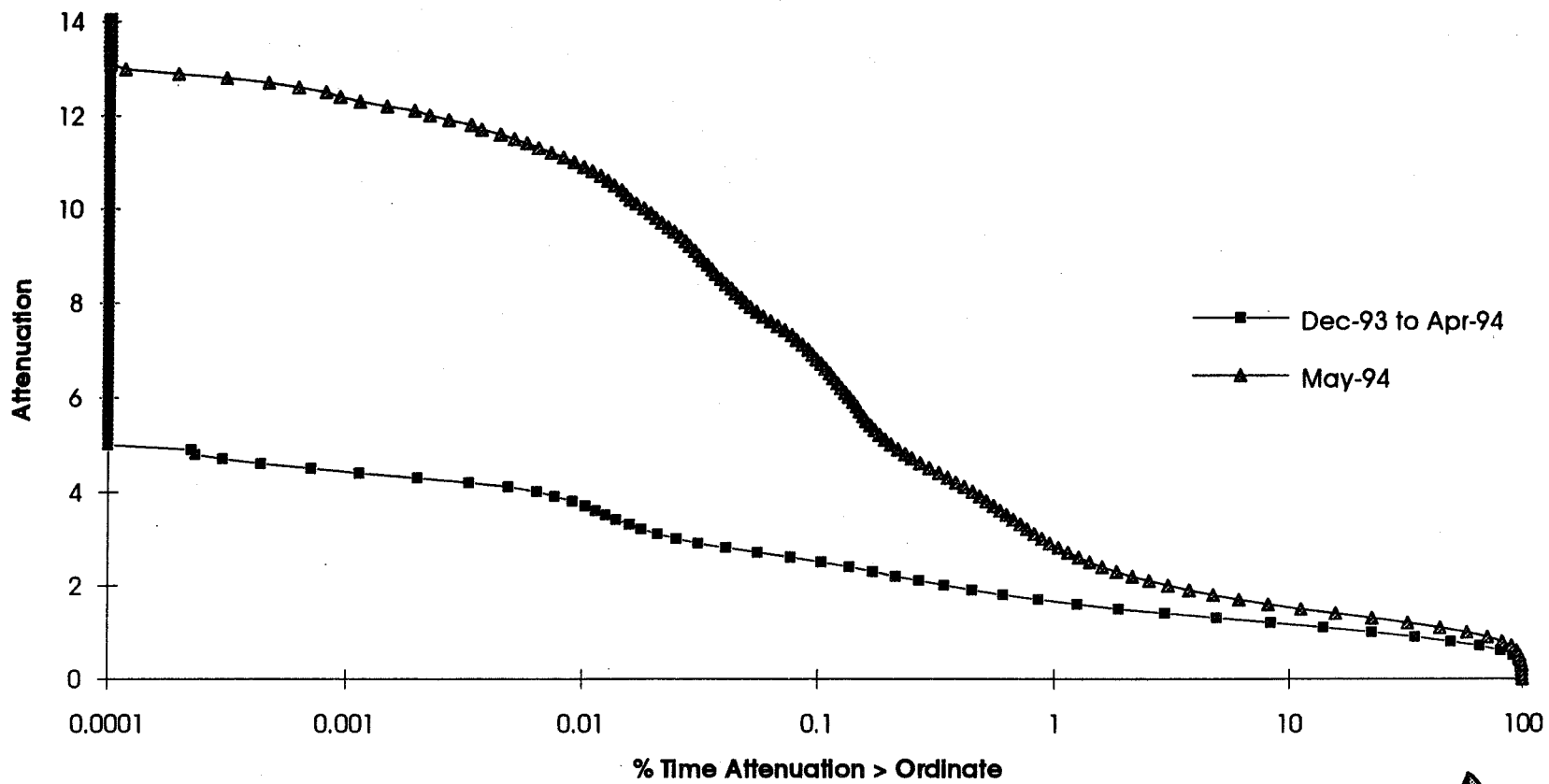
302



Alaska ACTS Propagation



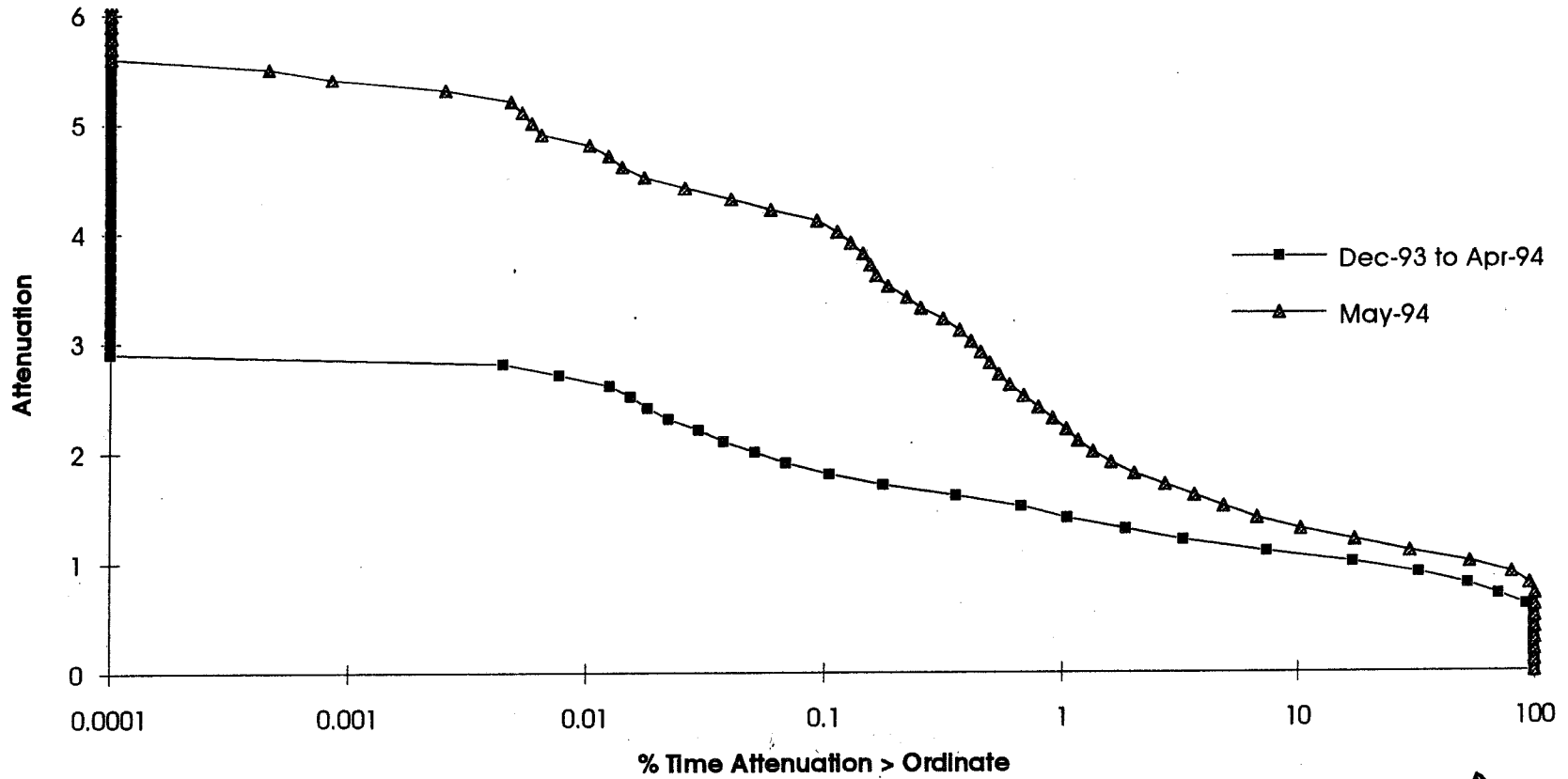
27.505 GHz Beacon CDFs



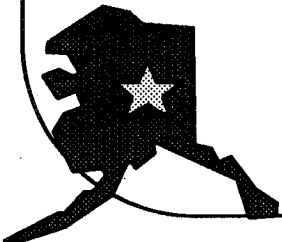
Alaska ACTS Propagation



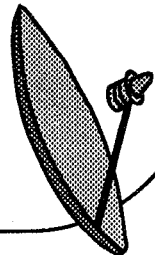
27.505 GHz Radiometer CDFs



304

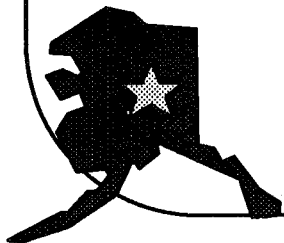
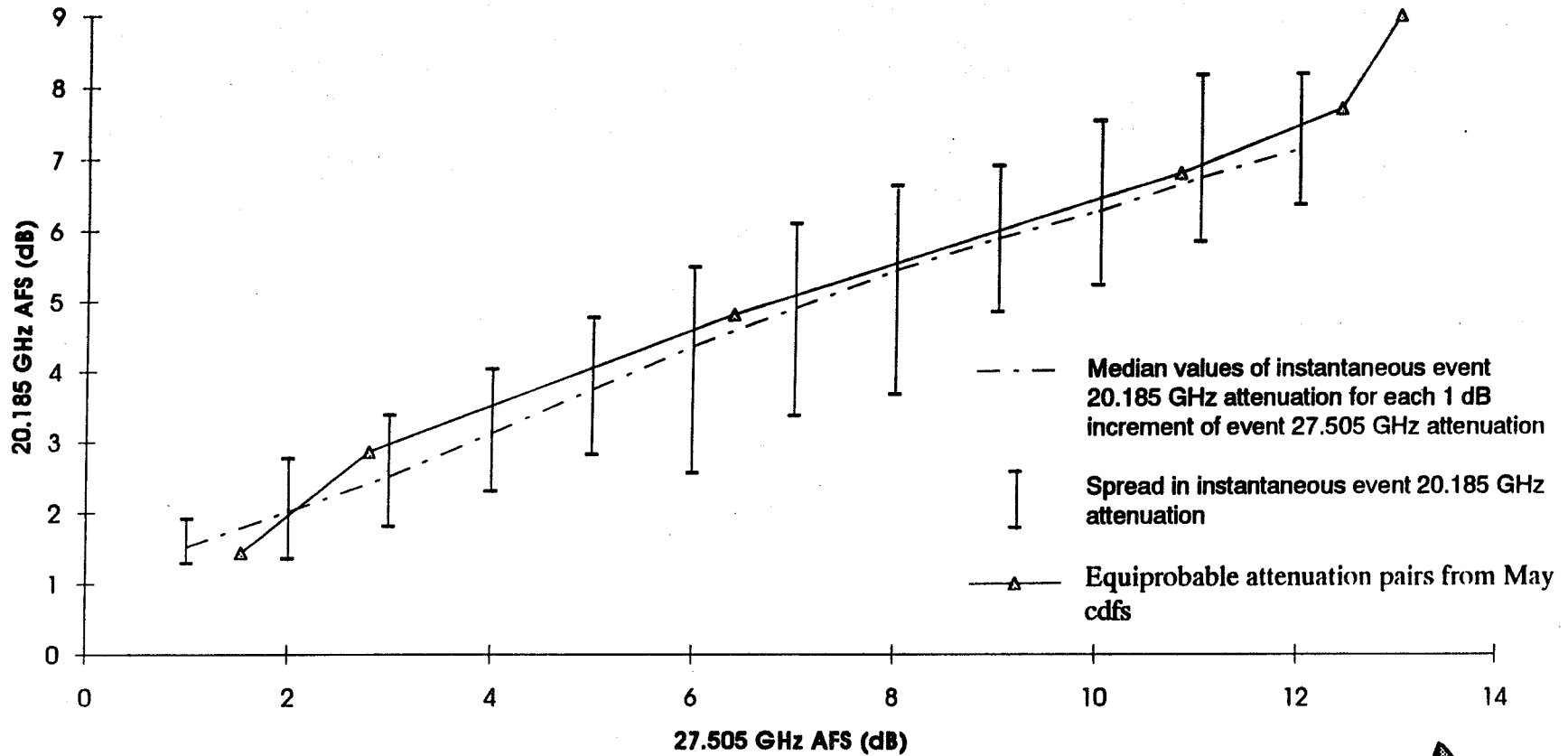


Alaska ACTS Propagation



20.185GHz AFS vs 27.505 GHz AFS 5/24/94 11-12 H GMT

305

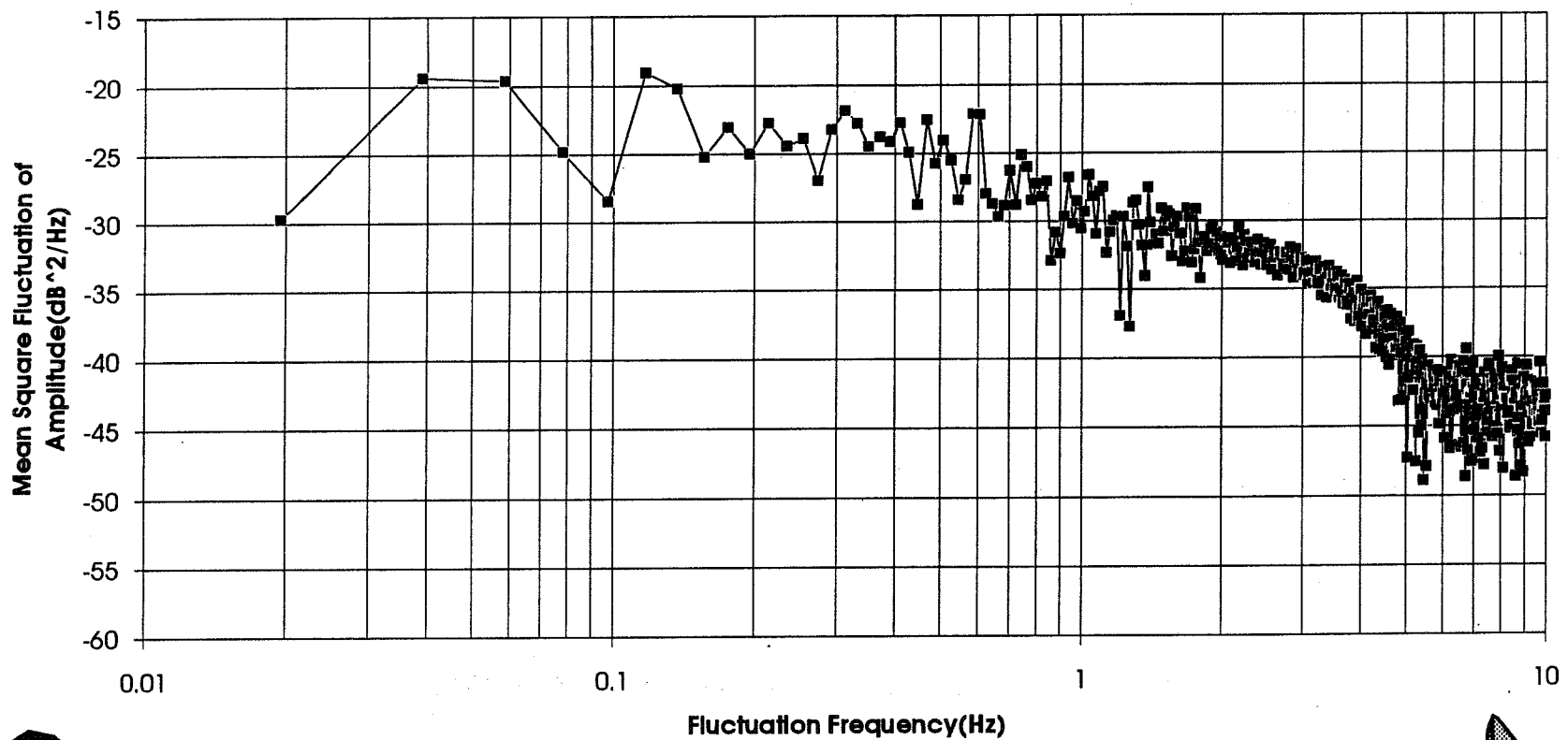


Alaska ACTS Propagation



27.505 GHz Scintillation Spectrum

Scintillation Intensity of 0.19 on 5/25/94 07:41:51-07:42:42.2 GMT



908

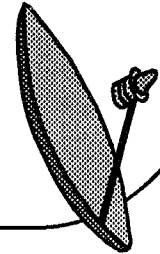
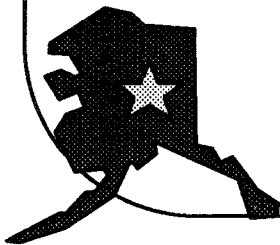
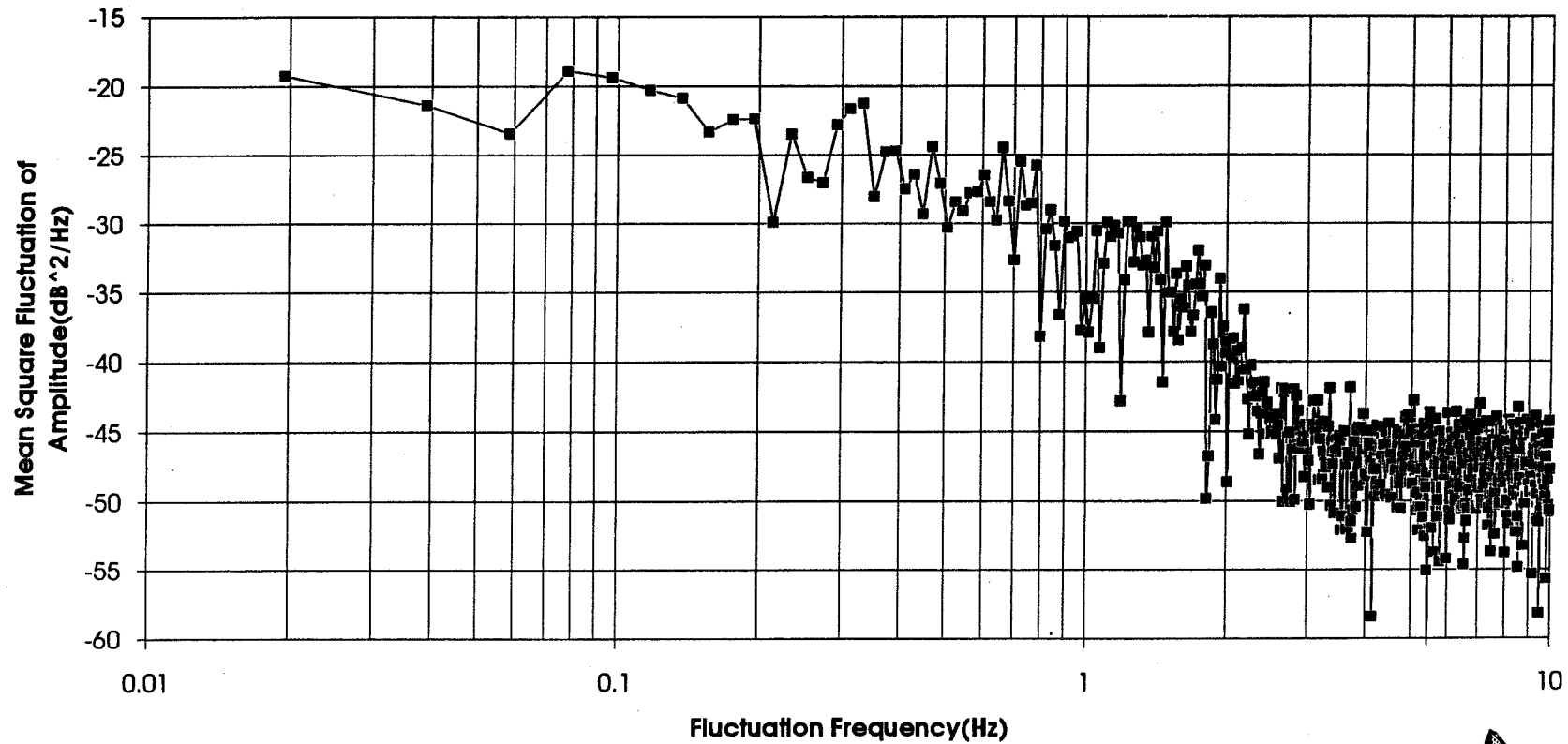


Alaska ACTS Propagation

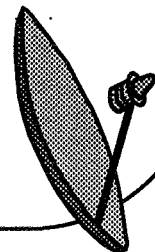
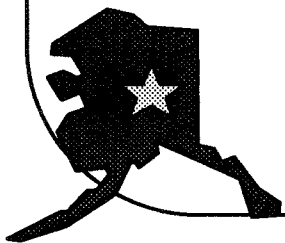
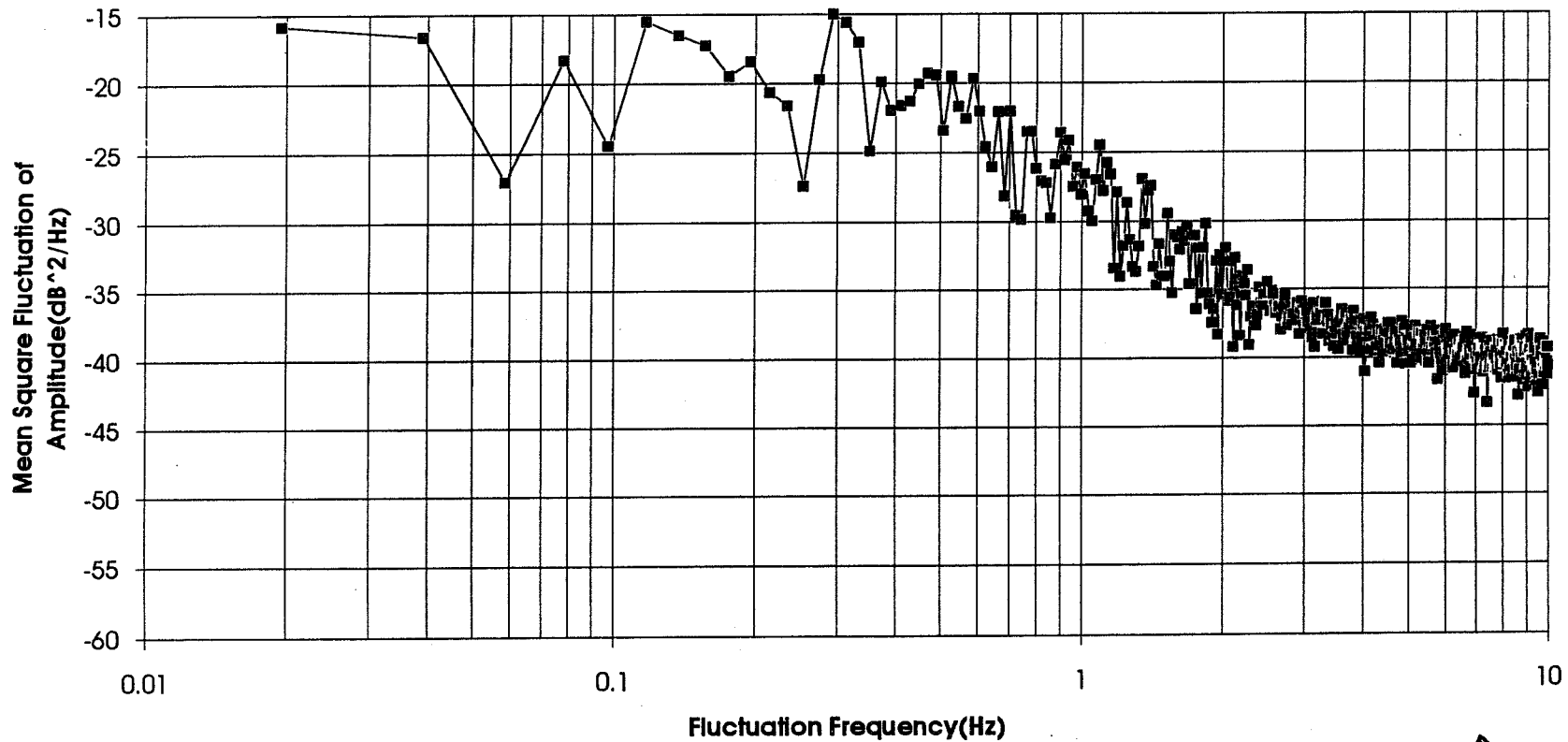


27.505 GHz Scintillation Spectrum

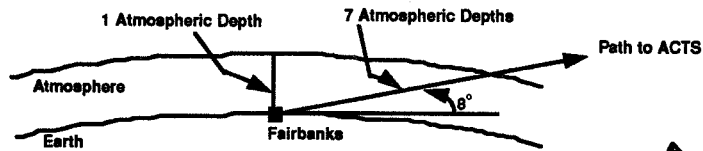
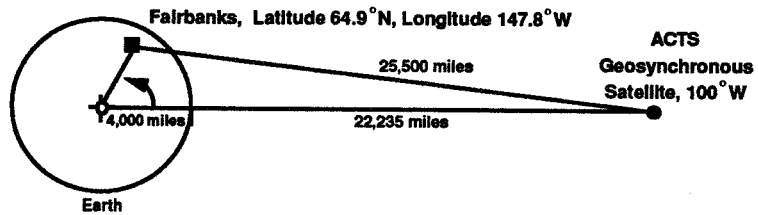
Scintillation Intensity of 0.50 on 5/25/94 22:57:04-22:57:55.2 GMT



27.505 GHz Scintillation Spectrum
Scintillation Intensity of 0.51 with 3.4 dB AFS on 5/27/94 23:14:42-23:15:33.2 GMT

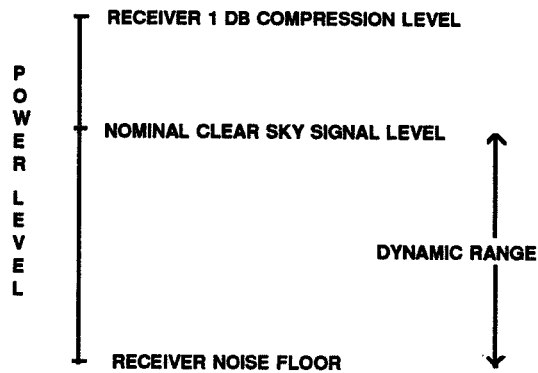
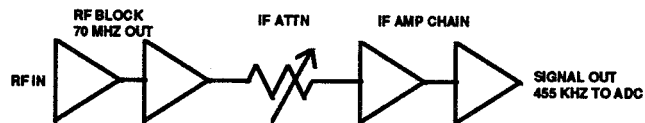


SATELLITE TO EARTH GEOMETRY



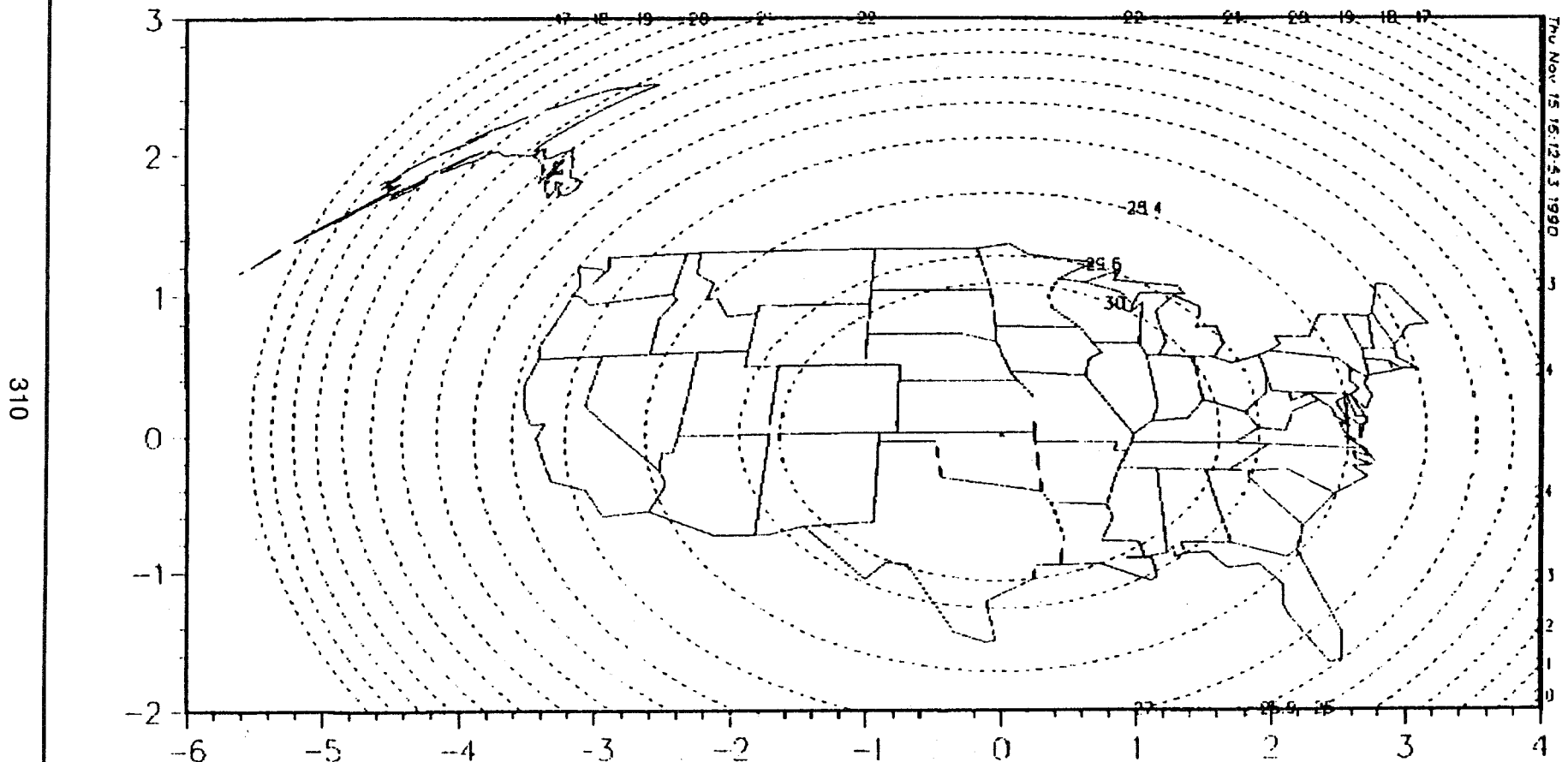
Alaska ACTS Propagation

DYNAMIC RANGE OF APT

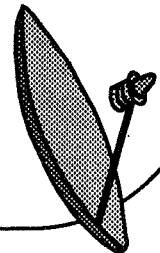
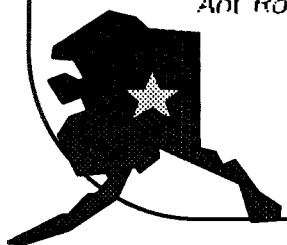


Alaska ACTS Propagation

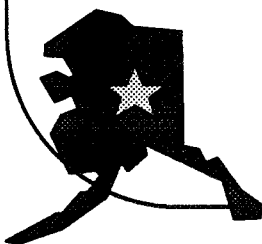
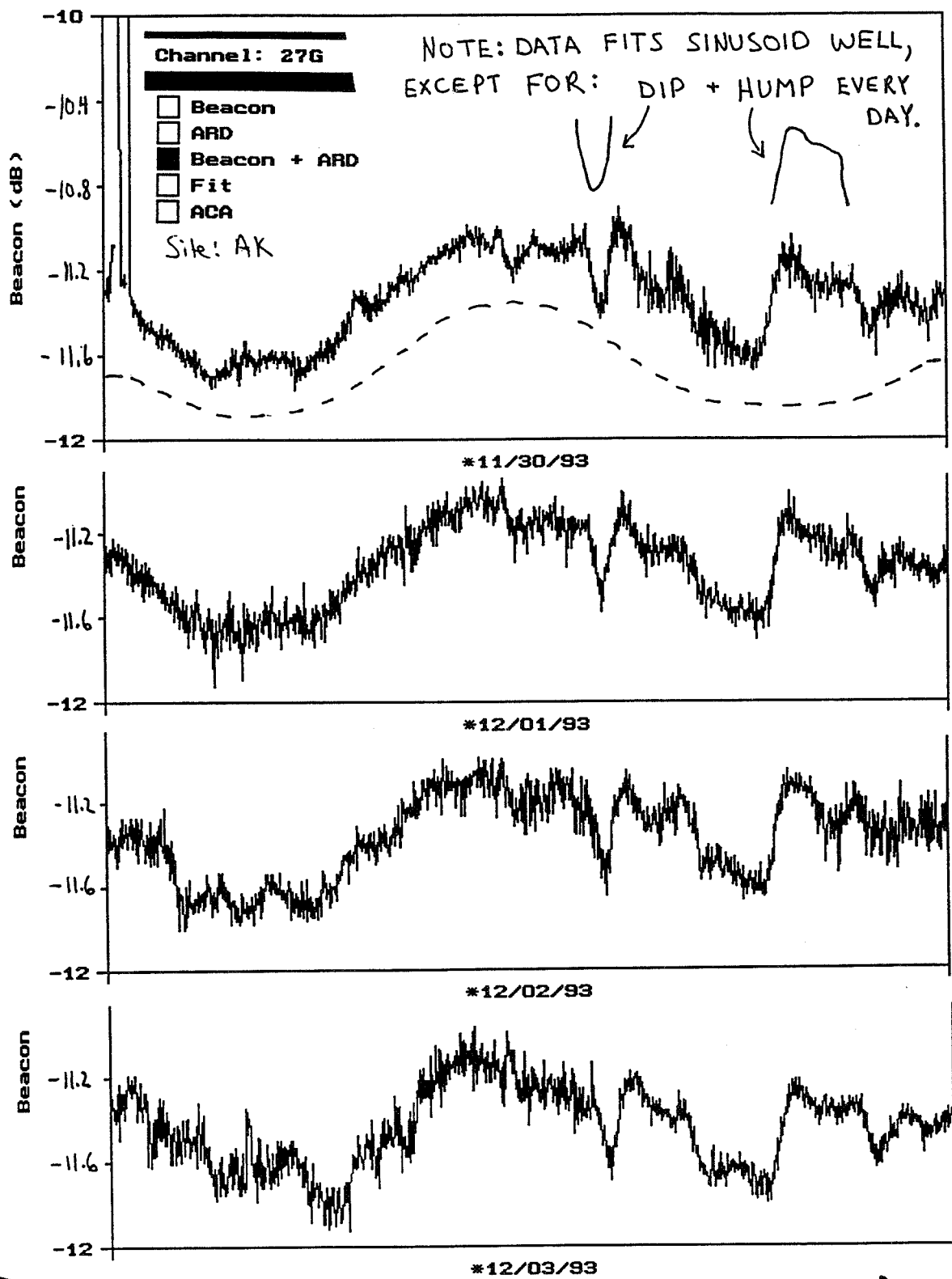
ACTS 20 GHz EIRP Contours



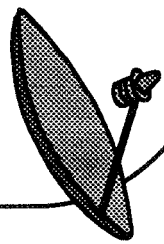
Sat Long=-100 Nadir at -0.50 Az/-5.87 El/Bore Long=-96.4 Lat=36.9
Ant Rot=0 Freq=20.185 GHz V-POL Conv Factor=-0.93 dB Peak=30.99 dB



Alaska ACTS Propagation

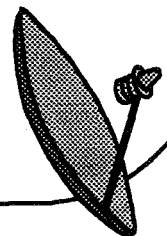
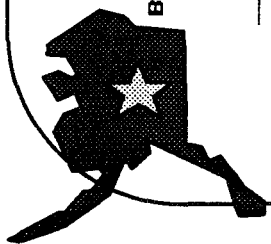
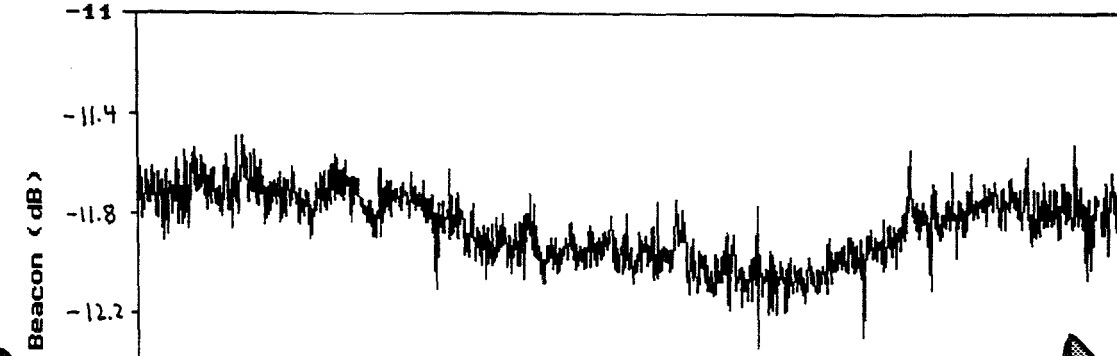
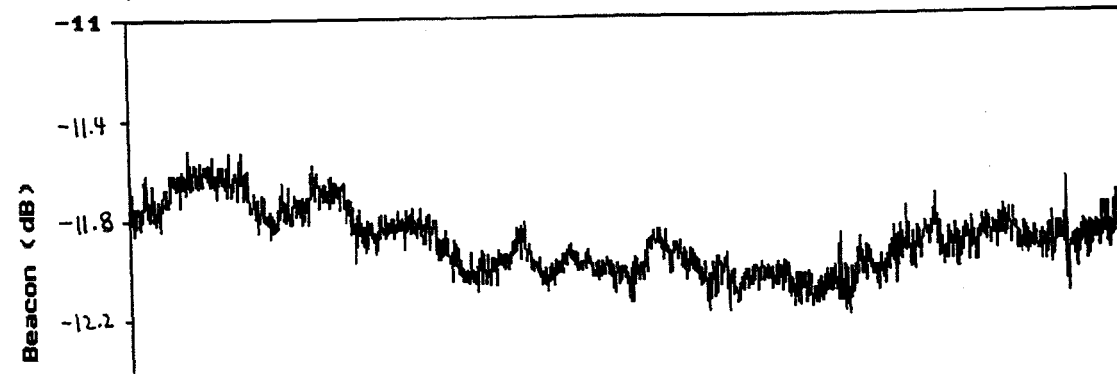
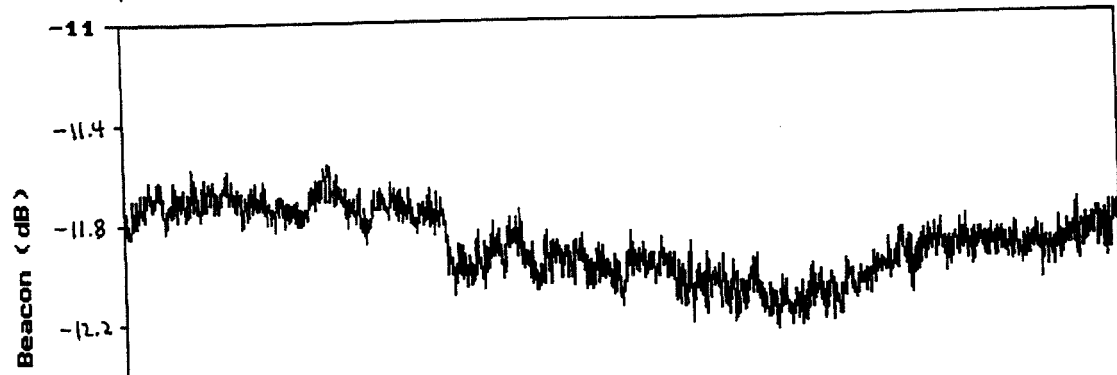
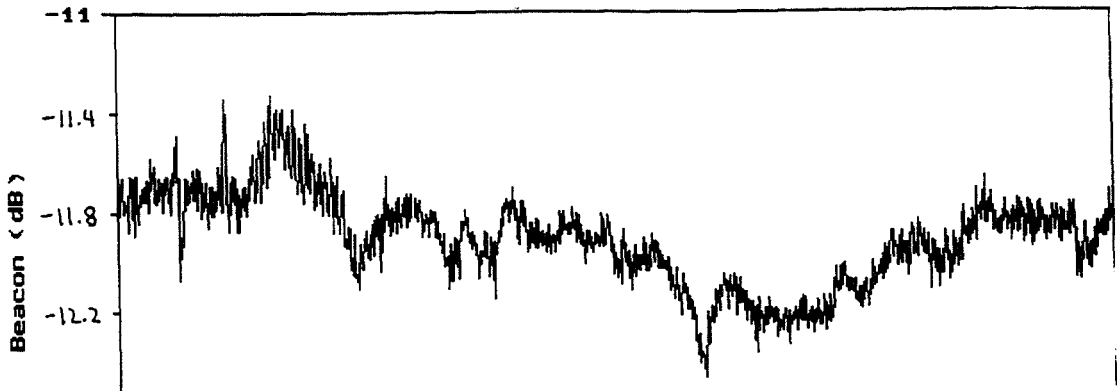


Alaska ACTS Propagation



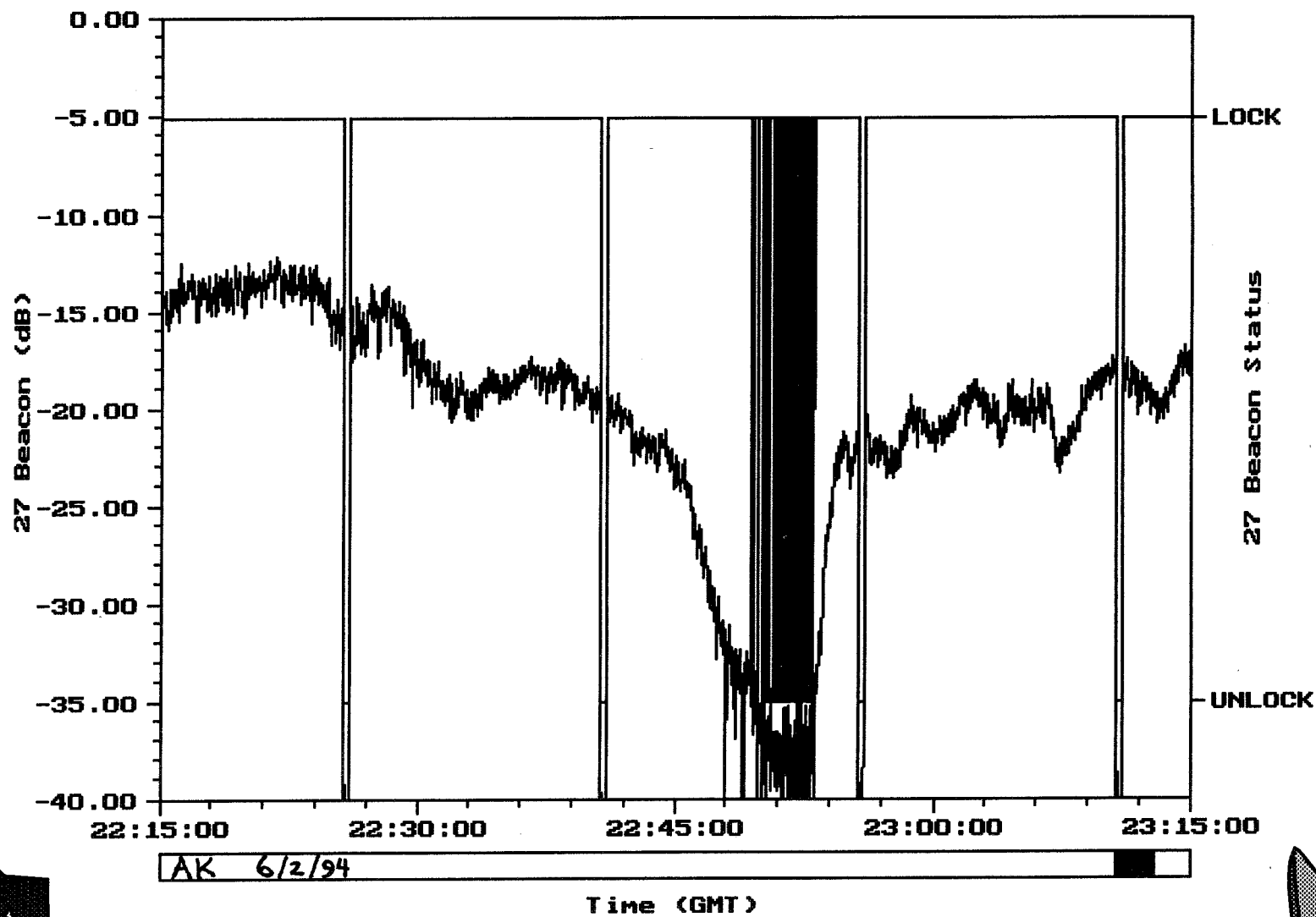
27 GHz Beacon + ARD
0.4 dB/tick mark

2/20-23/94
Site: AK



Alaska ACTS Propagation

AK Dynamic Range Limitation

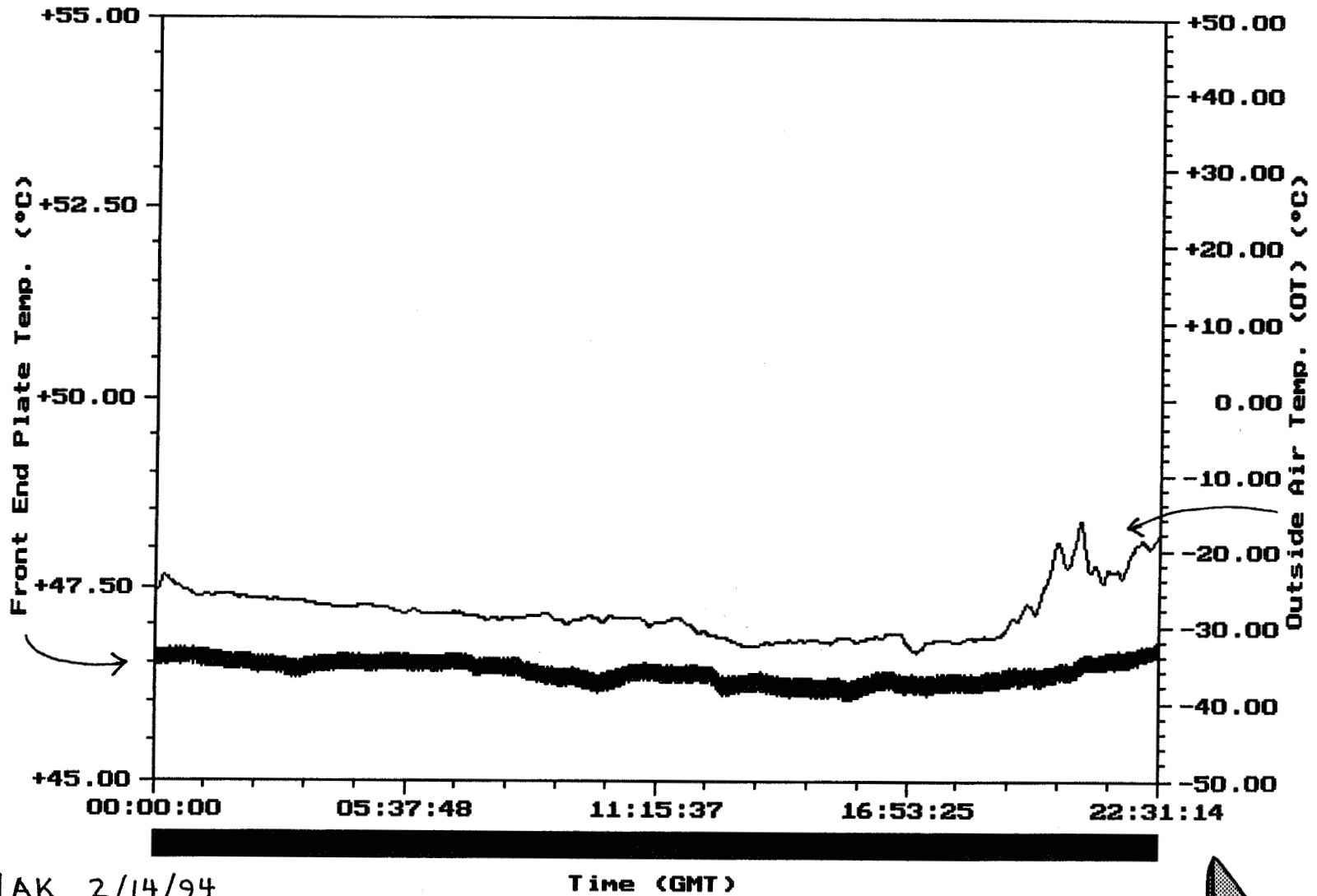


313



Alaska ACTS Propagation

Outside Air and Front End Plate Temperatures



314

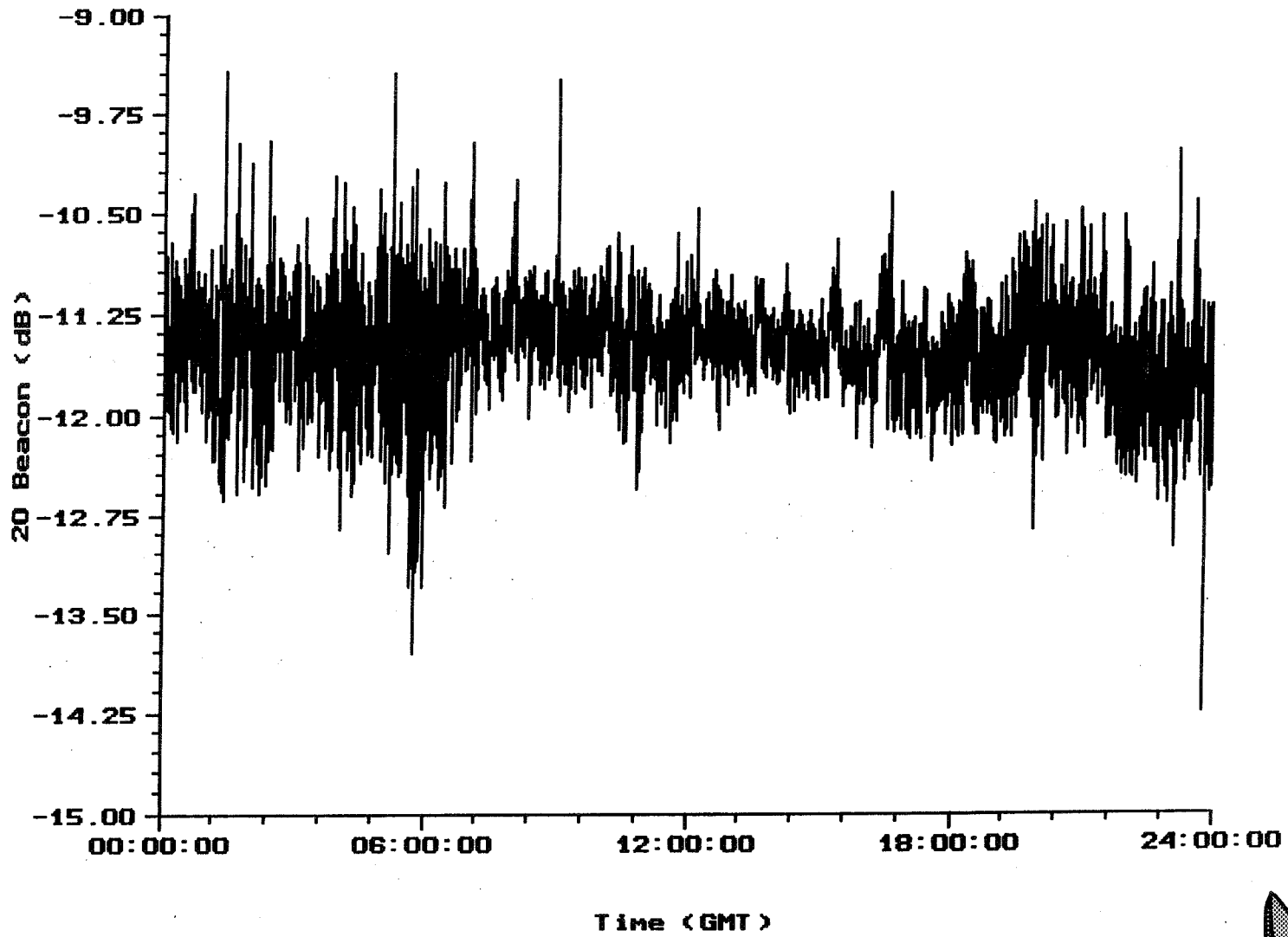
AK 2/14/94

Time (GMT)

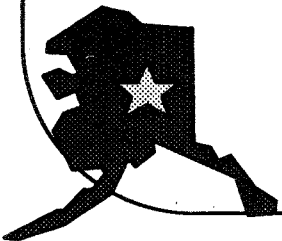
Alaska ACTS Propagation



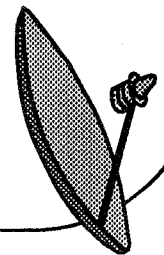
20.185 GHz Beacon 5/14/94 0-24 H GMT



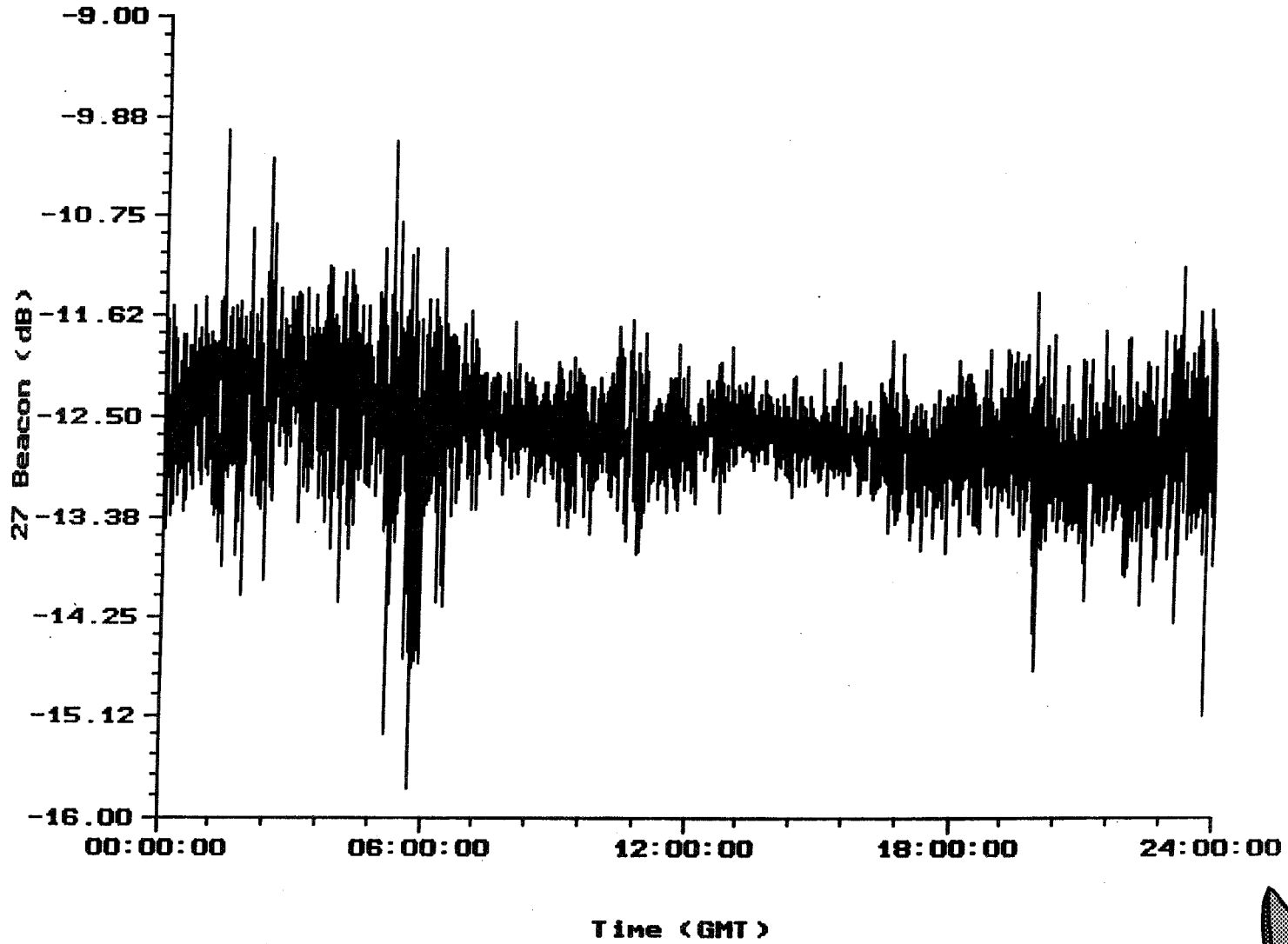
315



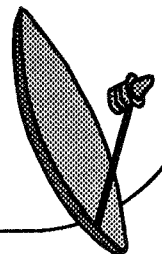
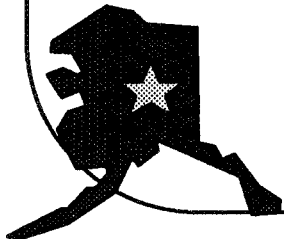
Alaska ACTS Propagation



27.505 GHz Beacon 5/14/94 0-24 H GMT

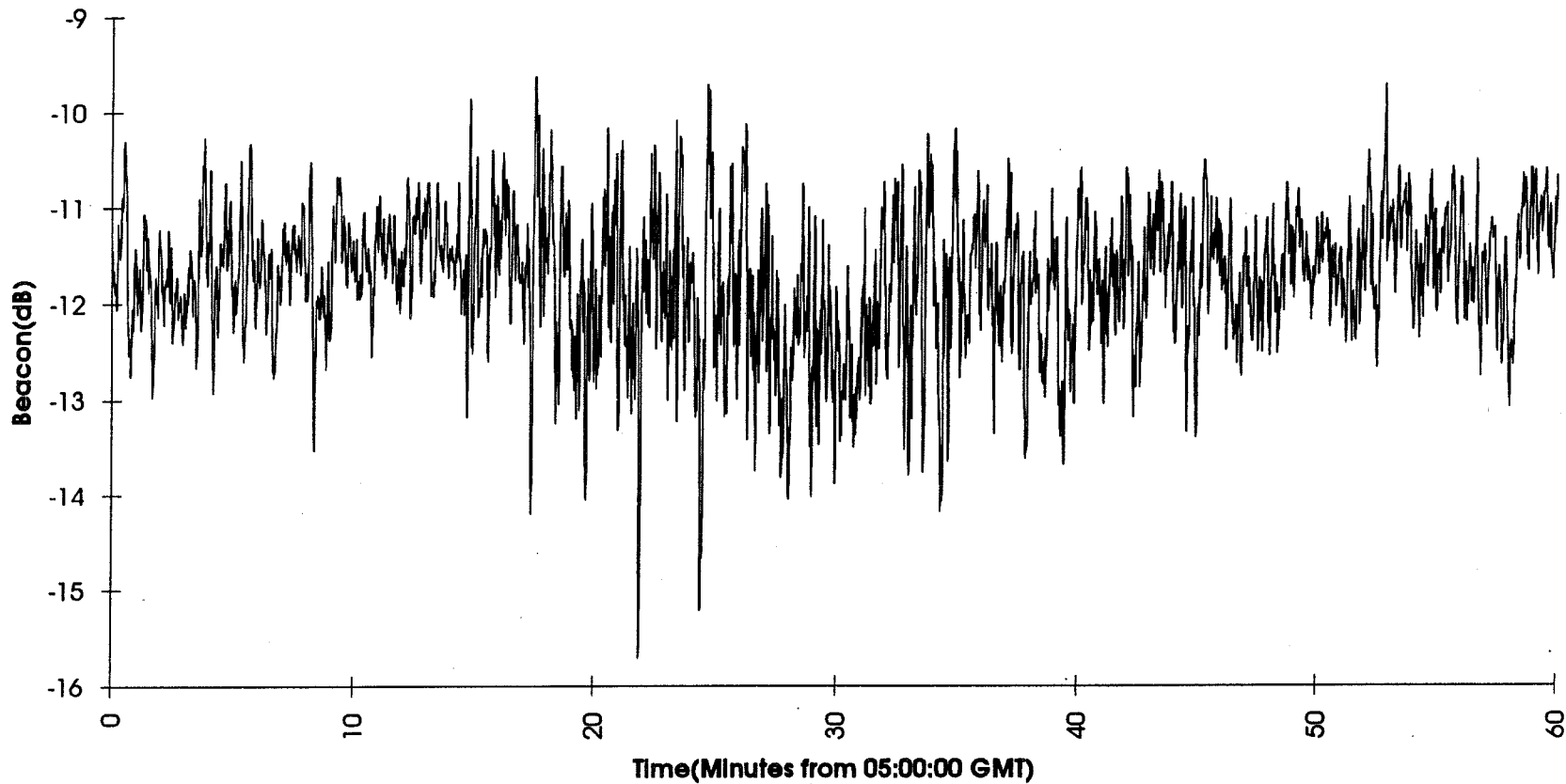


316

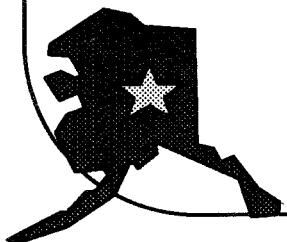


Alaska ACTS Propagation

20.185 GHz Beacon 5/14/94 5-6 H GMT

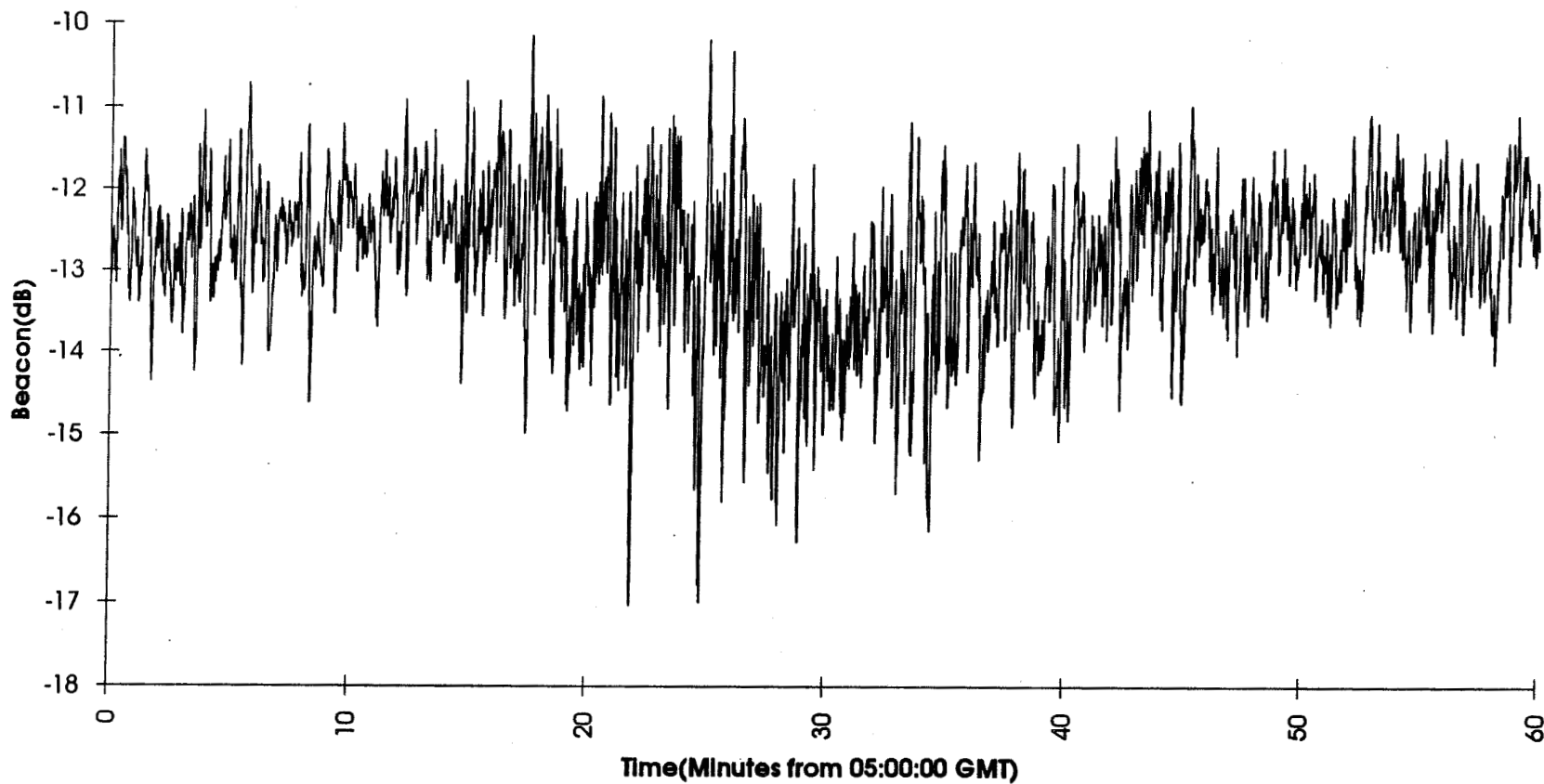


317



Alaska ACTS Propagation

27.505 GHz Beacon 5/14/94 5-6 H GMT



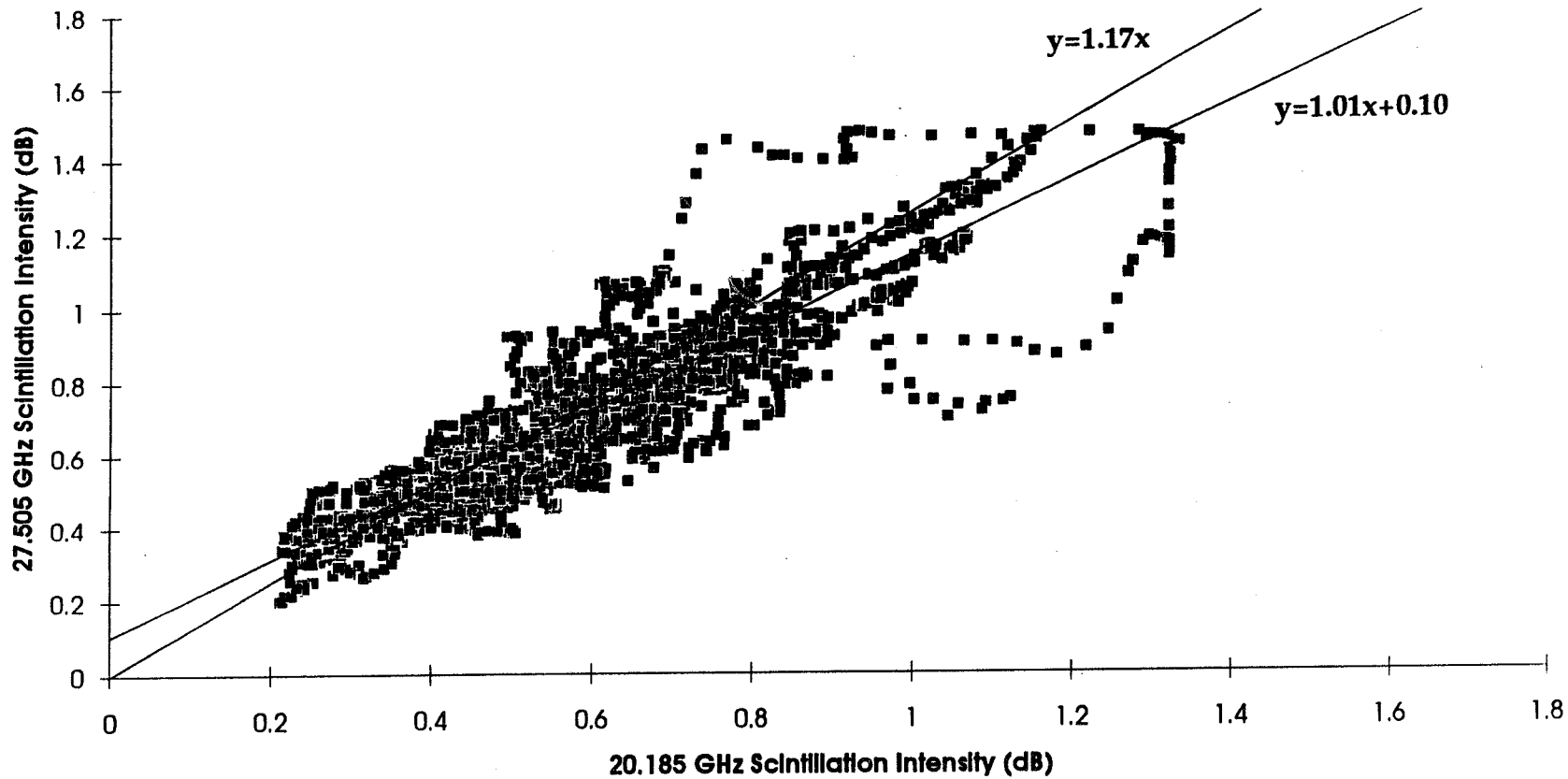
318



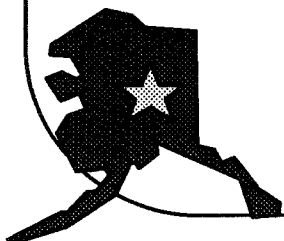
Alaska ACTS Propagation



Scatter Plot of Scintillation Intensity 5/14/94 5-6 H GMT



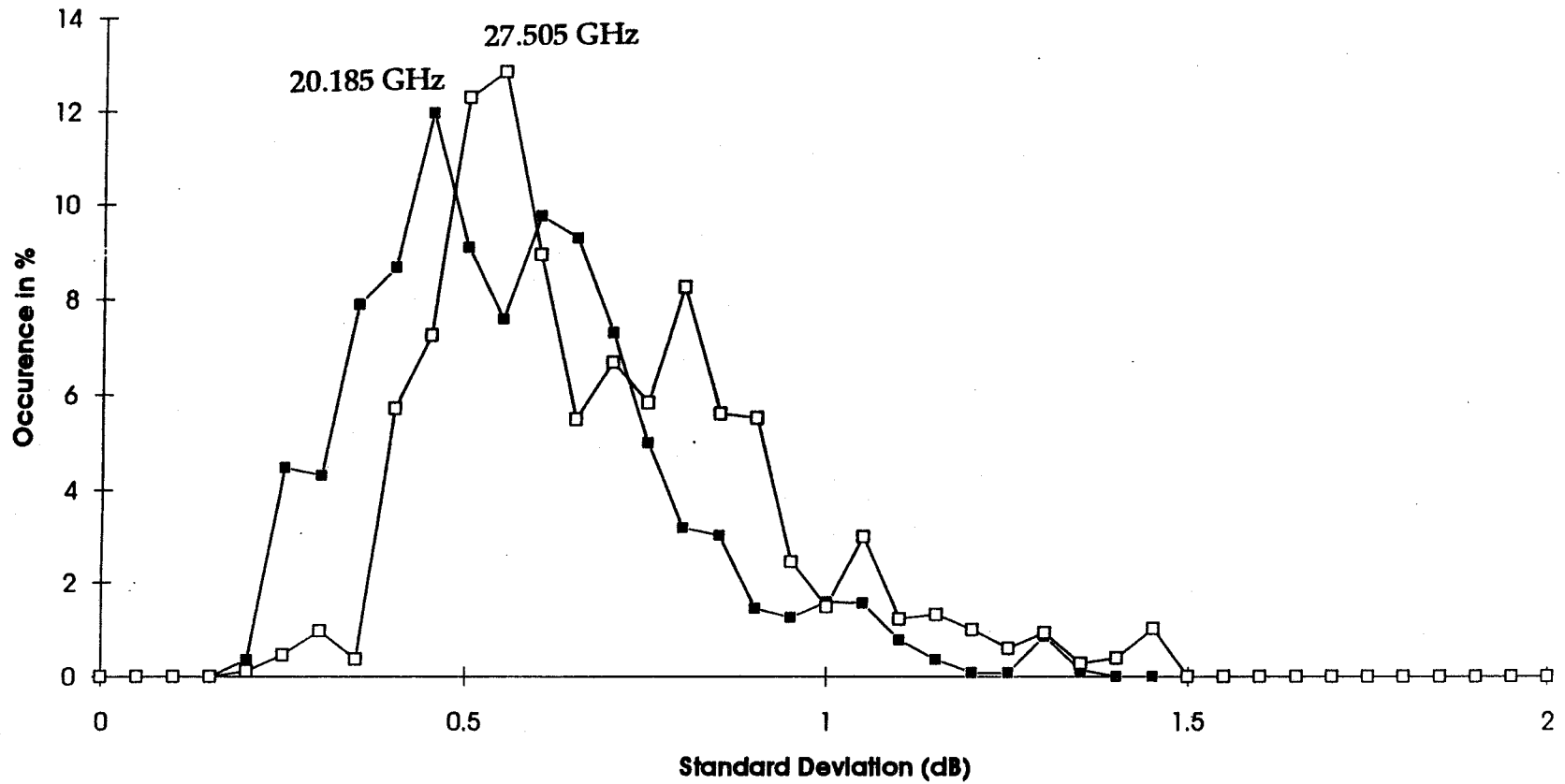
319



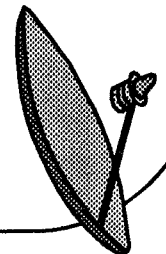
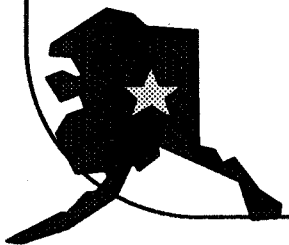
Alaska ACTS Propagation



Measured p.d.f. 5/14/94 5-6 H GMT



320



SCINTILLATION RATIO PREDICTIONS

- **FREQUENCY RATIO, 27.5/20.2 GHZ**
 - **FOR 1.22-M ANTENNA**
 - » 1.19
- **ANTENNA SIZE RATIO, 1.5"/1.22-M**
 - **FOR 20.2 GHZ FREQUENCY**
 - » 1.03
- **USED CCIR/CRANE MODEL**



Alaska ACTS Propagation



III. FUTURE PLANS

- **INSURE INTEGRITY OF DATA**
- **RAIN SEASON**
- **SCINTILLATION SEASON**
- **CONTINUE ANALYSES**
- **CLOUD EFFECTS**
- **DEVELOP MODELS OF PROPAGATION PHENOMENA**



Alaska ACTS Propagation



U.B.C. ACTS PROPAGATION EXPERIMENT

By:

I. Dommel
R. Hulays
M. Kharadly

Electrical Engineering Department
University of British Columbia

June 16, 1994

OUTLINE

- STATUS
- SOME PROBLEMS
- SOME OBSERVATIONS
- PRESENT AND FUTURE WORK

STATUS

- LATEST DACS SOFTWARE UPDATE INSTALLED ON JUNE 7, 1994
- RAW DATA, PRE-PROCESSED DATA AND EVENT AND FAULT LOGS UP TO, AND INCLUDING APRIL 1994 WERE SENT TO ACTS DATA CENTER. MAY DATA IS NOW COMPLETE
- ELEVATION TILT SCAN
 - ◇ Weather has not been cooperative!
 - ◇ No local sounding stations. The closest stations are:

* Quillayute (Olympic peninsula): 220 km, S.W.

* Port Hardy (Northern Vancouver island): 360 km, N.W.

* Vernon (Okanagan): 300 km, E.

◇ Possibility of interpolating between the three sounding sites

◇ Results thus obtained may not be valid at our site up to a height of 2 km.

◇ Attempting to arrange for a sounding on Campus

- **HYDROPHOBIC PAINT TEST**

- ◇ This has been tested, loss is hardly measurable, less than 0.1 dB signal loss at 29.6 GHz

- ◇ Has not yet been applied to antenna

- **SURVEILLANCE CAMERA AND TIME-LAPSE RECORDER**

- ◇ Installed to keep track of antenna surface conditions (e.g., Icing) and weather conditions (e.g., Rain, Snow)

- ◇ Records are obtained every 8 seconds with tape lasting 40 days

ADDITIONAL RESOURCE

- AIRPORT WEATHER STATION

- ◇ Approx. 8 km from APT site

- ◇ Close to propagation path

- ◇ Will use their monthly statistics to compare to ours

SOME PROBLEMS

- 27 GHz RADIOMETER STEPS CAUSING RADIOMETER RESTARTS, Fig. 1
- RADIOMETERS VOLTAGE DRIFT, Fig. 2
 - ◇ A manual reboot, at times, corrects the problem
- ACTSEEDIT PROBLEMS
 - ◇ Inability of software to remove certain spikes (e.g. Fig. 3)

◇ This causes error in the attenuation cumulative distribution function plots (Fig. 4)

● DR. CRANE'S EDITING PROGRAM

◇ We have not yet been able to make it work

SOME OBSERVATIONS

- TYPICAL FADES AT VANCOUVER, Figs. 5 and 6
 - ◇ Long duration
 - ◇ Low fade
 - ◇ Radiometer-derived attenuation generally agrees with Beacon-derived attenuation

- **ATYPICAL FADES AT VANCOUVER, Figs. 7 and 8**
 - ◇ **Strong fade - System lost lock**
 - ◇ **Radiometer-derived attenuation does not agree with Beacon-derived attenuation (Radiometer saturates at 10 dB?)**
 - ◇ **20 GHz attenuation > 27 GHz attenuation, Fig. 9**
 - * **Some snow-fall was recorded**
 - * **Possible cause (defocusing due to snow layer on antenna surface?)**

- **MONTHLY ATTENUATION STATISTICS**

- ◇ For the Month of January, Figs. 10 and 11

- ◇ For the Month of March, Figs. 12 and 13

- ⇒ 20 GHz attenuation reaches higher values than 27 GHz attenuation!

- **SCINTILLATIONS**

- ◇ Clear weather, Fig. 14

- ◇ Rain, Fig. 15

PRESENT AND FUTURE WORK

- ANALYSIS PACKAGE

- ◇ Exceedance statistics

- ◇ 27 GHz attenuation vs 20 GHz attenuation

- ◇ Fade-duration statistics

- ◇ Fill in missing data

- **MELTING LAYER**

- ◇ Estimation of the excess attenuation caused by the presence melting layer

- **SCINTILLATIONS**

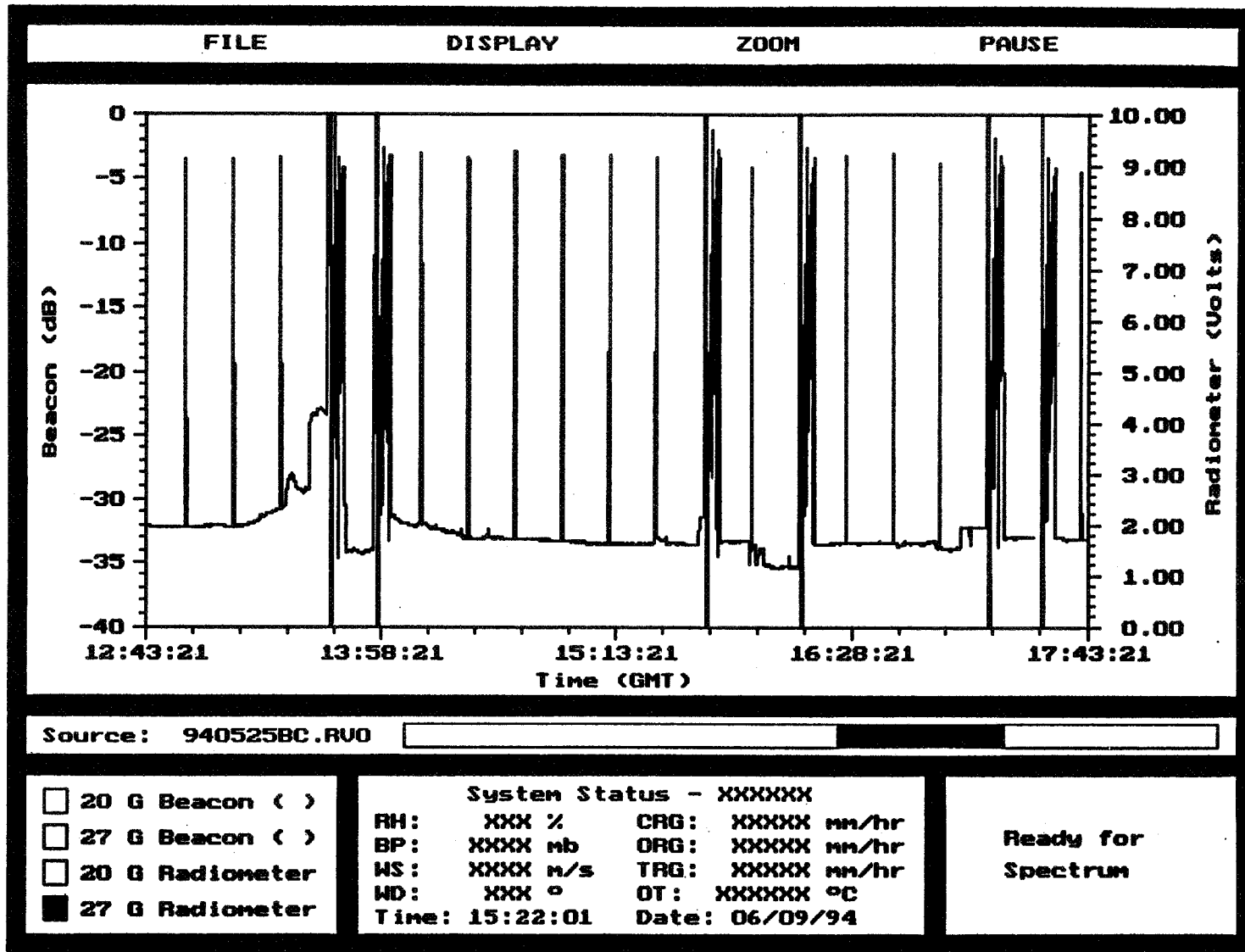


Fig.1: Typical 27 GHz radiometer steps causing automatic restart

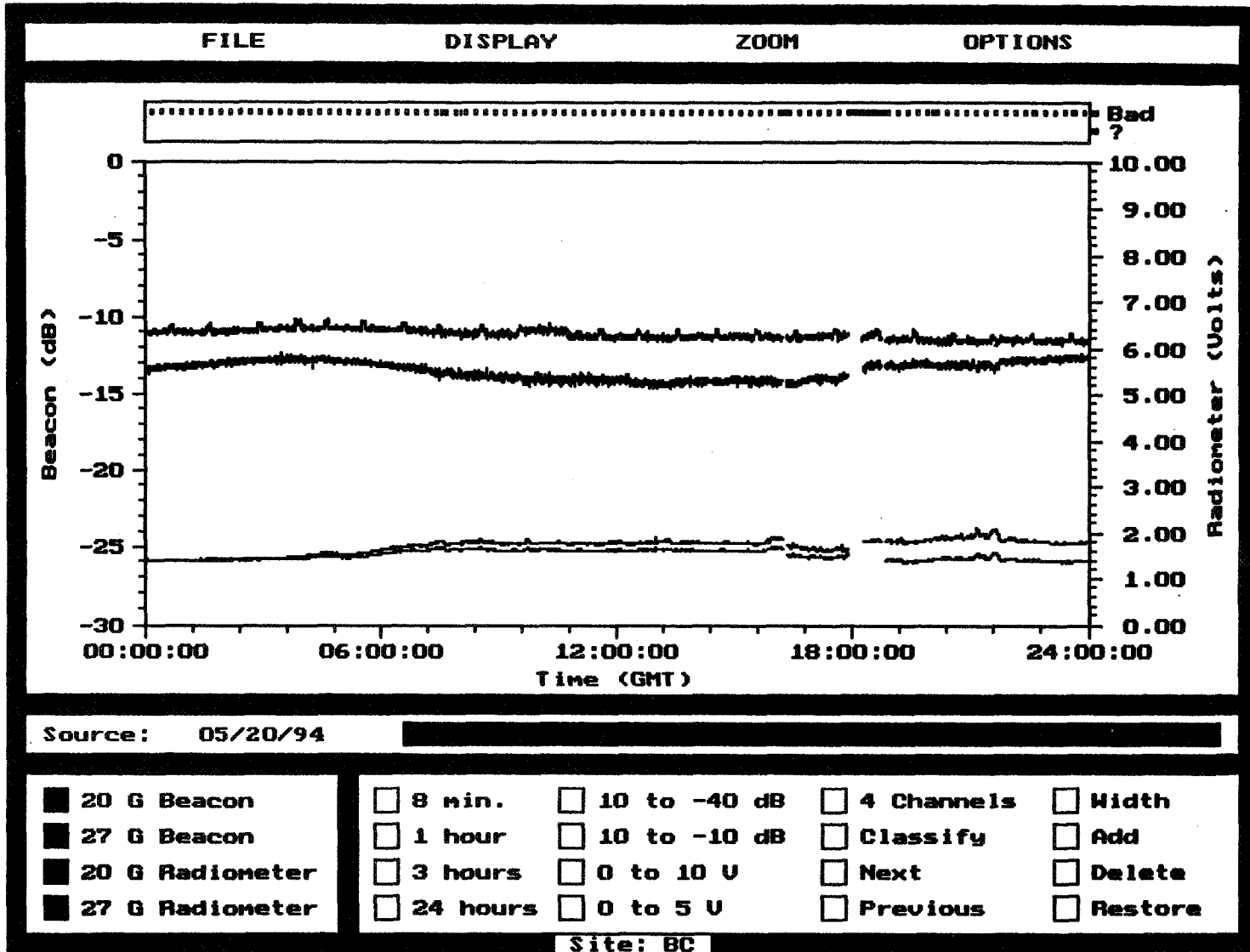


Fig. 2: Radiometer voltage drift

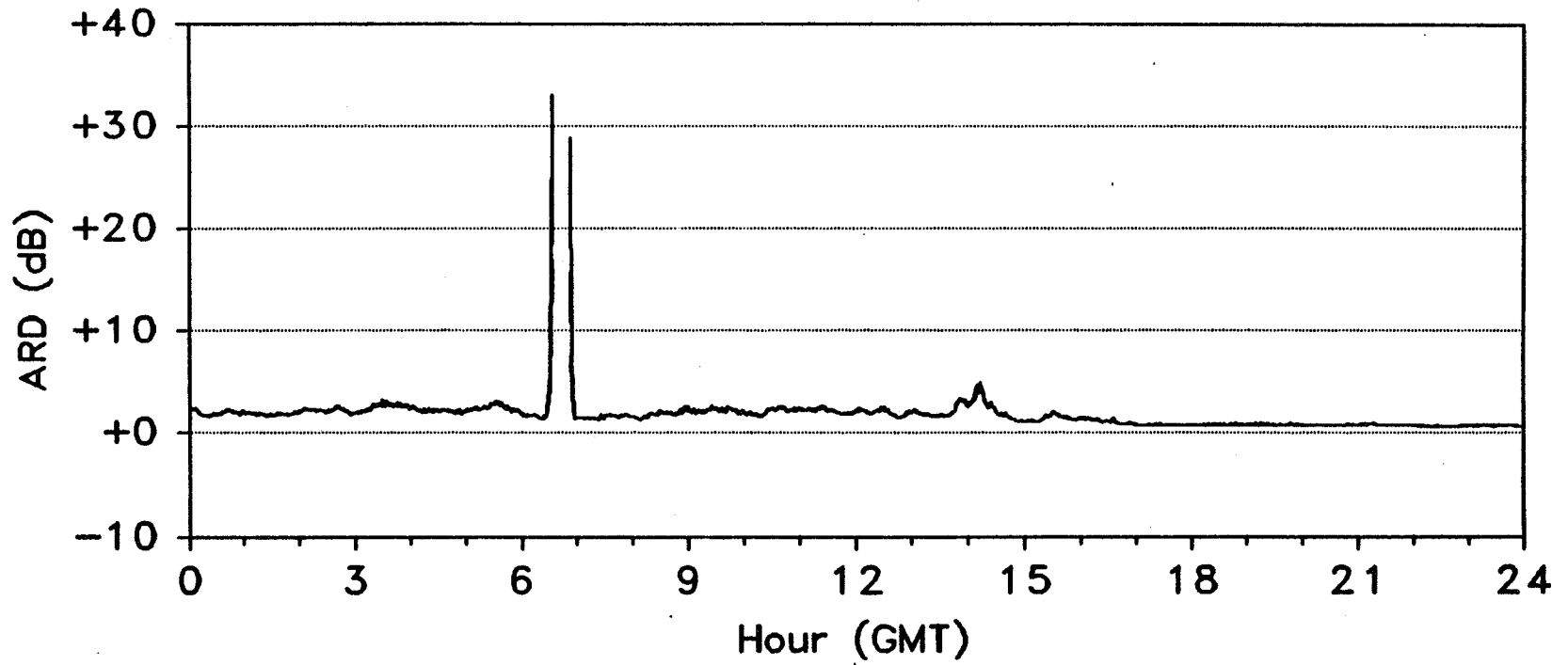


Fig. 3: Pre-processing software was unable to remove spike in 27 GHz radiometer-derived attenuation

FEB 1994 - 20 GHz AND 27 GHz RADIOMETER - BC

339

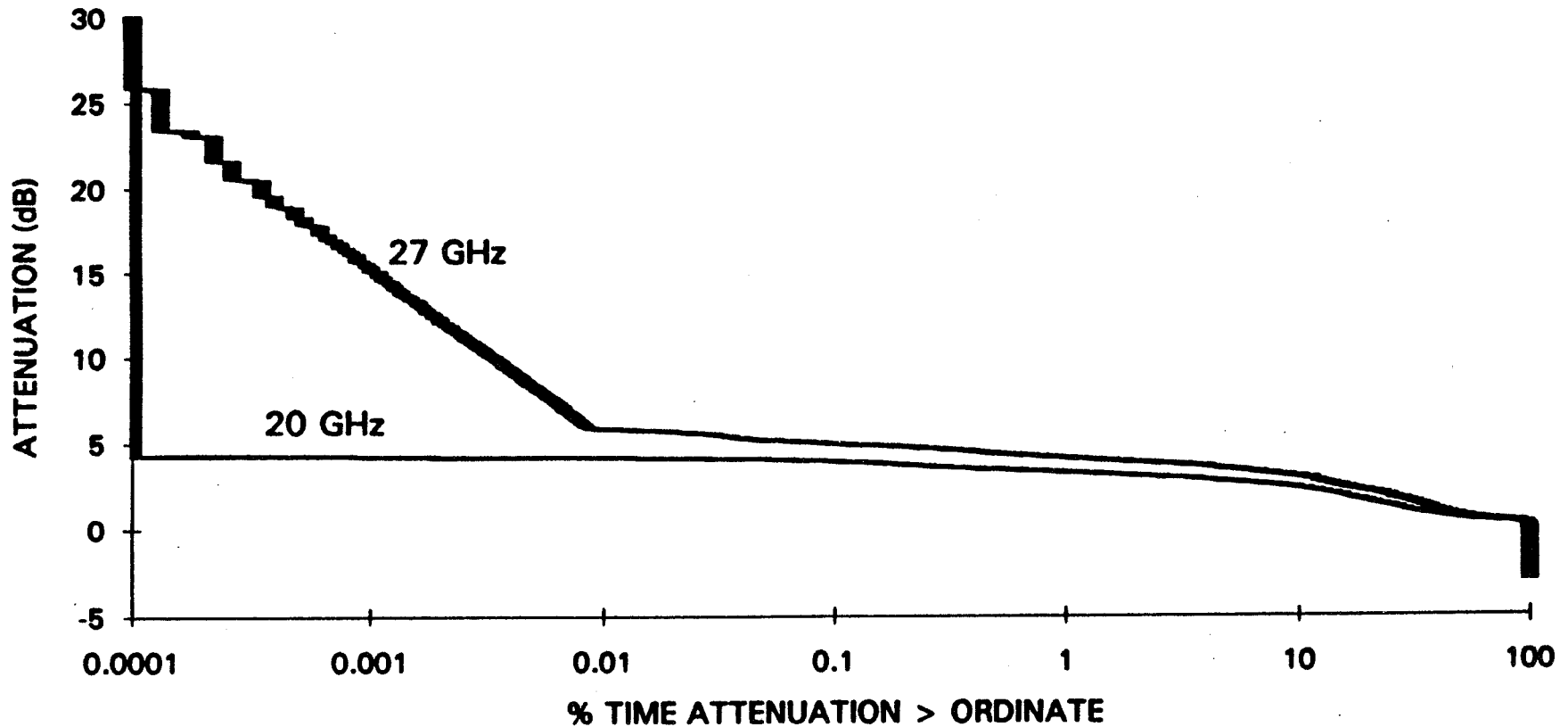


Fig. 4: Effect of the spike in Fig. 3 on the Cumulative Distribution Function of the 27 GHz radiometer-derived attenuation

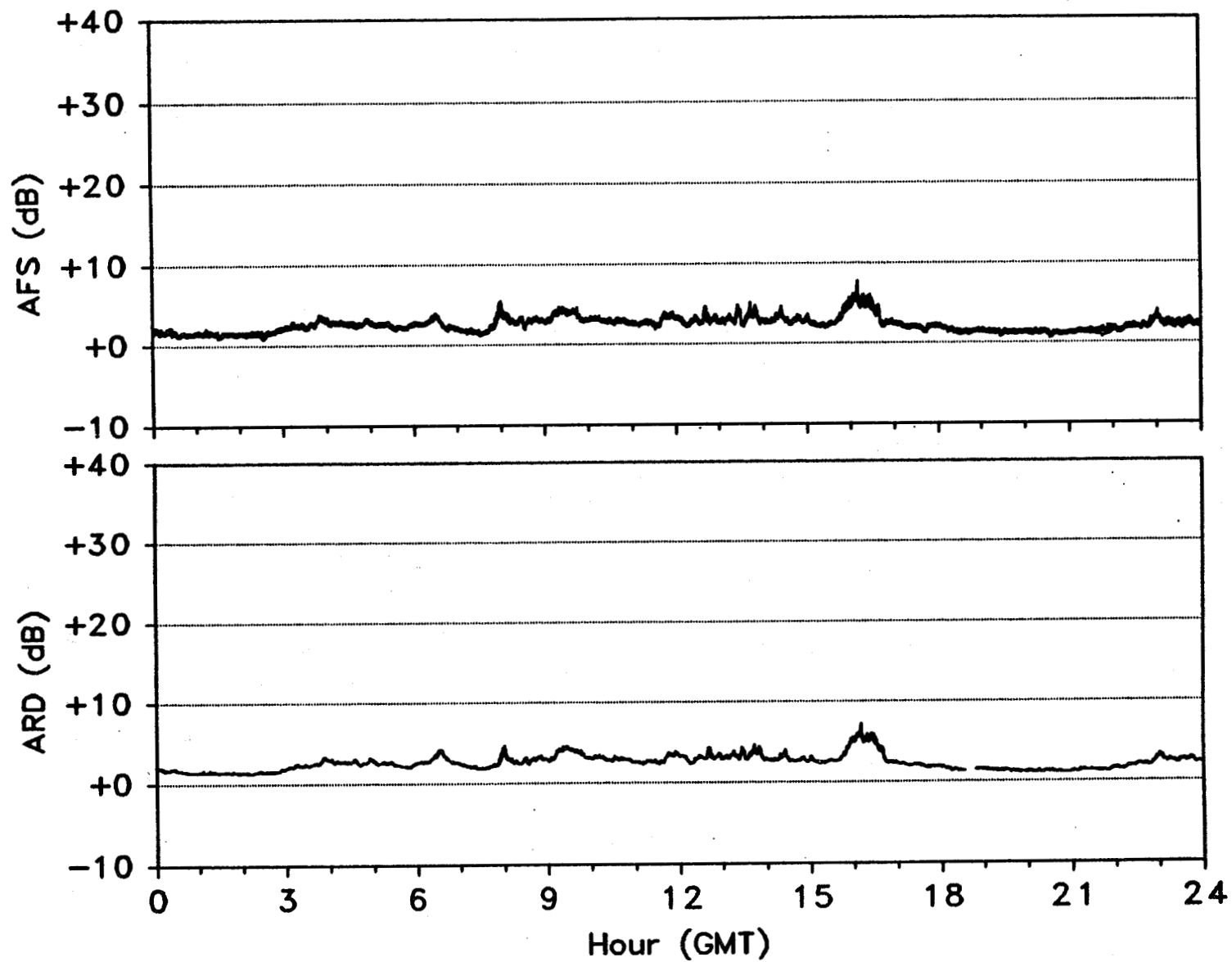


Fig. 5: 20 GHz attenuation for March 1, 1994

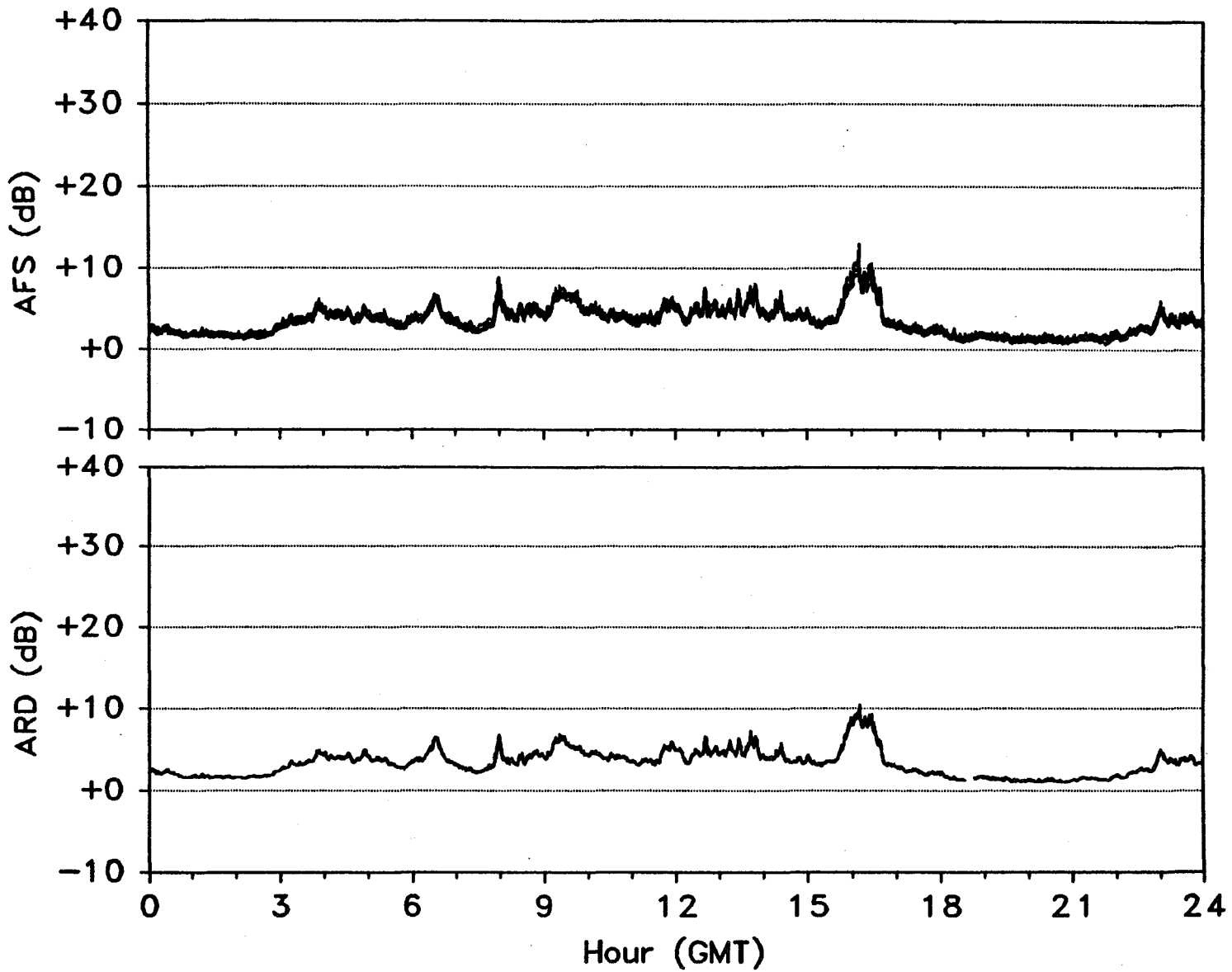


Fig. 6: 27 GHz attenuation for March 1, 1994

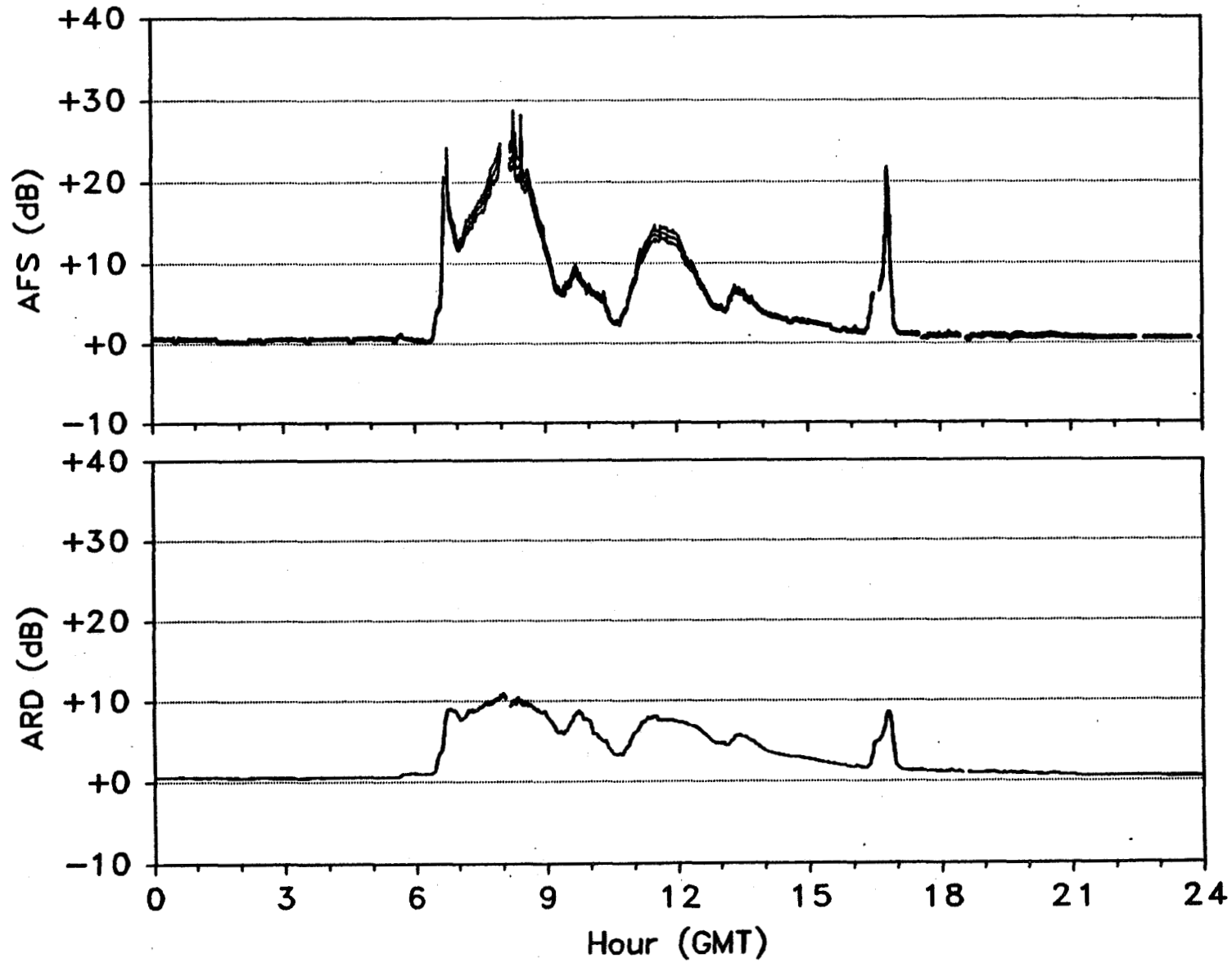


Fig. 7: 20 GHz attenuation for March 22, 1994

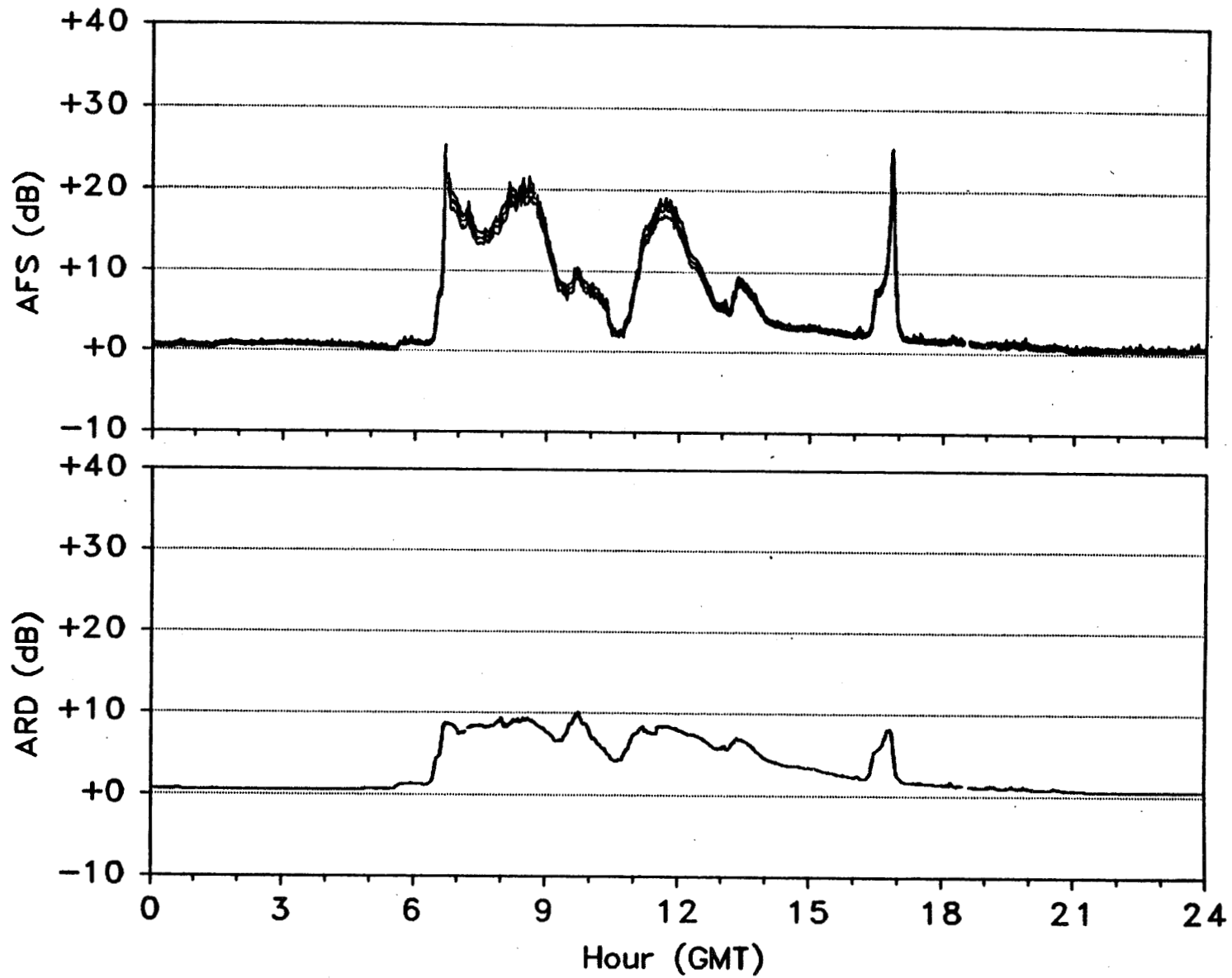


Fig. 8: 27 GHz attenuation for March 22, 1994

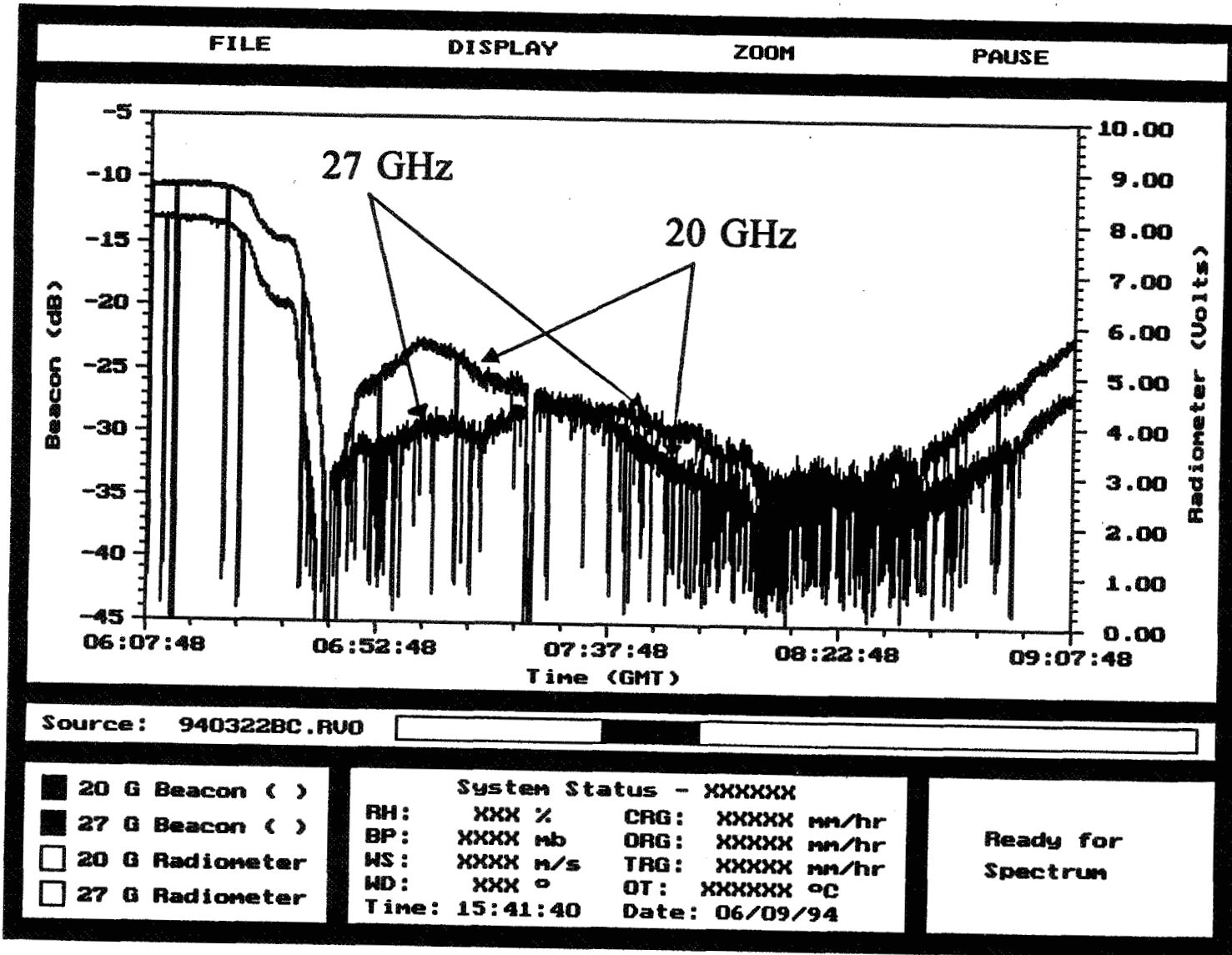


Fig. 9: 20 and 27 GHz signal level during a deep fade on March 22, 1994.

JAN 1994 - 20 GHz and 27 GHz BEACON - BC

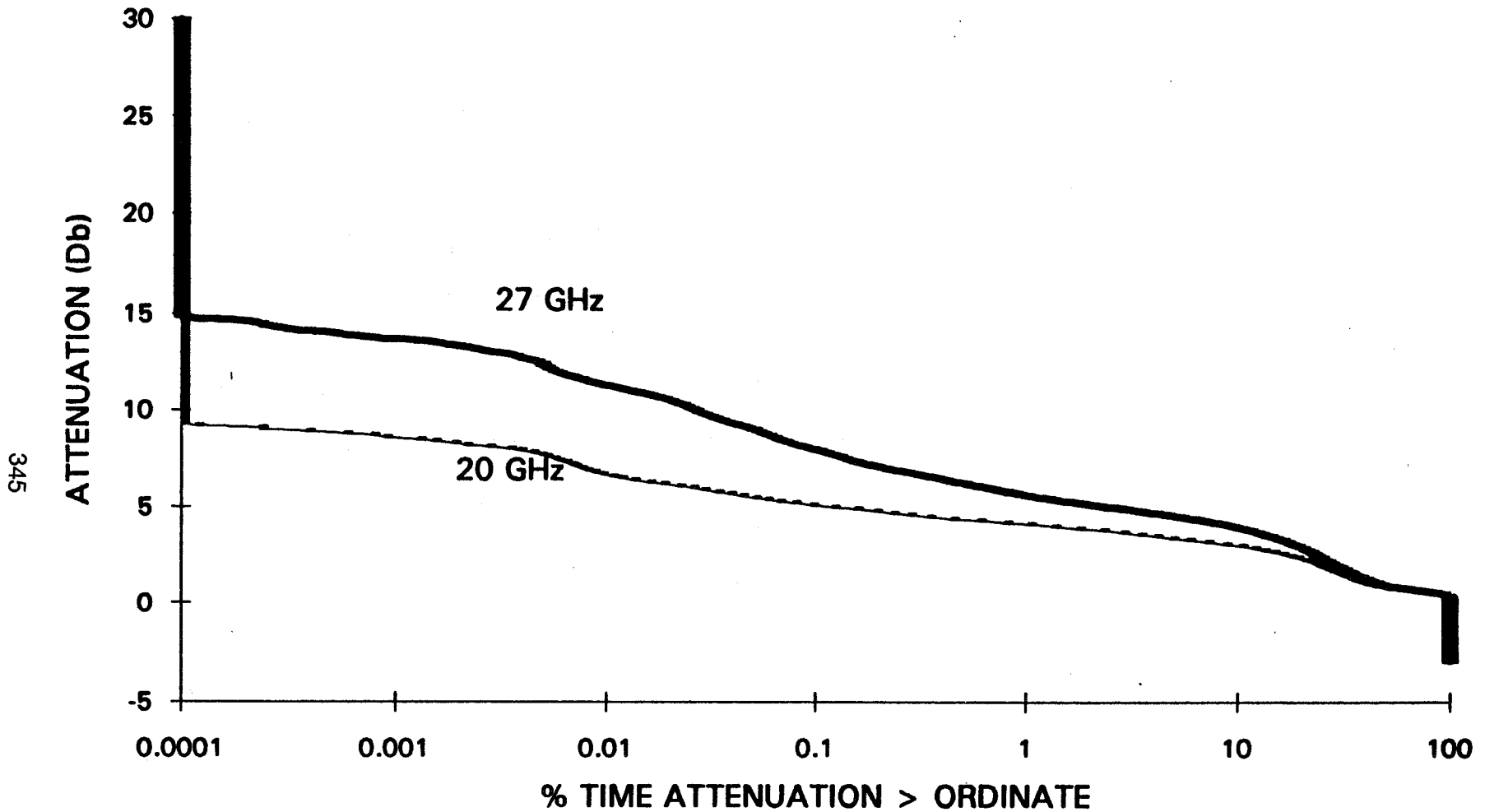


Fig. 10: Cumulative distribution functions of the 20 and 27 GHz beacon-derived attenuation for the month of January, 1994

JAN 1994 - 20 GHz AND 27 GHz RADIOMETER - BC

346

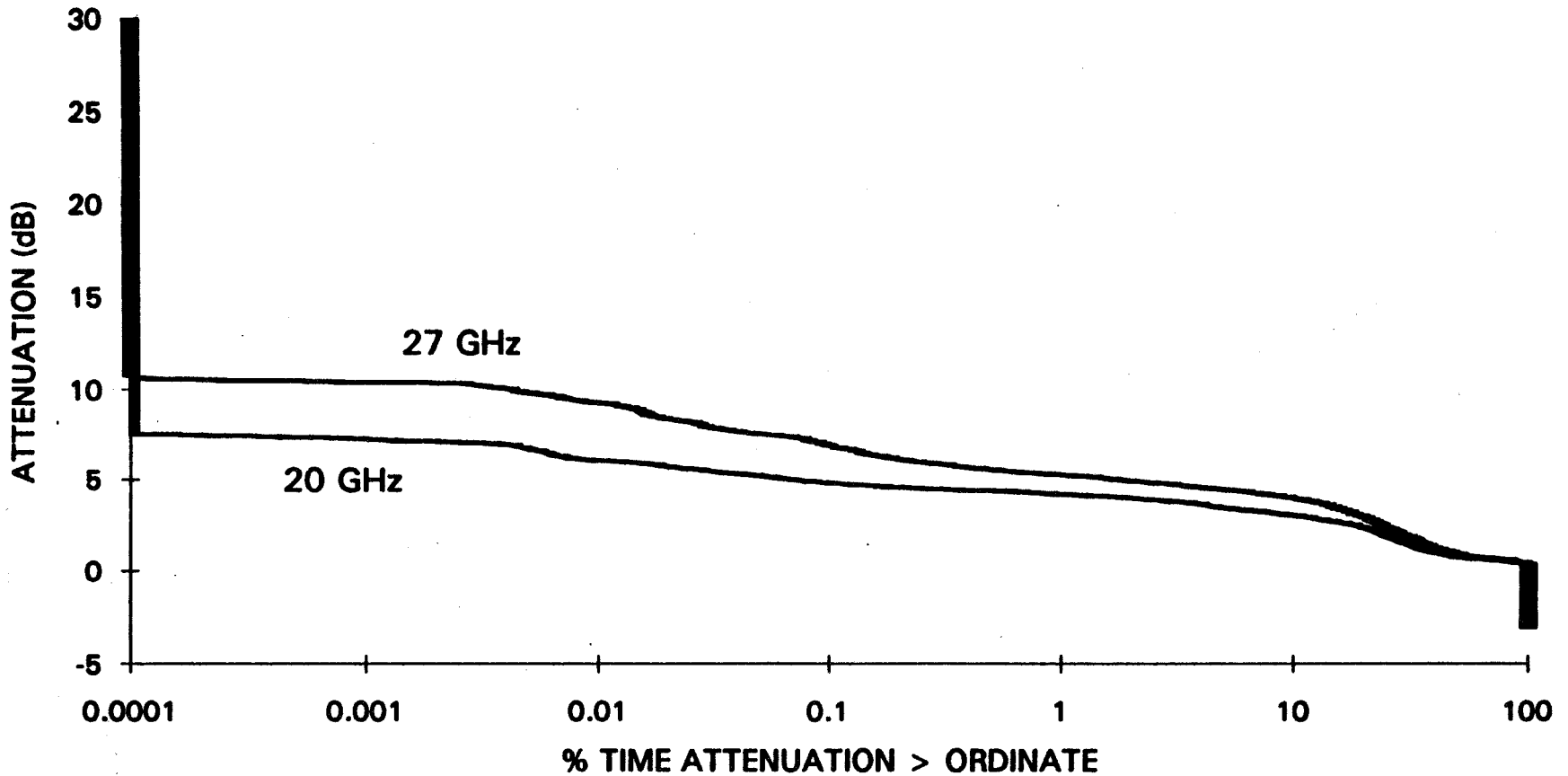


Fig. 11: Cumulative distribution functions of the 20 and 27 GHz radiometer-derived attenuation for the month of January, 1994

MAR 1994 - 20 GHz AND 27 GHz BEACON - BC

347

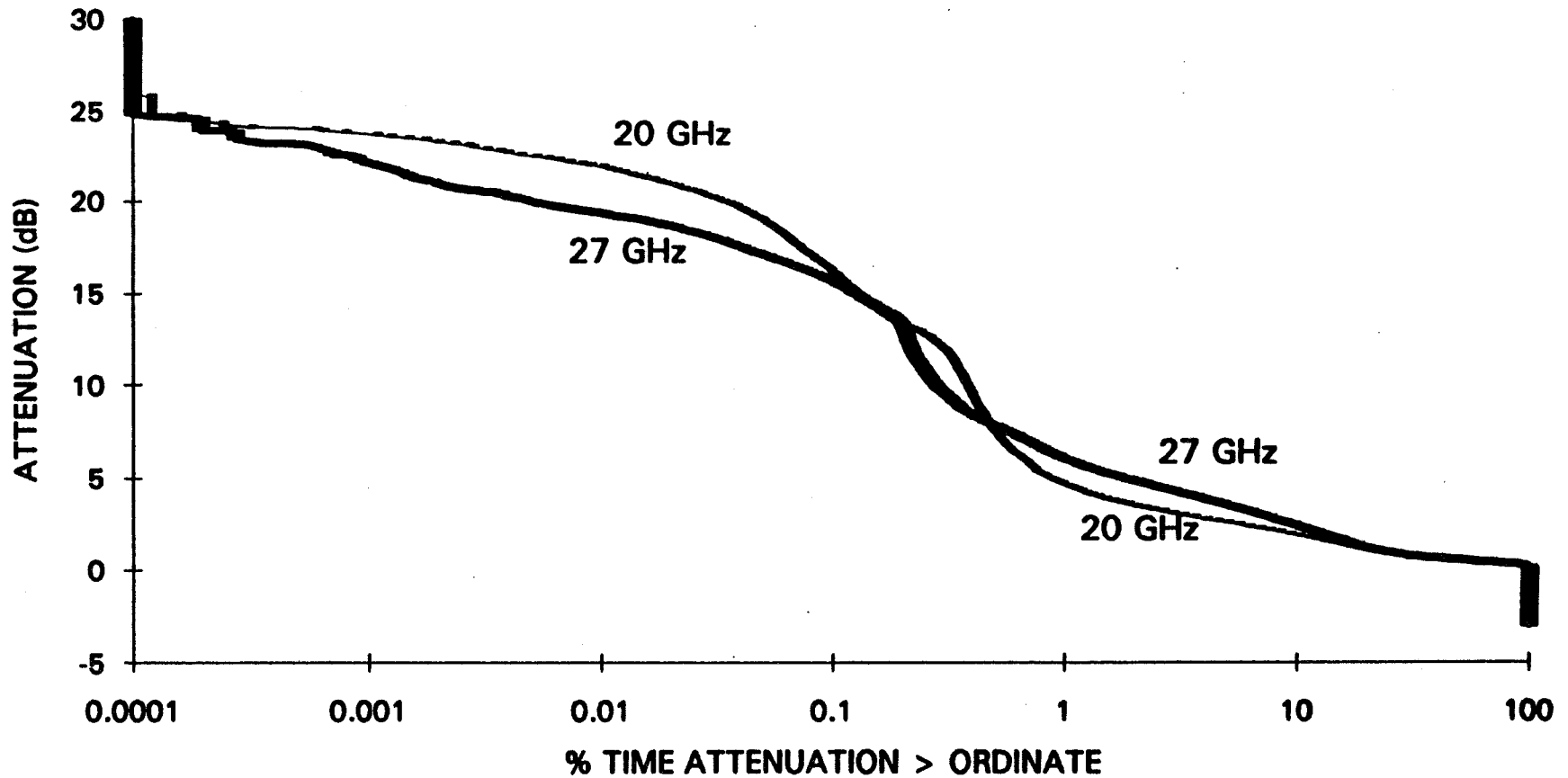


Fig. 12: Cumulative distribution functions of the 20 and 27 GHz beacon-derived attenuation for the month of March, 1994

MAR 1994 - 20 GHz AND 27 GHz RADIOMETER - BC

348

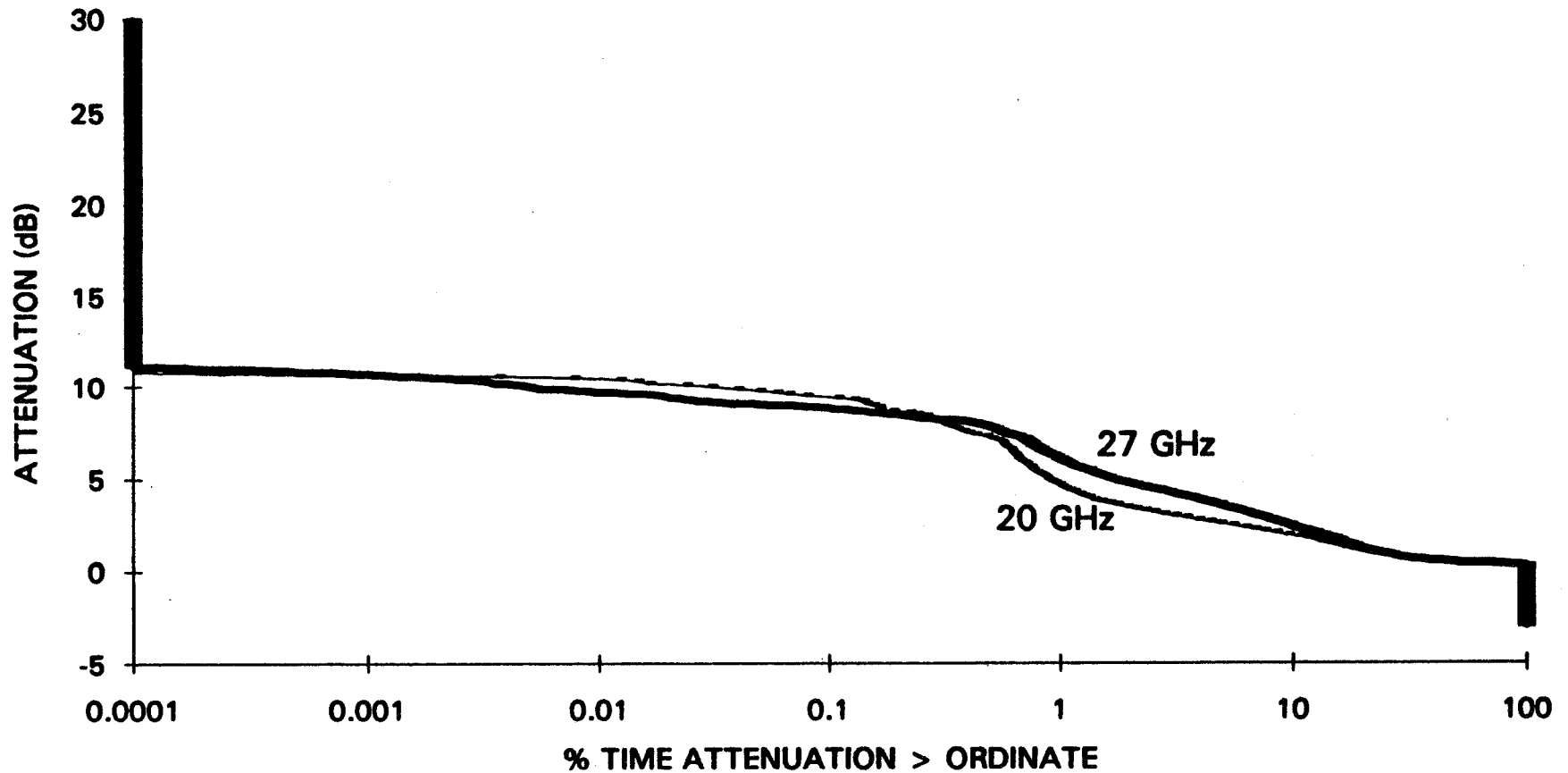


Fig. 13: Cumulative distribution functions of the 20 and 27 GHz radiometer-derived attenuation for the month of March, 1994

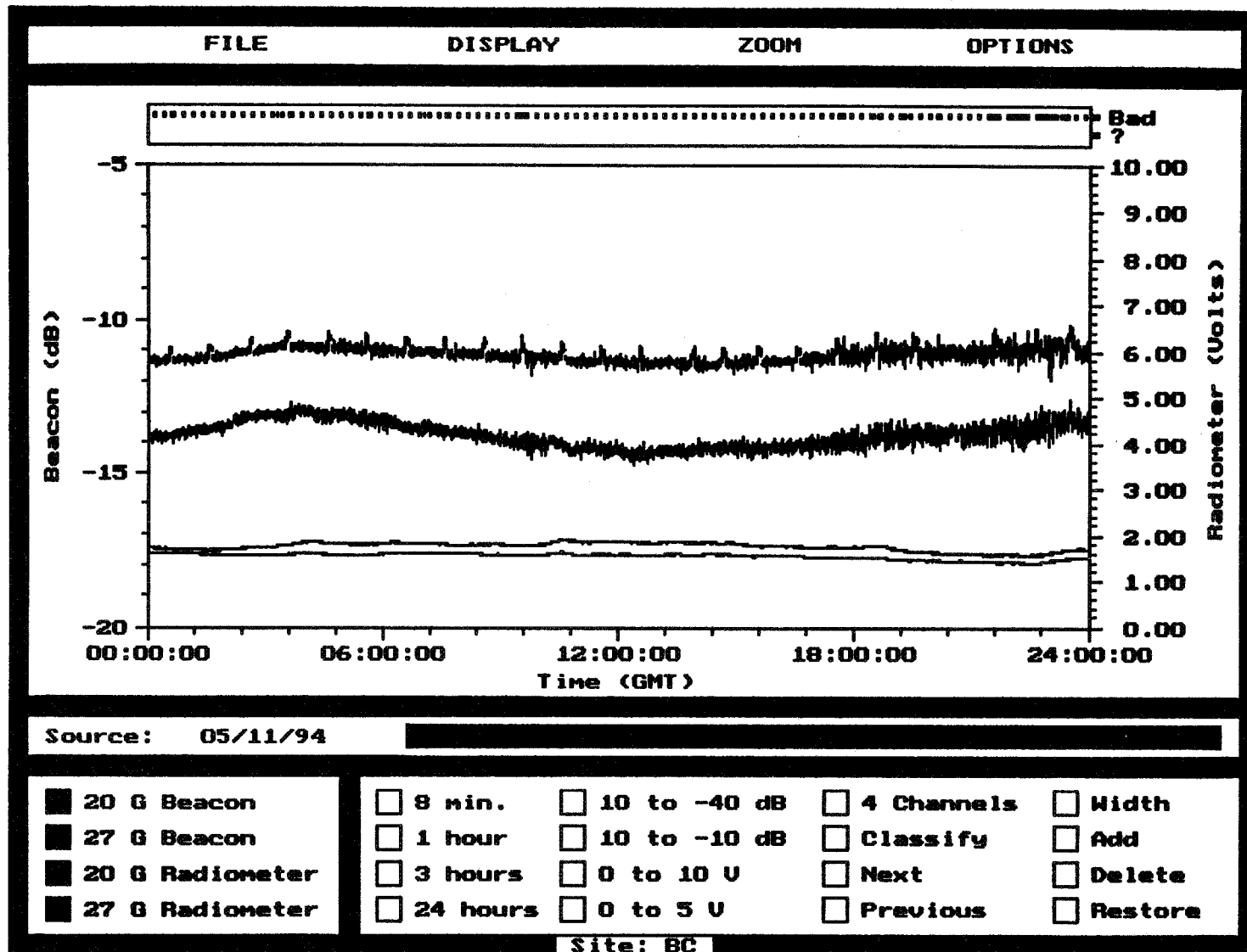


Fig. 14: Clear air scintillation on May 11, 1994

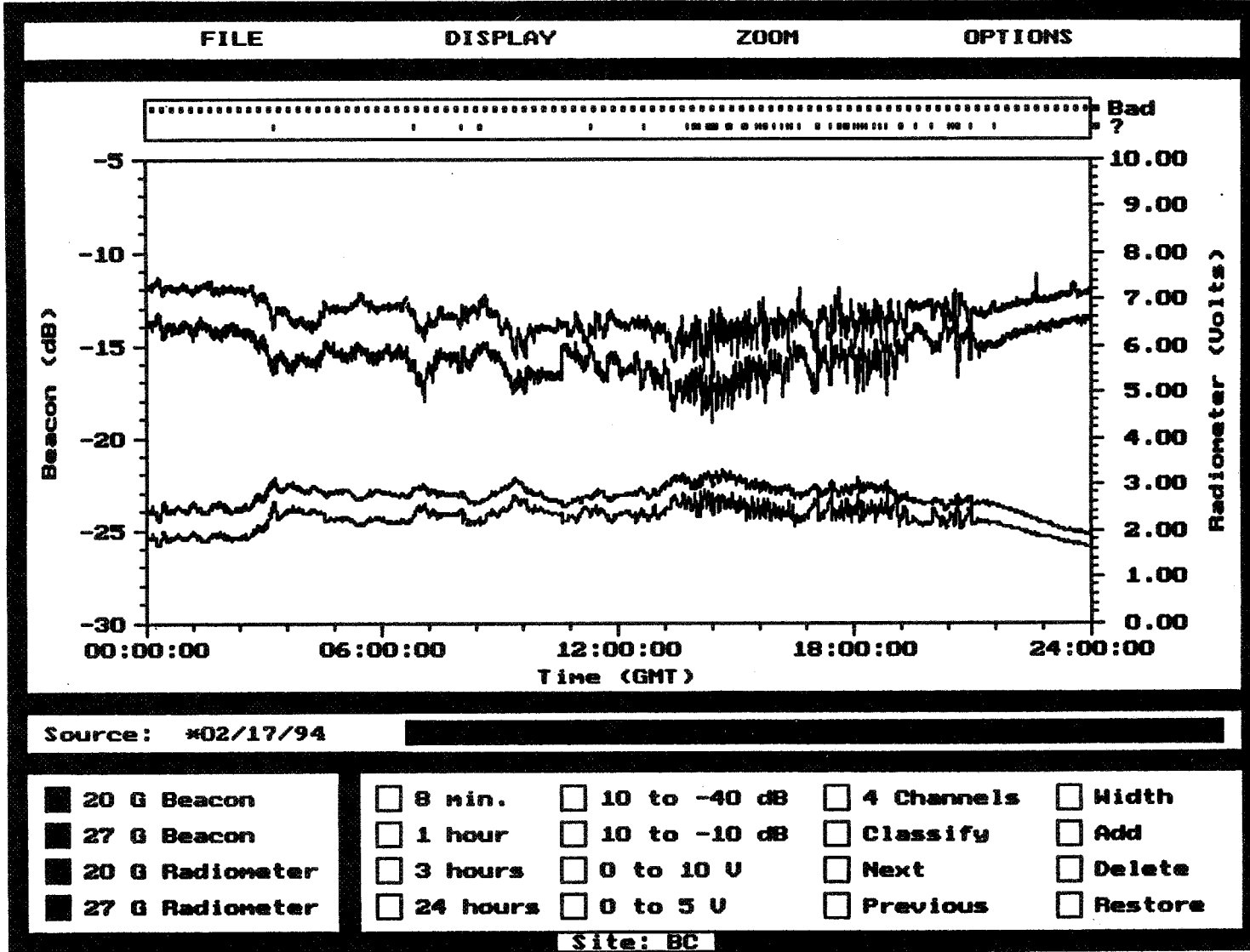


Fig. 15: Rainy weather scintillation on February 17, 1994

**Ka-band Propagation Measurements
Using the ACTS Propagation Terminal
and the CSU-CHILL Multiparameter Radar**

Experimenters

Colorado State University
Department of Electrical Engineering
Ft. Collins, CO 80523

Investigators

V.N. Bringi, Professor
John Beaver, Ph.D. Candidate
Joseph Turk, Research Associate

**ACTS Propagation Studies Mini-Workshop
June 16, 1994**

Outline

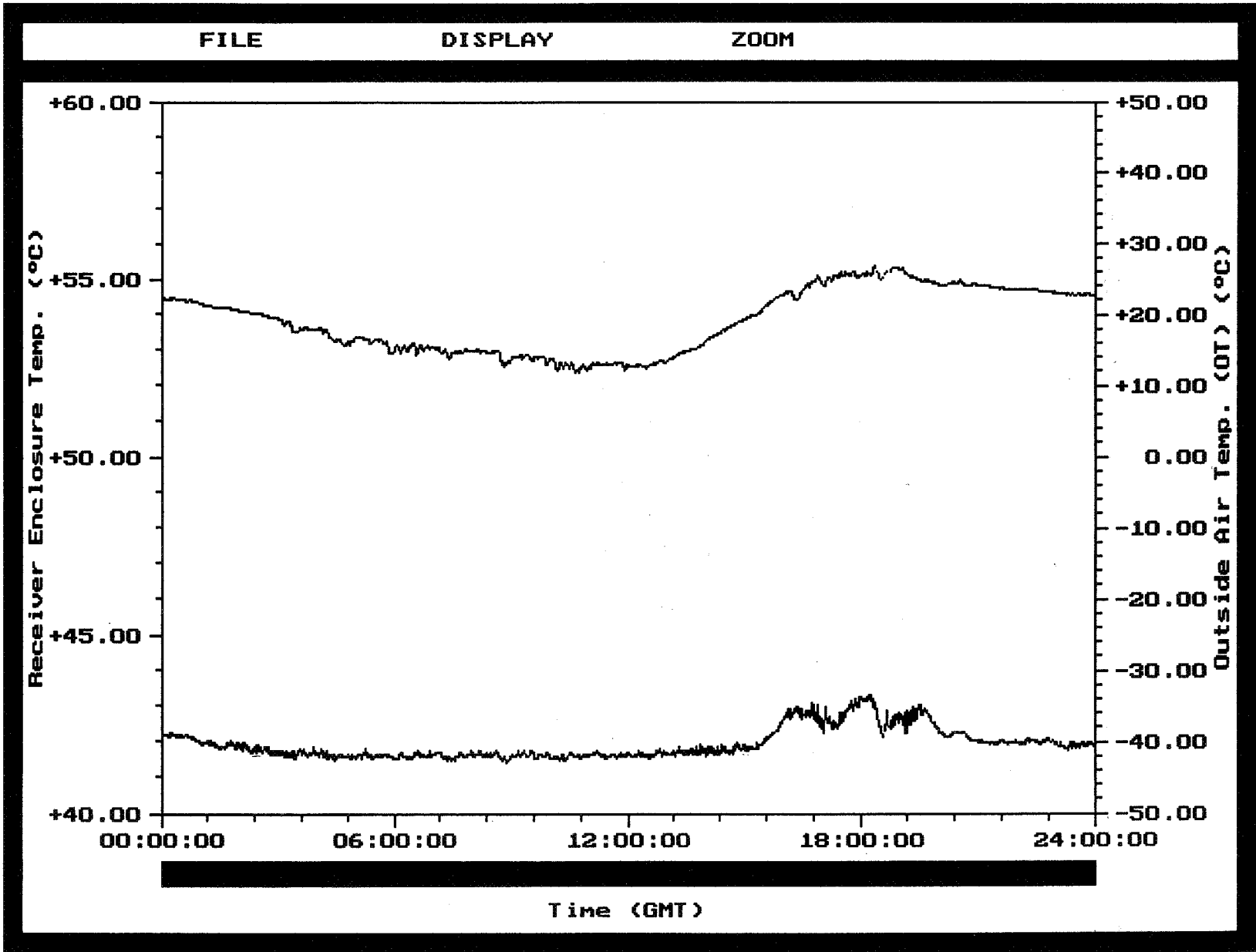
- CSU – ACTS Propagation Terminal Status
 - Hardware Problems and Solutions
 - Software Discussion

- ACTS Propagation Measurements
 - ACTS and CSU – CHILL measurements

- Modelling Efforts

Hardware Problems and Solutions

- Snow accumulation on the antenna surface
 - Installed a heating unit on the back surface of antenna
- Frequent system crashes and reboots
 - Reduced the receiver enclosure temperature to 40° Celcius
- Loss of 27GHz beacon signal
 - Lost lock on February 28, 1994.
 - After retuning the Master Oscillator, reacquired signal on March 4.

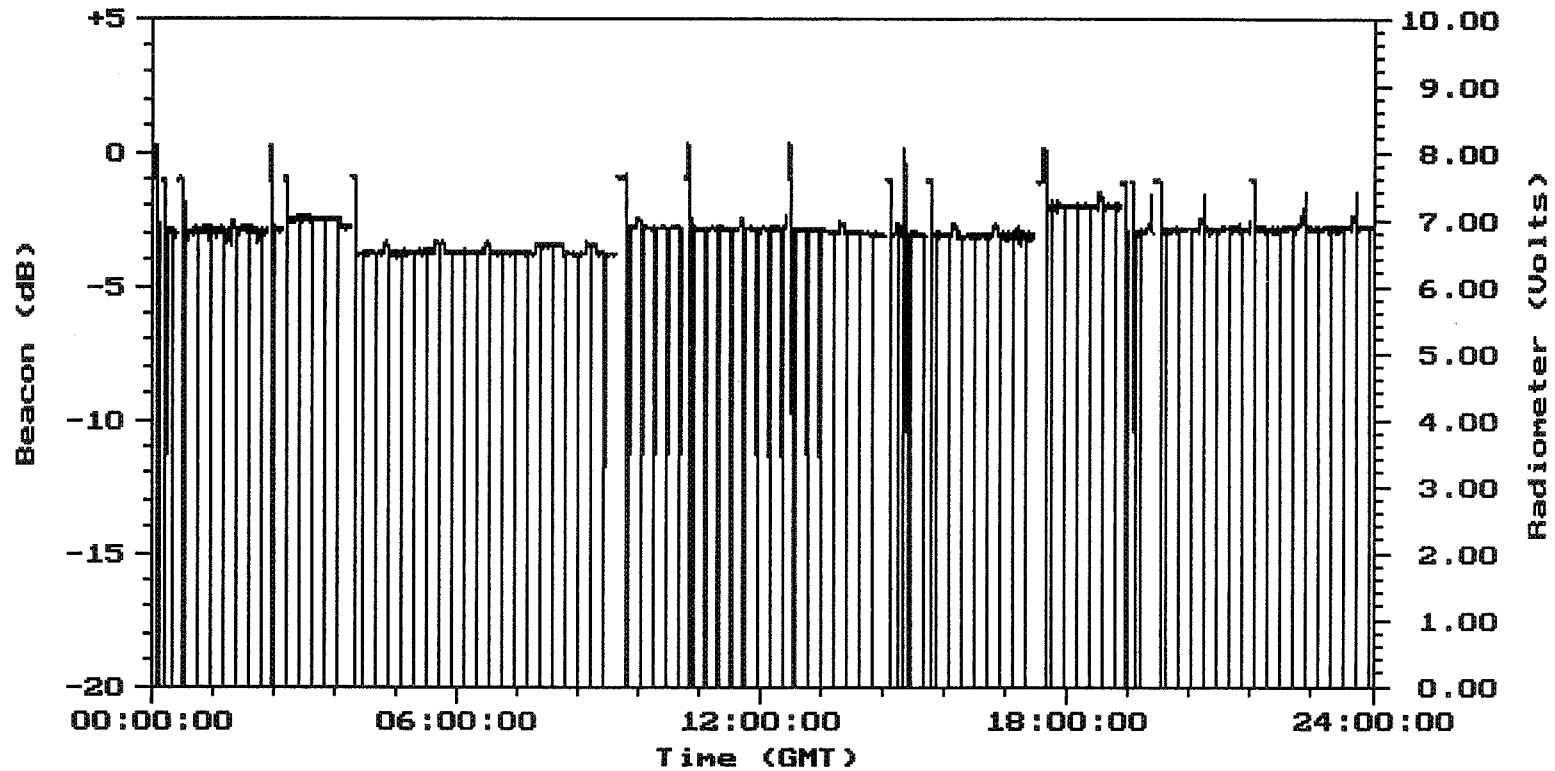


FILE

DISPLAY

ZOOM

PAUSE



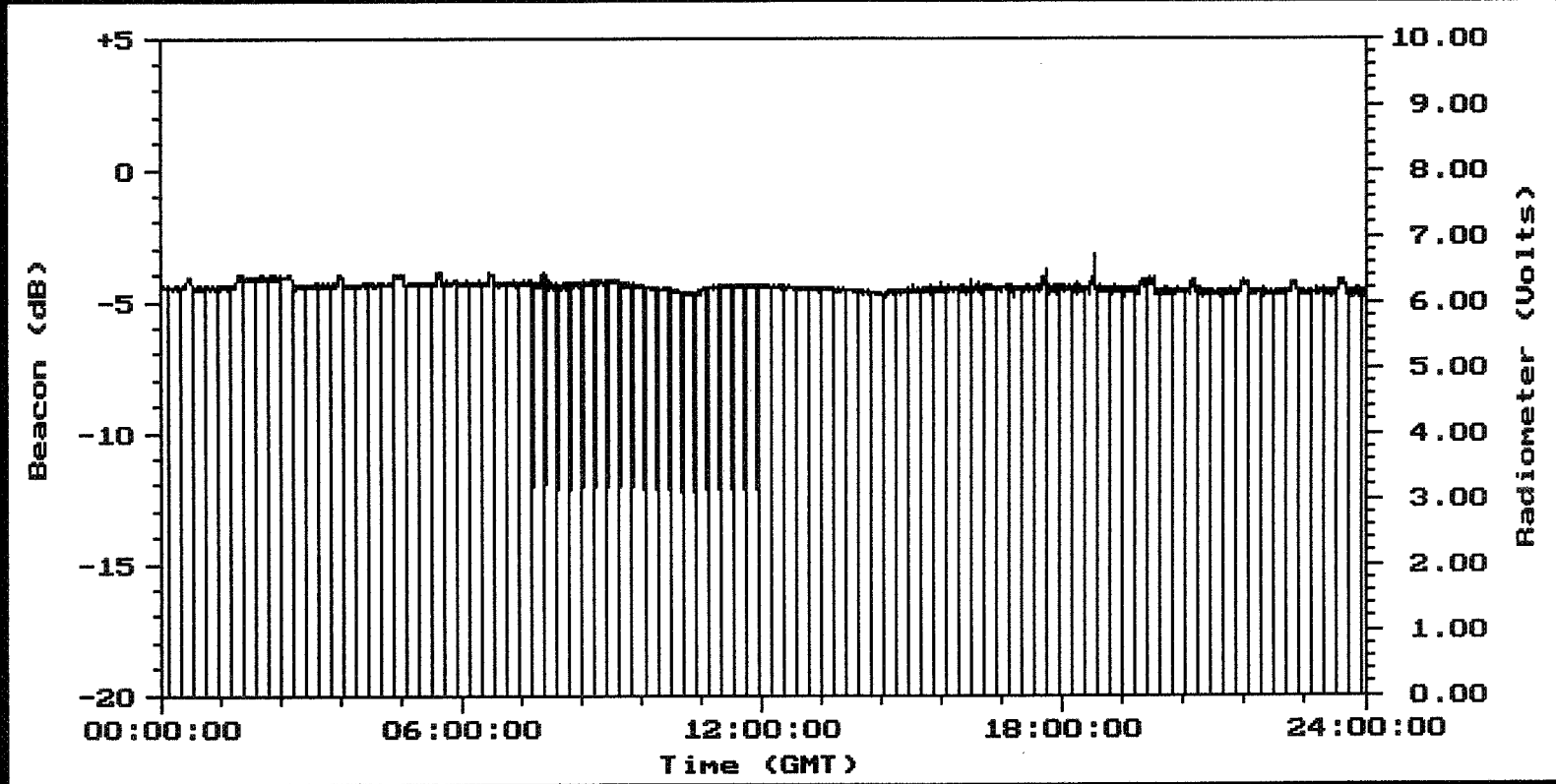
Source: 940424C0.RU0

- 20 G Beacon ()
- 27 G Beacon ()
- 20 G Radiometer
- 27 G Radiometer

System Status - XXXXXX
 RH: XXX % CRG: XXXXX mm/hr
 BP: XXXX mb ORG: XXXXX mm/hr
 WS: XXXX m/s TRG: XXXXX mm/hr
 WD: XXX ° OT: XXXXXX °C
 Time: 00:25:29 Date: 06/15/94

Ready for
Spectrum

FILE DISPLAY ZOOM PAUSE



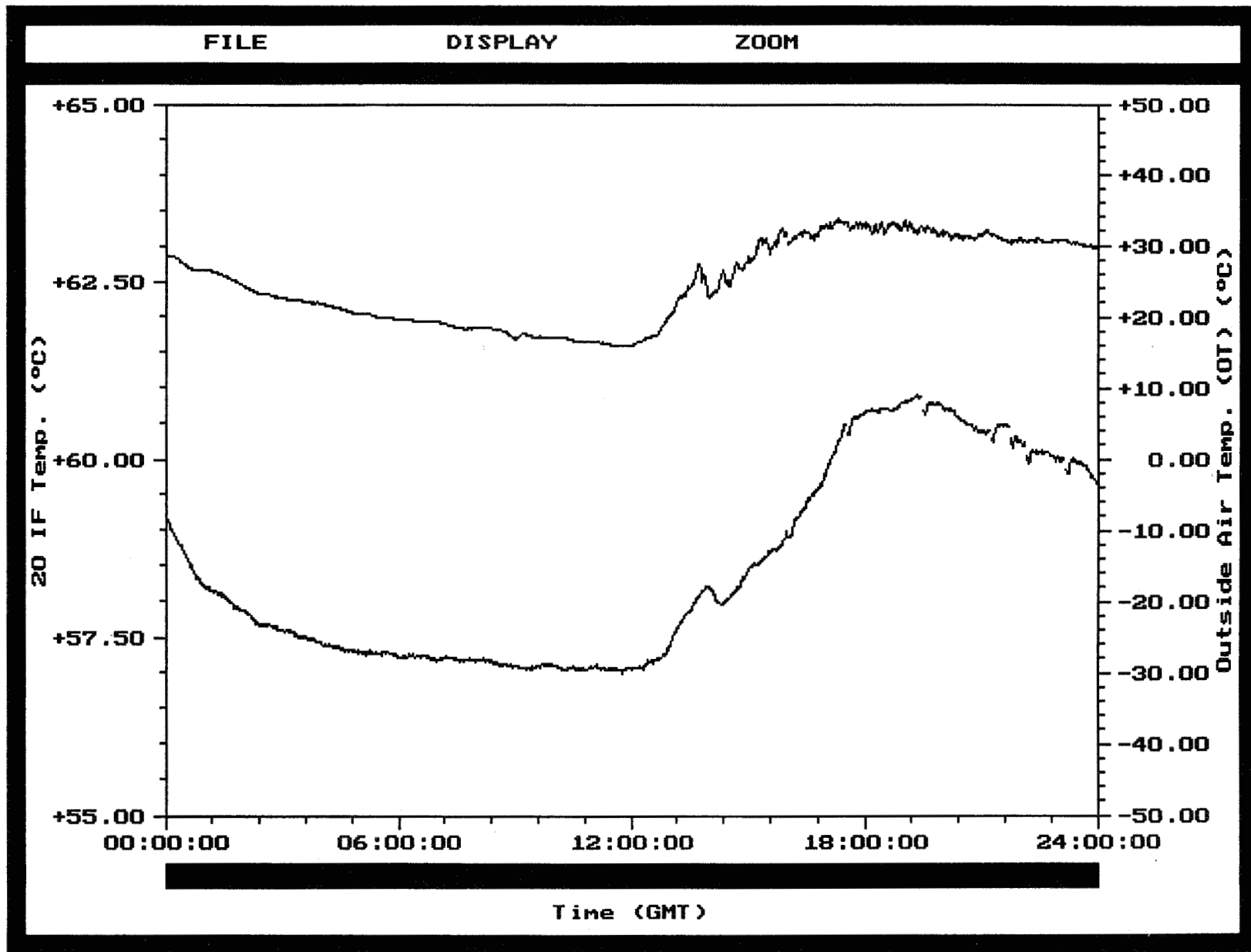
Source: 940611C0.RVD

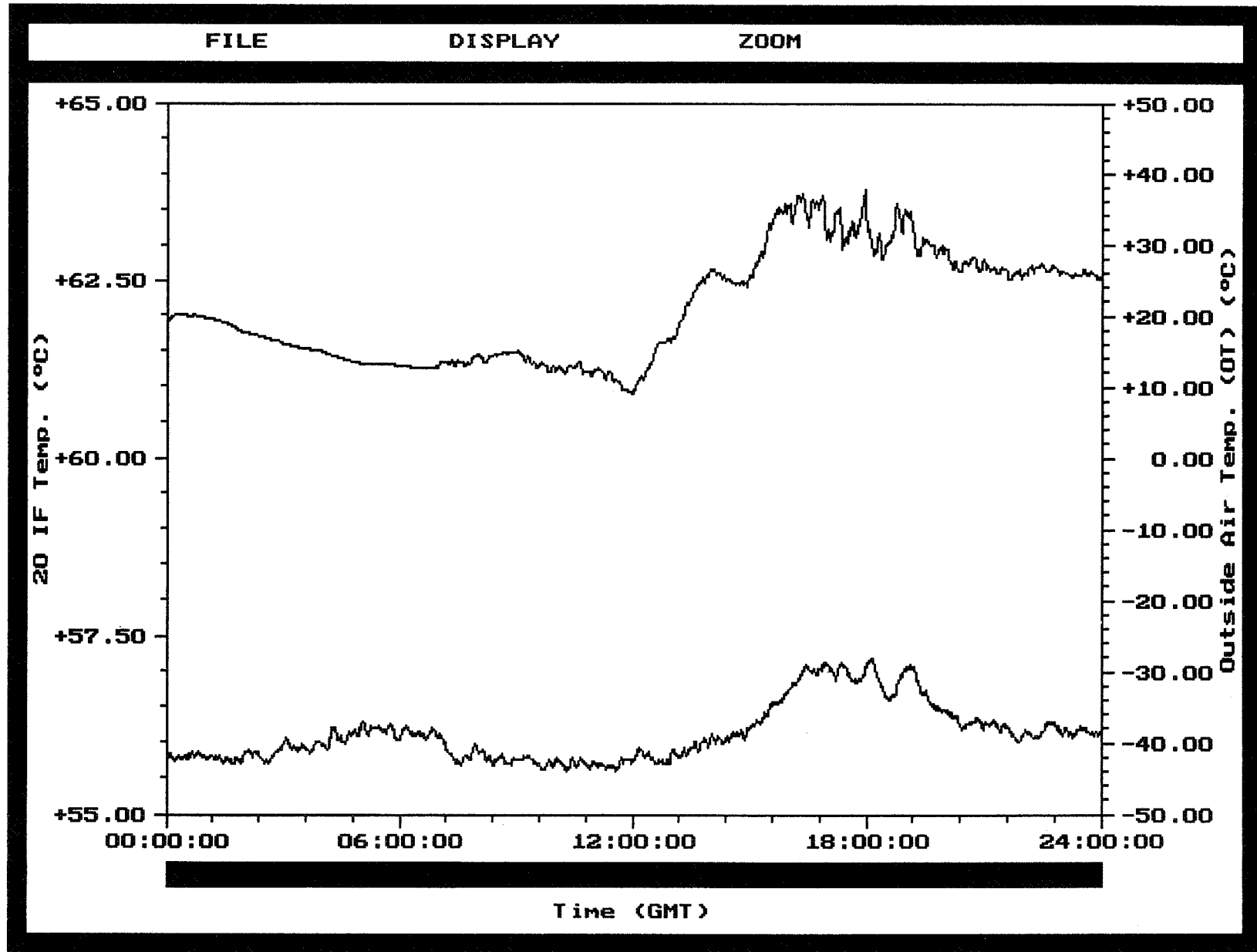
- 20 G Beacon ()
- 27 G Beacon ()
- 20 G Radiometer
- 27 G Radiometer

System Status - XXXXXX

RH: XXX %	CRG: XXXXX mm/hr
BP: XXXX mb	ORG: XXXXX mm/hr
WS: XXXX m/s	TRG: XXXXX mm/hr
WD: XXX °	OT: XXXXXX °C
Time: 01:42:12	Date: 06/15/94

Ready for Spectrum



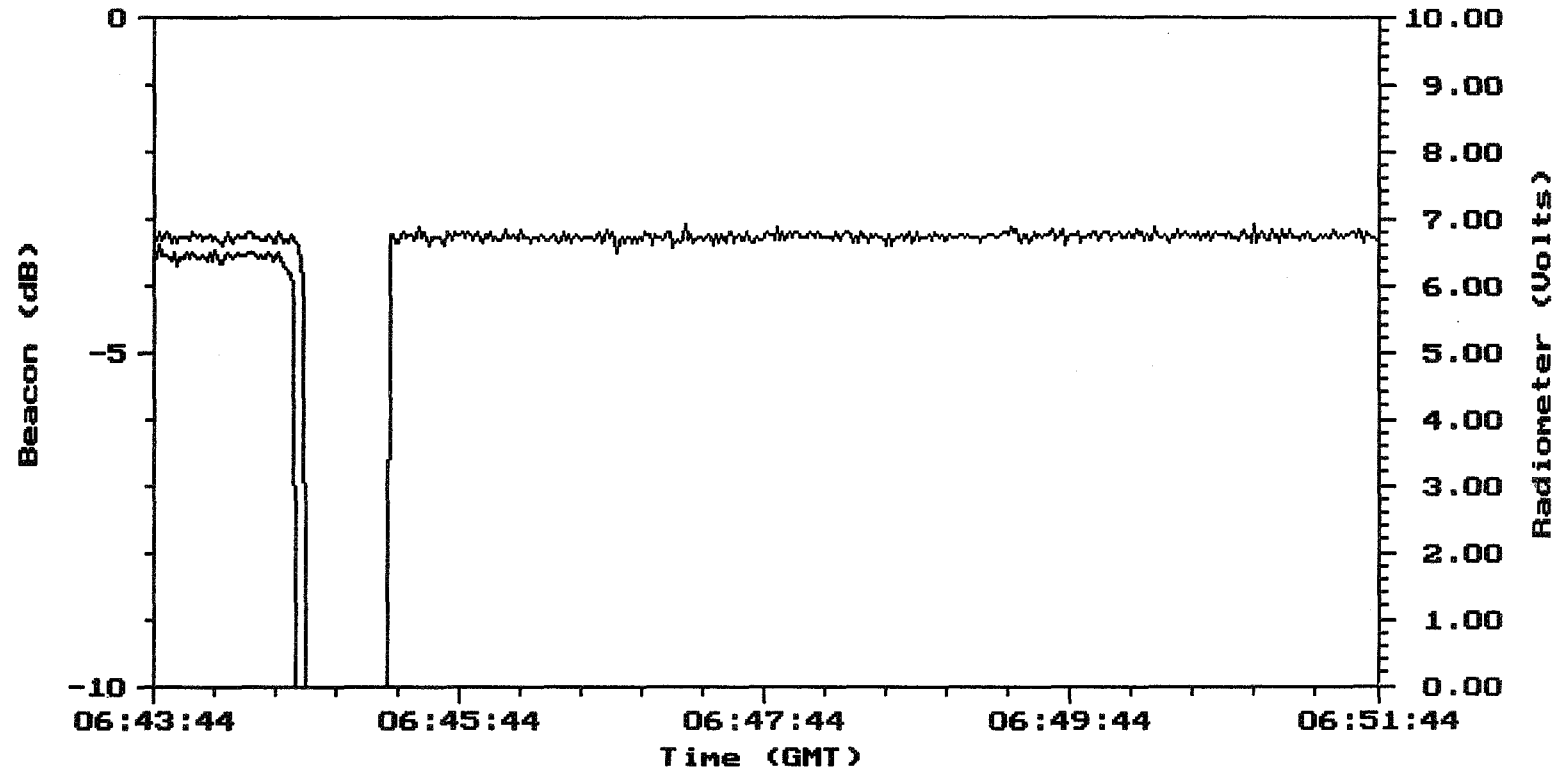


FILE

DISPLAY

ZOOM

PAUSE



Source: 940227co.RU0

- 20 G Beacon ()
- 27 G Beacon ()
- 20 G Radiometer
- 27 G Radiometer

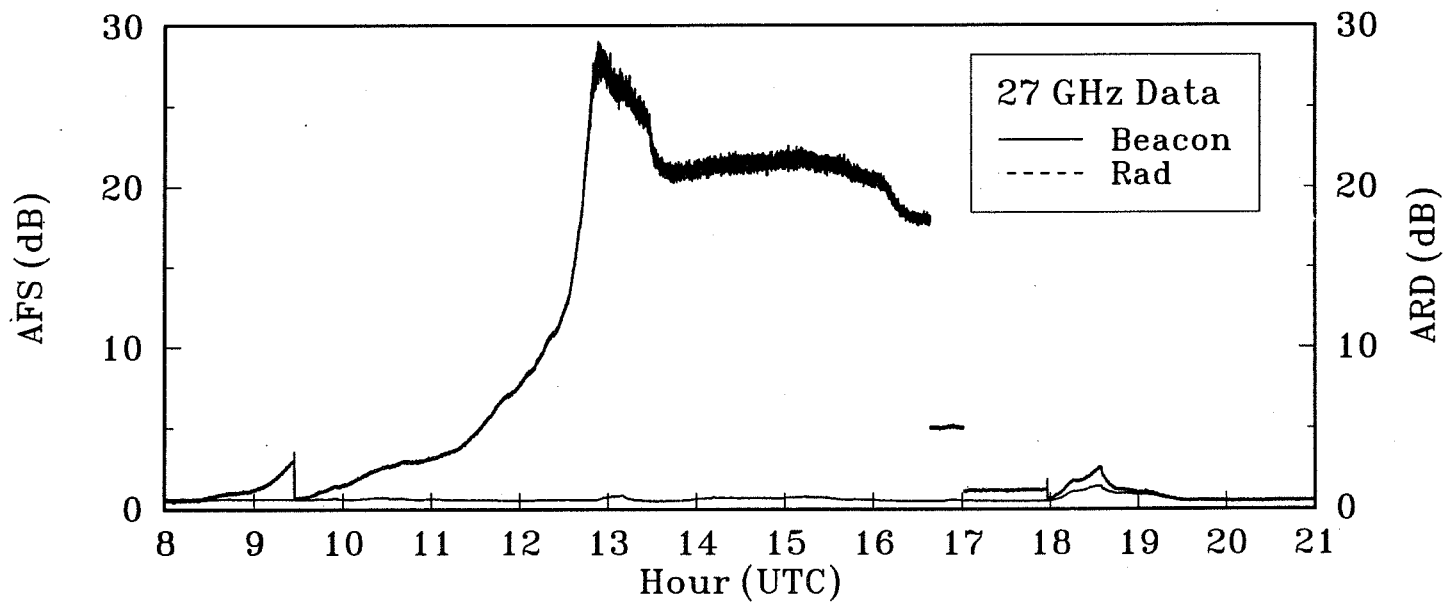
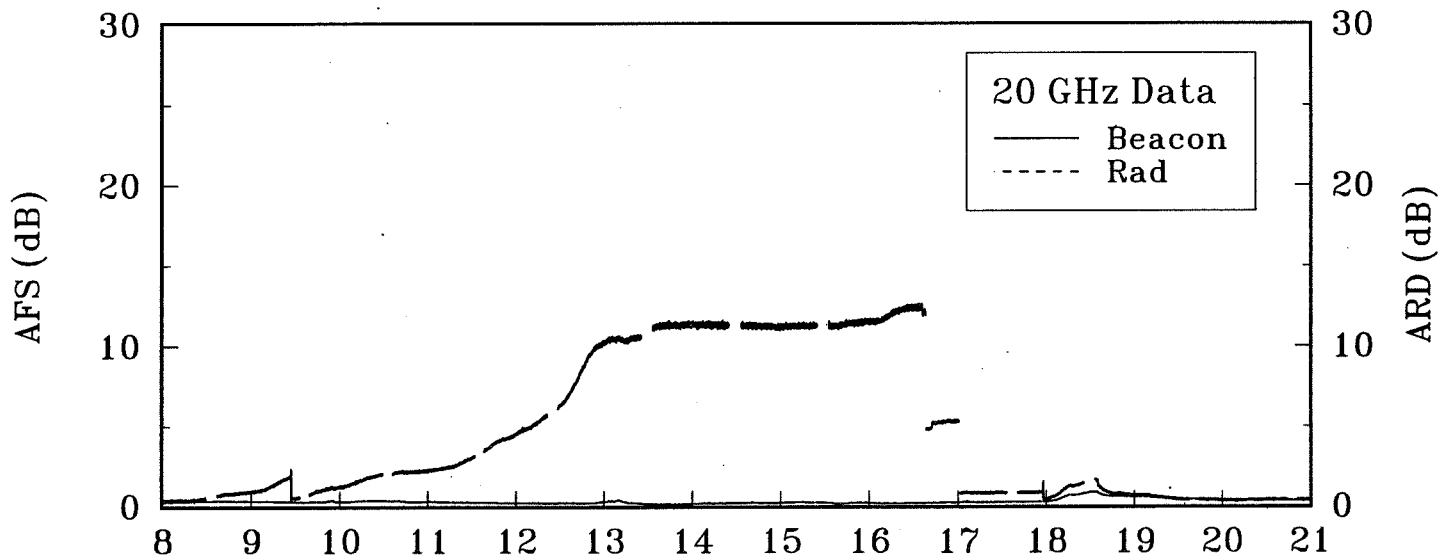
System Status - XXXXXX

RH: XXX % CRG: XXXXX mm/hr
 BP: XXXX mb ORG: XXXXX mm/hr
 WS: XXXX m/s TRG: XXXXX mm/hr
 WD: XXX ° OT: XXXXXX °C
 Time: 10:05:50 Date: 06/14/94

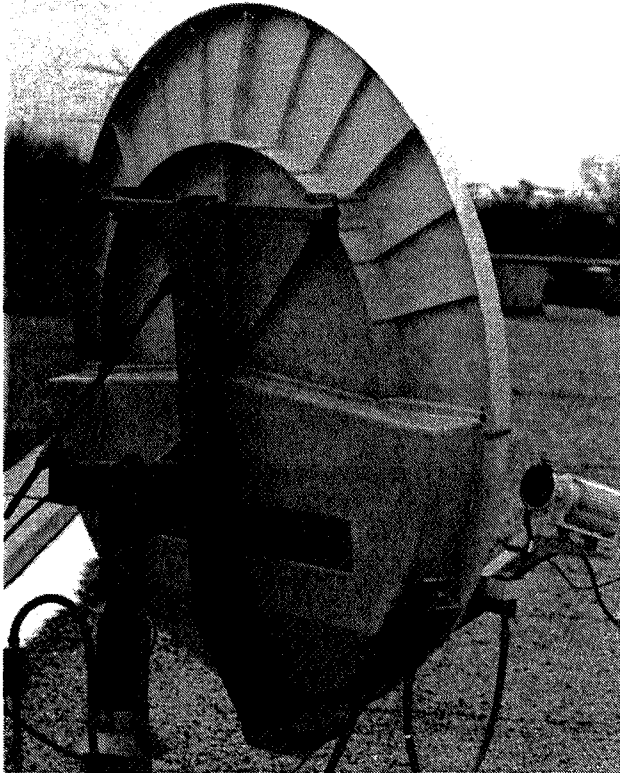
Ready for Spectrum

Snow Accumulation on Antenna Surface

ACTS Propagation Data (C0)



For Prodelin 1.2m, 1.8m
and 2.4m Earth Stations



Model RAD-P18H-1-S-53 mounted on Prodelin 1.8m Reflector

The SoftHeat Radiant Anti-Icing System family comprises models for the Prodelin 1.2m, 1.8m, and 2.4m reflectors. Field installation is simple, making them ideal for either initial installation or subsequent retrofit applications. Through the use of self-regulating heating elements, sufficient thermal power is delivered to the front surface of the antenna for effective anti-icing, while the uniform radiant heat minimizes reflector distortion.

Self-Regulating Performance

The polymer heater element used in SoftHeat Radiant Anti-Icing Systems is self regulating, allowing the thermal power delivered to the antenna to vary depending on the environmental conditions the antenna experiences: as ambient temperature decreases, heat output increases.

Radiant Heating Simplicity

Radiant heat transfer, as applied to antenna anti-icing, provides special benefits due to its inherent uniformity. Furthermore, SoftHeat Radiant systems respond differently to varying heat transfer conditions across the reflector surface, so that no mechanical means are required for even heat distribution. Thus the system has no moving parts other than controller contacts.

Ease of Installation

The SoftHeat Radiant Anti-Icing System is designed for quick and simple installation. It is complete and ready for installation

as shipped, requiring no special structural adaptations or additional framing.

High Thermal Flux

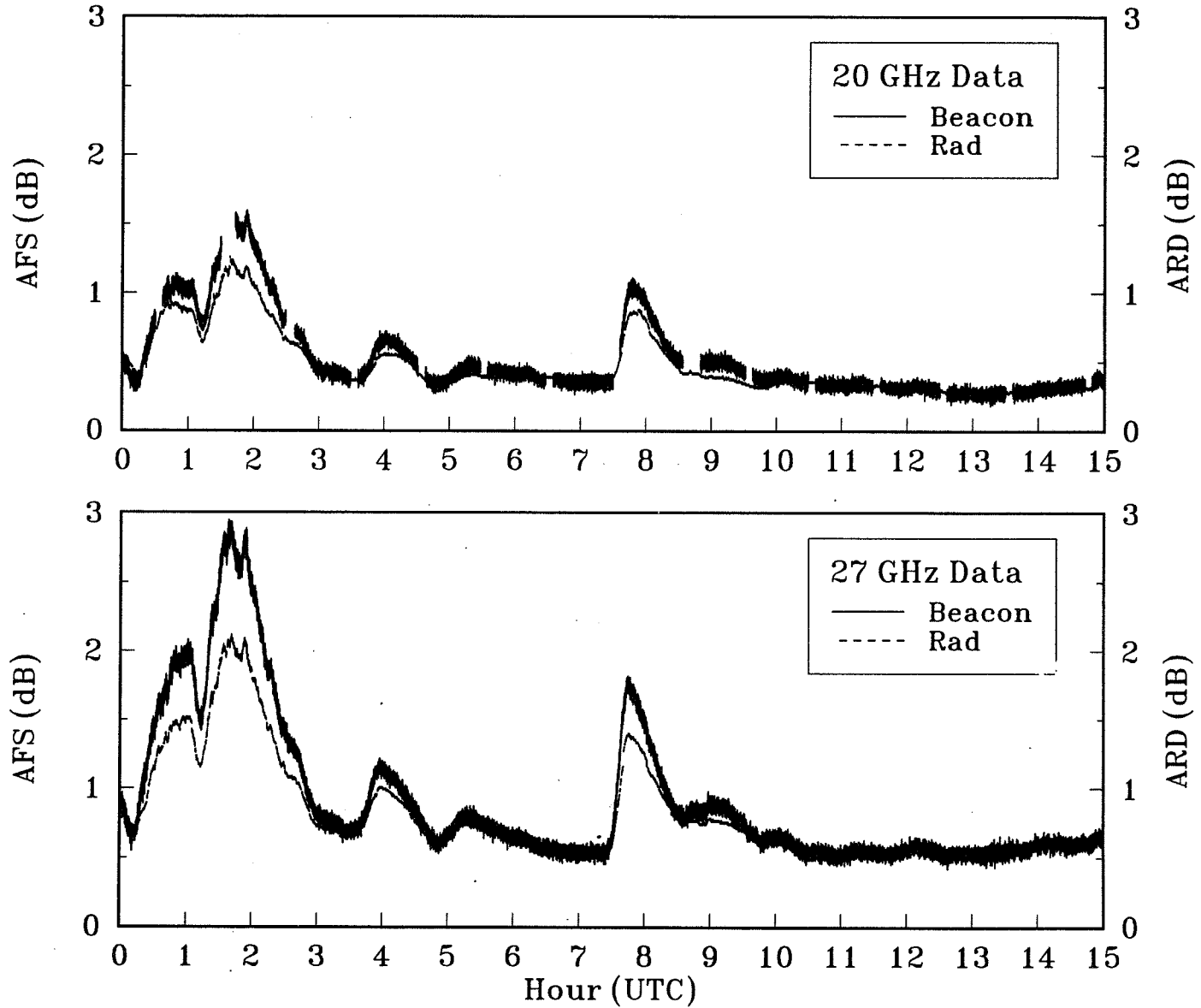
SoftHeat Radiant Anti-Icing Systems provide a high thermal flux, strongly biased **forward**, where snow and ice accumulation can cause severe signal attenuation. SoftHeat/Prodelin systems have demonstrated greater than 85% thermal efficiency toward the front of the antenna.

Features

SoftHeat Radiant Anti-Icing Systems are designed specifically for Prodelin 1.2m, 1.8m, or 2.4m reflectors. All systems operate on 120 volt A.C.; power connection for 1.2m and 1.8m systems uses a simple plug and cord. A feedhorn heating system reduces outages from ice and snow accumulation in the critical feedhorn window. An advanced solid state moisture/temperature sensor reduces energy consumption on 1.8m and 2.4m systems.

Measured Snow Event after De-Icing Unit was Installed

ACTS Propagation Data (CO)



Software Discussion

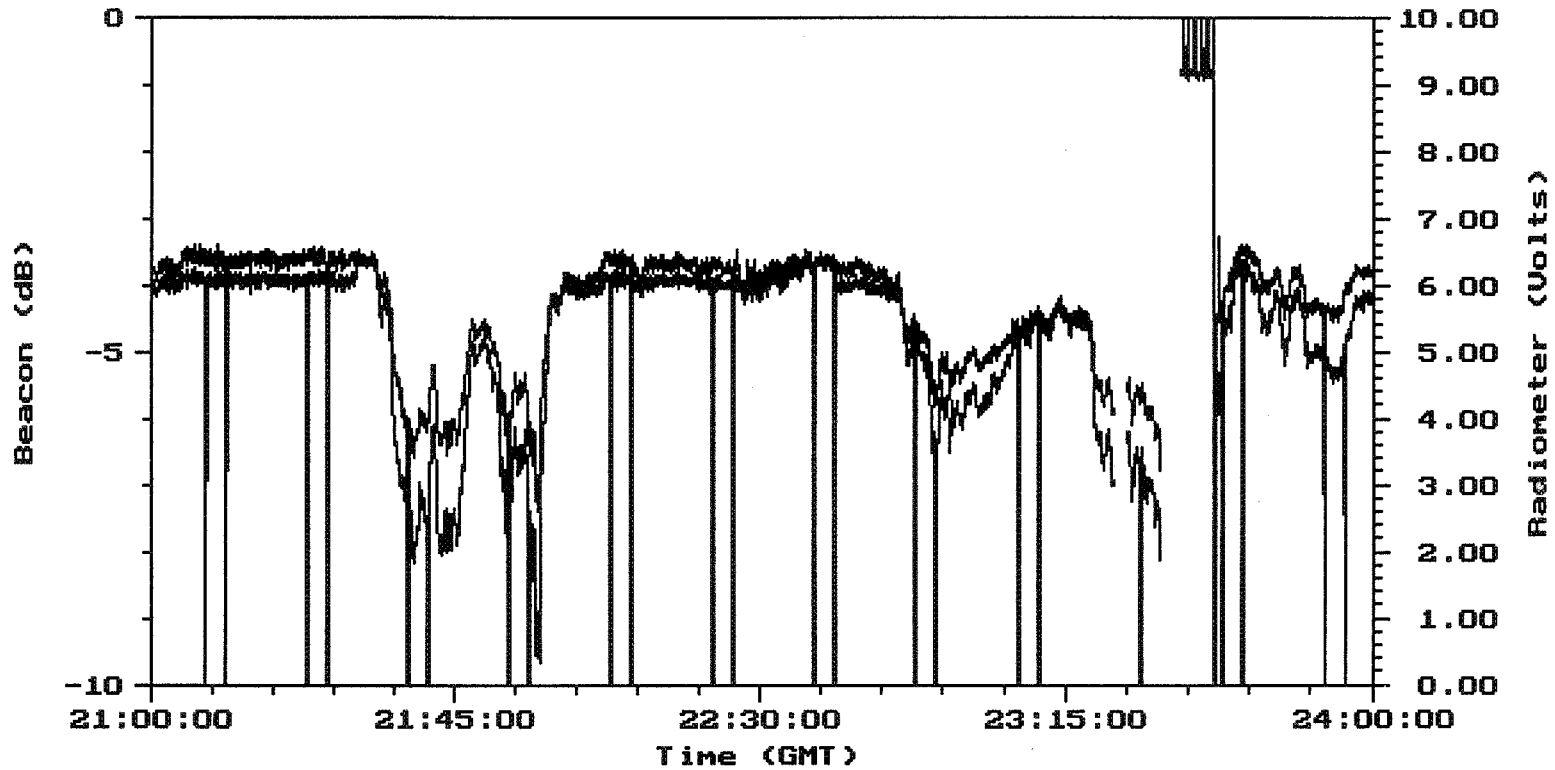
- Shorter set up times
- Level shifts in data after set ups
- Time axis in bias removal

FILE

DISPLAY

ZOOM

PAUSE



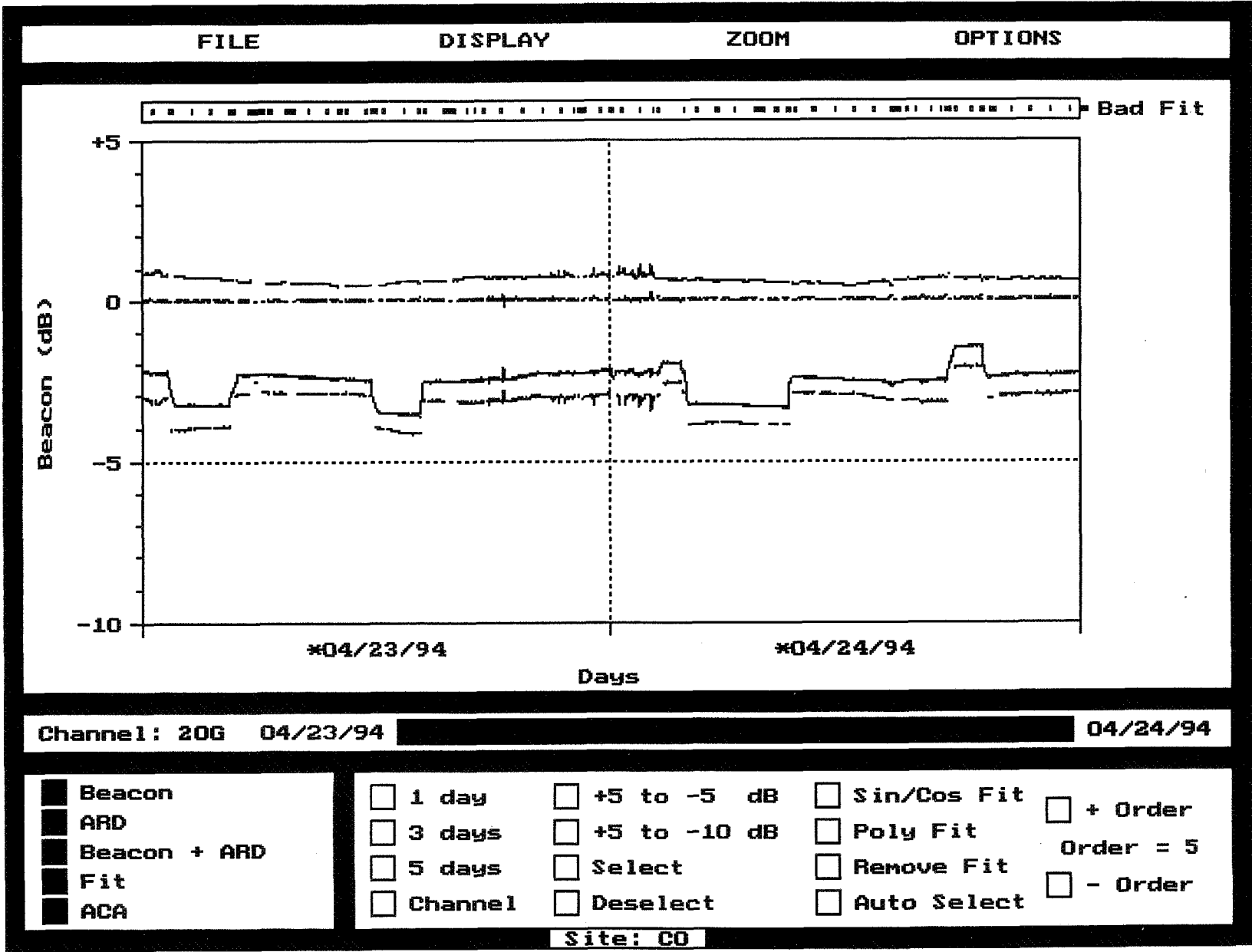
Source: 940513C0.RVD

- 20 G Beacon ()
- 27 G Beacon ()
- 20 G Radiometer
- 27 G Radiometer

System Status - XXXXXX

RH: XXX % CRG: XXXXX mm/hr
 BP: XXXX mb ORG: XXXXX mm/hr
 WS: XXXX m/s TRG: XXXXX mm/hr
 WD: XXX ° OT: XXXXXX °C
 Time: 01:14:34 Date: 06/15/94

Ready for
Spectrum

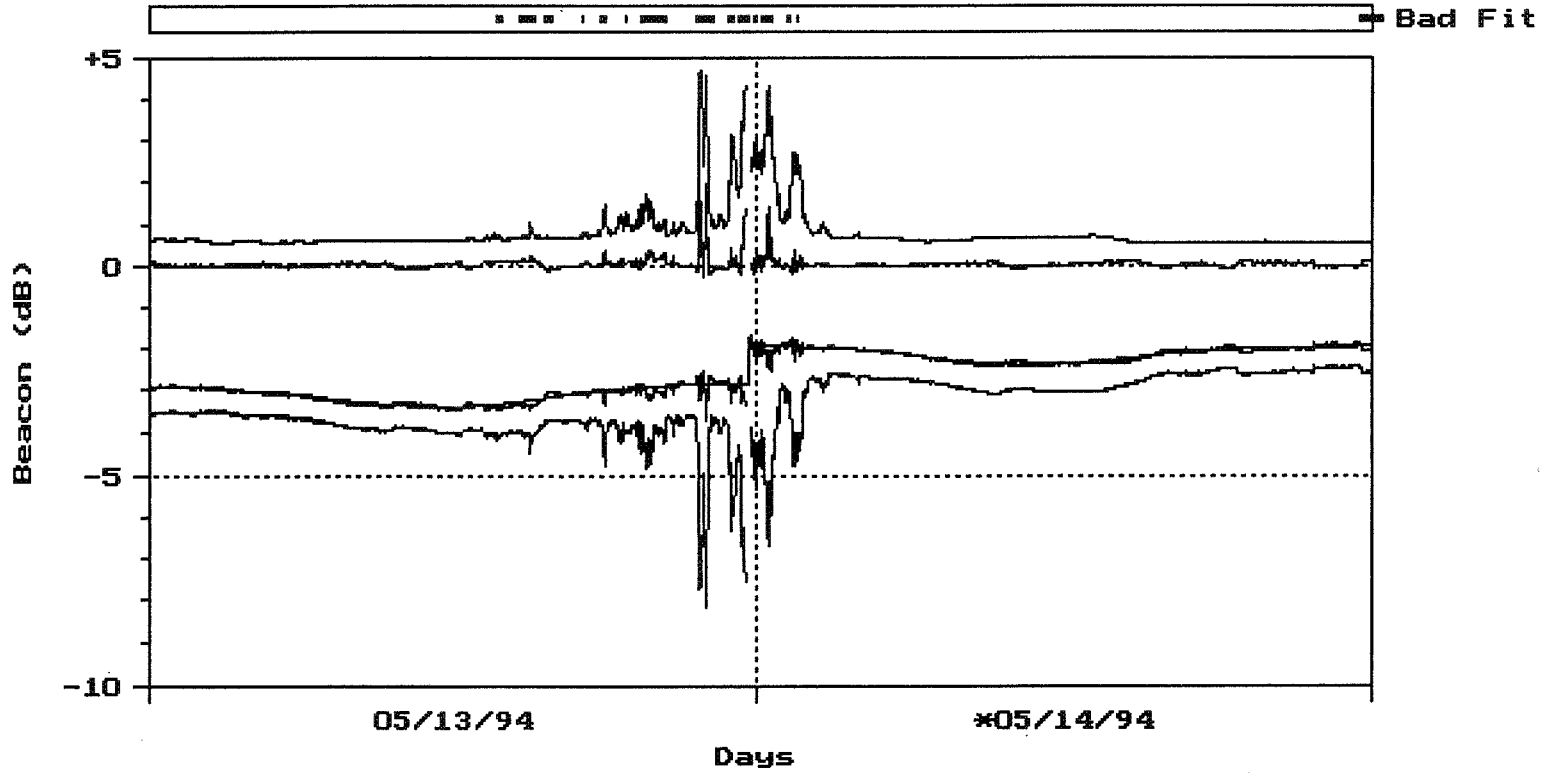


FILE

DISPLAY

ZOOM

OPTIONS



Channel: 27G 05/13/94

05/14/94

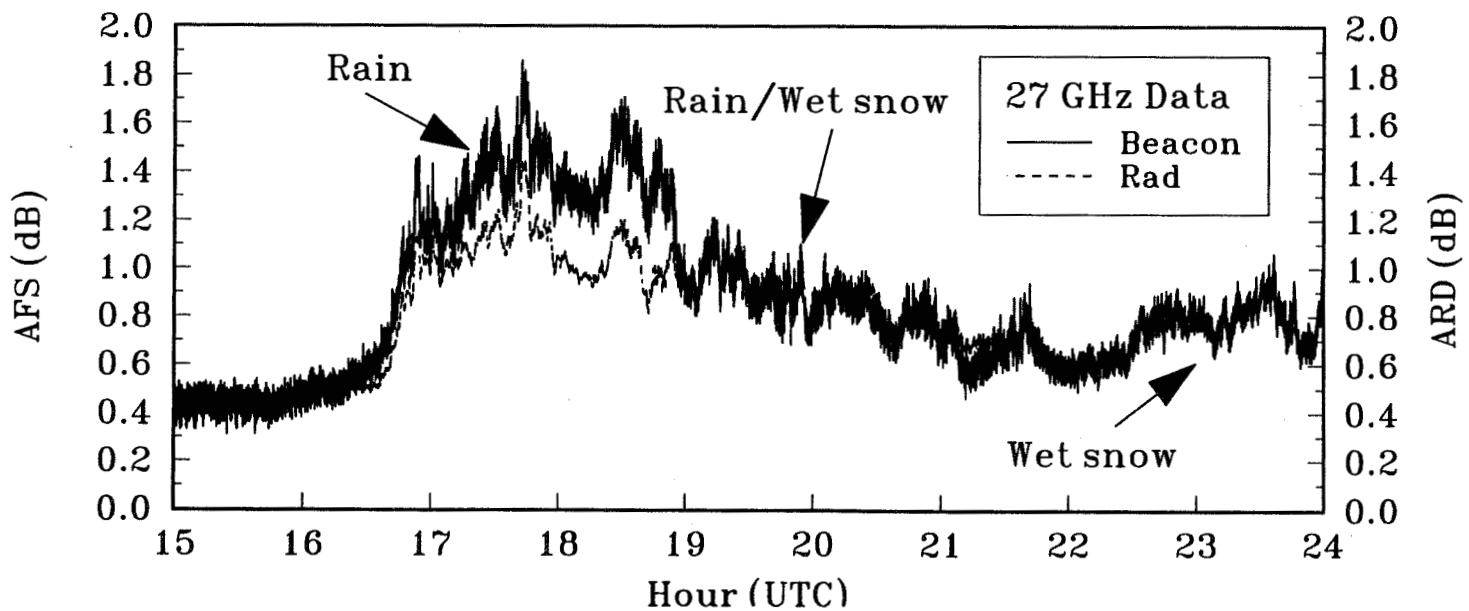
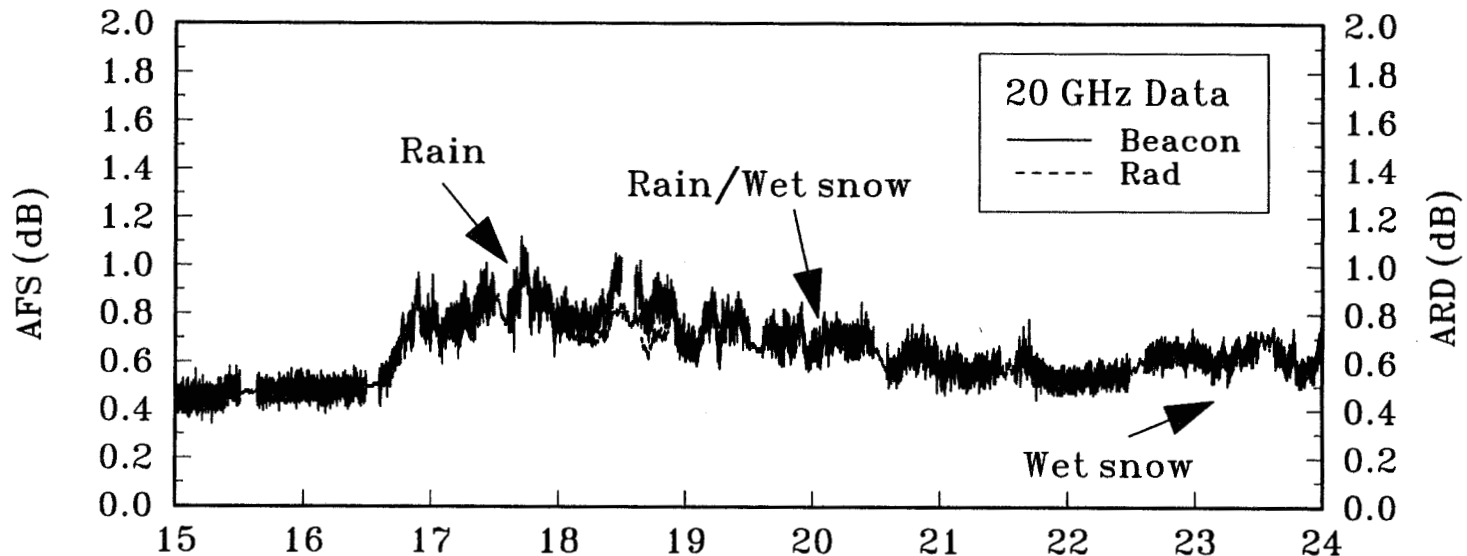
- Beacon
- ARD
- Beacon + ARD
- Fit
- ACA

- 1 day
- 3 days
- 5 days
- Channel
- +5 to -5 dB
- +5 to -10 dB
- Select
- Deselect
- Sin/Cos Fit
- Poly Fit
- Remove Fit
- Auto Select
- + Order
- Order = 5
- Order

Site: CO

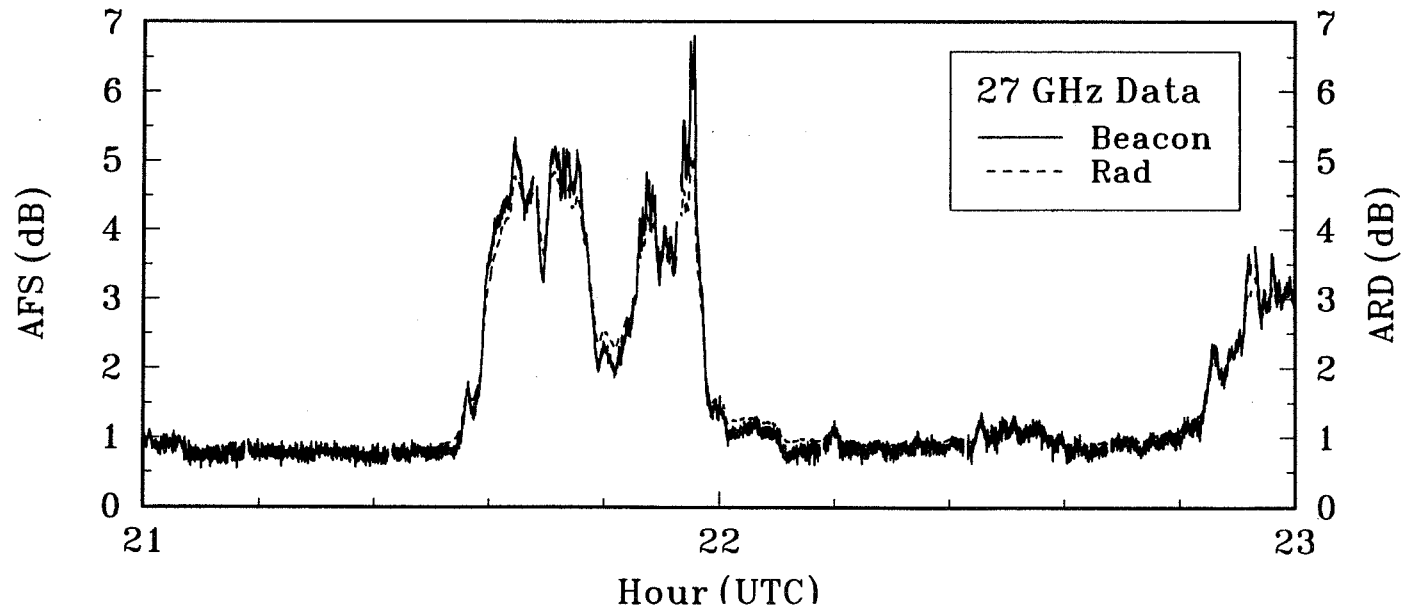
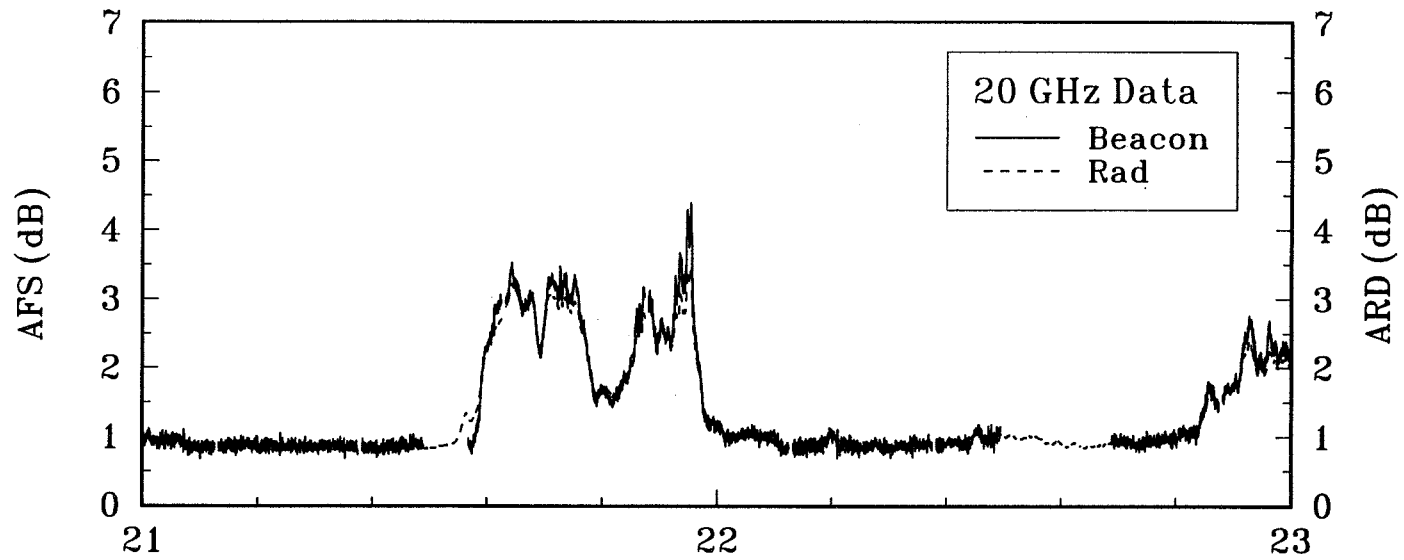
Rain / Wet Snow Event

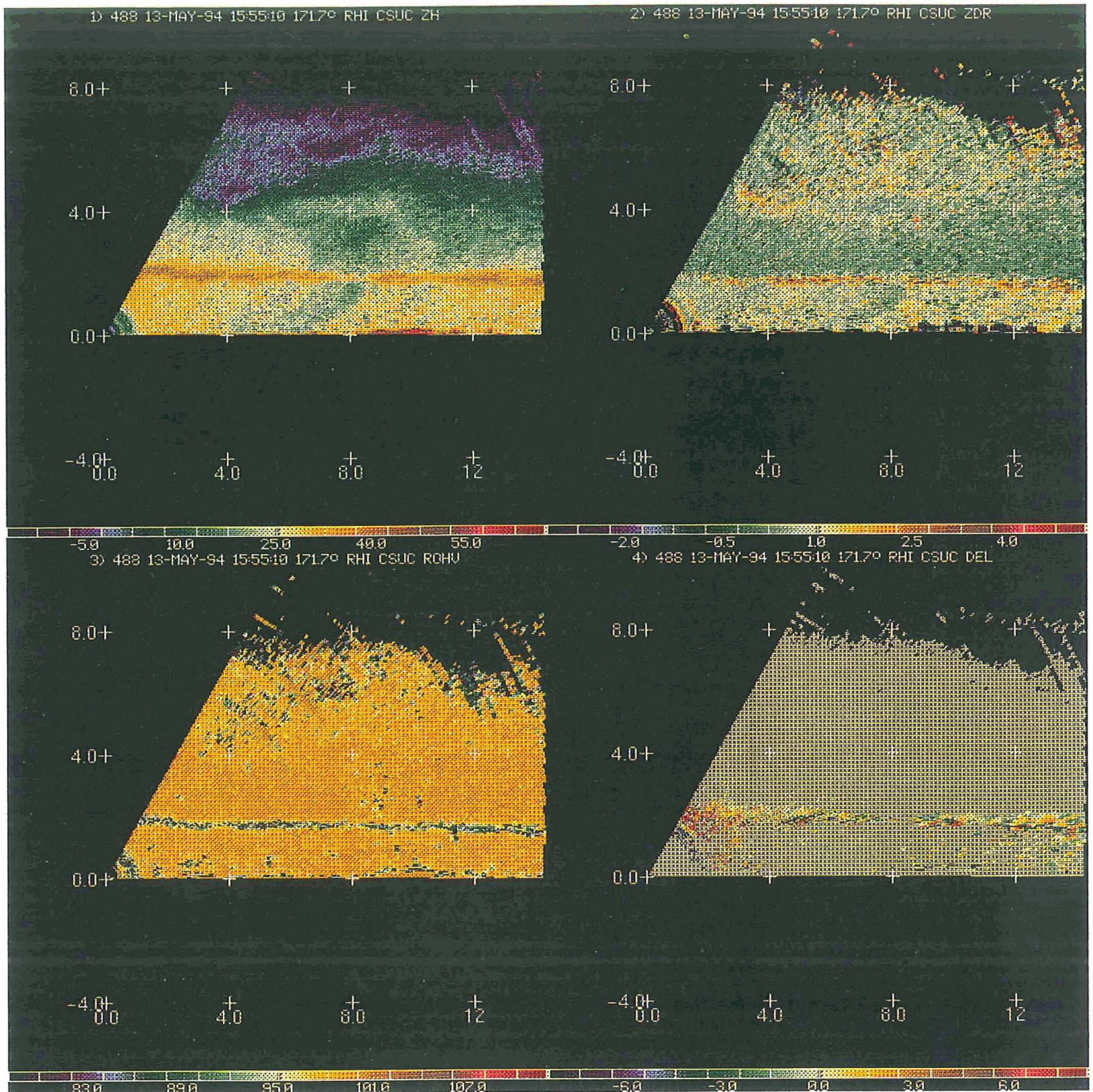
4/9/94 ACTS Propagation Data (C0)



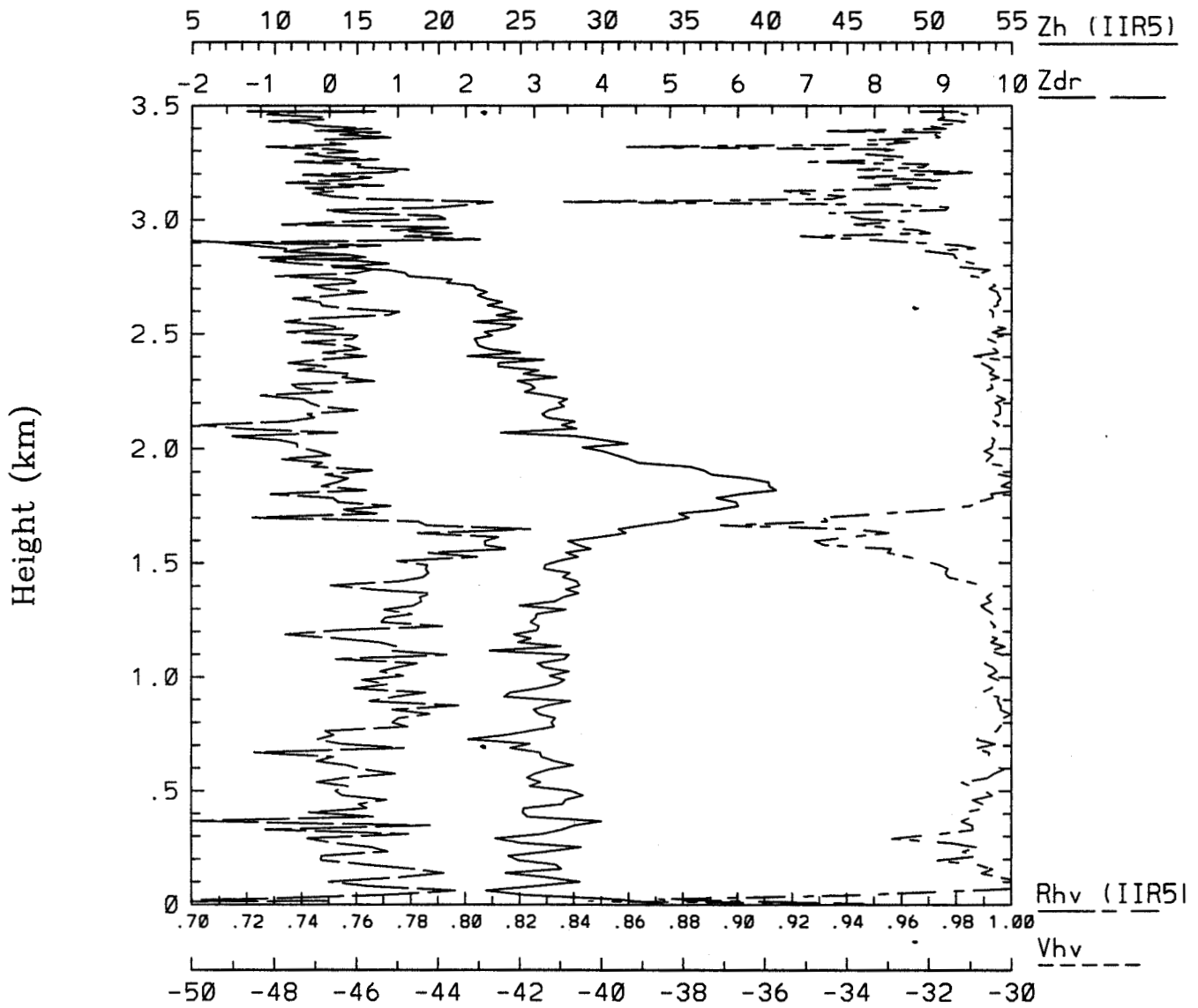
ACTS/CSU CHILL Data (Bright Band Case)

5/13/94 ACTS Propagation Data (CO)





Date: 51394 Time: 155540 Azim: 173.69
 Start RAY#: 484, total: 225 rays from 4. to 4. km CSU-CHILL



Phidp.T= 3.deg
 Dfr.T = 0.dB
 Ldr.T = 0.dB

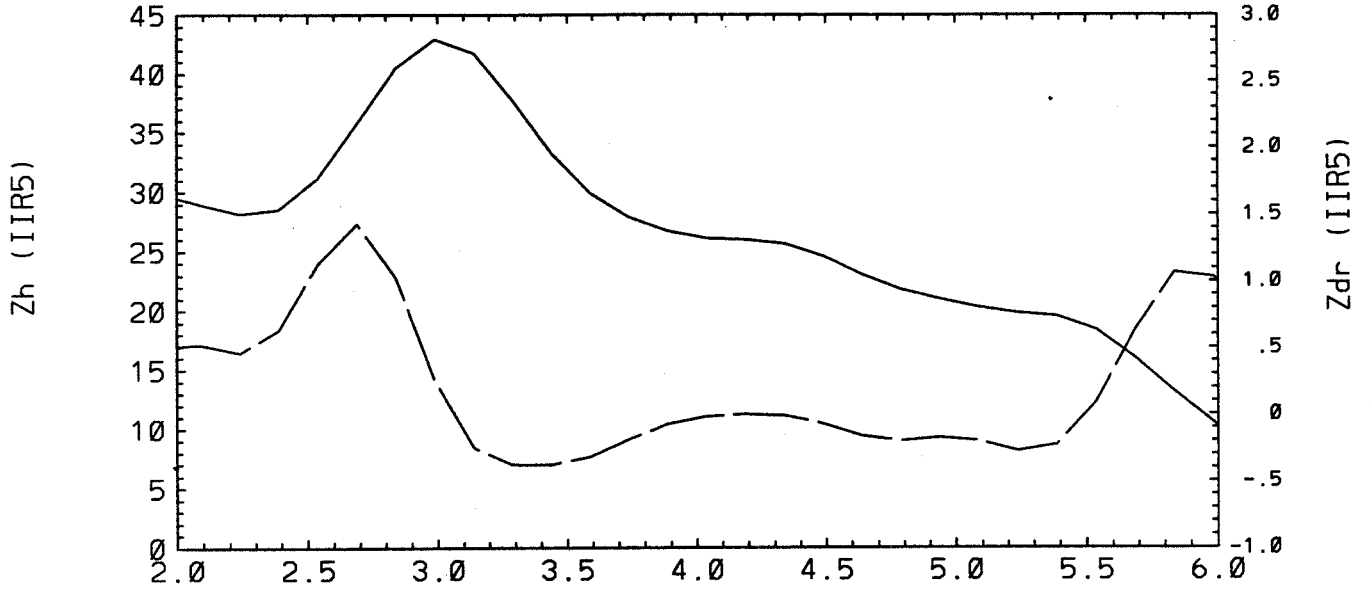
Ro.T= 0.80
 Zh.T= 40.dB

Zslope= 40.dB
 Madflt = 2

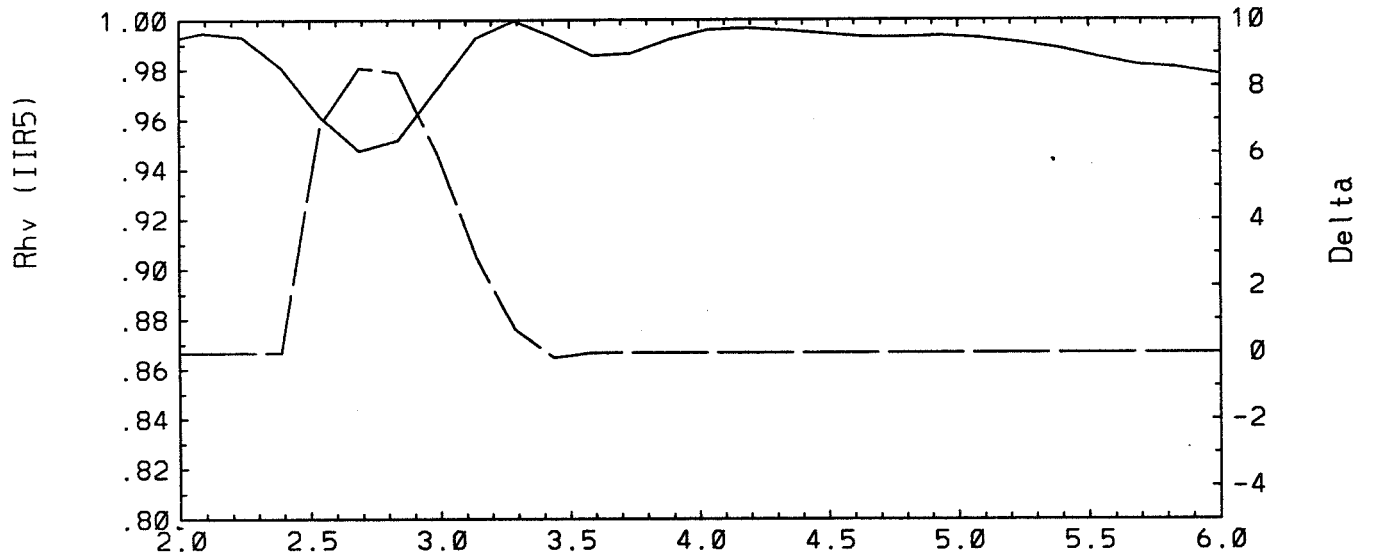
RCcf= 0.00dB
 DfrC= 0.00dB

may1394v117

Date: 51394 Time: 155518 AZ: 171.97 to 171.97 EL: 43.50 to 43.50



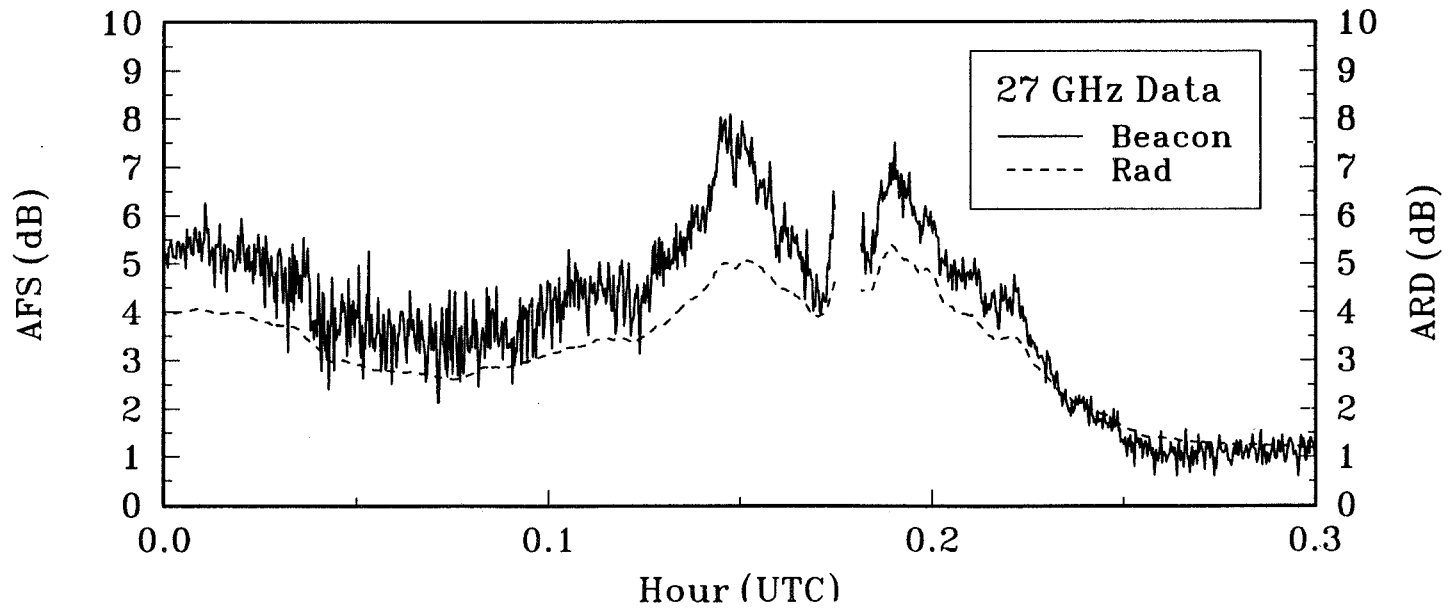
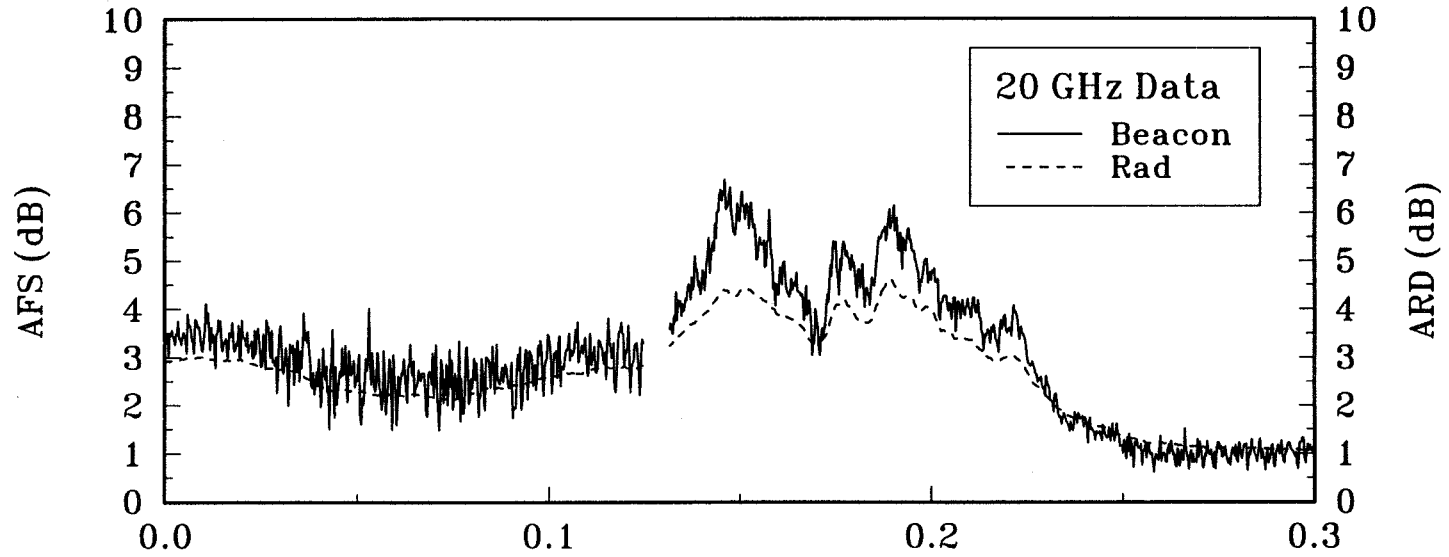
RAY NO. = 548 CSU-CHILL Range (km)

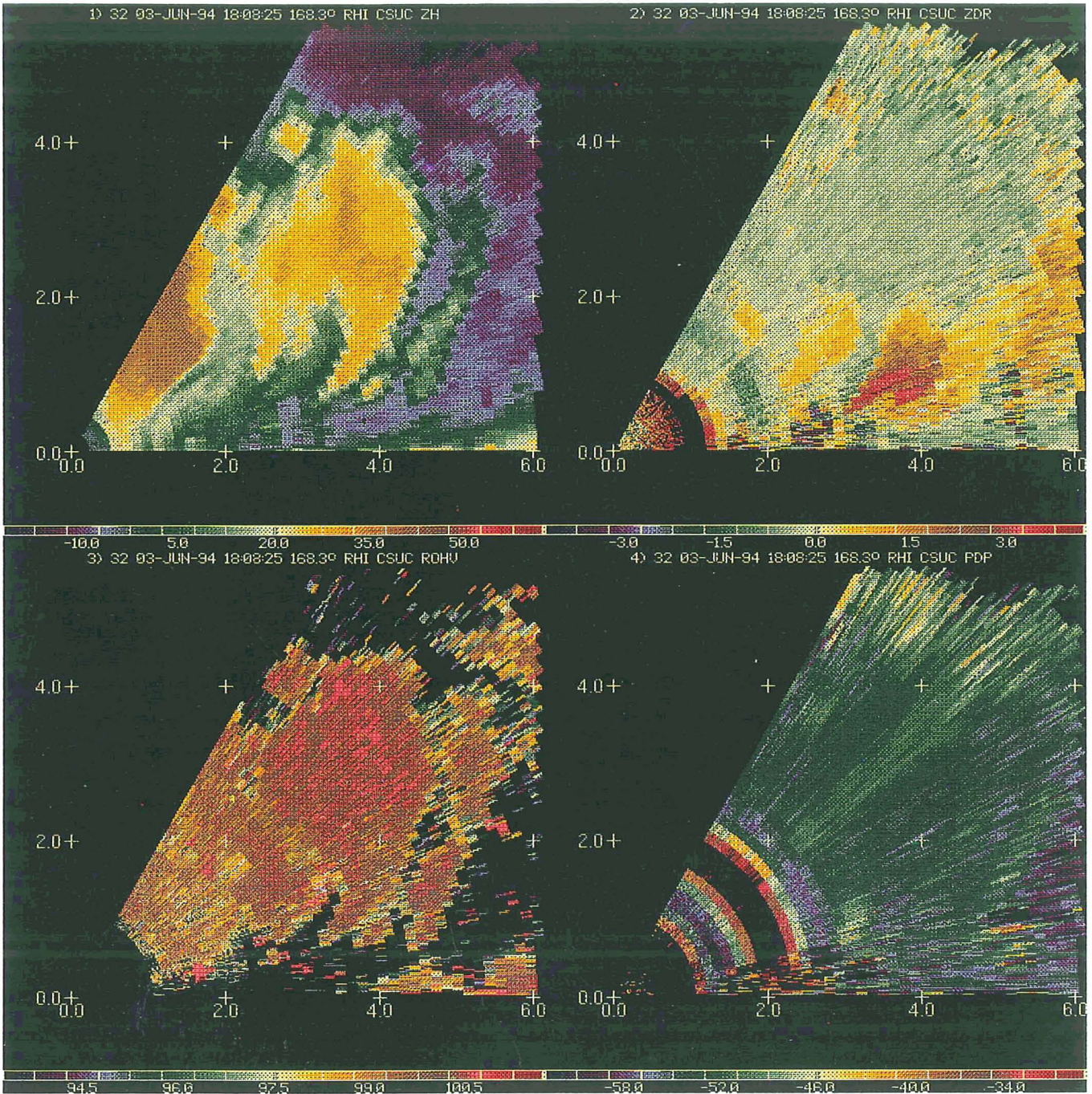


Phidp.T= 3.deg Ro.T= 0.80 Zslope= 40.dB RCcf= 0.00dB may1394v117
 Dfr.T = 0.dB Zh.T= 40.dB Madfit = 2 DfrC= 0.00dB

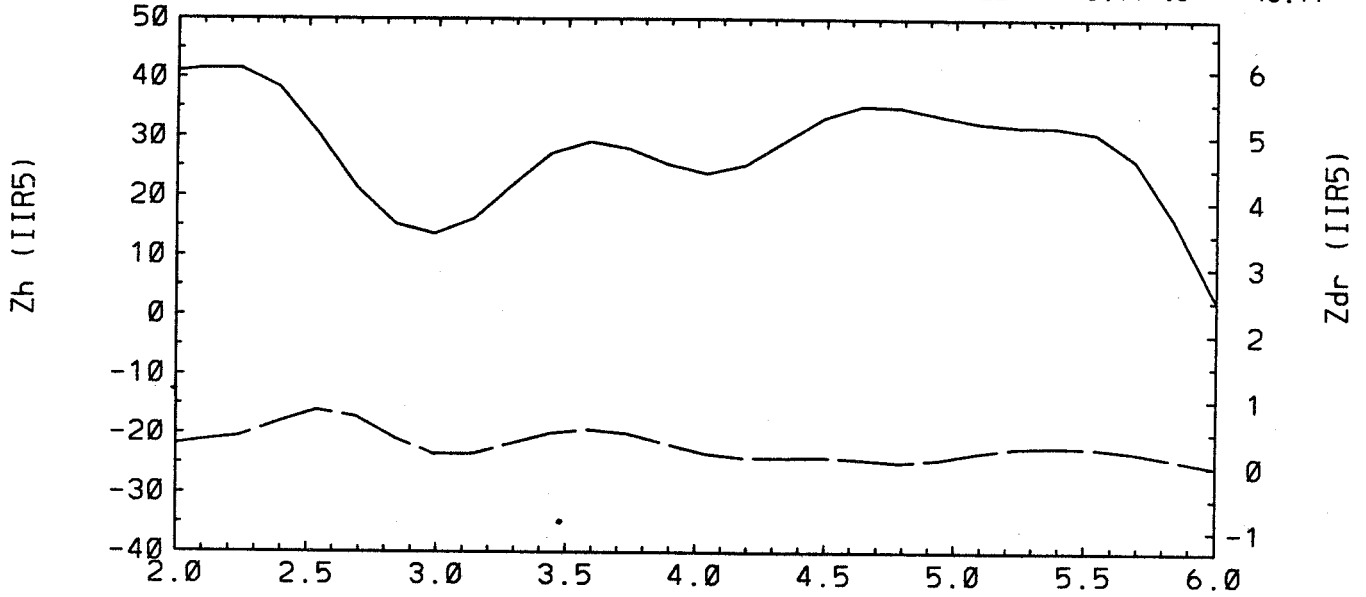
ACTS/CSU CHILL Data (Convective Case)

6/3/94 ACTS Propagation Data (C0)



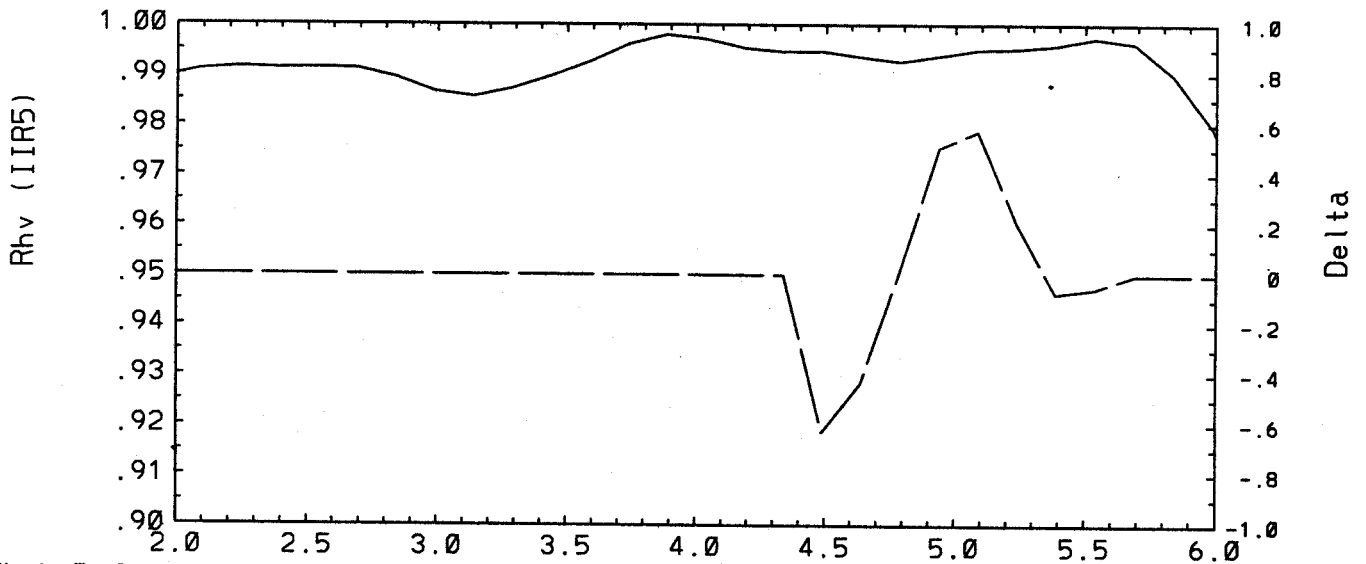


Date: 60394 Time: 180714 AZ: 171.98 to 171.98 EL: 43.11 to 43.11



RAY NO. = 681

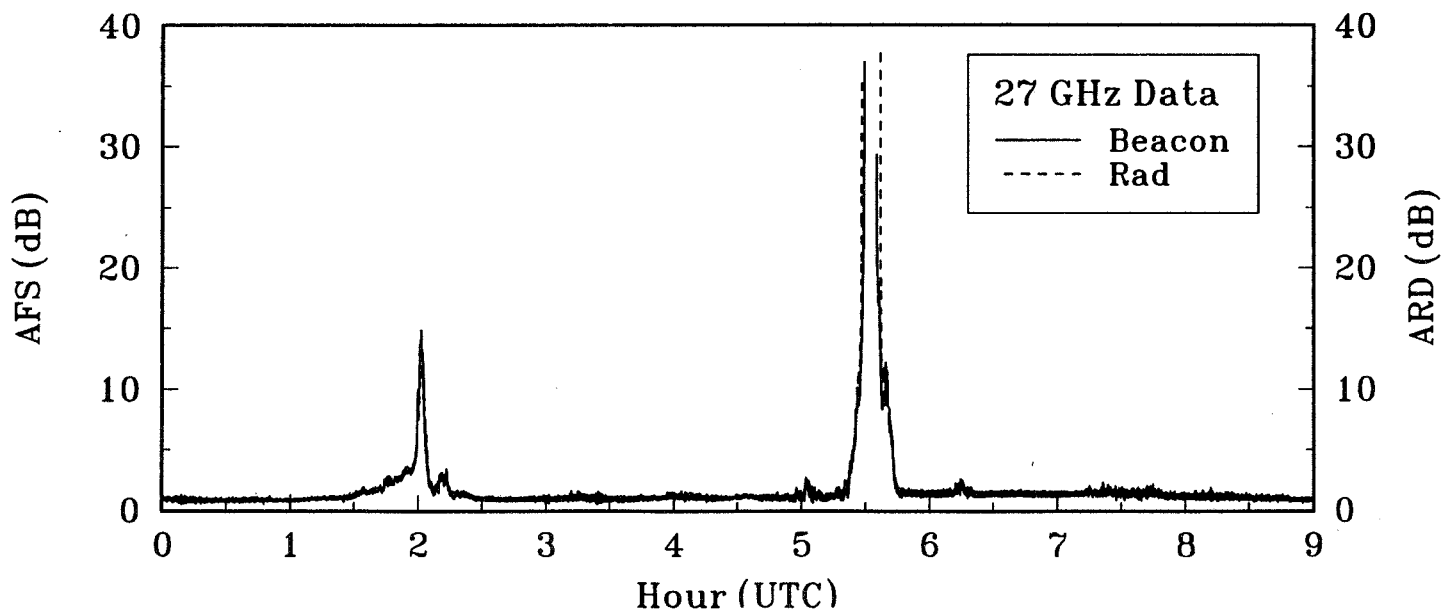
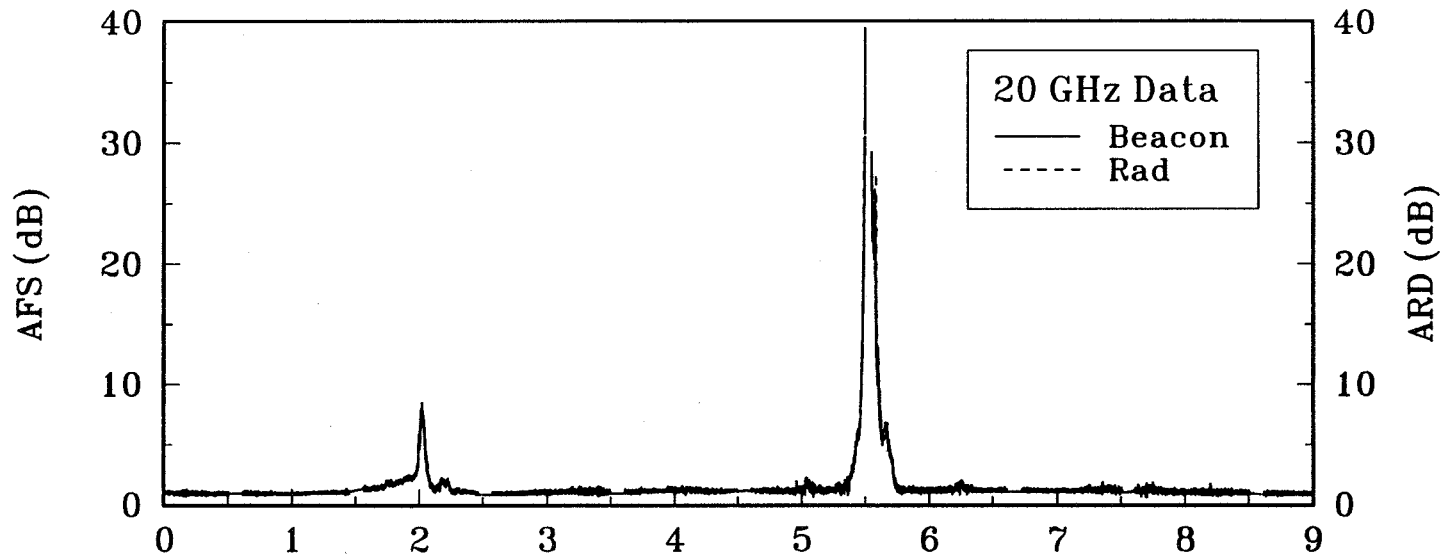
CSU-CHILL Range (km)



Phidp.T= 3.deg Ro.T= 0.80 Zslope= 40.dB RCcf= 0.00dB jun0294.v129
 Dfr.T = 0.dB Zh.T= 40.dB Madflt = 2 DfrC= 0.00dB

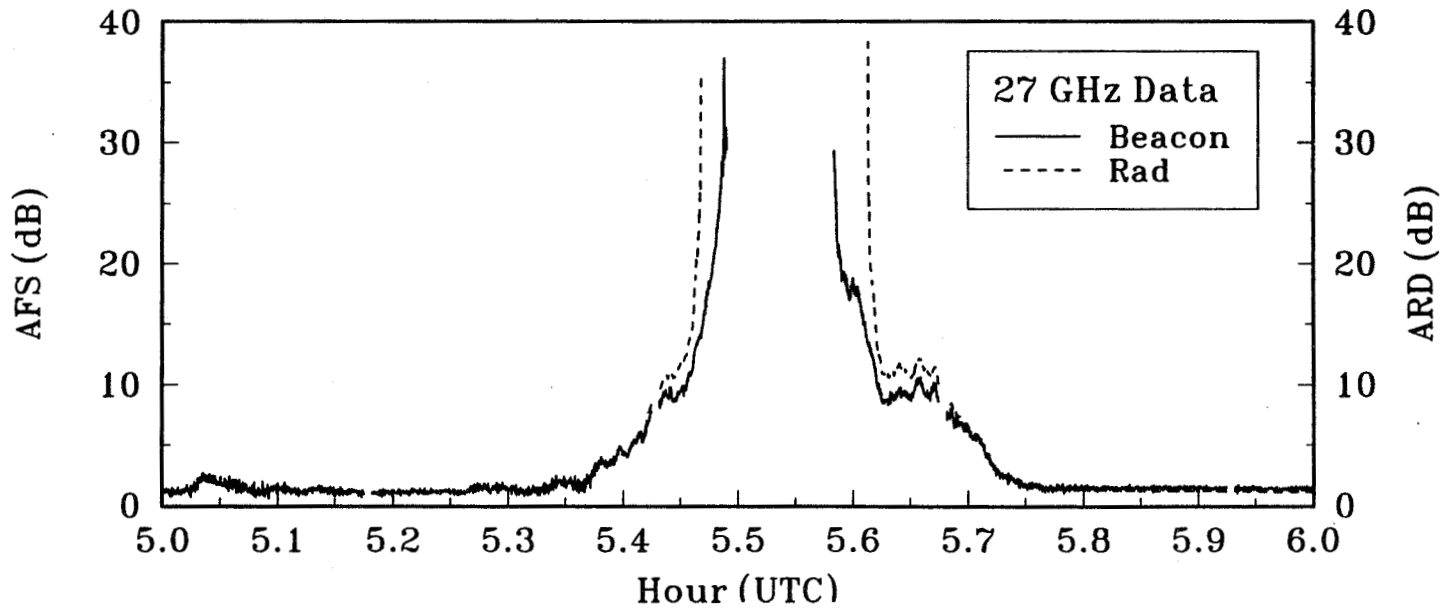
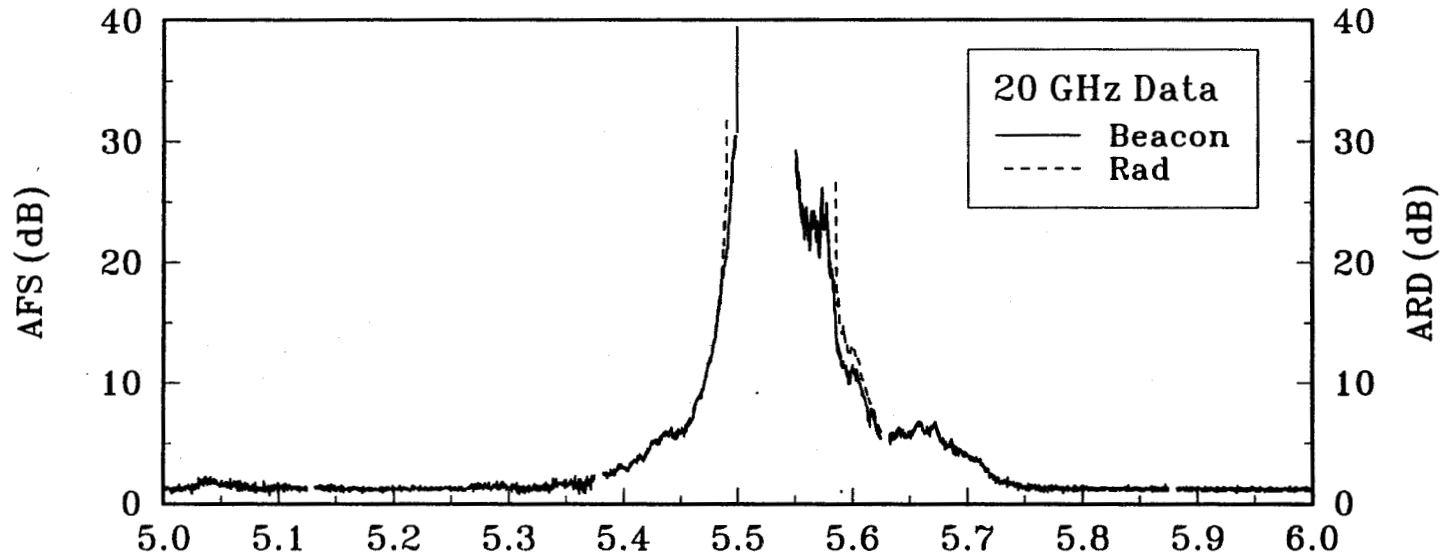
Loss of Both Signals due to Rain Event

6/1/94 ACTS Propagation Data (CO)

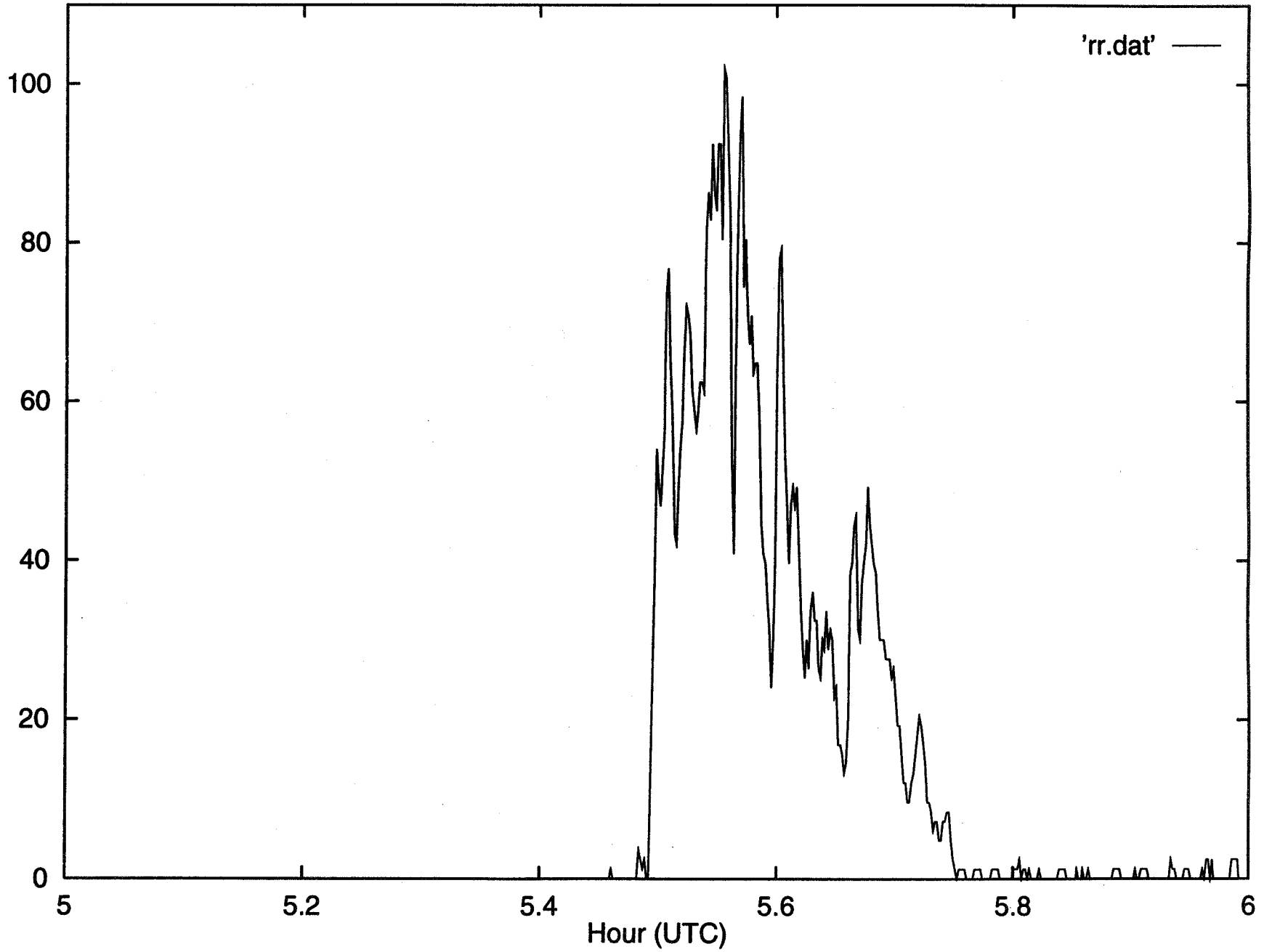


Loss of Both Signals due to Rain Event

6/1/94 ACTS Propagation Data (CO)



Rain Rates for 6/1/94 data



377
D.D.

Propagation Models

- Mueller Propagation Model (Wayne Adams, NCAR)
 - The variation of the electric field along the propagation path is given by

$$\frac{dE_v}{ds} = (ik + M_{vv})E_v + M_{vh}E_h$$

$$\frac{dE_h}{ds} = M_{hv}E_v + (ik + M_{hh})E_h$$

where

$$M_{ij} = \sum_p n_p \frac{2\pi i}{k} f_{ij}(\hat{k})$$

- f_{ij} are the forward scattering amplitudes
- n_p is the number concentration

Propagation Models

- The equations for the variation of the electric field along the propagation path can be used to obtain differential equations in terms of the modified Stokes parameters

$$\frac{dI_v}{ds} = 2\text{Re}(M_{vv})I_v + \text{Re}(M_{vh})U + \text{Im}(M_{vh})V$$

$$\frac{dI_h}{ds} = 2\text{Re}(M_{hh})I_h + \text{Re}(M_{hv})U - \text{Im}(M_{hv})V$$

$$\begin{aligned} \frac{dU}{ds} = & 2\text{Re}(M_{hv})I_v + 2\text{Re}(M_{vh})I_h + [\text{Re}(M_{vv}) \\ & + \text{Re}(M_{hh})]U - [\text{Im}(M_{vv}) - \text{Im}(M_{hh})]V \end{aligned}$$

$$\begin{aligned} \frac{dV}{ds} = & -2\text{Im}(M_{hv})I_v + 2\text{Im}(M_{vh})I_h + [\text{Im}(M_{vv}) \\ & - \text{Im}(M_{hh})]U + [\text{Re}(M_{vv}) + \text{Re}(M_{hh})]V \end{aligned}$$

where

$$I_v = \frac{|E_v|^2}{\eta}$$

$$I_h = \frac{|E_h|^2}{\eta}$$

$$U = \frac{2\text{Re}(E_v E_h^*)}{\eta}$$

$$V = \frac{2\text{Im}(E_v E_h^*)}{\eta}$$

Propagation Models

- Solutions of the four differential equations yield four eigenvalues and eigenvectors

$$\beta(\hat{s}) = \begin{bmatrix} \beta_1(\theta, \phi) \\ \beta_2(\theta, \phi) \\ \beta_3(\theta, \phi) \\ \beta_4(\theta, \phi) \end{bmatrix} = \begin{bmatrix} 2ImK_1 \\ iK_2^* - iK_1 \\ iK_1^* - iK_2 \\ 2ImK_2 \end{bmatrix}$$

where

$$\begin{aligned} K_1 &= k - \frac{i}{2} [M_{vv} + M_{hh} + r] \\ K_2 &= k - \frac{i}{2} [M_{vv} + M_{hh} - r] \end{aligned}$$

and

$$r = \left[(M_{vv} - M_{hh})^2 + 4M_{hv}M_{vh} \right]^{\frac{1}{2}}$$

Propagation Models

The eigenmatrix is given by

$$\mathbf{H} = \begin{bmatrix} 1 & |b_2|^2 & b_2 & b_2^* \\ |b_1|^2 & 1 & b_1^* & b_1 \\ 2\text{Re}(b_1) & 2\text{Re}(b_2) & 1 + b_1^*b_2 & 1 + b_1b_2^* \\ -2\text{Im}(b_1) & 2\text{Im}(b_2) & i(1 - b_1^*b_2) & -i(1 - b_1b_2^*) \end{bmatrix}$$

where

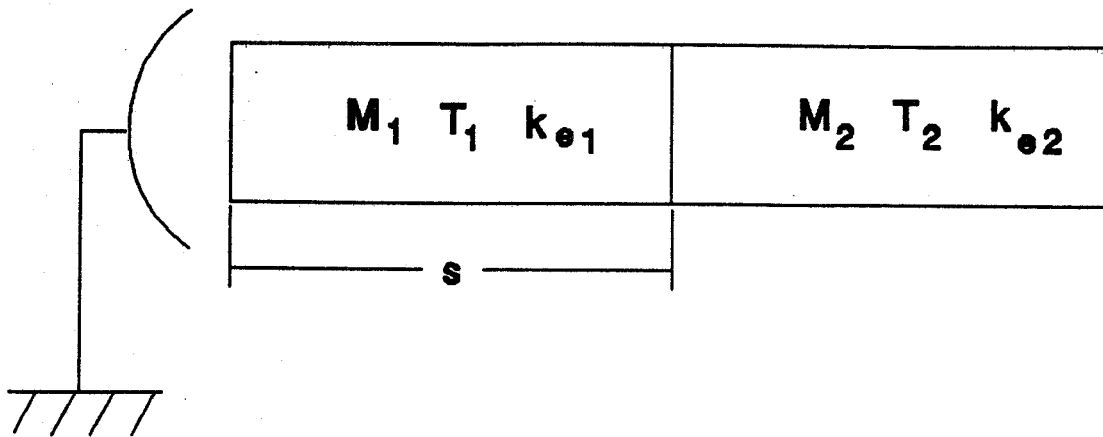
$$b_1 = \frac{2M_{hv}}{M_{vv} - M_{hh} + r}$$

$$b_2 = \frac{2M_{vh}}{-M_{vv} + M_{hh} + r}$$

The extinction matrix is defined as

$$\kappa_e = \begin{bmatrix} -2\text{Re}(M_{vv}) & 0 \\ 0 & -2\text{Re}(M_{hh}) \\ -2\text{Re}(M_{hv}) & -2\text{Re}(M_{vh}) \\ 2\text{Im}(M_{hv}) & -2\text{Im}(M_{vh}) \\ -\text{Re}(M_{vh}) & -\text{Im}(M_{vh}) \\ -\text{Re}(M_{hv}) & \text{Im}(M_{hv}) \\ -(\text{Re}M_{vv} + \text{Re}M_{hh}) & (\text{Im}M_{vv} - \text{Im}M_{hh}) \\ -(\text{Im}M_{vv} - \text{Im}M_{hh}) & -(\text{Re}M_{vv} + \text{Re}M_{hh}) \end{bmatrix}$$

Propagation Models



The transmission matrix \mathbf{T}_1 is given by

$$\mathbf{T}_1 = \mathbf{HPH}^{-1}$$

where

$$\mathbf{P} = \begin{bmatrix} e^{-\beta_1 s} & 0 & 0 & 0 \\ 0 & e^{-\beta_2 s} & 0 & 0 \\ 0 & 0 & e^{-\beta_3 s} & 0 \\ 0 & 0 & 0 & e^{-\beta_4 s} \end{bmatrix}$$

Propagation Models

- The Mueller matrix in resolution volume 2 is then modified to take into account the propagation effects of resolution volume 1.

$$\mathbf{M}'_2 = \mathbf{T}_1^t \mathbf{M}_2 \mathbf{T}_1$$

- Radar parameters that are normally computed using the Mueller matrix, can now be computed with the new Mueller matrix (\mathbf{M}'_2).



COMSAT

COMSAT Laboratories

ACTS Propagation Experiments

ACTS Up-link Power Control Experiment

A. Dissanayake

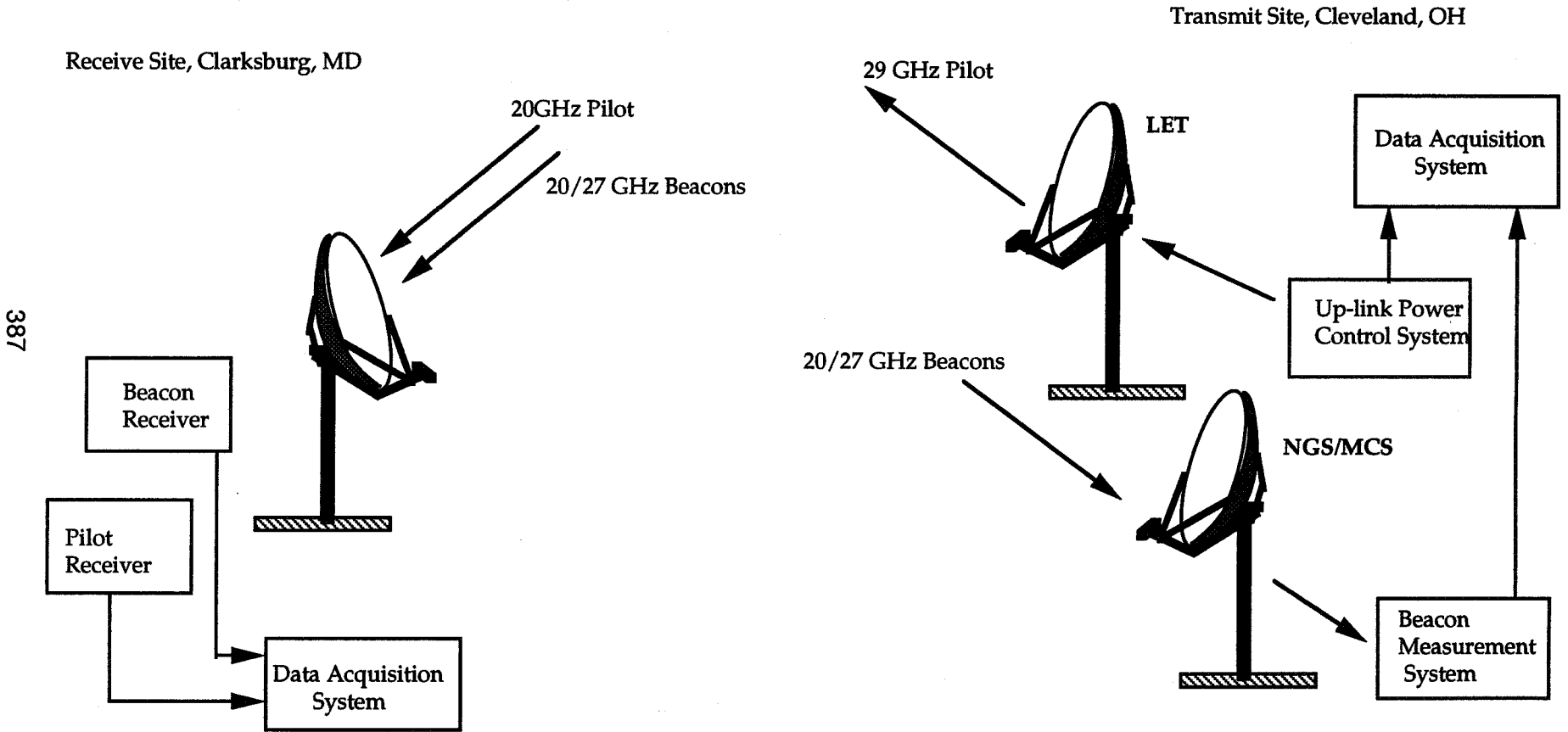
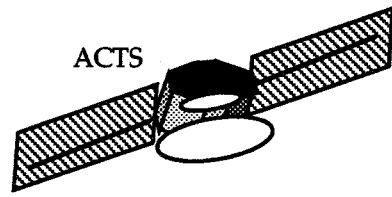
June 16, 1994

385

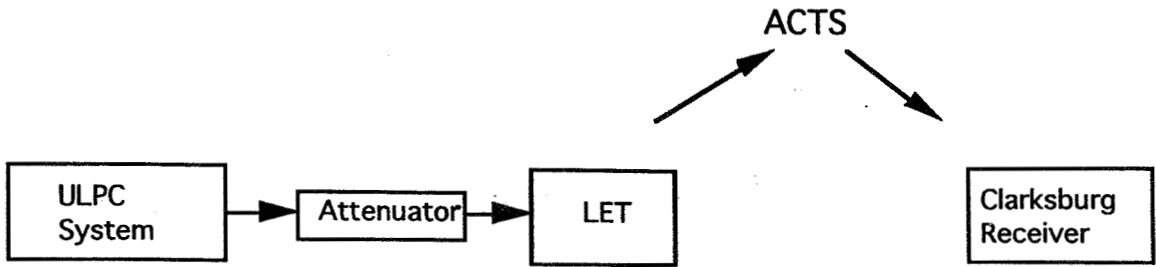
PREVIOUS PAGE BLANK NOT FILMED

Ka-band Up-link Power Control

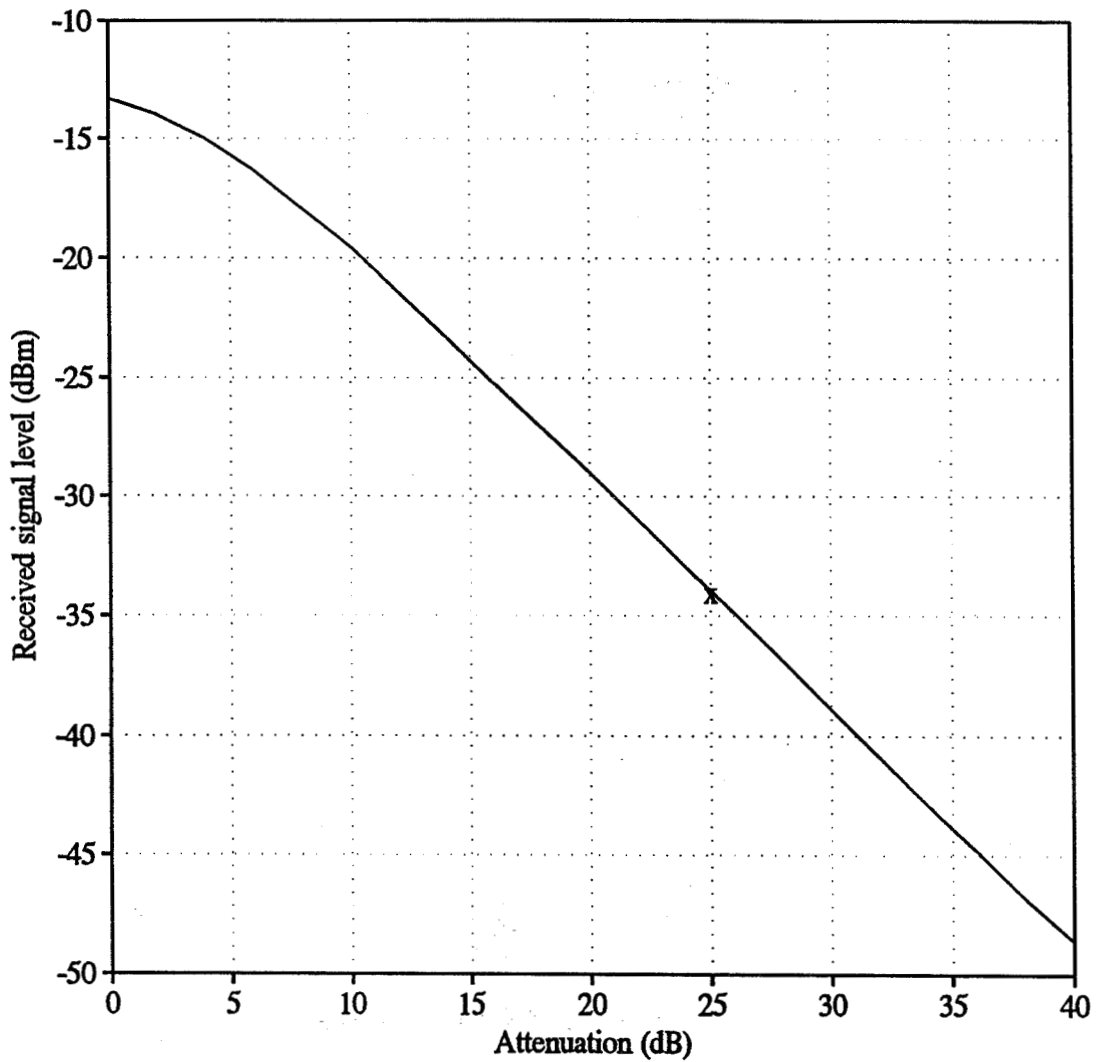
- * Power control carried out using a 27 GHz pilot carrier transmitted from the LET at Lewis Center in Cleveland; transponded carrier received at Clarksburg.**
- * Power control based on down-link attenuation measurements at 20 GHz**
- * Beacon reception and pilot transmission are done on separate antennas; antenna separation ~ 15 ft.**
- * Control applied at IF; power control resolution: 0.2 dB; update rate 5 Hz**
- * Maximum power control range: 25 dB; however, investigation will be limited to a control range of 15 dB.**
- * Several safety features incorporated into the power controller design to protect space segment**



ACTS Up-link Power Control Experiment Configuration



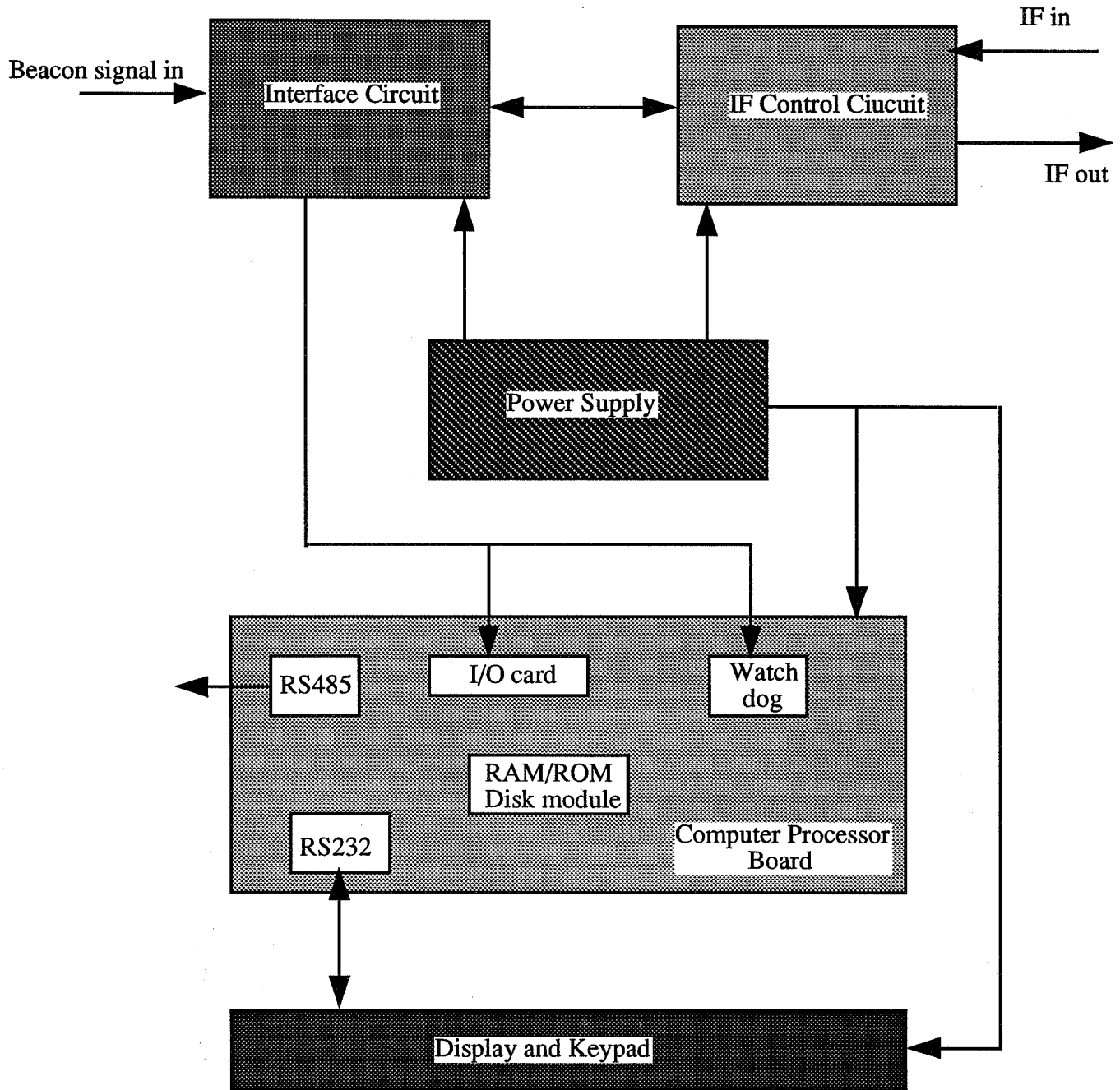
Measurement Configuration



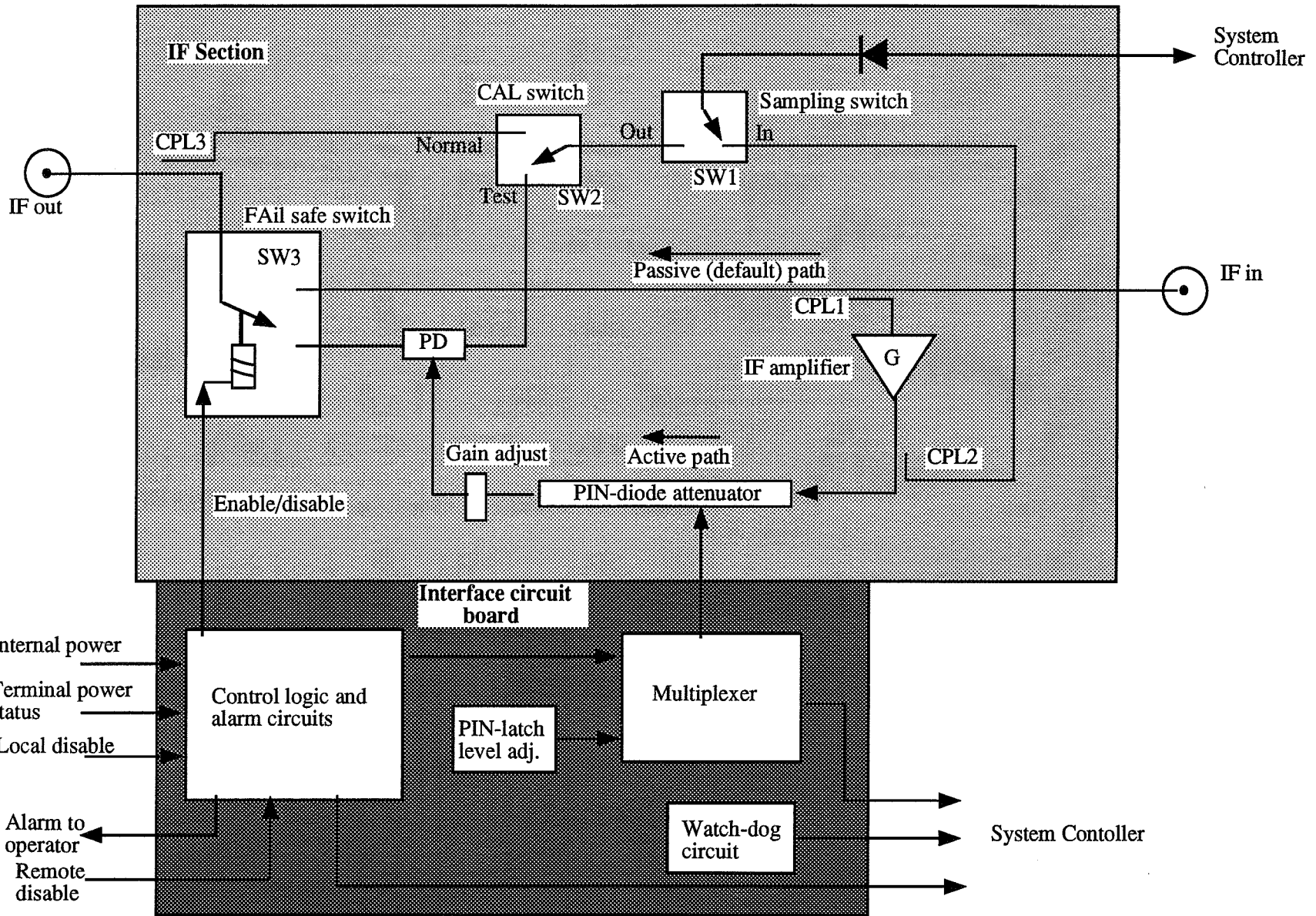
*Transponder/LET linearity test; attenuator setting vs. signal strength received at Clarksburg
x - nominal operating point*

Power Control System

- * Power control applied via a linearized PIN attenuator
- * A default path without power control available in case of a system failure; this path is also activated under exceptional conditions (beacon failure, beacon level jump or unacceptable drift)
- * Intel 386 based PC used as the system controller; system controller and control circuitry housed in a standard rack unit.
- * Controller parameters programmed through a front panel keypad and display.



Functional Block Diagram of the Up-link Power Controller



391

Control and Interface Circuits

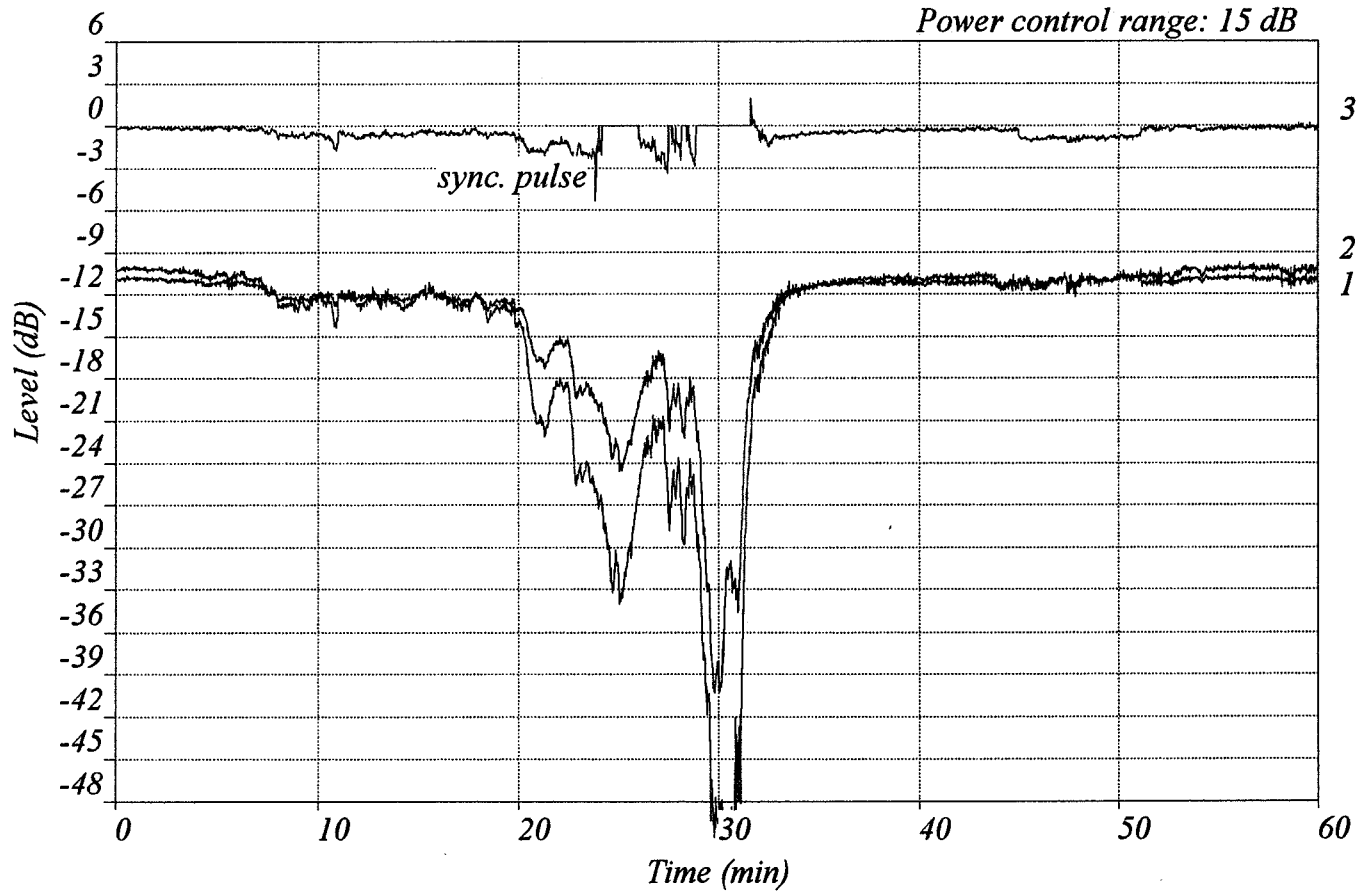
Power Control Algorithm

- * Detect down-link fade after establishing the reference level; reference level based on long-term observations using an adaptive filter with a time constant of the order of 1 hour**
- * Down-link fade separated in to rain fade and scintillation components; n averaging time of 20 sec. used in estimating the rain fade.**
- * Current level of rain fade predicted using an adaptive filter**
- * Frequency scaling of rain and scintillation fades to 27 GHz**

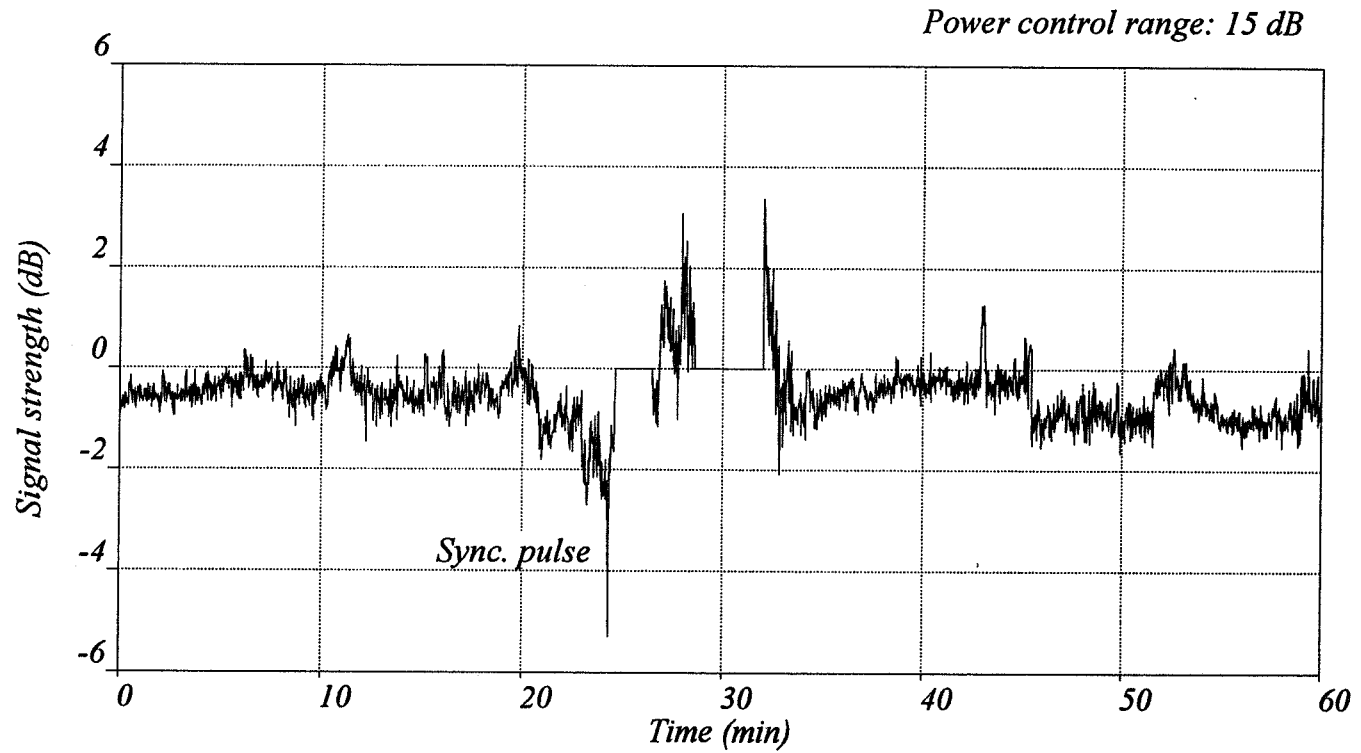


Initial Results

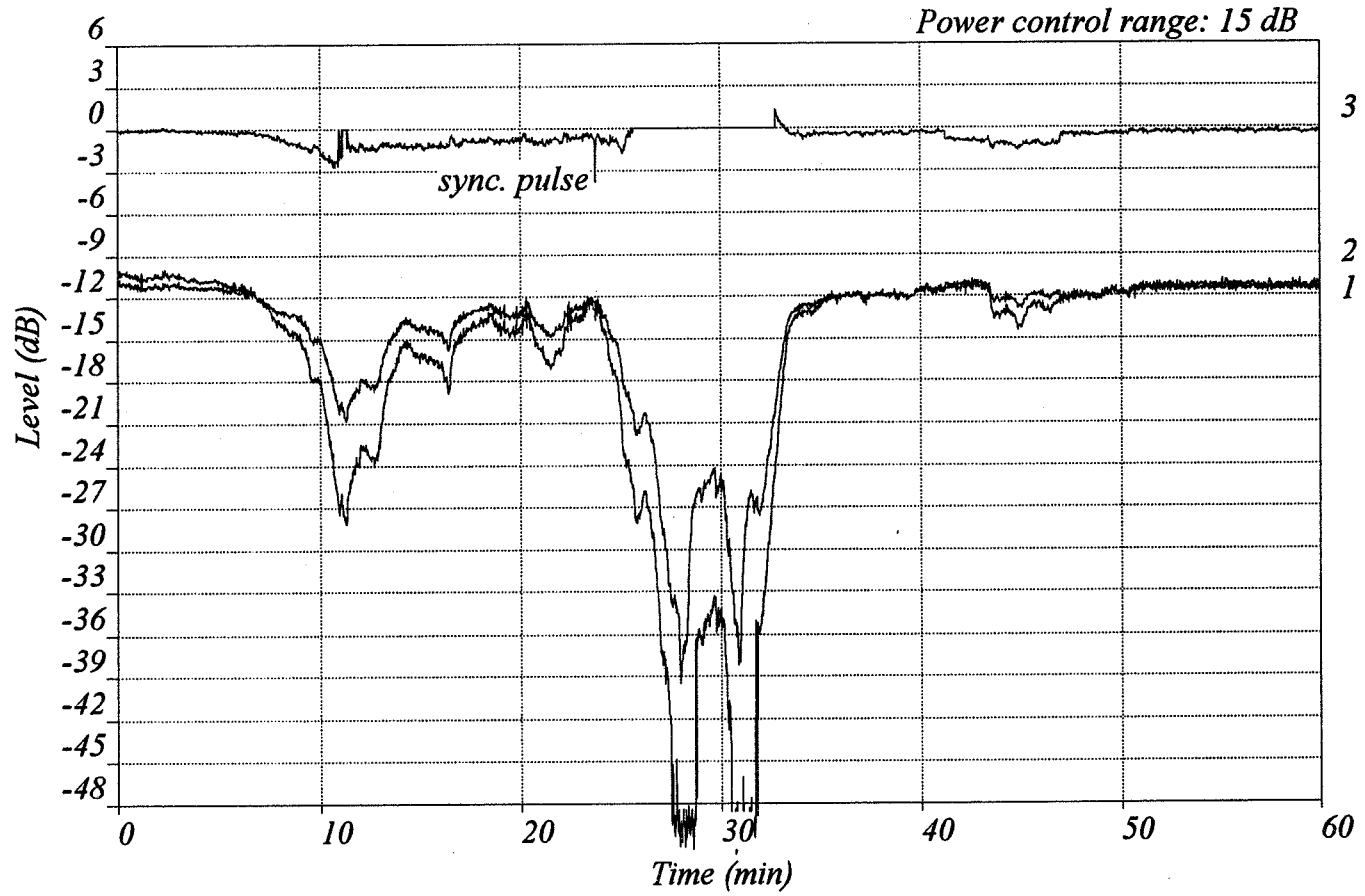
- * Separate transmit and receive antennas do not allow meaningful investigation of scintillation compensation.**
- * Approximately 24 hours of pilot transmissions completed; three severe rainstorms encountered during this period.**
- * Algorithm appears to underestimate the up-link fade.**
- * When restricted to a power control range of 15 dB, the control accuracy can be maintained within ± 3 dB.**



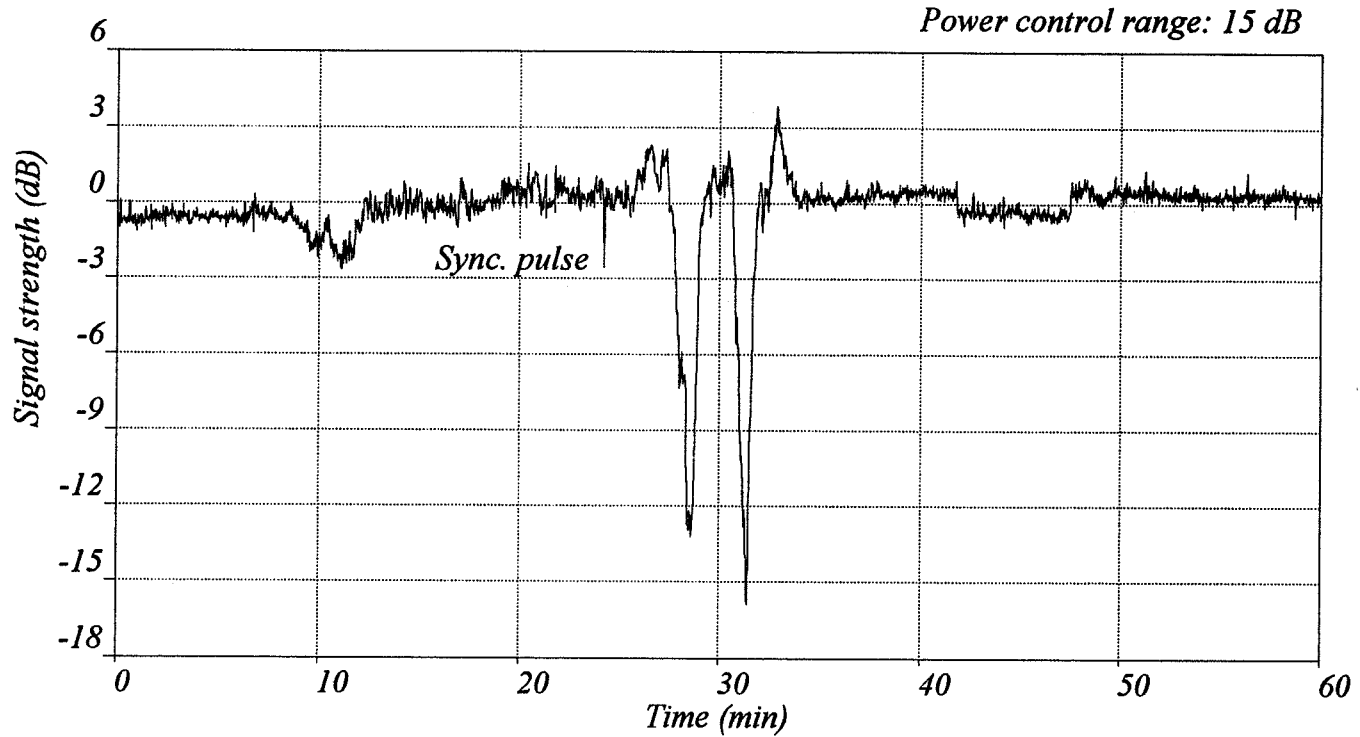
ACTS up-link power control experimnet
Rain event 1 on 31 May, 1994; 1: 20GHz, 2: 30GHz, 3: control error



*ACTS up-link power control experimnet
Rain event 1 on 31 May, Pilot level at Clarksburg*



ACTS up-link power control experiment
Rain event 2 on 31 May, 1994; 1: 20GHz, 2: 30GHz, 3: control error



*ACTS up-link power control experimnet
Rain event 2 on 31 May, Pilot level at Clarksburg*

FLORIDA'S PROPAGATION REPORT

309315

Participating Universities and Faculty Contacts:

Florida Atlantic University
 Boca Raton, FL 33431
 Dr. Henry Helmken
 Tel. 407-367-3452

University of South Florida
 Tampa, FL 33620
 Dr. Rudolf Henning
 Tel. 813-974-4782

P.D

Coordinates: Lat. 26.33, Long. 80.07

Lat. 28.06, Long. 82.42

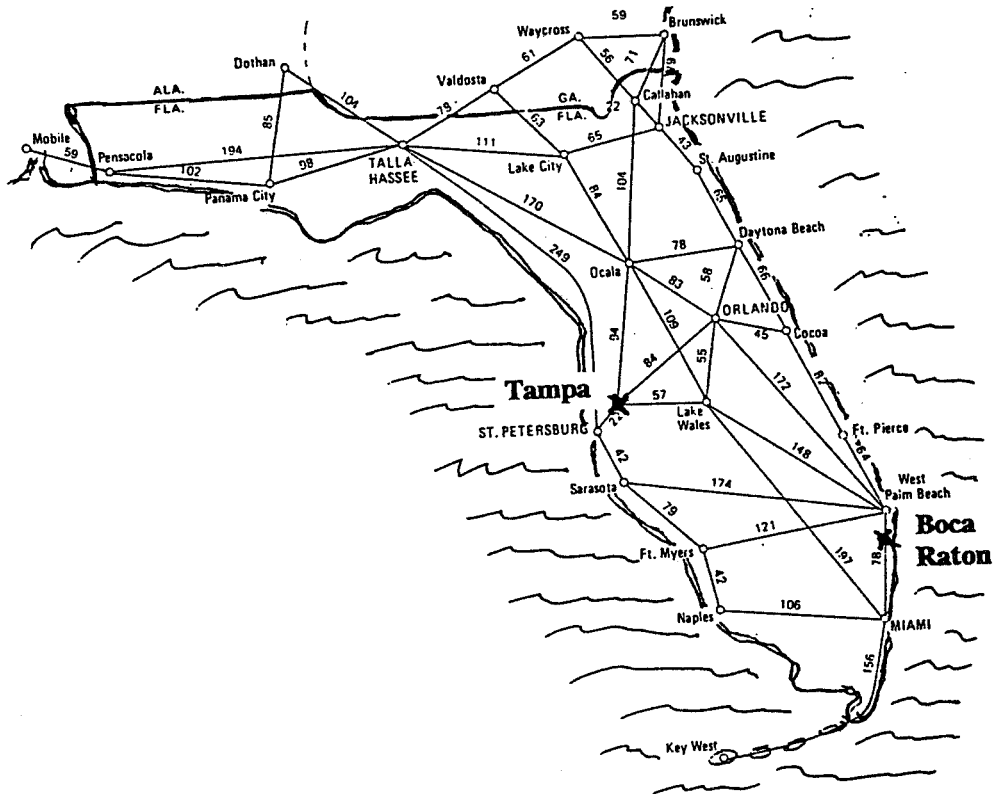
Angle to ACTS: El. 52.1°

El. 52.1°, Az. 214.0°

Tasks: Propagation Modeling
 Obtain supplementary Data
 Measure ACTS Beam Response
 Data Analysis & Validation

Obtain Continuous Data for Florida
 Submit Pre-processed Data to Un. of TX
 Data Analysis

Locations:



Terminals: "Custom" Terminal
 20 GHz RF Section,
 3.36 GHz I.F.,
 Spectrum Analyzer, Macintosh
 Computer, 1.2 m Antenna

"Standard" ACTS Propagation Terminal
 20 & 27 GHz RF Section,
 70 MHz I.F.,
 Digital Receiver, IBM-Compatible
 Computer, 1.2 m Antenna

I. UNIVERSITY OF SOUTH FLORIDA

A. FOCAL POINTS:

1. Equipment Operation:

Major effort is still being expended on obtaining reliable data and on establishing confidence that the data obtained is truly valid. Section C discusses a number of still outstanding issues in some further detail. On the hardware side this includes the meteorological instruments, proper operation under power-outage conditions, and verifying that the equipment is sufficiently temperature stable. On the software side, verifying that pre-processing (and its relation to equipment calibrations) is sufficiently reliable still needs to be established.

2. Sub-tropical Weather and Climate Related Information:

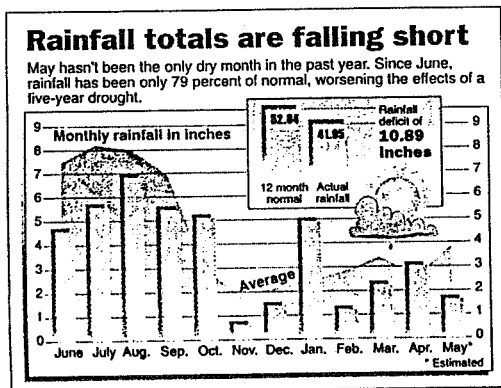
One of the key goals of the Florida Center is to obtain a maximum of useful information on propagation behavior unique to its sub-tropical weather and sub-tropical climate. Such weather data and information derived therefrom is of particular interest when it is (or has the potential to become) useful for developing and implementing techniques to compensate for adverse weather effects. Florida's unique climate, with its tropical summer pattern provides an opportunity to obtain significant tropical data, which is currently scarce. Its winter climate more closely resembles that of moderate climate zones. The combination appears to have the potential of providing a basis for evaluating designs and equipment destined to function in both climate environments. Some of the data presented in Section B. begins to address this area. We need to warn the reader that our weather in the last year has been quite abnormal, with much lower than normal rainfall. Thus the data presented cannot be considered truly representative of the statistical behavior for this area. See Figure I-1 below.

ampa bay AND state

section **B**

... WEDNESDAY, JUNE 1, 1994

This dry May was the driest of all



■ Last month was the exclamation point on the region's sentence of dry weather.

By SUE LANDRY
Times Staff Writer

Drought-weary residents looking to the skies for relief instead got the driest May on record. Barely enough rain fell at Tampa International Airport last month to be recorded by the rain gauge. The official May total amounted to a scant 0.07 inches of rain, which makes May 1994 the driest May this century in the Tampa Bay area. It was nearly as dry in nearby counties. The average May rainfall across Swiftmud's 16-county district was just 0.85 inches, nearly matching a record for the district. "May is when we typically see our driest conditions because it's at the end of the eight-month dry season," said Gary Florence, resource

data director with Swiftmud, the Southwest Florida Water Management District. "But to see a very dry May during our driest time of the year is particularly alarming."

The news that May was extremely dry might come as a surprise to residents whose Memorial Day picnics were drowned by heavy thunderstorms, but the showers were scattered, at best.

Swiftmud offices in Brooksville, for example, got no rain. Less than 10 miles north, a site on U.S. 98 got 2.98 inches during the holiday storms. An area in Tampa got just 0.03 inches of rain, while another area just east of Tampa got 1.74, according to Swiftmud records.

It's an area had inches, drought. Rain below normal. Rainfall for the past five years is 30 inches below normal. entire of 3.82 for the inches. The drought has hit especially hard in Tampa and most

Please see DRIEST 5B

Figure I-1

3. Rapid Signal Variations:

While equipment design must strongly consider longer term, statistically based information, equipment operation will be distinctly influenced by rapid (short-term) signal behavior (time intervals from milliseconds to several hours). Very little data seems to be available in this area. Obtaining such information on our unique summer weather, with its sudden, highly local, intense storms, is considered very important. Therefore we are focusing particular attention on rapid signal variations caused by both "weather" and "scintillation". Data presented in Section B. also begins to address this area.

B. DATA OBSERVATIONS:

1. Sub-Tropical Weather and Climate Related:

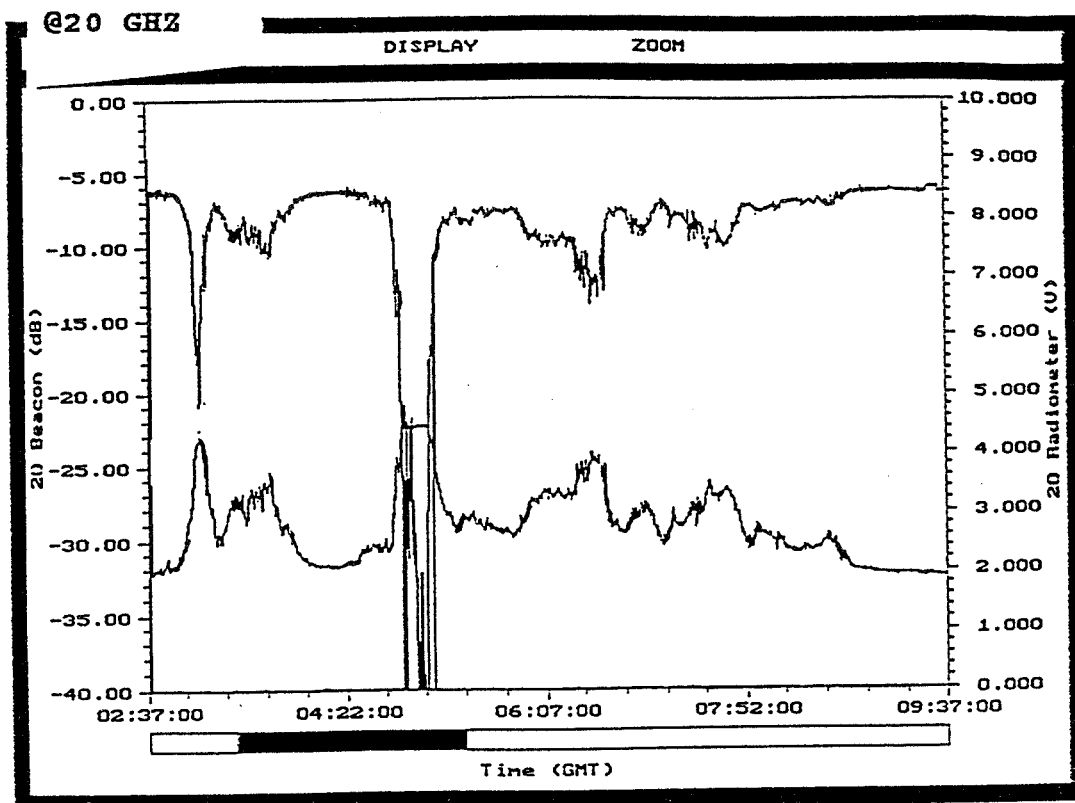
This section provides brief comments on the observed data presented in the figures that follow.

Figure I-2. presents an example of a winter weather "event", typically caused by a continental weather front reaching into and passing across Florida. Passing of a "front" normally lasts from several hours to over a day. Our (limited) observations to date show that there is only a brief interval (normally a few minutes) in which the beacon signal was completely lost (> 35 db increase in attenuation). The 27.5 GHz signal is invariably lost sooner and for a longer time interval than the 20.2 GHz signal.

Figure I-3. presents the first severe summer thunderstorm. It is an example of a typical summer weather "event". These storms are formed locally, are very high, but cover only a small areas at any one time. Rainfall rates of several inches/hour commonly exist in their center. Thus the observed long-time loss of signal (> 35 db increase in attenuation for 32 minutes at 20.2 GHz and for 40 minutes at 27.5 GHz) is not surprising.

Figure I-4. presents data on the first thunderstorm of the season. It occurred while a weak weather front was passing through - thus is representative of a weather "event" in the transition from winter to summer climate conditions.

Figures I-5 and I-6 provide a composite of all weather "events" in the winter-to-summer climate transition. Dates of occurrence have been typed in. The small number of May events is explained by the fact that May 1994 was the driest May ever encountered (see Figure I-1).



WINTER WEATHER FRONT, 01/18/94

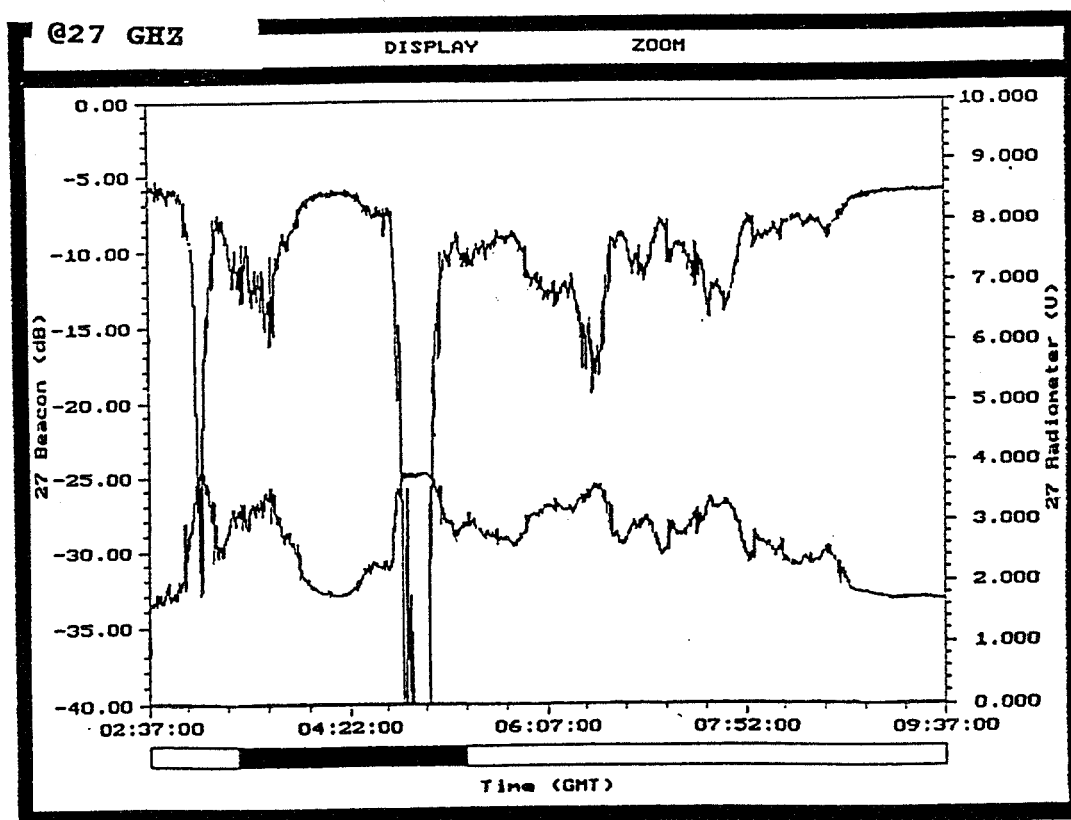


Figure I-2

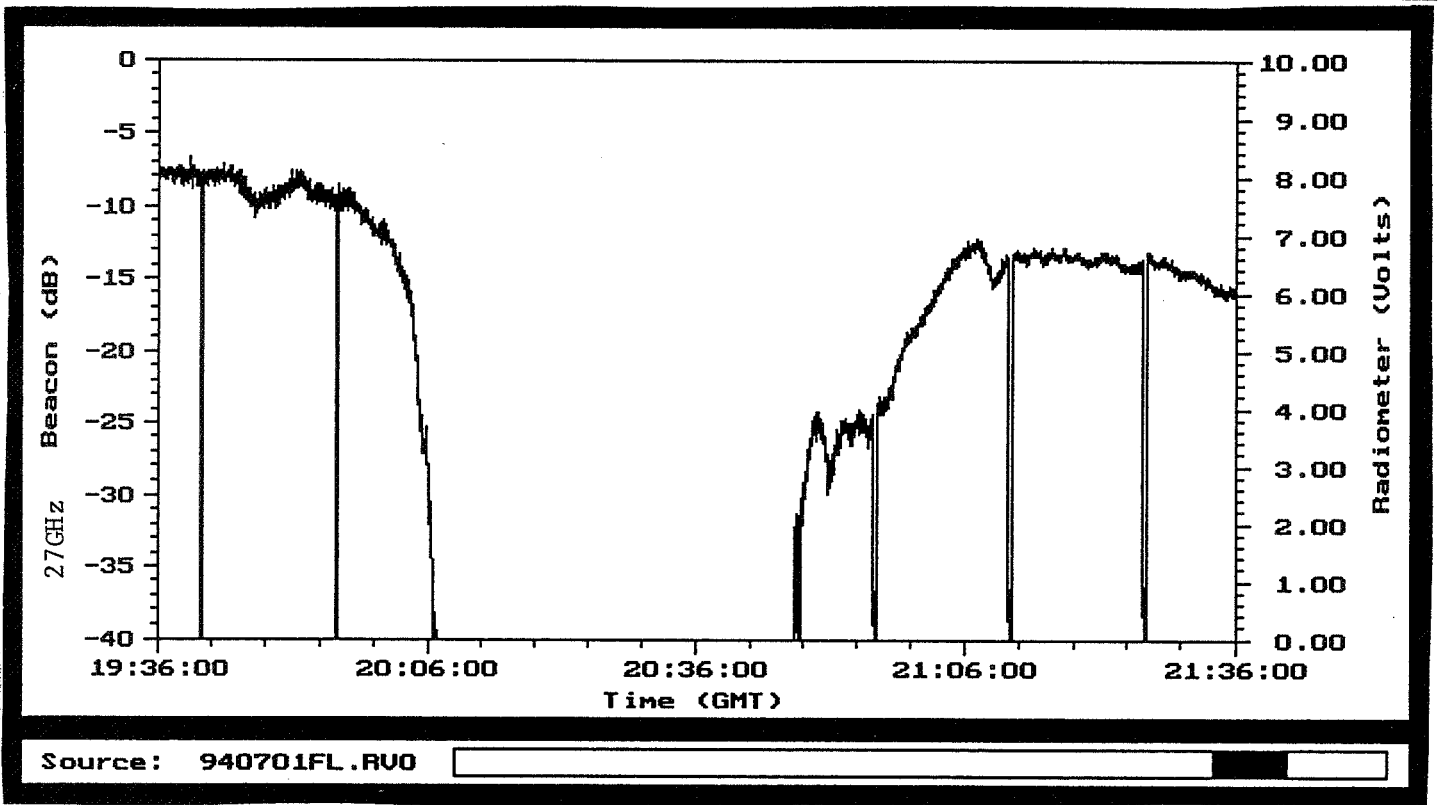
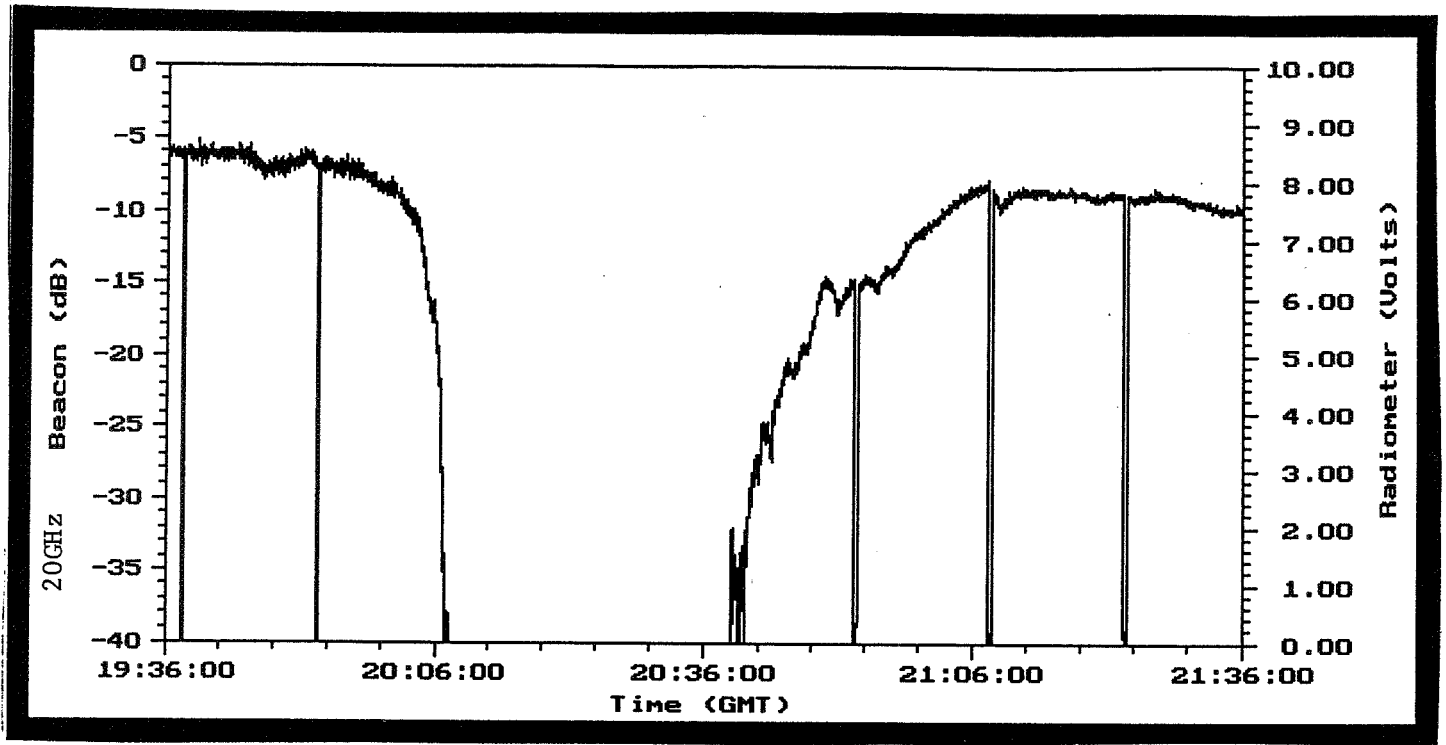
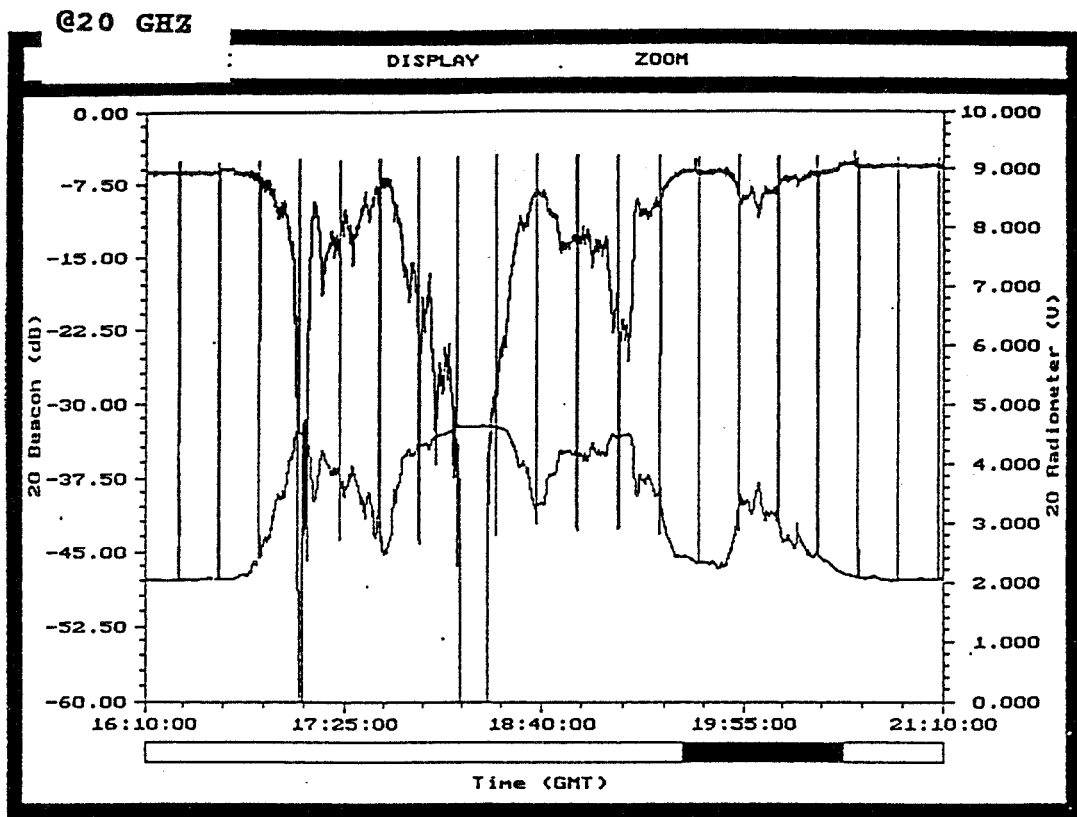


Figure I-3: SEVERE SUMMER THUNDERSTORM



FIRST 1994 THUNDERSTORM, (04/23)

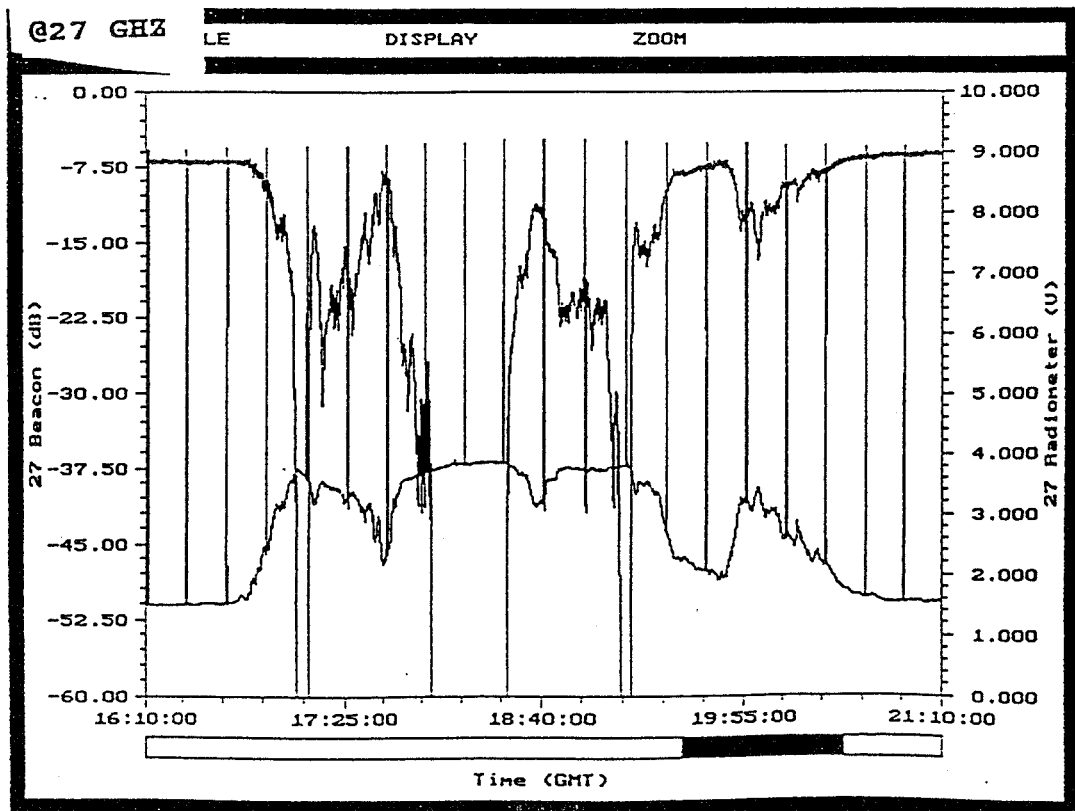


Figure I-4
404

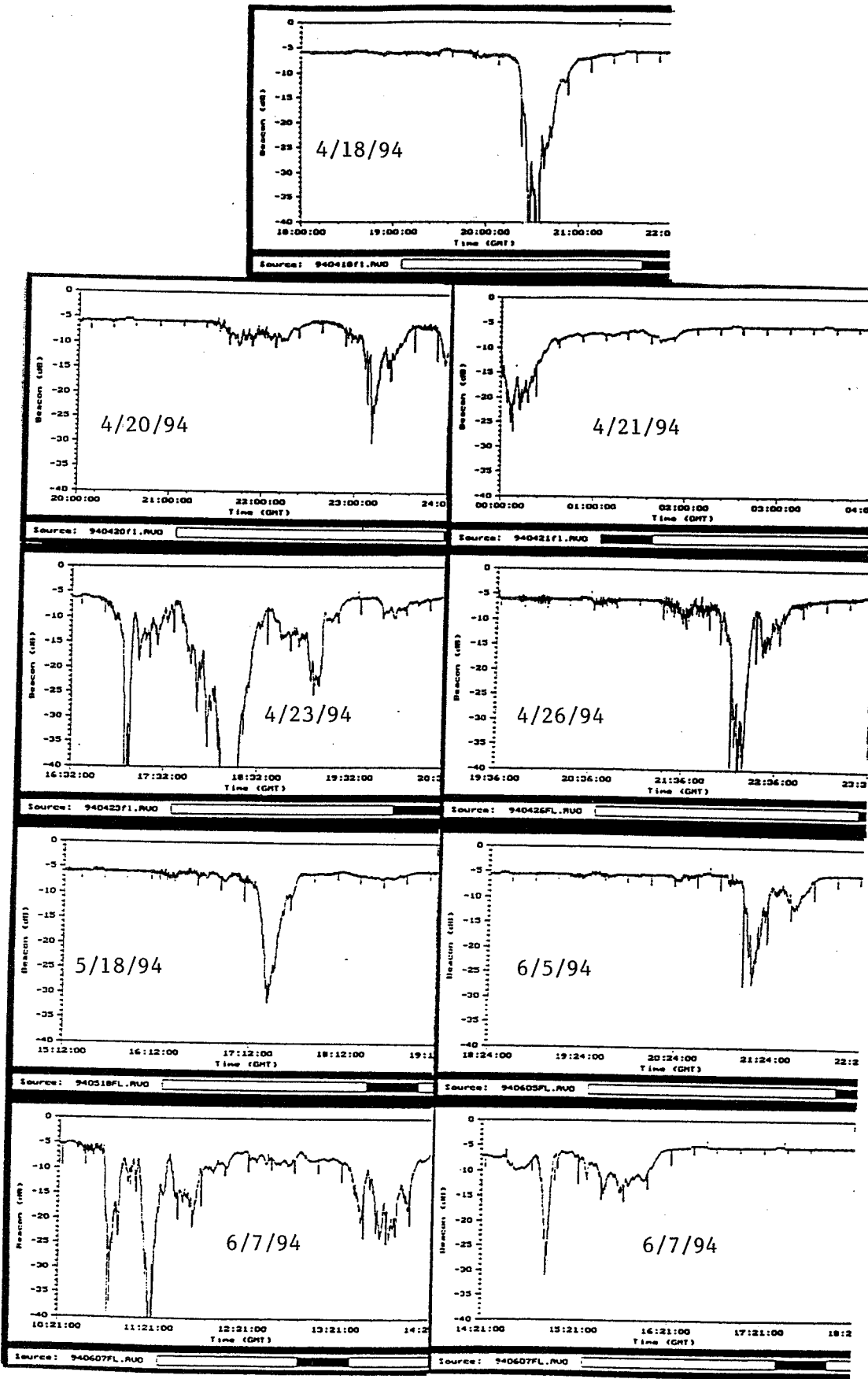


Figure I-5

**IMPACT ON 20 GHz SIGNALS BY
LOCAL RAINS AND THUNDERSTORMS, 04/18 TO 06/07**

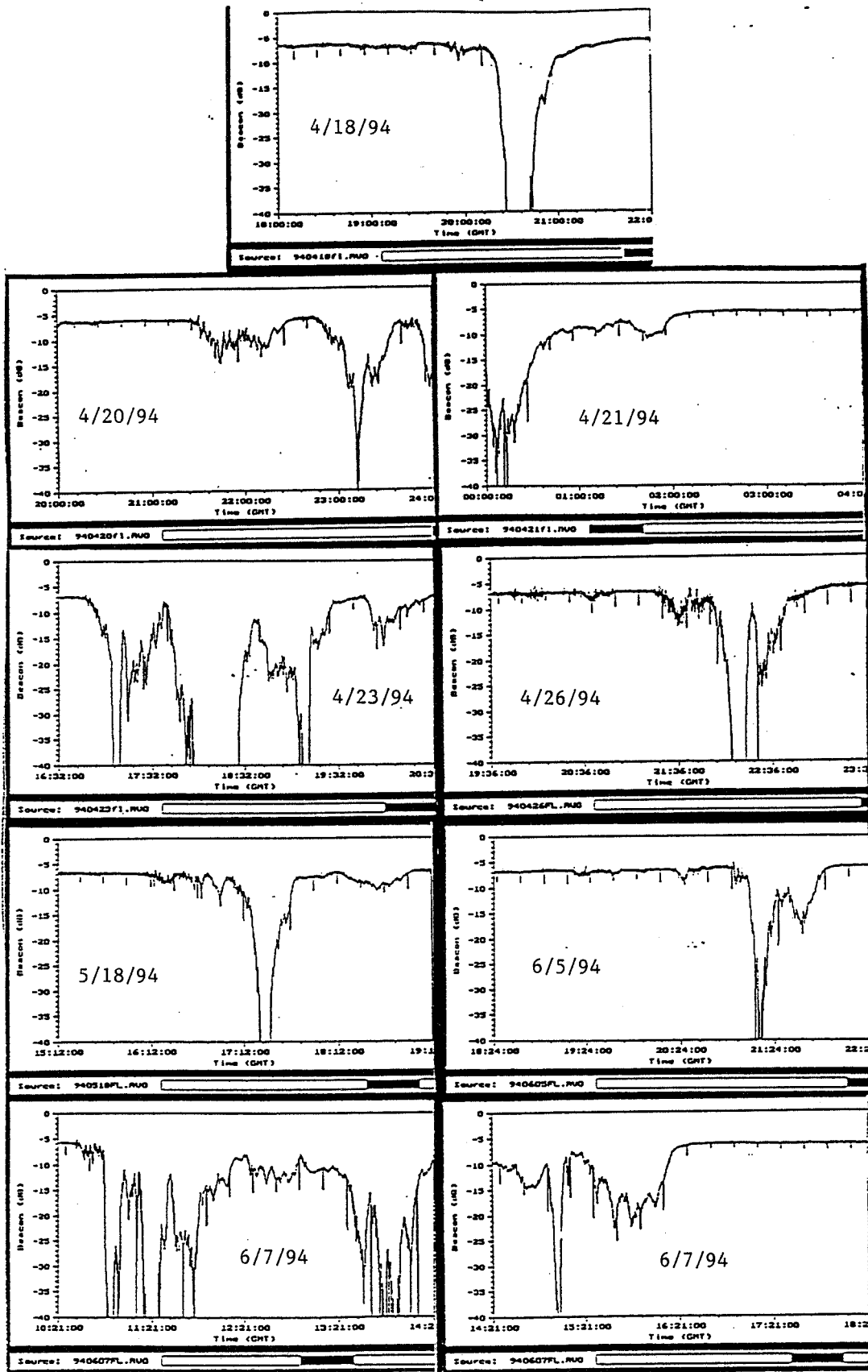


Figure I-6

**IMPACT ON 27 GHz SIGNALS BY
LOCAL RAINS AND THUNDERSTORMS, 04/18 TO 06/07**

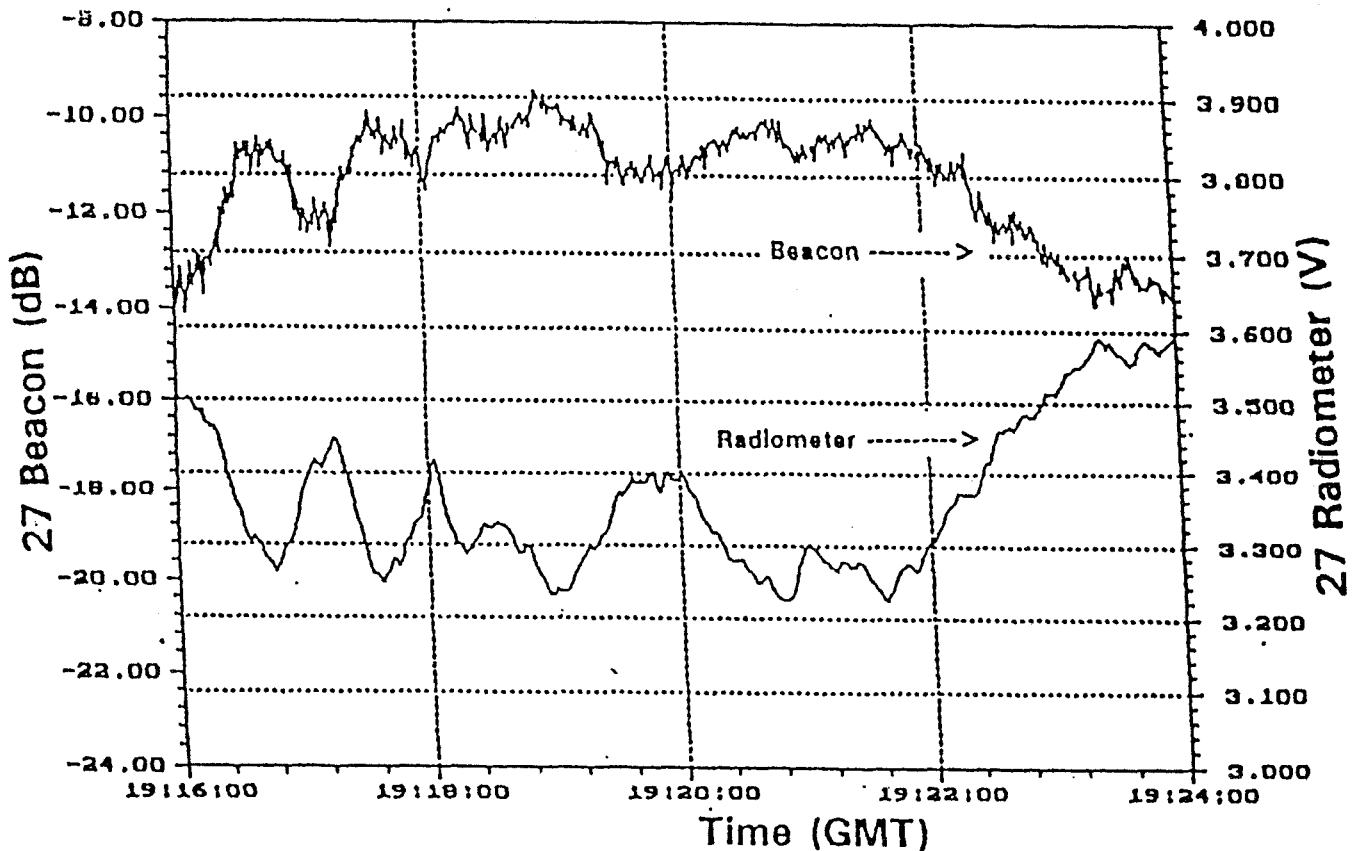
2. "Fast" Signal Variations Related:

The data presented here may on casual inspection be somewhat surprising, but actually confirms conclusions one would reach after a little thought.

Figure I-7 crushes any thought one might harbor that scintillation, being a type of random phenomena, shows no correlation between two independent signals at different frequencies. This scintillation-type data is presented on a time scale of 3 seconds = one small division. Extremely close correlation between the 20.2 and 27.5 GHz beacon signals is clearly visible. (Since this scintillation is weather induced, i.e., the signals travel through the same clouds, this is really not surprising.)

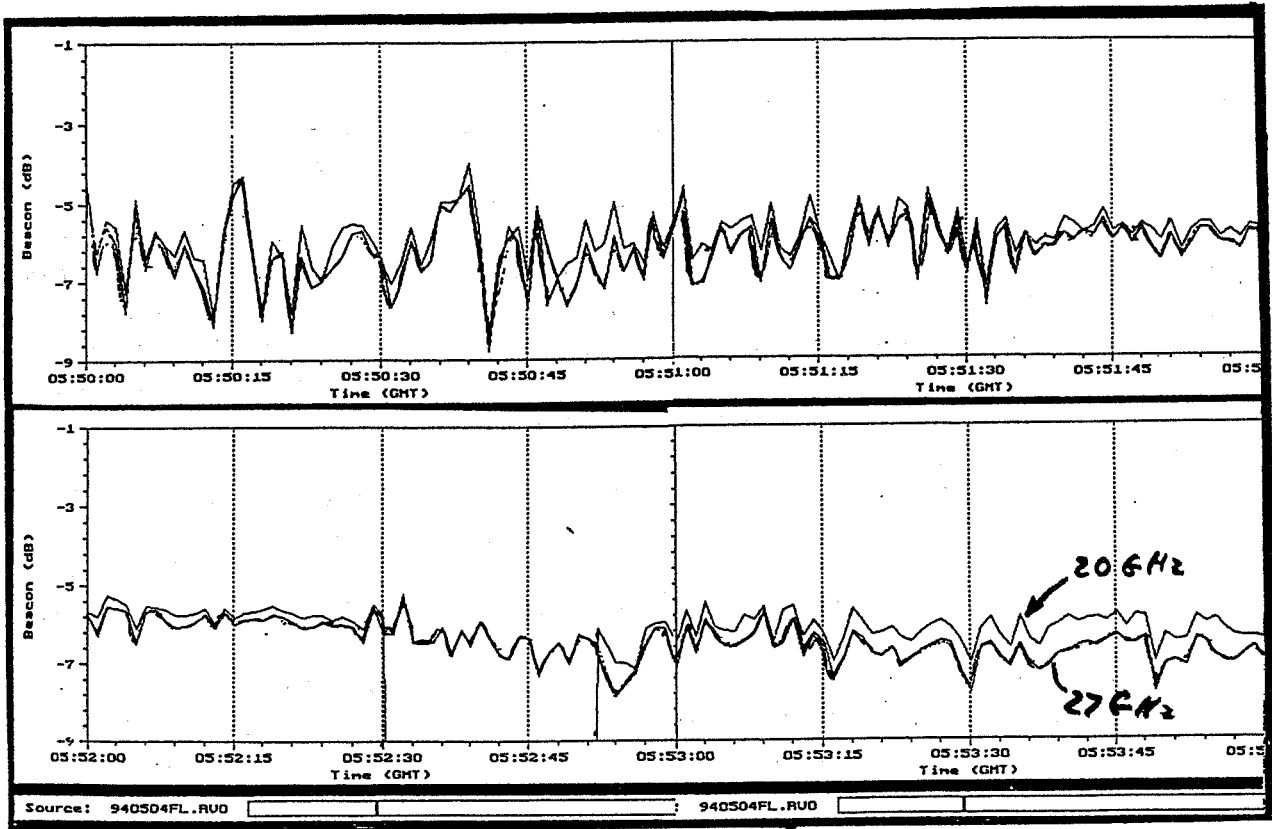
Figure I-8 spoils any illusion that propagation losses coincide with rainfall at the point of reception. A time delay of approx. 3 minutes between signal loss and heavy rainfall at the point of reception is clearly evident. In this case, heavy rainfall at a nearby location through which the beam passed was sufficient to cause loss of signal.

Figure I-9 confirms that close time-correlation exists between Beacon signal loss variations and radiometer output voltage (or sky temperature) variations. (Note that one small time division = 24 seconds.)



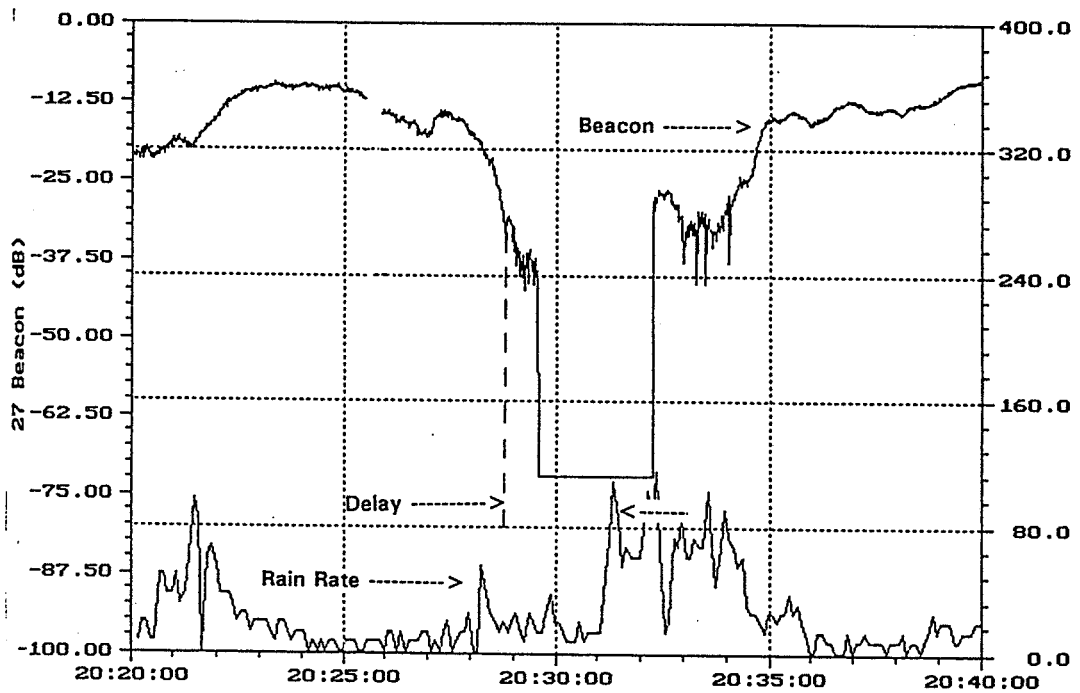
RADIOMETER/BEACON SIGNAL CORRELATION

Figure I-9



FOUR MINUTES OF 20 & 27 GHZ BEACON SIGNALS

Figure I-7



BEACON-SIGNAL/SITE-RAINFALL CORRELATION

Figure I-8

C. CURRENT "CHALLENGES"

1. Meteorological Instruments:

We are experiencing continuing problems in this area. Specifically:

a. Our Rain Gauge (As monitored on ACTSVIEW) rarely supplied information agreeing with "looking-out-the-window" data. It is very noisy, including off-scale readings, and often does not record rainfall or records rain when there is none. We are currently checking the complete set-up for the third time, including another laboratory calibration check of the rain gauge alone.

Any system-recorded rain data should be ignored. We are in the process of collecting rainfall information based on local data from other sources which we plan to compile and submit to the University of Texas' data center when completed.

b. The Humidity Gauge exhibited until very recently readings that made all data supplied suspect. (Example: readings well above 100% and step-function jumps in humidity which violate the laws of nature.) We finally traced the problem to the fact that the APT does not provide a dc voltage to the gauge in the range specified by its manufacturer. Adding a 6 volt battery in series with the APT-provided d.c. cleared up the problem and gives us temporary fix.

c. We believe that our wind velocity indication is consistently much lower than the actual wind velocity at its location. To-date other more urgent tasks have kept us from investigating this further.

d. If a need for uniform and systematic reporting of operational situations, such as outages, exists, it may be desirable to establish a "procedure" and "format" for reporting such information.

2. Power Failures:

We installed a backup system to the NASA-provided UPS to handle power outages up to a day or longer. The system works fine whenever it is tested. It provides power to our equipment when the building or campus is without power (as has happened twice). But --- data flow from the outside receiver enclosure to the inside lab computer is lost. We suspect major transients are the culprit -- unfortunately we cannot shut off the college's or campus' power to test details of this theory.

3. System "Crashes":

For months the system ran rather trouble-free. Then we began encountering "crashes". Observation that they always occurred at about the same time led to relating them to the sun moving into a position where it directly illuminated the fiber-optic input at the back of the PC. Black plastic blocking the sunlight provided a simple cure for this very high frequency EMI.

3. Water on the Antenna Dish:

We delayed applying the recommended hydrophobic paint to take data on the effect of dew (which frequently occurs in the spring) on attenuation data. Information has been collected and a brief report will be issued.

4. Enclosure Temperatures:

We are concerned about possibly significant temperature gradients between components in the temperature-controlled enclosures, measured at the same time . (A typical recent day shows at any one time the following differences: 27 vs. 20 Reference Loads: +1.94°, 27 vs. 20 IF's: -5.79°, 27 vs. 20 Radiometers: -2.34°, Front End Plate vs. Air: +2.84°, Front End Plate vs. 27 GHz Ref. Load: -2.50°.)

Similarly, we are concerned about the min/max daily variations in components or assemblies, whose performance is likely to be temperature sensitive. Temperature variations in degree centigrade on a typical recent day were:

Outside Temperature (for ref.)	13.0°	Receiver Enclosure	1.9°
20 GHz Reference Load	2.1°	27 GHz Reference Load	1.2°
20 GHz Radiometer	1.2°	27 GHz Radiometer	1.7°
20 GHz I.F.	3.8°	27 GHz I.F.	5.4°
Front End Plate	0.5°	Front End Air	4.6°

5. New Doppler Radars:

The Tampa Weather Bureau is currently checking out its new long range NEXRAD radar. Installation of a shorter range Doppler radar, particularly devoted to detect severe weather cells, including windshear, at Tampa's airports, has commenced. Thus within a year there will be two modern Doppler radars "on the air" which will cover our ACTS beam, and concurrently provide new opportunities for more precisely assessing weather effects on mm propagation.

II. FLORIDA ATLANTIC UNIVERSITY

1. CDF's:

On the next page CDF data plots are presented. Figure 1 is a composite CDF of the 20 GHz and 27 GHz beacon attenuation data for the period December 1993 to February 1994. Figure 2 illustrates the corresponding radiometer CDF's. Subsequent data has been processed but not included due to unresolved questions in calibration. These must be resolved first, since this will impact some observations which exhibit higher attenuation values at 20 GHz than at 27 GHz.

2. SUN MOVEMENT:

A computer program has been written to trace the apparent sun movement across the terminal field of view and a graphical output is illustrated in Figure 3 (below). We would be happy to supply similar graphs for other sites.

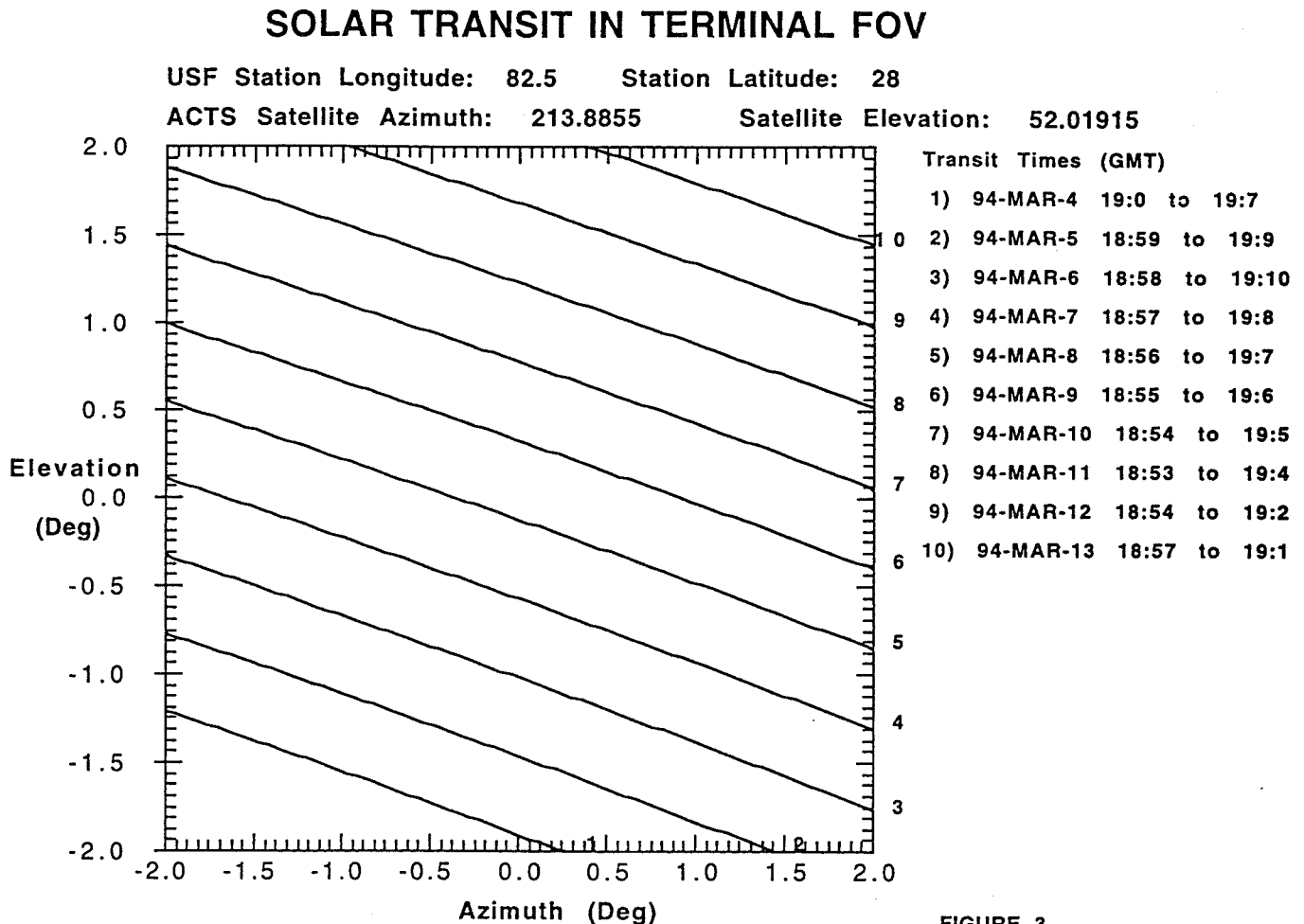
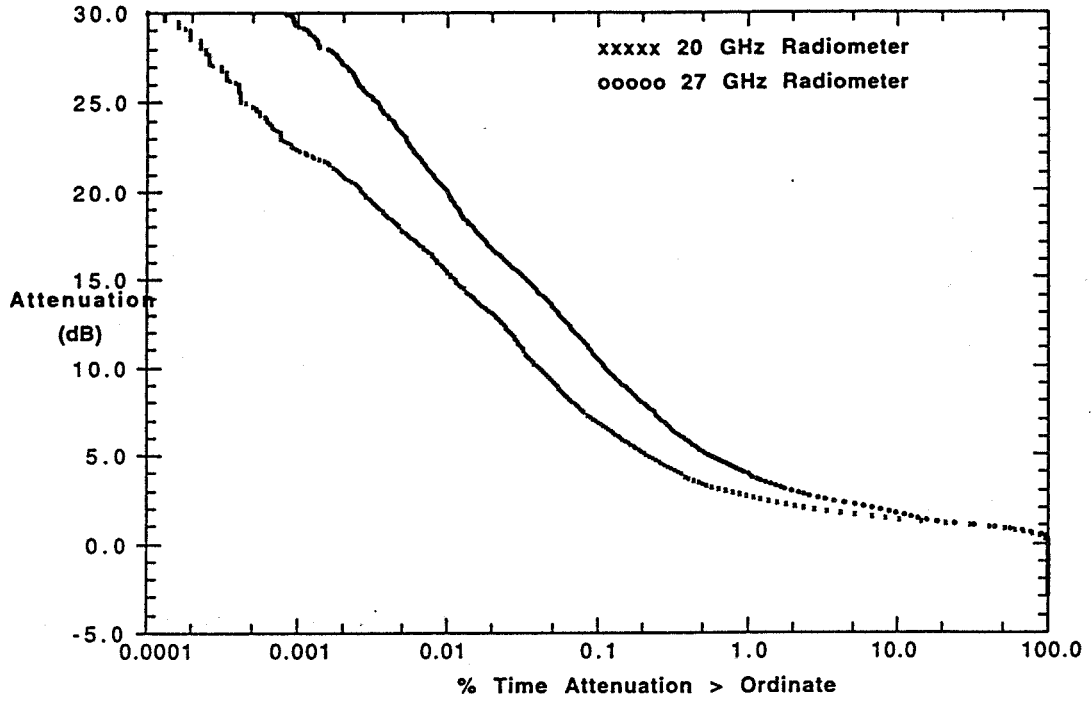


FIGURE 3

12/93 - 2/94 CUMULATIVE DISTRIBUTION

ACTS Propagation Terminal - Tampa, Florida

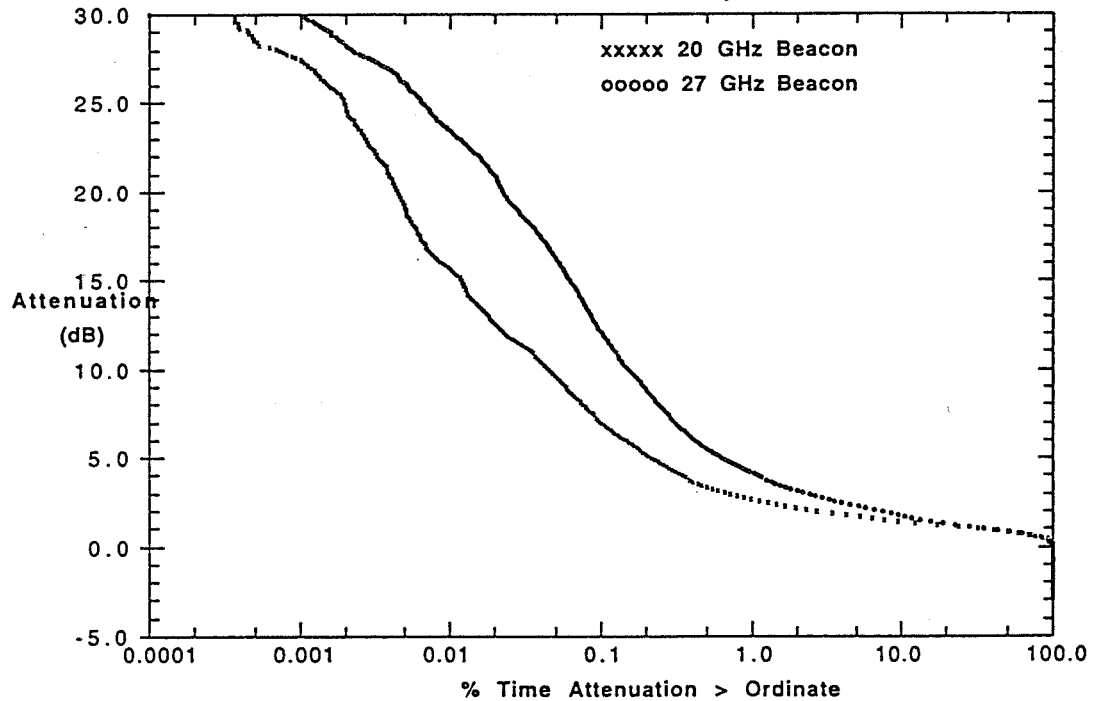
Diurnal Fit - 4th Order Polynomial



12/93 - 2/94 CUMULATIVE DISTRIBUTION

ACTS Propagation Terminal - Tampa, Florida

Diurnal Fit - 4th Order Polynomial



3. DIVERSITY EXPERIMENTS:

A series of diversity experiments are planned for later this year. Figures 4 and 5 below exhibit the rationale and the status of the receive-only transportable terminal. Initial measurements and calibration will occur adjacent to the ACTS terminal at USF in Tampa. Subsequent measurement sites will be in the range from 10 km to 30 km distant.

SITE DIVERSITY PROGRAM

- * GOAL
Diversity Measurements in a Sub-Tropical Weather Zone

- * PREVIOUS MEASUREMENTS
Tampa Triad: COMSTAR Beacon Experiments 1978-1979
19 GHz, Rainy Season Diversity
Sponsored by GTE

- * NASA ACTS Terminal Location
Campus of University of South Florida (USF)
Tampa, Florida (28° N, 82.5° W)

- * Possible Remote Locations
Within USF Campus - 2 km
Local School Areas 15 to 38 km

Figure 4

TRANSPORTABLE TERMINAL

- * Present Configuration
1.2 m Dish, Receive Only (RO) Terminal at 19 - 20 GHz
Downconvert to 3.3 GHz (LET IF) or 70 MHz
Record Signal Amplitude at -1 Hz via HP 8563A Analyzer

- * Upgrades in Progress
Downconvert 70 MHz to Baseband
Digital I & Q Demodulation
Sustained Recording at 8kHz rate

- * Possible Additional Upgrades
Add Noise Diode for Calibration
Add 30 GHz Channel

Figure 5

4. By way of reference, Figure 6 (below) illustrates the achievable Signal/Noise ratio when using only the terminal feed horn on an ACTS CW in-band signal. Data is useful for anyone planning to do shadowing, multipath or building measurements using ACTS in-band signals.

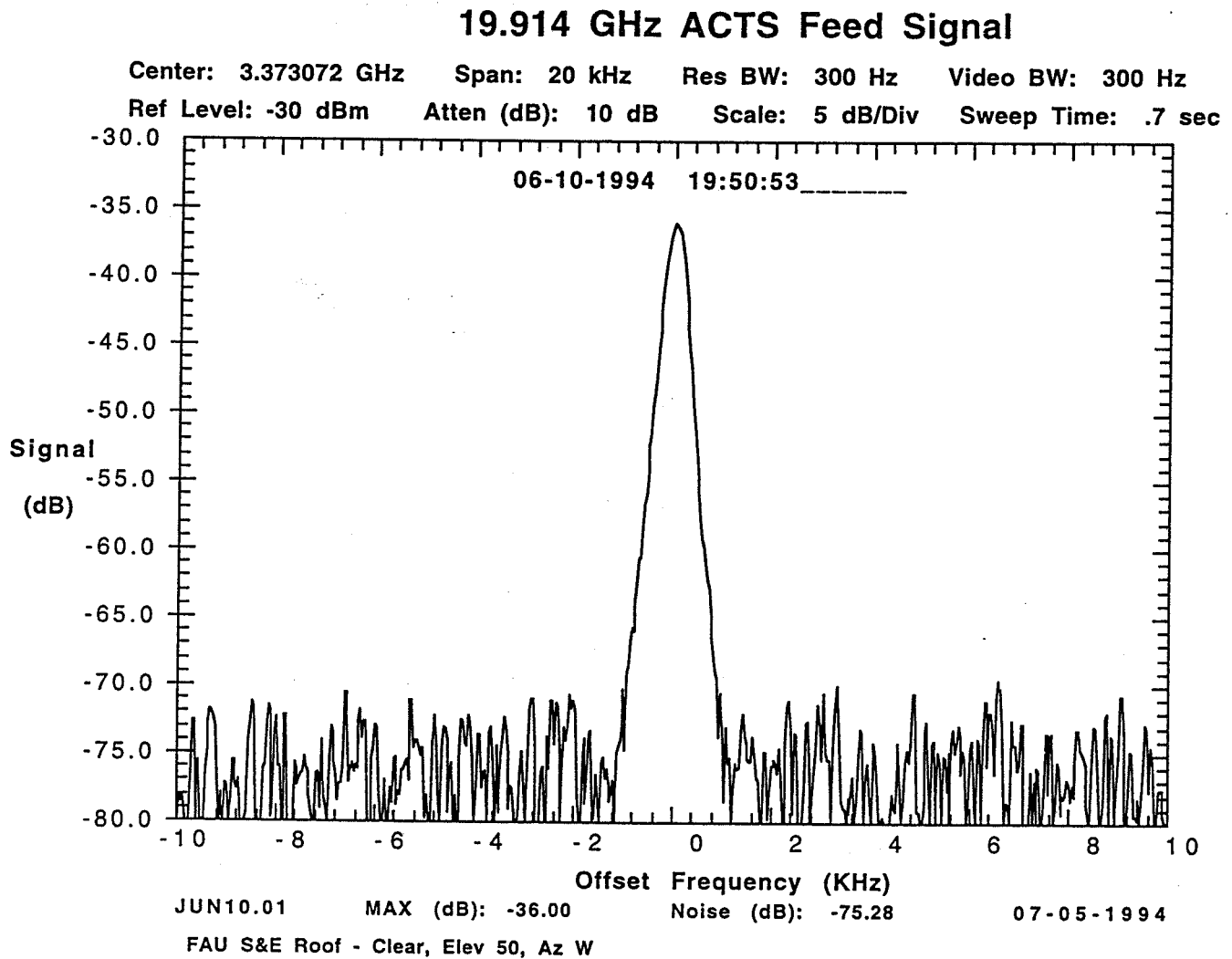


FIGURE 6

**NEW MEXICO ACTS PROPAGATION TERMINAL
STATUS REPORT**

1 DECEMBER 1993 - 31 MAY 1994

Prepared by

Stephen Horan and Glenn Feldhake
New Mexico State University
Department of Electrical and Computer Engineering
Las Cruces, NM 88003

June 15, 1994

I. TERMINAL OPERATING TIME AND RAIN EVENT DAYS

NEW MEXICO ACTS FIRST QUARTER SUMMARY

Month	Day	Las Cruces Sun News	NOAA	ACTS Terminal	NASA RainDance	DECEMBER	Days	Hr	Min	Sec	%
December	12	0.05	0.04	0.01	*	Up Time	28	15	27	22	92.4%
	13	0.00	0.02	0.00		Down Time	2	8	32	38	7.6%
	21	0.05	0.00	0.08	*	Hot/Cold Cal	3	17			
	22	0.24	0.32	0.35	*	Air Temp	10.9	18.4			
	23	0.01	0.00	0.00							
	29	0.32	0.10	0.00		JANUARY	Days	Hr	Min	Sec	%
30	0.03	0.29	0.00		Up Time	31	0	0	0	100.0%	
TOTAL RAIN ACCUM		0.70	0.77	0.44	N/A	Down Time	0	0	0	0	0.0%

417

Month	Day	Las Cruces Sun News	NOAA	ACTS Terminal	NASA RainDance	Hot/Cold Cal	Days	Hr	Min	Sec	%
January	29	0.04	0.05	0.85		Air Temp	6.6	22.0			
	30	1.78	0.00	0.00		FEBRUARY	Days	Hr	Min	Sec	%
	31	0.00	0.04	0.00		Up Time	24	9	59	2	87.2%
TOTAL RAIN ACCUM		1.82	0.09	0.85	0.00	Down Time	3	14	0	58	12.8%

Month	Day	Las Cruces Sun News	NOAA	ACTS Terminal	NASA RainDance	Hot/Cold Cal	Days	Hr	Min	Sec	%
February	8	0.12	0.00	0.00	*	Air Temp	14.1	19.2			
	9	0.05	0.17	0.00		TOTAL	Days	Hr	Min	Sec	%
TOTAL RAIN ACCUM		0.17	0.17	0.00	N/A	Up Time	84	1	26	24	93.40%
						Down Time	5	22	33	36	6.60%

* Represents Days NASA Rain Dance Data Indicates a Precipitation Event Occured. Accumulation and Rate Data were Not Provided.

NEW MEXICO ACTS SECOND QUARTER SUMMARY

Month	Day	Las Cruces Sun News	NOAA	ACTS Terminal	NASA Rain Dance	MARCH	Days	Hr	Min	Sec	%
March	8	0.02	0.01	0.00	*	Up Time	30	0	0	0	96.77%
	14	0.15	0.12	0.79	*	Down Time	1	0	0	0	3.23%
	20	0.00	trace	0.00							
TOTAL RAIN ACCUM		0.17	0.13	0.79	N/A						

Month	Day	Las Cruces Sun News	NOAA	ACTS Terminal	NASA Rain Dance	APRIL	Days	Hr	Min	Sec	%
April	20	0.00	0.00	0.00	*	Up Time	30	0	0	0	100.00%
	21	0.07	0.07	0.00	*	Down Time	0	0	0	0	0.00%
	22	0.10	0.00	0.00							
	23	0.16	0.27	0.00	*						
	24	0.00	0.03	0.00							
TOTAL RAIN ACCUM		0.33	0.37	0.00	N/A						

418

Month	Day	Las Cruces Sun News	NOAA	ACTS Terminal	NASA Rain Dance	MAY	Days	Hr	Min	Sec	%
May	8	0.00	0.01	0.00	N/A	Up Time	31	0	0	0	100.00%
	21	0.02	0.00	0.00	N/A	Down Time	0	0	0	0	0.00%
	22	0.00	0.01	0.00	N/A						
	23	0.30	0.29	0.00	N/A						
	24	0.00	0.04	0.00	N/A						
	25	0.03	0.16	0.00	N/A						
	26	0.15	0.00	0.00	N/A						
TOTAL RAIN ACCUM		0.50	0.51	0.00	N/A	TOTAL	Days	Hr	Min	Sec	%
						Up Time	91	0	0	0	98.91%
						Down Time	1	0	0	0	1.09%

* Represents Days NASA Rain Dance Data Indicates a Precipitation Event Occured. Accumulation and Rate Data were Not Provided.

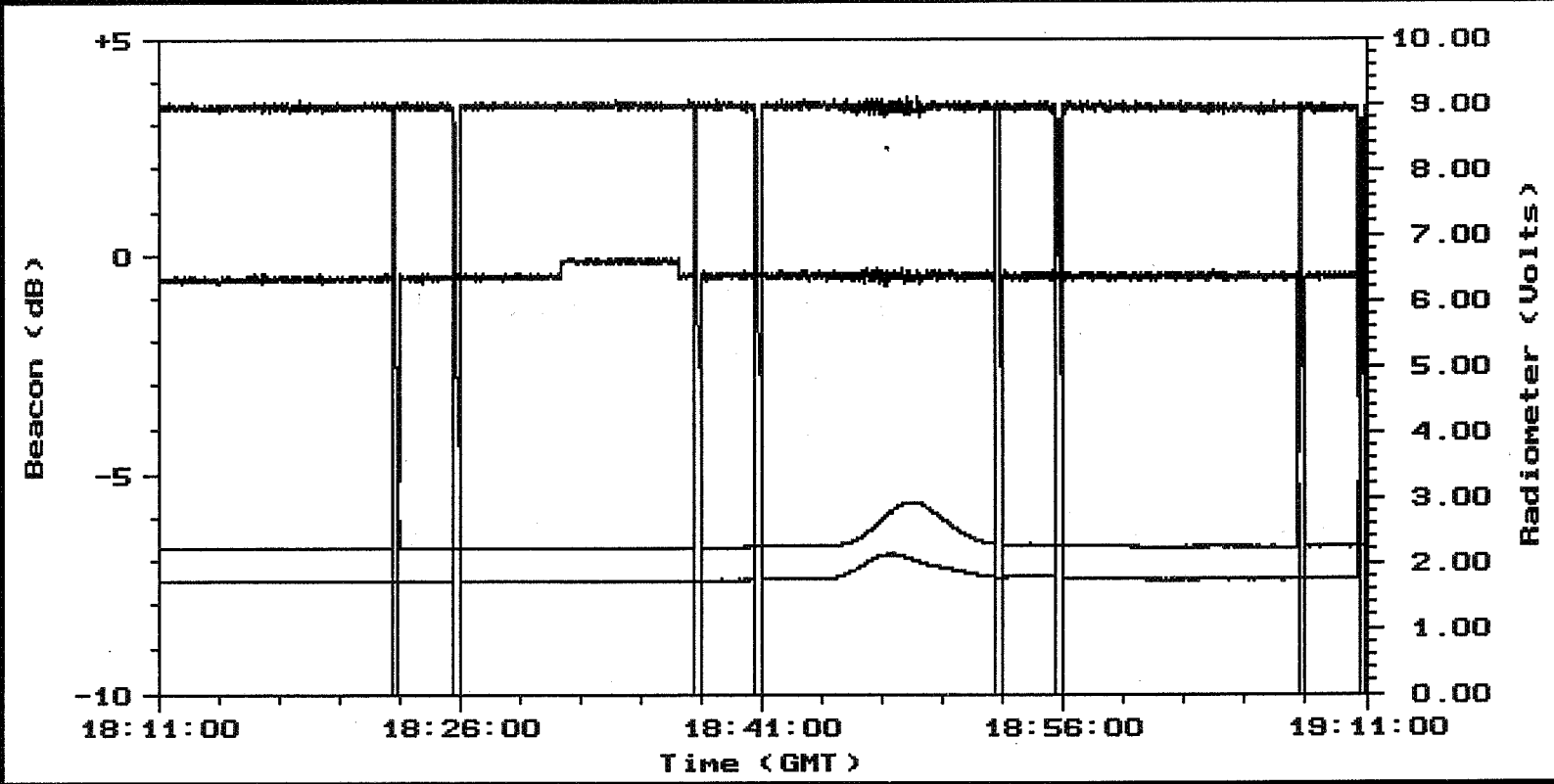
Up and Down Times are based on processable data RV0 files may be present with unprocessable data.

II. SUN TRANSIENT EVENTS

Daily events on March 3 through March 9, 1994

- beacons did not have maximum noise at the same time in each channel!
- radiometer saturated on one day

FILE DISPLAY ZOOM PAUSE



Source: 940304nm.RVD

- 20 G Beacon ()
- 16:32:00 Beacon ()
- 20 G Radioneter
- 27 G Radioneter

System Status - XXXXXX
 RH: XXX % CRG: XXXXX mm/hr
 WS: XXXX m/s TRG: XXXXX mm/hr
 WD: XXX ° OT: XXXXXX °C
 Time: 22:56:51 Date: 05/07/94

R: 16:47:00
 Spectrum

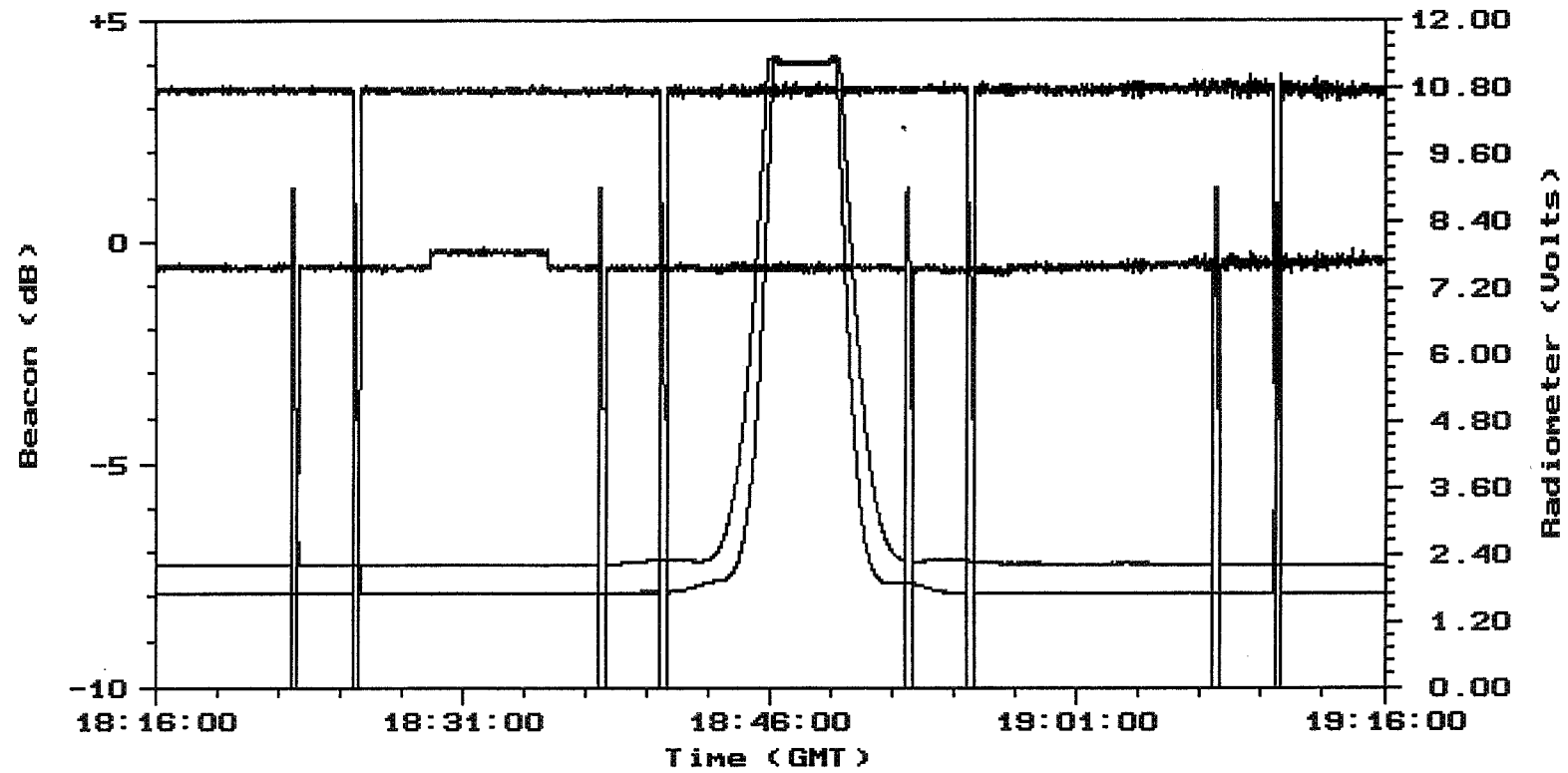
421

FILE

DISPLAY

ZOOM

PAUSE



Source: 940306nm.RVO

- 20 G Beacon ()
- 16:32:00 Beacon ()
- 20 G Radiometer
- 27 G Radiometer

System Status - XXXXXX

RH: XXX % CRG: XXXXX mm/hr
 WS: XXXX m/s TRG: XXXXX mm/hr
 WD: XXX ° OT: XXXXXX °C
 Time: 23:00:01 Date: 05/07/94

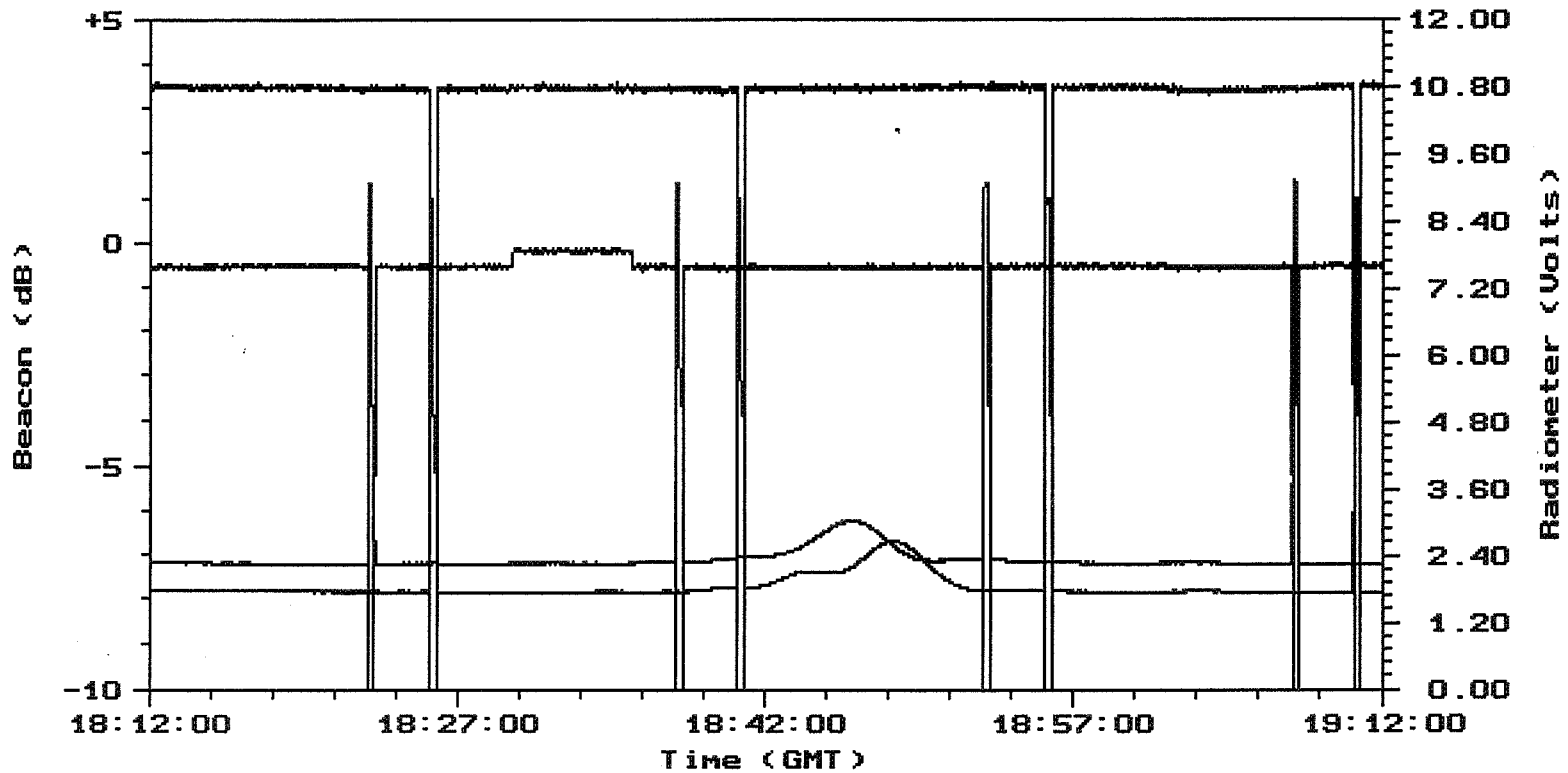
Rd 16:47:00
Spectrum

FILE

DISPLAY

ZOOM

PAUSE



Source: 940309nm.RV0

- 20 G Beacon ()
- 16:32:00con ()
- 20 G Radiometer
- 27 G Radiometer

System Status - XXXXXX

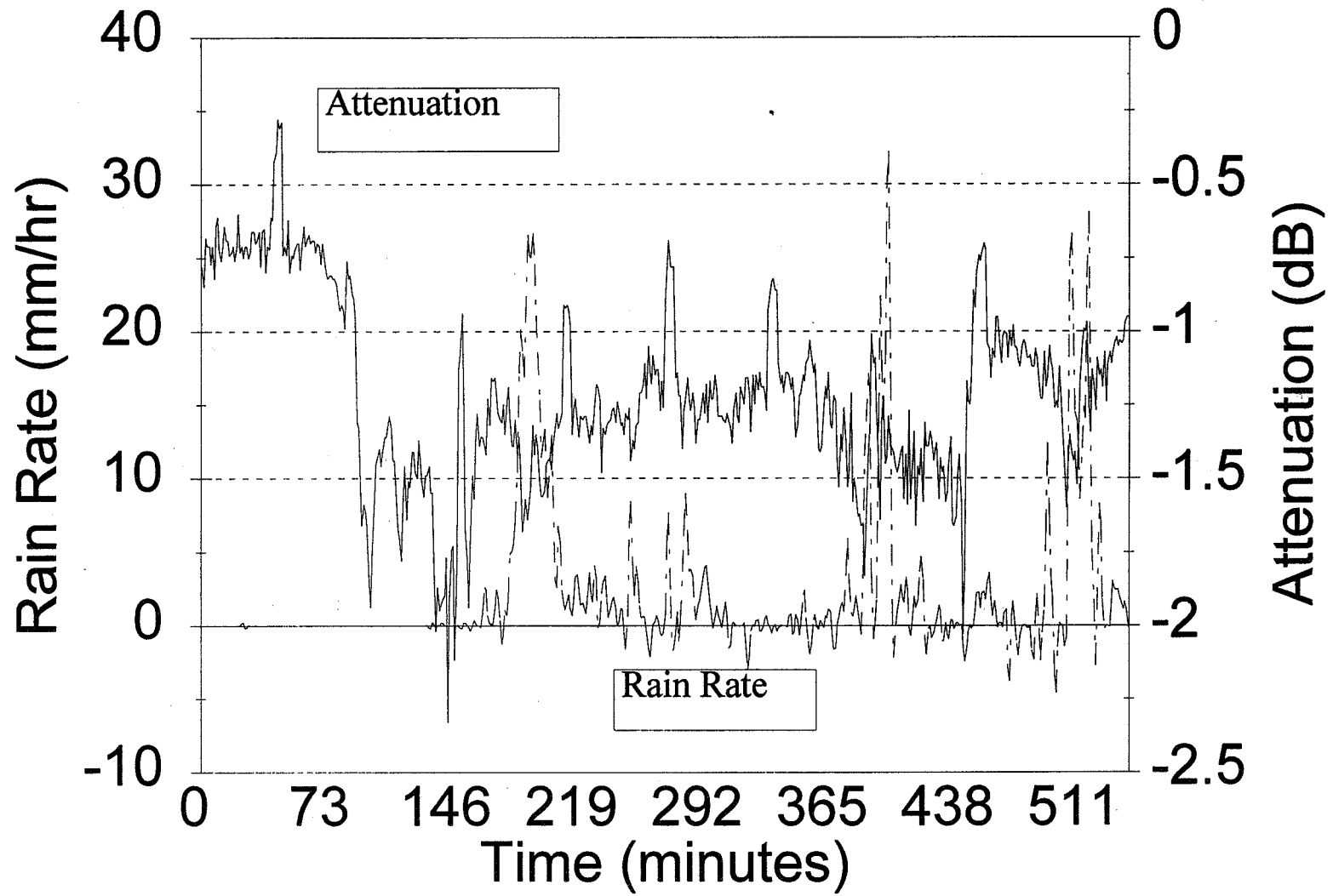
RH: XXX %	CRG: XXXXX mm/hr
MS: XXXX m/s	TRG: XXXXX mm/hr
WD: XXX °	OT: XXXXXX °C
Time: 23:03:14	Date: 05/07/94

Rq16:47:00
Spectrum

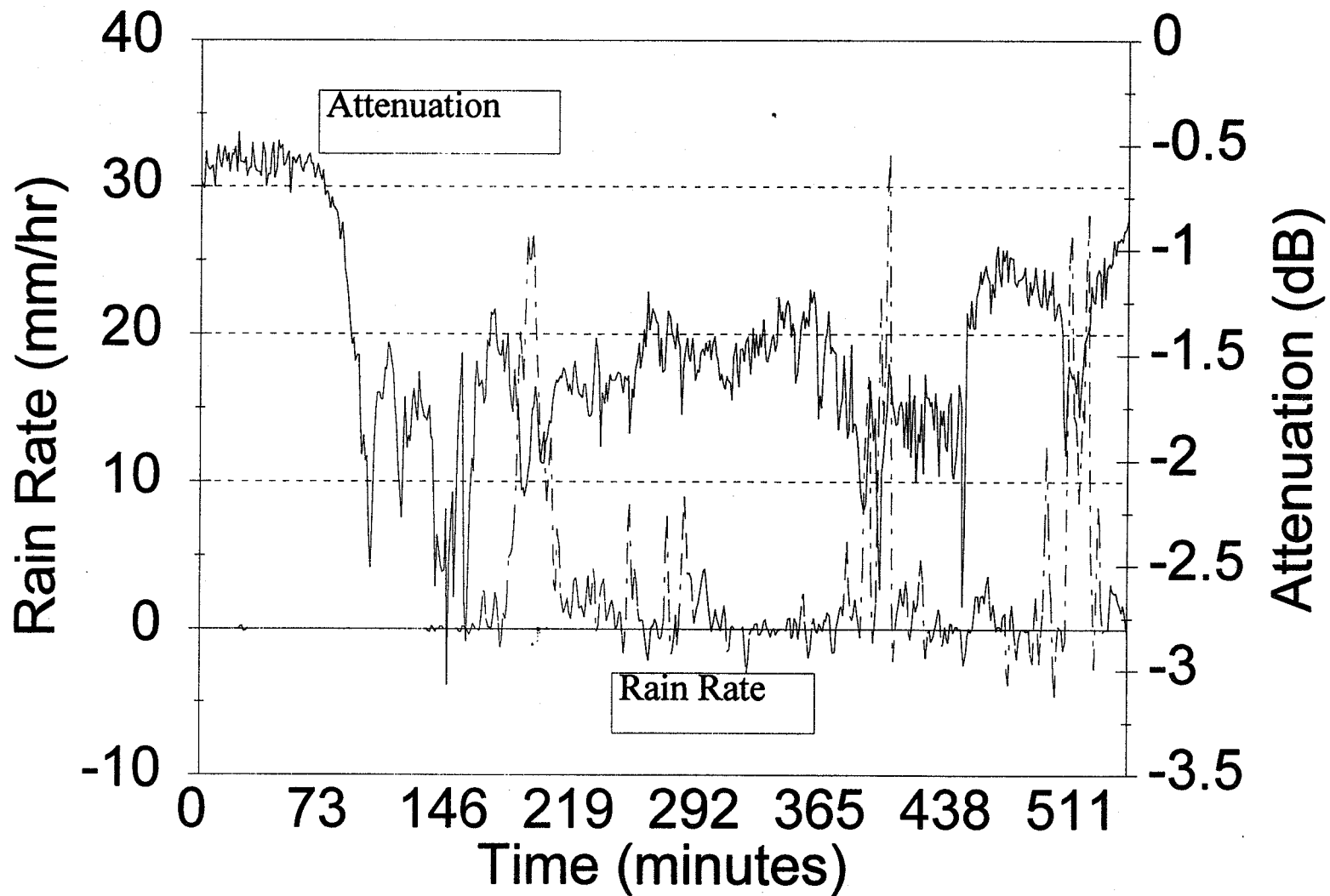
III. RAIN RATE MEASUREMENTS

- Rain gauge did not give reliable results this reporting period
- Tried 2-minute smoothing and numerical fitting for rain rate
- Only one day found with reasonable results - other days the rain reporting did not match fades

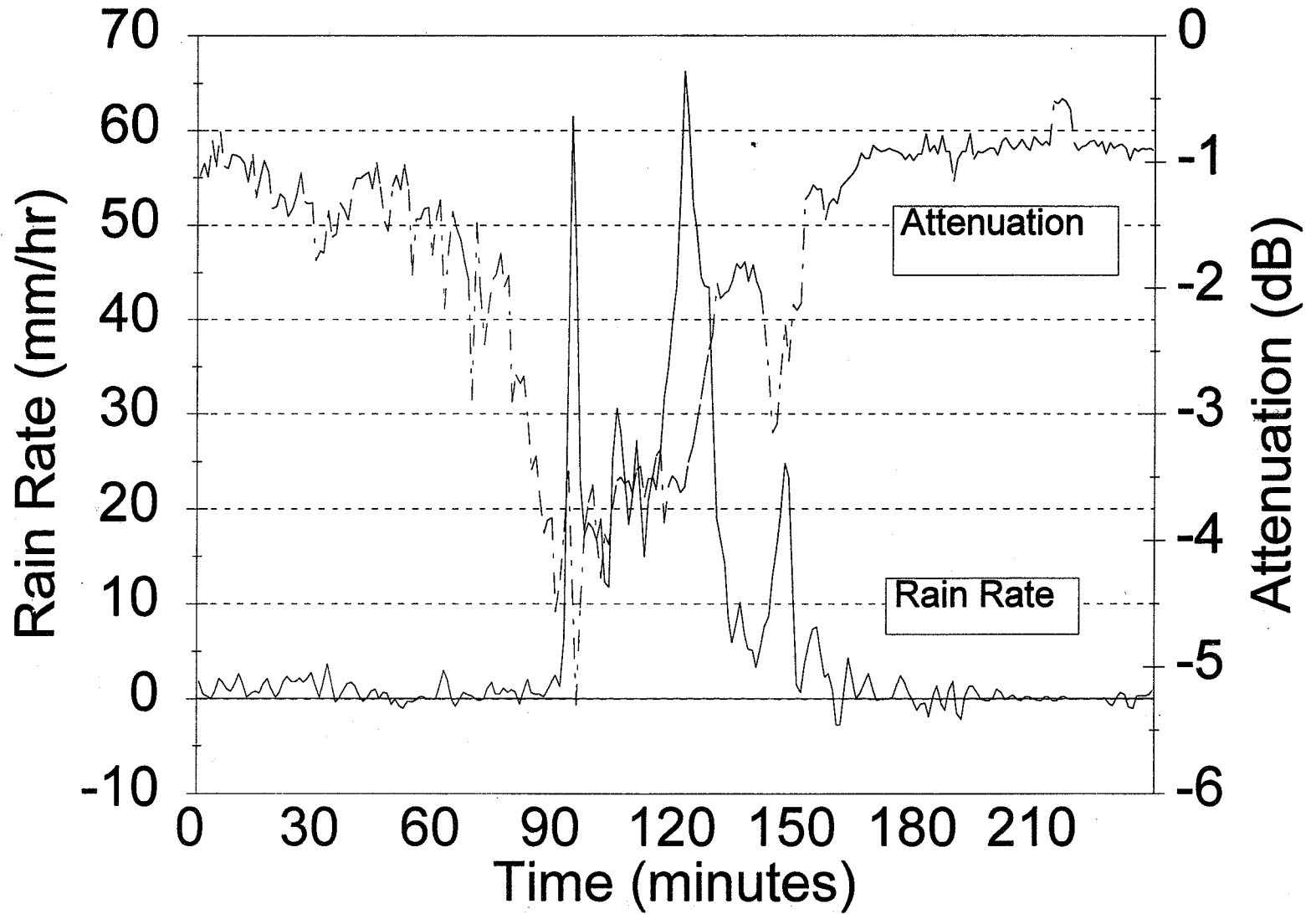
3-14-94 20 GHz



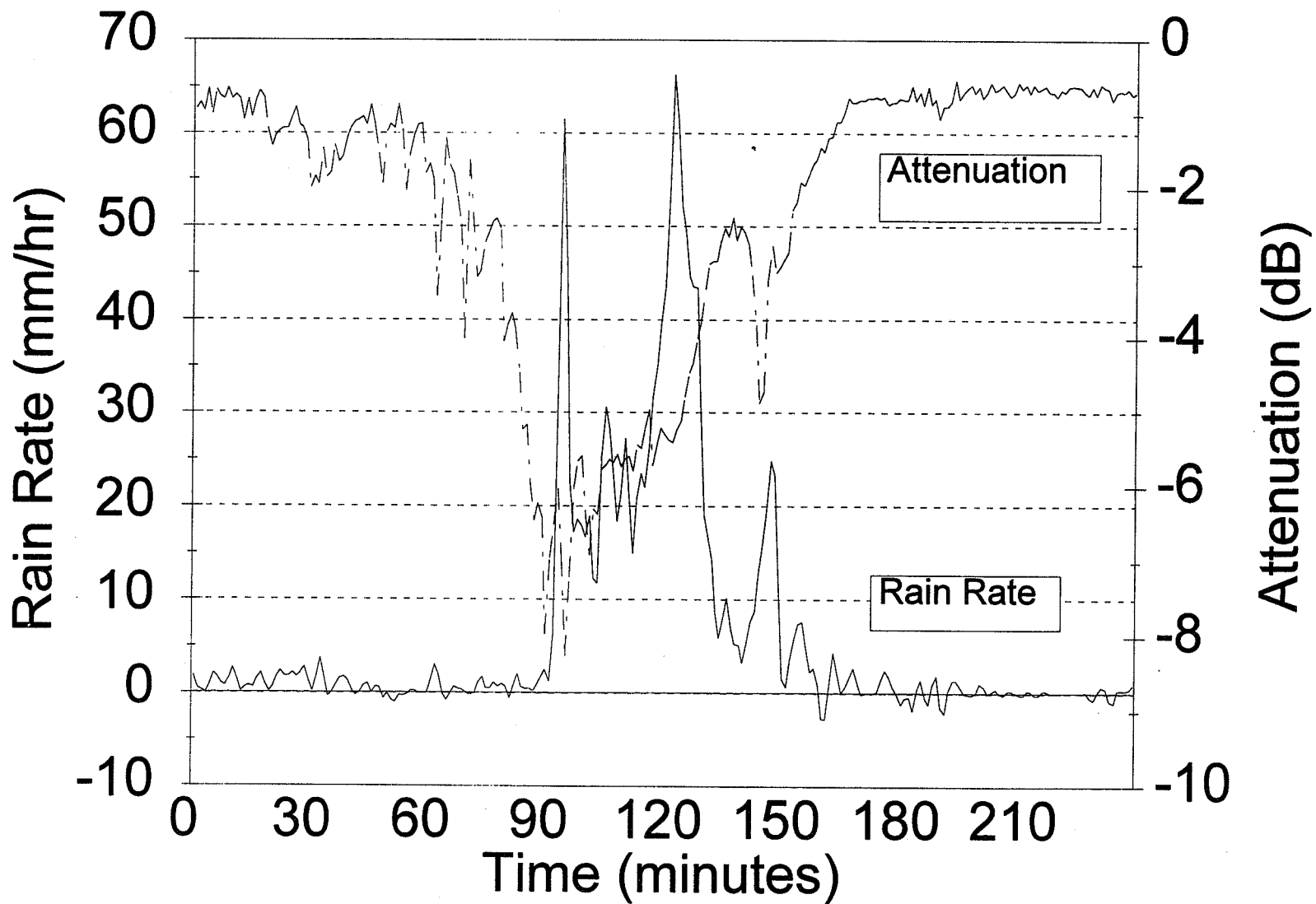
3-14-94 27 GHz



4 June 94; 20 GHz



4 June 94; 27 GHz



Stanford Telecommunications / New Mexico State University

**ACTS PROPAGATION MEASUREMENTS
PROGRAM**

Louis J. Ippolito

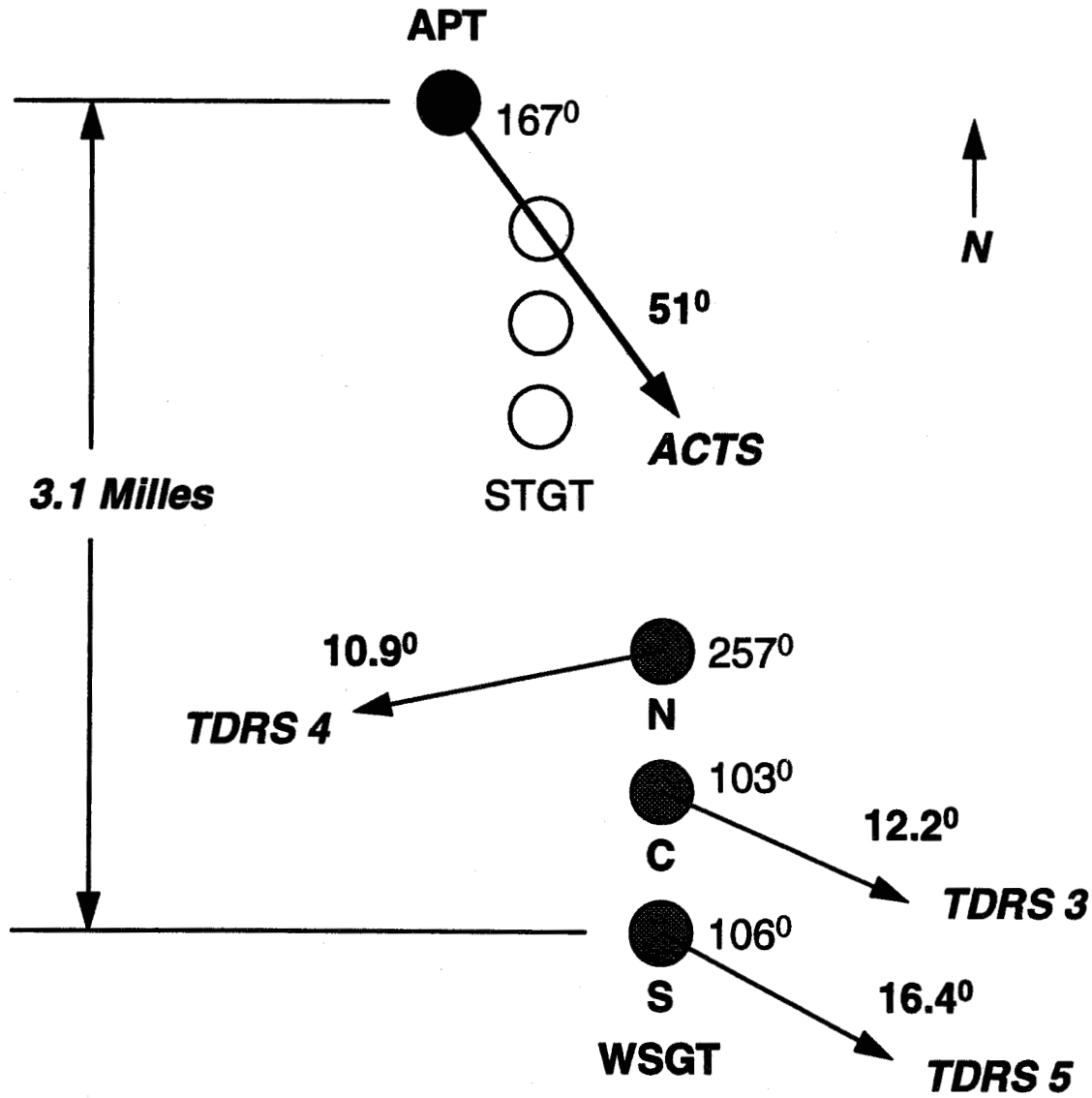
Data Analysis Summary

**NAPEX XVIII
NASA PROPAGATION EXPERIMENTERS MEETING
and
ACTS PROPAGATION STUDIES WORKSHOP
Vancouver, B.C.
June 16, 1994**

MEASUREMENTS

- **ACTS PROPAGATION TERMINAL (APT) AT STGT**
 - **ELEVATION ANGLE ANGLE: 51° TO ACTS**
 -
- **ANCILLARY MEASUREMENTS WITH TDRS**
 - **13.5 GHz SPACE-TO-GROUND LINK (SGL) FADE SUMMARIES FOR 3 ANTENNA SYSTEMS AT WSGT (RAINDANCE)**
 - **ELEVATION ANGLES RANGE FROM 7° TO 18° FOR TDRS CONSTELLATION**

SITE CONFIGURATION

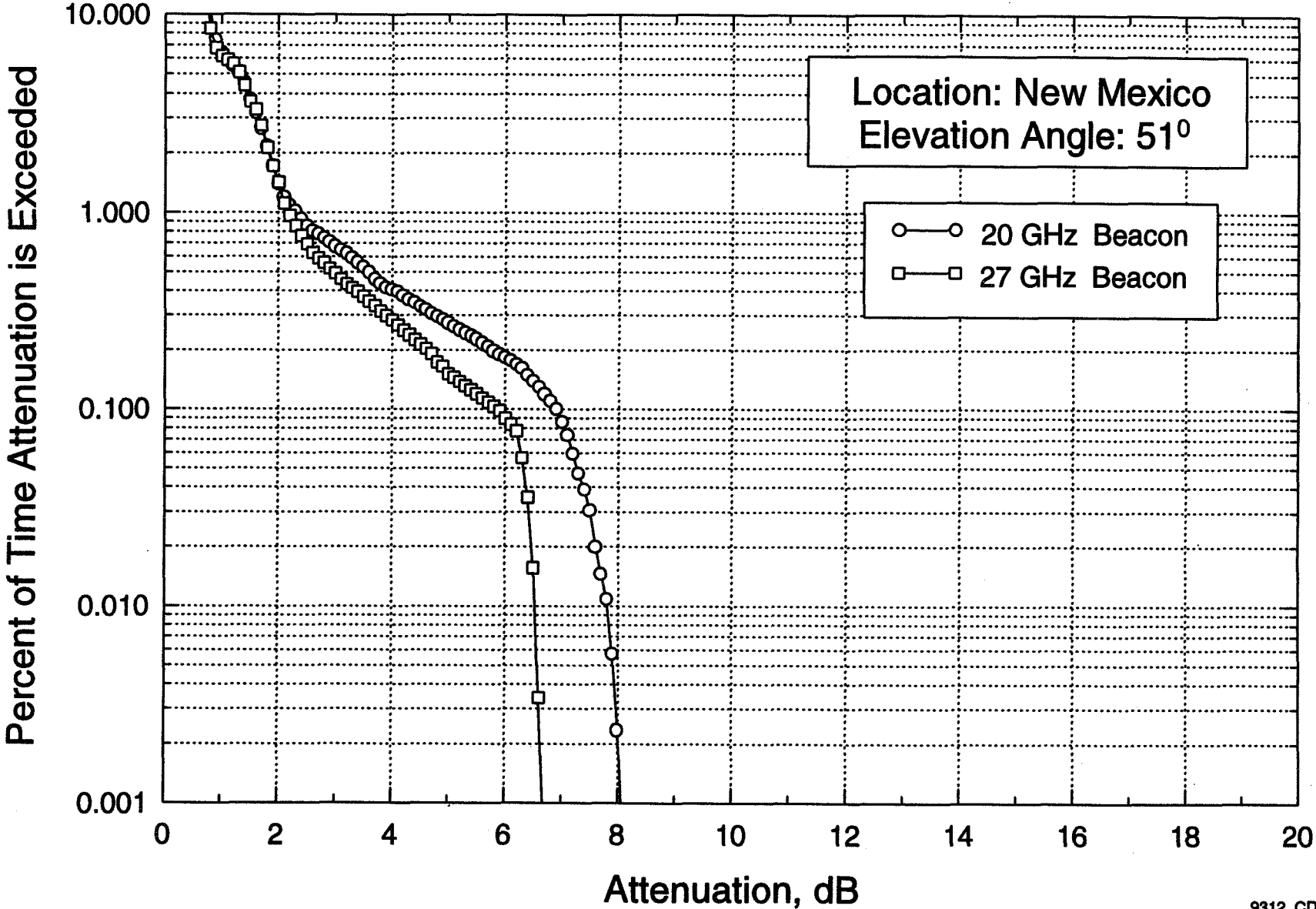


DATA ANALYSIS PRESENTATIONS

- MONTHLY CUMULATIVE DISTRIBUTIONS
- 4-MONTH CUMULATIVE DISTRIBUTIONS
- SUN PASS EVENTS, MARCH 1994
- ACTS \ TDRS FADE EVENTS
- ACTS \ TDRS CDF EXTRAPOLATIONS

Monthly Cumulative Distributions

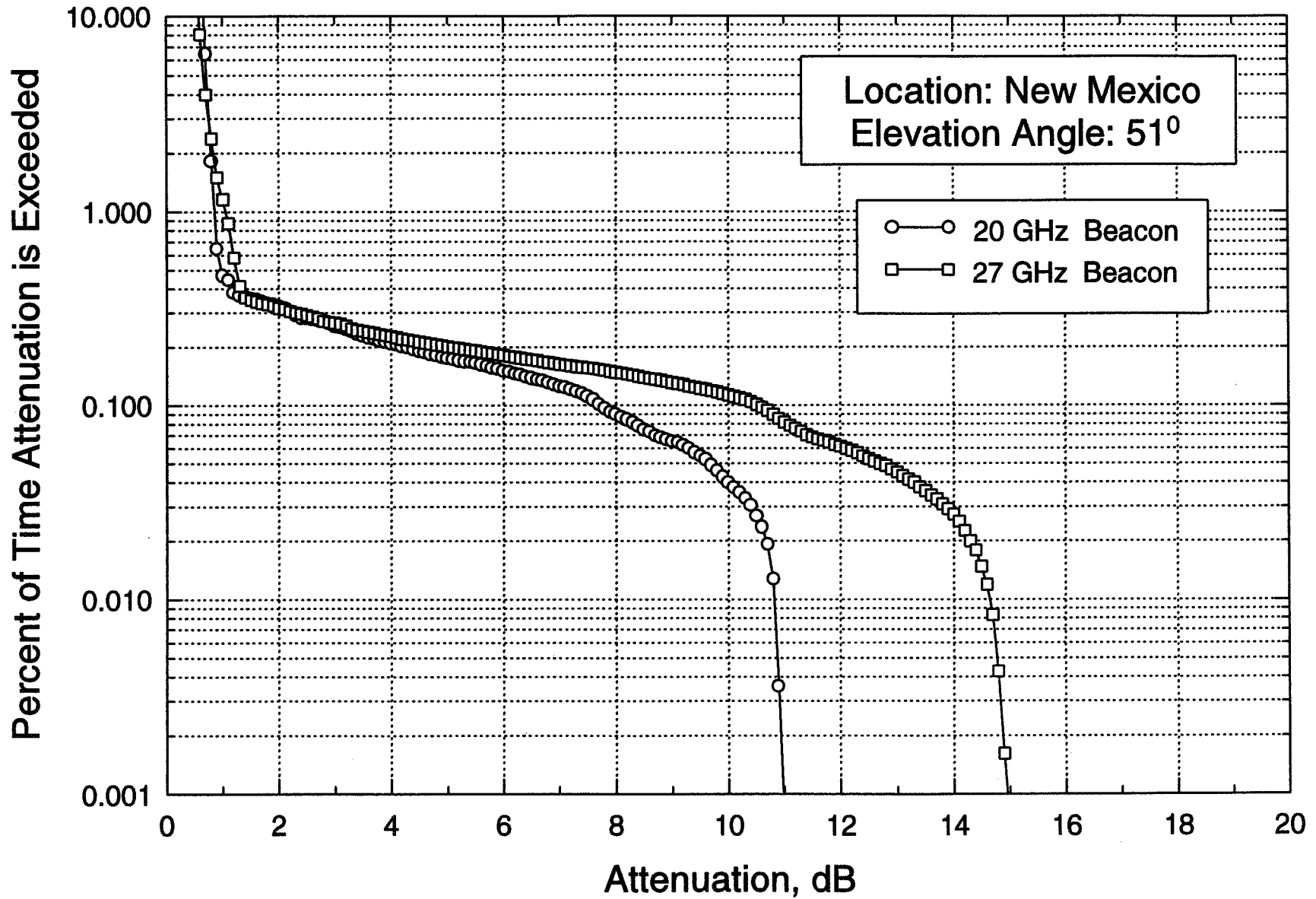
December 1993



433

Monthly Cumulative Distributions

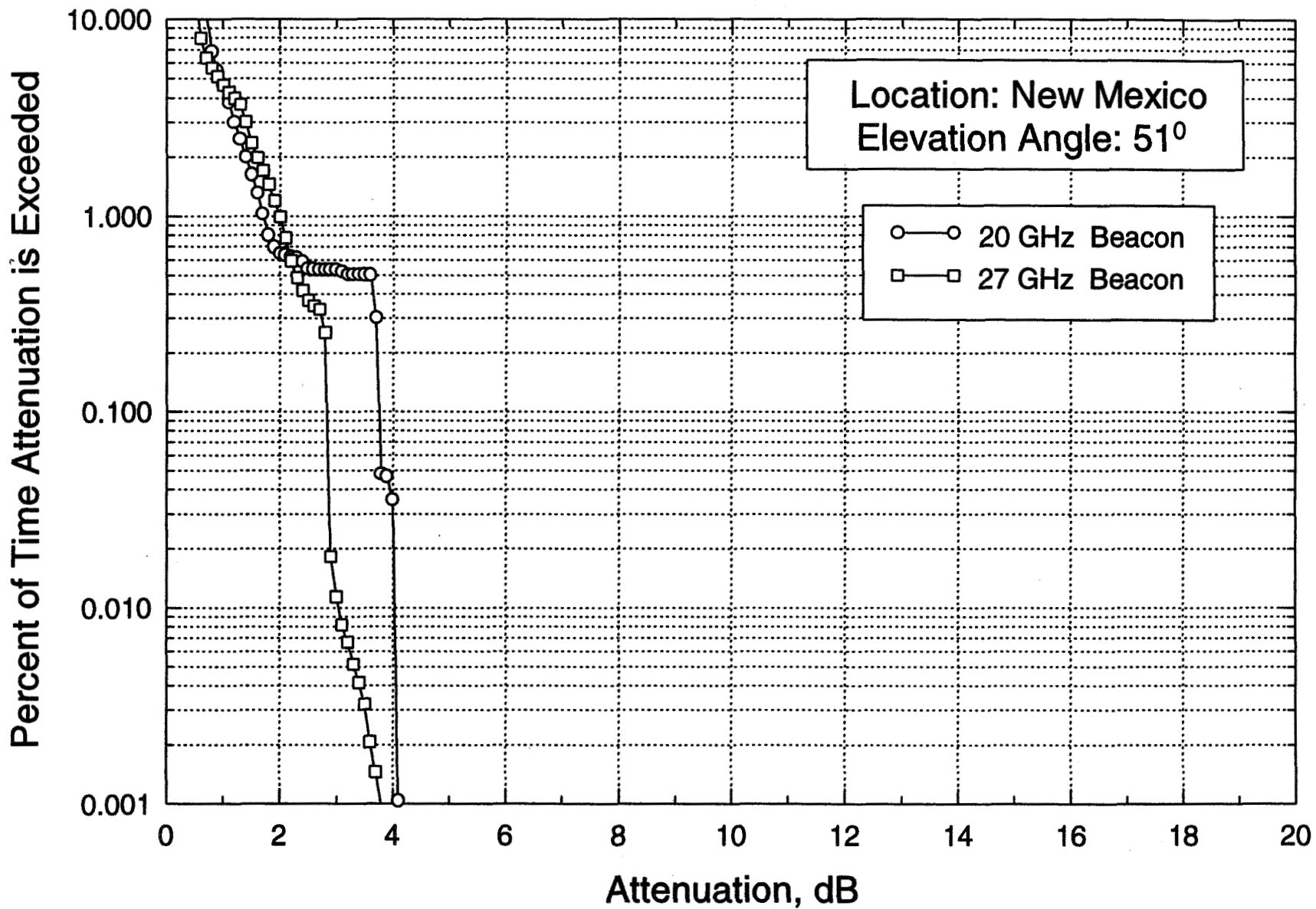
January 1994



434

Monthly Cumulative Distributions

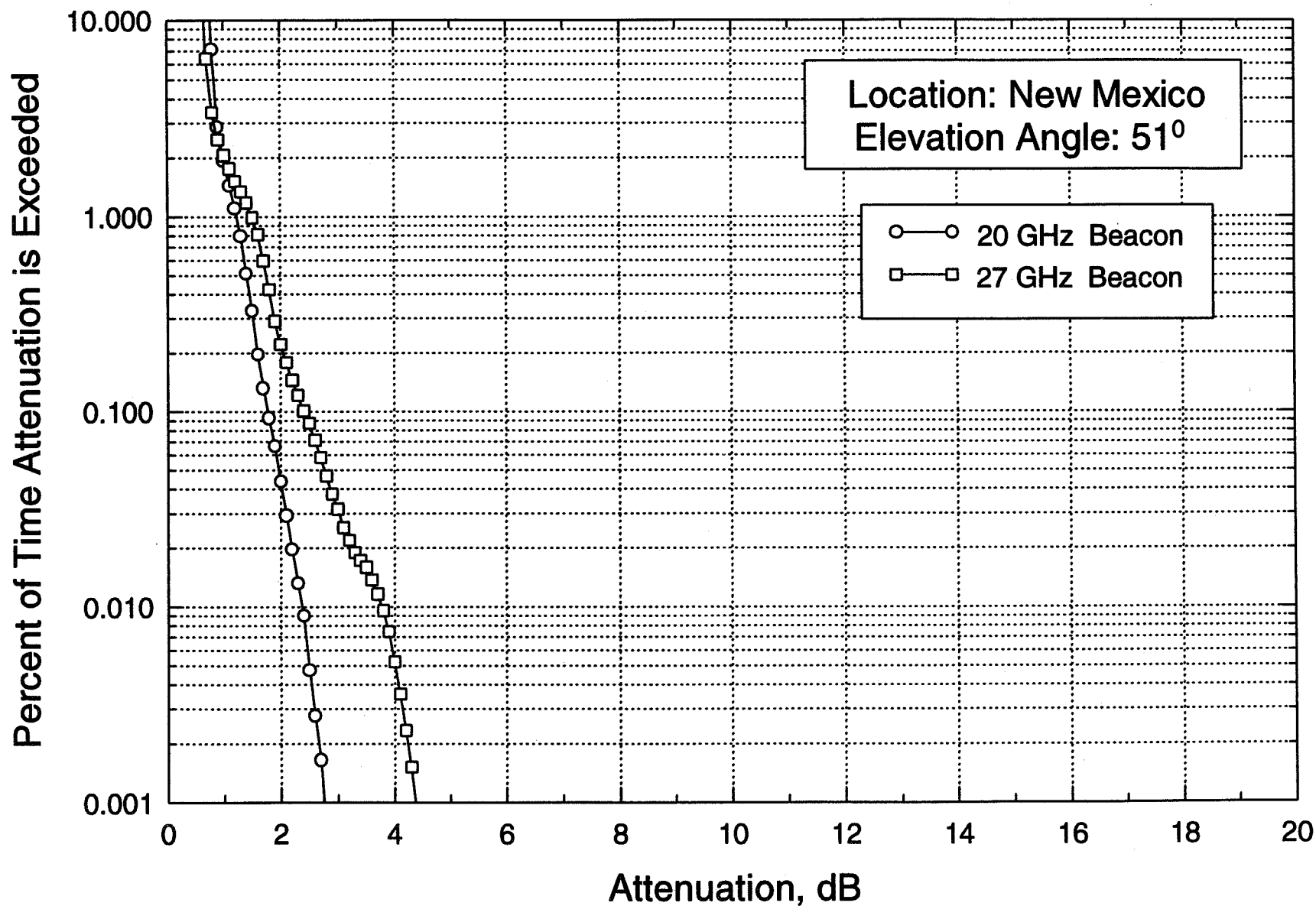
February 1994



435

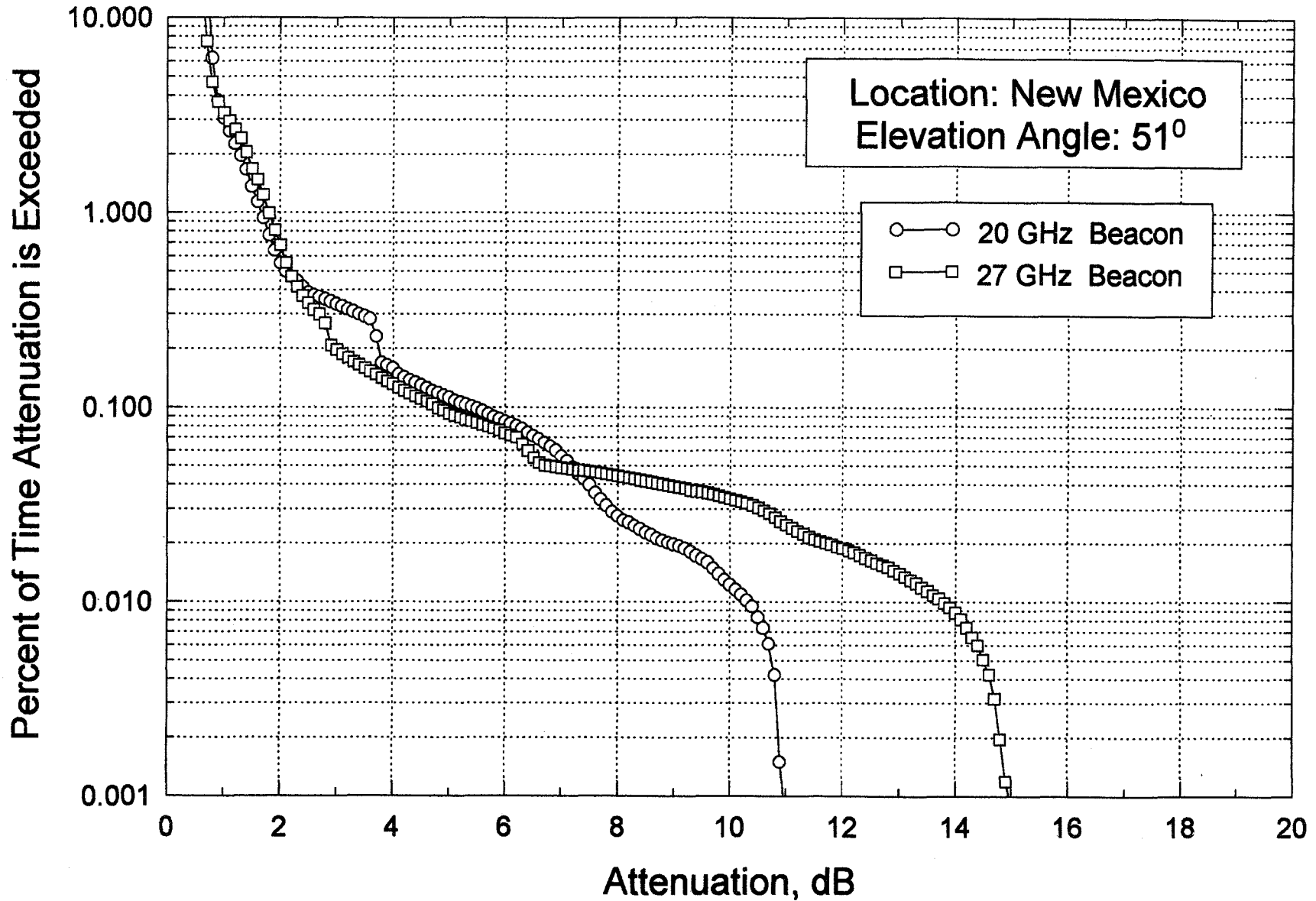
Monthly Cumulative Distributions

March 1994



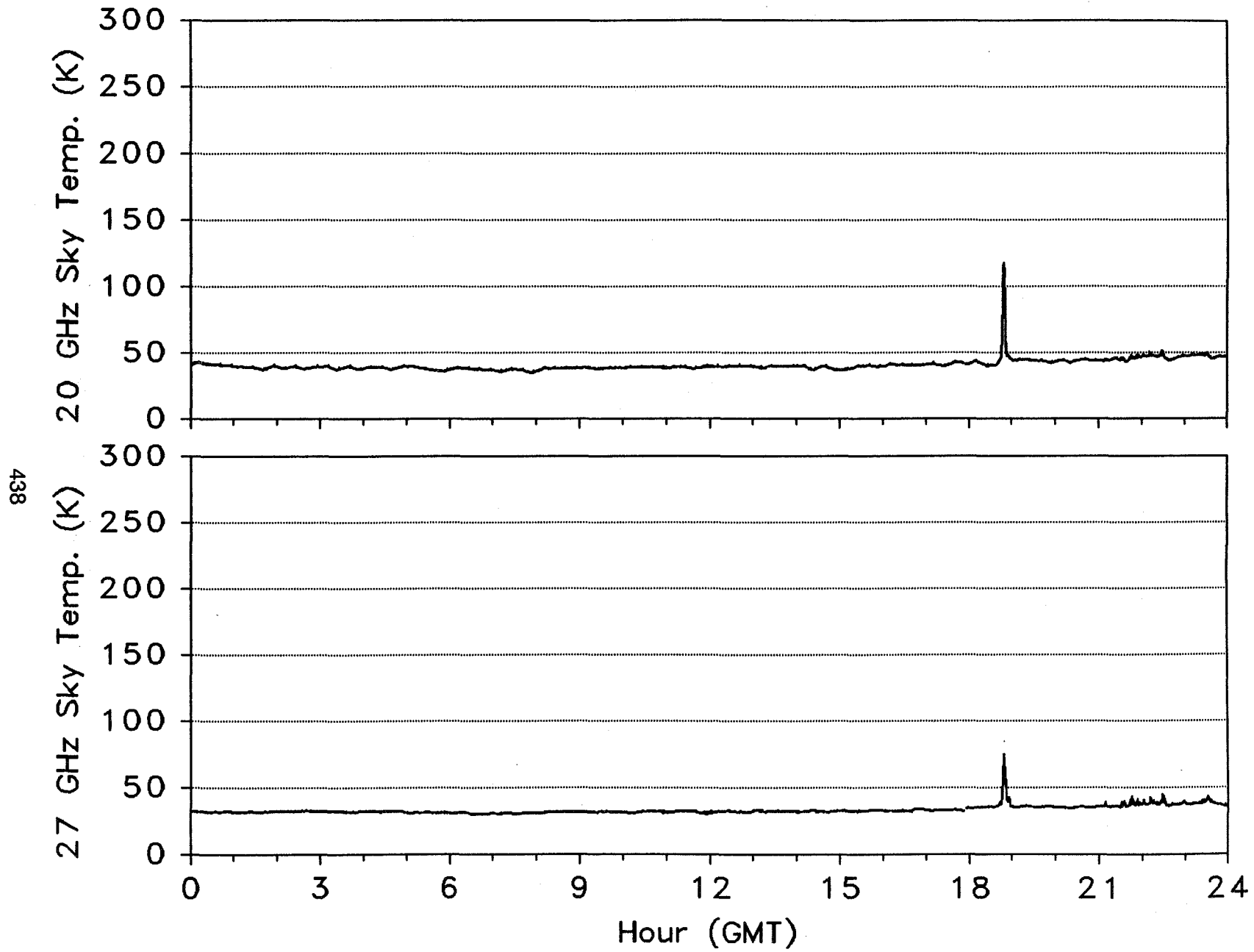
436

Four-Month Cumulative Distribution December 1993 - March 1994



437

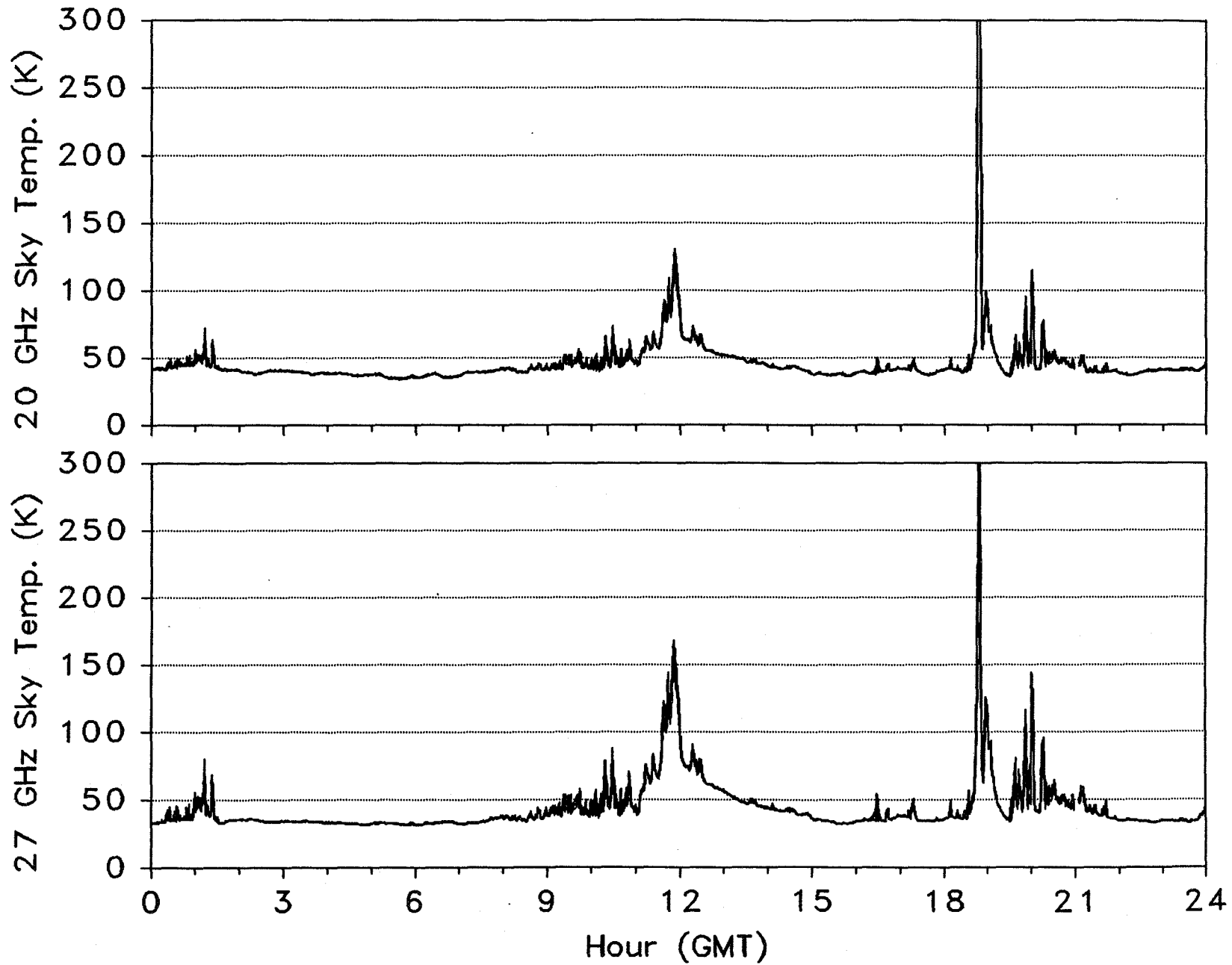
Propagation Data from the ACTS Experiment (NM)



4 March 1994

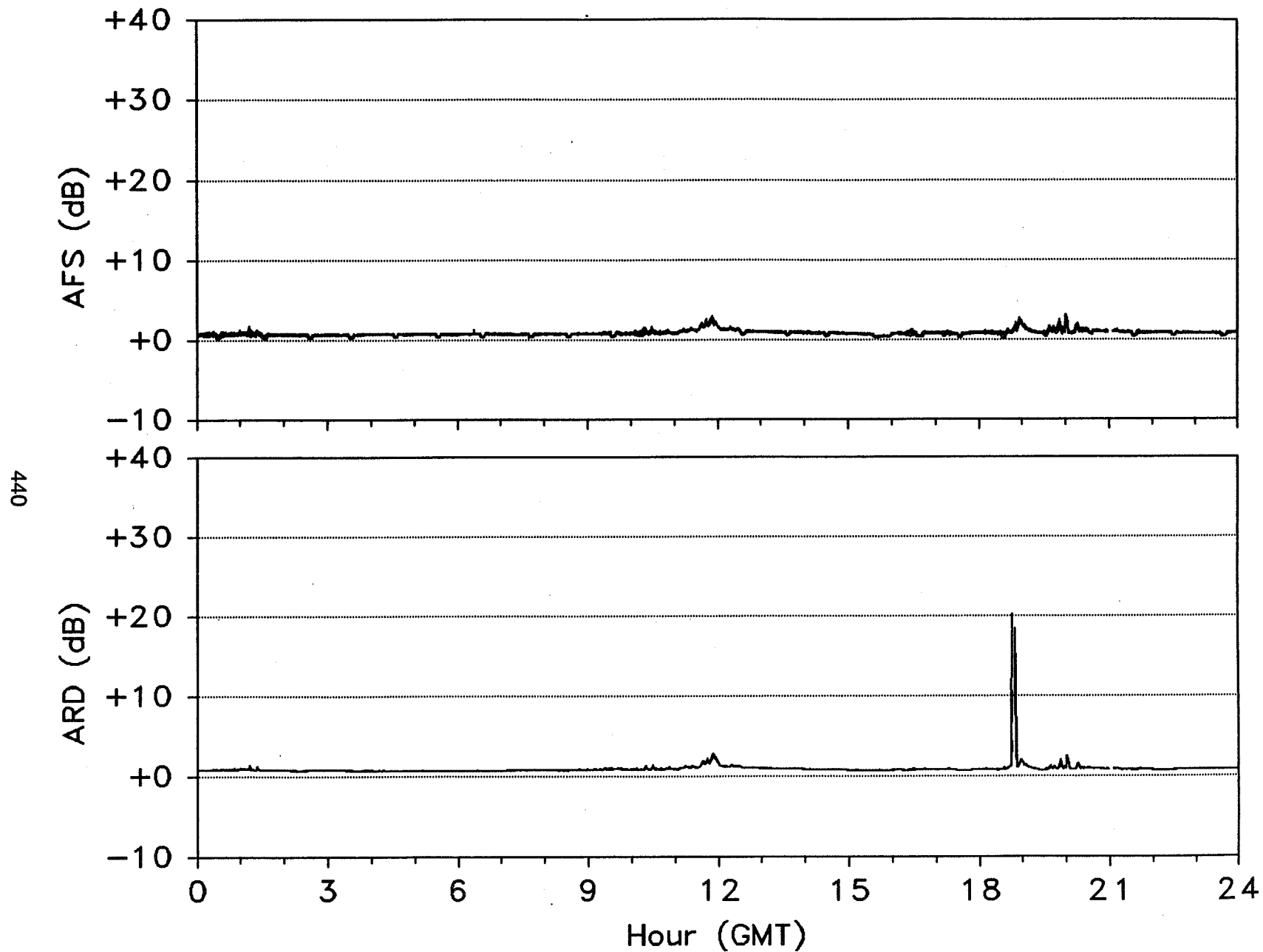
Propagation Data from the ACTS Experiment (NM)

439



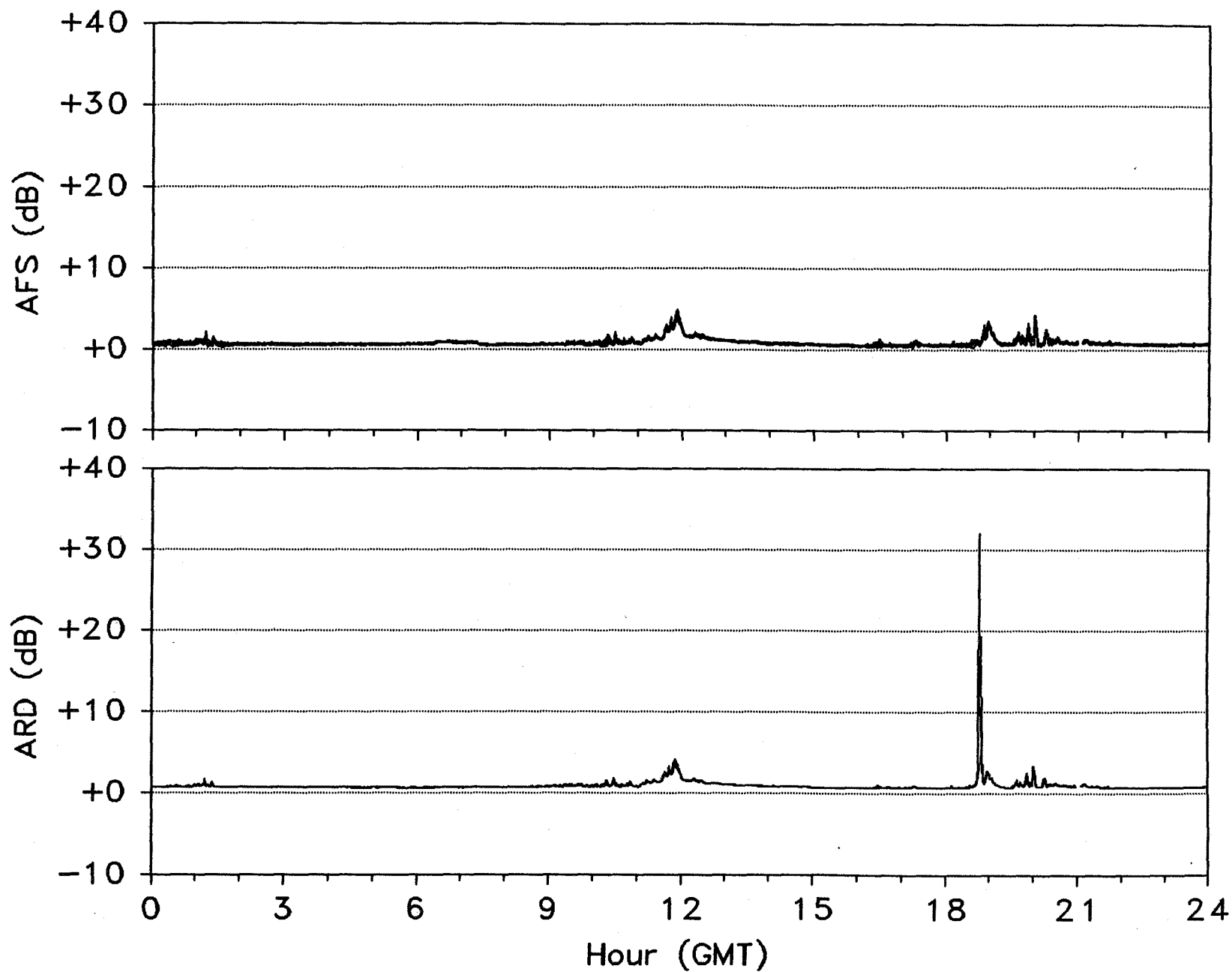
8 March 1994

20 GHz Propagation Data from the ACTS Experiment (NM)



8 March 1994

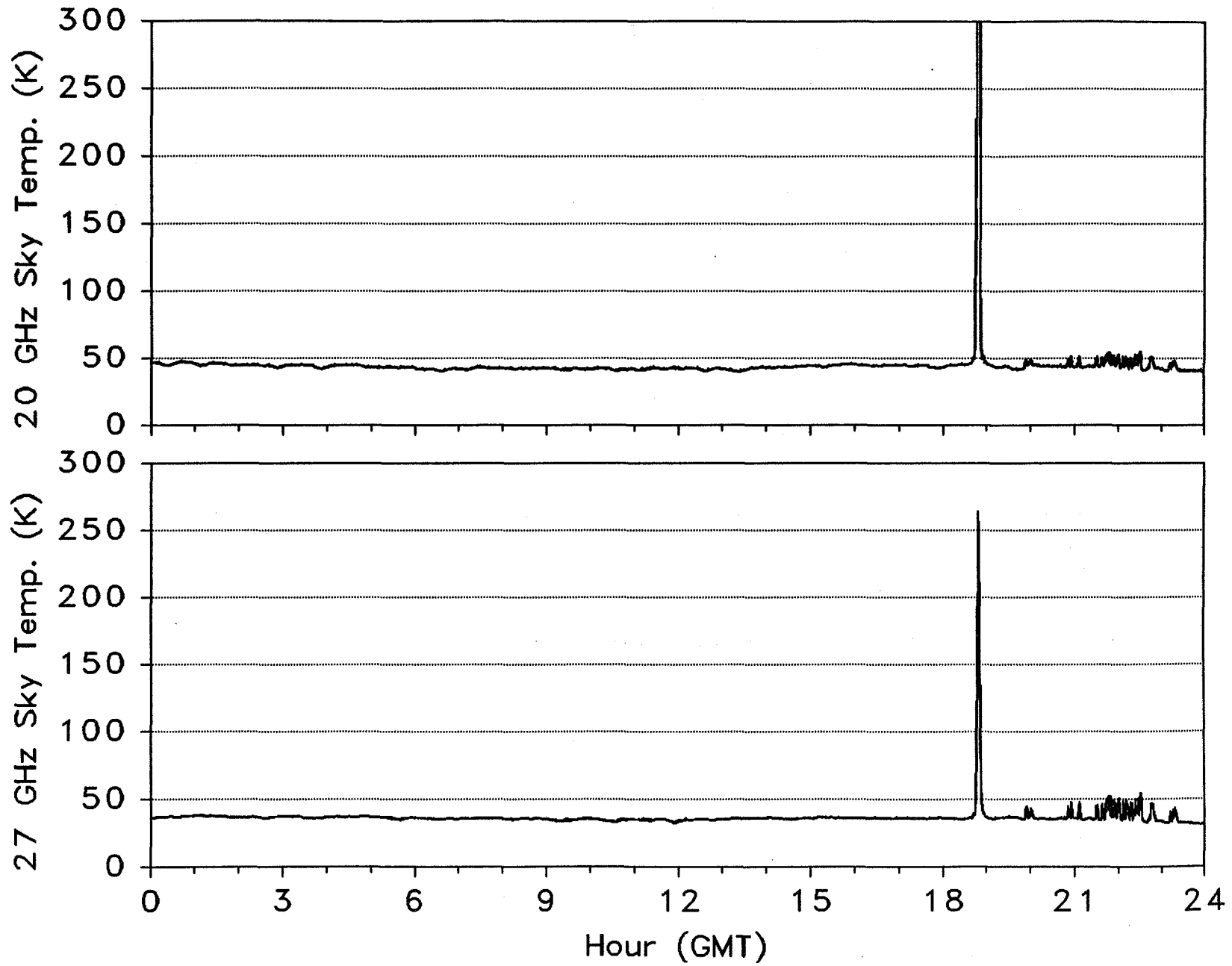
27 GHz Propagation Data from the ACTS Experiment (NM)



8 March 1994

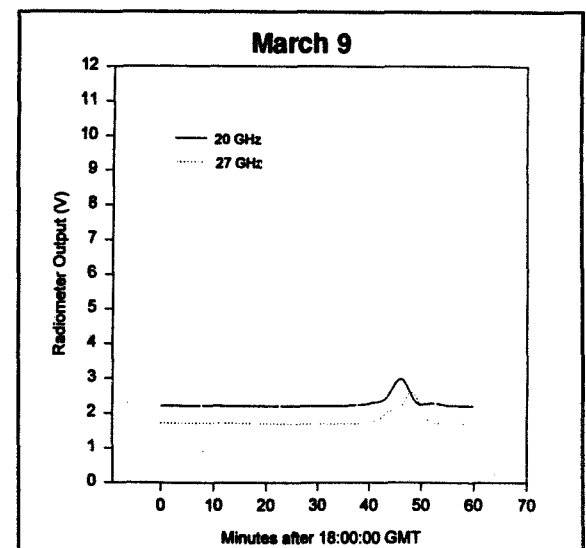
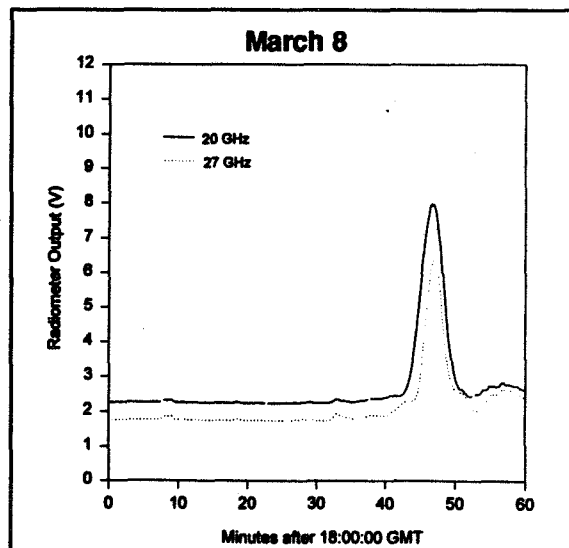
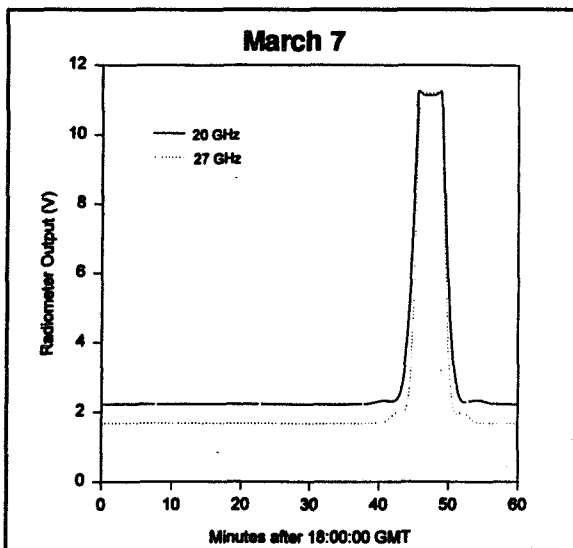
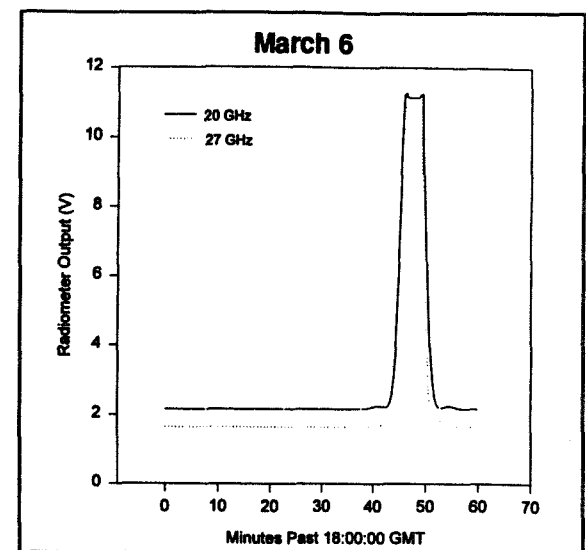
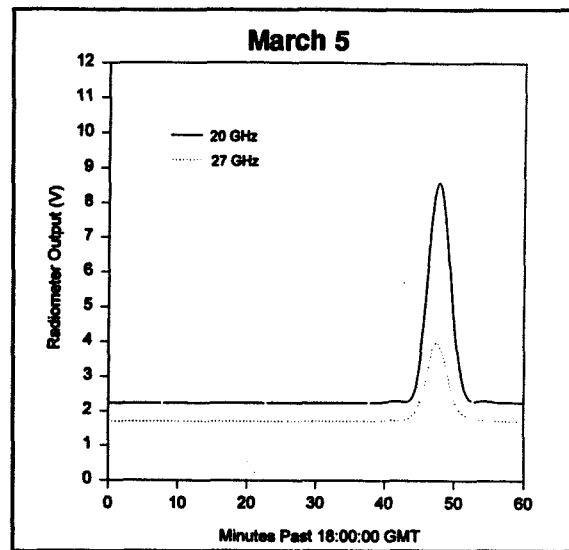
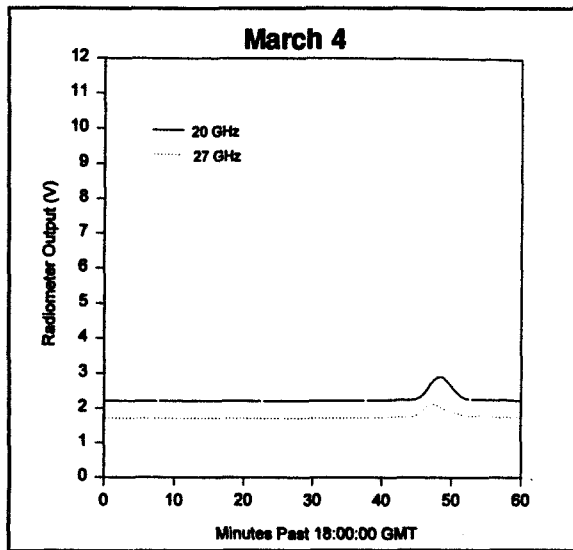
Propagation Data from the ACTS Experiment (NM)

442



5 March 1994

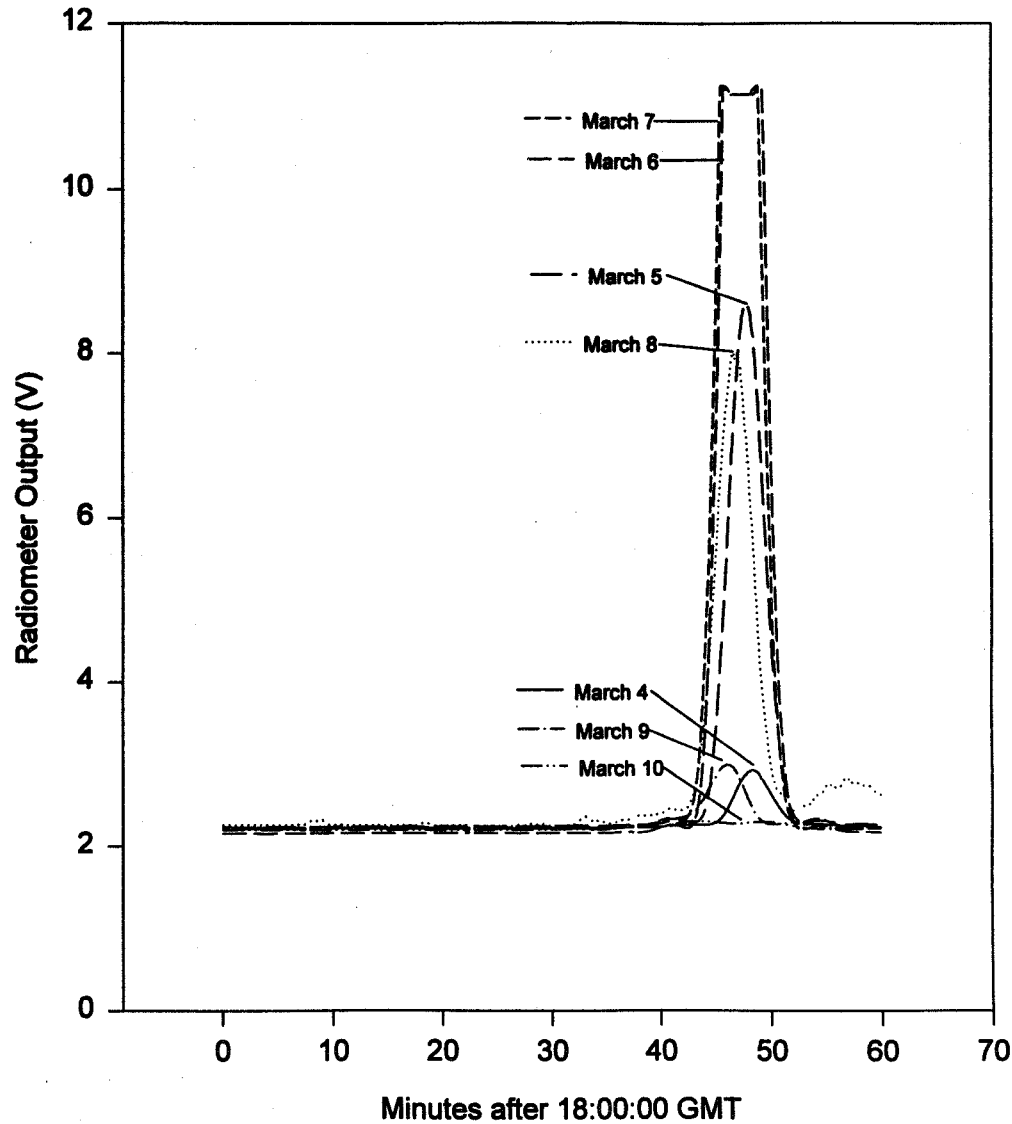
Summary of Sun Pass, March 1994



443

Summary of Sun Pass, March 1994

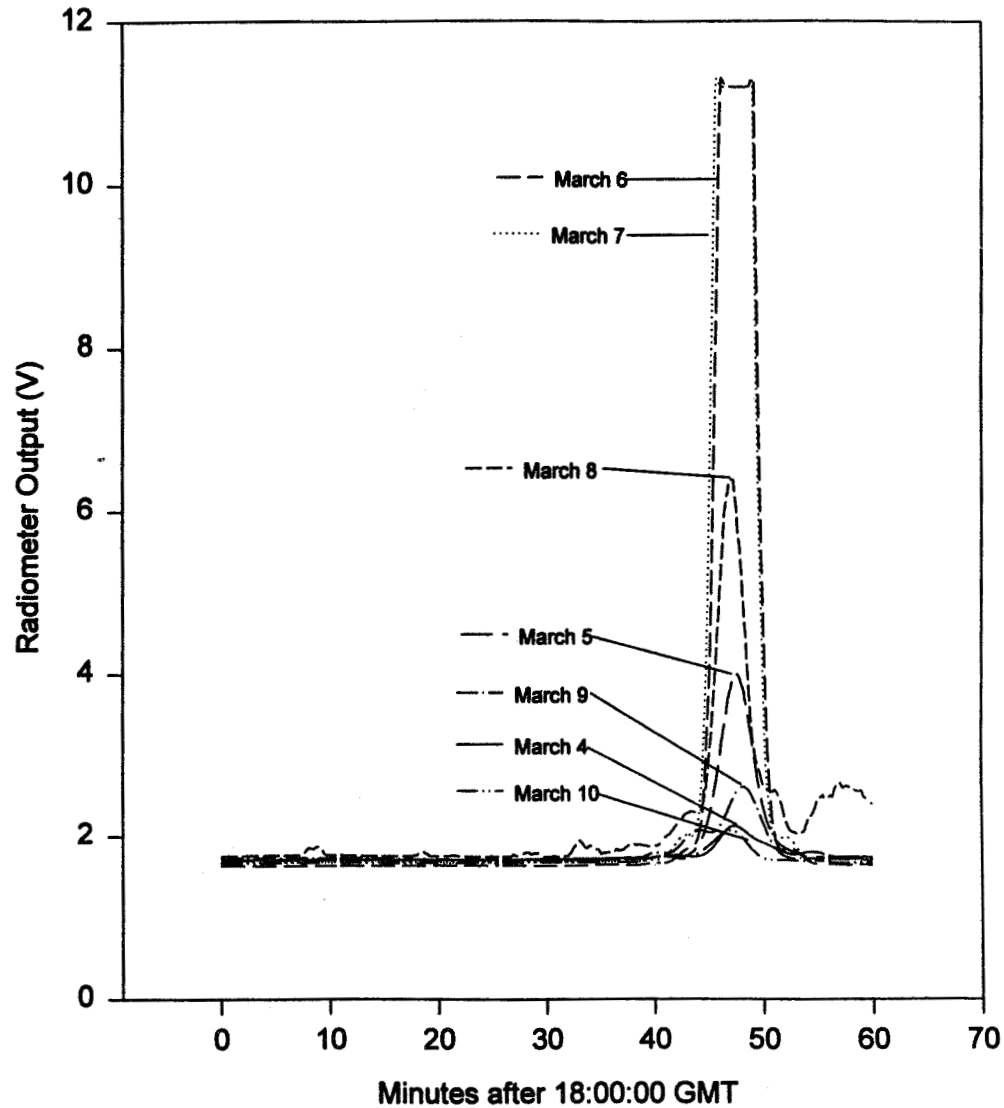
Comparison of 20GHz



444

Summary of Sun Pass, March 1994

Comparison of 27GHz



445

Summary of Sun Pass, March 1994

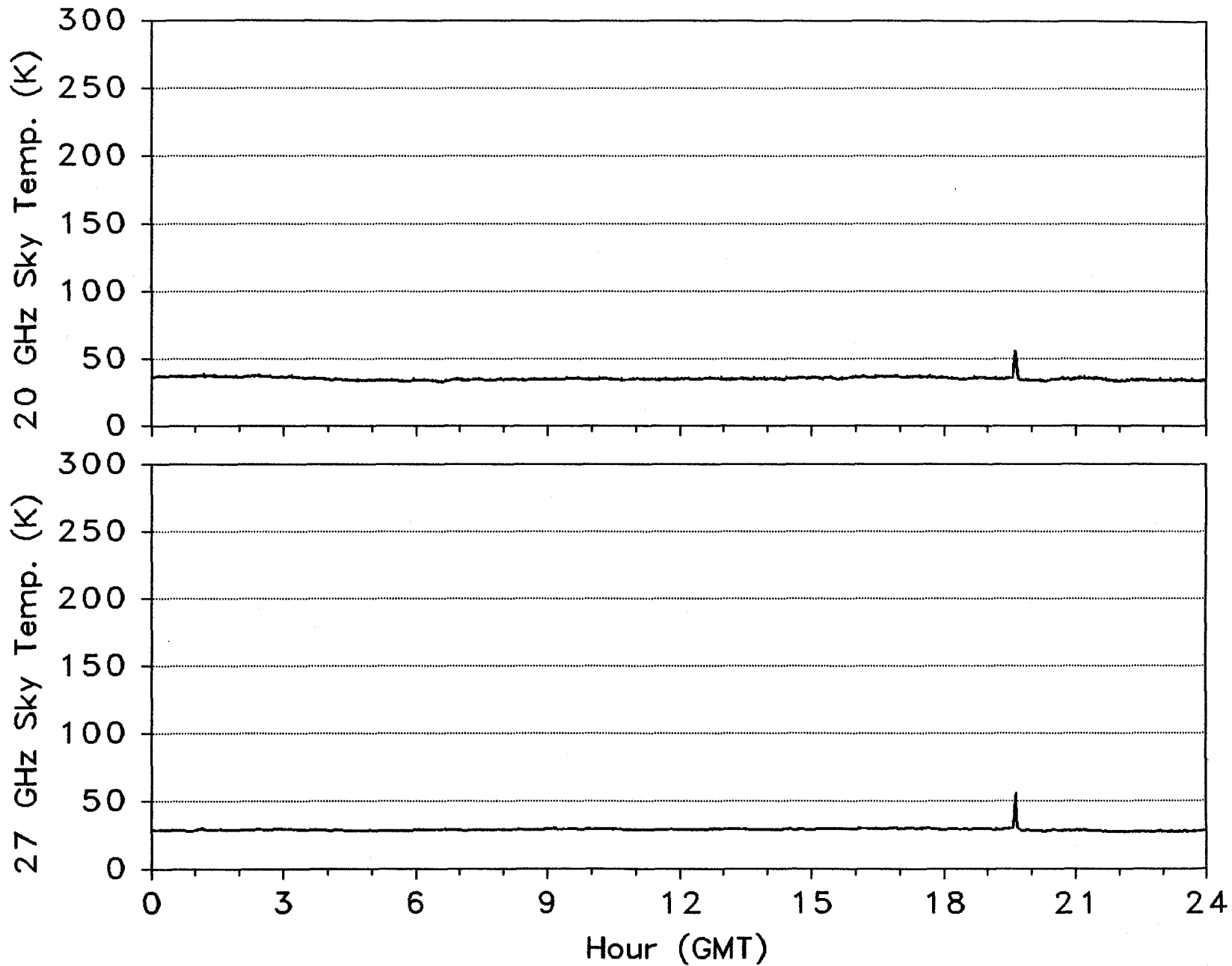
Location: New Mexico

Date	20 GHz				27 GHz				27 GHz Lead Time
	Duration	3-dB Time	Peak Time	Peak Temp.	Duration	3-dB Time	Peak Time	Peak Temp.	
3-4	6:35	3:50	18:48:25	120K	7:35	4:25	18:47:20	75K	0:00:55
3-5	8:50	5:50	18:47:45	400K	9:35	3:25	18:47:35	270K	0:00:10
3-6	11:40	5:00	18:47:30	> 450K	11:50	4:10	18:47:35	> 450K	-0:00:05
3-7	11:45	5:00	18:47:15	> 450K	13:05	4:20	18:47:10	> 450K	0:00:05
3-8	14:35	3:45	18:46:50	350K	15:50	2:50	18:47:10	300K	-0:00:20
3-9	8:45	3:45	18:46:10	120K	11:35	3:40	18:48:05	125K	-0:01:50
3-10	2:15	xx	18:43:40	50K	6:30	xx	18:47:05	70K	-0:03:25

446

Propagation Data from the ACTS Experiment (NM)

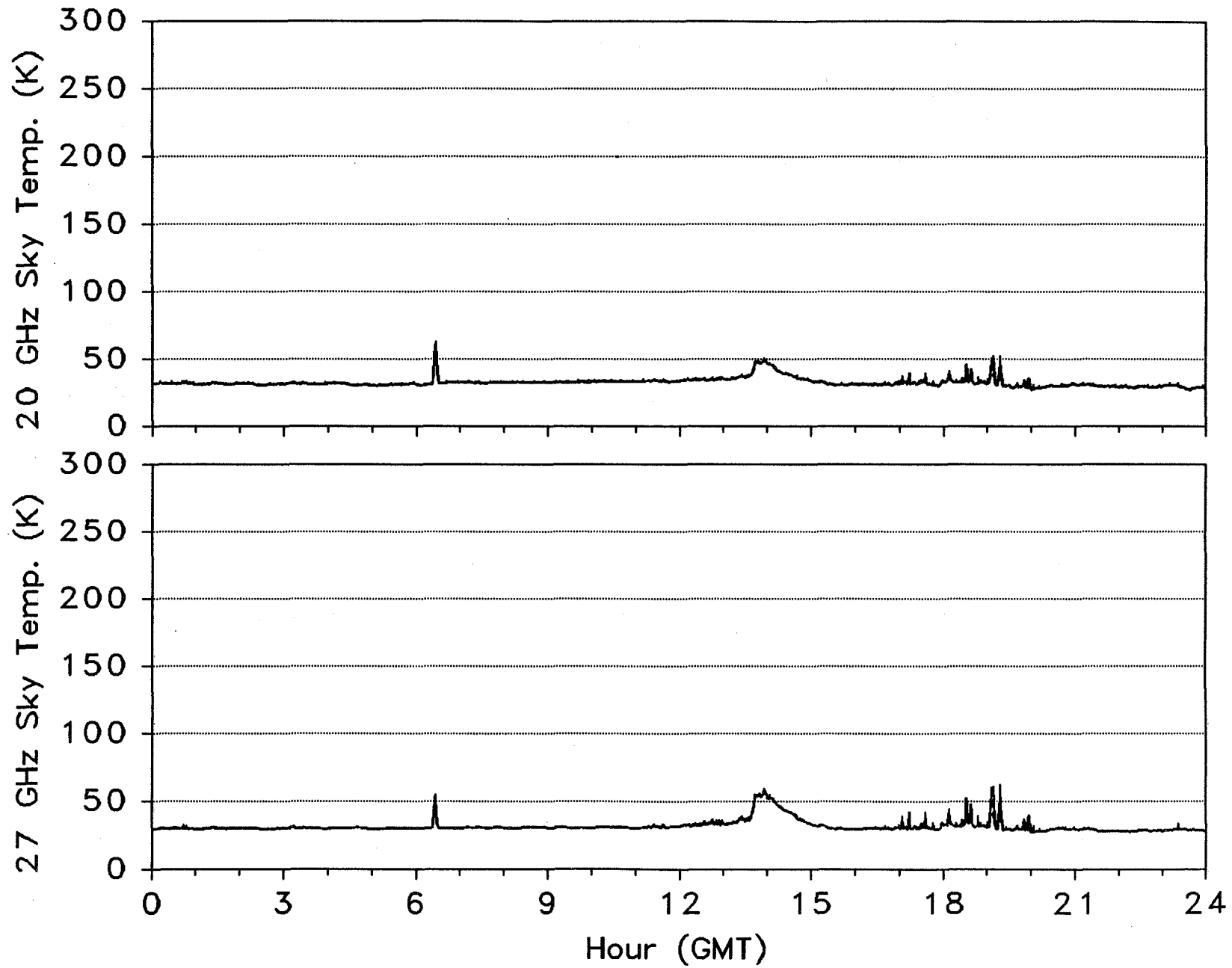
447



11 February 1994

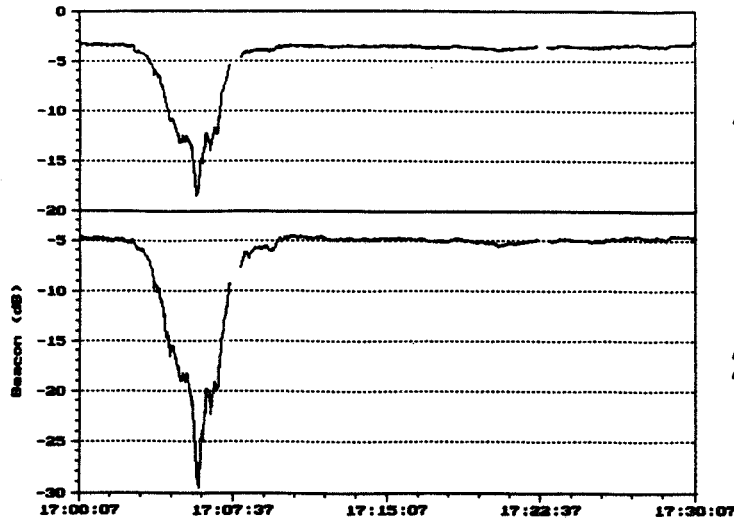
Propagation Data from the ACTS Experiment (NM)

448



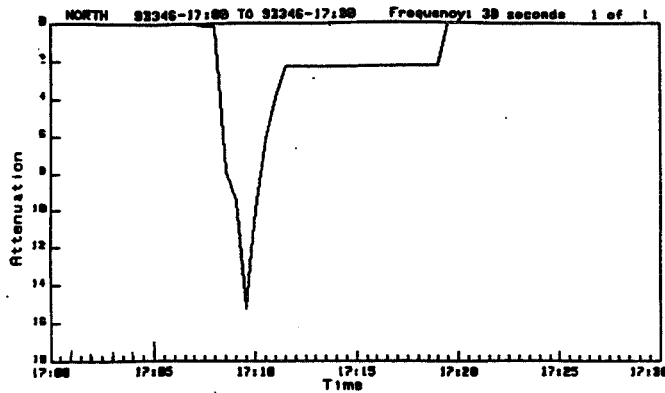
27 March 1994

RAIN EVENT, WHITE SANDS GROUND TERMINALS, Dec. 12, 1993

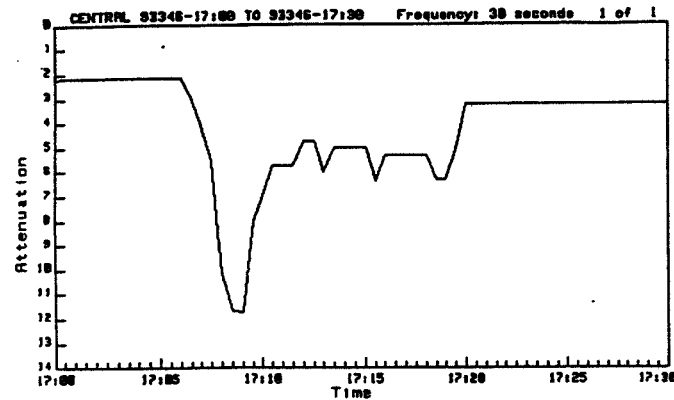


20 GHz

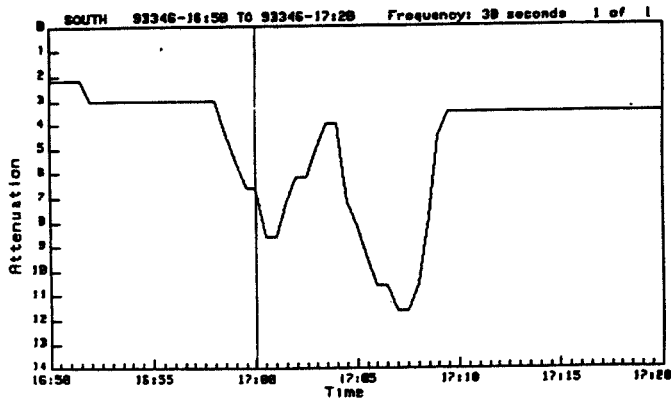
27 GHz



13.5 GHz N



13.5 GHz C

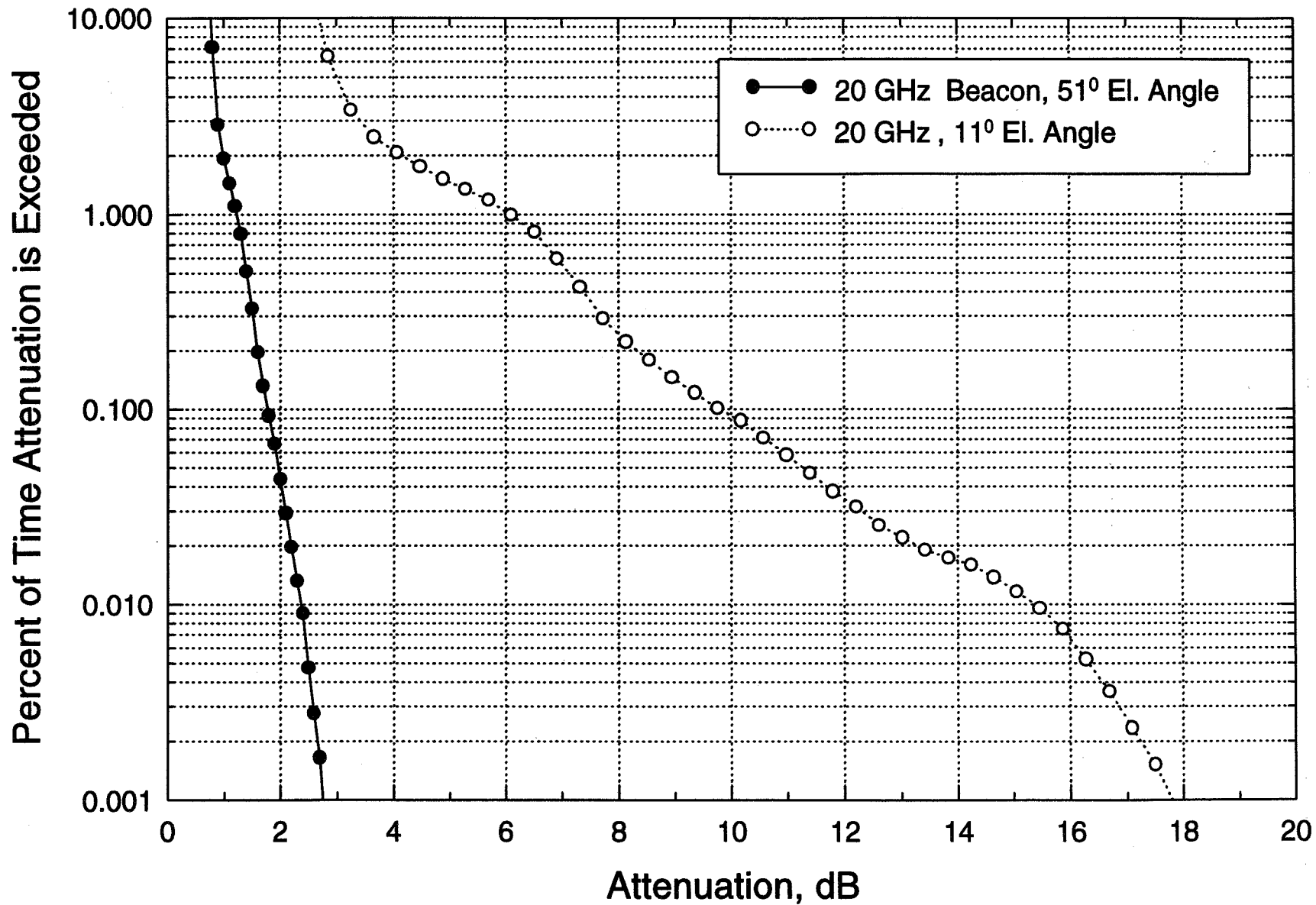


13.5 GHz S

EXTENSION OF ACTS MEASUREMENTS TO TDRS LINKS

March 1994

450



PLANS FOR NEXT REPORTING PERIOD

- RESOLUTION OF 'RAINDANCE" DATA TIME TAGS AND EVENT ANALYSES WITH ACTS DATA
- GENERATION OF DYNAMIC FADE STATISTICS FOR AVAILABLE DATA FILES
- FURTHER MODEL DEVELOPMENT AND SIMULATIONS FOR LOW ELEVATION ANGLE AND VARIABLE ELEVATION ANGLE STUDIES
- EVALUATION OF RAIN RATE MEASUREMENTS AND INCLUSION IN DATA STATISTICS
- DEVELOPMENT OF LONG TERM STATISTICS MODELING FOR TDRS LINKS

Georgia Tech ACTS Experiments

by

Daniel Howard

NOTE:

Georgia Tech has only recently joined the ACTS Propagation experimenter community. Consequently, no presentation was scheduled for Georgia Tech in this meeting. However, the following two charts have been provided to us for inclusion in the Proceedings by Daniel Howard, the principal investigator at Georgia Tech.

Georgia Tech ACTS Experiments

Daniel Howard

Assemble transmit/receive earth station from spare parts from Lewis and Ga Tech for a Class II Experiment

Use standard and custom waveform generation and reception equipment to perform RF Tests & Measurement through MSM in Loopback Mode

- Analog Measurements (ETE Noise Figure, Frequency and Phase Response, etc.)
- Digital Measurements (BER, Jitter, etc.)

Correlate RF signal measurements with weather data

- Use same weather monitoring equipment as Class I Experiments if possible
- Augment with additional weather data:
 - Doppler radar maps
 - Downloaded data from National Weather Service
 - Additional weather measurements in propagation path

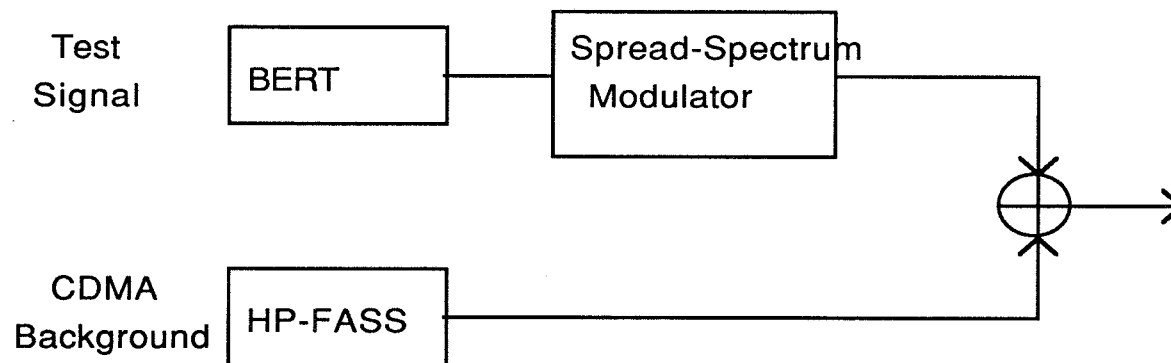
GT ACTS Experiment Phases

Phase I : Terminal and link RF Measurements:

- CW, Swept CW, noise, PSK, SBM modulations used for typical end-to-end link characterization measurements in two environments:
 - Clear Air
 - Inclement weather

Phase II : CDMA Measurements

- Use lab equipment to generate CDMA test signal with background CDMA traffic:



- Build code deinterleaver for BER measurements
- Use Spectrum Analyzer and Digital Waveform Capture for signal snapshots
- Scintillation effects on CDMA as key point of interest

REPORT OF THE WORKING GROUPS PLENARY MEETING

D.V. Rogers and R.K. Crane

As is customary at ACTS Propagation MiniWorkshops, the Science and Systems Working Groups met in Plenary Session to discuss issues related to the experiments being conducted with the ACTS Propagation Terminals. The main issues addressed were terminal/sensor calibration and data preprocessing. Results of this meeting are provided here.

I. Meteorological Sensor Calibration

A. Capacitance Rain Gauge

Much of the calibration discussion concerned the Young capacitance rain gauge that is supplied with the ACTS Propagation Terminal (APT). Several experimenters reported difficulties with the gauge, ranging from readings during periods of no rain, to an absence of readings on occasion in spite of clear evidence (*e.g.*, wet ground and reports from observers) of rain at the site. J. Goldhirsh (APL) reported good performance for many months with two gauges, and emphasized the importance of maintenance and frequent calibration of these devices for quality control.

ACTIONS:

After some discussion, the WGs prescribed a rain gauge calibration procedure to be performed once-per-week as follows:

- i) fill and purge rain gauge with water and allow at least 1.5 min for gauge to completely purge;
- ii) fill gauge (500 ml capacity) in five equal increments of 100 ml (data will be recorded by the data collection system);
- iii) ensure that rain gauge is purged of water at conclusion of test.

Experimenters should evaluate and record the performance of their rain gauge. S. Horan (NMSU) offered to receive weekly calibration data for each site on a monthly basis to evaluate the overall performance of the rain gauges. R.K. Crane (U. Oklahoma) will collaborate with D. Westenhaver (Auburn CCDS) to address the corresponding ACTSEdit issues.

B. Humidity Sensor

Some experimenters reported erroneous readings from the humidity sensors (*e.g.*, readings in excess of 100%). R. Henning (USF) noted that the DC voltage (≈ 17 V) supplied to the humidity sensor by the APT is below the

minimum (≈ 20 V) specified by the manufacturer. He was able to improve the performance by placing a battery in series with the supply voltage.

C. Mayer (U. Alaska) observed that the humidity sensor has a limited range of operating temperature, and that the sensor at the Alaska site was unable to operate during the coldest part of the winter. J. Goldhirsh asked if there are elements within the unit that should be replaced periodically, or if calibration were required. It was noted that the sensor should be placed so that it is out of direct sunlight. R. Henning stated that the manufacturer supplies an enclosure for the humidity sensor (\approx \$200) that seems to improve operation of the sensor. (The temperature sensor can also be placed in the same enclosure.)

ACTIONS:

D. Westenhaver stated that 20 VDC can be supplied by a barrier strip in the APT. He will determine and specify the appropriate modification to the experimenters.

Westenhaver will also distribute information on sensor enclosures provided by R. Henning and W. Vogel (U. Texas/ACTS Data Center). All sites should purchase or otherwise implement a suitable enclosure for the humidity sensor.

C. Anemometer

Some experimenters reported occasions when wind speeds recorded by the anemometer clearly appeared to be lower than actual speeds. R. Crane noted that the sensor cover can apparently be penetrated by water during rainfall, and that provision of drain holes might be necessary.

ACTION:

R. Crane will determine suitable locations to drill drain holes in the sensor enclosure, and specify the locations for the other experimenters.

II. *Beacon and Radiometer Calibrations*

Based on his presentations, "Radiometer Calibration Procedure" and "Beacon Attenuation Estimation Reference Level," which addressed calibration methodology in detail, R. Crane stated that the main remaining issue was what should be done with ACTSEdit to support reliable APT beacon and radiometer calibration procedures. (This item is also related to the preprocessing issues discussed below.)

The merits of establishing appropriate reference levels for the beacon and radiometer channels by essentially automatic means were emphasized. Iteration between beacon and radiometer readings improves the accuracy of both calibration sequences. Procedures can be defined to accomplish

beacon and radiometer calibrations in the desired automatic fashion, but they must be supported by ACTSEdit.

ACTION:

R. Crane and D. Westenhaver will collaborate to implement suitable automatic calibration procedures into ACTSEdit.

III. *Data Preprocessing*

A variety of data preprocessing issues were discussed, including reference-level estimation (calibration); removal of ranging spikes and level shifts from the 20-GHz beacon data; checking for extraneous bits in the cumulative distribution bins for beacon, radiometer and meteorological data; and formats for preprocessed data output from ACTSEdit to be used for data analysis.

R. Crane stated that the data flags should permit more designations than just the "good" or "bad" labels provided at present. At least a 2-bit status identifier should be provided. W. Vogel observed that data units greater than the current 16-byte limit could be used if desirable.

As the data preprocessing procedures are still under development, R. Hulays (UBC) asked what procedures should be followed in the meantime. There was additional discussion regarding importation of APT data into various spreadsheets for analysis support. Limitations were identified with some commercial spreadsheets for the data formats used in the data preprocessing software.

ACTIONS:

A Task Group composed of R. Crane, W. Vogel and D. Westenhaver was established to specify a fix for the data flagging and handling problems. Specifications for preprocessing procedures will address removal of 20-GHz beacon level variations caused by switches to/from ranging tones and radiometer and beacon calibrations via the iterative process (R. Crane). Data outputs for the beacon and radiometer channels will be final decibel levels for each channel.

A new program will be provided to automatically perform the preprocessing tasks and to supply summary information needed for the beacon and radiometer calibrations. The time required to preprocess one day of data should be less than 15 min. This program will generate a .PV1 file (format different from the .PVO file currently generated by ACTSEdit).

In the meantime, currently-available data preprocessing procedures should continue to be used to assist in identifying data glitches, etc. Once

the automated procedures are available in software, it will be a simple matter to reprocess these data.

IV. *Other Issues*

C. Mayer observed that the 20-Hz fast data sampling rate planned to be used for some tropospheric scintillation events is not available, having been deleted in its original form when the software filter was modified. As summer is the season of maximum scintillation activity, this feature should be provided soon if it is to be most beneficial.

Although weekly status reports from experimenters are no longer requested by NASA, D. Westenhaver stated that he has found frequent reports from the experimenters to be very helpful in monitoring APT operation and keeping aware of field problems. He requested that frequent reporting continue.

ACTIONS:

D. Westenhaver will address the implementation of 20-Hz sampling capability as a priority item. He will continue to maintain close contact with the experimenters via the existing communication channels to stay apprised of terminal operation and to keep experimenters informed.